112 | Springer Proceedings in Physics

T. Schanz
(Ed.)

Experimental Unsaturated Soil Mechanics

Springer

SPRINGER PROCEEDINGS IN PHYSICS 112

SPRINGER PROCEEDINGS IN PHYSICS

91 **The Dense Interstellar Medium in Galaxies**
Editors: S. Pfalzner, C. Kramer, C. Straubmeier, and A. Heithausen

92 **Beyond the Standard Model 2003**
Editor: H.V. Klapdor-Kleingrothaus

93 **ISSMGE**
Experimental Studies
Editor: T. Schanz

94 **ISSMGE**
Numerical and Theoretical Approaches
Editor: T. Schanz

95 **Computer Simulation Studies in Condensed-Matter Physics XVI**
Editors: D.P. Landau, S.P. Lewis, and H.-B. Schüttler

96 **Electromagnetics in a Complex World**
Editors: I.M. Pinto, V. Galdi, and L.B. Felsen

97 **Fields, Networks, Computational Methods and Systems in Modern Electrodynamics**
A Tribute to Leopold B. Felsen
Editors: P. Russer and M. Mongiardo

98 **Particle Physics and the Universe**
Proceedings of the 9th Adriatic Meeting, Sept. 2003, Dubrovnik
Editors: J. Trampetić and J. Wess

99 **Cosmic Explosions**
On the 10th Anniversary of SN1993J (IAU Colloquium 192)
Editors: J. M. Marcaide and K. W. Weiler

100 **Lasers in the Conservation of Artworks**
LACONA V Proceedings, Osnabrück, Germany, Sept. 15–18, 2003
Editors: K. Dickmann, C. Fotakis, and J.F. Asmus

101 **Progress in Turbulence**
Editors: J. Peinke, A. Kittel, S. Barth, and M. Oberlack

102 **Adaptive Optics for Industry and Medicine**
Proceedings
of the 4th International Workshop
Editor: U. Wittrock

103 **Computer Simulation Studies in Condensed-Matter Physics XVII**
Editors: D.P. Landau, S.P. Lewis, and H.-B. Schüttler

104 **Complex Computing-Networks**
Brain-like and Wave-oriented Electrodynamic Algorithms
Editors: I.C. Göknar and L. Sevgi

105 **Computer Simulation Studies in Condensed-Matter Physics XVIII**
Editors: D.P. Landau, S.P. Lewis, and H.-B. Schüttler

106 **Modern Trends in Geomechanics**
Editors: W. Wu and H.S. Yu

107 **Microscopy of Semiconducting Materials**
Proceedings of the 14th Conference, April 11–14, 2005, Oxford, UK
Editors: A.G. Cullis and J.L. Hutchison

108 **Hadron Collider Physics 2005**
Proceedings of the 1st Hadron Collider Physics Symposium, Les Diablerets, Switzerland, July 4–9, 2005
Editors: M. Campanelli, A. Clark, and X. Wu

109 **Progress in Turbulence 2**
Proceedings of the iTi Conference in Turbulence 2005
Editors: M. Oberlack et al.

110 **Nonequilibrium Carrier Dynamics in Semiconductors**
Proceedings
of the 14th International Conference, July 25-29, 2005, Chicago, USA
Editors: M. Saraniti, U. Ravaioli

111 **Vibration Problems ICOVP 2005**
Editors: E. Inan, A. Kiris

112 **Experimental Unsaturated Soil Mechanics**
Editor: T. Schanz

113 **Theoretical and Numerical Unsaturated Soil Mechanics**
Editor: T. Schanz

Volumes 66–90 are listed at the end of the book.

T. Schanz (Ed.)

Experimental Unsaturated Soil Mechanics

With 299 Figures and 67 Tables

Springer

Professor Dr. Ing. habil. Tom Schanz
Bauhaus-Universität Weimar
Laboratory of Soil Mechanics
Coudraystrasse 11c
99421 Weimar, Germany
tom.schanz@bauing.uni-weimar.de

ISSN 0930-8989

ISBN 978-3-540-69872-2 Springer Berlin Heidelberg New York

Library of Congress Control Number: 2007920611

Springer is a part of Springer Science+Business Media
springer.com

Typesetting: Integra Software Services Pvt. Ltd., Pondicherry, India
Cover design: WMX-Design, Heidelberg

Printed on acid-free paper SPIN: 11661139 42/Integra 5 4 3 2 1 0

Foreword

The event is a continuation of the series of International Conferences on Unsaturated Soils in Germany. The first International Conference was held during September 2003 in Bauhaus-University Weimar, Weimar, Germany. The current event is the second one in the series entitled "Mechanics of Unsaturated Soils." The primary objective of the Conference has been to discuss and understand unsaturated soil behaviour such that engineered activities are made better with times in terms of judgement and quality. We all realise by now that in addition to the knowledge on the classical concepts, it becomes an enormous challenging task to adapt convincing new concepts and present them in such a way that it could be used in engineering practices. During the last six years or so (2001–2007), scientific research works were extensively taken up by five scientific research teams from five German universities, whose scientific leaders are Wolfgang Ehlers (Universität Stuttgart), Jens Engel (HTW Dresden), Rainer Helmig and Holger Claas (Universität Stuttgart), Tom Schanz (Bauhaus Universität Weimar), Christos Vrettos, Helmut Meissner and Andreas Becker (Universität Kaiserslautern). The research studies involved theoretical and numerical approaches along with experimental studies on unsaturated soils. These two volumes present recent research findings obtained within this collaboration by the above research groups along with excellent contributions from several research groups throughout the World.

The experimental studies reported herein primarily focussed on the role of microstructure and fabric for the complex coupled hydro-mechanical behaviour of cohesive frictional materials. Several papers considered the relevance of temperature affecting the constitutive behaviour of clays. A careful reader may recognise that in both the topics there is an ambiguity with regard to the conclusions derived. Common features of state of the art theoretical and numerical approaches, including TPM (theory of porous media) and mixture theory, intend to describe the complex multi-field problems of fully coupled thermo-hydraulic-mechanical-chemical initial-boundary value problems. Additional important field of research includes optimization of numerical schemes to gain better computational performance. Applications include

highly toxic waste disposals, slope stability problems and contaminants transport in porous media. Some major significant contributions from the invited and keynote speakers are also included.

I would like to extend my deep sense of appreciation as the editor and the Head of the organizing committee, to many persons who have contributed either directly or indirectly to organize the International conference and to finalize these lecture notes. I would like to congratulate the authors for their very interesting presentations and the reported results and advances in the topics of the conference. I would like to thank all of those who promoted the conference in their respective home countries. These two volumes would have been not possible without financial support by the German Research Foundation (DFG, Deutsche Forschungsgemeinschaft) through grant FOR 440/2. We gratefully acknowledge the support of ISSMGE, especially TC6 "Unsaturated Soils" with its chairman Eduardo Alonso. I appreciate the effort of the members of the Technical committee and reviewers, who have spent their time to select the valuable contributions and to suggest the changes improving the presentation of the submitted papers. Finally, I wish to convey my thanks to all the keynote and invited speakers, authors, and delegates attending the conference.

I would like to express my deep sense of gratitude for the outstanding work performed by those involved in the technical and administrative organization of these proceedings. Special thanks go to Yvonne Lins. Typesetting of the proceedings was done by Venelin Chernogorov (alias Wily, Sofia University, Bulgaria, `wily@fmi.uni-sofia.bg`) in cooperation with Maria Datcheva. Last but not least we appreciate the fruitful cooperation with Springer publishers, especially the guidance provided by Thomas Ditzinger.

Weimar, *Tom Schanz*
March 2007

Contents

Part I

Microstructure and Fabric

Influence of Relative Density and Clay Fraction on Soils Collapse

Khelifa Abbeche[1], Farid Hammoud[1], and Tahar Ayadat[2]

[1] Civil Engineering Department, LARHYA, University of Batna, Avenue Chahid Boukhlouf, Batna 05000, Algeria abbechek@yahoo.fr, hammoud_farid@yahoo.fr
[2] Civil Engineering Department, University of Concordia, Sir George Williams Campus, 1515 St. Catherine West, EV002. 139, Montreal Quebec, Canada H3G-2W1 tayadat@yahoo.com

Summary. Most of the works conducted to investigate the parameters likely to govern the behavior of collapsible soils, have been dedicated to initial dry density, water content, degree of saturation and applied load. On the other hand, relatively few works have been oriented towards the study of the influence of clay fraction and relative density on the collapse of this type of soils. The experimental study, about reconstituted soils, presented in this paper, aims at highlighting the effect of relative density and clay fraction on the rate and magnitude of collapse.

Key words: collapsible soils, relative density, clay fraction, consolidation, oedometer test, inundation

1 Introduction

Rapid growth in arid and semiarid regions has brought increased focus on volume change characteristics of moisture sensitive unsaturated soils. One such type of concern is collapsible soil. The latter is likely to undergo a rearrangement of its grains, and a loss of cementation, upon wetting, resulting in substantial and rapid settlement under relatively low loads. Collapsible soils occur as naturally debris flows, rapid alluvial depositions, and wind-blown deposits. These soils are typically silt and sand size with a small amount of clay. The collapse phenomenon is also likely to occur in the case of compacted fills, used in man made structures such as earth dams, road subgrades, and embankments, which are also placed in an unsaturated state.

Some investigations were aimed at developing identification and stabilization methods (e.g. Jennings and Knight 1975, Ayadat and Belouahri 1996, Ayadat et al. 1998, Abbeche et al. 2005, etc). On the other hand, some other researchers (e.g. Ganeshan 1982, Ayadat et al. 1998, Cui and Magnan 2001, etc) have concentrated their works on the collapse mechanism.

Most of the work carried out on the parameters that govern the collapse behavior, has focused on the initial dry density, the water content, the degree of saturation and the applied load. Few studies have been conducted regarding the influence of the relative density and the clay fraction on the collapse of soils. The main interest of this paper lies in the study of the effect of these parameters on the soil collapse.

2 Materials, Equipment and Testing Procedure

In the present study eleven reconstituted samples composed of sand and clay in different proportions were tested. The proportions were chosen in order to obtain samples which meet the collapse criteria proposed by Lutenegger and Saber (1988) which distinguish between collapsible soils and non collapsible soils.

The sand used is washed river sand, whose characteristics are summarized as follows:

- sand equivalent, $E_s = 70\%$
- grain size distribution situated between 0.08 mm and 2.0 mm, of which $3.8\% < 0.08$ mm
- coefficient of uniformity, $C_u = 2.5$
- coefficient of curvature, $C_c = 0.56$

The clay used has the following characteristics:

- liquidity limit, $w_L = 41.50\%$
- plasticity limit, $w_P = 28.90\%$
- specific gravity of soil solids, $G_s = 2.7$
- percentage of particles finer than 2 µm (clay fraction), $CF = 32\%$

The reconstituted soils have the geotechnical characteristics given in Table 1 and the grain size distribution curves presented in Fig. 1.

Table 1. Geotechnical characteristics of soils

Soil	S1	S2	S3	S4	S5	S6	S7	S8	S9	S10	S11
Sand (%)	100	90	80	70	60	50	40	30	20	10	0
%PF < 80 µm	0	10	20	30	40	50	60	70	80	90	100
$e_{\max}$	0.765	0.773	0.817	0.828	0.846	0.913	0.955	1.007	1.035	1.184	1.472
$e_{\min}$	0.458	0.452	0.436	0.408	0.403	0.396	0.383	0.367	0.350	0.333	0.327
w_L (%)	–	13.7	15.1	16.1	19.3	21.4	26.8	34.0	34.3	40.6	41.5
w_P (%)	–	8.4	10.9	11.4	11.9	13.6	15.2	22.0	22.6	23.7	28.9
w_{opt} (%)	9.64	7.86	7.94	8.29	8.64	11.08	13.01	14.89	16.48	18.66	22.14

%PF < 80 µm percentage of particles finer than 80 µm

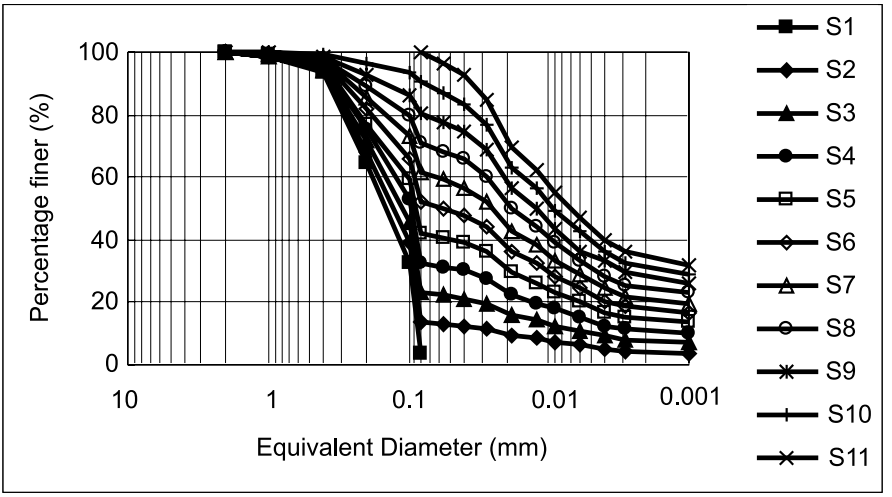

Fig. 1. Grain size distribution curves of reconstituted soils used

The soils studied was compacted at a given water content and a dry unit weight in a standard oedometric mold, in one layer, due to the small height of the ring (20 mm). The equipment used for the compaction procedure, which was made at the laboratory, is composed of a disk having a diameter slightly smaller than that of the ring, which is fixed to a stem of guidance and a disk shaped weight. The weight, having a mass of 152 g, sliding along the stem and that falls from a 15 cm height, comes to strike the disk, thus compacting the material in the oedometer ring.

The initial stage of sample preparation involves mixing the two components so as to obtain a well homogenized soil. Then it is absolutely necessary that meticulous preparation of a sample should be carried out to ensure a near perfect fit in the oedometer ring. This is achieved by first kneading the soil evenly in the oedometric mold and then compacting it with a certain energy (number of weight drops) following the procedure described above. The sample was then struck off level with the top of the ring with a rigid steel blade, to get a plane surface. After weighed, the specimen was put back in position in the oedometer so as to carry out the compressibility test described by Jennings and Knight (1975), for determining the collapse potential. The loading stage of a sample, at an initial water content and an initial unit weight, took place incrementally up to a pressure of 0.2 MPa and then flooded with water and left for 24 hours, and the consolidation test is carried on to its normal maximum loading limit. The sample settlements, before inundation and after, at different time intervals had been measured. Figure2 shows the stages of the collapse potential test. The collapse potential C_p is then defined as follows:

$$C_P\ (\%) = \frac{\Delta e_C}{1 + e_0} \times 100 \tag{1}$$

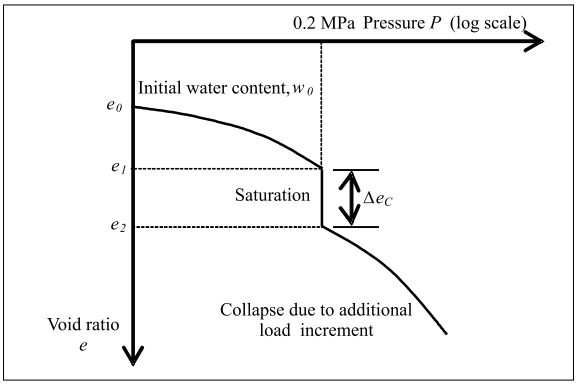

Fig. 2. Typical collapse potential one dimensional consolidation test

where Δe_C is the change in void ratio of the sample upon flooding and e_0 is the initial void ratio before loading.

The tests were conducted on soils at different water contents and relative densities. The relative density is defined as

$$D_r = \frac{e_{\max} - e_0}{e_{\max} - e_{\min}} \tag{2}$$

The retained values of initial water content and relative density are:

- relative density, D_r: 10%, 30% and 50%
- initial water content, w_0: 2%, 4% and 6%

Each soil sample was tested at the values of D_r given above and for each value, the initial water content was varied three times (i.e. 2%, 4% and 6%). As explained below, soils S2, S3, S4 and S5 were also tested at a relative density of 70%. Therefore, in all, 111 tests were carried out.

3 Results and Discussion

The results obtained clearly indicate that the collapses of the different soils are in keeping with the classification of Jennings and Knight (1975) and agree with the known properties of natural collapsible soils. For soils S1 to S11 the collapse potential C_p was found to vary from 0.16% to 12.55% for a water content $w_0 = 2\%$, from 0.13% to 5.73% for a water content $w_0 = 4\%$ and from 0.045% to 3.63% for a water content $w_0 = 6\%$. These results correspond to the categories ranging from "no problem" to "severe trouble" (Table 2). On the other hand, when the water content increases, the collapse potential decreases or even can be equal to zero above a certain value. It is also noted that, at a given water content, the collapse potential decreases with the increase of the initial unit weight. These results are in agreement with those obtained

Table 2. Relation of collapse potential to the severity of foundation problem

C_P (%)	Severity of problem
0–1	No problem
1–5	Moderate trouble
5–10	Trouble
10–20	Severe trouble
> 20	Very severe trouble

by Lawton et al. (1989) and Ayadat et al. (1998). Consequently, it is noticed that the artificially prepared soils possess a behavior analogous to those met in situ, which justifies the tests program adopted.

The influence of the relative density on the collapse potential of soils is presented in Figs 3**a**, 3**b** and 3**c**. It can be seen that C_P decreases when the relative density increases, whatever the soil type and the water content considered. It is also noticed that for a given relative density, the collapse potential decreases when the water content increases. For $D_r = 50\%$ and $w_0 = 6\%$, Figure 3**c** shows that except soils S2, S3, S4 and S5, all tested soils have a value of $C_P < 1$ and are therefore not susceptible to collapse. It is also noticed that the initial water content (i.e. 6%) is close to the values of the optimum water content w_{opt} of the collapsible soils studied (i.e. S2, S3, S4

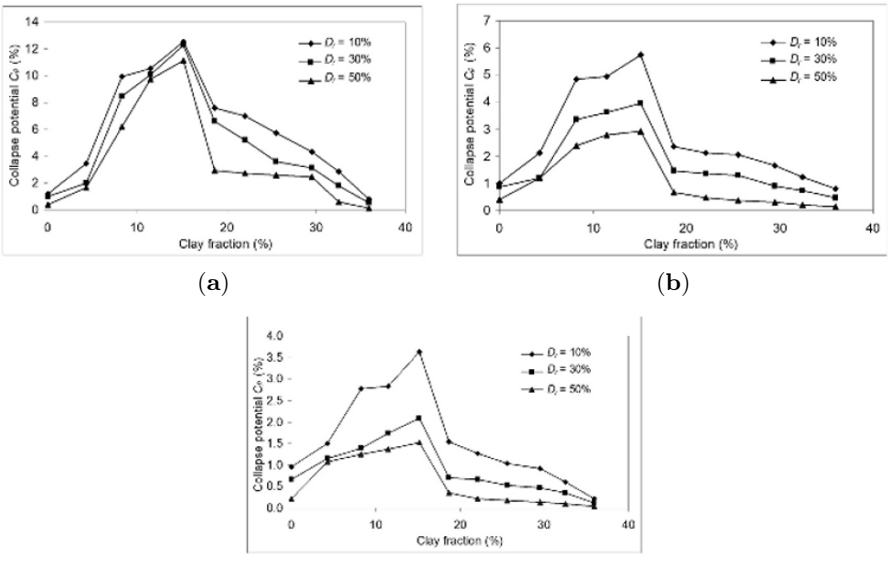

Fig. 3. Changes of collapse potential versus clay fraction, **(a)** for $w_0 = 2\%$, **(b)** for $w_0 = 4\%$, **(c)** for $w_0 = 6\%$

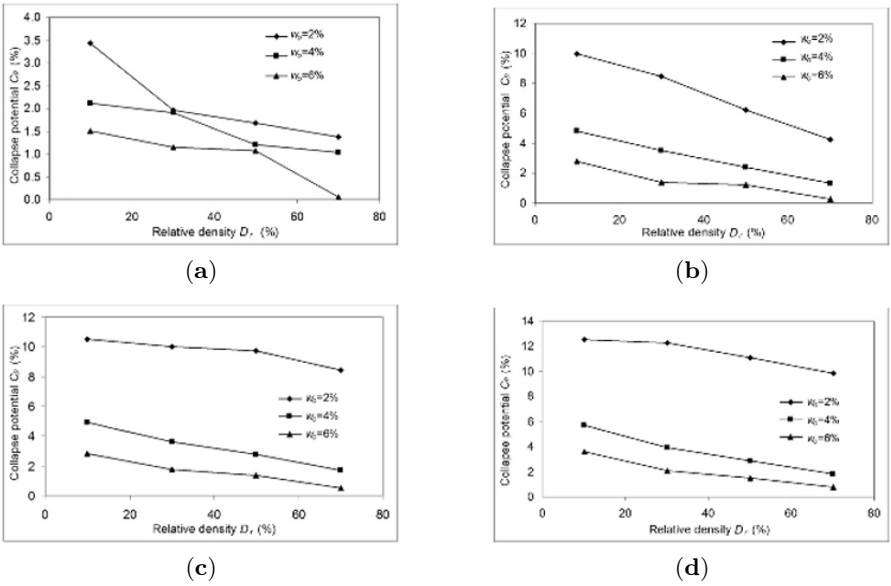

Fig. 4. Collapse potential variation versus relative density, **(a)** for soil S2, **(b)** for soil S3, **(c)** for soil S4, **(d)** for soil S5

and S5) given in Table 1. Consequently, it was judged useful to test these four soils with a more important relative density ($D_r = 70\%$). The results obtained are presented in Figs 4**a**, 4**b**, 4**c** and 4**d**. It can be noticed from these figures that, for a water content $w_0 = 6\%$, the collapse potential is negligible when the relative density is superior to 65%. It is also noticed that the more the soils are loose and have low initial water content and the more the increase of the collapse potential is important.

Figures 3**a**, 3**b** and 3**c**, which illustrate also the influence of the clay fraction on C_P, show that the collapse of soils depends on the clay content present in their structure, which confirms the observation made by Lawton et al. (1992). From these curves, it is clear that the collapse potential is negligible when the clay percentage is greater than 30%. Below 5%, a collapse settlement, which remains small, is likely to take place, while maximum collapse is reached for about 15%. This result is in keeping with the interval established by Lawton et al. (1992) who indicated that maximum collapse potential, for the natural soils studied, is obtained when of the clay fraction is situated in the range 10% and 40%. The classification proposed in Table 3 allows identifying the soils that are subjected to the collapse phenomenon.

Table 3. Proposed classification of collapsible soils

Clay Fraction CF ($\% < 2\,\mu m$)	Probability of collapse
$5\% < CF < 15\%$	High probability
$15\% < CF < 30\%$	Probability of collapse
$CF > 30\%$	No collapse

4 Conclusions

This paper has presented results of one-dimensional oedometer collapse tests using the procedure described by Jennings and Knight (1975). The main conclusions that can be drawn on the basis of the test results are as follows:

- It is possible to assess the soil collapsibility in the laboratory by means of the relative density, on the one hand, and the clay fraction, on the other hand.
- It is estimated that a soil is not subjected to collapse if its relative density is superior to 65% with initial water content close to the optimum water content.
- A soil is not susceptible to collapse if its clay fraction is greater than 30%.

References

Abbeche K, Mokrani L, Boumekik A (2005) Contribution à l'identification des sols effondrables, Revue Française de Géotechnique, 110:85–90

Ayadat T, Belouahri B (1996) Influence du coefficient d'uniformité sur l'amplitude et le taux de l'affaissement des sols, Revue Française de Géotechnique, 76:25–34

Ayadat T, Belouahri B, Ait Ammar R (1998) La migration des particules fines comme approche d'explication du mécanisme de l'effondrement des sols, Revue Française de Géotechnique, 83:1–9

Ayadat T, Ouali S (1999) Identification des sols affaissables basée sur les limites d'Atterberg, Revue Française de Géotechnique, 86:53–56

Cui YJ, Magnan JP (2001) Affaissements locaux dus à l'infiltration d'eau en géomécanique environnemental, Hermes, pp. 139–164

Ganeshan V (1982) Strength and collapse characteristics of compacted residual soils. Master Thesis, Asian Institute of Technology, Bangkok

Jennings JE, Knight K (1975) The additional settlement of foundation due to collapse of sandy soils on wetting, Proc 4th Inter Conf on Soil Mechanics and Foundation Engineering, 1:316–319

Lawton EC, Fragaszy RJ, James HH (1989) Collapse of compacted clayey sand, J Geotechnical Engineering, ASCE 155(9):1252–1267

Lawton EC, Fragaszy RJ, Hetherington MD (1992) Review of wetting-induced collapse in compacted soil, J Geotechnical Engineering 118(9):1376–1394

Lutenegger AJ, Saber RT (1988) Determination of collapse potential of soils, Geotechnical Testing J 11(3):173–178

Microstructure Features in the Behaviour of Engineered Barriers for Nuclear Waste Disposal

Pierre Delage

Ecole Nationale des Ponts et Chaussées, Paris (CERMES, Institut Navier), 6–8 av. B. Pascal, F–77455 Marne–la–Vallée cedex 2, France
pierre.delage@enpc.fr

Summary. Engineered barriers made up of bricks of compacted swelling clays are considered as potential barriers for the isolation of high activity nuclear waste at great depth. To better understand their coupled hydro-mechanical response, the microstructure of engineered barriers has been studied by various authors by using most often scanning electron microscope observations and mercury intrusion pore size distribution measurements (MIP). These studies confirmed that the microstructure of compacted bentonites was made up of aggregates with two classes of pores: inter-aggregates pores and intra-aggregate pores. Further investigation conducted by using X-Ray diffractometry at low angles conducted more recently provided deeper insight into the hydration mechanisms that occur during hydration. This paper presents some results obtained by various authors by using these techniques. It shows how the hydration mechanisms occurring at the level of the clay particles inside the aggregates help interpreting existing MIP data. Some conclusions about the water retention properties of compacted bentonites with or without swelling allowed are given. Some consequences on the water transfer properties of compacted bentonites are also drawn. In both cases, the clogging of inter-aggregate pores due to particle exfoliation has a significant effect.

Key words: engineered barrier, bentonite, hydration, microstructure, radioactive waste, swelling, coupling

1 Introduction

Isolation of high activity nuclear waste at great depth is designed according the concept of multibarrier system aimed at safely isolating the waste from the biosphere. In this system, the placement of engineered barriers made up of compacted swelling clay between the waste canister and the geological barrier (host rock) as shown in Fig. 1 is considered as a possible option.

In this option, bricks of clay are statically compacted at given water content, often to unit masses as high as 1.8–2 $\mathrm{Mg/m^3}$. Bricks are placed all around

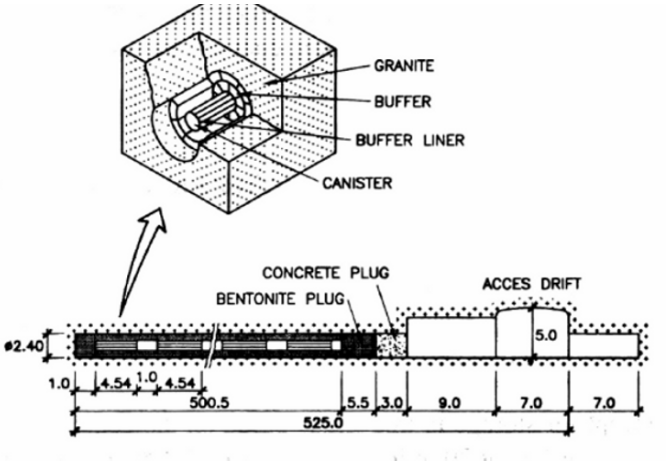

Fig. 1. Typical scheme of a deep geological repository for nuclear waste disposal (Gens and Olivella 2001)

the canister as shown in the figure, in order to fill the annular space between the canister and the excavation. Engineered barriers are submitted to complex thermo-hydro-chemo-mechanical actions due to the heat emitted by the nuclear waste, to infiltration by pore water coming from the host rock, to the movement of radionuclides through the barrier and to the emission of gas due to the anaerobic degradation of the canister, among other things. A typical feature that characterises the condition of engineered barriers is that they are hydrated with very small swelling permitted in the volume between canister and host rock. We will see later on that this particular situation is interesting in terms of microstructure changes.

For these reasons, intense investigation has been carried out in the past decades on the behaviour of engineered barriers. Researches clearly showed that microstructure features played an essential role. Some effects of microstructure on the behaviour of engineered barriers are described in this paper.

2 The Microstructure of Compacted Soils

2.1 Low Plasticity Soils

Following the initial Lambe's model (1958) of the microstructure of compacted soils that was based on the double layer theory, experimental observations of the microstructure of compacted soils based on scanning electron microscopy (SEM) and mercury intrusion porosimetry (MIP) afterwards provided a more realistic description of the real microstructure. Pioneering works in this field were provided by Barden and Sides (1970), Diamond (1970), Sridharan et al.

(1971). In mercury intrusion porosimetry, mercury, a non wetting fluid, is progressively intruded in a porous medium by increasing its pressure. As shown by Laplace's equation (1), the applied pressure can be related to an entrance pore radius as follows:

$$p_{\mathrm{Hg}} = \sigma \cos\theta \left(\frac{1}{r_1} + \frac{1}{r_2} \right) \tag{1}$$

where r_1 and r_2 are the radius of curvature of the interface. Under the hypothesis of a cylindrical pore of radius r, the air-water interface is spherical and $r_1 = r_2 = r$. Laplace's relation between the mercury pressure and the corresponding radius reduces to the following equation (sometimes called Washburn's equation, from Washburn 1921):

$$p_{\mathrm{Hg}} = \frac{2\sigma \cos\theta}{r} \tag{2}$$

The interfacial capillary parameters of the mercury/solid phase/vacuum system are the interfacial tension $\sigma = 0.484\,\mathrm{N/m}$ and the contact angle $\theta = 141.3°$ (Diamond 1970). Mercury intrusion tests are performed by running a progressive mercury pressure increase from vacuum up to 200 MPa. Tests have to be performed on dehydrated samples. Most often, dehydration is made by freeze-drying, where the sample is firstly quickly frozen by rapid immersion in cooled liquid nitrogen and then sublimated in a freeze-dryer (Sridharan et al. 1971, Tovey and Wong 1973, Gillott 1973, Delage and Pellerin 1984). To avoid any boiling when plunging samples, liquid nitrogen needs to be cooled to its freezing point (−210°C) by applying vacuum. Also, samples have to be small enough to allow high speed freezing, that leads to a cryptocrystalline structure with no volumetric expansion.

Ahmed et al. (1974) presented the pore size distribution (PSD) curves of three samples of grundite compacted on the dry side, the wet side and at optimum water content, as shown in Fig. 2.

The aggregate structure already suspected in soils compacted on the dry side of the optimum (Barden and Sides 1970, Diamond 1970) was confirmed by the bimodal shape of the PSD curve. This curve defines two pore populations, namely the inter-aggregate and the intra-aggregate populations respectively. In the figure, the entrance pore diameter of the inter-aggregate pores is defined by the inflection point at 30 µm, which is quite large. Above the corresponding pressure, mercury fills all the inter-aggregate porosity, finally surrounding the aggregates themselves. Mercury starts to penetrate the aggregates at a pressure that corresponds to the entrance diameter of 0.05 µm. On each curve, the degree of saturation of the compacted sample is also plotted, showing the inflection point corresponds to porous volume that was full of water. This confirms that the inter-aggregate pores in the dry sample are full of air. Results similar to that of Ahmed et al. (1974) have been obtained by Delage et al. (1996) and Romero et al. (1999), among others.

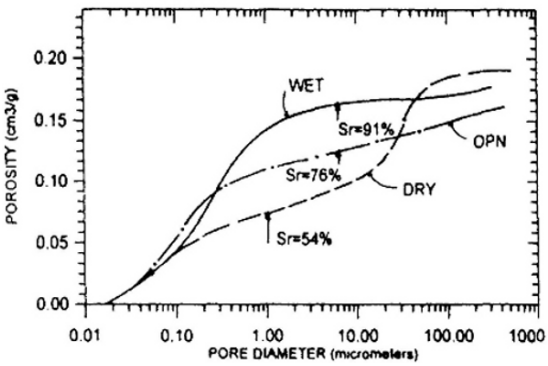

Fig. 2. PSD curves of a grundite statically compacted at various points of the Proctor curve (Ahmed et al. 1974)

A SEM photo of a dry compacted silt of low plasticity (Jossigny silt) is presented in Fig. 3. To ensure a well defined observation surface, samples have been freeze-fractured just before being sublimated. In this technique (Delage et al. 1982), the observation plane is defined by the fracture ice that works like an impregnation resin. It does not follow any possible weakness path in the microstructure and directly cross the different microstructure levels.

In Figure 3, the aggregates made up silt grains (10 to 20 µm in diameters) are clearly apparent together with the inter-aggregate pores. In the dry state, the clay fraction of Jossigny silt is not very apparent because platelets are closely stuck to the silt grains. As commented previously, large inter-aggregates pores are full of air and hence physico-chemical effects involving clay water interactions take place inside the aggregates. Based on this photo, the question of the location of air water menisci is interesting and indeed can

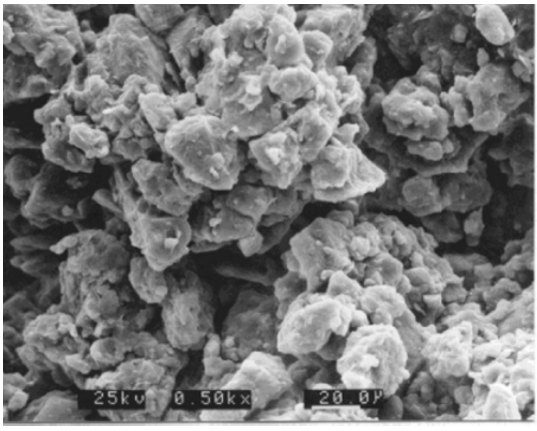

Fig. 3. SEM micrograph of a compacted Jossigny silt, dry side (Delage et al. 1996)

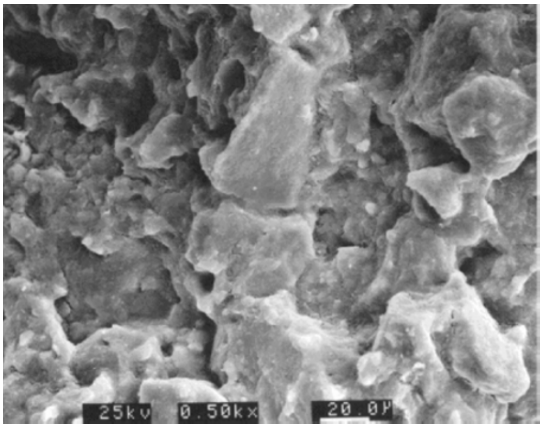

Fig. 4. SEM micrograph of a compacted Jossigny silt, wet side (Delage et al. 1996)

be further elucidated by using an environmental scanning electron microscope in which observation is carried out on wet samples and where the ambient relative humidity can be increased. It is probable in Fig. 3 that menisci are located inside the aggregates and that the connecting links between aggregates, that govern the overall macroscopical resistance, are made up of hydrated clay links.

A significantly different microstructure is observed on the wet side, as shown in Fig. 4. The microstructure is more of a matrix type with dominant appearance of clay platelets that constitute a matrix containing the silt grains. Neither aggregates nor the corresponding pore population can be observed. In other words, even in low plasticity soils, hydration makes the clay particles become much more voluminous and visually apparent. The unimodal PSD curve of Fig. 2 (also observed in the Jossigny silt) is compatible with the matrix microstructure.

Going back to MIP investigation, an interesting feature relating microstructure changes when volume is decreased has been obtained from the results of Sridharan et al. (1971), as presented in Fig. 5 (Delage and Graham 1995). The figure, that compares samples statically compacted at $w = 21\%$ at various void ratios included between 0.85 and 0.56, shows that the decrease in volume at constant water content only concerns the largest pores that exist prior to compression. With the pore volume saturated by water in smallest pores at $w = 21\%$ being represented on the figure, the figure also shows that compression affected the pores full of air. The PSD of saturated pores smaller than $0.2\,\mu$m in diameter is remarkably unaffected by the decrease in volume. Note that a similar mechanism had been observed in a natural sensitive clay of moderate plasticity by Delage and Lefebvre (1984). It appears here that compression at void ratio smaller than 0.56 would concern a quasi-saturated microstructure with build-up and subsequent dissipation of pore pressures.

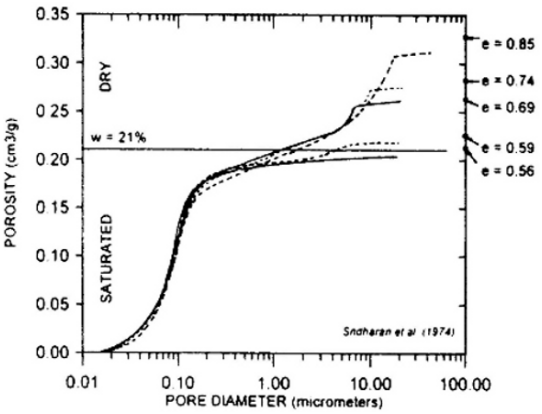

Fig. 5. Effect of increased compaction on the pore size distribution of a compacted soil (Delage and Graham 1995, after Sridharan et al. 1971)

2.2 Compacted Plastic Clays, Engineered Barriers

In common geotechnical engineering, compaction studies rather concerned low plasticity soils able to constitute earthworks like embankments or earthdams, with little attention given to plastic soils. This tendency has changed in the past decade with increased attention given to the behaviour of engineered barriers made up of heavily compacted swelling clays considered as possible barrier to be used in the multibarrier concept of isolating at great depth high activity nuclear waste. Investigations carried out on engineered barriers progressively showed the importance of microstructure effects for a sound understanding of the coupled hydro-mechanical behaviour of engineered barriers. In this context, the pioneering works conducted on low plasticity clay described above have been extended to high plasticity compacted clays.

Microstructure units

Swelling clays (that include bentonites, a term used in practice) are made up a significant amount of smectites, the active clay mineral responsible for swelling when hydrated. As compared to less plastic clays like kaolinite, the specificity of smectites (or montmorillonites) is related to the mineralogical composition of the elementary layer, depicted in Fig. 6. Whereas kaolinite is made up of the juxtaposition of one tetrahedral and of one octahedral layer (see the figure where the composition and structure of these layers are represented), a octahedral layer is located between two tetrahedral layer in smectites. Whereas two adjacent kaolinite particles will be strongly linked together because of possible hydrogen bridges acting between the oxygen and hydroxyls ions on top and bottom side of the layer, no such strong link exists between the two montmorillonite planes where oxygen atoms are located. As

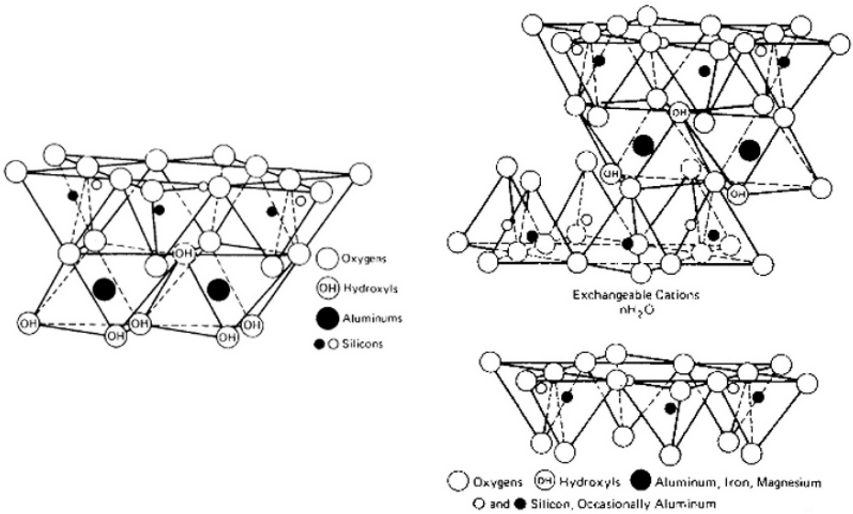

Fig. 6. Structure of clay minerals (from Mitchell and Soga 2005). Left: kaolinite; Right: montmorillonite

shown schematically in the figure, exchangeable cations with their hydrating water molecules shells can penetrate this space due to the electrical attraction caused by the electrical deficiency that is typical of clay minerals.

Note that in the case of illite that has the same structure as montmorillonite, the stability of the stacking of various elementary layers is strongly ensured by potassium ions K^+. In other words, the main difference between kaolinite and illite on one side and montmorillonite on the other side is related to the stability of the clay platelet made up of stacks of elementary layers stuck together. The various terms used to describe clay microstructure are now recalled:

- The *elementary layer*, represented in Fig. 6, is defined for montmorillonite by a 9.6 Å (96 nm) thickness in the direction perpendicular to the plane (called $d_{(001)}$). This level can be observed indirectly by standard X-Ray diffraction analysis. Direct observation can also be conducted by transmission electron microscope (see for example Ben Rhaïem et al. 1985).
- The clay *platelet* or *particle* (*crystal* or *quasicrystal* are somewhat found in the literature, see Aylmore and Quirk 1962), made up the stacking of elementary layers, with a number comprised between several (in the case of clay suspensions) to several hundreds in dry states. This important feature will be described further on in more detail. Clay particles can be observed using scanning electron microscope techniques.
- The aggregate made up of clays particles aggregated together, and somewhat similar with those previously observed. Aggregates can be observed

using scanning electron microscope and detected by MIP, as discussed above.

The microstructure of compacted bentonite

Figure 7 presents a SEM photo of a compacted Kunigel clay (Cui et al. 2002) obtained on a freeze fractured and freeze-dried sample. Kunigel clay (Komine and Ogata 1994) is a Japanese clay made up of 64% Na smectite with a liquid limit w_L equal to 474 ($w_P = 27$) and a specific surface of 687 m^2/g. The sample observed in the figure was statically compacted at a unit mass of 2 Mg/m^3 and a water content of 8%, giving rise to an as-compacted suction of 57 MPa.

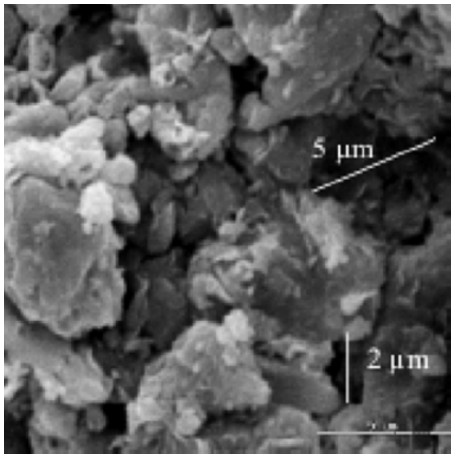

Fig. 7. SEM photo of a compacted Kunigel clay (Cui et al. 2002)

In spite of the high compaction density, aggregates made up of aggregated particles of clays are clearly apparent. Aggregates are separated by inter-aggregates pores that appear to be significantly large with a diameter up to 2–5 µm. Aggregates are composed of clay platelets made up of stacks of elementary layers as described in Fig. 6. Advanced investigation based on low angle X-Ray diffractometry on similar compacted bentonites by Saiyouri et al. (2000) that will be discussed further on provide interesting further precisions on the structures of the aggregates and on their changes during hydration and swelling. Observations carried out using an ESEM have also been published by Lloret et al. (2003) and Agus and Schanz (2005), among others.

MIP investigation conducted by various researchers (including Romero et al. 1999, Cui et al. 2002, Lloret et al. 2003, Agus and Schanz 2005 and Delage et al. 2006) showed PSD curves similar to that of Ahmed et al. (1974) showed in Fig. 2, evidencing the inter-aggregate and the intra-aggregate pore

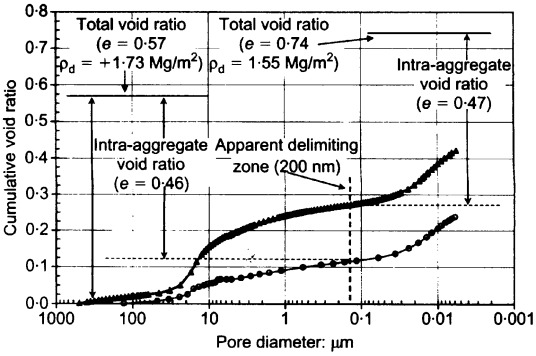

Fig. 8. Intruded pore volume in compacted Almeria clay (Lloret et al. 2003)

populations (see Fig. 8). By comparing the intruded mercury volume at the maximum mercury pressure to the total pore volume, as suggested in Delage and Lefebvre (1984), it is possible to check whether or not the sample porosity has been entirely filled by mercury. This appeared to be the case in low plasticity soils as for instance in the grundite of Ahmed et al. (1974) or the silt of Delage et al. (1996). This is no longer true in the case of plastic soils because of the presence of montmorillonite minerals and of the very thin pores that exist inside the aggregates. As shown in Fig. 6, the clay platelets are not stable with changes in water content and they may become quite thin at higher water contents. The fineness of the platelets gives rise to thin pores that are much thinner than the smaller entrance diameter accessible in MIP, close to 6 nm (60 Å).

This point is illustrated in the PSD curve of compacted Almeria clay presented in Fig. 8 (Lloret et al. 2003). In this figure, the total intra-aggregate void ratio appears to be much larger than the intruded one, due to an important amount of pores of very small entrance diameter. Interestingly, the value of this unintruded porosity is the same at the two densities considered in the figure (dry unit mass of 1.55 and 1.73 Mg/m^3 respectively, water content of 13%).

Observation of Fig. 8 also shows that the entrance inter-aggregate diameter is in the order of 18 μm whereas the intra-aggregate entrance diameter is close to 0.012 μm. Note also that the two curves are similar in shape for the pores that are smaller than 1 μm. A presentation of the same curves as done in Fig. 5 would also show more clearly that compression from a void ratio equal to 0.57 down to 0.47 only affected the largest existing inter-aggregate pores with no effect on the intra-aggregate porosity. In other word, no compression of the aggregates occurred between these two void ratios.

3 Effect of Changes in Water Content

Swelling soils are known to be sensitive to changes in water content with swelling when hydrated and shrinkage when dried. A common explanation is generally based on the ability of water molecules that hydrate exchangeable cations to penetrate in the interlayer planar spaces inside the platelets, as mentioned in Fig. 6. The most commonly used theory of soil swelling is based on the diffuse double layer theory and is based on the hypothesis of regularly scattered individual clay layers, as suggested by Bolt (1956). Although hydration mechanisms appear not to respect this hypothesis, this theory gave some interesting results, mainly in the case of Na^+ montmorillonite (see for instance Sridharan and Jayadeva 1982, Tripathy et al. 2004, Schanz and Tripathy 2005). The calculations of repulsion due to electrical interaction is very dependent of the valence of the cations, with significant differences between Na^+ and Ca^{++} for example. Indeed, the behaviour of swelling soils also depend of the valence of the dominant exchangeable cation with swelling properties enhanced with Na^+, but in a different fashion from what the DDL theory predicts. No more considerations on DDL approaches will be made in this paper, and interested readers are invited to read the papers mentioned previously.

Figure 9 shows the PSD curve of two compacted MX 80 bentonites (MX 80 is a Wyoming montmorillonite with $w_L = 520$ and $S = 700\,\mathrm{m^2/g}$) compacted at the same moderate density ($1.32\,\mathrm{Mg/m^3}$) at two different water contents (12.5 and 28.5%) with suction respectively comprised between 2 and 7 MPa at 12.5% and higher than 50 MPa at 28.5% (Delage et al. 2006). The figure

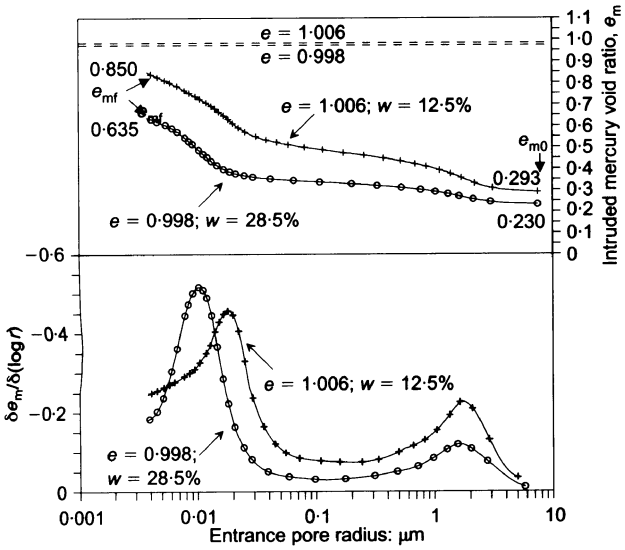

Fig. 9. Effect of initial water content on two compacted MX 80 bentonite samples at the same density (Delage et al. 2006)

shows that, whereas the two PSD curves are similar in shape – with however a smaller entrance pore radius in the wettest sample – the unintruded porosity is twice larger for the wettest sample at low suction.

The observation of the effect of drying and swelling on a heavily compacted ($\rho_d = 2\,\mathrm{Mg/m^3}$) sand bentonite mixture (50–50) made up of Calcigel bentonite (50–60% in montmorillonite) at a water content of 11% has been carried out by Agus and Schanz (2005). Sample was afterwards equilibrated using the vapour equilibrium technique under a suction of 22.7 MPa that gave an equilibrated value of water content equal to 9%. The swollen sample was obtained by lefting a compacted specimen above distilled water in a desiccator for 180 days and a final water content of 19% was reached. Results are presented in Fig. 10 in terms of PSD curves. As compared to the bimodal PSD curve of the as-compacted sample that defines an inter-aggregate entrance pore diameter close to 10 µm and an intra-aggregate entrance pore diameter close to 0.12 µm, the PSD curve after swelling shows two points:

- A new pore population around 1 µm appears, at a diameter smaller than that of the inter-aggregate porosity and larger than that of the intra-aggregate porosity. The corresponding pore volume corresponds to 44% of the total pore volume.
- A large amount of porosity is created below the limit of MIP, defining an unintruded porosity approximately equal to the intruded one. This feature is compatible with that observed on samples at higher water content in Fig. 9, showing that samples under low suction have a large very small porosity.

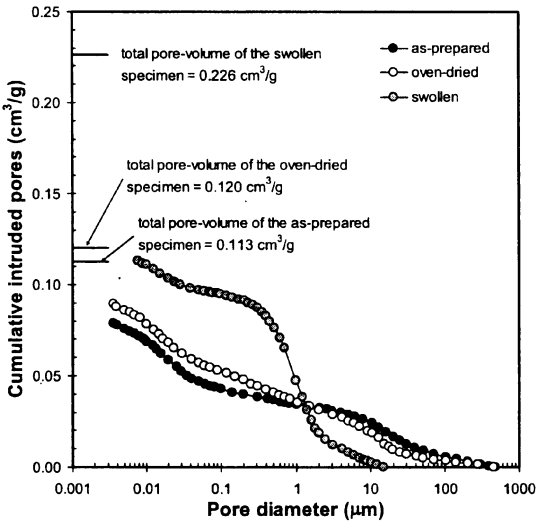

Fig. 10. Effect of wetting and drying on a heavily compacted Calcigel – sand mixture (Agus and Schanz 2005)

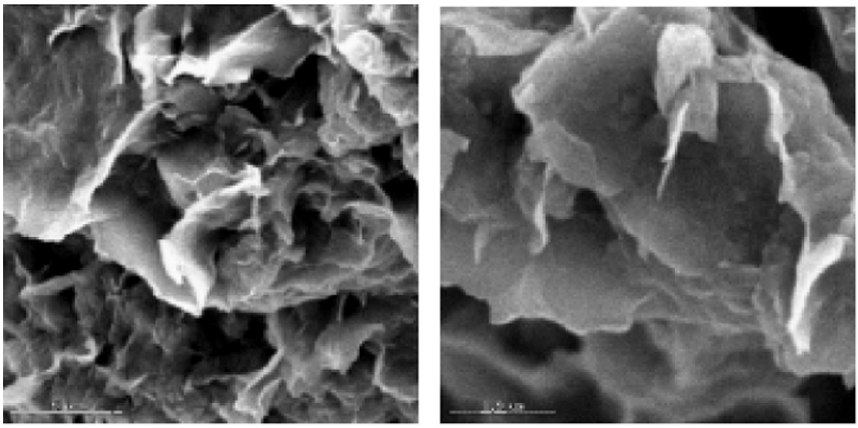

Fig. 11. SEM observation of Kunigel clay at zero suction (Cui et al. 2002)

As already observed by Ahmed et al. (1974) on samples compacted dry of optimum with bimodal porosity, there is little difference between the freeze-dried as-compacted sample (suction 22.7 MPa) and the oven-dried sample (suction estimated at 1 GPa according to Fredlund and Rahardjo 1993). Note also that the unintruded porosities detected in the two curves are similar. This shows that the suction of 22.7 MPa is high enough to already mobilize all the shrinkage potential of both the aggregates themselves and the assemblage of aggregates.

Figure 11 (Cui et al. 2002) presents two SEM photos carried out on samples of compacted Kunigel clay (described in the as-compacted state in Fig. 7) after hydration and swelling under zero suction. Aggregates appeared to be much less apparent in the various SEM observations conducted, as seen in the figure. Typically, the microstructure rather appears to be of a honeycomb type (Collins and McGown 1974) with clear presence of rather thin clay particle that form the walls of pores with a diameter of various micrometers. Similar microstructure also typical of clay gels have been observed in swollen bentonite (Marcial et al. 2002). The question arises as whether these pores could correspond or not to the 1 µm entrance diameter observed in the PSD curve of the swollen sample of Fig. 10.

4 Hydration Mechanisms in Smectites

Detailed investigations carried out on the hydration of dry smectites (Mooney et al. 1952, Calvet 1972, Prost 1975, Sposito and Prost 1982, Bird 1984, among others) showed that hydration initially occurred in the hydrophilic sites of the clay, i.e. on the mineral surface and around the exchangeable cations in the inter-layer spaces inside the particles. This first stage of hydration is called homogeneous hydration and it occurs by the ordered and progressive placement

of water molecules along the clay surface, layer after layer up to 4 layers. Detailed observation using transmission and scanning electron microscope also showed that smectite particles change with changes in water content, with a number of stacked clay layers that decreases when the clay is hydrated (Tessier 1990).

More recently, investigations using X-ray diffraction at low angles conducted on samples of compacted MX 80 and FoCa 7 clays hydrated at various suctions (Saiyouri et al. 1998, 2000, 2004) have been carried out. These results, based on Pons' probabilistic model (Pons et al. 1981), provided essential information on the hydration mechanism occurring at the particle level in compacted clays similar to that considered here. Results obtained on compacted MX 80 are presented in Fig. 12 **a** and **b**.

Starting from a high value of suction, hydration occurs in an organised manner with the progressive placement of 1, 2, 3 and 4 layers of water molecules along the clay monolayers in the interlayer spaces inside the particle. The corresponding distances between the clay monolayers (see Fig. 13) start from 9.6 Å with no water (see also the clay layer structure represented in Fig. 6) and are equal to 12.6, 15.6, 18.6 and 21.6 Å with 1, 2, 3 and 4 layers of adsorbed water molecules, respectively. Note that the basal spacing $2d$ is obtained by subtracting from the interlayer distance the clay thickness (9.6 Å), giving $2d = 3$, 6, 9 and 12 Å for 1, 2, 3 and 4 water layers, respectively.

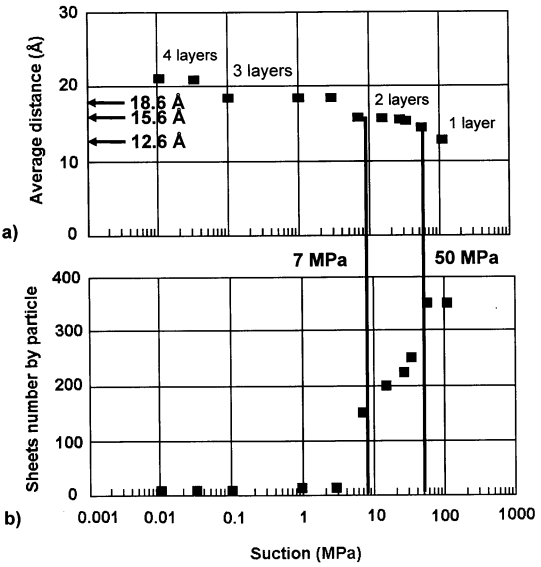

Fig. 12. Effect of a suction decrease (hydration) on the MX 80 particles (after Saiyouri et al. 1998, 2004): **a**) increase in the number of adsorbed water layers; **b**) decrease in the number of stacked layers per particle

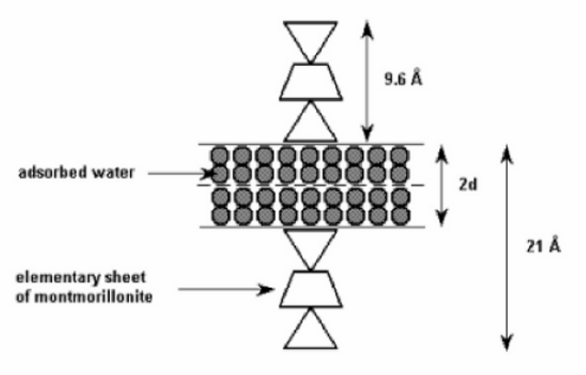

Fig. 13. Schematic distance between two layers of montmorillonite (Saiyouri et al. 2000)

As seen in Fig. 12**a**, the placement of water molecules is a function of suction, with only one layer above 50 MPa ($d = 1.5$ Å), a second water layer ($d = 3$ Å) when passing from 50 to 7 MPa, a third layer between 7 MPa and 60kPa ($d = 4.5$ Å), and a fourth layer below 60 kPa ($d = 6$ Å). Similar results were obtained on FoCa clay by the same authors and on other bentonites by Delvaux et al. (1992). Simultaneously, the number of clay layers per particle decreases with suction (Fig. 12**b**) starting with thick particles made up of 350 clay monolayers above a 50 MPa suction with a number of layers progressively decreasing down to 150 layers at 7 MPa and 10 layers at 3 MPa. Hence, the swelling mechanism starting from high suction is the result of two combined phenomena:

i) the progressive insertion of successive layers of water molecules in the interlayer spaces inside he particles;
ii) the subdivision of particles into thinner ones that are made up of a smaller number of stacked layers. Note that the observation of the compacted Kunigel clay submitted to zero suction in Fig. 11 where thin clay particles are observed is compatible with this mechanism.

In terms of changes in pore morphology inside aggregates in zones that cannot be investigated by mercury intrusion, these mechanisms have the following consequences :

i) the enlargement of the planar spaces located inside the clay particles at given distances that are function of the suction applied;
ii) the progressive creation inside the saturated aggregates of larger interparticles pores that are not necessarily planar.

By considering at various given suctions the value of the specific surface of the clay, the number of layers of adsorbed water along the clay layers and the number of clay layers stacked in a particle, Saiyouri et al. (2000, 2004)

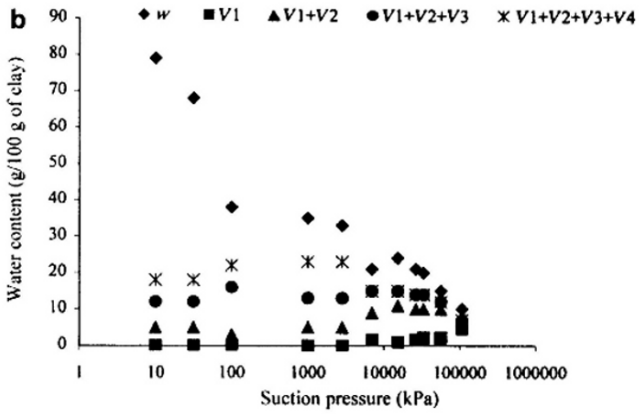

Fig. 14. Water distribution in MX 80 compacted sample as a function of suction. W is the water content, V_1 to V_4 are the water amounts in the interlayer spaces containing 1 to 4 water layers (Saiyouri et al. 2004)

were able to distinguish, in the total water content of the clay, the interlayer water from the interparticle water, as seen in Fig. 14. Comparison beetwen the V_4 points (that correspond to the totality of the interlayer water) and the points representing the total water content gives an indication of quantity of the interparticle water with respect to suction. The figure shows that a significant amount of interparticle water starts to appear during hydration when suction goes down below 60–70 MPa. This means that above 70 MPa, swelling is mainly due to the interlayer water. At 1 MPa, 22 g/100 g of water are located between layers whereas approximately 13 g/100 g of water are located in interparticle pores, with distances between particle larger than 21.6 Å. At a suction of 10 kPa, close to the fully swollen state, the maximum distance is estimated close to 150 Å. The authors also stated that these interparticle distances were large enough to allow for the development of diffuse double layers close to particle surfaces inside the aggregates. In other words, the DDL theory could be able to play a significant role in swelling at suctions below 5 MPa where it could account for approximately 25% of the total amount of absorbed water. Conversely, DDL phenomena could account for approximately 70% of the volume of absorbed water under a suction of 10 kPa, i.e. in the swollen state.

Considering the change in aggregate microstructure with suction, it can be said that aggregates in a drier sample are made up of a smaller number of thicker particles whereas aggregates in a wetter sample are made up of a larger number of thinner particles, giving rise to a larger proportion of inter-particle porosity. As derived from Fig. 12, suction changes have a well defined effect on the intra-aggregate porosity. The values of suction at which changes in the number of adsorbed water layers occur apparently do not depend on the

bentonite considered. These data will help interpreting the very thin porosity that is detected in pore size distribution curves below 3.5 nm.

The data of Fig. 12 also suggest that the threshold values of suction (or water potential) evidenced in the figure correspond to energetic barriers that separate the various levels of water molecules adsorbed in the inter-layers spaces. Physically, this correspond to a quite strong adsorption links for the first layer (water potential higher than 50 MPa) and to a weak one for the third layer (water potential smaller than 7 MPa). These values are apparently independent of the smectite considered (Saiyouri et al. 2004, Delvaux et al. 1992).

5 Application to Compacted Bentonites

5.1 About the Intra-Aggregate Porosity

In an attempt to extrapolate pore size distribution curves in the range of pores smaller than 3.5 nm in radius, it appears useful to deduce from previous data the dimensions that correspond to the two intra-aggregates pore populations that have been investigated by X-Ray low angle diffractometry, as follows:

- Interparticle pores radii deduced by Saiyouri et al. (1998, 2004). In a first approximation, it seems reasonable to approximate these pores as cylindrical pores as in standard mercury intrusion analysis. Interparticle distances estimated between 20 and 100 Å corresponds in Fig. 15 to pore radii of 10 and 50 Å, i.e. 1 to 5 nm.
  Planar interlayer pores located inside the particles. In this case, r_2 in equation (1) is infinite and Laplace's law writes:

$$p_{\mathrm{Hg}} = \frac{\sigma \cos\theta}{r} \tag{3}$$

Consequently, the x scale of the pore size distribution curves in zones where planar pores are suspected to exist should be divided by two. As commented earlier, the adsorption of 1, 2, 3 and 4 water layers correspond to d distances of 1.5, 3, 4.5 and 6 Å, respectively.

These approximate estimations can be used to better understand the pore morphology at dimensions smaller than 3.5 nm, as shown in Fig. 15. They help to interpret the trend shown by the pore size distribution curves in this zone.

In the figure, the representation of the range of size of interparticle pore estimated using XRD at low angle size (radii between 10 and 50 Å) is reasonably compatible with the order of magnitude of the intra-aggregate porosity given by the PSD curve.

The morphology inside the aggregate is now depending of the sample suction in the way defined in Fig. 12. In this regard, the interlayer distances

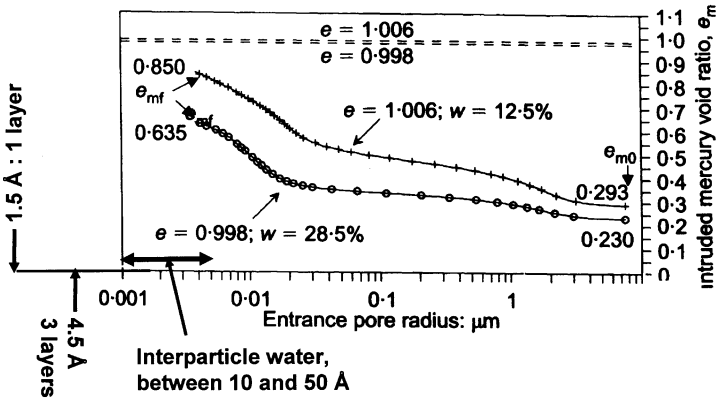

Fig. 15. Integration of XRD low angle data in PSD

corresponding to 3 layers (4.5 Å) and 1 layer (1.5 Å) of water molecules have been plotted in an extended logarithmic x axis in the PSD graph of Fig. 15.

The higher value of the very thin porosity ($r < 3.7$ nm) observed in the looser sample at $w = 28.5\%$ can be related to a low initial value of suction (approximately 4 MPa) that corresponds to a higher number of thinner particles that contain between 10 and 100 clay layers. The particle division at this suction is compatible with the development of a significant inter-particle porosity, corresponding to the high value of very thin porosity of the sample. The smaller amount of very thin porosity observed in the sample at $w = 12.5\%$ can be related to a higher suction (> 50 MPa) characterised by less numerous thicker particles (350 layers) that have only one layer of adsorbed water molecules.

Figure 14 can also be used to interpret some aspects of the change in microstructure observed in Fig. 10 in swollen Calcigel clay subsequently to suction reduction to zero. As suggested by the mechanism illustrated in Fig. 12, the zero suction hydrated state is composed of thin particles with a significant amount of interparticle pores. Observation of the corresponding PSD curve in Fig. 10 indeed shows a considerable pore volume of small dimensions suggested by the shape of the curve at pore diameters smaller than 10 nm (100 Å). Besides the change observed at a diameter of 1 μm, the swollen volume at small pores in Fig. 10 corresponds to the two kinds of swelling mechanisms identified in Fig. 14, i.e. inter and intra-particle mechanisms. In this figure, the disappearance of the inter-aggregate porosity can be related to the filling of these pores by the exfoliation of the aggregates limiting the inter-aggregate pore. Actually, the exfoliation process can also be interpreted with similar mechanisms of reduction in thickness and separation of particles in thinner particles. This process helps filling the inter-aggregates pores with a gel honeycomb structure similar to that observed in Fig. 11.

5.2 On the Retention Properties of the Confined Engineered Barrier

As commented earlier, very little expansion is allowed to the engineered barrier submitted to hydration between the canister and the wall in the host rock. This situation has been suspected to have some effects on the retention and transfer properties of the engineered barrier. A specific experimental device aimed at determining the retention properties of the engineering barrier with no volume changes allowed has been proposed by Yahia-Aissa et al. (2001). In this device, compacted clay samples are inserted in rigid cells that are specially designed to allow vapour exchanges. The water retention properties with no volume changes have been determined by placing the cells in desiccators with saturated saline solutions at constant temperature.

The data in Fig. 16 show firstly the retention properties obtained in a standard manner in desiccators with volume changes allowed (see Delage et al. 1998 for more details). The graph gathers experimental data from a compacted FoCa 7 bentonite and that of FoCa 7 powder. There is very little difference between the two data set, showing negligible influence of the sample density and indicating the predominant effects of physico-chemical actions, since no particular pore configuration can be invoked to justify any capillary effect in the case of the powder. The threshold values of suction (50 and 7 MPa) derived from the analysis of Fig. 12 are also reported in the y log axis. Starting from an initial suction of 110 MPa, it is possible to indicate on the water retention curve the number of intra-particle water layers, defining three zone with 1, 2

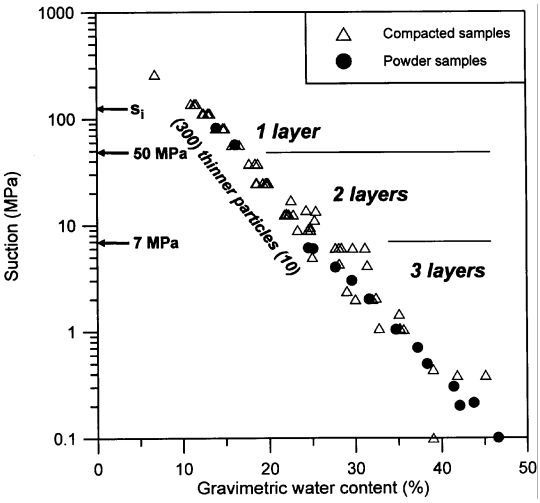

Fig. 16. Water retention properties of FoCa 7 engineered barrier (Yahia-Aissa et al. 2001)

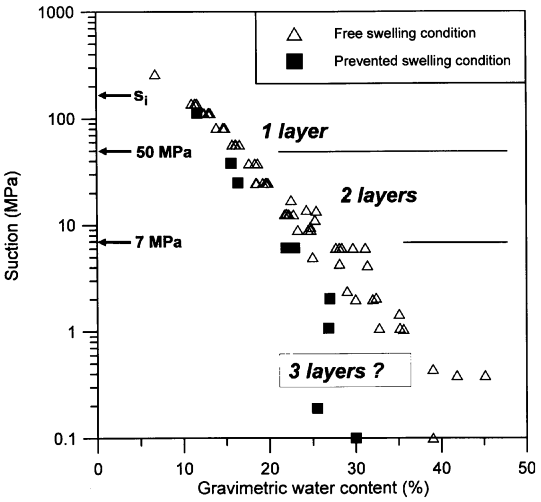

Fig. 17. Effect of volume constraint on the retention properties of FoCa 7 barrier

and 3 layers. Simultaneously, as indicated in the figure, the number of layers in the clay particles decreases from 300 down to 10.

The effect of volume constraint is described in Fig. 17. One can observe that the constant volume condition does not allow anymore the adsorption of third layer, whereas the adsorption of the two first layers of water seems to occur, like in the free swelling condition, from the initial state ($s = 110\,\text{MPa}$) down to a suction of 7 MPa. As suggested previously, this seems to indicate that the adsorption of the two first layers that occurs with a number of clay layers decreasing from 350 down to 150 in the case of compacted FoCa 7 clay (Saiyouri et al. 1998) corresponds to a significantly higher level of energy than the third layer, when also the number of layers per particle goes down to 10 with significant creation of inter-particle pores. In other words, the main effect of volume constraint is to prevent the separation of particles into thinner ones and the corresponding development of inter-particle voids. It is also likely that the creation of extra particles when passing from 350 layers to 150 clay layers progressively clog the initial inter-aggregate porosity.

6 Concluding Remarks

Microstructure studies of engineered barriers have been developed in various research groups in Europe in the last decade to better understand the coupled hydro-mechanical behaviour of compacted bentonites used as engineered barriers to isolate high activity nuclear waste at great depth. The examination of some results published in the literature and their interpretation based on the careful description of the process of hydration of smectites allowed

to complete the understanding of the changes in microstructure that occur in compacted bentonite during hydration. The description of the changes in shape of the smectite particles with suction allow to describe more precisely what occurs inside the aggregates of the compacted bentonite. As compared with compacted low plastic soils in which an analysis in terms of aggregates made up of stable particles is sufficient, the precise description of the change in shape with suction of the clay particles inside the aggregates give significant complementary information.

Some consequences have been drawn in this paper in terms of retention properties. Other important consequences also affect transfer properties, as suggested by Loiseau et al. (2002) who also showed that the changes in water permeability of a compacted bentonite during infiltration was not as expected in standard unsaturated soil mechanics analysis. Similar mechanisms also help understanding some ageing effect observed in compacted bentonite (Delage et al. 2006).

Obviously, the high sensitivity of the smectite microstructure to changes in water content invites to some precautions when using standard approaches of describing the retention and transfer phenomena in unsaturated compacted bentonites. This is particularly true in numerical calculations aimed at predicting the rate of infiltration of the engineered barriers.

References

Agus SS, Schanz T (2005) Effect of shrinking and swelling on microstructures and fabric of a compacted bentonite-sand mixture, In: Proc Int Conf on Problematic Soils, Cyprus 2:543–550

Ahmed S, Lovell CW, Diamonds S (1974) Pore sizes and strength of compacted clay, ASCE J Geotechnical Eng 100:407–425

Aylmore LAG, Quirk JP (1962) The structural status of clay systems, In: Proc 9th Nat Conf on Clays and Clay Minerals. Pergamon, Oxford, pp 104–130

Barden L, Sides GR (1970) Engineering behaviour and structure of compacted clay, ASCE J Soil Mech Found Div 96:1171–1200

Ben Rhaïem H, Pons CH, Tessier D (1985) Factors affecting the microstructure of smectites: role of cations and history of applied stresses, In: Schultz et al. (eds) Proc Int Clay Conf, Denver, The Clay Mineralogical Soc, pp 292–297

Bird P (1984) Hydration phase diagrams and friction of montmorillonite under laboratory and geologic conditions with implications for shale compaction, slope stability and strength of fault gauge, Tectonophysics 107:235–260

Bolt GH (1956) Physico-chemical analysis of the compressibility of pure clays, Géotechnique 6:86–93

Calvet R (1972) Adsorption de l'eau sur les argiles; Etude de l'hydratation de la montmorillonite, Bull Soc Chimique de France 8:3097–3104

Cui YJ, Loiseau C, Delage P (2002) Microstructure changes of a confined swelling soil due to suction controlled hydration, In: Proc 3rd Int Conf on Unsaturated Soils, UNSAT'2002. Recife, Brazil, Balkema 2:593–598

Collins K, McGown A (1974) The form and function of microfabric features in a variety of natural soils, Géotechnique 24(2):233–254

Delage P, Pellerin FM (1984) Influence de la lyophilisation sur la structure d'une argile sensible du Québec, Clay Minerals 19:151–160

Delage P, Tessier D, Marcel-Audiguier M (1982) Use of the Cryoscan apparatus for observation of freeze-fractured planes of a sensitive Quebec clay in scanning electron microscopy, Can Geotech J 19(1):111–114

Delage P, Audiguier M, Cui YJ, Howat MD (1996) Microstructure of a compacted silt, Can Geotech J 33:150–158

Delage P, Graham J (1995) The mechanical behaviour of unsaturated soils, In: Alonso EE, Delage P (eds) Proc 1st Int Conf on Unsaturated soils Paris, Balkema 3:1223–1256

Delage P, Lefebvre G (1984) Study of the structure of a sensitive Champlain clay and its evolution during consolidation, Can Geotech J 21(1):21–35

Delage P, Howat M, Cui YJ (1998) The relationship between suction and swelling properties in a heavily compacted unsaturated clay, Eng Geology 50(1–2):31–48

Delage P, Marcial D, Cui YJ, Ruiz X (2006) Ageing effects in a compacted bentonite: a microstructure approach, Géotechnique 56(5):291–304

Delvaux B, Tessier D, Herbillon A, Burtin G, Jaunet AM, Vielvoye L (1992) Morphology, texture and microstructure of halloysiticsoil clays as related to weathering and exchangeable cations, Clays and Clay Min 40(4):446–456

Diamond S (1970) Pore size distribution in clays, Clays and Clay Min 18:7–23

Diamond S (1971) Microstructure and pore structure of impact compacted clays, Clays and Clay Minerals 19:239–241

Fredlund DG, Rahardjo H (1993) Soil mechanics for unsaturated soils. Wiley, New-York

Gens A, Olivella S (2001) Clay barriers in radioactive waste disposal, Revue Française de Génie Civil 5(6):845–856

Gillott JE (1973) Methods of sample preparation for microstructureal analysis of soil, In: Soil Microscopy, Proc 4th Int Working Meeting on Soil Micromorphology, Kingston, pp 143–164

Komine H, Ogata N (1994) Experimental study on swelling characteristics of compacted bentonites, Can Geotech J 31:478–490

Lambe TW (1958) The structure of compacted soil, J Soil Mech Found Div 84(SM2):1–34

Loiseau C, Cui YJ, Delage P (2002) The gradient effect on the water flow through a compacted swelling soil, In: Proc. 3rd Int Conf Unsaturated Soils, UNSAT'2002 Recife, Brazil, Balkema 1:395–400

Lloret A, Villar MV, Sanchez M, Gens A, Pintado X, Alonso EE (2003) Mechanical behaviour of heavily compacted bentonite under high suction changes, Géotechnique 53(1):27–40

Marcial D (2003) Comportement hydromécanique et microstructural des matériaux de barrières ouvragées. PhD Thesis, Ecole des Ponts, Paris

Marcial D, Delage P, Cui YJ (2002) On the high stress compression of bentonites, Can Geotech J 39:1–9

Mitchell JK, Soga K (2005) Fundamentals of soil behaviour. John Wiley, New-York

Mooney RW, Keenan AC, Wood LA (1952) Adsorption of water vapor by montmorillonite. II. Effect of exchangeable ions and lattice swelling as measured from X-ray diffraction, J Amer Chem Soc 74:1371–1374

Nalezny CL, Li MC (1967) Effects of soil moisture and thixotropic hardening on the swell behaviour of compacted expansive soils, Highway Research Record No 209. Highway Research Board, Washington DC

Pons CH, Rousseaux F, Tchoubar D (1981) Utilisation du rayonnement synchrotron en diffusion aux petits angles pour l'étude du gonflement des smectites, Clay Minerals 16:23–42

Prost R (1975) Interactions between adsorbed water molecules and the structure of clay minerals: hydration of smectites. In: Bailey SW (ed) Proc Int Clay Conf 1975: Mexico City, Mexico. Applied Pub, Wilmette IL:351–359

Romero E, Gens A, Lloret A (1999) Water permeability, water retention and microstructure of unsaturated compacted Boom clay, Eng Geology 54:117–127

Saiyouri N, Hicher PY, Tessier D (1998) Microstructural analysis of highly compacted clay swelling, In: Proc. 2nd Int Conf on Unsaturated Soils Academic publishers, Beijing, China 1:119–124

Saiyouri N, Hicher PY, Tessier D (2000) Microstructural approach and transfer water modelling in highly compacted unsaturated swelling clays, Mech Cohesive Frictional Mater 5:41–60

Saiyouri N, Tessier D, Hicher PY (2004) Experimental study of swelling in unsaturated compacted clays, Clay Minerals 39:469–479

Schanz T, Tripathy S (2005) Soil-water characteristic curves of clays from physicochemical concepts, In: Proc Int Conf on Problematic Soils. Famagusta, Cyprus 1:219–228

Sposito G, Prost R (1982) Structure of water adsorbed on smectites, Chem Rev USA 82:552–573

Sridharan A, Altschaeffl AG, Diamond S (1971) Pore size distribution studies, ASCE J of the Soil Mech Found Div 97:771–787

Sridharan A, Jayadeva MS (1982) Double layer theory and compressibility of clays, Géotechnique 32(2):133–144

Tessier D (1990) In: Decarreau A (ed) Matériaux Argileux, Structure, Propriétés et Applications. Soc. Fr. Minéralogie et Cristallographie, Paris, France 1:387–445

Tovey NK, Wong KY (1973) The preparation of soils and other geological materials for the scanning electron microscope, In: Proc Int Symp on Soil Structure, Gothenburg, Sweden, pp 176–183

Tripathy S, Sridharan A, Schanz T (2004) Swelling pressures of compacted bentonites from diffuse layer theory, Can Geotech J 41:437–450

Washburn EW (1921) A method of determining the distribution of pore sizes in a porous material, Proc of the National Academy of Science 7:115

Yahia-Aissa M, Delage P, Cui YJ (2001) In: Adachi, Fukue (eds) Suction-water relationship in swelling clays, Clay Science for Engineering, IS-Shizuoka Int Symp on Suction, Swelling, Permeability and Structure of Clays, Balkema, pp 65–68

Microstructure of Gypsiferous Crust and Its Importance to Unsaturated Soil Behaviour

Ghazi Mokdad[1], Omran Alshihabi[1], and Leo Stroosnijder[2]

[1] Faculty of Agriculture, Damascus University, Syria ghazi57@scs-net.org, omran-alshihabi@hotmail.com
[2] Department of Irrigation and Soil & Water Conservation, Wageningen Agricultural University, The Netherland Leo.Stroosnijder@wur.nl

Summary. Formation of gypsiferous crust in agriculture lands deters seedling emergence, which constitutes a major problem around the world. The objective of this study is to investigate the micro-morphology of gypsiferous crust and its influence on unsaturated soil behavior. Samples containing 47% of gypsum were taken from Granada (North Syria), then left to dry under natural conditions. Undistributed soil samples (8×8 cm) of the crust and underlying soil material were taken in tins and impregnated with polyester resin. Thin sections were prepared, and examined with a petrographic microscope (Olympus) in plane and polarized light. The microstructure of these samples showed the distribution of soil materials and the types of pores. The crust consisted of clay, silt, calcite and gypsum attributed to the mechanical impact of raindrops. The main effect of raindrops on the soil surface layer was clogging the pores by means of the mentioned materials, which was the dominant mechanisms of crust formation. According to the structure of these soils, the infiltration rate reached a very low value and a remarkable increase in stiffness was observed.

Key words: undistributed soil, unsaturated soil, microstructure, gypsiferous crust, infiltration rate

Introduction

Gypsiferous soils Make up 22% of Syrian agricultural soil, with gypsum content of 1–80% (Ilaiwi 1983). A crust forms when these soils are exposed to rainfall or irrigation (Stroosnijder 1995). This crust hinders seed germination, and possible recultivation and planting. This study was initiated to describe the micromorphology of gypsiferous crust.

Gypsum crusts have been reported from many (semi-) arid regions. Their geographic distribution closely coincides with the areas receiving less than 250 mm rainfall per year (Watson 1982). Extensive gypsum crusts have been described in Middle East countries, where they are a major limitation for crop production because water infiltration rate, seedling emergence and crop

growth are largely controlled by the thickness and gypsum content of the crust (Nafie 1989). The severity of the mechanical hindrance that gypsum crusts oppose to crop development can be assessed by measuring penetration resistance. Morphological and micro morphological study of gypsiferous soils from the Middle Euphrates Basin (Syria) have been studied (Habib and Robert 1992). The effect of moisture and gypsum content on the penetration resistance of gypsiferous horizons has been studied by Poch and Verplancke (1997) but gypsum crusts developing on the soil surface have not been given yet the same attention (Jafarzadeh 1991). The objective of the present paper is to investigate the microstructure of gypsiferous crust in the soil surface.

Materials and Methods

Soils: The soils chosen for this study from Granada which are located in North-East Syria (35°57′9″N – 38°48′4″E and 290 m above the sea). The mean annual rainfall is 250 mm, distributed in winter season with high rainfall intensity (47 mm/h) and long period of drought. The soils were silty loam (gypsiferous soil). Soil samples are taken from the top layer (0–20 cm) of uncultivated area, The samples were characterized for particle size distribution using hydrometer method (Gee and Bauder 1986), calcium carbonate content using the volumetric calcimeter method (Nelson 1986), and organic matter content by wet combustion (Nelson and Somers 1986). Results are presented in Table 1. Gypsum content in the soil is high (47%). The organic matter content in the soil was low (1.2%). Other undistributed samples are taken, packed with boxes and then coated by cotton to maintain the crust surface with no alterations.

Thin sections preparation: Undistributed soil samples (8 × 8 cm) of the crust and underlying soil material were packed with boxes and coated with cotton to maintain the crust surface with no alterations. To study the micro morphology of the soil crust in Wageningen university (Holland). Thin sections preparation were made according to the method of (FitzPatrick 1993), the samples were oven dried (40–50°C) for 48 hours to remove hydroscopic water. Then the samples were taken in tins and impregnated with polyester resin, and it is included at vacuum for four weeks, to be given the cohesion. After that samples were cut, polished, trimmed with oil used, and lastly covered and in examined with a petrographic microscope (Olympus) in plane and polarized light. The micro morphological description used the terminology of Bullock et al. (1985).

The determination of the mineralogical gypsum crust was carried out with X-ray diffraction technique. For that a Philips PW 1710/1820 diffraction equipped with a co X-ray tube was used ($\lambda = 1.7889$ Å).

Table 1. Physical and chemical analysis of Granada soil

Symbol soil	USDA Texture.T	Granulo. Analysis			pH 1:2.5	ECs dS/m	Organic matter OM%	$CaCO_3$ %	Gypsum %
		Clay	Silt	Sand					
G	Si.L	35.4	55.9	8.5	7.8	4.2	1.2	13.0	47.0

Results and Discussion

Crust Formation

The crust consists of two layers (layer 1 and layer 2, Fig. 1), which are parallel oriented to each other. Each layer displays a textural fining upward towards the soil surface

Layer 1 is situated at the soil surface. The upper part is 100 µm thick (Fig. 2) densely packed and it consists of a mixture of clay and silt sized calcite particles (< 10 µm). Occasional gypsum crystals of similar sizes are present. The microstructure is compact grain microstructure, macro voids (> 10 µm) are absent.

The lower part (Fig. 3) is built up of denticular gypsum crystals (100–300 µm) and micro aggregates consisting of a mixture of clay and calcite crystals (< 10 µm). Occasionally calcite crystals ranging in size from 10–150 µm are present. Voughs (50–150 µm) frequently occur showing that the lower part of layer 1 is more porous than the upper part.

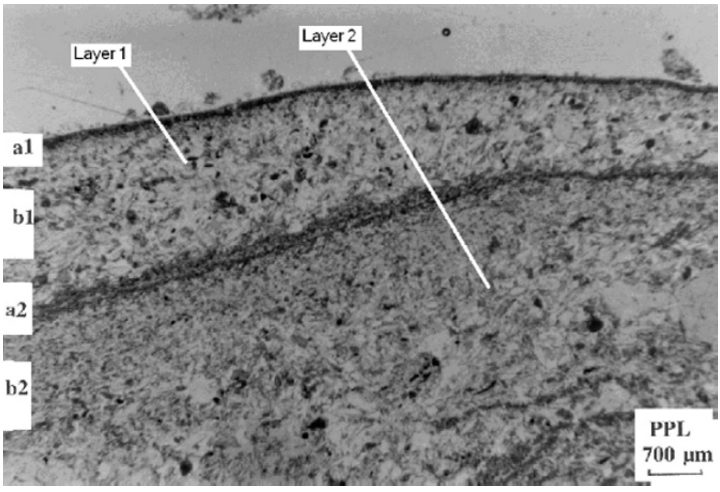

Fig. 1. General overview of the crust

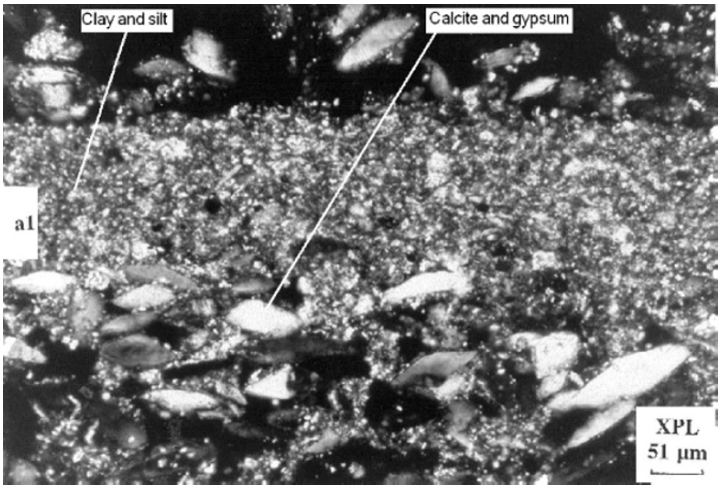

Fig. 2. Detail of the upper part of layer 1

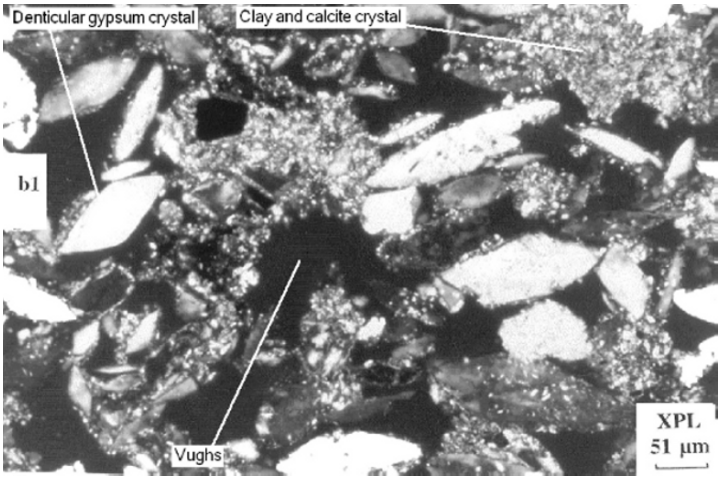

Fig. 3. Detail of the lower part of layer 1

Layer 2 is situated below layer 1.

The upper part (Fig. 4) is similar to the upper part of layer 1 regarding the grain size distribution, mineralogy, density and microstructure. The thickness of the upper part ranges from 150 to 250 µm.

The lower part (Fig. 5) is built up of denticulated gypsum crystals smaller sized than those of layer 1 (50–100 µm). In addition micro aggregates (50–100 µm) consisting of clay and fine (< 10 µm) calcite crystals are present. Occasionally calcite crystals (50–100 µm) occur. Few voughs (< 50 µm) are present, the microstructure is compact grainy. Layer 2 is finer textured, sig-

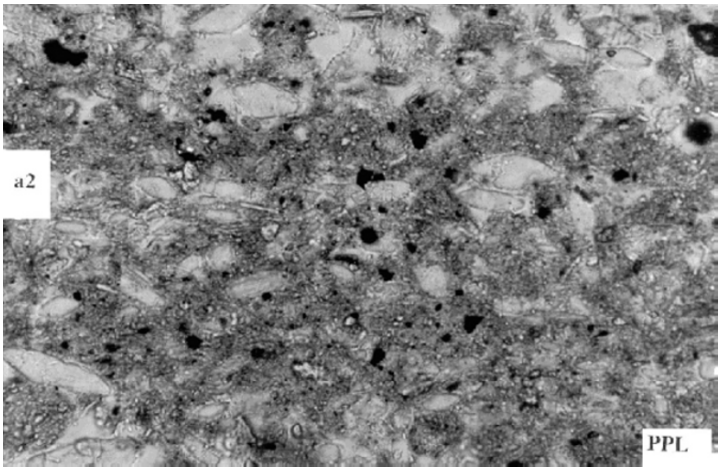

Fig. 4. Details of the upper part of layer 2

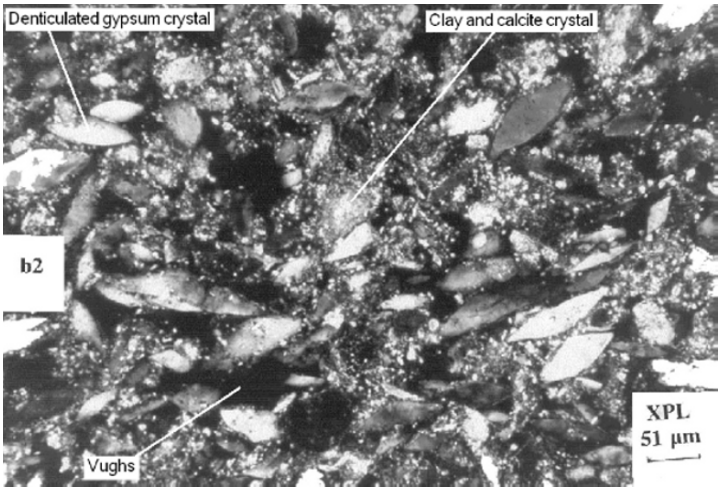

Fig. 5. Detail of the lower part of layer 2

nificant less porous than layer 1. Some plant tissues are present. The boundary between layer 1 and layer 2 is within 50 µm. The total thickness of the crust is approximately 2–3 mm.

The Soil Groundmass

As it is shown in Fig. 6, the groundmass consists of gypsum crystals and gypsum aggregates up to 1 cm. Occasionally calcite crystals occur. The fine material ($< 10\,\mu m$) consists of clay and calcite particles. The distribution

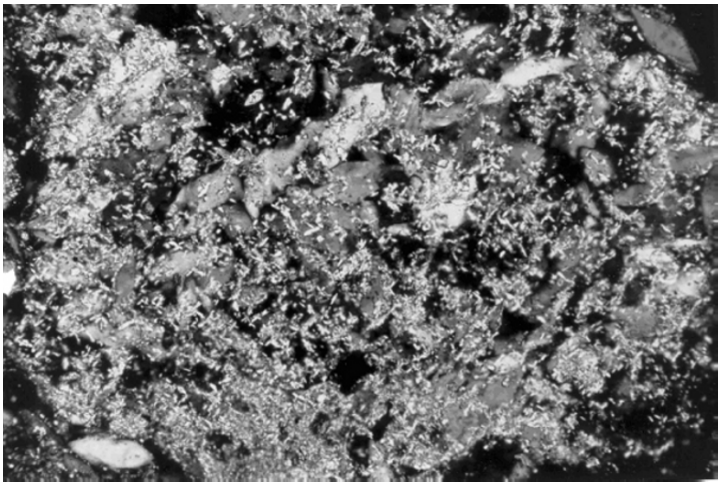

Fig. 6. Detail of the soil groundmass

pattern of the gypsum crystals and the fine material is random. Fragments of crusts are frequently found. They reflect previous stages of crust formation.

The results of X-ray diffraction analysis of undistributed samples of gypsum crusts are presented very much gypsum on the crust, much calcite, moderate amounts of quartz and few clay minerals.

The two distinguished layers within the observed crust represent two different stages of surface crust formation. Lenticular gypsum crystals are produced under semiarid conditions by gypsum weathering.

Eswaran et al. (1981) reported the occurrence of many very fine, lenticular crystals of gypsum, very closely packed. A petrogypsic horizon surface crust is governed by a complex sequence of soil particle detachment and transport processes at the soil surface. First particle detachment is achieved by various mechanisms:

- Disaggregation by entrapped air compression upon moistening of aggregates.
- Disaggregation by rain drop impact and/or flow turbulence.
- Micro cracking by shrinking and swelling.
- Physicochemical dispersion, resulting in the detachment of aggregates which individually greatly vary.

The textural fining upward within one layer in the crust is typical for water deposition: first sedimentation of the coarse particles continuously followed by deposition of the finer particles.

Both layers depend on particle transport and sedimentation modes, which determine two main morphological types, i.e structural crust and deposition crust (Chen et al. 1980). Compaction due to raindrop impact may play a great

part in soil crusting. McIntyre (1958) attributed skin seal formation to this process.

Capillary Barrier

Considering the porosity of the crust, it is condensed but especially the fine textured, dense packed upper part of both layers could hinder water conductivity.

Current polarized light one insert two polarized filters in the microscope. All lights waves are observed, but a crystalline mineral placed between the polarizer's results in birefringence.

The loss of porosity in the upper part of layer one and two and the smallest volume of it is considered as a clear incidence of the rainfall energy. This energy is reduced the volume of macroporisity and elongated porosity. The loss porosity by clogging it with disintegration of aggregate soils to smaller and finer units. As gypsum and calcite (Poch and Verplancke 1997). As a result the crust strength will be increased and the infiltration are decreased. Also for vughs are presented in the lower part of layer one and two in microstructure crust have irregular shape, and some of it are spherical and it is correlated with escaping of compressed air under the surface, and the soil ponding with rainfall, and the fine grains these factors are limited the air from escaping and substituted with water infiltration which limited. Microstructure of crust formation reduced the porosity from 30 to 90% (West et al. 1990).

Conclusions

Morphological descriptions of gypsiferous crusts are a useful tool to help explain crust behavior and to provide direct evidence of processes that have been important to the development of the crust. Pore size, shape, and amount in the crust as compared to uncrusted soil, layers of micromass accumulation and it consist of gypsum, calcite, silt and clay mineral. Additionally, these characteristics when coupled with crust thickness, low porosity and crust strength may help to explain the decline infiltration and seedling emergence in gypsiferous crust behavior observed.

References

Bullock P et al. (eds) (1985) Handbook for thin section description. WAINE Research Publications. Albrighton, Wolverhampton, UK

Chen Y, Tarchitzky J, Brouwer J, Morin J, Banin A (1980) Scanning electron microscope observations on soil crusts and their formation, Soil Sci 130:45–55

Eswaran H, Ilawi M, Osman A (1981) Mineralogy and micromorphology of aridsols. In: Proc 3rd Int Soil Classification Workshop, ACSAD/SS/P17, Damascus, Syria:153–174

FitzPatrick EA (1993) Soil microscopy and micromorphology. ohn Wiley & Sons, New York

Gal M, Arcan L, Shainberg I, Keren R (1984) Effect of exchangeable sodium and phosphogypsum on crust structure-scanning electron microscope observations, Soil Sci Soc Am J 48:872–878

Gafarzadeh AA, Zinck JA (2000) Penetration resistance of gypsum crust from laboratory experiments. Thesis, Wyecollege, University of London, UK

Gee GW, Bauder JW (1986) Particle size analysis. In: Klute A (ed) Methods of soil analysis, Part 1, 2nd ed. Agron Monogr No 9, ASA and SSSA, Madison, WI:383–409

Gooderham PT (1973) Soil physical conditions and plant growth. PhD Thesis, University of Reading, UK

Habib H, Robert M (1992) Morphological study of som gypsiferous soils from the Middle Euphrates Basin (Syria)

Ilaiwi M (1983) Contribution to the knowledge of the soils of Syria. PhD Thesis, University of Ghent, Belgium

Jafarzadeh AA (1991) Experimental studies of gypsum migration and deposition in soil profiles. PhD Thesis, Wye College, University of London, UK

McIntyre DS (1958) Permability measurements of soil crusts formed from raindrop impacts, Soil Sci 85:185–189

Nafie FAA (1989) The properties of highly gypsiferous soils and their significance for land management. PhD Thesis, Wye College, University of London, UK

Nelson RE, Somers LE (1986) Total carbon, organic carbon and organic matter. In: Page AL, Miller Rh, Keeny DR (eds) Methods of Soil Analysis, Part 2, 2nd ed. Agron Monogr No 9, ASA and SSSA, Madison, WI:539–577

Nelson RE (1986) Carbonate and gypsum. In: Page AL, Miller Rh, Keeny DR (eds) Methods of Soil Analysis, Part 2, 2nd ed. Agron Monogr No 9, ASA and SSSA, Madison, WI:181–196

Poch RM, Verplancke H (1997) Penetration resistance of gypsiferous horizons, Eur J Soil Sci 48:535

Stroosnijder L (1995) Crust formation, crust properties and crust control. Lecture 2. In processes and models in soil and water conservation. K200–507. Department of irrigation and soiul & water conservation, Wageningen Agricultural University, The Netherland

Watson A (1982) The origin, nature and distribution of gypsum crusts in deserts. PhD Thesis, University of Oxford, UK

West LT, Bradford JM, Norton LD (1990) Crust morphology and infiltrability in surface soils from the southeast and Midwest U.S.A. In: Douglas LA (ed) Soil micromorphology: A basic and applied science. Elsevier, Amesterdam, Developments in soil science 19:107–113

Fabric Changes in Compacted London Clay Due to Variations in Applied Stress and Suction

Rafael Monroy[1], Lidija Zdravkovic[1], and Andrew Ridley[2]

[1] Imperial College London, UK
rafel.monroy@imperial.ac.uk, l.zdravkovic@imperial.ac.uk
[2] Geotechnical Observations Ltd, UK andrew@geo-observations.com

Summary. In this study, the evolution of fabric in compacted London Clay has been studied in detail. Samples were statically compacted to the same initial conditions and taken along a number of stress paths – involving both wetting and loading – to different final conditions. Wetting and loading was conducted using both conventional and osmotic oedometers (the latter allowed the suction to be varied in a controlled manner). The study of micro-fabric involved a combination of quantitative measurements of the pore space, using Mercury Intrusion Porosimetry, with qualitative observations of the overall arrangement of particles, using Environmental Scanning Electron Microscopy. The study showed important changes to take place in the soil micro-fabric during wetting, whereas the effect of loading was seen to be less severe. The results suggest that changes in the overall micro-fabric of a compacted clayey soil are strongly stress path dependent.

Key words: fabric, compaction, clay, suction, oedometer

Introduction

Fabric plays a fundamental role in defining the hydro-mechanical response of a soil. It is now widely recognised that this parameter is even more relevant when partly saturated soils are being considered (Alonso et al. 1987, Cui et al. 2002), particularly so in those that contain a significant amount of expansive clay minerals. Current elasto-plastic models, such as the one proposed by Gens and Alonso (1992), try to include explicitly the effect of fabric on the overall soil behaviour by considering the interactions that take place between the micro and macro structural levels. This requires an understanding of the initial soil fabric, as well as its evolution along loading-unloading and wetting-drying paths. While many studies have looked at the initial fabric of a partly saturated soil, both in the intact and compacted states, less is known about the overall effect of changes in applied stress and matrix suction on the subsequent

evolution of micro-fabric (Al-Mukhtar 1995, Cui et al. 2002, Romero et al. 2005). The aim of this paper is to present experimental evidence on some of the changes that take place in the micro-fabric of compacted London Clay along a number of different stress paths.

Materials and Methods

The material selected for the study consisted of brown, weathered London Clay, extracted from a number of boreholes in north London, at a depth of 4–6 m. The liquid limit and plasticity index correspond to 83% and 54%, respectively.

The soil was initially dried at 70°C, mechanically grinded, and made to pass through a 425 μm (ASTM No. 40) aperture, before being mixed with the correct proportion of distilled water. The powder and water were thoroughly mixed and sealed in a plastic bag, after all the air had been removed with a vacuum pump. This was stored in a laboratory under controlled temperature for a minimum hydration period of three months. A comprehensive account of the method of sample preparation can be found in Monroy (2006).

A total of eight samples were statically compacted – to the same initial conditions, corresponding to dry of optimum in a Proctor plot – directly into an oedometer ring. These conditions corresponded to a moisture content of 23.61%, dry density of 1.384 Mg/m^3, void ratio of 0.952, degree of saturation of 67.1%, and matrix suction of 1000 kPa. The numbers quoted above represent average values measured in 87 samples compacted to the same initial conditions, as explained in Monroy (2006).

The samples were taken along different stress paths, as shown in Fig. 1: some of the samples were wetted under a nominal load of 7 kPa and allowed to swell and to reach equilibrium under different values of matrix suction (mta–7, mta–8, mta–9, mta–2); a further sample was wetted under confined conditions of constant volume (mta–5); another sample was loaded at a constant moisture content to a maximum vertical stress of 550 kPa (mta–3); and a final sample was loaded and then wetted at a constant high stress of 220 kPa (mta–6). Figure 1 shows the estimated location of the LC yield line (Alonso et al. 1987), as suggested in Monroy (2006).

A combination of conventional and osmotic oedometers was used to load and wet the samples. The latter set of equipment allowed the independent measurement and control of the matrix suction by means of the IC suction probe (Ridley and Burland 1993) and an osmotic system (Dineen and Burland 1995).

There were three reasons for the selection of the stress paths shown in Fig. 1:

1. To assess in detail the effect of a reduction in suction under a nominal load on the progressive change in the soil micro-fabric.

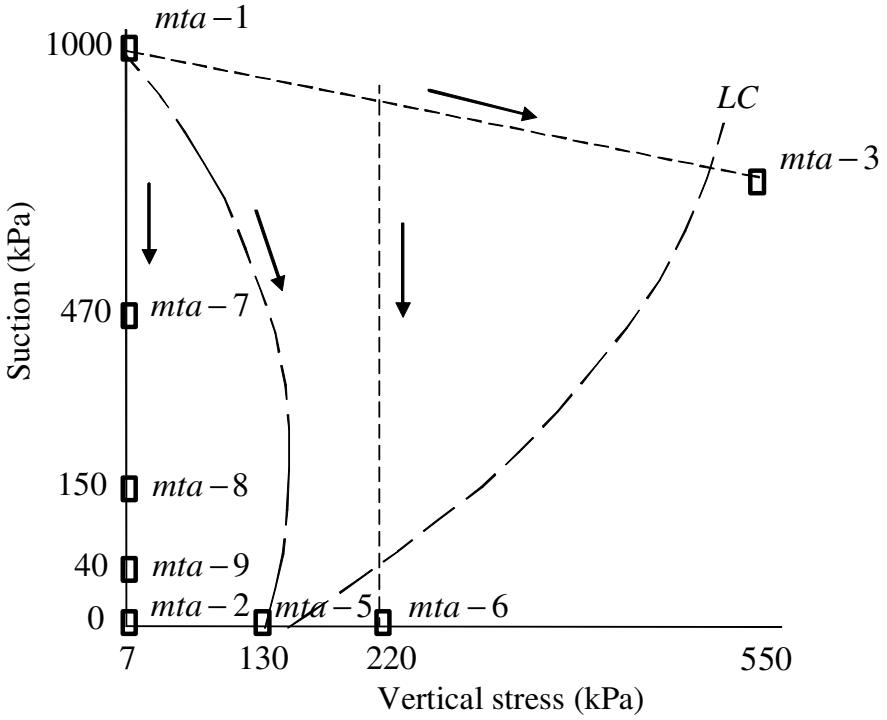

Fig. 1. Stress paths followed by the compacted samples

2. To compare the effect of unconfined versus confined hydration on the final soil fabric.
3. To determine the effect of stress path on the final fabric of samples undergoing similar levels of compressive strains.

After reaching equilibrium, the samples were unloaded, removed from the oedometer, and sealed in the way described above. They were then taken to the Universidad Politécnica de Cataluña in Barcelona, where a detailed study of their fabric was carried out using both Mercury Intrusion Porosimetry (MIP) and Environmental Scanning Electron Microscopy (ESEM).

Results

Due to limitations in space, only those results derived from the MIP are presented in this paper. The evolution of the pore space during unconfined swelling (mta–2, mta–7, mta–8, mta–9) is presented in Fig. 2, in the form of a pore size density function versus an equivalent pore diameter. This distribution is obtained by taking the derivative of the pore size distribution obtained directly from the MIP, as explained in Romero et al. (2005). The fabric of

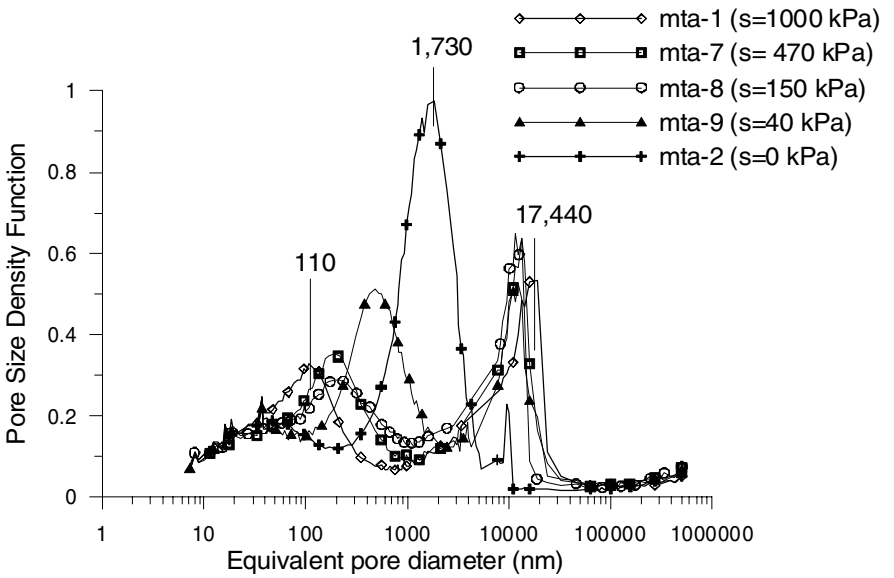

Fig. 2. Evolution of fabric along a free-swelling path

the initial as-compacted sample (mta–1) was found to have two dominant pore sizes, with peaks centred at around 110 nm and 17,440 nm. This pore distribution would correspond to a soil composed of large aggregations of clay particles separated by well defined macro-voids. The larger porosity would represent the inter-aggregate porosity, whereas the smaller pore size would refer to the intra-aggregate porosity (Alonso et al. 1987).

Figure 2 shows how suction decrements to 470 kPa (mta–7) and 150 kPa (mta–8) did not result in significant variations in the distribution of the pore space. It is only when the suction was reduced to 40 kPa (mta–9) and 0 kPa (mta–2) that a significant change in the shape of the pore size density function was observable. The final fabric of the saturated sample presents a single dominant pore size, centred at around 1,730 nm. This fabric is characteristic of a soil consisting of a matrix of elementary particle arrangements (consisting of groupings of clay minerals arranged in a semi-parallel configuration), in which there is a single intra-matrix pore space (Alonso et al. 1987).

Figure 3 presents a comparison between the pore size density functions displayed by samples mta–2 and mta–5 (corresponding to free and confined hydration, respectively). Both distributions have similar shape: there is a dominant pore size in both cases, which in sample mta–5 is centred at around 840 nm. The decrease in the dominant pore size in sample mta–5 with respect to mta–2 would be due to the effect of the confining stress in the former, which was measured to be 130 kPa.

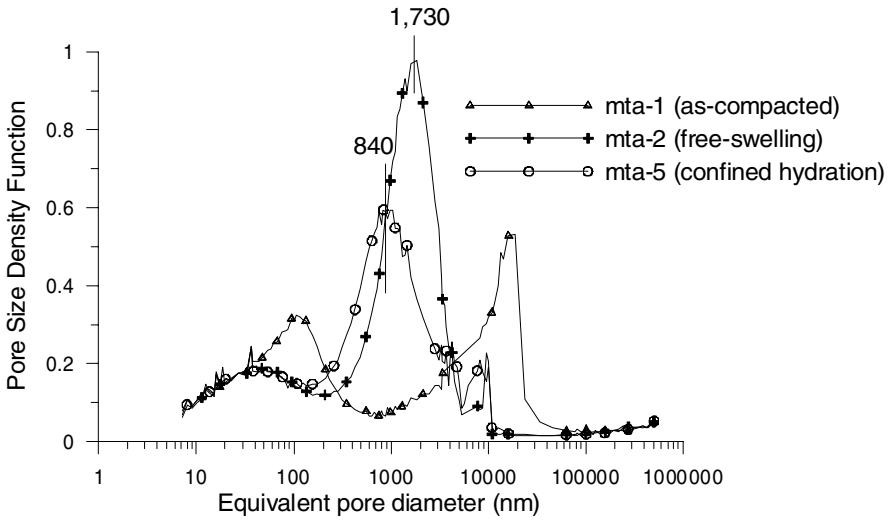

Fig. 3. Evolution of fabric during free-swelling and confined (constant volume) hydration

The results on samples mta–3 (loaded to 550 kPa) and mta–6 (loaded to 220 kPa and saturated under a constant load) are presented in Fig. 4. The

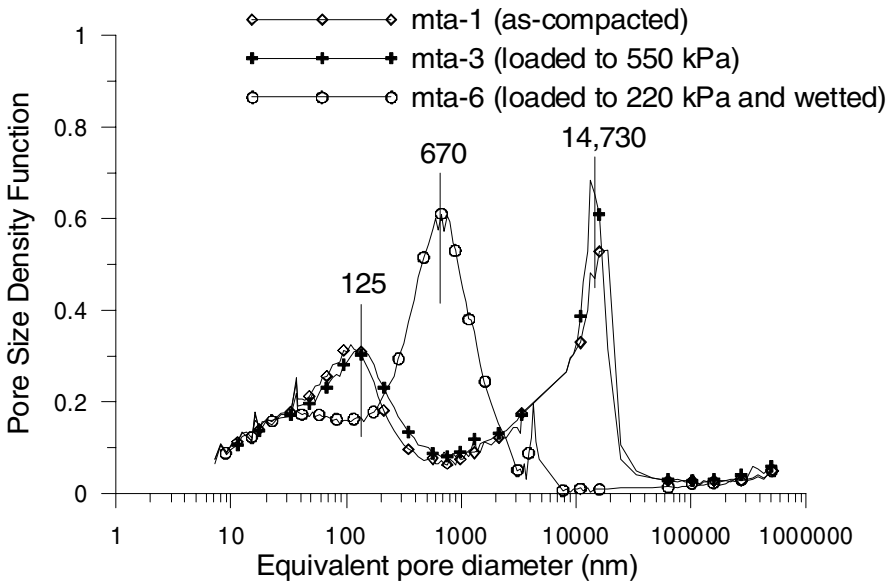

Fig. 4. Evolution of fabric along loading and wetting paths

distribution of the pore space in sample mta–3 remained virtually unchanged, despite the loading having continued beyond the yield stress: there is clear indication of an inter-aggregate pore size centred at around 14,730 nm, and an intra-aggregate porosity at around 125 nm. This result is consistent with earlier findings Delage and Lefebvre (1984), Lapierre et al. (1990), Al-Mukhtar et al. (1996), and suggests that the loading process affected mainly the larger inter-aggregate porosity, leaving the aggregations practically unchanged. Wetting of sample mta–6, on the other hand, resulted in the characteristic evolution from an aggregate into a matrix type fabric: the pore space in sample mta–6 can be seen to have been dominated by a single pore space centred at around 670 nm.

Samples mta–3 and mta–6 underwent similar degrees of compressive strains, although the mechanism behind these was different in each case. Whereas sample mta–3 experienced collapse on loading, sample mta–6 underwent collapse on wetting. This difference in the stress path determined in an unequivocal way the final soil fabric, as Fig. 4 clearly demonstrates.

Comparison of the dominant pore sizes in samples mta–2, mta–5 and mta–6 (Figs. 3 and 4) appears to indicate that an increase in load in the fully saturated state was accompanied by a reduction in the dominant entrance size of the intra-matrix pore space (1,730, 840 and 670 nm, respectively).

Table 1 summarises total volumetric strains, ε_{vol}, from each of the above experiments, with positive sign indicating compression.

Table 1. Volumetric strains

Test	*mta–7*	*mta–8*	*mta–9*	*mta–2*	*mta–5*	*mta–3*	*mta–6*
ε_{vol} (%)	−1.0	−4.0	−7.0	−9.0	0.0	2.0	1.0 (4.0)

Discussion and Conclusions

The research presented here was aimed at providing further evidence on the changes that take place in the fabric of a compacted, partly saturated clayey soil, when subjected to changes in stress and suction. In order to do so, samples were compacted to similar initial conditions and were subsequently loaded and wetted along different stress paths. A number of important findings have been reported:

- The initial as-compacted fabric consisted of well defined aggregations, separated by large, inter-aggregate voids.
- Hydration to full saturation, both under confined and unconfined conditions, resulted in the homogenisation of the pore space: the aggregations

swelled and eventually occupied the entirety of the inter-aggregate void space. This is reflected in the shape of the pore size density function derived from the MIP, which shows a single dominant pore size.

- The most significant changes in the soil fabric are believed to have taken place as the suction was reduced to low values. This was at least the case when the soil was hydrated under a nominal load.
- Loading at constant moisture content beyond the yield stress resulted in a (minimal) reduction in the size of the inter-aggregate porosity, with no significant visible modification in the overall distribution of the pore space.
- The evolution of fabric was found to be strongly stress path dependent: two samples undergoing similar amounts of compression, but which followed different paths, showed marked differences in their distribution of pore space.

Some of the above results are in close agreement with those reported in the literature in the past, and appear to indicate that fabric is a property that can experience significant changes during a test, particularly so when the suction is reduced. Fabric is known to play an important role in determining the behaviour of partly saturated expansive soils, and it is felt that future experimental research should play closer attention to this important topic.

Acknowledgements

The first author would like to acknowledge the financial support from the Royal Academy of Engineering (UK), the Soil Mechanics section at Imperial College London, and Geotechnical Observations Ltd.

References

Al-Mukhtar M (1995) Macroscopic behaviour and macro structural properties of a kaolinite clay under controlled mechanical and hydraulic state, In: Proc 1st Int Conf on Unsaturated soils, Paris, France 1:3–9

Al-Mukhtar M, Belanteur N, Tessier D, Vanapalli SK (1996) The fabric of a clay soil under controlled mechanical and hydraulic stress states, Applied Clay Science 11:99–115

Alonso EE, Gens A, Hight DW (1987) Special problem soils. General Report. In: Proc 9th Eur Conf on Soil Mechanics and Foundation Engineering, Dublin, Ireland 3:1087–1146

Cui YJ, Loiseau C, Delage P (2002) Micro-structure changes of a confined swelling soil due to suction controlled hydration. In: Proc 3rd Int Conf on Unsaturated Soils, Recife, Brazil 2:593–598

Delage P, Lefebvre G (1984) Study of the structure of a sensitive Champlain clay and of its evolution during consolidation, Can Geotech J 21:21–35

Dineen K, Burland JB (1995) A new approach to osmotically controlled oedometer testing. In: Proc 1st Int Conf of Unsaturated Soils, Paris, France 2:459–465

Gens A, Alonso EE (1992) A framework for the behaviour of unsaturated expansive clays, Can Geotech J 29:1013–1032

Lapierre C, Leroueil S, Locat J (1990) Mercury intrusion and permeability of Louiseville clay, Can Geotech J 27:761–773

Monroy R (2006) The influence of load and suction changes on the volumetric behaviour of compacted London Clay. PhD Thesis, University of London (Imperial College), London, UK

Ridley AM, Burland JB (1993) A new instrument for the measurement of soil moisture suction, Geotechnique 43(2):321–324

Romero E, Hoffmann C, Castellanos E, Suriol J, Lloret A (2005) Microstructural changes of compacted bentonite induced by hydro-mechanical actions. Advances in understanding engineering clay barriers. In: Alonso EE, Ledesma E (eds) Proc Int Symp on Large Scale Field Testing in Granite, Sitges, Barcelona (Spain). A.A. Balkema Pub pp 193–202

Microstructure of a Lime Stabilised Compacted Silt

Giacomo Russo, Sebastiana Dal Vecchio, and Giuseppe Mascolo

Facoltà di Ingegneria, Università di Cassino, Via G. Di Biasio 43, 03043 Cassino, Italy giarusso@unicas.it, s.dalvecchio@unicas.it, mascolo@unicas.it

Summary. Lime stabilisation of fine-grained soils is a well tested technique, traditionally used to improve clay subgrades for road pavements. The lime treated soils show a deep modification of the physical and mechanical properties (e.g., grain size distribution, plasticity, compressibility, shear strength). A deeper insight into the above mentioned behaviour has been achieved by investigating the changes of microstructure taking place after the addition of lime. In the paper, results from Mercury Intrusion Porosimetry (MIP) on a lime stabilised dynamically compacted natural silty soil are reported. Those results highlight the time dependency of modifications induced by lime on the microstructure, which is strongly related to the initial moulding water content of the sample.

Key words: lime stabilisation, compaction, microstructure

1 Introduction

Lime stabilisation of fine grained soils is widely recognized as a suitable ground improvement technique, since it allows the reuse of soils normally inadequate to be involved in earthworks (Croce and Russo 2002).

The effectiveness of the improvement is mainly due to the mineralogical and physical properties of natural soil, but also the treatment procedures play an important role. Therefore the lime stabilisation practice is based on some laboratory analyses concerning relevant physical and chemical properties of the soil, such as grain size distribution, Atterberg limits, organic matter, sulphate content, in order to state the suitability of lime stabilisation, and others tests in order to set up the treatment procedure (lime percent by weight, initial water content, curing time, type and energy of compaction) in order to gain the expected mechanical properties of the improved soil.

When lime is added to soil, two main phenomena take place: the cation exchange and the pozzolanic reactions (Bell 1996). These two mechanisms, referred to as modification and stabilisation of treated soils respectively (Rogers and Glendinning 1996), develop at different interval on the time scale. The

cation exchange between calcium ions and clayey minerals takes place very rapidly inducing the flocculation of the fine-grained fraction. On a macroscopic scale, this structural modification results in a different grain size distribution of the treated soil, characterized by a reduction of the finer fraction. As a further consequence of the cation exchange, the plasticity index of the treated soil is considerably reduced. The development of the pozzolanic reactions, with the formation of stable compounds as hydrated calcium silicates and hydrated alumina silicates, is slower than the cation exchange on the time scale, and it is responsible for the improvement of the mechanical properties of the treated soil (Diamond and Kinter 1965, Sherwood 1993). The considerable increase of shear strength is strongly dependent on curing time (Bell 1996, Croce and Russo 2003a). Otherwise the reduction of the soil compressibility measured after the addition of lime seems to be less influenced by the curing time (Russo and Croce 2001).

The treated soil is compacted and stabilised and both the improvement techniques change the physical state of the natural soil and his mechanical behaviour. Furthermore, the unsaturated state of the treated soil plays a relevant role in affecting his mechanical behaviour. The time dependency of the mechanical improvement of lime stabilised soils represents an additive complexity in the analysis of the effectiveness of this technique. The time scale over which the reactions take place is not well established, and there is not a wide agreement about the exact sequence of the chemical reactions (Boardman et al. 2001). From the practical point of view, it is relevant to appreciate the longevity of lime stabilised soils with respect to the mineralogy of the soil and to the treatment parameters.

Microstructural investigations allow a deeper insight in the complex of phenomena taking place after the addition of lime, as already observed for soils stabilised by cement (Ye 2003). In this perspective, in this paper some results of an experimental analysis on remoulded natural and lime stabilised specimen of an alluvial silty soil are reported. In order to highlight the time–dependency of the microstructure of a lime treated soil, Mercury Intrusion Porosimetry (MIP) on both natural and lime stabilized samples compacted at different initial water content and cured at different times have been performed. Other relevant parameters influencing the effectiveness of lime stabilisation (e.g. type and percent by weight of lime, compaction energy) were fixed in order to reduce the complexity of the data analysis.

2 Experimental Procedures

Laboratory tests were performed on remoulded samples of an alluvial silty soil. The physical characteristics (grain size distribution, specific weight, plastic limit, liquid limit) of the natural soil were determined and standard Proctor tests were performed. Lime treated samples were prepared by hand mixing the oven dried soil with 3% quicklime powder and distilled water, allowing the

quicklime to hydrate for 24 hours. The selected percent by weight of quicklime allowed the development of pozzolanic reactions (Rogers et al. 1997). The samples were then compacted at three different water contents, namely dry of optimum (w_{dry}), optimum (w_{opt}) and wet of optimum (w_{wet}). The initial water contents for samples compacted dry and wet of optimum were selected in order to obtain very similar densities.

Samples were then dehydrated by freeze-drying (Delage and Pellerin 1984), that is rapid freezing in liquid nitrogen (boiling point −196°C) followed by sublimation in a true vacuum. Freezing was accelerated using small pieces of soil (1–2 g in weight). In such condition the 9% volume expansion of the water does not take place, preserving the microstructure of the soil.

The dehydrated lime stabilised samples were cured for fixed time intervals under controlled conditions before performing MIP tests. The repeatability of the procedure was carefully verified performing several MIP test on samples taken from the same specimen. The curing intervals of time selected were $t = 0$, 7, 28 days, traditionally considered in order to evaluate the effectiveness of stabilisation. Only for the optimum stabilised samples curing times of $t = 0$, 7, 14, 21, 28 days were considered. Since the duration of the freeze drying procedure takes about 24 hours, all the time intervals are nominal.

3 Results

3.1 Physical Properties

In Table 1 the main physical characteristics of both natural and lime treated samples are reported. The plasticity of lime stabilised sample has not been reported since the plasticity limit w_P was not determinable.

The grain size distribution of both natural and lime stabilised samples is reported in Fig. 1**a**. The addition of 3% of quicklime changes the grain size distribution, shifting and rotating the distribution towards an increase of the medium-grained fraction of the sample. This change takes place immediately after the addition of lime, as evidenced by the two distributions determined by dry sieving and sedimentation respectively after the addition of lime ($t =$ 0 days) and after a curing time of 7 days. The compaction curves of lime-treated samples (Fig. 1**b**) are shifted with respect to those of natural samples, showing an increase of the optimum water content and a reduction of the

Table 1. Physical properties of the alluvial silty soil

	γ_s [kN/m^3]	w_L [%]	IP [%]	w_{opt} [%]	γ_{dmax} [kN/m^3]
natural	26.4	25.0	8.0	14.5	18.6
3% lime	26.1	24.0	—	17.5	17.3

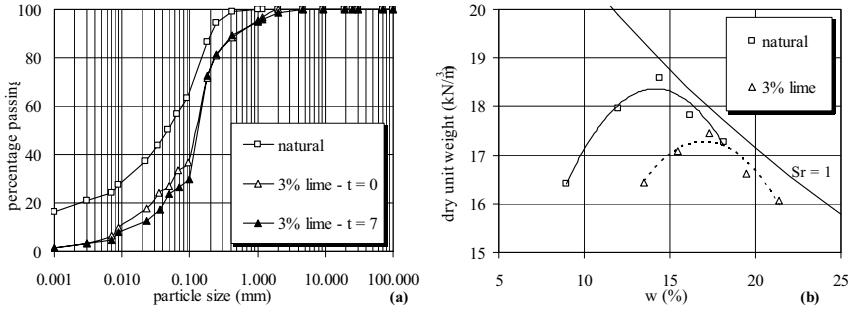

Fig. 1. Grain size distributions (**a**) and compaction characteristics (**b**) of natural and stabilized samples

maximum dry weight. The shape of the curve remains unchanged. Stabilised samples show an increase of the optimum water content w_{opt} restricted to 3% with respect to natural samples, while the reduction of maximum dry density is about $1.0 \div 1.3\,\mathrm{kN/m^3}$ after the addition of lime. The latter results are in good agreement with those reported in literature for other fine-grained soils (Croce and Russo 2003b).

3.2 Pore Size Distributions

The influence of initial water content of the natural samples has been firstly investigated. As expected, the cumulative intruded volume of mercury is lower for the optimum water content sample, characterized by the highest density (Fig. 2**a**). The percent porosity of the sample is about 21.4%. The other two samples show a similar porosity after compaction. The higher frequency of pore size of the sample compacted at optimum water content take place around an average entry values of $1\,\mu\mathrm{m}$ (Fig. 2**b**). The pore size distribution is unimodal. Both dry and wet samples are characterized by higher frequency

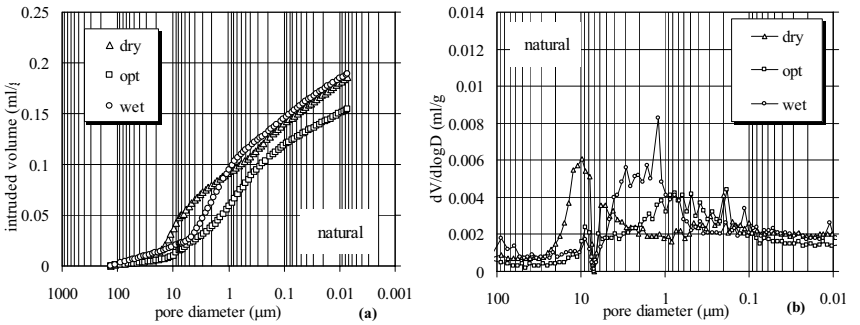

Fig. 2. Cumulative volume intruded (**a**) and pore size distribution (**b**) of natural samples

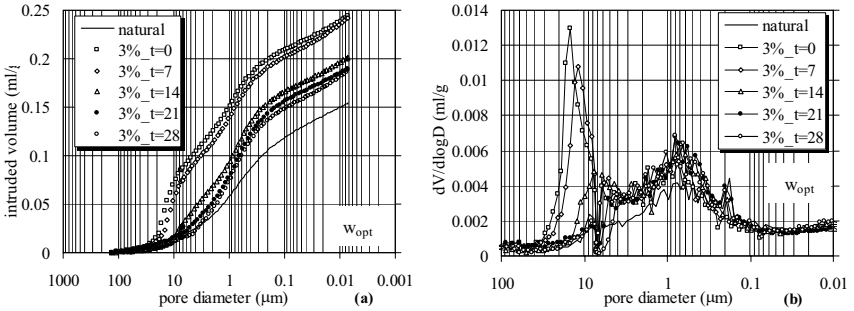

Fig. 3. Cumulative volume intruded (**a**) and pore size distribution (**b**) of optimum stabilised samples

of larger pores than the optimum sample. The dry sample show a pore size distribution slightly bimodal. The curves are qualitatively similar to those obtained by Delage et al. (1996) on different soils.

In Figure 3**a** the cumulative volumes of mercury intruded for the stabilised optimum samples are reported. Each curve corresponds to different curing time of the sample. A relevant increase of the intrusion is shown by the $t = 0$ days stabilised sample, corresponding to an increase of 33% of the natural sample percent porosity. This result is in agreement with the change of the grain size distribution and the shift of the Proctor curve induced by lime. The increase of porosity diminishes gradually for longer curing time, and the sample cured for 28 day shows only a porosity raise of 7% with respect to natural sample. At curing time of $t = 0$ days, the pore size distribution (Fig. 3**b**) shows a new peak not present in the natural sample curve around average entry values of 15 μm and a slight increase of the porosity contained between 6 and 0.3 μm. This peak disappear at curing time higher than 21 days, while the increase of porosity around 1 μm becomes stable and the curve unimodal again. The intra-aggregate porosity (average entrance entry values smaller than 0.3 μm) seems to be not affected by the addition of lime.

The behaviour shown by the wet stabilised samples is similar to the optimum stabilised samples. The percent porosity at curing time of $t = 0$ is 16% higher than the natural wet sample porosity, and it reduces for longer curing time (Fig. 4**a**). The pore size distribution becomes bimodal after the addition of lime ($t = 0$), but the new peak detected around 10 μm disappears after a curing time of 7 days, and the curve becomes unimodal again (Fig. 4**b**). The samples show a distribution characterised by higher frequency of pores contained between 3 μm and 0.3 μm.

Slight differences in cumulative volume of mercury intruded are shown by dry stabilised samples cured for different times (Fig. 5**a**). Negligible variations of percent porosity are detected in function of the curing time. Dry stabilised samples show a bimodal distribution also after the addition of lime with a reduction in the average entry values from 10 to 3 μm (Fig. 5**b**). Samples

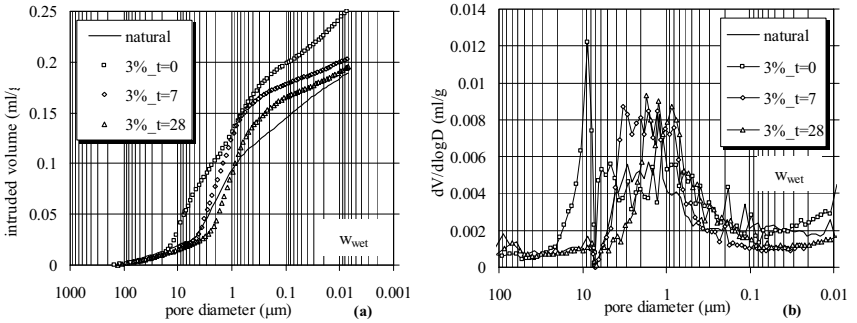

Fig. 4. Cumulative volume intruded (**a**) and pore size distribution (**b**) of wet stabilised samples

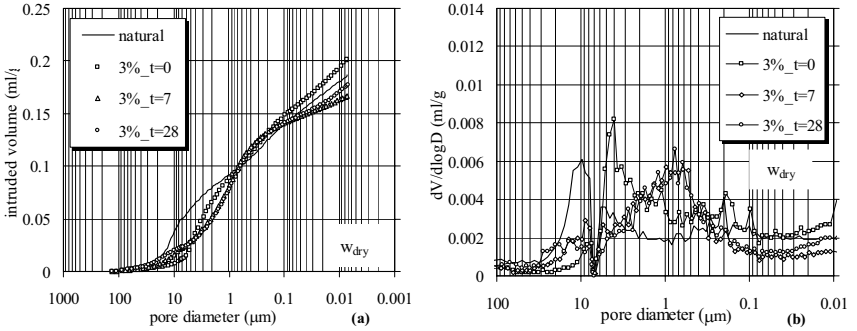

Fig. 5. Cumulative volume intruded (**a**) and pore size distribution (**b**) of dry stabilised samples

cured 7 days and more are characterised by a unimodal distribution, with a marked increase of diameters contained between 3 and 0.3 μm.

Variations in porosity induced by lime addition depend on the initial water contents of samples. In order to highlight the time-dependency of this variations, in Fig. 6 the curves representing cumulative volumes of mercury intruded in stabilised samples at different initial water content and equal curing time ($t = 0$, 28) are reported. It can be seen that lime affects the microstructure of the soil immediately after his addition. The more relevant effects are mainly detected in stabilised optimum samples, that show an increase of porosity (Fig. 6**a**) and, differently from the natural samples, a bimodal distribution of pore sizes (Fig. 6**b**). The less effective changes, at the same curing time, pertain to dry stabilised samples. Representing the intruded volume of all the three samples (namely dry, optimum and wet) cured for 28 days, a very slight difference in percent porosity (Fig. 6**c**) and a quite similar distribution of pore sizes (Fig. 6**d**) can be noted.

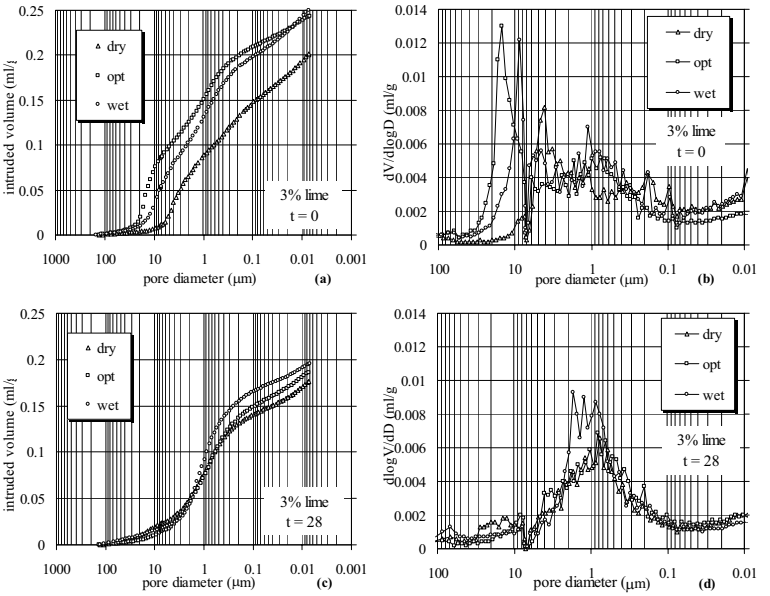

Fig. 6. Cumulative volume intruded (**a**) and pore size distribution (**b**) of stabilised samples cured for $t = 0$ and cumulative volume intruded (**c**) and pore size distribution (**d**) of stabilised samples cured for $t = 28$

4 Conclusions

A study of the microstructure induced by compaction and lime stabilisation on an alluvial silt was carried out by means of mercury intrusion porosimetry on freeze-dried samples.

The moulding water content plays a relevant role on the microstructure of compacted natural samples. The lesser porosity pertains to samples compacted at optimum water content, in agreement with results reported in literature (Delage et al. 1996) on different soils.

The time-dependency of the stabilised samples microstructure was clearly detected by means of MIP results. Addition of lime mainly affects the inter-aggregate porosity. A relevant modification of porosity for samples stabilised at 3% by weight and compacted at optimum water content of quicklime takes place immediately after the addition of lime. In particular, an increase of pores of relatively large diameter is detected. A subsequent reduction of this effect occurs for longer curing time of the stabilised samples, bringing back the pore size distribution towards the distribution of the natural samples. Similar behaviour is shown by the wet stabilised samples, while the microstructure of dry samples is less affected by the addition of lime. After a curing time of 28 days the stabilised samples show a very similar porosity and pore size distribution, irrespective of the moulding water content.

Cation exchange induced by lime takes place immediately after the addition of lime, producing the flocculation of grains and increasing the porosity of the stabilised sample. This effect is relevant for optimum and wet moulding water contents but decays for longer curing time, probably due to changes of the pH of pore water (Eades and Grim 1966). The similarity of pore size distribution of samples compacted at different water content and cured for 28 days may suggest that the development of pozzolanic reactions and the consequent cementation of the aggregates contributes to reduce porosity induced by flocculation and increases the frequency of pores of small diameters. In the long term, this effect may be more valuable on the microstructure than the moulding water content.

References

Bell FG (1996) Lime stabilization of clay minerals and soils, Engineering Geology 42:223–237

Boardman DI, Glendinning S, Rogers CDF (2001) Development of stabilisation and solidification in lime-clay mixes, Géotechnique 50:533–543

Croce P, Russo G (2002) Reimpiego dei terreni di scavo mediante stabilizzazione a calce. In: XXI Convegno Nazionale di Geotecnica, L'Aquila, Patron Editore, pp 11–216

Croce P, Russo G (2003a) Experimental investigation on lime stabilized soils. In: Proc XIII European Conference of Soil Mechanics and Geotechnical Engineering, Prague

Croce P, Russo G (2003b) Soil-water characteristic curves of lime stabilised soil. In: Vermeer, Schweiger, Karstunen, Cudny (eds) Proc Int Workshop on Geotechnics of Soft Soils – Theory and Practice. Noordwijkerhout

Delage P, Audiguier M, Cui YJ, Howat MD (1996) Microstructure of a compacted silt, Canadian Geotechnical Journal 33:150–158

Delage P, Pellerin FM (1984) Influence de la lyophilisation sur la structure d'une argile sensible du Québec, Clay Minerals 19:151–160

Diamond S, Kinter EB (1965) Mechanisms of soil-lime stabilization: an interpretative review, Highway Research Record 92:83-96

Eades JL, Grim RE (1966) A quick test to determine lime requirements of lime stabilization, Highway Research Record 139:61–72

Rogers CDF, Glendinning S (1996) Modification of clay soils using lime. In: Rogers CDF, Glendinning S, Dixon N (eds) Lime Stabilisation, Thomas Telford, London, pp 99–114

Rogers CDF, Glendinning S, Roff TEJ (1997) Modification of clay soils for construction expediency, Geotechnical Engineering 125:1–8

Russo G, Croce P (2001) Indagini sperimentali sui terreni stabilizzati a calce. In: Incontro Annuale dei Ricercatori di Geotecnica – IARG 2001, Milano

Sherwood PT (1993) Soil stabilization with Cement and Lime: State-of-Art Review. HMSO, London

Ye G (2003) Experimental study and numerical simulation of the development of the microstructure and permeability of cementitious materials. Ph.D. thesis, Delft University

Part II

Measuring Suction

Errors in Total Suction Measurements

Setianto Samingan Agus[1] and Tom Schanz[2]

[1] Civil and Environmental Engineering Consultants, Singapore
agus72indo@yahoo.com
[2] Laboratory of Soil Mechanics, Bauhaus-University Weimar, Germany
tom.schanz@bauing.uni-weimar.de

Summary. Suction as one of the stress state variables of unsaturated soils is usually either imposed to the soil or measured. Measurements of suction therefore become commonly practiced when dealing with unsaturated soil problems. Unlike the measurement of matric suction, whereby one can arrive at a sufficient accuracy, the accuracy in total suction measurements is questionable. Total suction measurements involve equilibration of sensors used with the relative humidity of the vapour space in or above the soils. Many factors have been cited to cause inaccuracy in the total suction measurements such as temperature gradient and the inaccuracy of the sensors used to measure total suction. In this paper, the total suction measurement inaccuracy of several sensors commonly used is discussed. It is found that the total suction measurements can only be performed to lowest suction of 1000 kPa when sufficient accuracy is to be obtained.

Key words: total suction, measurement error, accuracy, suction characteristic curve, temperature fluctuation, bentonite–sand mixture

Introduction

Suction is one of the stress state variables of unsaturated soils and is defined as the ratio of the partial energy of water vapor in the soil voids to that of free pure water (Aitchison 1965). Suction or total suction consists of capillary component or matric suction and osmotic component. In clays, capillary force can present with sorptive forces due to the presence of ions to form matric component of suction while osmotic component is associated with salt concentration of the free pore fluids. At completely dry conditions (i.e., oven-dry conditions), suction in the soil is 1,000,000 kPa (Croney and Coleman 1961 and Fredlund and Rahardjo 1993).

The relationship between suction and water content (either gravimetric or volumetric basis) in the soil following drying or wetting process is termed as soil-water characteristic curve (Fredlund and Rahardjo 1993). Soil-water characteristics curve can be used as a tool to derive other unsaturated soil

properties such as shear strength, compressibility, and coefficient of permeability provided the soil properties at saturated state are known.

Another relationship between suction and water content can be established when soil is mixed with water to reach several targeted water contents and the measurement of suction is performed for the soil at those water contents. Such a relationship is called suction characteristic curve. The two terms – the soil water characteristic curve and suction characteristic curve should not be mixed up. The soil-water characteristic curve is usually determined for the soil starting from saturated conditions whereas this condition is not necessary in the determination of the suction characteristic curve. In the case of clay soils, the effects of initial fabric are more pronounced in the soil-water characteristic curve but it is not clearly seen in the suction characteristic curve (Agus 2005).

Matric and total suctions are commonly measured while osmotic suction is normally inferred from the two values in spite of the availability of techniques to measure it. Many suction measurement methods are available and the methods can be broadly grouped into two main categories – direct method and indirect method.

The direct method of suction measurement refers to direct measurement of negative pore-water pressure in the soil, e.g., using tensiometer and null-type axis-translation techniques. Since the techniques essentially need the sensor used to be in intimate contact with the soil, matric suction component is measured. As long as the good contact between the soil and the sensor used is warranted, one can arrive at sufficient accuracy using this technique as far as the engineering accuracy is concerned. However, it is nearly impossible to maintain good contact between the soil and the sensor at high suctions. Moreover, cavitation poses another drawback to the technique. Thus, the direct method is not applicable for the measurement of high suctions.

Indirect methods can be considered as alternatives. The indirect methods of suction measurement are applicable for both matric and total suction measurements. For total suction measurement, only the indirect technique is applicable. It is called the indirect method for measuring total suction because it requires the measurement of other parameters such as water content or relative humidity to be performed for inferring the measured total suction.

Generally, it is more difficult to measure total suction than matric suction as far as the accuracy is concerned, since the error involved is generally greater. Although the accuracy of most sensors used in the total suction measurement in terms of the measured parameters (i.e., water content, relative humidity, etc.) is quantifiable, the error likely involved in the measurement in terms of total suction value has not been mentioned in most literature on total suction measurements. Arifin et al. (2006) discussed errors in the measurement of total suction of bentonite–sand mixtures using different types of sensor. However, the extent to which the errors affect the measurement results was not comprehensively discussed in the paper.

This paper focuses on the indirect measurement of total suction using commonly used sensors. The main discussion brought out in this paper is the error

associated with several total suction measurement sensors; namely, filter paper, psychrometer, capacitance sensor, warmed-head capacitance sensor, and chilled-mirror hygrometer. An interesting discussion on the extent to which the measurement error affects the results is presented at the end of the paper.

Total Suction Measurement Techniques

Various methods have been used to indirectly measure total suction of soils. Filter paper technique is among the available methods whereby filter paper water content is used to infer total suction of the soil. Other sensors like psychrometer and capacitance sensor are among the famous methods for measuring suction together with chilled-mirror hygrometer which has recently been introduced in geotechnical engineering. The sensors measure relative humidity of the vapour in the soil pores. The relative humidity is converted to total suction using Kelvin's equation (Fredlund and Rahardjo 1993):

$$s_t = \frac{-RT}{M_w(1/\rho_w)} \ln(\mathrm{RH}) \tag{1}$$

where R is the universal gas constant (i.e., 8.31432 J/mol/K), T is the absolute measured temperature in degrees K, M_w is the molecular weight of water (i.e., 18.016 kg/kmol), ρ_w is the unit weight of water in kg/m^3 as a function of temperature, and RH is the measured relative humidity defined as u_v/u_{vo} where u_v is the partial pressure of pore-water vapour in the specimen and u_{vo} is the saturation pressure of water vapor over a flat surface of water at the same temperature.

When a filter paper is placed without contact with a soil specimen in a closed container, the vapour space above the soil specimen acts as a true semi-permeable membrane which is only permeable to water vapour but not to ions from the pore-water. Therefore, in the (non-contact) filter paper technique, total suction is measured. The calibration curve for the filter paper technique for total suction measurement is normally established using vapour equilibrium technique (e.g., Chandler and Gutierrez 1986 and Leong et al. 2002). Ridley and Wray (1996) found that the filter paper technique is insensitive when used for measuring low total suctions due to possible vapour and temperature non-equilibrium during measurement.

The psychrometer technique has been widely used by many researchers for measuring total suction (see Ridley and Wray (1996) for literature review in this technique). There are many positive aspects, but few drawbacks associated with the accuracy of psychrometers for measuring total suction. The psychrometer technique can be used to measure total suction as high as 8500 kPa. The measurement of low total suctions (i.e., lower than 1000 kPa) using this technique requires an accurate means to maintain temperature at a constant value. Ridley and Wray (1996) noted that inaccuracies of the psychrometer technique may be caused by the insensitivity of psychrometer due

to temperature effects. On the other hand, variability in the electromotive force generated induces error in high suction range. Furthermore, there exists a possibility of deterioration in the sensitivity of psychrometer due to corrosion problem (Hamilton et al. 1981 and Zerhouni 1995). Unlike the filter paper method, no reports of hysteresis of the psychrometer technique for total suction measurement have been found in literature.

The capacitance sensor has been used for measuring high total suction by Albrecht et al. (2003). The capacitance of the sensor changes as the thin polymer film within absorbs water from its surrounding. Polymer capacitance technology is recently used in this type of sensors as the technology provides high reliability to the relative humidity measurement, insignificant hysteresis, and insensitivity to temperature fluctuation where measurement is conducted (Wiederhold 1997). Arifin et al. (2006) used similar sensor and found that the sensor also works at high temperature.

The warmed-head capacitance sensor generally has better performance than the capacitance sensor without warming function. When measurement is performed in an environment where relative humidity and temperature change very rapidly, condensation occurs resulting in overestimation of relative humidity or underestimation of total suction. In this case, the warming function in the warmed-head capacitance sensor plays its role in minimizing the effects of condensation.

The chilled-mirror hygrometer technique has been used to measure suction by Leong et al. (2003), Albrecht et al. (2003) and Schanz et al. (2004). The device measures dew point and temperature of the head space or essentially the relative humidity of the head space above the specimen. The description of the chilled-mirror hygrometer can be found in Leong et al. (2003). The equipment has a small chamber where the soil specimen is placed. The temperature of the soil specimen, the vapour space, and the measuring device is controlled and monitored very accurately using an infra-red thermometer. Considering the way the control during measurement is performed, the technique can be considered to be the most accurate method for measuring total suction to date (Leong et al. 2003 and Agus 2005).

Total Suction Measurement Errors

This section discusses errors in the total suction measurement using the filter paper technique (for Whatman 42 filter paper), the psychrometer (thermocouple type PCT-55 with HR-33T voltmeter from Wescor Inc.), the capacitance sensor (PSF102 series from BC component), the warmed-head capacitance sensor (Humicap® HMP 243 from Vaisala Oyj), and the chilled-mirror hygrometer (type 3TE from Decagon Devises Inc.). The first two devices have long been used for measuring suction whereas the other three devices were introduced in geotechnical engineering as total suction measuring techniques not longer than 15 years ago.

Since the measurement of low total suction is more difficult than the measurement of high total suction, the error is often related to how low total suction can be measured by the sensors. Errors in the total suction measurements can generally be divided into four categories:

1. Errors which are induced by inaccuracy of the equipment (or sensor) used. This type of errors exists in all sensors.
2. Errors due to isothermal non-equilibrium between the vapour space, the soil, and the sensor used (or temperature gradient). This type of error can be found in the filter paper (when the size of vapour space is not minimized) and in the total suction measurement using the psychrometer, the capacitance sensor, and the warmed-head capacitance sensor.
3. Errors due to excessive condensation of water vapour on the measuring device as mentioned as a result of rapid temperature and relative humidity fluctuations. The excessive condensation causes a drop in the temperature of water vapour in the vapour space and therefore this type of error can also be regarded as an isothermal non-equilibrium in the measuring system. This type of error can be found in the filter paper, psychrometer technique and in the capacitance sensor.
4. Errors due to handling of the sensor and procedures adopted by operator. This type of error is most pronounced in the filter paper technique.

Errors due to inaccuracy of the devices and temperature gradient can be quantified and are discussed further in the following sections while errors due to excessive water vapour condensation on the measuring devices and the operator-related errors cannot be simply quantified.

Errors Due to the Inaccuracy of the Measuring Devices

The error of total suction measurement due to the inaccuracy of the measuring devices which measures relative humidity of the vapour space in soil is calculated from ratio of the first derivative of Equation (1) with respect to relative humidity to the measured total suction:

$$\text{Error}(\%) = \frac{100\Delta\text{RH}}{\text{RH}\ln(\text{RH})}\% \tag{2}$$

For the filter paper technique, the inaccuracy of the device used is in essence the accuracy of the weighing balance used to measure the weight of wet and dry filter papers to obtain the water content of the filter paper. Considering the ASTM calibration curve for Whatman 42 filter papers (ASTM 1997) and 0.0002 g accuracy of the weighing balance (i.e., the one with 0.0001 g least count), an accuracy of 10.5% and 2% of measured total suction is obtained for the standard-sized 55-mm diameter filter paper (i.e., with an average dry mass of 0.065 g) water content ranging from 0% to 45.3% and 45.3% to 90%, respectively. Since water content of the filter paper is related to suction of

the soil, the accuracy of the filter paper technique in terms of total suction is a function of the soil-water characteristic curve or the suction characteristic curve of the soil. Assuming that the 45.3% filter paper water content corresponds to a total suction of 100 kPa, the error of 10.5% and 2% total suction is expected for the measured total suction ranging from 1,000,000 to 100 kPa and from 100 to 0 kPa, respectively.

For Wescor thermocouple psychrometer type PCT-55 with HR-33T voltmeter, the accuracy is equal to 2% reading (in microvolt) (Wescor 1986). Since total suction is linearly related to the psychrometer reading (with a factor of 0.75 μV/bar), the error in the measured total suction is also equal to 2%. However, the device exhibits a maximum noise of 0.1 μV. The error due to the noise is greater than that due to the reading inaccuracy and one can work out that this error can be quantified using the following expression with s_t in kPa.

$$\text{Error}(\%) = \frac{1333.33}{s_t} \tag{3}$$

Based on Equation (3), it is clear that the percentage of error reduces as measured total suction increases.

For the capacitance sensor PSF102 series, the accuracy is a function of measured sensor capacitance and the value is equal to 0.4 pF/% measured RH (BC Components 1999). Since the capacitance of the sensor is also a function of the measured RH, the accuracy depends on the calibration curve obtained for the sensor. Arifin et al. (2006) noted that several capacitance sensors of PSF 102 series exhibit slight variability in the calibration curve for each individual sensor. The typical calibration curve for the sensors used by Arifin et al. (2006) follows the equation below which is different from that of the sensor of the same type obtained by Albrecht et al. (2003).

$$\text{RH}(\%) = -2442.12 + 19804C_p - 49542C_p^2 + 38978C_p^3 \tag{4}$$

where C_p is the capacitance of the sensor in nF.

The error due to the inaccuracy of the capacitance sensor can be determined by taking the first derivative of Equation (4) with respect to C_p and substituting it to Equation (2).

The warmed-head capacitance sensor Humicap® HMP 243 essentially also measures the capacitance of the sensor. However, since the sensor normally comes with a digital display which can show directly the measured RH value, only the accuracy in terms of measured RH is of concern. Like the capacitance sensor PSF 102 from BC Components, the accuracy of the warmed-head capacitance sensor is also a function of the measured RH, which follows the equation below (Vaisala 2002).

$$\text{RH Error}(\%) = (0.5 + 0.025\text{RH})\% \tag{5}$$

Equation (5) can be directly substituted to Equation (2) to obtain the error in the measured total suction for this sensor.

The chilled-mirror hygrometer type 3TE is a very accurate device for measuring total suction. Leong et al. (2003) found that the device can measure total suction of as low as 150 kPa. However, the value was determined by considering the readability of the device which is 0.1% RH instead of its accuracy. The actual accuracy of the device is equal to 0.3% RH as described by the manufacturer although Agus (2005) found that the device has as low as 0.2% RH accuracy when used to measure relative humidity above standard salt solutions. The 0.3% RH accuracy can be substituted to Equation (2) to obtain the accuracy of the device in terms of measured suction.

Figure 1 shows a graphical representation of total suction measurement error for different sensors assessed in this paper. It is seen that by considering 30% total suction error due to the inaccuracy of the sensors only, the lowest total suction that can be measured using the psychrometer is about 50 kPa, the capacitance sensor is 150,000 kPa, the warmed-head capacitance sensor is 15,000 kPa, and the chilled-mirror hygrometer is 1500 kPa. The error of the total suction measurement using filter paper is much lower than that of the other four sensors.

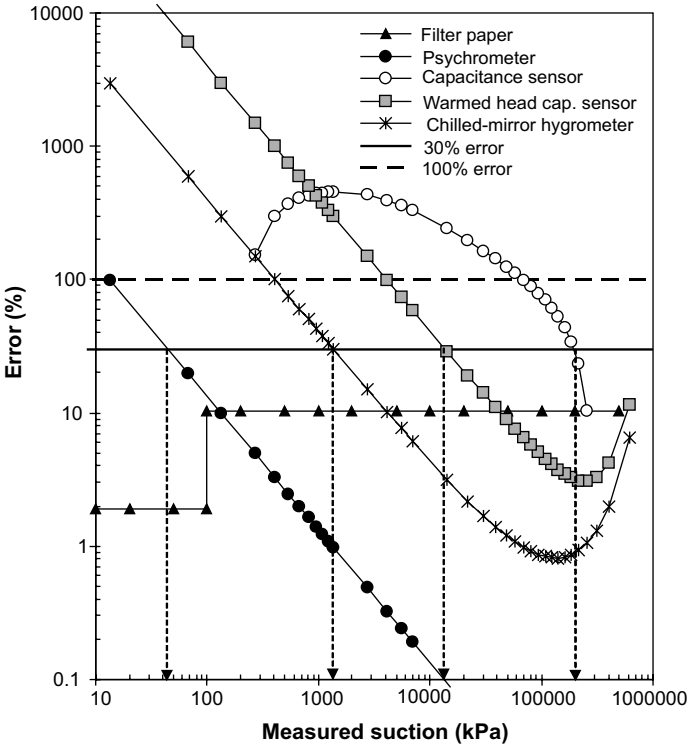

Fig. 1. Error in the total suction measurement due to the inaccuracy of the sensor used only

Errors Due to Temperature Gradient

The total suction measurement errors due to temperature gradient depend on how an isothermal equilibrium between the specimen, the vapour space, and the sensor used in the measurement can be maintained. In a closed system, the amount of water vapor is constant and thus the partial pressure of water vapor (u_v) is also constant. A difference in temperature (or a temperature gradient) between the specimen and the vapour space causes movement of water resulting in a change in the saturated water vapour (u_{vo}) while the change in u_v is zero. A change in the total suction (or the error in total suction measurement) due to temperature gradient can be estimated by rearranging Equation (1) and taking its first derivative with respect to temperature (Croney et al. 1952 and Agus and Schanz, in press).

$$\frac{\mathrm{d}(\ln s_t)}{\mathrm{d}T} = \frac{1}{T} - \frac{1}{u_{vo}\ln(\mathrm{RH})}\frac{\mathrm{d}(u_{vo})}{\mathrm{d}T} \tag{6}$$

The change in total suction or the error in total suction measurement due to different values of temperature gradient is shown in Fig. 2 (Agus and Schanz, in press). If the error is limited, for instance, to 30% of the measured value, the measurement of total suction will be limited to a value of about 850 kPa assuming that a 0.5°C temperature gradient exists in the system.

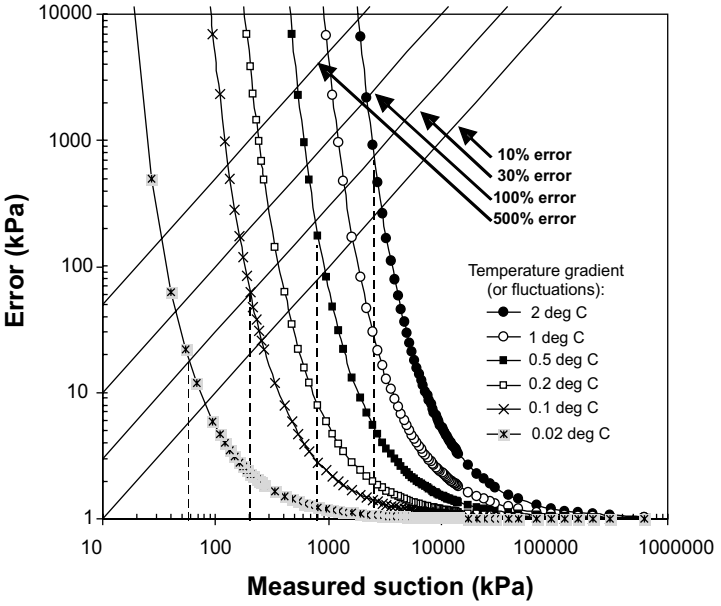

Fig. 2. Error in the total suction measurement due to temperature gradient only (Agus and Schanz, in press)

The temperature gradient of 0.5°C can likely be maintained in a temperature-controlled laboratory. Based on Equation (6), the accurate measurement of total suction to as low as 100 kPa with 30% error requires a means to control temperature within ±0.04°C.

Effects of Total Suction Measurement Errors

To illustrate the effects of total suction measurement errors, a suction characteristic curve plotted as bentonite water content versus total suction relationship that has been obtained for loose bentonite–sand mixtures is considered. The properties of the materials can be found in Agus (2005). The suction characteristic curve presented was measured using the chilled-mirror hygrometer type 3TE. The procedures adopted were described in Agus (2005). The data obtained have been best-fitted using a simple power function for simplicity (Fig. 3). The possible envelopes where the measured total suction data may be obtained using each sensor discussed above have been computed based on the error due to sensor accuracy and that due to temperature gradient and also drawn in Fig. 3. For the filter paper, psychrometer, capacitance sensor, and warmed-head capacitance sensor, a temperature gradient of 0.5°C has been considered. The error due to temperature gradient does not exist in the chilled-mirror hygrometer. It must be noted that the errors due to condensation problems and operator-related factors are not considered. These errors, although cannot be simply quantified cannot be ignored and may govern the overall accuracy of the total suction measurement.

It can be seen from Fig. 3(**a**) that for the filter paper technique, the measurement of total suction is accurate to a lowest total suction of about 1000 kPa. More erratic measurement data can be expected at lower range of total suction as the temperature gradient effects become more pronounced. Similar trend is seen for the psychrometer (Fig. 3(**b**)).

Generally, the capacitance sensor has poor performance almost in the entire range of total suction (Fig. 3(**c**)). A slightly better performance may be expected when measuring total suction of greater than 200,000 kPa using the capacitance sensor (Fig. 3(**c**)) and greater than 20,000 kPa using the warmed-head capacitance sensor (Fig. 3(**d**)) considering errors due to both the sensor accuracy and temperature gradient.

The chilled-mirror hygrometer has the best performance. The sensor can be used to measure total suction as low as 1000 kPa with sufficient accuracy (Fig. 3(**e**)). It is depicted in the figure that some of the data are located outside the envelopes for the chilled-mirror hygrometer technique. The reason for this may be possible errors in the measurement of water content of the specimens. Since the chilled-mirror hygrometer is the most accurate means of measuring total suction, the sensor can be regarded as a benchmark for assessing the accuracy of other sensors for measuring total suction greater than 1000 kPa.

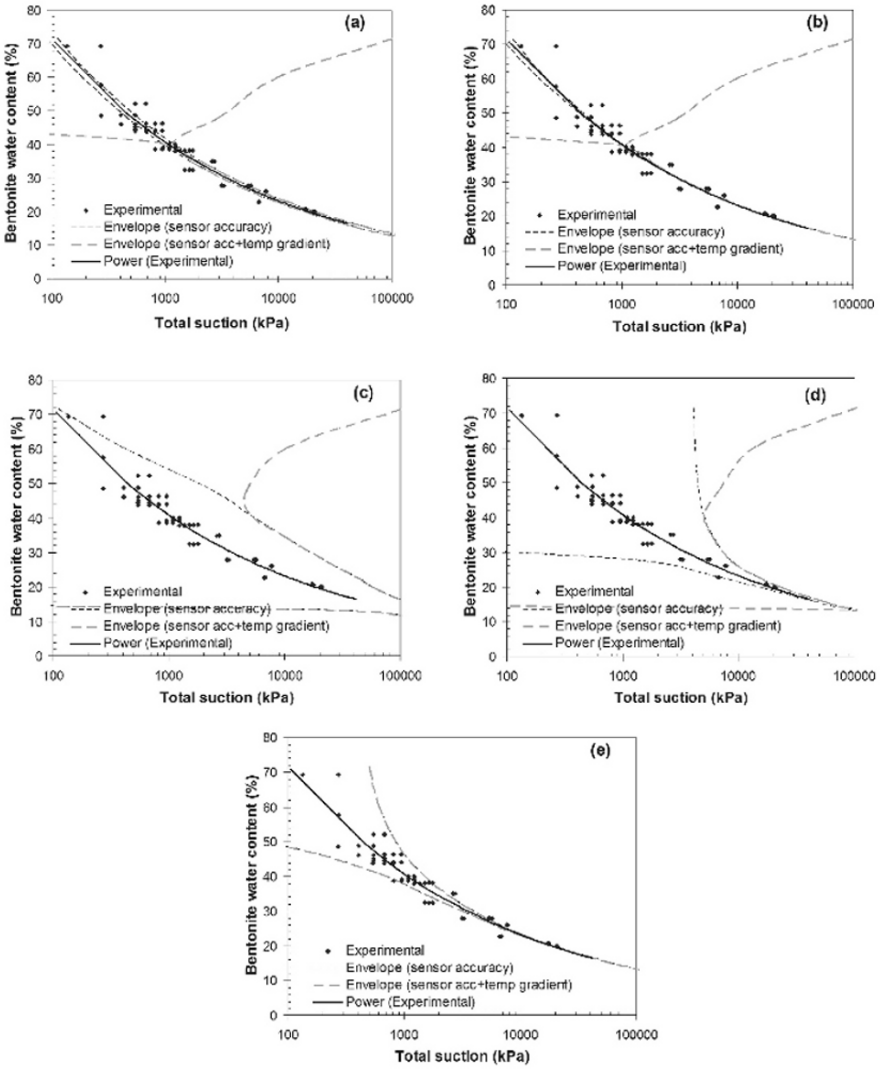

Fig. 3. Suction characteristic curve of loose bentonite–sand mixtures and the envelope of possible measured data for: (**a**) filter paper; (**b**) psychrometer; (**c**) capacitance sensor; (**d**) warmed-head capacitance sensor; and (**e**) chilled-mirror hygrometer

Considering the possible significant errors involved in the total suction measurement, it is recommended to measure matric suction instead of total suction, for suction less than 1000 kPa. When significant amount of contaminant and/or salts are expected to exist in the soil pore-water, there will be significant difference between matric and total suction. Therefore, for suction less than 1000 kPa, measurement of osmotic suction is recommended and

total suction can be computed by adding up the measured matric and osmotic suctions.

Conclusions

A total suction measurement error analysis has been presented and the following conclusions can be drawn:

1. Measurement of low total suction measurement involves great errors. Two quantifiable errors are noted; namely, errors due to the measuring sensor accuracy and errors due to temperature gradient.
2. The chilled-mirror hygrometer possesses the best accuracy and, therefore, can be regarded as a benchmark for assessing other sensors.
3. Total suction measurement can only be performed in the range of suction greater than 1000 kPa, if sufficient accuracy is to be obtained.
4. For suction less than 1000 kPa, matric and osmotic suction measurements are recommended to be performed and total suction is computed from the two values.

References

Agus SS (2005) An experimental study on hydro-mechanical characteristics of compacted bentonite–sand mixtures. PhD Thesis, Bauhaus-University Weimar, Germany

Agus SS, Schanz T (In press) Discussion of paper "Free energy of water-suction-in filter papers" by R. Bulut and W.K. Wray, Geotechnical Testing Journal, 29(6)

Aitchison GD (1965) Moisture equilibria and moisture changes in soils beneath covered areas. In: Aitchison GD (ed) A symposium in Print, Australia, Butterworth

Albrecht BA, Benson CH, Beuermann S (2003) Polymer capacitance sensors for measuring gas humidity in drier soils, Geotechnical Testing Journal, 26(1):3–11

Arifin YF, Agus SS, Schanz T (2006) Temperature Effects on Suction Characteristic Curve of Bentonite-Sand Mixtures. In: Miller GA, Zapata CE, Houston SL, Fredlund DG (eds) Proc 4th Int Conf on Unsaturated Soils, 2006, Carefree, Arizona, USA:1314–1325

ASTM (1997) Annual Book of Standards. Volumes 04.08 and 04.09, Soil and rock, ASTM International, West Conshohocken, PA

BC Components (1999) Humidity Sensor Brochure

Croney D, Coleman JD, Bridge P (1952) The suction of moisture held in soil and other porous materials, Road Research Technical Paper, 24

Croney D, Coleman JD (1961) Pore pressure and suction in soil. In: Proceedings of Conference on Pore Pressure and Suction in Soils, London, Butterworths:31–37

Chandler RJ, Gutierrez CI (1986) The filter paper method of suction measurement, Geotechnique 36:265–268

Fredlund DG, Rahardjo H (1993) Soil mechanics for unsaturated soils. John Willey & Sons, Canada

Hamilton JM, Daniel DE, Olson RE (1981) Measurement of hydraulic conductivity of partially saturated soils. In: Zimmie TF, Riggs CO (eds) Permeability and Groundwater Contaminant Transport, ASTM Special Technical Publication 746, ASTM:182–196

Leong EC, He L, Rahardjo H (2002) Factors affecting the filter paper method for total and matric suction measurements, Geotechnical Testing Journal, 25(3)321–332

Leong EC, Tripathy S, Rahardjo H (2003) Total suction measurement of unsaturated soils with a device using the chilled-mirror hygrometer technique, Geotechnique 53(2)173–182

Ridley AM, Wray WK (1996) Suction measurement: a review of current theory and practices. In: Alonso EE, Delage P (eds) Proc 1st Int Conf on Unsaturated Soils (UNSAT 95), Paris, 1995, Balkema, Rotterdam:1293–1322

Schanz T, Agus SS, Tscheschlok G (2004) Determination of hydro-mechanical properties of Trisoplast®. Research Report Bo-015/03. Laboratory of Soil Mechanics, Bauhaus-University Weimar, Weimar, Germany

Vaisala (2002) HMP240 series transmitters. User's guide. Vaisala Oyj., Helsinki, Finland

Wescor Inc. (1986) HR 33T Dew point microvoltmeter: Instruction/service manual. Wescor Inc., Utah

Wiederhold PR (1997) Water vapour measurement—methods and instrumentation. Marcel Dekker, NY

Zerhouni (1995) Triaxial testing using psychrometers (In French). In: Alonso EE, Delage P (eds) Proc 1st Int Conf on Unsaturated Soils (UNSAT 95), Paris, 1995, Balkema, Rotterdam:673–678

Application of a Dew Point Method to Obtain the Soil Water Characteristic

Gaylon S. Campbell, David M. Smith, and Brody L. Teare

Decagon Devices, Inc., 950 NE Nelson Ct., Pullman WA. USA
gaylon@decagon.com, daves@decagon.com, brody@decagon.com

Summary. The dew point method, which determines suction by measuring sample temperature and dew point temperature of air equilibrated with the sample, provides a quick and accurate method for measuring suction in the range 1 to 400 MPa (pF 4 to pF 6.6). We present a procedure, using the dew point method, to prepare samples in the relevant suction range, measure suction and water content, and obtain an equation describing the soil water characteristic (SWC). Characteristics for four soil samples ranging in texture from sand to bentonite are presented. All show a linear relationship when water content is plotted vs. logarithm of suction. The slope of the characteristic is easily obtained for use in expansive soil identification.

Key words: soil water characteristic, chilled mirror dew point, expansive soil identification

Introduction

The soil water characteristic (SWC) relates total suction to water content for a particular soil, and is of fundamental importance to unsaturated soil mechanics. In spite of its importance, few methods exist for quickly and accurately determining the SWC. Traditionally axis translation methods (pressure plates) have been used to equilibrate samples at preset matric suctions, and then the water content of the equilibrated samples is determined by oven drying. The assumption is made that samples equilibrate in the axis translation apparatus at the preset pressures. Both models and measurement confirm that this is a bad assumption at suctions drier than 200 to 300 kPa (Campbell 1988, Gee et al. 2002). Beyond these suctions the hydraulic conductivity of both the sample and sample-plate contact become so low that even weeks are not sufficient for equilibrium. Outflow decreases rapidly with time because of the decreasing hydraulic conductivity giving an appearance of equilibrium, but in fact the sample stays far from it.

Tensiometers provide another popular method to measure matric suction. Most are limited to the range 0 to 80 kPa (Lu and Likos 2004), though special

designs and pretreatments allow some units to reach 1500 kPa. Such units are not widely available. A tensiometer can be used, along with oven drying, to determine the wet end of the SWC. A different method is required for the dry end of the curve.

Vapor pressure methods are ideal for measuring suction of samples drier than the axis translation or tensiometer range. Suction is determined by equilibrating a sample with a head space, measuring the head space vapor pressure and the sample saturation vapor pressure, and then using the Kelvin equation to compute total suction:

$$\psi_t = \frac{R(T + 273.16)}{V_w} \ln\left(\frac{p}{p_o}\right). \tag{1}$$

Here R is the gas constant (8.3143 J/mol), T is Celsius temperature, V_w is the molar volume of water (1.8×10^{-5} m^3 mol^{-1}), p is the equilibrium vapor pressure in the head space and p_o is the saturation vapor pressure at sample temperature. The units of ψ_t are J m^{-3} or N m^{-2} or Pa. The head space vapor pressure can be measured by determining wet bulb depression, as with the thermocouple psychrometer (Rawlins and Campbell 1986) or the dew point temperature as with the dew point potentiometer (Gee et al. 1992).

Because the vapor gap between the sample and the sensor is a perfect semi permeable membrane, vapor pressure methods measure total suction. Axis translation methods and tensiometers measure matric suction. The difference between these is the osmotic suction. To determine matric suction from a vapor pressure measurement one needs to have an independent measurement of osmotic suction. Methods for making this measurement are discussed elsewhere (Rawlins and Campbell 1986, Leong et al. 2003).

The Dew Point Method

The Dew Point Potentiameter (Model WP4, Decagon Devices, Inc., Pullman, WA 99163 USA) determines total suction by measuring the dew point temperature of the head space above a sample. This is done by cooling a mirror whose reflectance is carefully monitored by an optical sensor. The mirror temperature is controlled to maintain a constant thickness of dew. The mirror temperature is measured with a thermocouple. Sample temperature is monitored by infrared thermometry. The vapor pressure of the air is the saturation vapor pressure at dew point temperature. Saturation vapor pressure is only a function of temperature:

$$p_o(T) = 0.611 \exp\left(\frac{17.502T}{240.97 + T}\right) \tag{2}$$

Substituting T_d in Eq. (2) to get vapor pressure (saturation vapor pressure at dew point temperature) and T_s to get saturation vapor pressure at sample temperature, and substituting these into Eq. (1) gives

$$\psi_t = \frac{R(T + 273.15)17.502}{V_w}\left(\frac{T_d}{T_d + 240.97} - \frac{T_s}{T_s + 240.97}\right) \quad (3)$$

Note that Eqs. (1) and (3) give negative values. The water potential, or potential energy of the water with reference to pure free water is negative. The term *suction* has an implied negative, so the suction values we report here are positive values. Equation (3) shows two things. First, suction measurement accuracy depends mainly on a correct measurement of temperature difference, not on knowing the absolute temperatures. Second, suction is roughly proportional to the difference between dew point and sample temperature. A rough sensitivity analysis using Eq. (3) shows that 0.1°C difference between sample and dew point temperature is approximately equal to 1 MPa. The WP4 has a temperature resolution of approximately 0.01°C giving a water potential resolution of 0.1 MPa.

Performance Verification

The dew point measurement is a primary measurement in the sense that its prediction of suction comes from fundamental thermodynamic relationships and measurements of temperature. The temperature measurements, of course, need to be accurate for the results to be accurate. Factory calibration of the instrument involves setting the sensitivity of the thermopile using a black body radiator with an embedded temperature standard, and making minor adjustments to the thermocouple sensitivity using unsaturated salt standards of known suction. To verify the performance of the WP4 over its measurement range we tested a standard unit using saturated salts of known suction (Greenspan 1977). These were independent of the solutions used for setting the thermocouple sensitivity. Readings for one unsaturated salt are also shown to indicate performance at low suction. The results are shown in Table 1.

Table 1. WP4 measurements on standard salt solutions. The mean and standard deviation for three readings on each salt are shown. Measurements are at 25°C

	Suction (MPa)	WP4 Mean ± SD (MPa)
0.5 mol KCl	2.22	2.19 ± 0.08
Sat. KCl	23.37	23.41 ± 0.11
Sat. NaCl	39.09	39.16 ± 0.07
Sat. $Mg(NO_3)_2$	87.76	88.62 ± 0.04
Sat. $MgCl_2$	153.75	155.28 ± 0.05
Sat. LiCl	300.20	302.06 ± 0.80

The measurements agree with the standards to within 1% or better for all of the saturated salts indicating excellent accuracy over that entire range.

The resolution is 0.1 MPa, which is 5% of the reading at 2 MPa and 10% of the reading at 1 MPa. We point this out to make sure the reader is aware of the limitations of vapor pressure methods on the wet end. They are not a substitute for axis translation and tensiometer measurements. For the SWC data we will present we will avoid using values wetter than 1 MPa.

Sample Preparation

Correct sample preparation methods are critical for obtaining good SWCs. The following methods have given reliable results in our laboratory. It should be pointed out that a wetting characteristic will be different from a drying characteristic because of moisture hysteresis. The methods here are for a wetting characteristic. Previous work has shown that, at the suction values covered by vapor pressure methods, bulk density has little if any effect on suction (Campbell and Gardner 1971). All measurements are therefore made on soil that has been air dried and sieved through a 2 mm sieve.

The range of water content for the SWC is strongly dependent on the clay content of the sample, as shown in Table 2. This table gives silt and clay fractions, 1.5 MPa water contents and air dry soil water contents for representative members of the 12 soil texture classes. It is important to point out that these are average values from many soils. They can serve as a guide, but many things in addition to texture can influence these values. Our objective is to obtain a set of samples with water contents roughly ranging between the values shown in the table.

The procedure for preparing samples is as follows. Begin with air dry soil (soil that has been exposed to the air for several days so that it is in moisture

Table 2. Representative silt and clay fractions and typical water content values at 1.5 MPa and air dry suction for the 12 soil texture classes

Texture	Silt (g/g)	Clay (g/g)	$w_{1.5}$ (g/g)	w_{ad} (g/g)
Sand	0.05	0.03	0.008	0.003
Loamy sand	0.12	0.07	0.015	0.005
Sandy loam	0.25	0.10	0.045	0.015
Sandy clay loam	0.13	0.27	0.143	0.048
Loam	0.40	0.18	0.106	0.035
Sandy clay	0.07	0.40	0.204	0.068
Silt loam	0.65	0.15	0.098	0.033
Silt	0.87	0.07	0.075	0.025
Clay loam	0.34	0.34	0.174	0.058
Silty clay loam	0.58	0.33	0.166	0.055
Silty clay	0.45	0.45	0.204	0.068
Clay	0.20	0.60	0.234	0.078

equilibrium with the air). The soil water content is defined as the mass of water divided by the mass of oven dry soil. This definition can be used to obtain the following equation for determining the mass of water to add to a given mass of air dry soil to get the desired water content:

$$M_w = M_{\mathrm{ad}} \frac{w - w_{\mathrm{ad}}}{1 + w_{\mathrm{ad}}} \tag{4}$$

where M_{ad} is the mass of air dry soil, w is the desired final water content, and w_{ad} is the air dry water content of the soil (from Table 2). To prepare samples, determine the soil texture by feel or particle size analysis and use Table 2 to find the approximate air dry and 1.5 MPa water contents. Weigh out five to ten 50 g samples of sieved, air dry soil into containers which can be sealed with a lid. Use Eq. (4) to compute amounts of water to add to the samples to produce a set of samples with water contents spanning the range from air dry to a little wetter than 1.5 MPa. Thoroughly mix the water with the samples, seal them and allow them to stand for 24 hours or longer to equilibrate. At the end of the equilibration period a sub sample of the soil is placed in a sample cup and its suction determined with the WP4. Discard samples with suctions wetter than 1 MPa. Determine the water content of all remaining samples by oven drying. If the stainless steel cups are used in the WP4, the same sample on which water potential was determined can be weighed, oven dried at 105°C, and reweighed to determine the water content. If polyethylene cups are used, a separate sub sample is dried using standard drying tins. The water content is computed as the mass of water (change in sample mass on drying) divided by the mass of the oven dry soil (dry mass of the sample and container minus the mass of the container). Extreme care is necessary, especially in coarse textured soils, to obtain accurate water content values. Once this initial set of samples is run, additional samples can be prepared with appropriate water contents to fill in where data are sparse.

An alternative approach, useful for high clay samples that can not be mixed with small quantities of water to give a uniform water content is to place approximately 5 g samples of air dry soil in WP4 sample cups, suspend the cups over water to take up water through vapor absorption, and remove the cups at intervals to get a range of suctions. Again, the cups need to be sealed and allowed to equilibrate for 24 hours or more before readings are taken.

Results

Data from samples measured using the WP4 with the technique just described are shown in Fig. 1. Soils from sand to clay are shown. Here the base 10 logarithm of the suction is plotted as a function of water content. Each data set except the sand contains data from 2 or 3 independent sample runs, indicating excellent agreement among samples. No systematic deviation from a straight

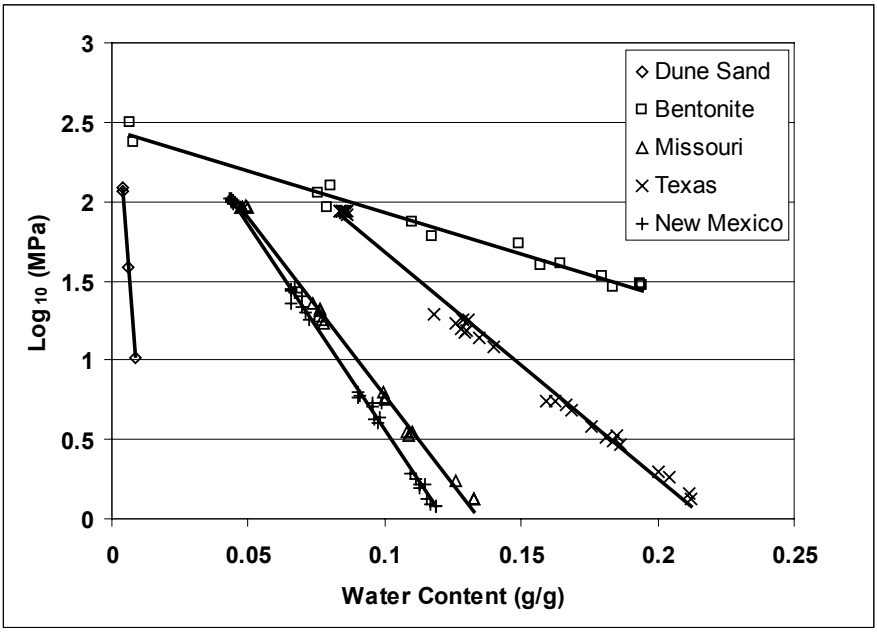

Fig. 1. Soil Water Characteristics for five soils. Each data set is for 2 or 3 samples. Lines are from linear regression

line is seen in any of the data, so the SWC model for the range of suctions shown in Fig. 1 is

$$\psi_t = 10^{aw+b} \tag{5}$$

where a and b are constants for the particular soil. Table 3 gives the values of a and b for the soils in Fig. 1. The slope, a can be used as an index to identify expansive soils (McKeen 1992) (note that McKeen used pF, which is the base 10 logarithm of the suction in cm of water; these units are no longer recommended). According to McKeen's classification, only the Missouri and Bentonite samples are expansive. The Missouri soil is low to medium, and the Bentonite is called "special case," beyond high.

Table 3. Coefficients for Eq. (5) for the five soils in Fig. 1

Soil	Texture	Slope a	Intercept b	r^2
Dune Sand	Sand	−224	2.94	0.999
New Mexico	Clay loam	−25.8	3.14	0.997
Missouri	Silty clay loam	−22.3	3.02	0.997
Texas	Clay	−14.2	3.10	0.993
Bentonite	Clay	−5.2	2.46	0.98

Conclusions

The dew point instrument is a primary method for measuring total soil suction in the range 1 to 400 MPa with an accuracy of about 1%. A measurement takes less than 5 minutes. This makes it a useful device for rapid determination of soil water characteristics in this range. Moisture characteristics can be efficiently obtained from a texture-based estimate of the range of water contents needed to cover the range of desired suctions. Plotting water content vs. logarithm of suction gives a linear relationship, the slope of which can be useful in detecting expansive soils.

References

Campbell GS (1988) Soil water potential measurement: an overview, Irrig Sci 9:265–273

Campbell GS, Gardner WH (1971) Psychrometric measurement of soil water potential: temperature and bulk density effects, Soil Sci Soc Am Proc 35:8–12

Gee GW, Campbell MD, Campbell GS, Campbell JH (1992) Rapid measurement of low soil water potentials using a water activity meter. Soil Sci Soc Am J 56:1068–1070

Gee GW, Ward AL, Zhang ZF, Campbell GS, J Mathison (2002) The influence of hydraulic nonequilibrium on pressure plate data, Vadose Zone J 1:172–178

Greenspan L (1977) Humidity fixed points of binary saturated aqueous solutions, J Res Nat Bureau Stds – A. Physics and chemistry 81A:89–96

Leong E–C, Tripathy S, Rahardjo H (2003) Total suction measurement of unsaturated soils with a device using the chilled-mirror dew-point technique, Geotechnique 53:173–182

Lu N, Likos WJ (2004) Unsaturated Soil Mechanics. Wiley, Hoboken, NJ

McKeen RG (1992) A model for predicting expansive soil behavior. In: 7th Int Conf on Expansive Soils, Dallas, 1:1–6

Rawlins SL, Campbell GS (1986) Water potential: thermocouple psychrometry. In: Methods of Soil Analysis, Part 1, 2nd Ed. Agron Monogr 9:597–618, Madison, WI

A Comparative Study of Soil Suction Measurement Using Two Different High-Range Psychrometers

Rafaela Cardoso[1], Enrique Romero[2], Analice Lima[3], and Alessio Ferrari[4]

[1] Instituto Superior Técnico, Portugal rafaela@civil.ist.utl.pt
[2] Universitat Politècnica de Catalunya, Spain enrique.romero-morales@upc.edu
[3] Universitat Politècnica de Catalunya, Spain analice.lima@ig.com.br
[4] Università degli Studi di Palermo, Italy ferrari@diseg.unipa.it

Summary. An extensive experimental study was performed to compare the measurement capabilities within different ranges of two total suction measurement equipment: SMI transistor psychrometers and a chilled-mirror dew-point psychrometer (WP4 Dewpoint PotentiaMeter). The equipment were used in a systematic way to determine the relative humidity of the environment surrounding different compacted clayey soils along drying paths and covering a wide total suction range (0.1 to 70 MPa). The equipment description and the calibration protocols followed are presented, as well as suggestions regarding the improvement of their performance. The water retention curves of two different compacted clayey soils are presented and commented by taking into account the corrections proposed for the readings. A possible explanation for differences in the measurements observed between both instruments in the high suction range is presented in terms of the hydraulic paths undergone by the soils during the measurement period.

Key words: total suction, transistor psychrometer, chilled-mirror dew-point psychrometer, calibration, water retention curve

1 Introduction

The determination of the water retention properties in a wide suction range of natural and compacted soils is a fundamental issue in many geoenvironmental and geotechnical applications, such as engineered barriers and liners, ground-atmosphere interactions and compacted fills used in man made structures – earth dams, road subgrades and embankments.

This paper focuses on a performance comparative study of two high-range psychrometers for total suction measurement, which have been widely used and their reliability widely accepted. One of these equipment is the SMI transistor psychrometer (Soil Mechanics Instrumentation, Adelaide, Australia), which has been used by several authors (e.g. Dimos 1991, Woodburn

et al. 1993, Truong and Holden 1995, Woodburn and Lucas 1995, Mata et al. 2002, Boso et al. 2004). The other one is a chilled-mirror dew-point psychrometer (WP4, Decagon Devices, Inc., Pullman, Washington, USA, `www.decagon.com`). The latter equipment has been developed in recent years to accurately determine the relative humidity in a wide range and involving a reduced time of reading. This equipment or a similar one has been used by Loiseau (2001), Leong et al. (2003), Tang and Cui (2005), and Thakur and Singh (2005).

To undertake such a study, two compacted clayey soils were used that are able to hold moisture in a wide range of total suctions (0.1 to 70 MPa). The drying branch of the water retention curves of these soils – compacted/destructured argillite and compacted scaly clay – were determined using both equipment. Careful and well-posed protocols were followed to calibrate the psychrometers and perform the measurements, which are discussed within the context of the determination of the water retention curves. Based on the results, suggestions for the calibration protocols and corrections for the readings are made. A possible explanation for differences in the measurements observed between both instruments in the high suction range is also discussed.

2 Equipment Used for Total Suction Measurement

A picture of the equipment used in this research is presented in Fig. 1. The working principle of the psychrometers is based on the measurement of the relative humidity of the air inside a small sealed chamber. At equilibrium, the relative humidity of the air in the chamber is the same as the relative humidity of the soil. The soil total suction, ψ, the equivalent suction derived

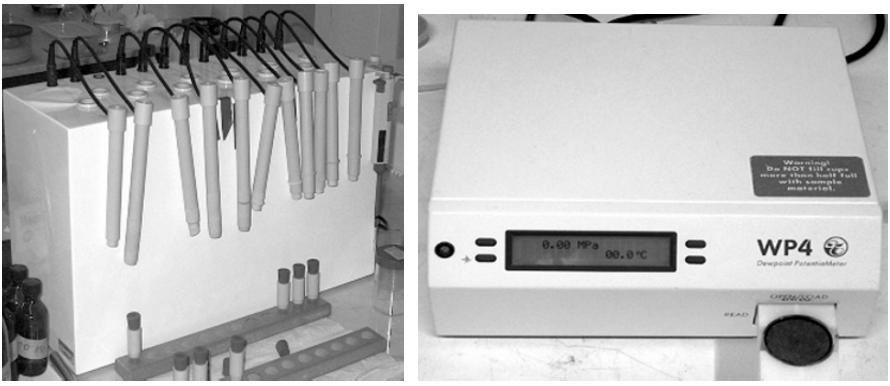

a) SMI transistor psychrometers

b) Chilled-mirror dew-point psychrometer, WP4

Fig. 1. Equipment used to measure total suction

from the vapour pressure, p, in equilibrium with the soil water, relative to the saturation vapour pressure, p_o, at the same temperature in equilibrium with free pure water, is related to the relative humidity, $RH = p/p_o$, by the psychrometric law (Fredlund and Rahardjo 1993):

$$\psi = -\frac{RT\rho_w}{M_w} \ln(RH) \tag{1}$$

where R is the gas constant (8.314 J/(mol K)), T is the absolute temperature, M_w is the molecular mass of water (18.016 kg/kmol) and ρ_w is the density of pure water (998 kg/m^3 at 293 K).

The psychrometers are known to have some variables and factors that can affect the measurement. One of these variables is temperature, which can induce fluctuations in relative humidity readings due to the temperature dependence of p_o. Readings should be taken at a constant temperature of the measurement environment in thermal equilibrium with the soil sample. In addition, hysteresis effect, change of calibration with time and equalisation period are also factors that affect the reliability of the readings.

The devices are presented schematically in Fig. 2. As shown in Fig. 2**a**, the SMI psychrometer probe consists of two bulbs, which act as 'wet' and 'dry' thermometers that are placed inside a sealed chamber in equilibrium with the soil sample (cylinder 12 mm high and 10 mm in diameter). A drop of distilled water with specified dimensions is used to wet the 'wet' thermometer. The rate of evaporation of the drop is inversely proportional to the quantity of vapour present in the atmosphere of the chamber: the drier the air, the quicker the evaporation. Evaporation from the 'wet' bulb lowers the temperature so that this thermometer shows a lower temperature than the one of the 'dry' bulb thermometer. The psychrometer measures indirectly the relative humidity by the difference in temperature between the 'dry' and the 'wet' bulbs – the output voltage can be related to the relative humidity (or total suction) through a suitable and extended calibration. The probe is installed

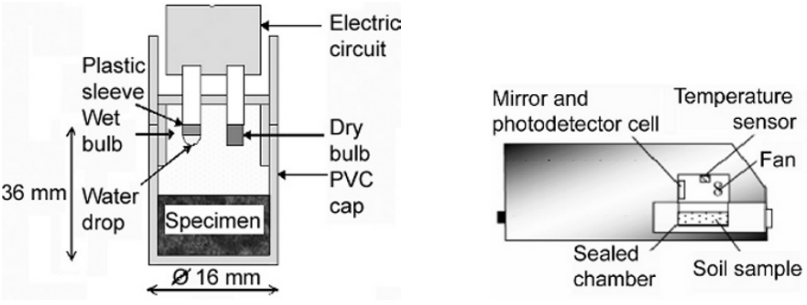

Fig. 2. Schema of **a**) SMI transistor psychrometer, and **b**) chilled-mirror dew-point psychrometer (Leong et al. 2003)

in a thermally insulated bath to minimise temperature induced fluctuations. The standard equilibration period is one hour.

The chilled-mirror dew-point psychrometer measures the temperature at which condensation first appears (dew-point temperature). As shown in Fig. 2b, a soil sample in equilibrium with the surrounding air is placed in a housing chamber containing a mirror and a detector of condensation on the mirror. The temperature of the mirror is precisely controlled by a thermoelectric (Peltier) cooler. The sensing of the condensation point is done with a photoelectric cell, which detects the presence of condensed water on the mirror through the reduction in the mirror's reflection. A thermocouple attached to the mirror records the temperature at which condensation occurs. The relative humidity is computed from the difference between the dew-point temperature of the air and the temperature of the soil sample, which is measured with an infrared thermometer. A fan is included in the sealed compartment to speed up the equalisation period between the sample and the surrounding air. The total suction measuring time is around 5 minutes. The device also has a temperature controller to set the temperature of the sample at which relative humidity measurement is to be made. It is assumed that since both dew-point and sample surface temperatures are simultaneously measured, the need for complete thermal equilibrium is eliminated (Decagon Devices, Inc. 2003). However, temperature gradients between the measurement environment and the sample, may result in unstable readings, and more accurate results are obtained by controlling the temperature difference between the sample and the chamber block – usually within 0.1°C of each other. More details are described in Decagon Devices, Inc. (2003).

Table 1 presents the comparison of both equipment concerning suction range, output, accuracy, measurement time and calibration. Calibration issues will be discussed further in this paper.

Table 1. Specifications of the psychrometers used

Equipment	SMI Psychrometer	Chilled-mirror dew-point WP4
Suction range	1 to 70 MPa (*)	1 to 60 MPa (max. 300 MPa)
Output reading	Voltage, suction (logger)	Suction and temperature
Accuracy	$< \pm 0.05$ pF ± 0.01 pF (repeatability)	$\pm$ 0.1 MPa from 1 to 10 MPa and $\pm$ 1% from 10 to 60 MPa
Measuring time	Usually 1 hour	3 to 10 minutes
Calibration	Multiple point calibration	Single point calibration
Sample geom.	$\phi = 15$ mm, $h = 12$ mm	Sample cup: $\phi = 37$ mm, $h = 7$ mm

(*) disconnecting the probe from the standard logger (Woodburn and Lucas 1995)

3 Calibration Protocols

The calibrations of the psychrometers were performed in a controlled-temperature room ($22 \pm 1°C$) at a relative humidity of $40 \pm 5\%$ by comparing the relative humidity measured to the one applied with standard salt solutions, and covering a wide total suction range (2–73 MPa). The following sections describe the calibration procedures adopted for each psychrometer.

3.1 SMI Psychrometer Calibration

The calibration of the SMI psychrometers – relationship between millivolts output and known relative humidity value – was performed adopting the standard procedure described by Dimos (1991) and Woodburn et al. (1993). The psychrometers were first equilibrated at zero total suction for one hour with distilled water and the output adjusted to the initial offset. Afterwards, the different outputs were recorded following a single step calibration of one-hour stabilisation period – each total suction step was applied after equalisation at zero total suction. Increasing suction steps were followed to avoid hysteresis effects. The operation range of the SMI was extended in the high total suction domain by disconnecting the equipment from the standard logger and using a millivoltmeter instead, as suggested by Woodburn and Lucas (1995) and Mata et al. (2002). The solutions used to apply the relative humidity were prepared with KCl, NaCl and $NaBr{\cdot}2H_2O$, covering a suction range from 2 to 73 MPa (Romero 2001, OIML R 121 1996). To fit the measured points, linear relationships were used. Figure 3 shows the calibration for one-hour equilibration time using a standard drop size. As observed, two linear relationships are necessary to best fit the results, one defined for the low total suction range (from 0 to 20 MPa) and the other for the high one (greater than 20 MPa).

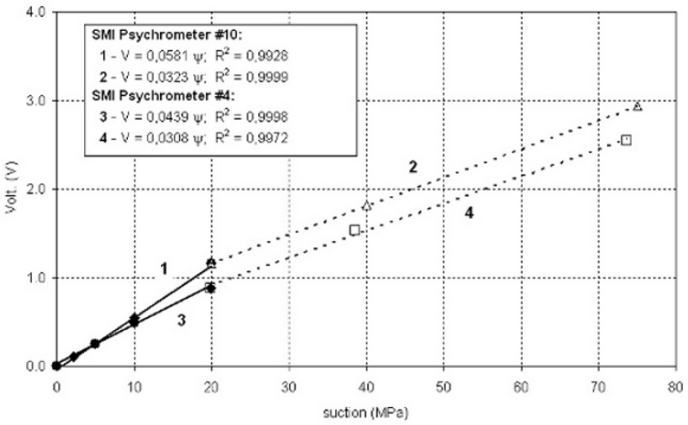

Fig. 3. Calibration of SMI psychrometers (one hour reading time and standard drop size)

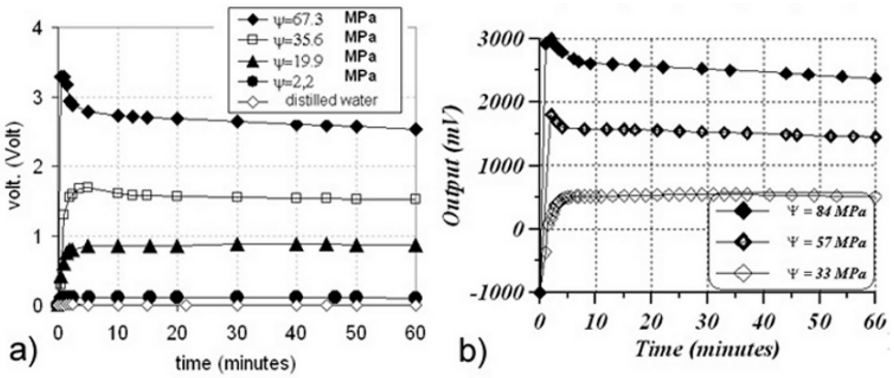

Fig. 4. Time evolution of output for the same psychrometer for different values of total suction applied using a standard drop size. **a**) Results from the present study, **b**) Results from Mata et al. (2002)

The time period adopted for equilibration has a major role on the calibration at high suctions since the readings are not constant in time, as illustrated in Figs 4**a** and 4**b** for a standard drop size. As observed in these figures, initially the outputs increase due to the influence of the measuring environment that maintains the relative humidity of the laboratory. At $\psi < 40\,\text{MPa}$, the outputs tend to rapidly level off without peak at the relative humidity in equilibrium with the soil sample. On the contrary, at $\psi > 40\,\text{MPa}$, the output at the quasi-equilibrated state with the soil sample is rapidly achieved after a peak in the transient evolution. In addition, the output evolution show a continuous decreasing shift after the quasi-equilibrated state, in which levelling out of the output does not occur when applying high total suctions ($> 40\,\text{MPa}$). This fact makes the selection of the final reading difficult and implies smaller voltages for the higher suctions after one hour, which explains the bilinear calibration relationship plotted in Fig. 3.

A reasonable explanation for the changes in the readings with time after equalisation can be the fact that the measuring chamber, where the soil sample is placed, is not completely closed. As a consequence, the measuring environment is affected by the relative humidity of the laboratory. At elevated soil total suctions, the water drop evaporates continuously demanded initially by the total suction of the soil and later by the influence of the relative humidity of the laboratory. An observation consistent with this statement is that the mass of the high-suction soil samples slightly increase along the reading period, indicating some small water transfer to the soil, and that the water drop evaporates. In fact, at ultimate conditions, the water drop can dry completely, and the voltage reading should return to the reading associated with zero total suction, i.e., no temperature difference between bulbs.

In order to amend the aforementioned problem, two procedures have been suggested to make readings in the high-suction range. A way to obtain a

more constant output from the instrument as the water drop evaporates is to increase the size of the standard drop. Woodburn and Lucas (1995) reported a flatter slope in the time evolution using 1.5 water drop size and one hour measuring time. Another possibility is to reduce the time for equilibrium and maintain the standard drop size as suggested by Mata et al. (2002), who proposed to change the measurement time according to the total suction range considered: 60 minutes for $1 \leq \psi \leq 33$ MPa; 30 minutes for $33 < \psi \leq 57$ MPa and 20 minutes for $57 < \psi \leq 84$ MPa. In this way, the linear relationship of the low-suction range could be extrapolated throughout the entire suction range, as shown in Fig. 5. The reduction in the measurement time depends on the prediction of the soil total suction before doing the measurement, which is not always easy to assume. In this paper, the bi-linear calibration with standard drop size presented in Fig. 3 is preferred to measure soil suction and perform the comparison with the chilled-mirror dew-point psychrometer.

Besides drop size and measurement time, temperature, hysteretic behaviour, change in calibration with time and gap size, are other factors that affect the results of transistor psychrometers, as extensively studied by Truong and Holden (1995).

3.2 WP4 Psychrometer Calibration

As suggested by the manufacturer, the single-point calibration of the WP4 is performed with dilute KCl or NaCl solutions (0.5 m) applying a total suction of 2.2 MPa at 20°C. The calibration slope is fixed during factory calibration and the user only adjusts the zero offset in the low-suction range (Decagon Devices, Inc. 2003). This single point will be named calibration point and indicated with sub-script 'cal' from now on. However, in addition to offset shift, sensitivity drifts over time are expected to occur, which make the single-point calibration inappropriate.

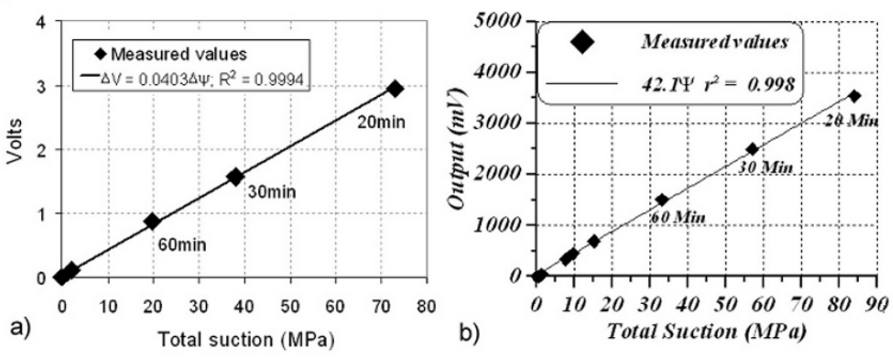

Fig. 5. Linear relationship for total suction applied and SMI psychrometer output for standard drop size and reduced measurement time. **a**) Results from the present study, **b**) Results from Mata et al. (2002)

To verify the calibration throughout the measurement range, in-dependent offset calibrations were performed at three different total suction levels, ψ_{cal} = 2.2, 19.4 and 38.2 MPa (22°C). Once the offset had been set, the verification of the calibration was carried out for each ψ_{cal} by checking the WP4 reading with different total suctions. Partially saturated solutions of NaCl were used along the verification programme. The relationship between the relative humidity, RH, and the molality, m, of the solute (mol of NaCl/kg of pure water, with molecular mass of the salt 58.443 kg/kmol) at 22°C is given by the following empirical expression (Horvath 1985, Romero 2001):

$$\begin{aligned} RH &= 1 - 0.035m - \chi m(m-3), \\ \chi &= 1.7147 \times 10^{-3} \text{ for } m \geq 3\text{mol/kg}, \\ \chi &= 1.1421 \times 10^{-3} \text{ for } m < 3\text{mol/kg}. \end{aligned} \tag{2}$$

Table 2 summarises the results of this verification programme.

Table 2. Results of the verification programme for different ψ_{cal}

Applied total suction (22°C)	Measured values for different ψ_{cal} (22°C)		
	2.2 MPa	19.4 MPa	38.2 MPa
6.0 MPa (NaCl 1.3 mol/kg)	5.5	4.4	4.8
10.5 MPa (NaCl 2.2 mol/kg)	9.8	8.7	9.1
19.4 MPa (NaCl 3.7 mol/kg)	20.4	19.5	19.7
38.2 MPa (NaCl 6.1 mol/kg)	37.4	37.5	38.1

The readings performed by adopting ψ_{cal} = 2.2 MPa display some shift when compared to the applied suctions, especially in the high-suction range. In a similar way, deviations in the readings performed in the low-suction range are detected for ψ_{cal} = 19.4 and 38.2 MPa. This situation highlights the importance of carrying out the offset calibration nearby the expected measurement range. Figure 6 shows the calibration results for different ψ_{cal}.

The sensitivities, b, of the calibrations, i.e., slope of the linear relationships shown in Fig. 6, are plotted in Fig. 7 for different ψ_{cal}. Results were fitted to the expression indicated in the figure (Fig. 7). In order to correct the WP4 psychrometer readings, the following expression can be used:

$$\psi = \psi_{WP4} - (\psi_{WP4} - \psi_{cal}) \left(1 - \frac{1}{b}\right) \tag{3}$$

where ψ is the soil total suction, ψ_{cal} is the calibration point, ψ_{WP4} is the measured value, and b is the sensitivity presented in Fig. 7. As observed in Eq. (3), maximum corrections are obtained for points distant from the calibration point. According to Fig. 7, the calibration point ψ_{cal} for $b = 1$ – no need for correction according to Eq. (3) – is 2.7 MPa, which is close to the value suggested by the manufacturer (ψ_{cal} = 2.2 MPa).

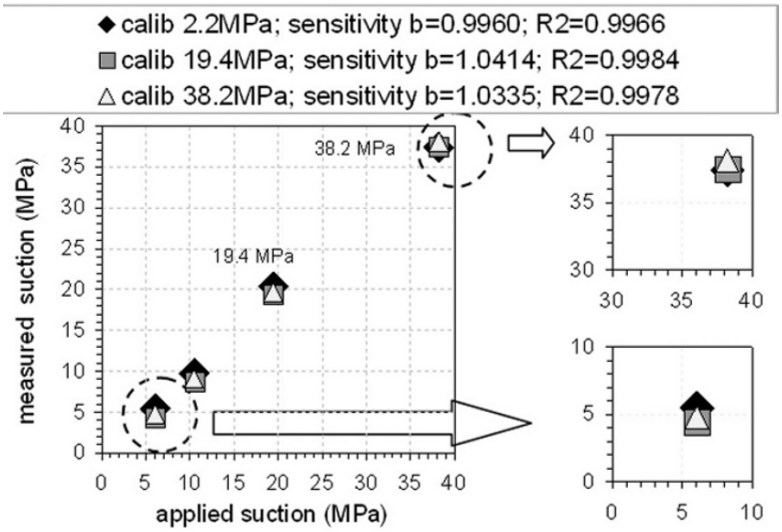

Fig. 6. Total suction readings for different ψ_{cal}

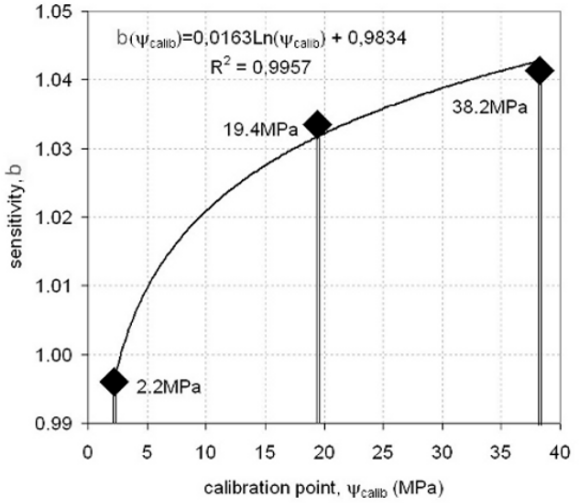

Fig. 7. Variation of the calibration sensitivity, b, for different ψ_{cal}

4 Water Retention Curves

Two different compacted clayey soils were used to study the performance of the psychrometers. Main properties of these soils – destructured argillite (Soil A) and compacted scaly clay (Soil B) – are presented in Table 3.

Only the drying branch of the retention curves of these soils was determined starting from the as-compacted water content. In this way, total suction

Table 3. Properties of the different soil samples (average values)

Sample	W (%)	γ_d (kN/m^3)	w_L (%)	PI (%)	γ_s (kN/m^3)
A. Compacted destructured argillite	12.4	17.2	37	16	27.4
B. Compacted scaly clay	15.3	17.4	58	30	27.7

determinations followed the same suction increase path used in the calibration of SMI psychrometers, and hysteresis effects (both of the soil and the equipment) were minimised. The suction range was limited to the equipment used, previously presented in Table 1. WP4 psychrometer readings were corrected according to Eq. (3).

Measured values using the two equipment are plotted in Figs 8 and 9 for soils A and B, respectively. Water retention results were fitted to a modified form of van Genuchten (1980) expression for water content, w, as a function of total suction, ψ (Romero and Vaunat 2000)

$$w = w_{\max} C(\psi - \psi_0) \cdot \left[\frac{1}{1 + (\alpha(\psi - \psi_0))^n}\right]^m , \tag{4}$$

$$C(\psi - \psi_0) = 1 - \frac{\ln\left[1 + \frac{\psi - \psi_0}{a}\right]}{\ln 2} \tag{5}$$

where $w_{\max}$ is the water content at saturation for total suction ψ_0. Parameters n, m and α are the same as used in van Genuchten's expression. The parameter α is mainly associated (inversely) with the air-entry value of the soil. The original van Genuchten's expression is not adequate to fit retention curve data for clayey soils. For this reason, the expression was modified by a correction function Eq. (5), which makes the curve tend to a linear relationship between

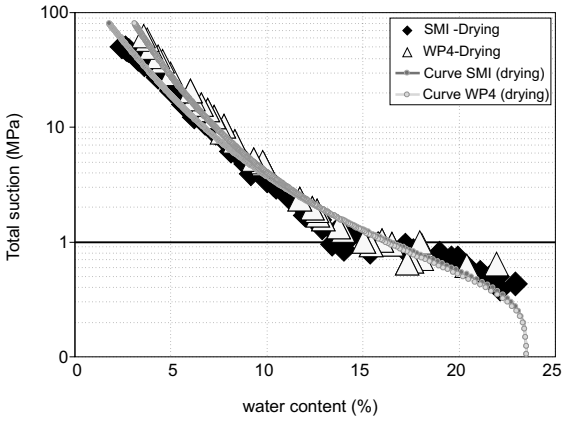

Fig. 8. Water retention curves of soil A (drying branch)

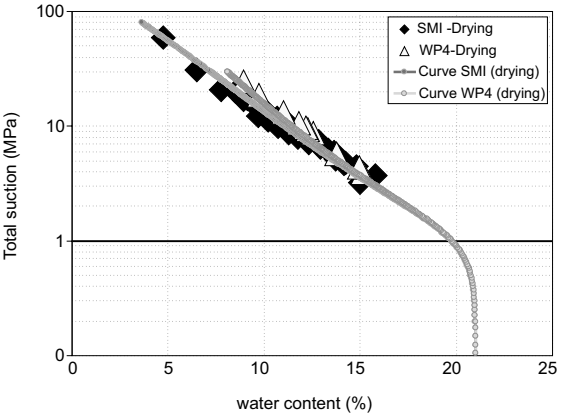

Fig. 9. Water retention curves of Soil B (drying branch)

the logarithm of ψ and w in the high-suction zone, with intersection parameter, a, at $w = 0$. Fitted parameters for the two soils are listed in Table 4.

Table 4. Constants for the definition of the water retention curves for the soils (drying branch)

Soil	Soil A		Soil B	
Equipment	SMI	WP4	SMI	WP4
$w_{\max}$ (%)	23.5	23.5	21.0	21.0
ψ_0 (MPa)	0.1	0.1	0.1	0.1
a (MPa)	200	600	200	300
α (MPa^{-1})	2.913	3.400	0.990	0.990
m	0.14	0.13	0.10	0.10
n	2.5	2.5	2.5	2.5

Comparing the retention curves for each soil obtained with the two psychrometers, it can be observed that a good agreement is found in the total suction range 0.5 to 7 MPa. Above this upper value the readings measured with WP4 psychrometer are systematically higher than the SMI ones and the difference between instrument measurements become larger for the highest total suctions.

The equipment were carefully calibrated and verified, so that differences in the high-suction range cannot be solely attributed to errors in the measurements. Nevertheless, the differences can be explained in terms of the hydraulic paths undergone by the soils during the measurement time. To help in this interpretation, Figure 10 shows the expected behaviour of the samples inside the measurement chamber of SMI and WP4 psychrometers.

Just after closing the chambers that house the samples, the relative humidity that prevails in the psychrometer chambers corresponds to the relative humidity of the laboratory ($HR_0 = 40\%$). In the case of SMI psychrometer, the water drop immediately evaporates increasing the relative humidity of the chamber to $HR_1 > HR_0$, as shown schematically in Fig. 10. The sample at a lower relative humidity HR_{soil} undergoes some wetting before reaching the equalisation state at $HR_{\text{eq SMI}}$, which is the state finally measured by the SMI psychrometer. In other words, it is expected that the soil housed inside the SMI chamber undergoes some wetting induced by the evaporation of the drop. On the contrary, the sample placed inside the equalisation chamber of the WP4 psychrometer undergoes some drying before reaching equalisation $HR_{\text{eq WP4}}$. The differences between the two psychrometers are readily observed in Fig. 11, in which the hydraulic paths 2–3 followed by the samples during equalisation in the measurement chambers are schematically plotted. The sample installed in the WP4 undergoes some small drying along the main drying curve during equalisation in the measurement chamber (path 2–3). On the other hand, the sample installed in the SMI measuring chamber undergoes some small wetting along a scanning wetting path 2–3. As a consequence, the total suctions measured and the final water contents are different, displaying slightly higher suctions and slightly lower water contents the sample equilibrated in the WP4 measuring chamber.

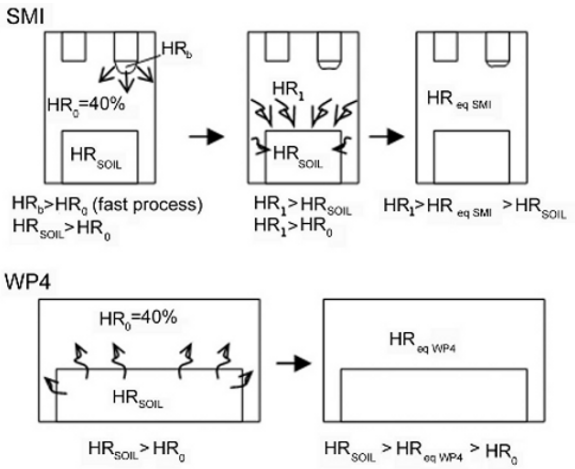

Fig. 10. Equalisation process in the measurement chamber of SMI and WP4 psychrometers. High-suction range for $HR_{\text{SOIL}} > HR_0$

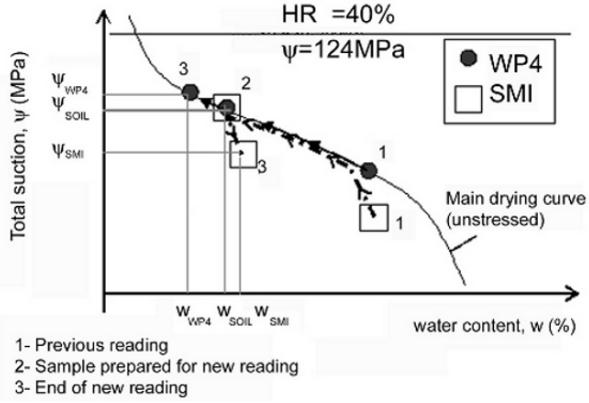

Fig. 11. Hydraulic paths followed by the samples during equalisation in the measurement chambers of SMI and WP4 psychrometers

5 Conclusions

This paper presents the equipment description and the calibration protocols followed for two high-range psychrometers, namely the SMI transistor psychrometer and the WP4 chilled-mirror dew-point psychrometer.

Regarding the improvement of the performance of the SMI psychrometer for measuring in the high-suction range (20 to 70 MPa), three different procedures were suggested: a) to use one-hour measurement time with the standard drop size; b) to reduce the measurement time with standard drop size in accordance to the total suction measured; and c) to use one-hour measurement time with 1.5 standard drop size. Procedures b) and c) reduce the shift in the time evolution of the output, since they minimise the interaction with the relative humidity of the laboratory –the measuring chamber is not a closed system and vapour is lost inducing the reduction of the drop size. Protocols b) and c) require a single linear calibration relationship along the measurment range. However, protocol b) can only be followed if the total suction is assumed before the reading. In the paper, procedure a) was used, which required a bi-linear calibration relationship.

Concerning the WP4 psychrometer, the manufacturer's calibration protocol that uses a single-point was found to be inappropriate. The calibration slope is fixed during factory calibration and the user only adjusts the zero offset in the low-suction range. A verification programme using different single-point calibrations was performed and contrasted with partially saturated salt solutions that applied different relative humidities. It was observed that some shifting in the readings occurred for points distant from the single calibration point. An expression to correct the readings was suggested based on the verification study performed.

The drying branches of the water retention curves of two different compacted clayey soils were determined by taking into account the corrections proposed for the different psychrometers. A good agreement in the equipment readings was observed, particularly in the low total suction range from 1 to 7 MPa. On the contrary, in the high-suction range (7 to 70 MPa) differences between the readings of both psychrometers were observed, which increased with the total suction of the soil. The paper presented a possible explanation for these differences in terms of the different hydraulic paths undergone by the soils along the measurement period, i.e., along the equalisation period inside each equipment chamber. Samples installed inside the WP4 chamber undergo some small drying, whereas the samples in the SMI psychrometric chamber experience some wetting. As a consequence, the total suctions measured and the final water contents are slightly different. WP4 total suction readings are slightly higher since the samples follow their main drying curves, whereas SMI readings are below these main drying curves.

Finally, the WP4 can be a promising alternative – it presents a reduced measuring time- in the total suction range where the readings do not present relevant differences with the SMI (1–7 MPa). However, this suction range can be different for other type of soils, and further research is needed to clearly state this range. The differences obtained in the high-suction range had shown the need for further studies in this range to increase the reliability of both psychrometers.

Acknowledgements

The authors would like to thank Dr Francesc Ferrer for lending to UPC the WP4 equipment and also for his useful comments regarding its calibration and use.

The first author acknowledges the financial support given by the Portuguese Foundation for Science and Technology, FCT (Ref. POCTI/ECM/59320/2004). The third author acknowledges the financial support given by ESV EURIDICE GIE Belgium contract (Ref. EUR-04-248).

References

Boso M, Romero E, Tarantino A (2004) The use of different measurement techniques to determine water retention curves. In: T. Schanz (ed) 93 Springer Proceedings in Physics. Unsaturated Soils: Experimental Studies. Springer, Berlin 1:169–181

Fredlund DG, Rahardjo H (1993) Soil Mechanics for Unsaturated Soils. John Wiley & Sons, New York

Decagon Devices, Inc. (2003) WP4 Water Dewpoint Potentiometer. Operator's Manual, Version 2.2. Decagon Devices, Inc., Pullman (`www.decagon.com`)

Dimos A (1991) Measurement of soil suction using transistor psycrometer. Internal Report IR/91–3, Special Research Section, Materials Technology Department, Vic Roads

Horvath AL (1985) Handbook of aqueous electrolyte solutions: physical properties, estimation and correlation methods. Ellis Horword Limited, John Wiley & Sons New York

Leong E-C, Tripathy S, Rahardjo H (2003) Total suction measurement of unsaturated soils with a device using the chilled-mirror dew-point technique, Géotechnique 53(2):173–182

Loiseau C (2001) Transferts d'eau et couplages hydromécaniques dans les barriers ouvragées. PhD thesis, École Nationale des Ponts et Chaussées, Paris

Mata C, Romero E, Ledesma A (2002) Hydro-chemical effects on water retention in bentonite-sand mixtures. In: Jucá JFT, de Campos TMP, Marinho FAM (eds) Proc 3rd Int Conf on Unsaturated Soils, Recife, Brazil. A.A. Balkema Lisse, The Netherlands 1:283–288

OIML R 121 (1996) Organisation Internationale de Métrologie Légale. International Recommendation. The scale of relative humidity of air certified against saturated salt solutions. Grande Imprimerie de Troyes, Troyes, France

Romero E (2001) Controlled-suction techniques. In: Gehling WY, Schnaid F (eds) 4th National Brazilian Symposium on Unsaturated Soils. ABMS, Brazil 535–542

Romero E, Vaunat J (2000) Retention curves of deformable clays. Experimental Evidence and Theoretical Approaches in Unsaturated Soils. In: Tarantino A, Mancuso C (eds) Proc Int Workshop on Unsaturated Soils, Trento, Italy. A.A. Balkema, Rotterdam 91–108

Tang A-M, Cui Y-J (2005) Controlling suction by the vapour equilibrium technique at different temperatures and its application in determining the water retention properties of MX80 clay, Can Geot J 42:287–296

Thakur VKS, Singh DN (2005) Swelling and suction in clay minerals. Advanced Experimental Unsaturated Soil Mechanics. In: Tarantino A, Romero E, Cui YJ (eds) Proc Int Symp (Experus 2005), Trento, Italy. A.A. Balkema, Rotterdam 27–31

Truong HVP, Holden JC (1995) Soil Suction Measurement with Transistor Psychrometer. In: Alonso EE, Delage P (eds) Proc 1st Int Conf on Unsaturated Soils (UNSAT 95), Paris. A.A. Balkema, Rotterdam 2:659–665

van Genuchten MTh (1980) A closed-form equation for predicting the hydraulic conductivity of unsaturated soils, Soil Sci Soc Am J, 49(2):143–159

Woodburn JA, Holden JC, Peter P (1993) In: Houston SL, Wray WK (eds) Unsaturated Soils. Geotechnical Special Publication No. 39. ASCE, New York 91–102

Woodburn JA, Lucas B (1995) New Approaches to the Laboratory and Field Measurement of Soil Suction. In: Alonso EE, Delage P (eds) Proc 1st Int Conf on Unsaturated Soils (UNSAT 95), Paris. A.A. Balkema, Rotterdam 2:667–671

Determination of the Soil Water Retention Curve with Tensiometers

Sérgio Lourenço[1], Domenico Gallipoli[1], David Toll[1], Fred Evans[2], and Gabriela Medero[3]

[1] School of Engineering, Durham University, South Road, Durham DH1 3LE, UK s.d.n.lourenco@durham.ac.uk, domenico.gallipoli@durham.ac.uk, d.g.toll@durham.ac.uk
[2] Wykeham Farrance Ltd, Chiltern House, Unit 4B, Knaves Beech Business Centre Loudwater, High Wycombe, Bucks HP10 9QY, UK Fred.Evans@wfi.co.uk
[3] Heriot Watt University, School of the Built Environment, Riccarton, Edinburgh EH14 4AS, UK G.Medero@hw.ac.uk

Summary. An alternative technique for the determination of the soil water retention curve has recently been proposed whereby a tensiometer is used to measure soil suction and a balance to record the water content variations. The soil water retention curve is obtained by drying the soil either continuously or by stages (i.e. each drying stage is followed by an equalization period). Initial results from tests on compacted soil suggest that the relatively fast evaporation rate during continuous drying affects the water retention curve whereas the stage drying procedure provides more accurate results. Factors such as sample geometry and tensiometer position (relative to the sample) are also likely to affect the response obtained during continuous drying. These are the object of future investigation.

Key words: tensiometers, soil water retention curve

Introduction

Recently, high capacity tensiometers have emerged as an alternative instrument for the determination of the soil water retention curve because they provide fast measurements and determine directly the water tensile stress unlike instruments based on the axis translation.

Cunningham (2000), Toker et al. (2004) and Boso et al. (2003) determined the soil water retention curve by using an electronic balance to record the progressive decrease of water content in a sample left to dry to the atmosphere while using a tensiometer to measure the corresponding increase of suction. Boso et al. (2003) presented a comparison between stage drying and continuous drying for a sample of reconstituted clayey silt. The evaporation rate

during continuous drying was slowed down by wrapping the sample in a geotextile. The results revealed no differences between the soil water retention curves determined using the two procedures. Cunningham (2000) investigated the influence of the evaporation rate for the continuous drying procedure applied to samples of reconstituted silty clay. In particular, he compared the soil water retention curves obtained by drying continuously the sample either to the atmosphere or inside a controlled humidity chamber. Similar results were obtained from the two procedures suggesting that the evaporation rate had little or no influence on the resulting soil water retention curve. These two studies also confirmed that tensiometers could be used to determine the soil water retention curve in a significantly shorter period of time in comparison to other conventional testing techniques (see also Toker et al. (2004)).

The stage drying procedure is expected to yield the most accurate results as the suction is measured after the sample has achieved equalization. On the other hand, continuous drying tends to be faster and simpler but it is likely to introduce inaccuracies due to the lack of equalization through the sample. These inaccuracies depend on factors such as sample size, shape, extent of surface exposed to drying and tensiometer position relative to the sample. Clearly, if the suction is measured on the surface of relatively large samples, the continuous drying procedure is expected to yield an incorrect water retention curve. Further study is therefore required to confirm the results obtained by Boso et al. (2003) and Cunningham (2000).

This paper presents some initial data from an experimental investigation on the particular drying procedure used (i.e. stage drying and continuous drying) for the determination of the soil water retention curve.

1 Experimental Set up

A sandy clay of intermediate plasticity with PL = 19.7%, LL = 43.3% and grain size distribution shown in Fig. 1 (Mendes 2006) has been used in this study. All samples were compacted according to the standard Proctor test at an initial water content of 25% (optimum water content is 18%).

The sample is enclosed in a metallic ring with a diameter of 100 mm and height of 30 mm and sealed by two (top and bottom) end plates, which include fittings to house tensiometers. The tensiometers used in this work have a nominal air entry value of 15 bar but they are capable of measuring suctions up to 1600 kPa (see Lourenço et al. (2006)). The water content decrease by the sample was measured by a digital balance logged into an acquisition system via a RS 232 interface.

For the case of stage drying, the soil water retention curve was determined by a sequence of independent drying phases and suction measurements on the same sample. For each stage, the soil was left to dry by evaporation to the atmosphere and, following an equalization period, the suction and sample mass were measured.

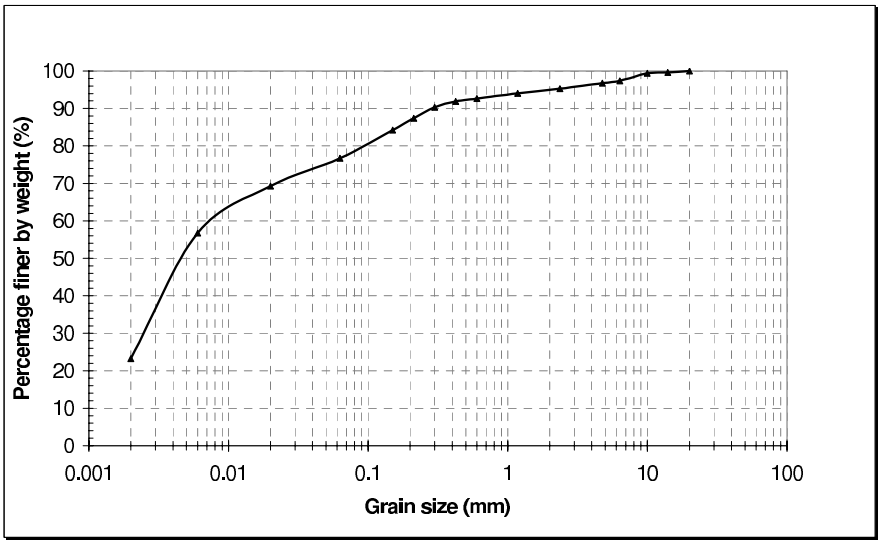

Fig. 1. Grain size distribution of the sandy clay soil (Mendes 2006)

The detailed procedure was as follows:

1) Drying. The sample is dried by removing the top plate of the measuring cell and allowing the pore water to evaporate to the air for a set period of time. Drying was accelerated by a fan located above the sample;
2) Equalization. The top plate is placed back to seal the sample allowing water redistribution within the soil mass;
3) Suction measurement. The tensiometer is inserted through the bottom plate in contact with the sample (a good contact is ensured by the own weight of the sample) and suction is continuously read;
4) Mass measurement. After suction becomes constant indicating equalization, the total weight of cell, sample and tensiometer is recorded.

Steps 1) to 4) are repeated for the number of data points required to define the entire soil water retention curve. The above sequence is illustrated for one selected data point in Fig. 3.

For the continuous drying procedure, a sample with the same dimensions and initial conditions as for the stage drying was placed on the balance together with the metallic ring as shown in Fig. 2. A tensiometer was gently pushed into the top surface of the sample to a depth of approximately 3 mm. The entire length of the tensiometer cable was also supported to minimize any influence of its stiffness on the mass measurements. Pore water was left to evaporate through the exposed top surface of the sample while the decrease of water content and increase of suction were continuously recorded by the connected PC. The initial sample conditions and a summary of the key results for all six tests performed are shown in Table 1.

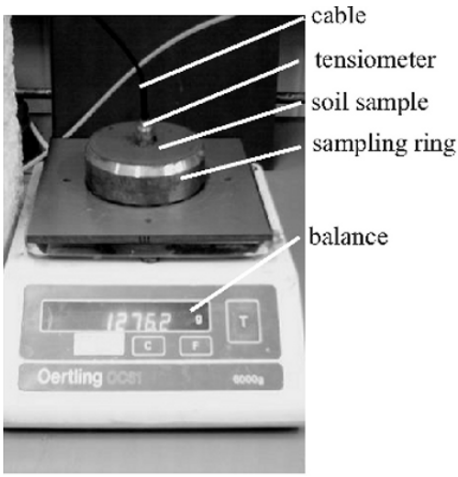

Fig. 2. Experimental set up for the continuous drying tests

Table 1. Initial and final physical indexes and summary of results

Test no.	Drying procedure	e_i	w_i [%]	w_f [%]	ΔM_w [g]	$s_{\max}$ [kPa]	Δt [h]
1	Stages	0.59	24.35	16.88	29.3	568.6	148.8
2		0.55	24.80	17.76	33.5	485.5	114.5
3		0.54	25.25	14.70	42.5	995.0	171.9
4	Continuous	0.52	24.70	18.37	26.0	376.0	25.1
5		0.56	24.76	17.25	30.0	745.2	32.5
6		0.55	24.17	17.23	27.9	584.6	28.44

e_i initial void ratio, w_i initial water content, w_f final water content, ΔM_w mass of water evaporated, $s_{\max}$ maximum suction of water retention curve, Δt test duration

2 Results

During all tests the soil significantly reduced in volume but such shrinkage was not measured. Therefore the corresponding variation of degree of saturation could not be calculated and the results are presented only in terms of gravimetric water content.

The entire test sequence for the definition of the soil water retention curve by using stage drying is shown in Fig. 3, which includes information of both gravimetric water content and suction for each of the nine drying stages. As expected, the suction equalizes at increasing values as the gravimetric water content decreases.

A similar set of information for a test performed by continuous drying is shown in Fig. 4, where suction and the gravimetric water content are plotted against the elapsed time. Inspection of Fig. 4 indicates that the decrease of

the gravimetric water content was linear ($R^2 = 0.9993$) with respect to time confirming that the influence of the stiffness of the tensiometer cable on the mass measurement of the balance can be considered negligible. The analysis of Table 1 also indicates that the tests using continuous drying were about five times faster than the tests using the stage drying, with the entire water retention curve obtained in less than two days.

The soil water retention curves for all six tests performed are shown in Fig. 5. All curves show a similar pattern but they tend to diverge for increasing values of suction. Some curves in Fig. 5 end at lower values of suction due to premature cavitation of the tensiometer.

Discussion

Data presented in the paper revealed a partial agreement with Boso et al. (2003) and Cunningham (2000) results, which suggested that the drying rate had no influence on the soil water retention curve. Inspection of Fig. 5 indicates that the curves obtained by continuous drying are slightly displaced upwards with respect to the curves obtained by stage drying. In other words, the suction measured by continuous drying is higher than that measured by stage drying at the same water content. This may be explained by the inhomogeneous distribution of suction and water content through the sample in the former case, with faster drying of the sample surface with respect to the core. The

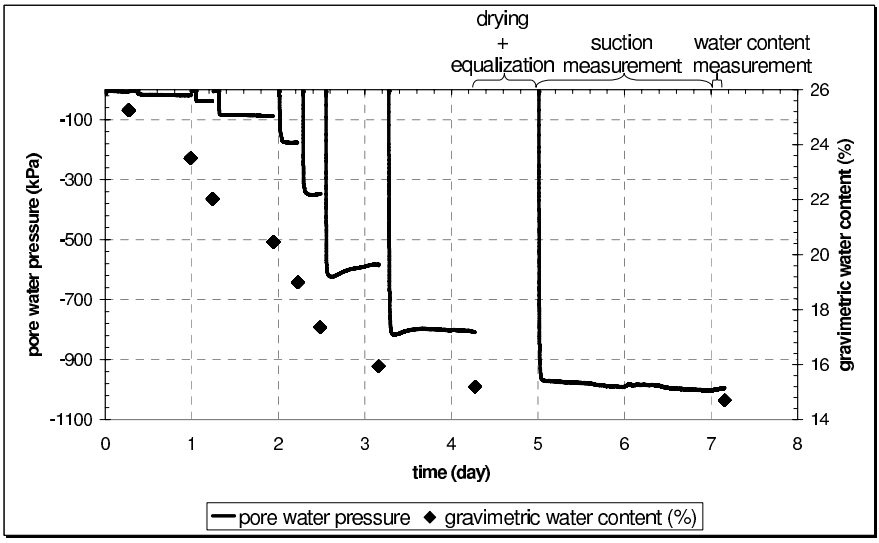

Fig. 3. Time sequence for the stage drying test 3, with the sequence of steps followed for each drying stage illustrated

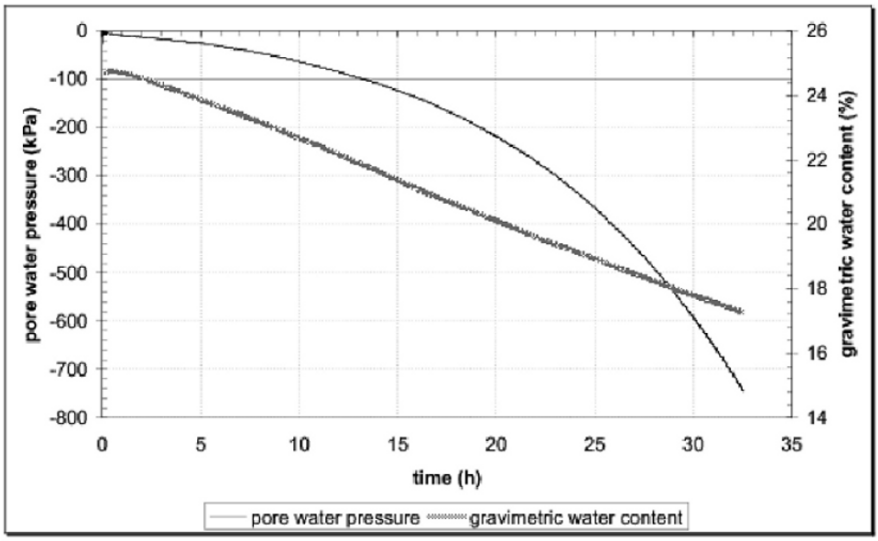

Fig. 4. Time sequence for the continuous drying test 5

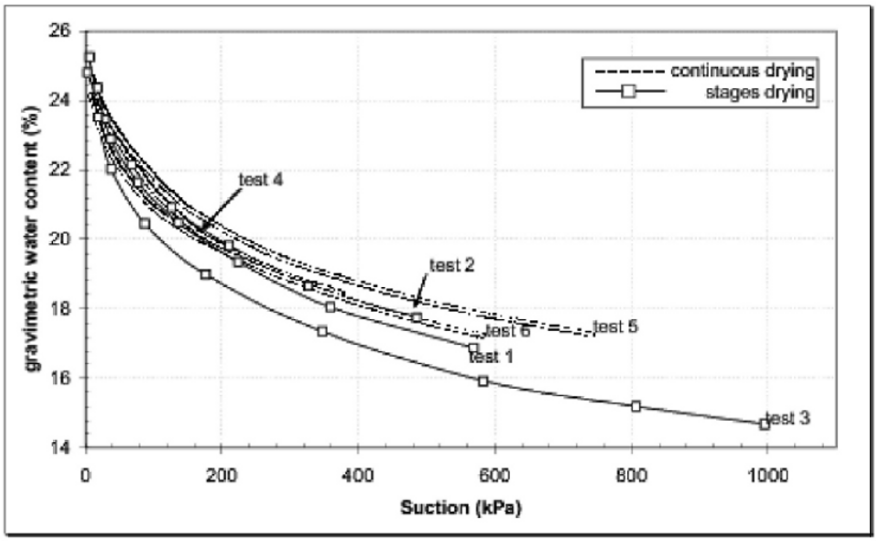

Fig. 5. All soil water retention curves

use of stage drying avoids such shortcoming and is therefore expected to yield more reliable results.

One limitation of both techniques is that volumetric measurements cannot be easily integrated in the experimental set up, preventing the determination of degree of saturation during the test (Toker et al. 2004).

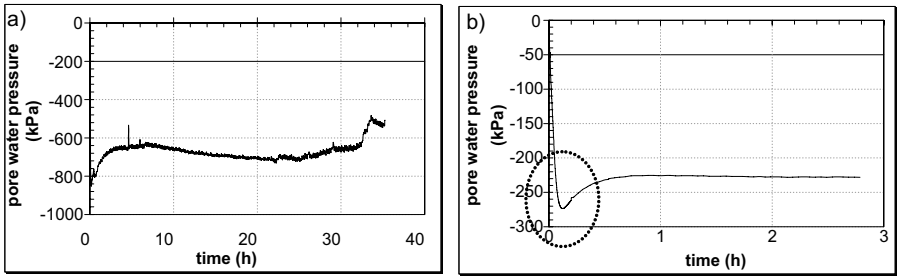

Fig. 6. Possible sources of error in the determination of the soil water retention curve by the stage drying procedure: **a**) poor contact of the tensiometer–soil interface and, **b**) insufficient equalization time

In the course of this study it was found that the following sources of errors had also a possible effect on the accurate measurement of suction and water content when using the stage drying procedure:

- When testing shrinkable soils, special care should be taken to ensure that the tensiometer remains in contact with the sample at all times during equalization of suction inside the measuring cell. In a preliminary test (Fig. 6**a**), the suction reading did not stabilize because the tensiometer was fixed to the top plate of the measuring cell and was, therefore, unable to follow the downward displacement of the soil sample as this shrunk. This problem was solved by moving the tensiometer to the bottom plate so that the sample's own weight was sufficient to ensure good contact of the soil with the probe.
- The gravimetric water content determination was affected by the low dry mass of the samples (approximately 400 g). For instance, an error of 2 g in the measurement of the mass of the dry sample would be enough to introduce an error in the water content of about 0.5%. It is possible that the scatter between the stage drying curves in Fig. 5 is due to the loss of little quantities of soil while opening and closing the measuring cell to let the sample dry out at the different water contents.
- For stage drying it is important to ensure achievement of equilibrium at the end of each stage. A suction rebound is sometimes observed after placing the tensiometer in contact with the soil, indicating lack of equalization (Fig. 6**b**). Hence, in order to avoid erroneous readings, enough time must be allowed for the stabilization of suction at a constant value.

Conclusions

The paper investigates the use of tensiometers for the determination of the soil water retention curve of a compacted sandy clay. The soil water retention curves determined by continuous drying show higher suctions than the curves

obtained by stage drying at the same water content. The former procedure is probably affected by incomplete equalization of the sample whereas the latter is expected to yield the most reliable results. Possible factors affecting the accuracy of continuous drying are also discussed and areas of further investigation are identified.

References

Boso M, Romero E, Tarantino A (2003) The use of different suction measurement techniques to determine water retention curves. In: Schanz T (ed) Unsaturated soils: Experimental studies, Springer-Verlag Berlin, pp 171–181

Cunningham M (2000) The mechanical behaviour of a reconstituted unsaturated soil. Ph.D. Thesis, Imperial College of Science, Technology and Medicine, London

Lourenço SDN, Gallipoli D, Toll DG, Evans FD (2006) Development of a commercial tensiometer for triaxial testing of unsaturated soils, Geotechnical Special Publication No. 147, ASCE, Reston, Vol. 2:1875–1886

Mendes J (2006) Personal communication

Toker N, Germaine J, Sjoblom K, Culligan P (2004) A new technique for rapid measurement of continuous soil moisture characteristic curves, Géotechnique 54(3):179–186

Tensiometer Development for High Suction Analysis in Laboratory Lysimeters

Cláudio Fernando Mahler and Abdoul Aziz Diene

COPPE/UFRJ – Cidade Universitário, Centro de Tecnologia, Programa de Engenharia Civil, Caixa Postal 68506, CEP 21945-970 RJ/RJ, Brazil
cfmahler@acd.ufrj.br, abdoulazizdiene@yahoo.com

Summary. This paper presents results when using a tensiometer designed in the Soil Mechanics Laboratory at COPPE/UFRJ, and several other instruments. This new instrument measures suction values up to 1500 kPa. In more typical tensiometers, the cavitation of the system hinders the measurement of suction with values over 100 kPa. Ridley and Burland (1993) designed a new model of tensiometer to measure suction of more than 100 kPa. Mahler et al. (2002) presented a new tensiometer with which suction values up to 350 kPa were measured. This paper introduces an updated model of a tensiometer, using a variation of the equipment proposed by Mahler et al. (2002). The updated model worked extremely well and cost little to build. The equipment used allows suction to be measured relatively quickly and, as previously stated, is economical to produce (about US$300). To date, the range of suction levels that can be measured reaches 1500 kPa with no difficulty. The tests were carried out in two boxes of $160 \times 50 \times 60$ cm under laboratory conditions. The equipment used included a 15 m.c.a. ceramic block pressure sensor, de-aerated water and a special acrylic tube specifically designed for this instrument. The results were compared to two simple automated tensiometers and equivalent tensiometers. In general very good results were obtained. The main final remarks so far are as follows:

- the high bubble air entry of the ceramic block inhibits the presence of air bubbles, but the response time is slower for suction values of more than 200 kPa;
- the saturation process used for the ceramic stone worked very well;
- as expected, the position of the equivalence tensiometer influences the value measured;
- the mini-lysimeter system proved to be a very good alternative for laboratory tests and for the development of instruments that measure suction;
- the new instrument presented herein proved to be a good and an economical alternative for measuring matrix suction in the soil.

Key words: suction, tensiometer, unsaturated soil, mini-lysimeter

1 Introduction

Tabor (1979) demonstrated theoretically that water resistance traction is around −500 MPa. On this hypothesis, Ridley (1993) and Ridley and Burland (1993) introduced the first equipment capable of measuring stress in soil of more than 1 MPa.

König et al. (1994) used a tensiometer for pore pressure in centrifugal Druck PDCR–81. This apparatus consists of an instrumented silicon diagram tied in an internal glass cylinder and connected at the porous elements by steel external box protector conform Fig. 1. Using a large-scale measuring device, with a porous stone of 15 bar of air entry, saturated at a pressure of 2000 kPa, Ridley (1993) was able to measure suctions of more or less 1370 kPa. He reported that the ample external strain of the diaphragm with broad negative pressure could compromise the integrity of the connection between the diaphragm and the glass cylinder support. Consequently, water is free to penetrate the cavities of the device, causing the suspect result of pressure measured for both negative and positive cases.

Ridley and Burland (1995) presented another prototype based on the principle of maximising the sustainable stress in tensiometers to measure high suctions in soil. This tensiometer makes it possible to measure onsite suctions of 1500 kPa. The equipment consists of an integrated strain-gauge diaphragm and a sealed ceramic porous element with a value of 15 bar of air entry, as shown in Fig. 2.

Guan and Fredlund (1997), likewise, introduced a tensiometer, which measured matrix suctions in soils of over 1250 kPa when saturated under a six-cycle pressure from 12000 kPa to −85 kPa (Guan and Fredlund 1997). The ceramic stone of high air entry value is sealed halfway in a box detachable from the device. Assembled in the water, the other half of the box acts as a compression element adjusting and sealing the commercial transducer in the water reservoir as showed in Fig. 3.

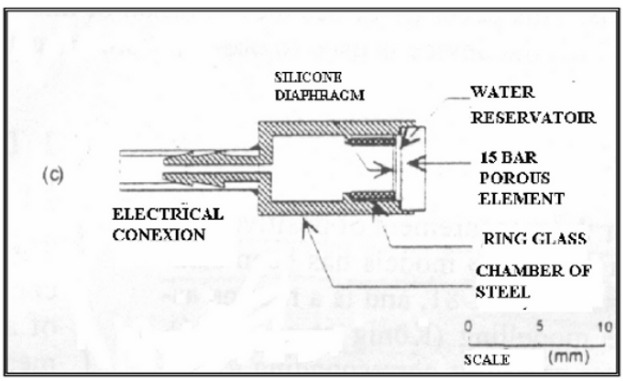

Fig. 1. Sketch of the tensiometer proposed by König et al. (1994)

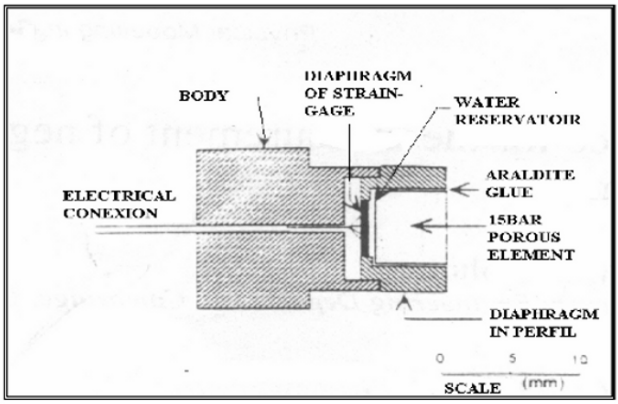

Fig. 2. Sketch of the Tensiometer proposed by Ridley (1995)

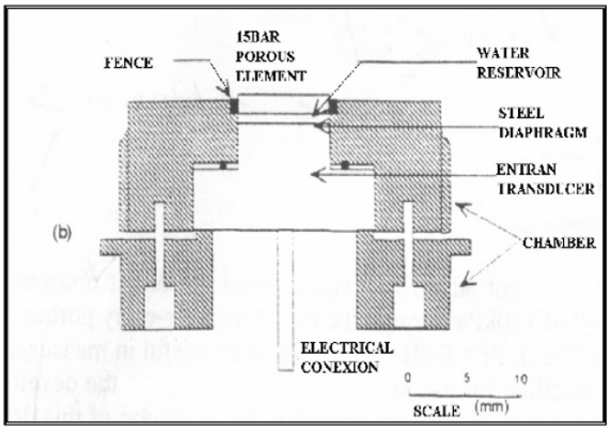

Fig. 3. Sketch of the Tensiometer proposed by Guan and Fredlund (1997)

Pacheco (2001) developed a low-cost tensiometer as shown in Fig. 4**a** and **b**, with measurements to even more than 3 atm without cavitation and concluded that: "the reduced water volume used in the transducer and porous stone interface of the new instrument and the saturation process inhibited the formation of air bubbles in the system, and permitted suction measurement up to 3 atm, with a time lag of a few seconds up to 1.5 atm."

Take and Bolton (2002) wanting to overcome the high loss of "Druck PDCR–81", conceived new more robust instruments for measuring negative pore pressure in centrifuge. They developed three prototypes introducing some format particularities for each. In common, the prototypes were fitted with an Entran (2000) EPB transducer with 7 bar air entry value and a porous stone of 15 bar, as shown in Fig. 5.

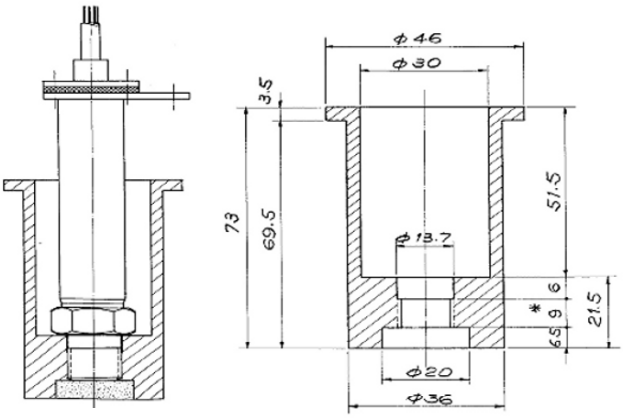

Fig. 4. Sketch of the First New Tensiometer (Pacheco 2001, Mahler et al. 2002)

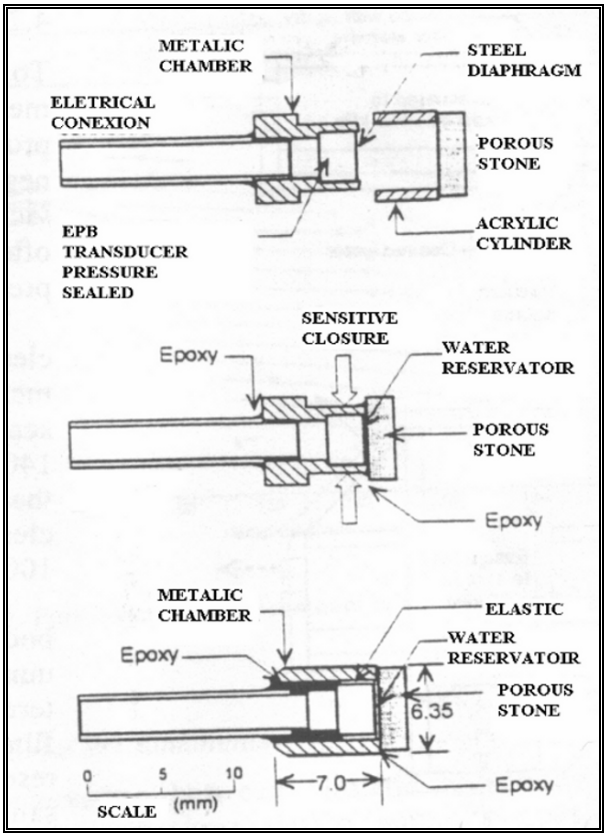

Fig. 5. Take and Bolton (2002) prototypes

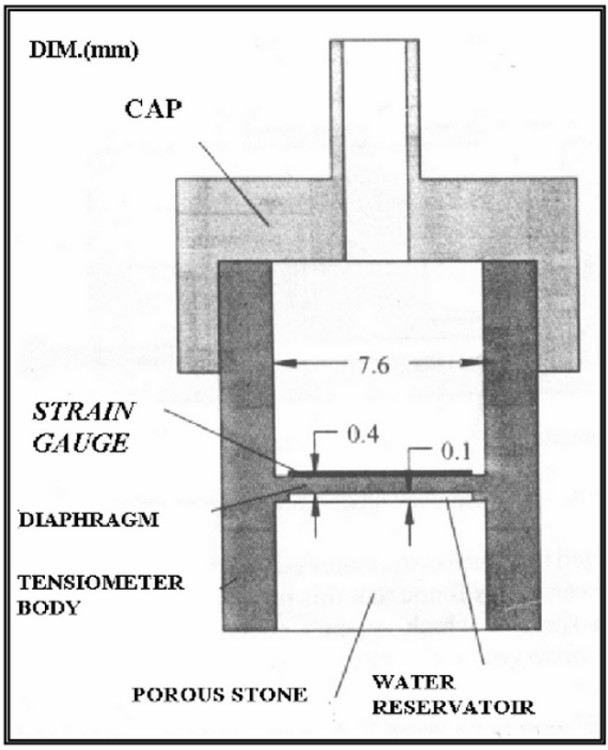

Fig. 6. Tarantino and Mongiovi (2002)

Tarantino and Mongiovi (2002) introduced a new tensiometer similar to the Ridley and Burland (1993) prototype, but with several modifications to the diaphragm diameter and thickness, to the water reservoir size and closing of the annular opening between the porous stone and tensiometer body (Fig. 6). This new equipment measured suction up to 1000 kPa for a period of time of more than 15 days and reached the maximum negative pressure of 2 MPa.

A problem common to all these items of equipment is the cavitation factor that is expressed when the transducer reading is interrupted, even momentarily. From the various models that explain water cavitation undergoing traction strain, the most acceptable is that proposed by Harvey et al. (1944): "it is supposed that cavitation arises from the non-dissolved gas nuclei in the space of the reservoir walls instead of in the free cavities of liquid;" this due to the fact that the spherical nucleus of free gas is generally unstable and tends to move into the liquid. On the contrary, the gas nucleus in the cavities of the container walls can remain indissoluble even under high water pressure. When the pressure decreases to negative values, these nuclei can expand and possibly cause cavitation. This process is controlled by gases spreading through the gas-liquid boundary and furtively moving into the solid-liquid-gas junction

determined by moving forward and back (inward contact angle). Physicians using glass or steel in a Berthelot tube determine the stress tests for the water. This tube is initially almost completely filled with water and the remaining volume consists of a mixture of steam and air. The tube is heated to expand the liquid content and force the air into the solution. After cooling, the liquid sticks to the walls of the tube and undergoes gradual increasing stress until breaking at the start of cavitation.

In order to inhibit the cavitation in the equipment, various solutions were proposed by a number of authors, which was summarised in procedures applied to assembly or saturation, or their calibration. these proposals gave rise to some conclusions on how to prevent cavitation. Ridley (1993) assumed that the maximum tension sustainable by the tensiometer is also a function of the air entry value of the porous element. "If the difference in pressure between the water volume reservoir and the measured pressure in the soil exceeds the air entry value, the air can be drawn into the water reservoir; a variation of external pressures that operate in the device will result in expansion or contraction of the air bubbles and the measured pressure is potentially detached from reality." Marinho and Chandler (1995) assigned the use of a small water volume in the suction measurement system as responsible for the non-occurrence of cavitation, and that the minimum volume possible is limited by the transducer diaphragm. The pre-pressurisation of water was considered essential for the saturation of tensiometers by Ridley and Burland (1993) and Guan and Fredlund (1997).

Some differences however do exist between the two pre-pressurisation methodologies.

Guan and Fredlund (1997) apply several pre-pressurisation cycles first under a vacuum of −85 kPa followed by higher positive pressures until 12 000 kPa. In fact, it was suggested that the rupture tension is initially affected by the number of cycles and magnitude of applied positive pressure (Guan and Fredlund 1997). Ridley and Burland (1993) affirmed that the pre-pressurisation procedure is less important. These authors proposed that a tensiometer be saturated by applying constant pressure of 4000 kPa maintained for at least 24 hours. Tarantino et al. (2000) made suction measurements higher than the air entry value of the porous element without cavitation and concluded that "cavitation may occur before the soil-equipment system equalizes, causing the interruption of the test and pre-saturation of the instrument; the knowledge of conditions that address cavitation is, therefore, essentially based on optimising the instrument's design and on determining a suitable experimental process."

Cavitation does not occur if the system is free from cavitation nuclei, which in short means the use of pure clean "de-aerated" water, extremely clean smooth surfaces, undergoing the vacuum system, cyclical application of positive and negative pressures and pre-pressurising the system at high pressures to dissolve the free air.

2 Description of the Equipment – Tensiometer

A traditional tensiometer usually consists of a porous stone in contact with the soil, a body containing the porous stone, de-aerated water and a transducer (in this case). The soil matrix suction is measured by excitation of the transducer.

The problems referring to cavitation that generally occur at approximately 80 kPa are very common to the traditional tensiometers mentioned above. Such problems were solved in this new form of building tensiometers due to:

- the use of porous stone with a high air entry value;
- the use of "de-aerated" water throughout the saturation process and assembly;
- the use of acrylic in constructing the tensiometer because of its smooth surface that prevents the formation of micro air bubbles during the saturation process of the system;
- the process of assembly, saturation and calibration of the prototype.

The equipment presented here consists only of these three elements – porous stone, transducer and acrylic body.

This is extremely simple equipment. It uses the stone and transducer in its original dimension. So this tensiometer can be tailor-made for each case.

Figures 7 and 8 presents respectively photographs of the prototypes designed and used in this research and the acrylic capsule design with different dimensions for each tensiometer used.

In the development of the current tensiometer prototypes, the following porous stone and transducers were used (Table 1).

All prototypes presented satisfactory behaviour, the time-lag variation in seconds, not significantly enough to negatively influence its use in laboratory or field.

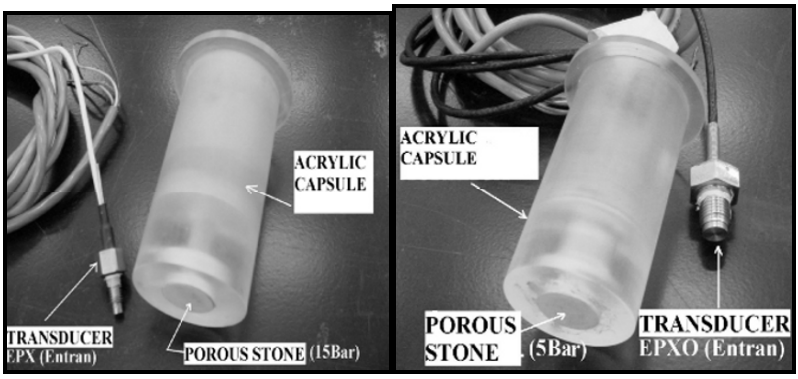

Fig. 7. Example of developed tensiometers – Tense EPX and Tense EPXO (Diene 2004)

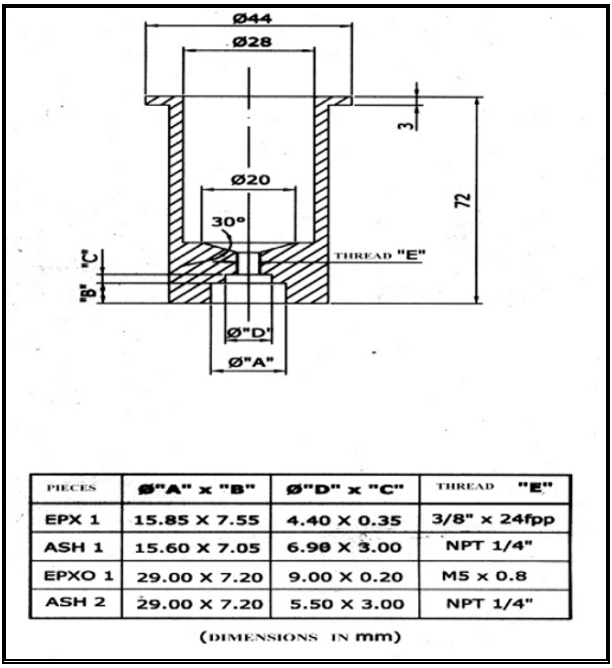

PIECES	Ø"A" x "B"	Ø"D" x "C"	THREAD "E"
EPX 1	15.85 X 7.55	4.40 X 0.35	3/8" x 24fpp
ASH 1	15.60 X 7.05	6.98 X 3.00	NPT 1/4"
EPXO 1	29.00 X 7.20	9.00 X 0.20	M5 x 0.8
ASH 2	29.00 X 7.20	5.50 X 3.00	NPT 1/4"

(DIMENSIONS IN mm)

Fig. 8. Design of the acrylic capsule prototype (Diene 2004)

Table 1. Dimensions and characteristics of the components of tensiometers (Diene 2004)

Tensiometer	Tense-EPX.1		Tense-ASH.1		Tense-EPXO.1		Tense-ASH.2	
	Diam.	Thickn.	Diam.	Thickn.	Diam.	Thickn.	Diam.	Thickn.
Stone	test		test		test		test	
Diam./Thickn. (mm)	15.85	7.55	15.6	7.05	29	7.20	29	7.20
Pressure (kPa)	1500		1500		500		500	

In this research, other equipment for control and monitoring, such as TDR and equitensiometers were used together with the tensiometers.

The equivalence tensiometer or equitensiometer consists of a Theta probe and acrylic body, as shown in Fig. 9.

The equitensiometer sensor consists of a Theta probe built in a special projected porous material (Fig. 9). The water content of this material enters into equilibrium with the matrix potential of the soil involved, where it is detected by the Theta probe, when absorbed. This operation is based on the equivalence of the matrix potential between the soil material and instrument's body.

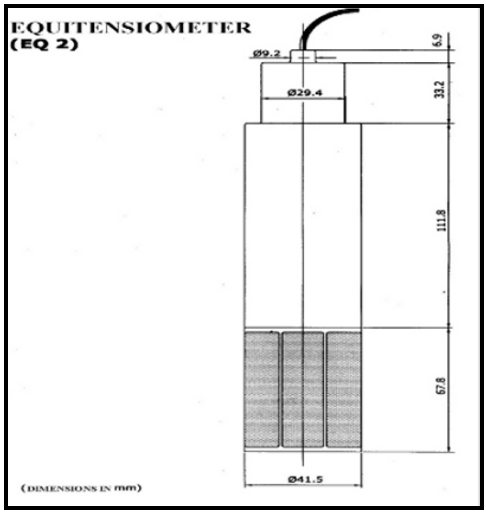

Fig. 9. Equivalence Tensiometer – Equitensiometer EQ2 (Diene 2004)

In principle, the EQ2 instrument response varies in a band from 0 to −1000 kPa. The best precision occurs between −100 kPa and −1000 kPa, with ± 5% error. Its reading precision in suctions from 0 to −100 kPa is ± 10 kPa.

Calibration and Saturation Process

The saturation and calibration process comprised the following actions and equipment (Fig. 10):

1. Check the inclusion of the porous stone in the acrylic body by applying three water pressure cycles, to check the water tightness of the contact (porous stone-acrylic);
2. The porous stone was saturated by applying a vacuum in the calibration chamber, which has no water content inside it for longer than 15 hours. Later, "air bubble free" water is introduced in the chamber (maintaining the vacuum application) until the water covers the porous element. The vacuum in the system should be maintained for another two hours;
3. Transfer the assembled set to the calibration/saturation chamber and apply pressure cycles varying from zero to 600 kPa, following the value of the bubbling pressure of the porous stone used to generate a water flow into the stone and remove any bubbles;
4. Install the pressure transducer in the system by screwing it to the acrylic body in "air bubble free" water and re-apply a vacuum to the system for three to four hours;
5. Calibrate the prototype using pots of mercury in three loading and unloading stages, with water pressure values until it reaches the calibration

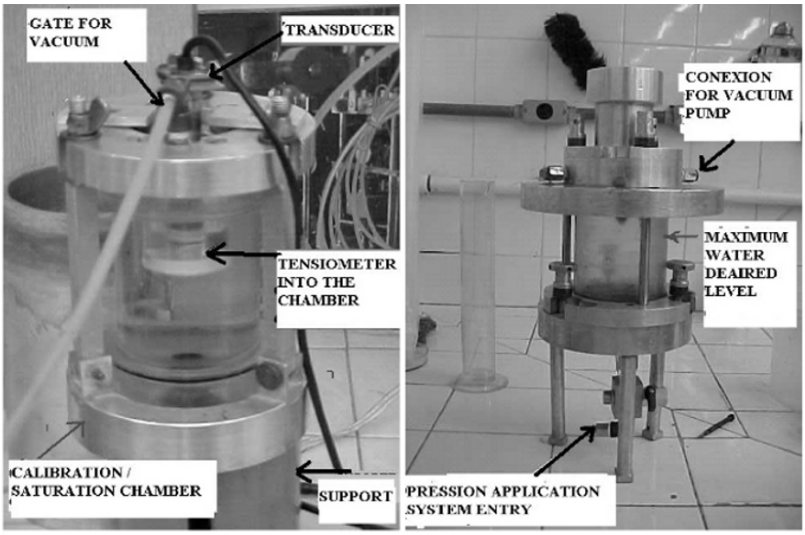

Fig. 10. Calibration/saturation chamber and porous stone saturation chamber (Diene 2004)

linear curve (these water pressure values vary according to the installed prototype).

3 Results

Figures 11 and 12 showed some of the results obtained in lysimeter laboratory tests (Diene 2004), compared with other automatic tensiometers and different suction measuring systems such as equitensiometers.

The Tense-ASH1 and 2 tensiometers behaved in a similar manner until reaching suction values of over −800 kPa, at which point a loss of pressure in the Tense-ASH2 tensiometer was observed. This loss of pressure is due to the fact that this tensiometer, with a porous stone of 500 kPa, reached the air entry pressure, and the system achieved the air entry value limit. Consequently, bubble air nuclei formation causes cavitation (Fig. 11). In this case, cavitation might also be called maximum water-ceramic adhesion stress.

The Tense-EPXO1 tensiometer measured soil suction values with sufficient precision and continuously until reaching higher values than air entry value of 500 kPa of the porous stone attached to it.

The Tense-EPX1 tensiometer inserted to 30 cm in depth measured quite similar suction values to those measured by the Tense-EPXO1 installed at a depth of 15 cm. The tensiometer measured suction values of up to −1465 kPa and when correlated to the Tense-EPXO inserted at a depth of 15 cm, showed a difference of decreasing pressure of 15 to 25 kPa (Fig. 12).

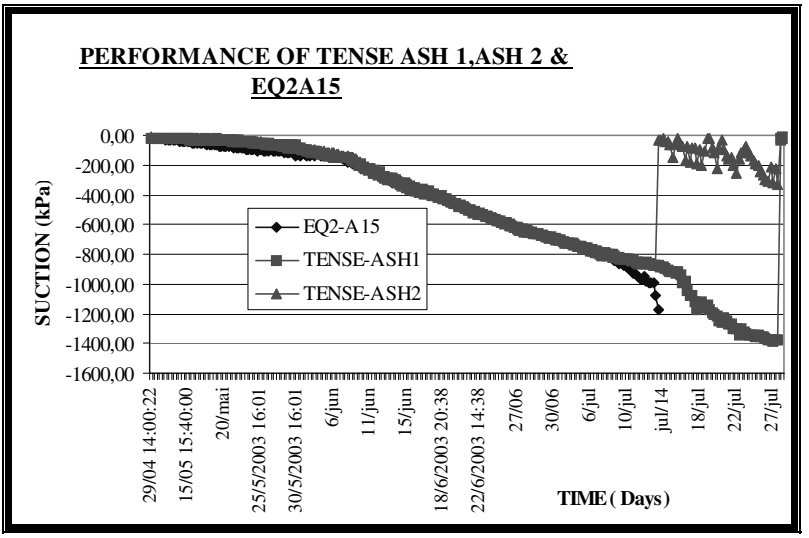

Fig. 11. Results of high suction tensiometers correlated with the equivalence tensiometer tested in lysimeters (Tank A) (Diene 2004)

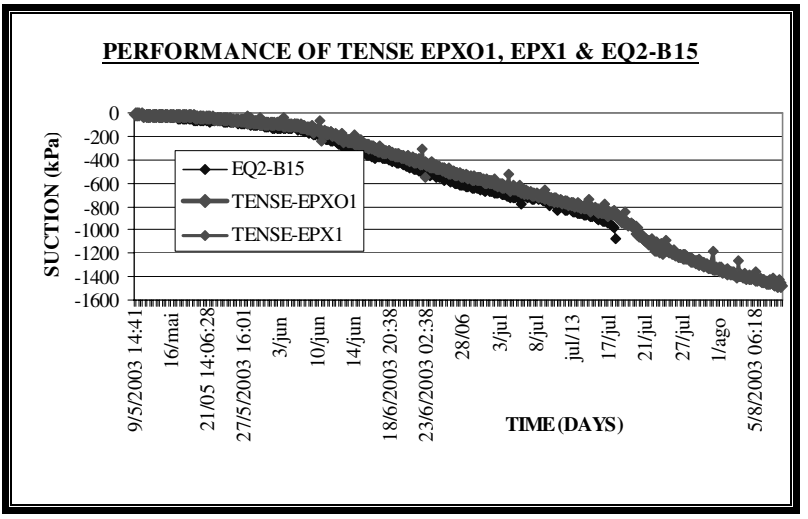

Fig. 12. Results of high suctions tensiometers correlated to the equivalence tensiometer tested in the lysimeter (Tank B) (Diene 2004)

4 Final Comments

The following conclusions can be made from the developed prototypes and their results:

1. With the manufacturing progress of porous stones and transducers there are no longer problems in developing tensiometers to measure high suction values;
2. The acrylic should be as smooth as possible, in order to prevent the accommodation of any micro-bubbles in irregularities of the walls;
3. The variation band of suction measurement to be achieved will be determined by the (air entry pressure) porous stone used and transducer capacity;
4. The obtained results show that the developed prototype may be employed in onsite measurements or in the laboratory with its adjustment, for example, to the cells of triaxial tests or odometer;
5. This is robust equipment. It is able to use the porous stone and transducer separately in other installations due to the easy handling of the proposed procedure.

Acknowledgements

The authors thank the National Research Council (CNPq), CAPES, Foundation Volkswagen and the Institute for Environmental System Research of the University of Osnabrück, Professor M. Matthies, for their constant support and interchange. They thank Ms. Elvyn Marshall for the revision of the English text.

References

Diene AA (2004) Tensiometers development for high suction measurement in laboratory lysimeters. MSc Thesis, Coppe-UFRJ, 173 pp (in Portuguese)

Entran® Pressure Sensors (2000) EPX Miniature Threaded Pressure Sensors, `www.entran.com`

Guan Y, Fredlund DG (1997) Direct measurement of high soil suction. In: Simpósio solos não saturados brasileiro, 3, Rio de Janeiro, 2:543–550

Harvey EN, Barnes DK, McElroy WD, Whiteley AH, Pease DC, Cooper KW (1944) Bubble formation in animals. I. Physical factors, J Cell Comp Physiol 24(1):1–22.

König D, Jessberger HL, Bolton MD, Phillips R, Bagge G, Renzi R, Garnier J (1994) Pore pressure measurement during centrifuge model test: experience of five laboratories. In: Leung, Lee, Tan (eds) Centrifuge'94. Balkema, Rotterdam:101–108

Mahler CF, Pacheco AC, Souza HG (2002) Development of an automatic tensiometer in laboratory using a Mini-Lysimeter. In: 3rd Int Conf on Unsaturated Soils, REcife, Brazil

Marinho FAM, Chandler RJ (1995) Cavitation and the Direct Measurement of Soil Suction. In: First Int Conf on Unsaturated Soils, Paris, France 2:623–630

Pacheco AC (2001) Development of a new tensiometer to measure suctions higher than one Atm. MSc Thesis, Coppe-UFRJ 93 pp (in Portuguese)

Ridley AM (1993) The measurement of soil moisture suction. PhD Thesis, University of London, Civil Eng Dept

Ridley AM (1995) Strength–suction–moisture content relationship for kaolin under normal atmospheric conditions. In: First Int Conf on Unsaturated Soils Unsat'95, Paris 2:645–651

Ridley AM, Burland JB (1993) A new instrument for measuring soil moisture suction. In: Technical Note, Geotechnique 43(2):321–324

Ridley AM, Burland JB (1995) Mesasurement of suction in materials which swell, Appl Mech Rev 48(10):727–732

Tabor D (1979) Gases, liquids and solids, 2nd ed. Cambridge University Press

Take WA, Bolton MD (2002) A Negative Devices for the Measurements of Negative Pore Water Pressure in Centrifuge Models, Physical Modeling On Geotecnics: 89–94

Tarantino A, Bosco G, Mongiovi L (2000) Response of the IC Tensiometer With Respect to Cavitation. Unsaturated Soils for Asia:309–313

Tarantino A, Mongiovi L (2002) Design and Construction of a Tensiometer for Direct Measurement of Matric Suction. Unsaturated Soils:319–334

Part III

Strength and Dilatancy

Dilatancy of Coarse Granular Aggregates

Eduardo E. Alonso, Enrique F. Ortega Iturralde, and Enrique E. Romero

Department of Geotechnical Engineering and Geosciences, Building D2,
Technical University of Catalunya, Jordi Girona 1–3, 08034 Barcelona, Spain
eduardo.alonso@upc.edu, enrique.francisco.ortega@upc.edu,
enrique.romero-morales@upc.edu

Summary. Coarse granular materials such as rockfill have been described in recent years by means of strain and work hardening plasticity models Oldecop and Alonso (2001), Chávez and Alonso (2003), Alonso et al. (2005) which require a proper definition of the flow rule. The paper presents experimental information on dilatancy rates obtained in suction controlled triaxial tests performed on large diameter (25 cm) specimens of compacted coarse gravels of hard limestone. Tests involved confining stresses in the range 0.3–1 MPa and Relative Humidity in the range 10–100%. Unloading-reloading during the tests provided information on the elastic response. Volumetric and deviatoric plastic strains rates were determined from records of total vertical and volumetric deformations. In general, a steady (critical) state was not found. Plots have been prepared showing the variation of the plastic flow direction, d, with a number of variables: vertical deformation, stress ratio, η, confining stress, p, plastic work, W^p, suction, s, and some derived normalized variables. It was found that the common framework of dilatancy being a function of the current stress ratio and the limiting stress ratio is far from being appropriate to describe the behaviour of the tested aggregates. It was found that relationships $d = f\left(\eta W^p/p, s\right)$, provide a good description of test results. The paper discusses the rationale behind this selection.

Key words: dilatancy, granular material, triaxial test, suction, relative humidity

Background

Information on dilatancy during shear is a fundamental contribution towards understanding stress-strain behaviour. It is also required to build elastoplastic constitutive models. Coarse granular aggregates differ from granular soils in one fundamental aspect: They are able to fracture under stress states common in engineering practice. The breakage of particles results in an enhanced compressibility under confining stress. The breakage of particles is not only controlled by the confining stress but also by the prevailing Relative Humidity (RH) or, alternatively, the total suction.

Oldecop and Alonso (2001) investigated the compressibility of rockfill by performing large scale oedometer tests under controlled RH. The material tested, a compacted gravel of quartzitic shale (Pancrudo shale), exhibited a substantial compressibility under K_0 conditions. Irreversible strains dominated the total strains ever since the application of the first loading increments. It was also shown that increasingly dry atmospheres resulted in a substantial reduction of compressibility. Oldecop and Alonso (2001) explained this macroscopic behaviour from the perspective of fracture mechanics concepts applied to the mechanisms of crack propagation in individual rock particles. Increasing suction retards the propagation of cracking in stressed particles and leads to an overall stiffer response. Likewise, a suction reduction accelerates the fracture propagation and this may lead, under appropriate stress conditions, to rapid compression phenomena, identified as collapse. No capillary action is invoked in this explanation.

Because of these effects, it turns out that modeling rockfill materials in hardening plasticity requires a "cap" to account for the relevant irreversible deformations in compression. The model developed by Chávez and Alonso (2003) is an example. It was based on a series of large scale suction controlled triaxial tests performed on compacted specimens of Pancrudo shale.

A fundamental reference for materials which dissipate energy (in compression and shear) in a frictional mode is Cam Clay (Schofield and Wroth 1968). In the original associated model, dilatancy is simply expressed as:

$$d = \frac{\dot{\varepsilon}_v^p}{\dot{\varepsilon}_s^p} = M - \eta \tag{1}$$

where $\dot{\varepsilon}_v^p$, $\dot{\varepsilon}_s^p$ are the plastic rates of volumetric and deviatoric strains, $\varepsilon_v^p = \varepsilon_1^p + 2\varepsilon_3^p$, $\varepsilon_s^p = 2/3(\varepsilon_1^p - \varepsilon_3^p)$ and $\eta = q/p'$; $q = \sigma_1' - \sigma_3'$; $p' = \sigma_1' + 2\sigma_3'$.

If equation (1) is integrated, the plastic potential of Cam Clay is obtained. If the plastic flow is associated, integration of (1) leads to the yield function (in triaxial stress states). Equation (1) is plotted in Fig. 1. For a stress ratio $\eta = 0$, (isotropic compression) Cam Clay predicts a finite dilatancy ($d = M$). This is not the behaviour observed in soils since isotropic loading leads mainly to volumetric deformations, which implies $d \to \infty$. On the other hand, in Cam Clay the rate of change of d with η is 1. Lagioia et al. (1996), aware of these limitations, proposed a more flexible dilatancy law:

$$d = \mu(M - \eta)\left(\frac{\alpha M}{\eta} + 1\right) \tag{2}$$

where α and μ are parameters. When η tends to zero, d tends to infinity and the plastic potential becomes rounded at its apex. The shape of the dilatancy relationship given by equation (2) is also indicated in Fig. 1 for a particular set of parameters. The authors showed that a few popular elastoplastic models (Modified Cam Clay – Roscoe and Burland 1968; Sinfonietta Classica – Nova 1988, 1991; the single hardening models of Kim and Lade 1988 and Lade and

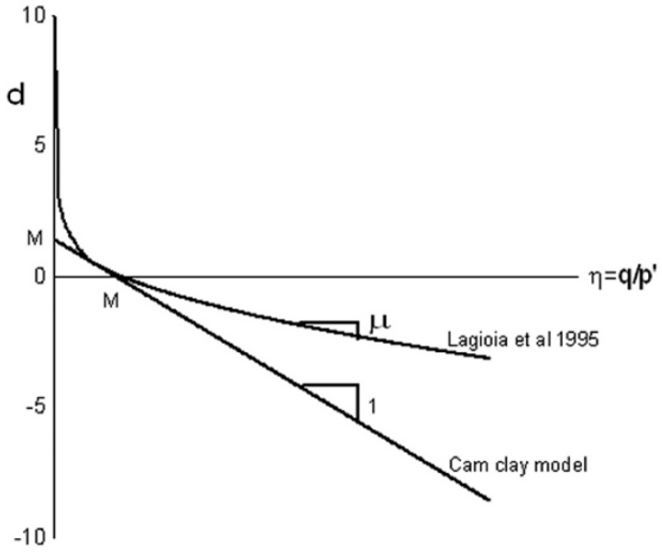

Fig. 1. Dilatancy in Cam Clay and Lagioia et al. (1996) models

Kim 1988) are well reproduced by particular combinations of parameters of equation (2).

Rowe (1962) analyzed the dilatancy of granular materials and the effect of applied stresses. He reached the conclusion, later supported by De Josselin de Jong (1976), that the dilatancy parameter d could be written as:

$$d = 1 - \left(\frac{\sigma_1}{\sigma_3}\right) \frac{1}{K_{\mathrm{cr}}} \tag{3}$$

where $K_{\mathrm{cr}} = \tan^2(45 + \phi_{\mathrm{cr}}/2)$ and ϕ_{cr} is the critical state angle. The principal stress ratio may be expressed as $\sigma_1/\sigma_3 = (3 + 2\eta)/(3 - \eta)$. Therefore, Rowe's equation, as well as equations (1) and (2), relates dilatancy with the current stress ratio, η, and the limiting value, M (or ϕ_{cr}).

In none of the equations (1), (2) and (3) there is an explicit consideration on the density of the material, or, alternatively, on the confining stress. Different initial densities are implicitly considered as different materials.

Wan and Guo (1998) modified Rowe's expression and introduced a parameter, $(e/e_{\mathrm{crit}})^{\alpha}$ where e is the current void ratio, e_{crit} is the corresponding void ratio at critical state and α is a constant, to take density into account. Accepting this proposal, Chávez (2004) and Chávez and Alonso (2003) described the results of suction controlled triaxial tests on Pancrudo shale and examined the effect of suction on dilatancy. Some results are reproduced in Fig. 2.

Note that, when $D = 1 - d = 1$, a zero dilatancy (critical state conditions) are reached. Tests represented in Fig. 2 did not reach critical state conditions

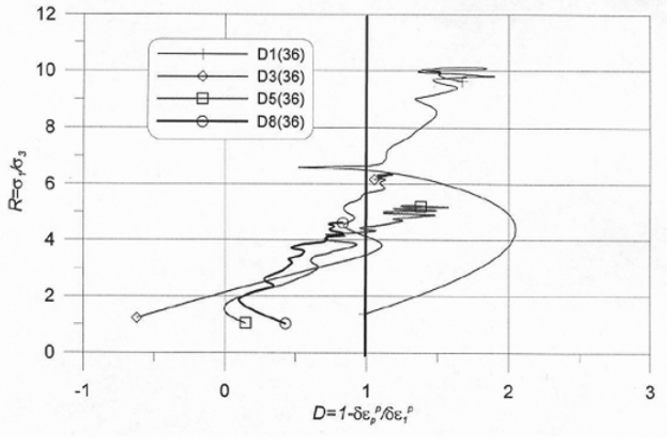

Fig. 2. Dilatancy observed in four triaxial tests performed at 0.1, 0.3, 0.5 and 0.8 MPa at a constant relative humidity of RH = 36% (Chávez 2004)

in all cases but they were close enough. Results were interpreted with the help of a modified Wan and Guo's equation, introducing suction as an additional controlling variable and taking critical state conditions as a reference.

Li and Dafalias (2000) argue that classical dilatancy theories do not include the static and kinematic constraints at particle contacts which in practical terms imply that density and stress levels effects are not properly included. To overcome these limitations they formulate dilatancy in terms of a state parameter ψ which expresses the difference between the current void ratio and the critical state void ratio:

$$d = d_1 \left(e^{m\psi} - \frac{\eta}{M} \right) \tag{4}$$

where d_1, m, and M are material parameters. Chiu and Ng (2003) adopt this formulation for the "shear" yield of their constitutive model for unsaturated soils simply recognizing that material parameters (and the critical state line) depend on suction. Suction now becomes an additional state parameter. They define an additional law for the "cap" yield function of their model, making sure that $d = \infty$ when $\eta = 0$. Cecconi et al. (2002) also criticize, on the basis of experimental observations, the one-to-one relationship between d and η implied by the classic models of dilatancy. Their study focuses on grain crushing of pyroclastic soils and its implications. They interpret that grain crushing leads to a progressive evolution of material parameters such as M and m in equation (2). In their elastoplastic model degradation induced by particle crushing occurs as plastic strains accumulate.

Dilatancy data in connection with suction controlled tests in soils has been reported in several papers. Some results of the triaxial tests reported by Cui and Delage (1996) on compacted Jossigny silt are shown in Fig. 3.

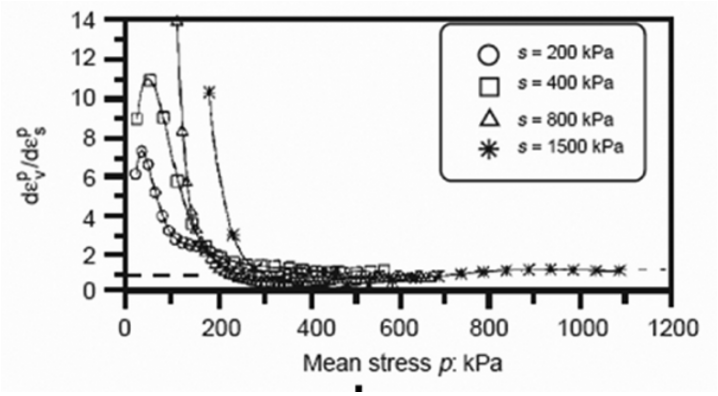

Fig. 3. Triaxial tests by Cui and Delage (1996) on compacted Jossigny silt. Measured dilatancy for a constant $\eta = 1$ value. Effect of confining stress and suction

For a constant $\eta = 1$ value, a significant effect of confining stress and suction was measured. Dilatancy decreases as the mean stress increases and suction decreases. Later, Cui and Delage (1998) proposed a simple dilatancy equation

$$d = \mu\eta + \alpha \tag{5}$$

where α depends on confining cell pressure. Equation (5), however, fails to reproduce the infinite d values associated with isotropic loading. Parameter μ has found to depend linearly on suction.

Ng and Zhou (2005) performed suction controlled direct shear tests on a compacted residual soil from granite and found that the maximum dilatancy depended strongly on suction and density. Further suction controlled tests on expansive clay were reported by Zhan and Ng (2006). Direct shear tests are not very useful to derive general relationships for dilatancy, but they also indicate that suction tends to increase negative dilatancy rates.

Cattoni et al. (2005) have recently reported the results of suction controlled triaxial tests on a silty sand. In their analysis the confining stress p also includes suction effects through a Bishop type of effective stress. Their dilatancy vs. η plots show also the role of p to inhibit dilatancy. They also found that dilatancy in bonded soils only develop significantly once the peak strength is reached.

Plastic flow rules are therefore more complicated than suggested by equations (1), (2), (3) or (4). In this paper, dilatancy measurements performed on large scale suction triaxial tests performed on a hard limestone gravel are reported. Pancrudo shale (Fig. 2), tested previously, was a low quality rockfill, currently being used to build the shoulders of an earth and rockfill dam. There was an interest, however, in testing a harder material, of very low porosity, probably not inter-connected. This material is generally used as ballast in railway construction and maintenance. Capillary effects on this rock

are unimportant and therefore suction induced effects are related to particle breakage and crack propagation phenomena.

Suction Controlled Triaxial Tests on Hard Limestone Gravel

The raw material is a gravel having sizes in the range 40–1.2 mm. Figure 4 shows a photograph of one of the specimens tested. Some identification rock parameters are given in Table 1.

Tests were performed in a double wall triaxial cell described in Chávez (2004) and Chávez et al. (2005). Relative humidity inside the specimens was maintained by means of a flow of moist air. Relative humidity was measured by means of a capacitive hygrometer located in the circuit of moist air at a point close to the specimen. Volume change was measured by local transducers by means of three rings located at three different horizontal sections. The instantaneous sample volume was calculated fitting a smooth interpolation through measurements. Independently, volume change was measured by a differential pressure transducer monitoring the excess water level inside the

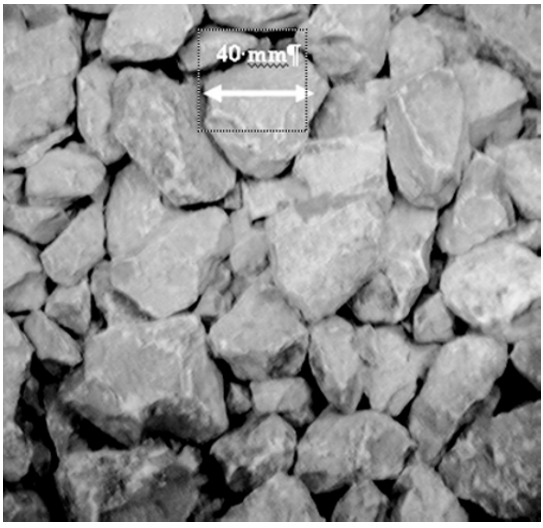

Fig. 4. Limestone gravel tested

Table 1. Identification parameters of limestone gravel

Unit weigth	Specific gravity of solids	Void ratio	Unconfined compression strength
17.73 kN/m^3	2.7	0.544–0.548	150 MPa

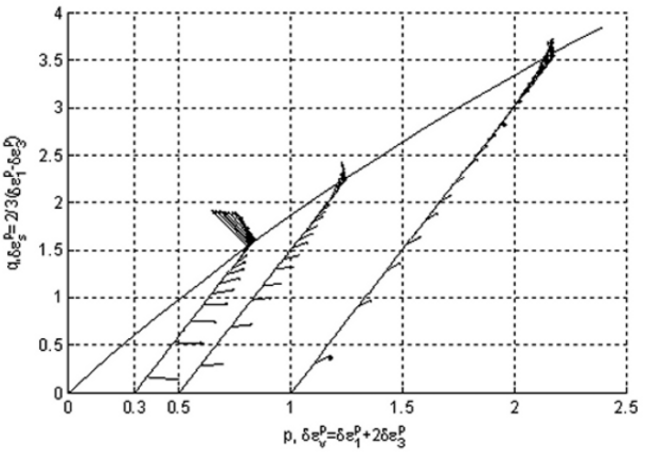

Fig. 5. Stress paths and plastic strain increment vectors in triaxial tests performed at RH = 50%

inner chamber. Specimens were compacted in six layers under an energy of compaction equivalent to the Standard Proctor. Neoprene membranes had a special inner coating to reduce friction at the particle-membrane contacts. Vertical deformations and vertical loading were also measured inside the cell.

Figure 5 shows the stress paths followed and the estimated nonlinear strength envelope for the tests performed at RH = 50%. Plastic strains develop in compacted gravel specimens during the entire stress path. Plastic strain vectors have been plotted in Fig. 5, during the deviatoric loading. It can be noticed that (negative) dilatancy develops only in the proximity of limiting strength conditions.

Figure 6 shows the stress-strain-volumetric behaviour of tests performed at a relative humidity of 50% and varying confining stress. Additional results for RH = 10% are shown in Fig. 7. At some stage during these tests specimens were wetted and the RH was increased to 100% (without changing the vertical deformation rate). The volumetric deformation rate changed in the sense of increasing the compression rate (collapse) and reducing the dilatancy rate. As a result, the deviatoric stress decreased suddenly but it later recovered again as the imposed vertical deformation increased. The final limiting strength corresponds to saturated conditions (RH = 100%).

Figures 6 and 7 show that specimens compress volumetrically during most of the loading curve. Dilatancy develops when the specimen is close to limiting conditions. It is worth noting also that triaxial tests on gravel specimens show a ductile behaviour, even if the "soil" has been well compacted. There are at least two reasons for this behaviour: the continuous breakage of particles during deformation and the relative dimensions of specimen size and par-

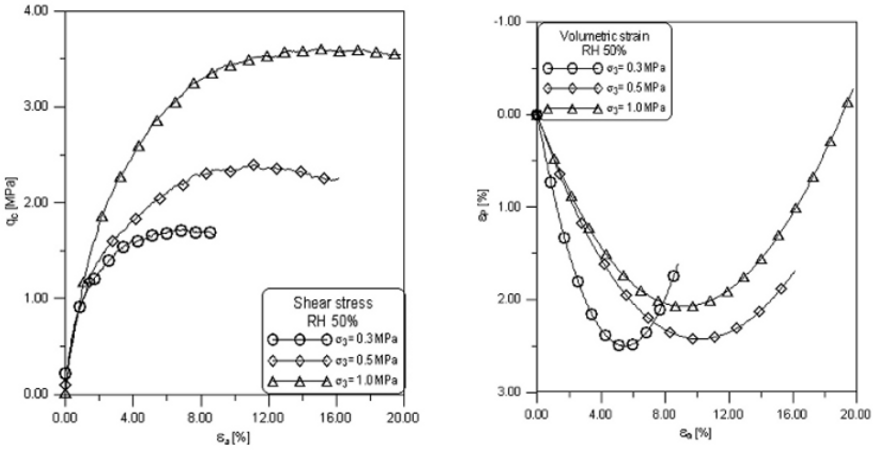

Fig. 6. Suction controlled triaxial tests on compacted limestone gravel. RH = 50%. Deviatoric-vertical strain curves (left) and volumetric-vertical strain curves (right)

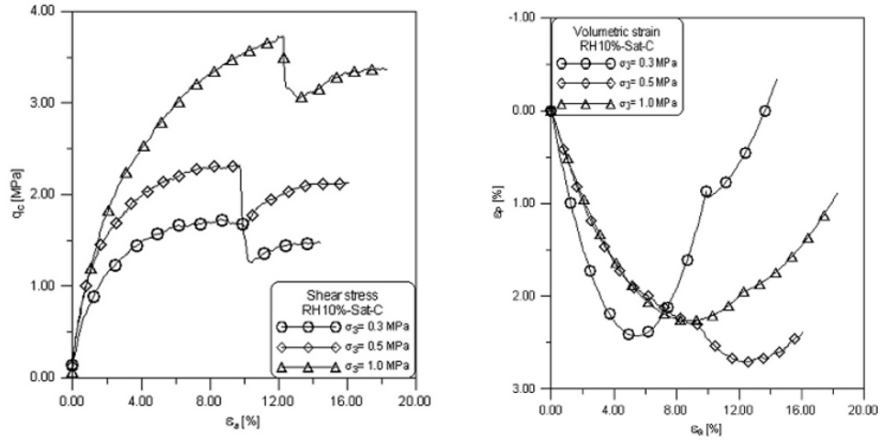

Fig. 7. Suction controlled triaxial tests on compacted limestone gravel. RH = 10%. Deviatoric stress-vertical strain curves (left) and volumetric-vertical strain curves (right). RH was increased to 100% at an advanced state of deformation

ticle dimensions which prevent strain localization. Note also that dilatancy maintains relatively high rates at the end of the test, at large vertical strains. In practically no case of the set of triaxial tests performed a condition close to critical state could be found. This is illustrated in Fig. 8, which shows the void ratio-mean stress paths of the three tests performed at RH = 50%. The plot shows the volumetric compression observed during most of the shear stage and the rapid development of dilatancy at the end of the test. However, the tests are far from reaching a constant volume condition. Therefore, no critical

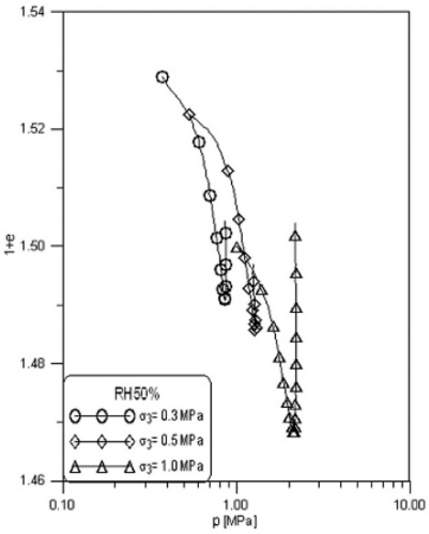

Fig. 8. Suction controlled triaxial tests on compacted limestone gravel at RH = 50%. Specific volume-mean stress during triaxial shearing

state condition could be defined in this case. These results were essentially repeated when other tests under different RH's (10%, 100%) were performed.

In the more compressible Pancrudo shale, in which the elongated particles broke more easily, critical state conditions could be found in triaxial tests performed in the same equipment (see Fig. 2, Chávez 2004). The harder nature of the limestone particles is apparently the reason for the change in behaviour. Presumably, if tested in much larger equipment so that the ratio of specimen diameter to particle size increases dramatically, the limestone gravels would exhibit a different behaviour. This result prevents the reference to critical state when describing the dilatancy of the tested gravel.

Dilatancy

Consider first simple dilatancy plots in which d is represented against the axial deformation. Figure 9 shows such a plot for two series of tests performed under RH = 50% and 10%, respectively. In the second series of tests, RH was increased to 100% when the vertical deformation was high (more than 8%). The zero reference for the axial deformation is the beginning of the deviatoric load application. As expected, dilatancy starts at a high positive value and decreases rapidly as deformation increases. However, negative values are reached after a large accumulation of axial strains. The confining stress controls also the dilatancy rate: low confining stresses lead to higher dilatancy rates.

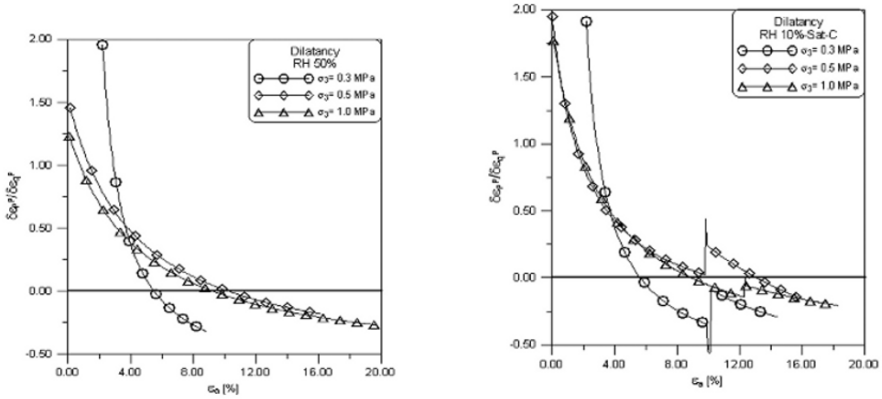

Fig. 9. Dilatancy measured in triaxial tests on compacted limestone gravel at RH = 50% (left) and RH = 10% (RH was increased to 100% at an advanced state of deformation) (right)

For a more fundamental appraisal, following traditional understanding, plots of dilatancy rate d in terms of the stress ratio η/M have been prepared for the set of suction controlled triaxial tests performed (Fig. 10). Due to the curvature of the strength envelope, the value of Mvaries with the particular test considered. Dilatancy rate, having initially a positive high value, decreases with stress ratio and reaches a zero value for stress states close to shear strength in most cases. The strong effect of confining stress dominates the plot. Increasing confining stress decreases the (positive) dilation rate. In comparison, the effect of RH for this hard gravel is less marked.

However, this type of plot is not very useful to interpret the negative dilatancy stage because dilation accumulates at an essentially constant η value. This is especially apparent when one considers the normalized η/M value in Fig. 10. Dilatancy is still active at the end of tests but it increases at a constant $\eta/M = 1$ value. All tests performed, irrespective of confining stress and suction, are superimposed at the end of the plot shown in Fig. 10.

An attempt has been made to introduce a state parameter, the void ratio, to explain the dilatancy rates observed. However, the initial void ratio of specimens tested, before the application of the deviatoric loading, was very similar because of the low isotropic compressibility of the material. During the test (Figure 11 for RH=50%) void ratio decreases first and then increases. For a given e (and confining stress), two dilatancy rates (positive and negative) may be found. If the difficulties to find a critical state in this material are added, it is concluded that void ratio does not help in this case to model the measured results.

In a coarse aggregate, deformations integrate two phenomena: the breakage of contacts and the particles themselves and the re-arrangement of the granular structure by means of rotations and displacements of particles. The

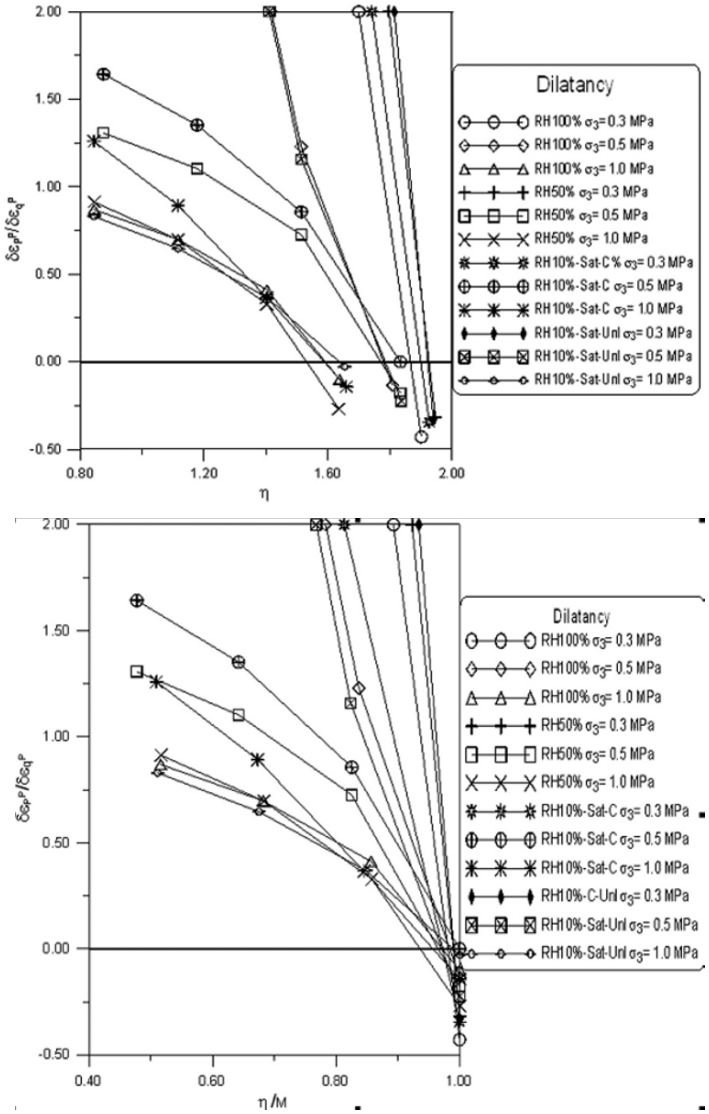

Fig. 10. Dilatancy rate, d, vs. stress ratio, η, and normalized stress ratio, η/M, for the set of triaxial tests performed on limestone gravel

positive dilatancy rates measured during the loading process are an indication of the dominant effect of contact and particle breakage during the increase of stress ratio. On the other hand, the dominant effect of confining stress and vertical deformation in all cases suggests that the work input into the specimen may be a suitable variable to integrate the stress and deformation processes taking place in the gravel. The plastic work spent during the tests, W^p, has

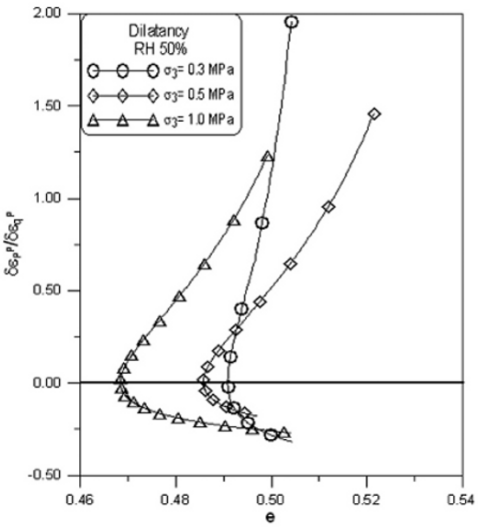

Fig. 11. Dilatancy rate, d, vs. current void ratio and confining stress for triaxial tests performed at RH = 50%

been calculated along the stress paths. Dilatancy was initially plotted against W^p for the different tests performed, but the effect of the current p value was still significant. Further regularization is achieved if the plastic work is normalized with respect to the mean stress (Fig. 12).

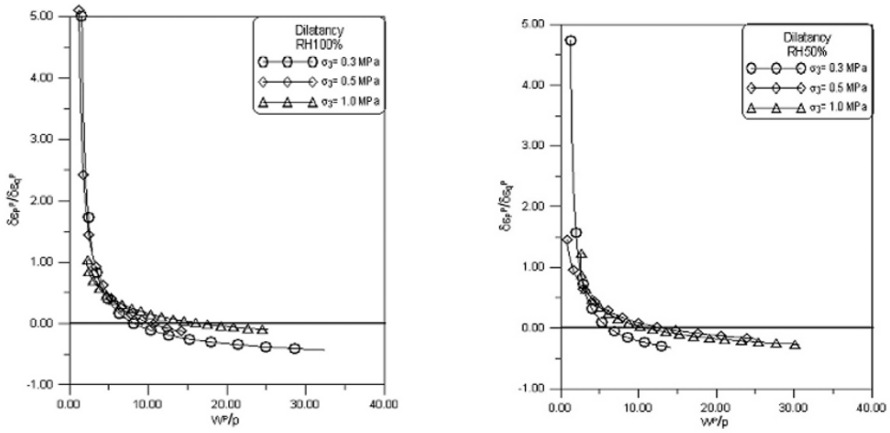

Fig. 12. Dilatancy rate, d, vs. normalized plastic work, W^p/p, and confining stress for triaxial tests performed at RH = 100% and RH = 50%

However, dilatancy cannot be made dependent only on the plastic work. In fact, in isotropic paths the accumulation of plastic work will lead towards a continuous reduction of dilatancy, if the plots in Fig. 12 are accepted as a general framework. It is clear that under isotropic loading, irrespective of the work input into the specimen, the dilatancy rate should maintain an infinite value (only plastic volumetric deformations are induced).

These considerations led to the proposal of dilatancy relations having the form

$$d = f(\eta W^p/p, s) \tag{6}$$

where s is the total suction. Dilatancy has been plotted against the variable $\eta W^p/p$ in Fig. 13 for triaxial tests performed at RH = 50% and RH = 10%.

All the tests performed seem now to plot into a common dilatancy relationship. If only isotropic stress paths are applied, $\eta = 0$, and irrespective of the work input into the aggregate, (positive) dilatancy maintains an infinite value. When η increases, dilatancy tends towards negative values but it is necessary to reach relatively high plastic work input values to really induce negative dilatancy. The effect of confining stress, in the sense of inhibiting dilatancy as it increases, is also included in the dimensionless parameter $\eta W^p/p$.

Plots in Fig. 13 suggest that empirical dilatancy equations of the type:

$$d = \left(\alpha + \frac{\beta}{(\eta W^p/p)^2}\right)^2 - \beta^2 \tag{7}$$

where α and β are constant parameters may reproduce the measured dilatancy. A comparison of calculations using equation (7) and measurements is given in Fig. 14 for two series of triaxial tests performed at RH = 100% and 50%, respectively.

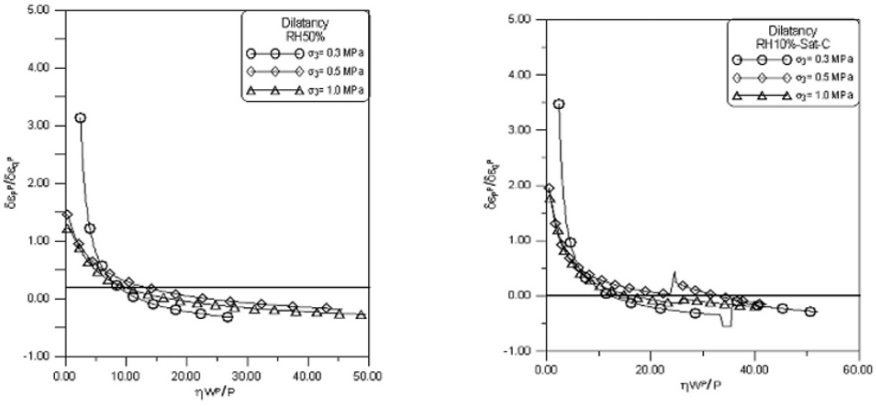

Fig. 13. Dilatancy rate, d, vs. normalized variable, $\eta W^p/p$, for triaxial tests performed at RH = 50% and RH = 10%

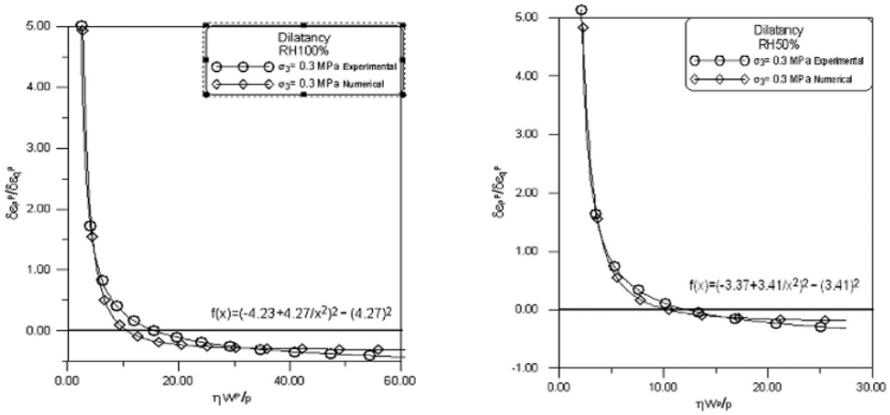

Fig. 14. Comparison of measured dilatancy and prediction through equation (7) for triaxial tests at RH = 100% and 50%, respectively

The effect of suction on dilatancy is small in the hard limestone tested. Tests performed at the same confining stress but different suctions are compared in Fig. 15. Despite the limited influence, when suction increases (negative) dilatancy also increases. However, for the extreme range of suctions tested (RH = 10% is equivalent to a total suction of 320 MPa) dilatancy maintains similar values.

The result that negative dilatancy tends to be higher (in absolute terms) when suction is high has been found when shearing unsaturated soils (Cui and Delage 1996, Ng and Zhou 2005, Cattoni et al. 2005). A similar result was also found by Chávez and Alonso (2003) and Chávez (2004) when testing specimens of compacted gravel of Pancrudo shale. The explanation for this

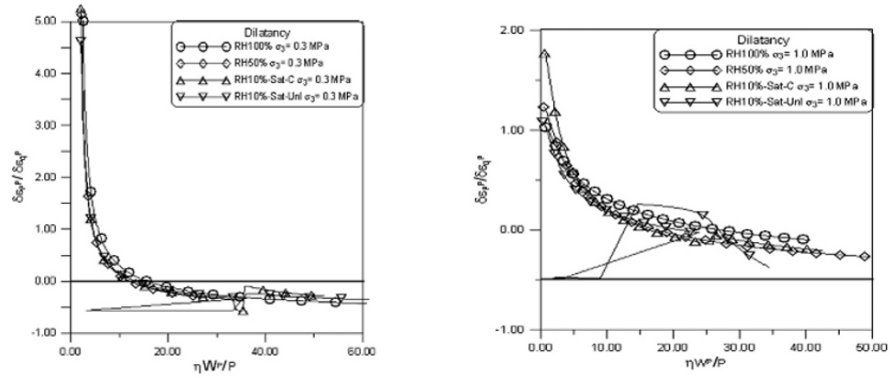

Fig. 15. Effect of Relative Humidity on dilatancy rate for two series of triaxial tests ($\sigma_3 = 0.3$ and 1.0 MPa, respectively)

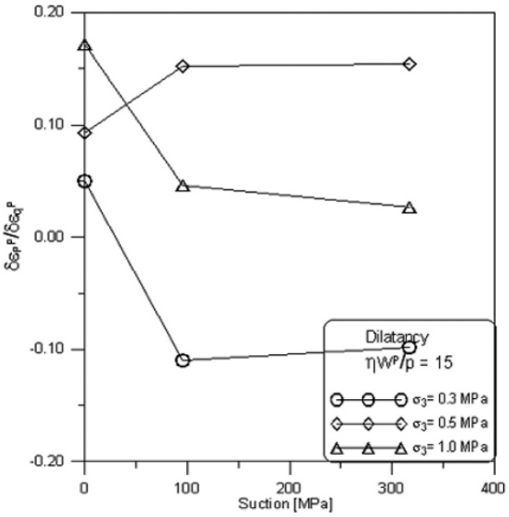

Fig. 16. Variation of measured dilatancy rates with Relative Humidity for a constant value of the controlling parameter $\eta W^p/p$

behaviour, in the case of granular aggregates, is that low RH's makes stronger particles which, in turn, favour dilation. However, in the case of the hard aggregates tested, small variations in specimen density or in the particular arrangement of grains may be as significant as the applied suction. The effect of suction on the hard limestone gravel tested may be observed in more detail in Fig. 16, which provides the variation of d with suction for a constant value of the controlling variable $\eta W^p/p$. With the exception of the test performed at $\sigma_3 = 0.5\,\mathrm{MPa}$, the data indicates an increase of (negative) dilation rate with increasing suction. Equation (7) may be used to take this small influence into account simply by making α and β functions of suction.

Summary and Conclusions

Large diameter suction controlled triaxial tests have been performed on compacted specimens of limestone gravel. The paper has focused on the development of dilatancy during shearing.

Several conclusions are reached:

Dilatancy was still active at the end of the tests performed, when axial deformations were high (in excess of 15%). Critical state conditions could not be found.

The common framework of dilatancy being a function of the current stress ratio and the limiting stress ratio is far from being appropriate to describe the behaviour of the tested aggregates. In particular, most of the observed

dilation takes place at constant stress ratio, very close or at the limiting state. For this reason, the variable η has limited discriminating capacity to describe dilatancy.

It has been found that the plastic work input into the specimens as well as the average stress should be introduced to describe the measured dilatancy for the range of stress ratios and confining pressures applied in the tests. Plastic work may explain the amount of contact and particle breakages that occur within the soil, a phenomena which is believed to control, to a large extent, dilatancy.

Dilatancy may be described by a variable which combines stress ratio, plastic work and mean stress. Relationships of the form

$$d = f(\eta W^p/p, s)$$

provide a reasonably good description of the tests performed.

Suction has a limited effect on the measured dilatancy. In any case, its effect, although noticeable and, in general terms consistent with observations in other suction controlled tests in soils and weaker gravels, is substantially smaller than the rest of variables mentioned.

Acknowledgements

The authors wish to acknowledge the financial support provided by the Consejo Nacional de Ciencia y Tecnologia (CONACYT) of México to the second author during the performance of the research described in this paper.

References

Alonso EE, Olivella S, Pinyol NM (2005) A review of Beliche Dam, Géotechnique 55(4):267–285

Cattoni E, Cecconi M, Jommi C (2005) Soil dilatancy and suction: some remarks on their mutual effects on the shear strength of granular soils. Proceedings of the 11th International Conference on Computers Methods and Advances in Geomechanics, Torino, Italy:19–26

Cecconi M, DeSimone A, Tamagnni C, Viggiani MBG (2002) A constitutive model for granular materials with grain crushing and its application to a pyroclastic soil, International Journal for Numerical and Analytical Methods in Geomechanics 26:1531–1560

Chávez C, Alonso EE (2003) A constitutive model for crushed granular aggregates which include suction effects, Soils and Foundations 43(4):215–227

Chávez C (2004) Estudio del comportamiento triaxial de materiales granulares de tamaño medio; con énfasis en la influencia de la succión. Tesis doctoral Universidad Politécnica de Cataluña, España

Chávez C, Romero E, Alonso EE (2005) Volume change measurement of partially saturated rockfill in triaxial test, Proceedings International Symposium on Advanced Experimental Unsaturated Soil Mechanics, Trento, Italy. Taylor & Francis Group, London:93–98

Chiu CF, Ng CWW (2003) A state-dependent elasto-plastic model for saturated and unsaturated soils, Géotechnique 53(9):809–829

Cui YJ, Delage P (1996) Yielding and plastic behaviour of an unsaturated compacted silt, Géotechinique 46(2):291–311

Cui YJ, Delage P (1998) Plastic flow of an unsaturated compacted silt, Proceedings of de 2nd international conference on unsaturated soils. Beijing, China vol. 1:467–472

De Josselin de Jong G. (1976) Rowe's stress–dilatancy relation based on friction, Géotechnique 26(3):527–534

Kim MK, Lade PV (1988) Single Hardening constitutive model for frictional materials. I. Plastic potential function, Computers and Geotechnics 5:307–324

Lade PV, Kim MK (1988) Single hardening constitutive model for frictional materials. II. Yield criterion and plastic work contours, Computers and Geotechnics 6:13–29

Lagioia R, Puzrin AM, Potts DM (1996) A new Versatile expression for yield and plastic potential surfaces, Computers and Geotechnics 19(3):171–191

Li XS, Dafalias YF (2000) Dilatancy for cohesionless soils, Géotechnique 50(4):449–460

Ng CWW, Zhou RZB (2005) Effects ofsoil suction on dilatancy of an unsaturated soil, Proceedings 16th International Conference on Soil Mechanics and Geotechnical Engineering. Asaka, Japan, Millpress, Rotterdam, vol. 2:559–562

Nova R (1991) A note on sand liquefaction and soil stability, Conf Constitutive Laws for Engineering Materials. ASME Press, Tucson, AZ

Nova R (1988) Sinfonietta classica: an exercise on classical soil modeling, Proc Int Symp Constitutive Eq for Granular Non-Cohesive Soils. Balkema-Rotterdam, Cleveland:501–520

Oldecop L, Alonso EE (2001) A model for rockfill compressibility, Géotechnique 51(2):127–140

Oldecop L (2000) Compresibilidad de escolleras influencia de la humedad. Tesis doctoral Universidad Politécnica de Cataluña, España

Roscoe KH, Burland JB (1968) On the generalised stress strain behaviour of "Wet" clay. Engineering plasticity, Cambridge University Press, Cambridge:535–609

Rowe PW (1962) The stress-dilatancy relation for static equilibrium of an essembly of particles in contact. Proc Roy Soc London A269:500–527

Schofield AN, Wroth CP (1968) Critical state soil mechanics. McGraw Hill, London

Wan RG, Guo PJ (1998) A simple constitutive model for granular soil: Modified stress–dilatancy approach, Computers and Geotechnics 22(2):109–133

Zhan TLT, Ng CWW (2006) Shear strength characteristics of an unsaturated expansive clay, Canadian Geotechnical Journal 43:751–763

A Laboratory Investigation into the Effect of Water Content on the CBR of a Subgrade soil

Samuel Innocent Kofi Ampadu

Kwame Nkrumah University of Science and Technology, Kumasi, Ghana
skampadu.soe@knust.edu.gh, sikampadu@yahoo.co.uk

Summary. Residual soils, most of which are lateritic serve as subgrade and even sub-base and base layers for road and highway pavements in the subregion. However, the material is known to undergo substantial strength reduction when they become saturated with water. An understanding of the dependence of the CBR strength of local soils on water content will contribute towards better design and maintenance practices. Samples of soil from a study site were prepared by laboratory compaction at the optimum water content using different levels of compaction to obtain samples at different densities. The remoulded samples were then subjected to different levels of wetting in a water tank and different degrees of drying in the laboratory and the CBR determined. The variation of the CBR with the water content is presented and discussed and related to the matric suction.

Key words: CBR, subgrade, matric suction, water content, remoulded sample, compaction

Introduction

The road pavement structure in many developing countries consists of relatively thin sub-base and base layers made of lateritic gravel with very thin water proofing surfacing, founded on a residual soil subgrade. The residual soils which are the decomposition products of the local geology occur at various degrees of laterization (Charman 1995) and are known to undergo substantial strength loss on soaking (Ampadu 2006).

The most common parameter used to evaluate pavement layer strength is the California Bearing Ratio (CBR). Even though the CBR is not a fundamental soil property, its significance lies in the fact that it is the basis of the CBR Method of Pavement design which is still, by far, the most popular pavement design method used in developing countries. The details of the CBR test are covered in ASTM D 1883-91. The CBR value is influenced by the water content and the dry density as well as the texture of the soil. Normally, the CBR test in the laboratory is conducted on test samples prepared at the

dry density and water content likely to be achieved in the field. Whereas the field dry density can be fairly well predicted the difficulty is to determine the stable moisture content at which to conduct the test. The local practice which is also used in many other countries is to use the 4-day soaked CBR. In other countries like the UK the design CBR is the CBR corresponding to the equilibrium water content. Recently, there have been attempts to interpret the results of CBR test in terms of concepts of unsaturated soil mechanics (Sanchez-Leal 2002).

The influence of the moulding water content on the CBR of local lateritic soils has been studied by Hammond (1970) This investigation seeks to contribute further towards a better understanding of the effect of water content on the CBR of local soils. Samples of a subgrade material were prepared by compaction using three different compactive efforts and then subjected to different conditions of drying and wetting. The CBR corresponding to each condition was determined. The soil-water characteristics were also estimated. The results of the CBR variation with the water content for the different dry densities are presented and discussed and modelled in terms of the matric suction.

Methodology

Bulk samples of decomposed granite were obtained from depths of 0.3 m to about 0.6 m in a trial pit. The samples were air-dried for two days and the index properties determined in accordance with BS 1377: Part 2:1990 using the wet sieving method for the grading analysis. The compaction characteristics were also obtained by ASTM D 1557-91 commonly referred to as the Modified AASHTO compaction using 55 blows of the rammer.

Three different test series were conducted. For Test Series 1, using the optimum moisture content (OMC) obtained from the compaction test, eight samples were prepared in the CBR mould by ASTM D 1557-91 except that 5 blows of the rammer per layer were used. After preparation, the first sample, designated "OMC", was covered in a black polythene bag to prevent moisture loss and stored for 24 hours to ensure moisture equilibriation. The next four samples, designated "wetting" were soaked in water for 1, 2, 3 and 4 days respectively while the last batch of three samples, designated "drying" was subjected to various degrees of drying by allowing the samples to dry out for 4, 6 and 8 days respectively. After each period of soaking and of drying, the samples were covered in black polythene bags for 24 hours to prevent further moisture loss and to equilibrate the moisture distribution within the sample. After that each sample was subjected to the CBR test in accordance with ASTM D 1883-91. After each test, the water contents at the top, middle and bottom of the specimen were determined. For Test Series 2 and Test Series 3 the same procedure was repeated except that 20 blows and 55 blows respectively of the rammer per layer were used in preparing the samples.

Discussion of Results

The index properties of the soil used for the investigation are shown in Table 1. In this study gravel is defined as particles larger than 2 mm. The soil used in this study may be described as a sandy clay of medium plasticity.

Table 1. Summary of Index Properties

Gravel (%)	Sand (%)	Silt (%)	Clay (%)	LL	PI	Gs	OMC (%)	MDD (Mg/m^3)
9	28	14	49	49	24	2.65	16.8	1.80

The summaries of results are shown in Tables 2 to 4 for Test Series 1 to 3, respectively. The initial states of the samples for the CBR tests are plotted on the compaction characteristics in Fig. 1. The dry densities refer to the values achieved after sample preparation which means that any effects of volumetric changes arising from drying and from wetting have been neglected. The mean dry densities achieved were 1.355, 1.649 and 1.706 Mg/m^3 with standard deviations of 0.013, 0.047 and 0.028 Mg/m^3 for Test Series 1, 2 and 3 corresponding to 75%, 92% and 95% level of compaction respectively based on the maximum dry density (MDD). The scatter in the dry density values may be due to variations in the moulding water content during compaction. It may be noted that in Test Series 3 the same 55 blows of the rammer achieved only a 95% level of compaction. This observation is consistent with the results of studies (Ampadu 1997) which show that at the optimum moisture content, this material gives lower MDD values when fresh samples are used for compaction than when samples are reused for each test point. The results of the water content distribution across the sample during testing showed that on the average the difference in water content across the sample was less than 6% and for Test Series 2 and 3, drying appeared to produce a more uniformly distributed water content across the sample than wetting. The water content values in the Tables are the average values across the samples.

The variation of the CBR with water content for all three test series are shown in Fig. 2. The similar values of CBR at higher water contents for both Series 2 and Series 3 may be due to similar dry density values. The results show that as the soil dries from the OMC condition, initially there is a rapid increase in CBR but this slows down as the water content reduces further especially for lower density samples. The rate of reduction in the CBR during wetting is relatively slower. In fact the rate of change in CBR per percentage change in water content was 3 to 7 times larger for drying than for wetting from the OMC. The practical implication of this is that there is tremendous benefit in terms of increase in CBR in ensuring that the subgrade is well drained to achieve equilibrium water content below the optimum value. The results also show that on soaking from the OMC condition, the CBR of the

Table 2. Summary of Test Results for Test Series 1

Test Condition	Average Water Content (%)	Dry Density (Mg/m^3)	Degree of Saturation (%)	CBR
	9.56	1.377	27.4	34
Drying	11.73	1.371	33.3	33
	13.37	1.362	37.4	25
OMC	16.58	1.348	45.5	8
	26.54	1.346	72.6	0.8
Wetting	26.81	1.348	73.6	0.6
	27.03	1.354	74.8	0.4
	28.88	1.338	78.0	0.3

Table 3. Summary of Test Results for Test Series 2

Test Condition	Average Water Content (%)	Dry Density (Mg/m^3)	Degree of Saturation (%)	CBR
	10.51	1.622	43.9	95
Drying	12.66	1.579	49.5	79
	13.54	1.643	58.5	52
OMC	16.09	1.595	64.5	28
	18.30	1.669	82.5	18
Wetting	19.35	1.684	89.4	16
	20.22	1.703	96.4	16
	21.26	1.694	99.8	15

Table 4. Summary of Test Results for Test Series 3

Test Condition	Average Water Content (%)	Dry Density (Mg/m^3)	Degree of Saturation (%)	CBR
	12.10	1.697	57.1	94
Drying	13.73	1.674	62.4	79
	14.89	1.670	67.2	59
OMC	16.45	1.743	83.8	28
	18.22	1.733	91.2	20
Wetting	18.30	1.719	89.5	18
	18.59	1.726	92.0	17
	21.63	1.688	100	15

subgrade drops and the relative reduction in CBR is between 46% and 98% for dry densities ranging between 1.71 and 1.36 Mg/m^3.

The logarithm of the CBR is plotted against water content in Fig. 3. The results quoted in Croney and Croney (1998) for soil B showing a linear variation of log CBR with water content over the likely field water content are superimposed. The limited results from this study do not show such a linear

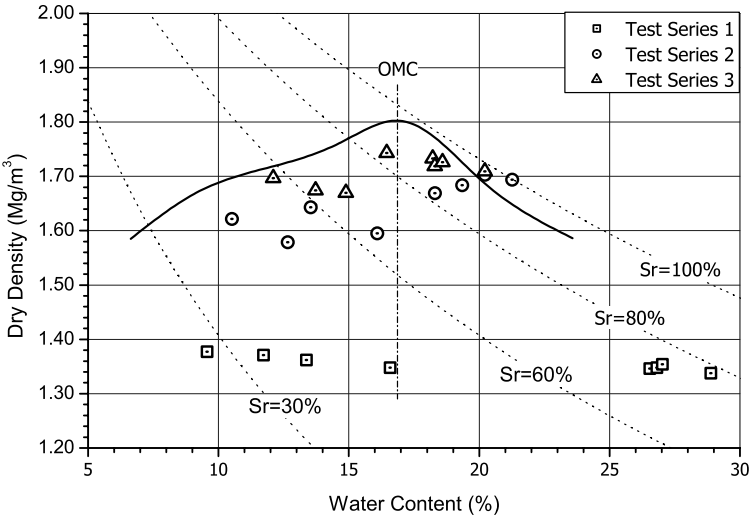

Fig. 1. Compaction characteristics and initial states of test samples

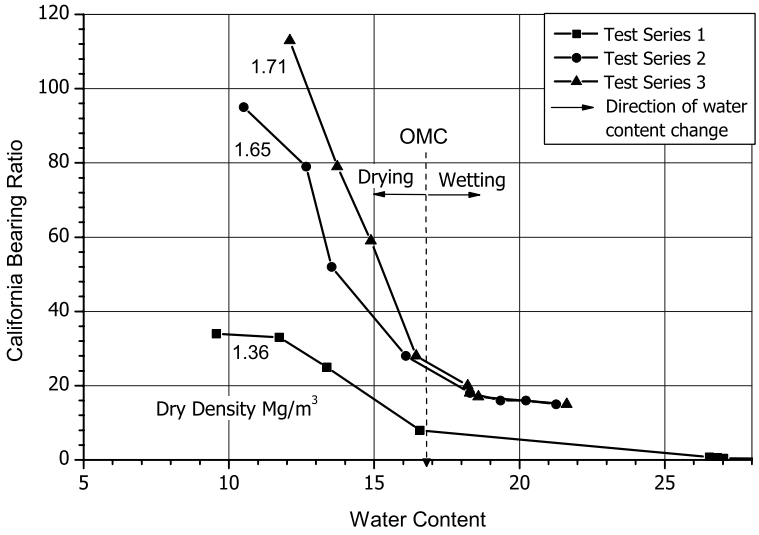

Fig. 2. Variation of CBR with water content for constant dry densities

relationship and suggest that hysteresis effect from wetting or drying may be important in defining the relationship.

The soil-water characteristics of the same material obtained from a parallel test programme using the filter paper method (ASTM D-5298-03) are shown in Fig. 4 for dry densities of 1.79 and 1.51 Mg/m^3. A linear relationship may be assumed within the range of saturation investigated with an average air entry

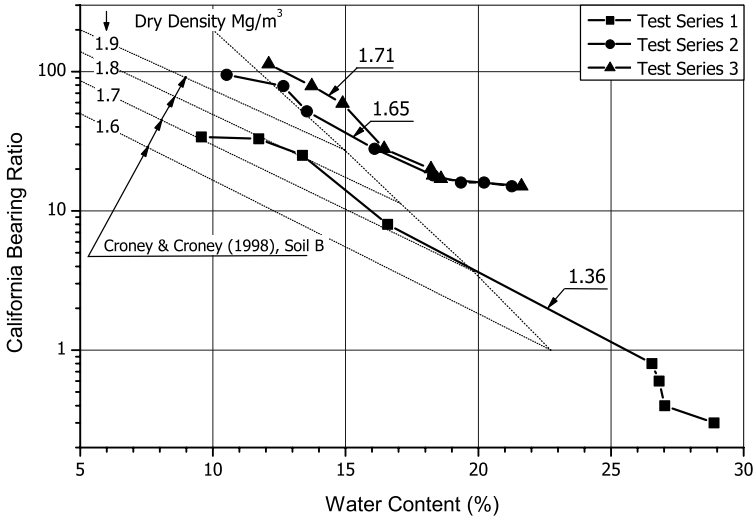

Fig. 3. Variation of log CBR with water content

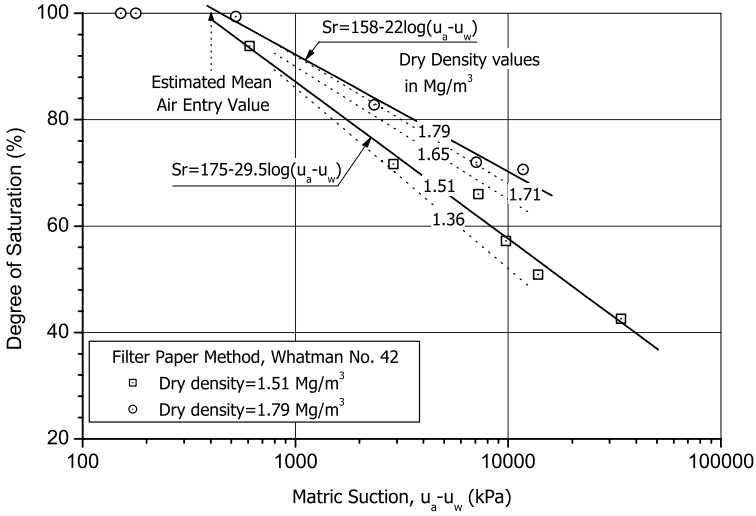

Fig. 4. Soil-Water characteristics for different densities

pressure of about 420 kPa. Based on this and interpolating and extrapolating for dry densities used in this study, the corresponding matric suction values, $(u_a - u_w)$, for all the test points were estimated. These are plotted against the unsaturated CBR, CBR_u on a log-log scale in Fig. 5. The results suggest a linear log-log model which can be expressed as

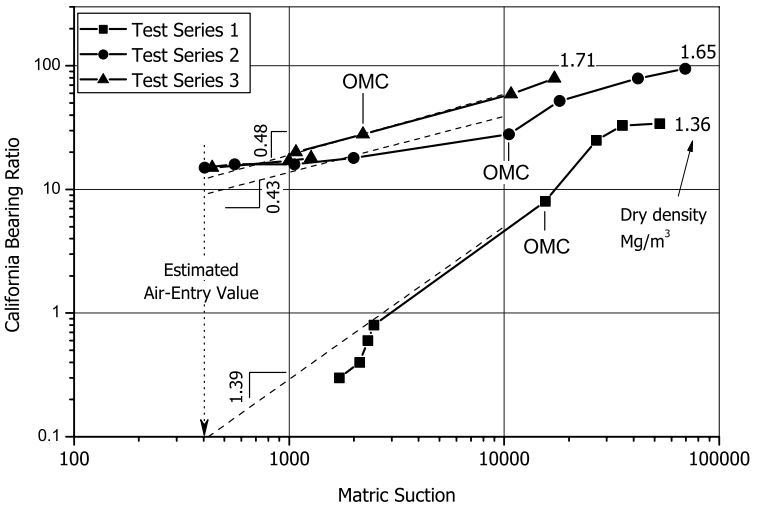

Fig. 5. CBR-matric suction relationship

$$\mathrm{CBR}_u = \mathrm{CBR}_s \times \left(\frac{u_a - u_w}{u_e} \right)^n$$

where CBR_s is the soaked CBR, u_e is the air-entry value and n is a constant which depends on the suction and the dry density.

For this study, n was of the order of 1.4 and about 0.5 for the lower and for the higher dry densities respectively, and constant for suction values up to about 15,000 kPa.

Conclusion

From the laboratory CBR test results on a subgrade material at different water contents for three different dry densities, it may be concluded that the rate of change in CBR per percentage change in water content during drying from the OMC was 3 to 7 times larger than during wetting from OMC. Soaking from the OMC condition, leads to a relative reduction in CBR of between 46% and 98% for dry densities ranging between 1.71 and 1.36 $\mathrm{Mg/m^3}$. A linear log-log relationship between CBR and matric suction is suggested for matric suction values of up to about 15,000 kPa.

References

Ampadu SIK (1997) The compaction characteristics of residual soils, In: Proc 3rd Int Conf on Structural Eng Analysis and Modeling, Accra, 7–11 September 1997

Ampadu SIK (2006) The loss of strength of an unsaturated local soil on soaking, Geotechnical Symposium, University of Rome, March 16-17, 2006 (in print)
ASTM D 1557-91 Standard Test Method for Laboratory Compaction Characteristics of Soil Using Modified Effort. Annual Book of ASTM Standards
ASTM D 1883-91 Standard Test Method for CBR of laboratory-compacted soils. Annual Book of ASTM Standards
ASTM D 5298-03 Standard Test Method for Measurement of Soil Potential (Suction) Using Filter Paper. Annual Book of ASTM Standards
BS 1377–1990 British Standard Methods of tests for Soils for civil engineering purposes, British Standards Institution
Charman JH (1995) Laterite in road pavements. CIRIA Special Publication 47. Transport Research Laboratory, Department of Transport
Croney D, Croney P (1998) Design and Performance of Road Pavements, 3rd Edn. McGraw Hill, pp 137–138
Hammond AA (1970) A study of some laterite gravels from the Kumasi district. Building and Road Research Institute, Project Report SM.5
Sanchez-Leal FJ (2002) Interpretation of CBR test results under the shear strength concept of unsaturated soil mechanics. In: Proc 3rd Int Conf on unsaturated soils (USAT 2002), Recife, pp 663–668

Shear Strength Affected by Suction Tension in Unsaturated Fine Grained Soils?

Carola Bönsch and Christof Lempp

Martin-Luther-University, D-06099 Halle (S.), Germany
carola.boensch@geo.uni-halle.de, christof.lempp@geo.uni-halle.de

Summary. Suction tension acts within the gas and liquid filled grain-pore-system in unsaturated fine grained soils and should partly control the shear strength. The development of pore pressure in a completely water saturated grain structure will reduce the shear resistance, whereas the suction tension within an unsaturated soil will cause additional grain-to-grain forces. These are changing with varying degree of water saturation and thus may influence the shear strength probably by favouring the formation of coarse grained aggregates.

An experimental approach was started to investigate this expected relation in overconsolidated Tertiary clay and in Quaternary loess (silt) using triaxial and direct shear test results and comparing them with the results of suction tension measurements obtained by using pressure membrane apparatus. Based on the common classifications, one should argue that shear velocity will control the shear strength due to pore pressure effects in the shear zone. However, the antagonistic effects of overpressure of the pore fluid and compression of grains due to suction tension act on a micro-scale in unsaturated fine grained soils and influence the shear behaviour differently.

Effects of suction tension are noticeable in triaxial and direct shear tests in unsaturated fine grained soils. Quantification is difficult because other stress influences like load level act more effectively.

Key words: suction tension, water saturation, shear strength, loess, clay

1 Expected Effects of Suction on Strength

Due to the interaction between the solid, fluid and gaseous phases, additional forces are effective in unsaturated pore systems. An unsaturated soil has the tendency to receive water and increase its saturation level. If the soil is more or less saturated, a certain force is required to remove water from the pore space and decrease the saturation level of the soil. These effects can be explained by the idea of suction tension.

Suction tension consists of both capillary and adsorptive parts. The capillary part depends on the pore size distribution. The adsorptive part of suction

tension is a function of the mineralogical composition of the solid part, as well as the chemical composition of the pore fluid (Bönsch 2006).

Normally, the water content or the saturation level is plotted against the logarithm of the tension in the pF curve. This, originally agricultural idea of suction, can be used because the natural water content and the connected suction tension of an unsaturated soil normally range in the same dimensions.

Water content-pF curves of fine grained soils can be simplified approximated by using a logarithmic regression of the following the form:

$$y = a + b \cdot \ln(x) \tag{1}$$

The amount of the variable a represents approximately the saturation water content. The term $b \cdot \ln(x)$ describes the form of curve. More precisely, the flatter the curve, the smaller $b \cdot \ln(x)$ is. The term $b \cdot \ln(x)$ has the range $-4 < b < 0$. y is the water content at suction x. The regression equations and some statistical parameters of the regression are given in Table 2. Using the inverse function of that regression one can estimate the suction tension corresponding to certain water content.

What are the explicit influences of the suction tension on strength and stiffness of the unsaturated soil? If the effective friction angle and the effective cohesion as well as the relation between suction tension and water content of a soil are known, the shear strength could be specified using the theory of Fredlund and Xing (1994). The shear stress is a function of net normal stress $(\sigma_n - u_a)$ and the suction s (Vanapilli et al. 1996). It can be written as:

$$\tau = c' + (\sigma_n - u_a) \cdot \tan\varphi' + s \cdot (\tan\varphi') \cdot \left(\frac{\theta_w - \theta_r}{\theta_s - \theta_r}\right) \tag{2}$$

where θ_w are the volumetric water content during shearing, θ_s the volumetric water content in case of saturation and θ_r the residual water content. There is still no agreement to find in literature what water content that residual water content is. It is not possible to measure the pore air pressure u_a directly so one can calculate it from the effective stress equation (Bishop 1959). This uses the normal stress, the corresponding shear stress and the suction curve of the soil:

$$u_a = -\left\{\frac{c'}{\tan\varphi'} - (u_a - u_w) \cdot \chi - \sigma_n\right\} \tag{3}$$

where the term $(u_a - u_w)$ is

$$(u_a - u_w) = \psi_m \,. \tag{4}$$

The suction tension s, as the equivalent of the matrix potential Ψ_m, could not be measured directly. Therefore after knowing the water content, s can be calculated from the inverse suction curve. The weighting factor χ depends on pore air and pore water pressures as well as saturation level (Vanapilli et al. 1996). Theoretically it is 0 in a saturated soil and 1 in a dry soil:

$$\chi = \frac{\theta_w - \theta_r}{\theta_s - \theta_r} \,. \tag{5}$$

Since the suction pressure s is equivalent to pore water pressure and negative, it can be added to the normal stress σ_n. Due to the fact that the suction level of residual water content is unknown it will be neglected. Using the assumption that the residual water content θ_r goes to 0, then χ is equivalent to the saturation degree s_R. Naturally the χ value will be smaller then s_R, but its linear influence will not change the general trend of effective suction neither it influences whether the calculated effective suction will be a pore water pressure.

Actually the partial pressure of pore water and air are disregarded in reference to the very slow shear velocity. In the assumption that the principle of effective stresses is applicable also for unsaturated soils, and there is no correlation between cohesion and suction tension, then the shear strength τ using Eqs. (2), (3) and (5) can also be written as

$$\tau = c' + \left[\sigma_n - \left(-\frac{c'}{\tan\varphi'} - s \cdot s_R - \sigma_n\right)\right] \cdot \tan\varphi' + s \cdot \tan\varphi' \cdot s_R \,. \tag{6}$$

Then Eq. (6) can be transformed into

$$\tau/2 - c' - \sigma_n \cdot \tan\varphi' = s \cdot s_R \cdot \tan\varphi' \,. \tag{7}$$

Finally the suction tension s can be estimated:

$$s = \frac{\tau/2 - c' - \sigma_n \cdot \tan\varphi'}{\tan\varphi' \cdot s_R} \,. \tag{8}$$

One can expect that the shear strength will increase with an increasing suction pressure, but theoretically there could be an influence from the shear velocity. If it is too fast the reallocation of pore water is detained and there could be a local increase of water content in the shear splice, which decreases the suction based part of shear strength. Otherwise a brittle behaviour increases the strength at fast shear tests, and creeping reduces the strength at very slow shear tests. The real dimension of these influences are unknown as long as the suction tension in the shear splice can not be measured. These effects are similarly described by Junge et al. (2000) for tensile tests. As a matter of fact the measured shear strength of an unsaturated soil is normally smaller than determined by Eq. (2) (Behrens and Neumann 2002, Schanz et al. 2004). Contrary to their opinion that neither suction tension nor shear velocity play roles for shear strength, we make two assumptions. First, there is a false estimation of the suction in shear splice, and second, in dependence on velocity deficient consideration of brittle behaviour or creeping processes.

2 Characterisation of the Tested Materials

Different fine grained soils were tested from locations around Halle/Saale. As example for clayey soils a slightly overconsolidated Tertiary clay from

Table 1. Characteristic properties (median of grain size distribution M, coefficient of unconformity U, particle density ρ_s, porosity n, content of organic matter c_{org}, total carbonate c_C and dolomite c_{Dol}, saturated water permeability k_f and specific surface S)

Sample:	M [µm]	$U = d_{60}/d_{10}$	ρ_s [g/cm^3]	n [%]	c_{org} [%]	c_C [%]	c_{Dol} [%]	k_f [m/s]	S [m^2/g]
Silt FB	25	20.1	2.65	32.3	2.81	1.54	0.39	1.6×10^{-8}	13.5
Silt PL	29	3.5	2.65	32.9	4.89	6.79	1.33	4.0×10^{-8}	13.2
Loess SM	32	5.4	2.71	38.1	0.28	20.7	7.45	5.9×10^{-7}	14.2
Clay SP	1.2	—	2.64	37.4	7.38	unverifiable		2.2×10^{-9}	27.1

Schiepzig (SP) was used. The silty soils were located in the north or north west from Halle: in an open pit near the village Ploetz (PL), the open pit Fuchsberg (FB) and the archaeological excavation site "Erdwerk Salzmuende" (SM). For a comparative overview over all characteristic properties of the different soils see Table 1. The material SM is a loess, the other PL and FB are leached loess-loams. The clay (SP) is emerged from a rhyolitic rock in situ as a result of intensive weathering.

3 Suction Measurements Results

To determine the suction tension in the range of 6 to 1,500 kN/m^2 a pressure membrane apparatus was used. As expected water retention curves of the silty soils are steeper than of the clay. The regression results of the pF curve are given in Table 2. If the residual water content is defined as the adsorbed water with a suction pressure of 10,000 kN/m^2 (Lu and Likos 2004), the residual water content can be estimated. With the assumption that the regression function is valid for higher suction pressures too, the residual water content in clay is about 19.5% and in silt it range from 0.1 to 2.1%.

Table 2. Regression results of the pF curves: equation, correlation coefficient and residual water content θ_r (assumption: the suction of adsorbed residual water is 10,000 kN/m^2)

Soil	pF function	Correlation coefficient	θ_r [%]
Clay (SP)	$y = 30.78 - 1.23 \ln x$	0.99	17.5
Silt (FB)	$y = 22.69 - 2.23 \ln x$	0.98	2.1
Silt (PL)	$y = 30.18 - 3.26 \ln x$	0.98	0.1

4 Shear Test Results

The shear velocity in triaxial and direct shear tests was 0.005 mm/min. The influence of effective suction tension on maximal shear strength is more important in direct shear tests as shown in Fig. 1. Higher effective suction pressures are linked with higher maximal shear strengths.

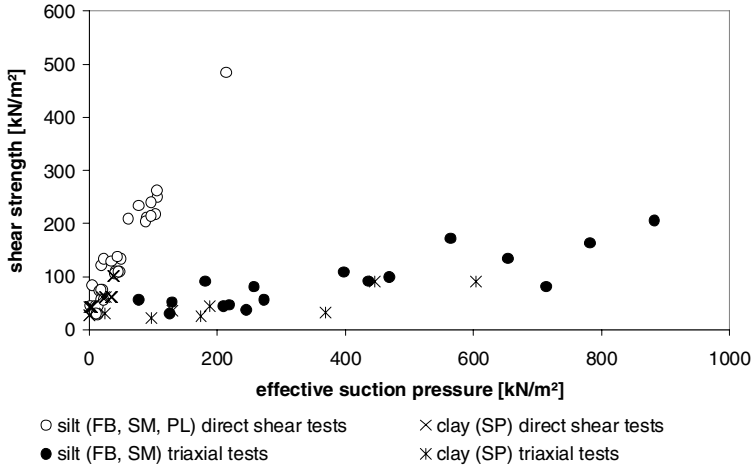

Fig. 1. Maximal shear strength versus effective suction pressure

4.1 Results of Triaxial Shear Tests

Estimating the shear strength parameters five single tests with cell pressures of $\sigma_3 = 25$, 50, 100, 200 and 400 kN/m^2 with one soil in similar saturation level were realized. All samples were isotropically consolidated at the same cell pressure as during shearing until there were no significant deformation. This consolidation took about half an hour to two hours in silt, and few hours in clay.

Generally friction angle decreases with increasing water saturation (see Table 3). There is no clear correlation between water saturation and effective cohesion. Effective suction tension correlates with water saturation degree as shown in Fig. 2. If the water saturation level is low, effective suction pressure increases.

There are two different fracture mechanisms in unsaturated fine grained soils. While in the clay a certain sloped plane is developed and the upper block slides along the lower, in the silt a more or less symmetric system of crossed shear planes, with two main directions, is formed (see Fig. 3). If the saturation level is near the complete saturation during the triaxial test, samples of both

soil types show a barrel-shaped body structure without macroscopically visible cracks.

Table 3. Average saturation degrees s_R, total and effective shear parameters of triaxial tests of unsaturated fine grained soils (shear velocity 0.005 mm/min)

Sample	s_R [%]	ϕ [°]	c_u [kN/m^2]	ϕ' [°]	c' [kN/m^2]
Clay (SP)	69	17.46	27.81	17.46	27.81
	78	1.78	21.20	7.65	19.19
Silt (FB)	41	35.37	64.03	35.37	64.03
	45	33.84	0.00	35.07	11.24
	53	31.29	4.90	38.60	11.54
Silt (SM)	37	40.45	23.46	40.45	23.46
	41	35.46	21.08	35.42	21.36
	88	17.11	10.45	39.85	7.15

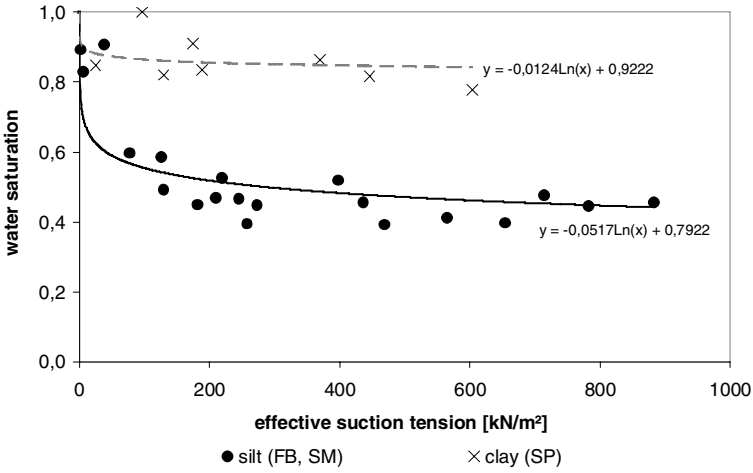

Fig. 2. Water saturation degree versus effective suction pressure (calculated after equation (8)) of three different soils in triaxial shear tests

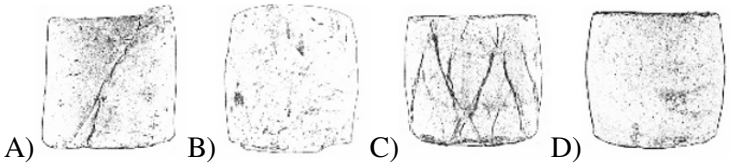

Fig. 3. Geometry of shear splices and sample deformation in triaxial shear tests with 25 kN/m^2 cell pressure: **A**) clay (SP) with 66% water saturation; **B**) clay (SP) water saturated (100 kN/m^2 cell pressure); **C**) silt (FB) with 39% water saturation, **D**) silt (FB) water saturated (200 kN/m^2 cell pressure)

4.2 Results of Direct Shear Tests

The cohesion and friction angle both seem to be dependent on saturation level. This should be an effect of the enforced shear splice, while in the triaxial tests the deformation can develop free. Even in case of very slow shear velocities a pore pressure partly can be effective in the shear plane, because the enforced movement causes turbulent water flow nearest to the shear plane. To calculate the effective suction after Eq. (8), the average saturation degree of the sample is used. But its influence is overlaid by dynamical forces of the water in the nearest area around the shear plane. As a result, the effective suction pressure does not correlate with water saturation. The effective suction pressure depends on the water allocation in the sample, more precisely, in the shear splice.

Table 4. Average water saturation s_R and effective shear parameters of direct shear tests of unsaturated fine grained soils (shear velocity 0.005 mm/min)

Sample	s_R [%]	ϕ' [°]	c' [kN/m^2]
Clay (SP)	69	23.88	5.60
Silt (FB)	29	23.61	34.52
	69	26.73	9.73
Silt (PL)	42	29.17	17.32
	63	26.09	8.13
Loess (SM)	26	31.91	13.14
	53	29.19	14.72
	70	27.64	4.66

Is there an influence of shear velocity? The clay is used to discuss the influence of shear velocity between 0.002 and 0.15 mm/min, because of its very low water permeability, the largest influence of pore water pressure is to be expected. In statistical tests the water saturation degree of the clay ranges from 70 to 85%.

On the one hand, the effective suction pressure decreases with higher shear velocities with a logarithmic correlation. On the other hand the maximal shear strength increases with increasing shear velocity until 0.03 mm/min. It is almost constant at higher shear velocities. Maximal shear strength increases with increasing suction pressure in statistical tests with the same velocity and vertical loads but different saturation degrees.

If the effective suction tension is bigger at low shear velocities, there must be another reason why the shear strength is lower at low velocities. Creeping processes and reduction of void ratio by compaction of the soil could explain these effects.

5 Conclusions

Suction tension is noticeable in unsaturated fine grained soils. Its effects can be measured in mechanical tests (triaxial compression tests and direct shear tests) by evaluating an effective suction pressure during shearing. This is based on theoretical assumptions as well as on the knowledge of the degree of saturation. The suction tension effect is quantified more likely in triaxial compression tests than in direct shear tests. That is why in the latter one, smaller samples are tested usually, and a distinct orientation of the shear splice is enforced.

Even at normal stresses of 50 to 200 kPa one can differentiate an increasing trend of suction tension as a distinct effect at the same stress level. Either way, the quantification is difficult due to various parameters influencing the strength. Consequently, the effect of suction tension on the strength of unsaturated soils may be even relevant at low stresses and median saturation degrees around 50% (40–70%). Low shear velocities apparently reduce the suction tension effects due to creeping with pore space reduction and increase of saturation degree. Clay and silt differ in their strength behaviour and in their relations between effective suction tension and saturation degree.

References

Behrens W, Neumann M (2002) Untersuchungsergebnisse zu einigen mechanischen Eigenschaften von TRISOPLAST. Müll und Abfall 2:86–89

Bishop AW (1959) The principle of effective stress. Teknisk Ukeblad 106/39:859–863

Bönsch C (2006) Weathering of partial saturated soft rock. In: Von Cotthem A, Charlier P, Thimus JF, Tshibangu JP (eds) Multiphysics coupling and long term behaviour in rock mechanics. Taylor and Francis London, pp 397–402

Fredlund DG, Xing A (1994) Equations for the soil water characteristic curve, Can Geotech J 31:521–532

Junge T, Gräsle W, Bensel G, Horn R (2000) Einfluss des Porenwasserdrucks auf die Zugfestigkeit von Bodenproben. J Plant Nutrition Soil Sci 163(1):21–26

Lu N, Likos WJ (2004) Unsaturated Soil Mechanics. John Wiley and Sons, New York

Schanz T, Agus SS, Tscheschlok G (2004) Hydraulischmechanische Eigenschaften einer polymerverbesserten Sand-Bentonit-Mischung beim Einsatz im Deponiebau, Geotechnik 27(4):344–355

Schick P (2004) Scherfestigkeit durch Kapillarität in unzementierten ungesättigten bindigen Böden, Bautechnik 81(1):90–104

Vanapilli SK, Fredlund DG, Pufahl DE, Clifton AW (1996) A model for prediction of shear strength with respect to soil suction, Can Geotech J 33:379–392

Shear Strength Behaviour of Unsaturated Silty Soil

Ali R. Estabragh[1] and Akbar A. Javadi[2]

[1] Faculty of Soil and Water Engineering, University of Tehran, Karaj 31587-77871, Iran a.estabragh@gmail.com
[2] School of Engineering, Computer Science and Mathematics, University of Exeter, EX4 4QF, UK a.a.javadi@exeter.ac.uk

Summary. This paper presents results of an experimental study on shear strength behaviour of an unsaturated silty soil. A comprehensive set of laboratory experiments have been undertaken in a double-walled triaxial cell (and a conventional cell for saturated samples) on samples of a compacted silty soil. In the experiments the soil samples were subjected to isotropic consolidation followed by unloading and subsequent anisotropic reloading (shearing) under constant suctions. Volume change and shear strength data for the samples were monitored continuously during the experiments. In this paper, the results of the experimental study will be presented and the effects of suction on the shear strength and volume change of unsaturated soil will be discussed in detail.

Key words: unsaturated soils, suction, shear strength, overconsolidation ratio, volume change

1 Introduction

There are vast areas of the world, particularly in tropical and subtropical regions, where the soils are generally unsaturated. In addition, even in many temperate regions, the soil above the water table remains unsaturated. Geotechnical engineers need to be able to assess the shear strength of unsaturated soils for safe and cost effective design of structures founded on unsaturated soils.

The first attempt to explain the shear behaviour of unsaturated soil was presented by Bishop (1959). The use of Bishop's equation for unsaturated soils was criticised by Jennings and Burland (1962) and Burland (1964). They pointed out that Bishop's equation, while appearing to explain shear strength behaviour, could not fully explain volume change behaviour. The importance of separating the stress state variables $(\sigma - u_a)$ and $(s = u_a - u_w)$ has been emphasized (where σ is total stress s is suction u_a is pore air pressure and u_w is pore water pressure) by many researchers such as Fredlund et al. (1978),

Matyas and Radhakrishna (1968) and Wheeler and Karube (1995). Fredlund et al. (1978) and Fredlund (1979) put forward concepts for unsaturated soil based on independent stress state variables, giving the shear strength relationship as:

$$\tau = c' + (\sigma - u_a)\tan\phi' + (u_a - u_w)\tan\phi^b \tag{1}$$

where τ is shear strength, c' is the effective cohesion, ϕ' is the angle of friction and ϕ^b is the angle of friction for changes in $u_a - u_w$. In this method ϕ^b is assumed to be constant for all values of matric suction $(u_a - u_w)$. This approach has been widely used in interpreting shearing behaviour of unsaturated soils. Fredlund et al. (1978) suggested that ϕ^b could be assumed to be equal to the effective stress angle of friction measured in saturated condition (ϕ'). This would suggest that it is constant for all values of matric suction. The use of a linear relationship between $u_a - u_w$ and ϕ^b (i.e., a constant value of ϕ^b) was shown to be in error by Escario and Saez (1986). This non-linearity was confirmed by Fredlund et al. (1978) who assumed ϕ^b varied as a function of suction. In what follows the results of an experimental study on the shearing behaviour of an unsaturated soil will be presented and the effect of suction on the shear strength of unsaturated soils will be discussed.

2 Test Procedure and Program

2.1 Preparation of Compacted Specimens

The soil used in the testing program was a silty soil with low plasticity. The soil comprised 5% sand, 90% silt and 5% clay and had a liquid limit of 29% and plasticity index of 19%. The results of the standard proctor compaction test indicated a maximum dry density of 1.74 $\mathrm{Mg/m^3}$ at an optimum water content of 14.5%. Compacted specimens were prepared using a compaction mould designed specially for static compaction. The purpose of using static compaction as opposed to dynamic compaction was to obtain a more homogenous specimen in terms of density and shear strength throughout the volume of the specimen. The soil mass was mixed at a water content of 10% (4% less than optimum from standard compaction test). The specimens were 76 mm high and 38 mm in diameter. Compaction was done in nine layers with each layer being compacted to a maximum vertical total stress of 1600 kPa. The specimens produced by this method were found to be very uniform and the interface between the layers was barely apparent.

2.2 Test Procedure and Program

A series of triaxial tests were conducted using a conventional triaxial cell for saturated and a modified cell for unsaturated soil testing Estabragh et al. (2004). Both triaxial cells were connected to GDS controllers for applying the

cell pressures, pore water pressure (u_w) and axial strain. All the experimental data were recorded continuously by a computer. The triaxial test program consisted of several stages as follows:

3.2.1 Equalisation

After setting the apparatus, the first step of each test was equalisation. At this stage by applying the required air and water pressures, the specimen was brought to the desired suction.

3.2.2 Ramp consolidation and unloading

After the equalisation stage each specimen was consolidated isotropically to the selected value of mean net stress (p') by ramp consolidation. The sample was then unloaded isotropically to a predefined lower value of mean net stress. Suction was maintained constant during loading and unloading.

3.2.3 Shearing

After the unloading stage, each specimen, with pre-defined overconsolidation ratio (OCR), was sheared by applying an axial load at a constant compressive strain rate Estabragh and Javadi (2006).

3 Results and Discussion

Typical results of the triaxial tests are presented in Figs. 1 and 2. The triaxial shear tests were performed under controlled suctions (0, 100, 200 or 300 kPa) and constant cell pressures (50, 100, 200, 300 or 400 kPa). Each series of tests was carried out at a specified overconsolidation ratio (OCR = 11, 5.5, 2.75, 1.38 and 1.1). Compression of a specimen during shearing is expressed using a negative sign, and a positive sign is used for dilation of the specimen in the graphs of volumetric strain versus axial strain. Figs. 1**a** and 2**a** show that in the shear tests the deviator stress increased with increasing cell pressure until a peak value and then remained nearly constant. Figs. 1**b** and 2**b** show that, generally, the volume of the samples decreased during shearing except for the samples with high overconsolidation ratios. For tests with $\sigma_3 = 50$ and 100 kPa at suctions of 100 and 200 kPa the deviator stress first increased and then slightly decreased. During shearing, the volume of these samples increased after a slight initial contraction. However, it is concluded from these results that the stiffness of the soil specimens generally increased with increasing confining pressure and decreasing the value of OCR. In the tests conducted on specimens with high OCR values of 11 and 5.5, the specimens exhibited a relatively brittle behaviour and during shearing, a slight increase

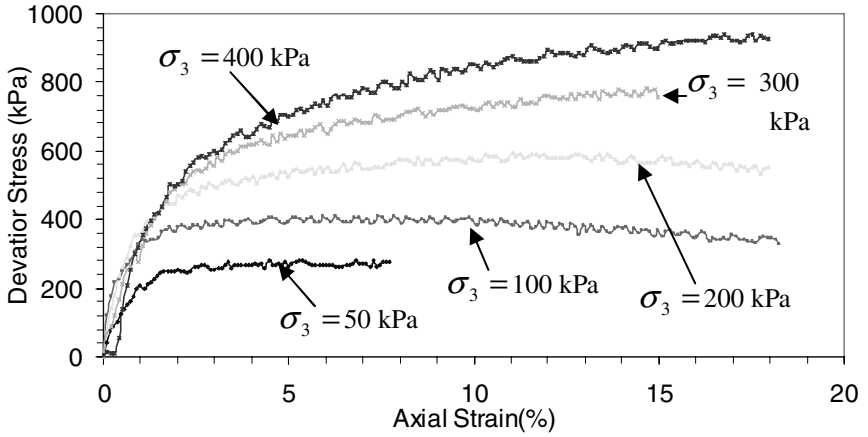

(a) Deviator stress with axial strain

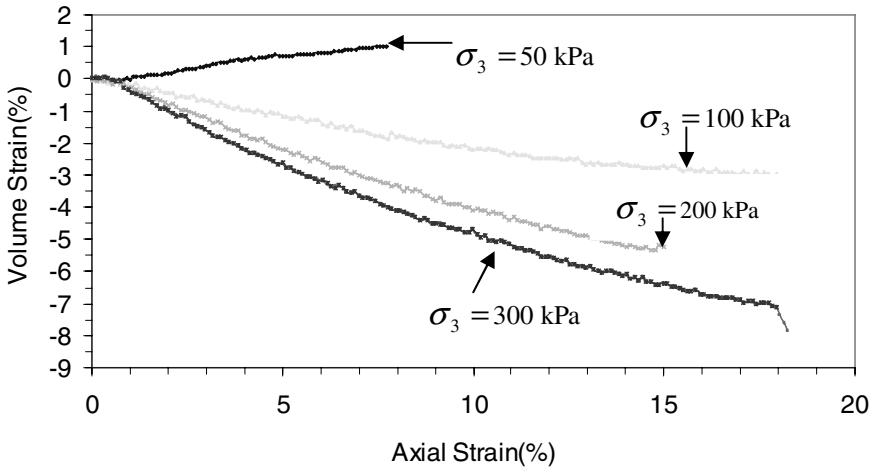

(b) Volumetric strain-axial strain curves

Fig. 1. (**a**) Stress-strain curves, (**b**) Volumetric strain-axial strain curves for samples tested at $s = 100$ kPa under various cell pressures

in total volume was observed after an initial compression. This behaviour can be attributed to the influence of matric suction on the stiffness, brittleness and dilatancy of the soil specimens, especially at low confining pressures. The exhibition of post softening behaviour is commonly observed in heavily over consolidated specimens.

Figure 3 shows typical results of variation of maximum deviator stress with suction at constant cell pressure. This figure shows that the deviator

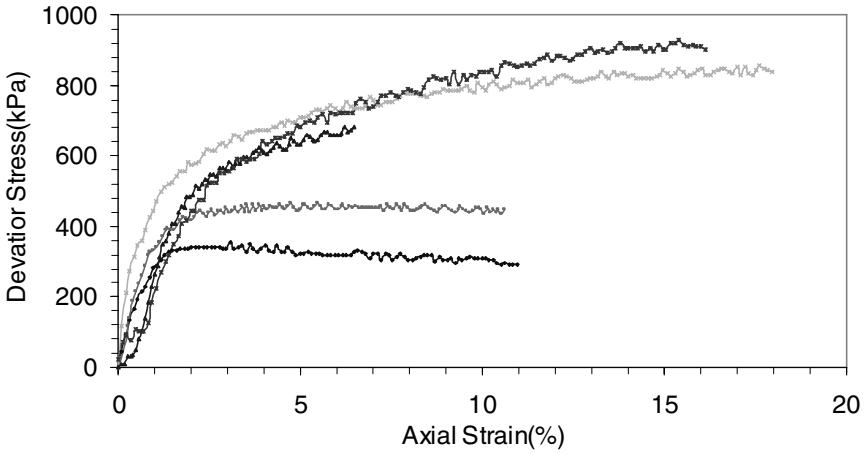

(a) Deviator stress-axial strain curves

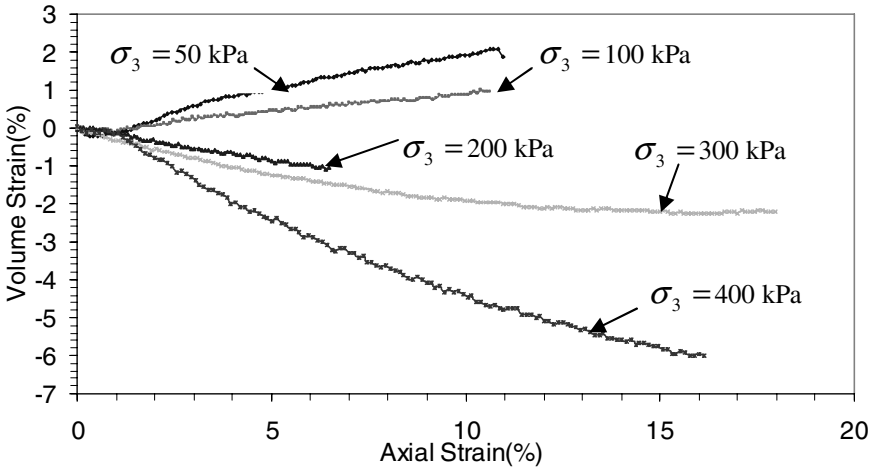

(b) Volumetric strain-axial strain curves

Fig. 2. (**a**) Stress-strain curves, (**b**) Volumetric strain-axial strain curves for samples tested at $s = 200\,\text{kPa}$ under various cell pressures

stress increased with increasing suction. Also, Figs. 1 and 2 show that the brittleness of the soil decreased with increasing confining pressure. It can be concluded that the strength of soil specimens increases with increasing suction but its variation is not linear. The increase in cell pressure causes

a progressive evolution from dilatancy to compression behaviour until the dilatancy completely disappears.

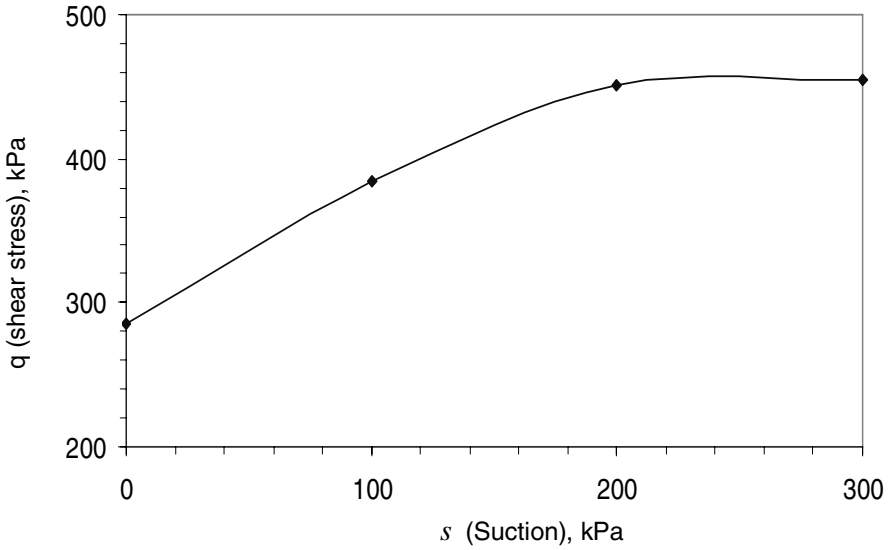

Fig. 3. Variation of maximum deviator stress with suction

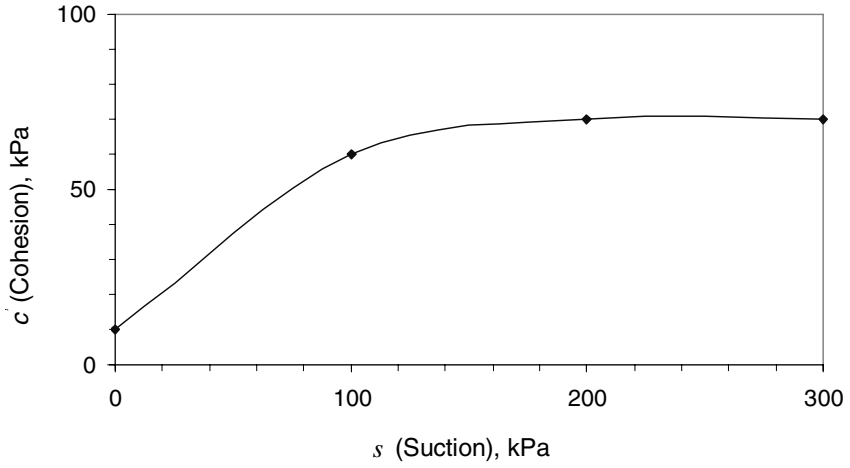

Fig. 4. Variation of c' with s

Figure 4 indicates a similar pattern of increase in cohesion intercept with increase in matric suction at the peak shear stress for all specimens tested under different confining pressures.

4 Conclusion

The experimental program on the saturated and unsaturated specimens provided some information on the shear strength behaviour of unsaturated compacted silty soils. The following conclusions are drawn.

Both confining pressure and suction affect the shear strength behaviour of unsaturated soil.

Softening and increasing the stiffness (hardening) of specimens for a given cell pressure depend on the value of suction.

Dilatancy or compression may occur during shearing; suction and OCR are important factors affecting dilatancy and compression.

The cohesion of soil is a function of suction and the relationship is nonlinear.

References

Bishop AW (1959) The principle of effective stress. Tek Ukeblad 39:859–863

Burland JB (1964) Effective stress in partly saturated soils, Géotechnique 14:64–68

Escario V, Saez J (1986) The shear strength of partly saturated soil, Geotechnique 36(3):453–356

Estabragh AR, Javadi AA, Boot JC (2004) Effect of compaction pressure on consolidation behaviour of unsaturated soil, Can Geotech J 41(3):540–550

Estabragh AR, Javadi AA (2006) Yielding of unsaturated silty soil under anisotropic condition. In: Miller GA, Zapata CZ, Houston SL, Fredlund DG (eds) Proc 4th Int Conf on Unsaturated Soils, Arizona, USA 1:1259–1266

Fredlund DG, Rahardjo H, Gan JKM (1978) The shear strength of unsaturated soils, Can Geotech J 15:313–321

Fredlund DG (1979) Appropriate concepts and technology for unsaturated soil, Can Geotech Eng J 16:121–139

Jennings JEB, Burland JB (1962) Limitation to the use of effective stress in partially saturated soils, Géotechnique 12(2):125–144

Matyas EL, Radhakrishna HS (1968) Volume change characteristics of partially saturated soils, Géotechnique 18(4):432–448

Wheeler SJ, Karube D (1995) State of the art report: Constitutive modellind in unsaturated soils. In: Alonso EE, Delage P (eds) Proc 1st Int Conf on Unsaturated Soils. Paris, France 3:1323–1356

Experimental Investigation on the Time Dependent Behaviour of a Multiphase Chalk

Grégoire Priol[1], Vincenzo De Gennaro[2], Pierre Delage[2], and Thibaut Servant[2]

[1] Geotechnical Department, NTNU, Trondheim, Norway
gregoire.priol@ntnu.no
[2] Ecole Nationale des Ponts et Chaussées, Paris (CERMES, Institut Navier), 6–8 av. B. Pascal, F–77455 Marne–la–Vallée cedex 2, France
vincenzo.degennaro@enpc.fr, pierre.delage@enpc.fr, servantt@eleves.enpc.fr

Summary. A series of high pressure oedometer compression tests were carried out on samples of Lixhe chalk (Belgium) containing various pore fluids: water, air (dry sample), oil (Soltrol) and oil/water under a controlled suction of 200 kPa. Strain curves with respect to time of tests carried out under a constant load were examined in a purpose of investigating the time dependent behaviour of chalk. A simple empirical exponential law able to account for the combined effects of stress and suction is proposed. Experiments show that it provides satisfactory results to predict a feature of multiphase chalk behaviour that is important in the study of the behaviour of oilfields.

Key words: chalk, multiphase, creep, water weakening, suction, collapse

Introduction

Investigations carried out on multiphase chalk (i.e. chalk that contains various non miscible pore fluids) as for example oil reservoir chalk (with gas, oil and water) or unsaturated chalk (with air and water) have evidenced a typical water weakening effect under water infiltration. Water weakening leads to: (i) instantaneous deformation (collapse) under constant load, (ii) strength reduction and (iii) increasing compressibility (see among others: Masson 1973, Schroeder et al. 1998, Gutierrez et al. 2000, Lord et al. 2002, De Gennaro et al. 2004). Research on oilfield chalks has shown that important physico-chemical interactions exist between water, oil and chalk involving collapse and time dependent behaviour (e.g. Newman 1983, Hellmann et al. 2002, Risnes et al. 2005). Delage et al. (1996) first suggested the reliability of the mechanical framework commonly used for unsaturated soils to study the coupled mechanical response of multiphase chalks provided oil is considered as a non wetting

fluid (like air in unsaturated soils). Instantaneous collapse during water injection in oil reservoir chalk was thus considered as a typical case of collapse due to wetting under constant load (Pasachalk 2001, 2004).

In this paper, results from oedometer tests performed on a chalk saturated with various pore fluids (oil, water and air) are presented. Particular attention has been paid to the time dependent behaviour of chalk that has been investigated by running creep tests. The effect of suction on the time dependent behaviour of chalk is investigated and the relevance of a simple empirical creep law accounting for suction effects is demonstrated.

Tested Material and Experimental Techniques

The chalk specimens used in this study come from blocks of an outcrop chalk extracted near Lixhe (CBR quarry, Belgium). This chalk originates from the same geological unit as some oil reservoir chalks of the North Sea (Ekofisk). Lixhe chalk is composed of almost pure calcite (with less than 1% of silica) with an average porosity $n \cong 43\%$. Oedometer tests were carried out on chalk specimens that were saturated with water and/or Soltrol 170 (Phillips Petroleum Company). Soltrol is a non polar organic liquid not miscible to water used as an oil analog. Oil–water–chalk interaction is believed to be mainly dependent on the capillary effects in the water menisci that are located in the small intergranular spaces close to grain contacts. By defining the two pressures u_o and u_w as the oil and water pressures respectively, the oil/water suction (called suction in the following) is defined as $s = u_o - u_w$ (to compare to the air–water suction in unsaturated soil $s = u_a - u_w$, being u_a the air pressure).

Four standard step loading oedometer tests have been performed on samples of 38 mm diameter and 20 mm high with total tests duration ranging from six months to more than one year. Tests were respectively performed on a water saturated sample, an oil saturated sample, a dry sample and the last test was carried out under controlled suction using the osmotic technique (Kassiff and Ben Shalom 1971, Delage et al. 1992, Dineen and Burland 1995). The dry sample was obtained after a heating period of 24 hours at 105°C. Based on the retention properties of Lixhe chalk a suction of 200 kPa was selected, corresponding to a degree of water saturation S_{rw} of about 30%.

Void Ratio–Time Relationship

In saturated soils, compression strains in oedometer tests are due to both pore pressure dissipation and creep (respectively primary and secondary consolidation). In a multiphase chalk with two pore fluids, compression affects the pore pressures and strain stabilisation corresponds with suction equilibration under the applied mean net stress ($\sigma'_v = \sigma_v - u_o$). In saturated soils, there is still

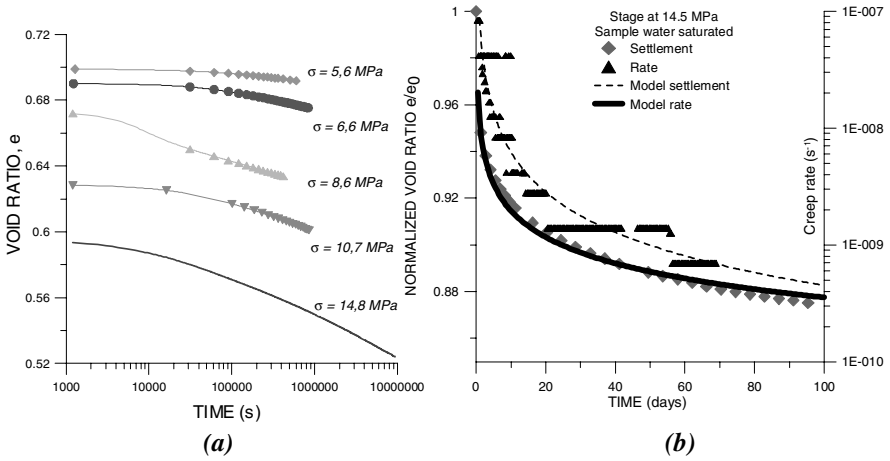

Fig. 1. (**a**) Consolidation curves under a suction equal to 200 kPa; (**b**) Analysis of the void ratio-time relationship during consolidation

no agreement how to distinguish the effect of viscous strain to that of excess pore pressure dissipation during primary consolidation (Mesri and Choi 1985, Leroueil 2006). Results from compression tests on two chalks (De Gennaro et al. 2005, Priol 2005) showed that neither Casagrande's nor Taylor's methods were helpful to identify any primary consolidation. Indeed, it seems likely that the low compressibility of the soil skeleton due to intergranular bonding effect together with the relatively high chalk permeability (about 10^{-8} m/s) are sufficient to prevent excess pore pressure generation (given that the amount of the applied total load instantaneously transferred to pore water pressure decreases when the drained bulk modulus increases, Biot 1941).

Indeed, the results of the suction controlled oedometer test ($s = 200$ kPa) presented in Fig. 1**a** show that, from the early beginning of the test, the curves giving the time dependent strain look very similar to creep curves. Hence, the time dependent volumetric strain of chalk should be essentially due to creep with the solid skeleton continuously settling under zero excess pore pressure. This result should obviously be confirmed by pore pressure measurements during initial loading.

The examination of a typical consolidation curve is presented in Fig. 1**b** in terms of normalised void ratio e/e_o plotted as a function of the elapsed time in a linear scale. This allows defining the following evolution law:

$$\frac{e}{e_{oi}} = \beta_i t^{\alpha_i} \tag{1}$$

where e_{oi} is the void ratio at the beginning of loading stage i. β_i represents the instantaneous strain whereas α_i controls the shape of the curve in Fig. 2, the

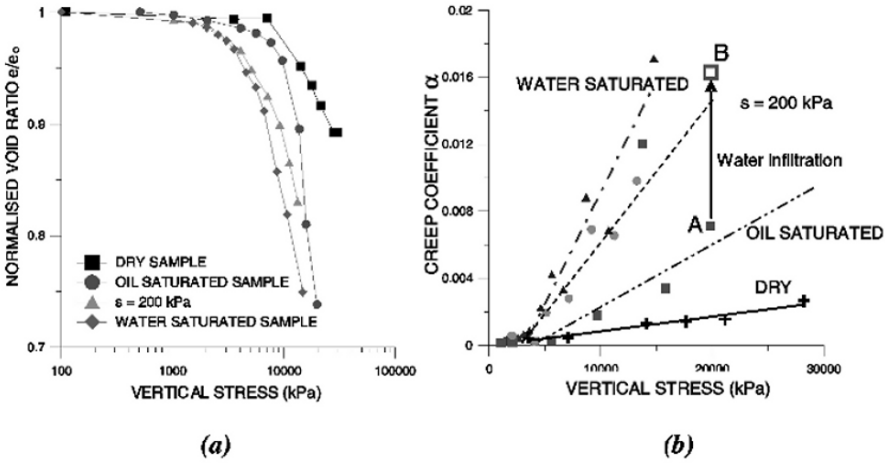

Fig. 2. (**a**) Compression curves of Lixhe chalk at various saturation states; (**b**) Influence of stress level and suction on the creep coefficient α

higher α_i the larger the time dependent strain. Typical values of α_i are between 0 (no time dependency) and 0.02. Note that equation (1) bears strong similitude with the common interpretation in term of creep coefficient $C_{\alpha e}$ when using a logarithmic time scale ($C_{\alpha e} = \Delta e / \Delta \log t$). As shown in Fig. 1**b**, the interpolation given by equation (1) satisfactorily fits the experimental data. This was verified, with minor exceptions, for all the analysed consolidation curves.

The creep strain rate evolution law presented in dotted line in Fig. 1**b** has been obtained by deriving equation (1) with respect to time. Good agreement is als observed with experimental data. This allows identifying the creep rate at each creep phase (right axis in Fig. 1**b**).

Stress-Void Ratio Relationship

In the absence of any apparent pore pressure dissipation phase, it was necessary to adopt a strain criterion to define the stress strain curves. In the case of isochronous time dependent behaviour (i.e. only dependent of the loading duration t_c), the strain after a loading duration t_c can be adopted (Bjerrum 1967). In the alternative case of isotach behaviour (i.e. only dependent on the strain rate $\dot{\varepsilon}$), the strain adopted corresponds to a given creep rate ($\dot{\varepsilon}_c$) (Šuklje 1957 in Leroueil 2006). This second approach was adopted here with $\dot{\varepsilon}_c = 10^{-10}\,\mathrm{s}^{-1}$. This value was chosen based on the accuracy limit of the LVDT used to measure the vertical displacement. The values of e determined at each loading stage with this approach correspond to given couples of α_i and β_i values.

The compression curves obtained are presented in Fig. 2**a**. Like in unsaturated soils, the higher the suction (i.e. the lower the degree of saturation in water S_{rw}), the higher the yield stress, in good agreement with the water weakening effect. In contrast to unsaturated soils, the plastic compression modulus appears to be slightly suction dependent. Note however that it is smaller in the case of the dry sample. This shows that the fluid chemistry and the chalk wettability to fluids (oil, water, air) influence the mechanical behaviour.

Creep Evolution

Since relation (1) is valid for all the saturation states, the α_i and β_i coefficients have been assessed at all the loading stages of the four tests of Fig. 2**a**. The values of the creep coefficients α_i are plotted with respect to the corresponding applied vertical stress in Fig. 2**b**. A careful examination of the plots (between 5 and 10 MPa) shows that they are bilinear with a change in slope that approximately corresponds with the yield stress observed in Fig. 2**a** (not shown here in more detail for lack of space). Above 5 MPa, α_i increases with increased stress and decreased suction, starting from a fully water saturated state ($s = 0$ and $S_{rw} = 100\%$), passing through a partially saturated state ($s = 200$ kPa and $S_{rw} = 30\%$) up to a dry state. This is again consistent with the water weakening effects discussed in the previous sections.

Relatively few creep tests on unsaturated materials have been presented in the literature. Similar effects of suction and stress on creep were also documented from oedometer tests carried out on a partially saturated rockfill (Alonso et al. 2005). However, the generalization of these findings to all possible stress states is an open issue.

The effect of water injection in a chalk sample saturated with oil under a constant vertical stress of 19.8 MPa is shown in Fig. 2**b**. This situation is somewhat similar to that prevailing during waterflooding, a technique of enhanced oil recovery used in the North Sea. The sample was injected under a 10 kPa water pressure and it exhibited a collapse that occurred within a few hours. A more pronounced creep characterised by a α_i coefficient of 0.0164 was then observed. Starting from the oil saturated plot of Fig. 2**b** with a α_i value of 0.0047 at point A, the path followed in this diagram leads to point B (0.0164). It is observed that point B is located close to the $s = 200$ kPa line. This is related to the residual saturation in oil ($S_{ro} = 30\%$) that probably has an effect on the macroscopic creep behaviour of the chalk through the physics of the intergrains bonds. In other words, there is apparently a difference between two samples at zero suction between a fully saturated sample and a sample with a residual oil content. Hysteresis effects may also play a role in this difference.

Conclusion

The experimental data presented in this paper were aimed at showing some effects of suction on the compressibility and on the time dependent behaviour of a sample used as a model of a multiphase oil reservoir chalk. Some similarities with the behaviour of unsaturated soils have been observed, the non wetting fluid in chalk being oil as compared to air in unsaturated soils. Chalk strength is increased by increasing the suction level, i.e. by decreasing the water content. Time dependent strains have been related to the changes in water saturation by means of the oil–water suction. Some aspects of the water weakening effect in chalk, including time effects, have been considered in a more comprehensive framework based on the use of the oil-water suction as an independent stress variable capable to account for the fluid-rock interactions.

Acknowledgements

The work carried out was conducted in relation with the European Project Pasachalk 2 (EC contract ENK6–2000–00089) in the framework of the first author's PhD thesis that was supported by a grant from Ecole des ponts, Paris. The first author is now in NTNU Trondheim with the support of the "Marie Curie" RTN "AMGISS" network (MRTN–CT–2004–512120). The second and third authors wish to acknowledge the support of the EU via the "Marie Curie" RTN "MUSE" network (MRTN–CT–2004–506861).

References

Alonso EE, Olivella S, Pinyol NM (2005) A review of Beliche dam. Géotechnique 55(4):267–285

Biot MA (1941) General theory of three-dimensional consolidation, J Appl Phys 12:155–164

Bjerrum L (1967) Engineering geology of Norwegian normally-consolidated marine clays as related to settlement of buildings, Géotechnique 17:81–118

De Gennaro V, Delage P, Cui YJ, Schroeder Ch, Collin F (2003) Time-dependent behaviour of oil reservoir chalk: a multiphase approach, Soils and Foundations 43(4):131–148

De Gennaro V, Delage P, Priol G, Collin F, Cui YJ (2004) On the collapse behaviour of oil reservoir chalk, Géotechnique 54(6):415–420

De Gennaro V, Delage P, Sorgi C, Priol G, Collin F (2005) Time dependent compression behaviour of two chalks, In: Proc 11th Int Conf Int Ass of Comp Meth Adv Geomech (IACMAG), Torino, Italy, June 2005:34–42

Delage P, Suraj De Silva GPR, Vicol T (1992) Suction controlled testing of non saturated soils with an osmotic consolidometer. In: 7th Int Conf Expansive Soils, Dallas:206–211

Delage P, Schroeder C, Cui YJ (1996) Subsidence and capillary effects in chalks. In: EUROCK'96, Prediction and performance on rock mechanics and rock engineering, Turin, Italy 2:1291–1298

Dineen K, Burland JB (1995) A new approach to osmotically controlled oedometer testing. In: Proc 1st Int Conf on Unsaturated Soils UNSAT95, Paris:459–465

Gutierrez M, Oino LE, Hoeg K (2000) The effect of fluid content on the mechanical behaviour of the fractures in chalk, Rock mech Rocks eng 33(2):93–117

Hellmann R, Renders PJN, Gratier J-P, Guiguet R (2002) Experimental pressure solution compaction of chalk in aqueous solutions. Part1. Deformation behaviour and chemistry. In: Hellmann, Wood (eds) Water-Rock Interactions, Ore Deposits, and Environmental Geochemistry: A Tribute to David A. Crerar; The Geochemical Society, Special Publication No 7:129–152

Kassiff G, Ben Shalom A (1971) Experimental relationship between swell pressure and suction, Géotechnique 21:245–255

Leroueil S (2006) The isotache approach. Where are we 50 years after its development by Prof. Sukjle? In: Proc 13th Danube-European Conf on Geotechnical Engineering, Ljubljana 2:55–88

Lord JA, Clayton CRI, Mortimore RN (2002) Engineering in chalk. CIRIA Eds

Masson (1973) La craie. Bulletin des Laboratories des Ponts et Chaussées, Special V190 pp

Mesri G, Choi YK (1985) The uniqueness of the End of primary (EOP) void ratio-effective stress relationship. In: Proc 11th Int Conf on Soil Mech and Found Eng, San Fransisco 2:587–590

Newman GH (1983) The effect of water chemistry on the laboratory compression and permeability characteristics of some North Sea chalks, J Petroleum Eng 976–980

Pasachalk1 (2001) Mechanical Behaviour of PArtially and Multiphase SAturated CHALKs Fluid-skeleton Interaction: Main Factor of Chalk Oil Reservoirs Compaction and Related Subsidence. Publishable Final report, European Joule III contract No JOF3CT970033

Pasachalk2 (2004) Mechanical Behaviour of PArtially and Multiphase SAturated CHALKs Fluid-skeleton Interaction: Main Factor of Chalk Oil Reservoirs Compaction and Related Subsidence. Part 2. Publishable Final report, Energy, Environment and Sustainable Development Programme, contract No ENK6–2000–00089

Priol G (2005) Comportement mécanique différé et mouillabilité d'une craie pétrolifère. ENPC, PhD Thesis

Risnes R, Madland MV, Hole M, Kwabiah NK (2005) Water weakening of chalk-Mechanical effects of water-glycol mixtures, J Petroleum Sci Eng 48:21–36

Schroeder Ch, Bois AP, Maury V, Halle G (1998) Water/chalk (or collapsible soil) interaction: Part II. Results of tests performed in laboratory on Lixhe chalk to calibrate water/chalk models. SPE/ISRM (SPE 47587) Eurock'98, Trondheim

Šuklje L (1957) The analysis of the consolidation process by the isotache method. In: Proc 4th Int Conf on Soil Mech and Found Engng, London 1:200–206

Testing Unsaturated Soil for Plane Strain Conditions: A New Double Wall Biaxial Device

Tom Schanz and Jamal Alabdullah

Laboratory of Soil Mechanics, Bauhaus-University Weimar, Germany
tom.schanz@uni-weimar.de, jamal.alabdullah@uni-weimar.de

Summary. In this paper a new experimental device for unsaturated soil testing is presented. The new Double Wall Biaxial Cell was designed to study the behavior of unsaturated granular material under plane strain conditions. The required calibration of the new device is presented in detail. Saturated soil samples were tested in the new device under isotropic consolidation conditions. The volume changes of the specimen were measured by two alternative methods to check the reliability of the new device. To verify the independent two stress state variables concept proposed by Fredlund and Morgenstern, Null-tests were performed on sand-kaolin mixture specimen. Axis translation technique was used for creating the desired matric suction. The details of the new device and the test procedures are described. The obtained result are presented and discussed in detail.

Key words: plane strain, biaxial, double wall cell, granular material

Introduction

For a saturated soil, one stress state variable is enough to describe the behavior of two phases (solid and fluid/or gas) of soil mass. The stress state variable σ' is defined as $\sigma' = \sigma - u_w$, where σ' is the effective stress, σ is the total stress, and u_w is the pore water pressure. The concept of the effective stress may be the most important principle in soil mechanics.

Unsaturated soil is normally considered as a three-phase system, i.e., solid, gas (air), fluid (water). In 1977 Fredlund and Morgenstern added the contractile skin as a fourth phase and these four phases were used by these two authors in the stress analysis of unsaturated soil on the basis of continuum mechanics.

Several authors tried to define a single stress state variable for unsaturated soil but soil properties were involved in the proposed equations (Corney et al. 1958, Bishop 1959, Richards 1966, Aitchison 1965, 1973). State variables used to describe the state of the stress have to be independent of soil properties (Fung 1977, Fredlund and Morgenstern 1977).

In 1961 Bishop and Donald performed a set of triaxial shear tests on unsaturated silt where the total stress (i.e., cell pressure) σ_3, pore-air pressure u_a, and pore-water pressure u_w were varied by equal amount keeping $(\sigma_3 - u_a)$ and $(u_a - u_w)$ constant. The result of these tests substantiate the concept of using $(\sigma_3 - u_a)$ and $(u_a - u_w)$ as valid stress state variables for this type of test.

Fredlund and Morgenstern (1977) discussed the stress state variables controlling the behavior of unsaturated soil, stated that the stress state variables have to be created from the individual forces components acting on the solid, water and air phases and the air-water contractile skin. The proposed variables are the net stress $(\sigma - u_a)$ and the matric suction $(u_a - u_w)$, where σ is the total stress. In the same work, Fredlund and Morgenstern validated this concept about the stress state variables by a set of null tests. In these tests it has been proven that changing the air, water, and the total pressures causes no changes in the state of the soil as long as the state variables remain constant. Tarantino et al. (2000) investigated these variables using a new laboratory apparatus. Using this apparatus, unsaturated kaolin samples were maintained under a constant state of strain and water content. Keeping the water pressure in the negative range, changes in net stress and matric suction were measure in response to applied changes in pore air pressure. The results confirmed the use of the net stress and the matric suction as stress state variables.

In practice, most common geotechnical problems involve unsaturated soils, such as embankments, earth dams, highways. The state of deformation in several structures (e.g., long retaining walls, strip foundations, embankments) is plane strain state. In fact, unsaturated soil testing equipment normally consist of odometer, shear box, or triaxial cell. There is no equipment (known to authors) to test unsaturated soil specimen in biaxial state. All the biaxial devices found in literature were designed to test saturated or dry soils (Duncan and Seed 1966, Desrues 1984, Vardoulakis and Graf 1985, Drescher et al. 1990, Alshibli et al. 2004).

The double wall cell concept is an important concept in unsaturated soil testing. Several equipment were designed according to the double wall concept. First double wall cell was presented by Bishop and Donald in 1961. Later, several researchers presented different designs of the double wall cell (Wheeler 1986, 1988, Cui and Delage 1996, Geiser et al. 2000, Toyota et al. 2001, Ng et al. 2002, Aversa and Nicotera 2002, Yin 2003, Sivakumar et al. 2004).

The New Biaxial Double Wall Cell

The new device consists of double-wall cell made of high quality acrylic where the outer cell is reinforced with metal bands, two immovable walls to attain the plane strain conditions, some accessories such as special mould for sample preparation, special rectangular membrane, and metal plates at the top and the base platen to insure the tightening of the membrane by the O-ring.

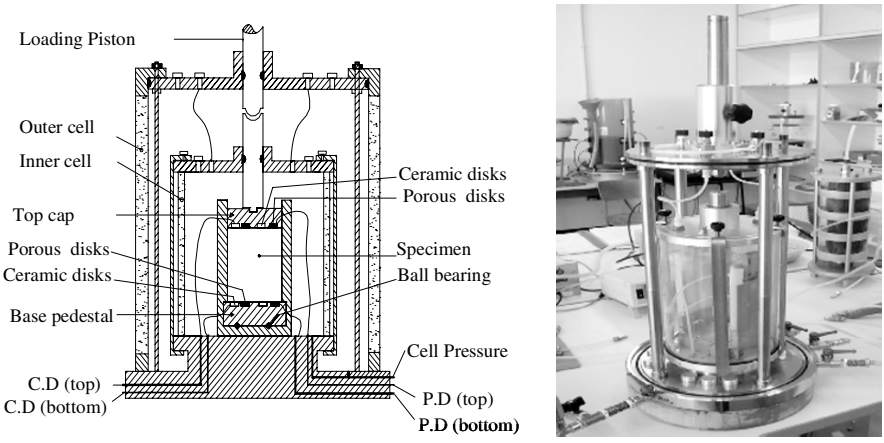

Fig. 1. Double wall biaxial cell

In order to reduce the friction between the base and the soil sample (i.e., end restraint) ball bearings are provided at the base of the sample (Vardoulakis and Goldscheider 1981, Han and Vardoulakis 1991, Alshibli et al. 2004). Teflon sheets with the thickness of 0.25 mm were used to reduce the friction between the membrane and the metal side walls. Figure 1 shows schematic diagram and a photograph of the new double wall biaxial cell.

The sample height is 12 cm and the cross section of the sample is 10 cm × 4 cm. The top pressure pad and the base carry metal plates, each of these metal plates are provided with two ceramic disks and two porous disks.

In the current equipment the ceramic disks have an air entry value of 100 kPa. The diameter of these disks is 1.5 cm and the thickness is 0.5 cm. It is possible to change these metal plates with other plates provided with different ceramic disks, giving the possibility to test the soil in a wide range of matric suction. The porous disks facilitate the application of air pressure, whereas the water pressure is applied through the fully saturated ceramic disks inducing the desired matric suction in saturated soil sample. Both of the water pressure u_w and air pressure u_a can be independently controlled at the top and the bottom of the specimen, so suction gradient can be applied during the test. Layout of the new system is shown in Fig. 2. The dimensions of the inner and outer cell are summarized in Table 1.

Table 1. The dimensions of the inner and outer cell

	Diameter (cm)	Height (cm)	Wall thickness (cm)
Inner cell	17.5	27	0.5
Outer cell	27.0	47	0.8

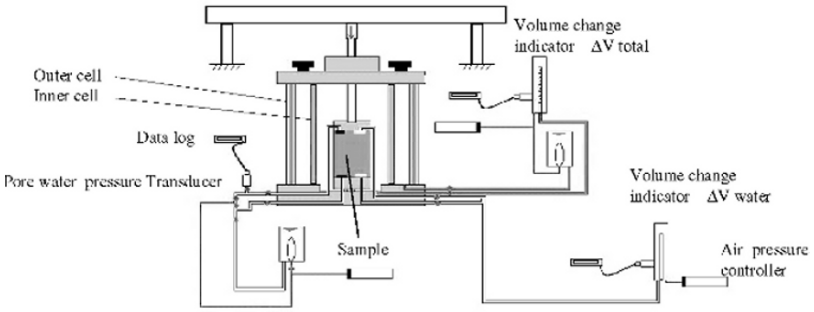

Fig. 2. Layout of the new double wall biaxial cell system

Calibration

Even though the confining pressure is supposed to be the same in the inner and outer cell, several factors may affect, resulting in volume changes of the inner cell. These factors are the flexibility of fittings, time lag in the equalization of the pressures between the inner and outer cell (Leong et al. 2003), compressibility of the water, temperature fluctuation, absorption of the water by the acrylic wall of the inner cell (Wheeler 1988, Sivakumar et al. 2004), and the creep effect of the acrylic inner cell. Another correction should also be considered due to the piston movement inside the inner cell during the compression stage of the test (Sivakumar et al. 2004, Ng et al. 2002).

Inner Cell Expansion Due to the Applied Pressure

The cell volume changes of the inner cell due to the applied pressure was determined by filling the two cells with de-aired water and a dummy metal sample was used. Pressure was applied stepwise. The immediate volume change was recorded five minutes after applying pressure. The calibration curve is presented in the Fig. 3. In the calibration of the inner cell, the pressure was chosen to cover relatively wide range of pressure (0–600 kPa). The hysteresis of the system was examined by performing a test in which the cell pressure was increased from zero to 600 kPa, then the pressure was reduced to zero following the same loading path. Figure 3 shows good repeatability of the inner cell volume change during the loading and unloading process, and no hysteresis was observed.

Calibration of the Inner Cell Using a Saturated Soil Specimen

The reliability of the system was checked by testing a saturated sample in isotropic consolidation test. For a saturated sample, the volume change of the

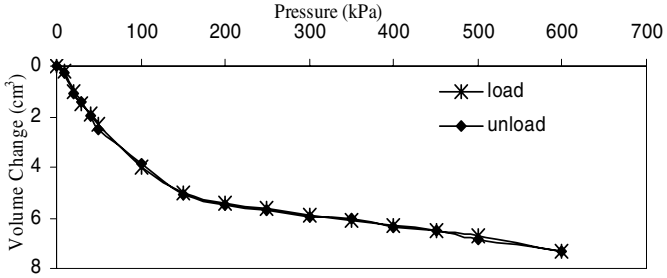

Fig. 3. Calibration of the inner cell (loading and unloading)

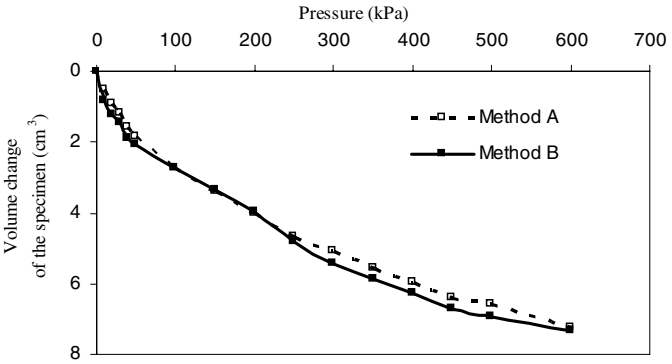

Fig. 4. Volume changes of saturated soil sample measured by two methods A, B

specimen during the test (i.e., total volume change) is equal to the volume of the water drained out of the specimen.

A saturated Hostun sand (Schanz 1998, Flavigny et al. 1990) specimen was prepared, the initial void ratio e_0 was 0.72. The cell pressure was applied simultaneously to the outer and inner cell (isotropic consolidation conditions). The volume changes of specimen were measured using two methods. In method A the double wall cell technique was used (i.e., by measuring volume changes of the inner cell). Whereas in method B the volume of the water expelled out of the specimen was measured using a burette with accuracy of 0.1 cm^3. Figure 4 shows the volume changes measured by the two methods. No significant differences were observed between both method A and B.

Verification of Two Independent Stress State Variables Concept

Two null tests were conducted for a equalized soil sample under specific stress state. The test is termed *null*, because the expected result is to measure no volume changes due to the change in the values of the individual pressures.

It is difficult to measure zero volume change over a long period of time, so it is expected to measure a slight volume changes due to several factors such as imperfect testing procedure, air diffusion through the ceramic disk, water loss of the specimen through the evaporation or diffusion, secondary consolidation (Fredlund and Morgenstern 1977).

Null tests were performed on Hostun sand-kaolin mixture specimen, the mixture consists of 10% kaolin and 90% sand. The initial void ratio was 0.56, coefficient of uniformity 1.95, and $d_{50} = 0.35\,\text{mm}$. The specimen was compacted in the special mold, then it was saturated using back pressure method. The back pressure value at the end of saturation stage was 60 kPa and cell pressure was 70 kPa. The axis translation technique was used to create the matric suction in the soil specimen. The specimen was equalized under these pressure: cell pressure of 80 kPa, air pressure of 70 kPa, and water pressure of 60 kPa. Thus the net stress $(\sigma - u_a) = 10\,\text{kPa}$, and the matric suction $(u_a - u_w) = 10\,\text{kPa}$.

Equilibrium was reached after four days (i.e., when neither volume changes of the specimen nor water volume changes were observed), then the individual pressures were changed with the same increment so that the stress state variables remain always constant and equal to their initial values. Air pressure was applied through the porous disks, while water pressure was applied through ceramic disks with high entry value of 100 kPa. Both of water and air pressure were applied at the top and the bottom of the specimen. Table 2 shows the different pressure values and the corresponding stress state variables used in the tests.

Table 2. Pressures values (kPa) in the null-tests

	σ	u_a	u_w	$(\sigma - u_a)$	$(u_a - u_w)$
Test 1	100	90	80	10	10
Test 2	250	240	230	10	10

Figure 5 shows the total volume changes and the water volume changes measured in a period of two days.

To check the effect of the possible creep of the inner cell, two tests without samples were conducted at constant cell pressure (100, 250 kPa), and the volume changes of the inner cell were recorded for two days.

Volume change versus time plots show that the volume of the specimen remain almost constant in the period of two days after taking into consideration the volume change due to the creep of the inner cell. The volume changes due to the creep of the inner cell were subtracted from the apparent volume changes.

The maximum measured overall volume change (i.e., volumetric strain ε_v) was 0.07%. The water volume changes which were measured as water leaving

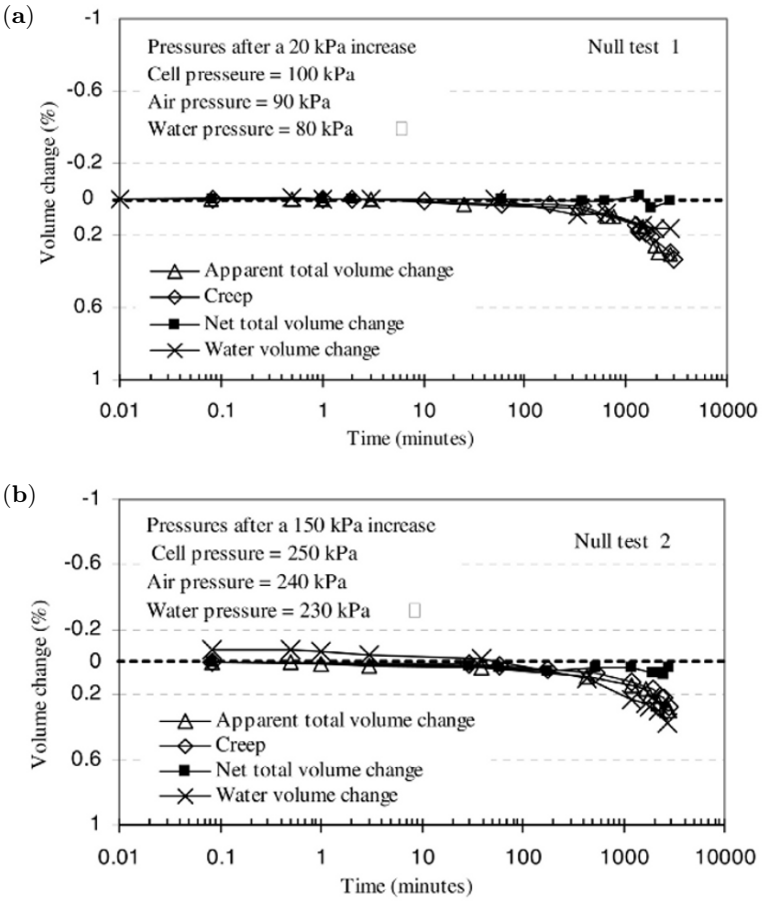

Fig. 5. (**a**) Volume change versus elapsed time in null test No. 1; (**b**) Volume change versus elapsed time in null test No. 2

the specimen during the test, could be contributed to the diffusion of the air to the water phase of the specimen (Fredlund and Morgenstern 1977). Figure 5 shows the measured volume changes due to the creep of the inner cell. The creep of the inner cell in this double wall cell system could be demonstrated by taking some factors into consideration such as the expansion of the tubing, the absorption of the water by the inner acrylic cell walls, and the compressibility of the walls of the inner cell due to the compressive stress applied at both sides of the wall.

To evaluate the accuracy of the volume change measurement, the corrected volumetric strain ε_v can be given by: $\varepsilon_v = \varepsilon_{vm} \pm \beta$, where ε_v is the corrected volumetric strain, ε_{vm} is the measured volume change, and β is the absolute

error. The value of $\beta = 0.1\%$ was proposed by Geiser et al. (2000) as an accepted absolute error in measuring the volumetric strain in triaxial tests on unsaturated soils Leong et al. (2003).

Conclusions

In this paper, the new developed double wall biaxial cell is presented with the required calibration tests. The calibration tests using saturated soil specimen show that the system is capable to measure the volume changes of the specimen according to the double wall cell technique. The observed error in measuring the volume changes of the saturates soil specimen was 0.01–0.07%. The maximum measured volumetric strain of the specimen in the null tests on sand-kaolin mixture specimen was about 0.07%. Regarding to the accepted absolute error proposed by Geiser et al. (2000), the measured values in the new device could be accepted.

The null tests results shown in Fig. 5, strongly support the use of the net stress and the matric suction as two independent stress state variables to describe the behavior of unsaturated soil. The significant amount of creep shown in Fig. 5 underlines that the creep of the inner cell in a double wall system should be taken into consideration in the analysis of the tests results regarding the volumetric strain.

Acknowledgements

The present work was carried out in the frame of the DFG-research project Mechanik teilgesättigter Böden (Mechanics of unsaturated soils). An acknowledgement is given to the research assistantship provided by the Bauhaus-Universität Weimar Germany through the research grant from Deutsche Forschungsgemeinschaft (DFG), FOR 444/2.

References

Aitchison GD (1973) The quantitative description of the stress deformation behavior of expansive soils. In: Proc 3rd Int Conf Expansive Soils (Haifa, Israel) 2:79–82

Aitchison GD (ed) (1965) Moisture Equilibria and moisture changes in soils beneath covered areas. A Symp in print. Butterworth, Australia, 278 pp

Alshibli KA, Godbold DL, Hoffman K (2004) The Louisiana Plane Strain Apparatus for Soil Testing, Geotech Test J 27(4):1–10

Aversa S, Nicotera MV (2002) A triaxial and oedometer apparatus for testing unsaturated soils, Geotech Test J 25(1):3–15

Bishop AW (1959) The principle of effective stress (Lecture delivered in Oslo, Norway, in 1955), Teknisk Ukeblad, 106(39):859–863

Bishop AW, Donald IB (1961) The experimental study of partly saturated soils in the triaxial apparatus, Proc 5th Int Conf on Soil Mechanics and Foundation Engineering, Paris 1:13–21

Corney D, Coleman JD, Black WPM (1958) Movement and distribution of water in soil in relation to highway design and performance. Water and Its Conduction in Soils, Highway Res Board, Special Report, Washington, DC, No. 40:226–252

Cui YJ, Delage P (1996) Yielding and plastic behaviour of an unsaturated silt, Geotechnique 46(2):291–311

Drescher A, Vardoulakis I, Han C (1990) A biaxial apparatus for testing soil, Geotech Test J 13:226–234

Duncan J, Seed HB (1966) Strength variation along failure surfaces in clay, Proc Am Soc Civ Engrs 94(SM6):81–104

Desrues J (1984) La localization de la deformation dans les materiuax granulaires, PhD Thesis, UJF–INP6 Grenoble

Flavigny E, Desrues J, Palayer B (1990) Note technique: Le sable d'Hostun RF, Rev Fran C Geotech 53:67–70

Fredlund DG, Morgenstern NR (1977) Stress state variables for unsaturated soils, J Soil Mech Found Div 103:447–466

Fung YC (1977) Afirst course in continuum mechanics, 2nd ed. Prentice-Hall, Englewood Cliffs, NJ 340 pp

Geiser F, Laloui L, Vulliet L (2000) On the volume measurement in unsaturated triaxial test, Proc Asian Conf Unsat Soil:669–679

Han C, Vardoulakis IG (1991) Plane-strain compression experiments on water-saturated fine-grained sand, Geotechnique 41(1):49–78

Leong EC, Agus SS, Rhardjo H (2003) Volume change measurement of soil specimen in triaxial test, Geotech Test J 27(1):47–66

Mokni M, Desrues J (1998) Strain localization measurements in undrained plane-strain biaxial tests on hostun RF sand, Mechanics of Cohesive-Frictional Materials 4:419–441

Ng CWW, Zhan LT, Cui YJ (2002) A new simple system for measuring volume changes in unsaturated soils, Can Geotech J 39:757–764

Richards BG (1966) The significance of moisture flow and equilibria in unsaturated soils in relation to the design of engineering structures built on shallow foundations in Australia. Symp on permeability and capillary, Amer Soc Testing Material, Atlantic City, NJ

Schanz T (1998) Zur Modellierung des mechanischen Verhatltens von Reibungsmaterialien, Mitteilung 45, Institut für Geotechnik, Universität Stuttgart

Sivakumar R, Sivakumar V, Blatz J, Vimalan J (2004) Twin-Cell Stress Path Apparatus for Testing Unsaturated Soils, Geotech Test J 29(2):175–197

Tarantino A, Mongiovi L, Bosco G (2000) An experimental investigation on the independent isotropic stress variables for unsaturated soils, Geotechnique 50(3):275–282

Toyota H, Sakai N, Nishimura T (2001) Effect of stress history due to unsaturation and drainage conditions on shear properties of unsaturated cohesive soil, Soils and Foundations 41(1):13–24

Vardoulakis I, Goldscheider M (1981) Biaxial apparatus for testing shear bands in soils, Proc 10th Int Conf Soil Mech Fndn Engng, Stockholm 4:819–824

Vardoulakis I, Graf B (1985) Calibration of constitutive models for granular materials using data from biaxial experiment, Geotechnique 35(3):299–317

Wheeler SJ (1986) The stress-strain behavior of soils containing gas bubbles. PhD Thesis, Oxford University, Oxford, U.K.

Wheeler SJ (1988) The undrained shear strength of soils containing a large gas bubbles, Geotechnique 28(3):399–413

Yin JH (2003) Double cell triaxial system for continuous measurement of volume change of an unsaturated or saturated soil specimen in triaxial testing, Geotech Test J 26(3):353–358

Yin ZZ (ed) (1998) Settlement and consolidation of soil mass. China Electric Publication House (in Chinese)

Influence of State Variables on the Shear Behaviour of an Unsaturated Clay

Viktoria Schwarz, Andreas Becker, and Christos Vrettos

Division of Soil Mechanics and Foundation Engineering, Technical University of Kaiserslautern, Kaiserslautern, Germany
vschwarz@rhrk.uni-kl.de, becker@rhrk.uni-kl.de, vrettos@rhrk.uni-kl.de

Summary. Suction is one important parameter affecting the shear behaviour of partially saturated soils. State variables such as void ratio and degree of saturation control the development of suction. A series of deviatoric triaxial tests on kaolinite clay with direct measurement of suction are reported. An appropriate elasto-plastic constitutive for this type of soil is presented and its parameters are determined from the test results.

Key words: clay, constitutive model, shear behaviour, triaxial tests

1 Introduction

The shear behaviour of partially saturated cohesive soils is strongly affected by the value of suction. Work done in the past on this subject refers mainly to triaxial tests with controlled value of suction (Blatz and Graham 2003). The constitutive laws derived from these tests are based on extended Cam-clay models whereby the suction is explicitly included as an independent stress component (Alonso et al. 1990, Wheeler and Sivakumar 1995).

An alternative formulation is adopted in the present study. Following Bishop's equation (Bishop 1959) the variation of effective stresses with suction is given by:

$$\sigma' = (\sigma - u_a) - (u_a - u_w) \cdot \chi \,. \tag{1}$$

In this equation σ' denotes the effective stresses, σ = the total stresses, u_a = the pore air pressure, u_w = the pore water pressure (negative valued) and χ = a factor that depends on soil type and degree of saturation. An appropriate elasto-plastic constitutive soil model for clays can thus be formulated directly in terms of effective stresses for different values of the degree of saturation. The model in its general form has been previously applied to describe the behaviour of unsaturated cohesionless soils, cf. Weckbecker (1993) and Becker (2002). A survey of models for unsaturated soils considering Bishop's stress representation is given by Khalili et al. (2004).

A series of triaxial tests have been carried out for this purpose whereby suction is directly measured during the tests and effective stresses are determined by equation (1).

In the following, the testing procedure is described, the proposed constitutive relation is presented and its appropriateness for modeling the material behaviour is shown.

2 Triaxial Tests

A series of triaxial tests using a kaolinite clay of high plasticity have been carried out. The material properties are summarized in Table 1.

Table 1. Material parameters of the kaolinite clay

Clay minerals	Kaolinite $> 40\%$ Illite $< 20\%$ Smectite $< 5\%$
Liquid limit	$w_L = 54.0\%$
Plastic limit	$w_P = 21.3\%$
Water absorption value after 4 h	$w_A = 73.5\%$

The triaxial apparatus developed especially for the study as well as the specimen preparation technique is described in detail by Schwarz et al. (2006). Shear behaviour has been investigated in dependency of the initial void ratio e_0 and the degree of saturation S_r at distinct values 0.68/0.78/0.83 and 0.85/0.9/1.0, respectively. This range has been chosen in order to avoid high initial suction values and the application of the time-consuming axis-translation-method.

Specimens were loaded up to the specified consolidation stress and then consolidated until the measured suction value reached an almost constant level. The consolidation stresses are defined in terms of the first stress invariant I_σ as follows

$$I_\sigma = \sigma_{11} + \sigma_{22} + \sigma_{33} \tag{2}$$

where σ_{11}, σ_{22} and σ_{33} are the principal stresses.

Tests at two values I_σ equal to 300 kPa and 900 kPa are reported herein. At the low stress level only compression tests have been conducted while at the high stress level both compression and extension tests were possible. All tests were performed under drained conditions with a strain rate of 0.01 mm/min for compression and 0.005 mm/min for extension, respectively.

3 Constitutive Relation

A conventional elasto-plastic model is adopted here that is based on a proposal by Stutz (1973). The yield surface has the general form

$$f = II_s^{\frac{1}{2}} - A \cdot I_\sigma \left(1 - B\frac{III_s}{II_s^{\frac{3}{2}}}\right)^{-m} = 0 \tag{3}$$

where

$$II_s = s_{ij} \cdot s_{ji} \tag{4}$$

and

$$III_s = s_{il} \cdot s_{lj} \cdot s_{ji} \tag{5}$$

with s_{ij} denoting the deviatoric stresses.

A, B and m are parameters to be determined from appropriate triaxial tests. Parameter A is a function of e_0 and I_σ. B is a constant while m is given by the following relation:

$$m = \frac{\zeta}{\ln\left(1 - \frac{B}{\sqrt{6}}\right)} \tag{6}$$

where ζ is a constant.

The stress-strain-relationship within the yield surface during unloading and reloading is assumed to be nonlinear elastic. Triaxial tests not reported herein have shown that the associated values of bulk modulus K as well as shear modulus G depend on the stress state, the void ratio, and the degree of saturation.

The parameter A strongly depends on the initial void ratio e_0, while the dependency on I_σ is neglected at the present stage. The following linear relation is assumed:

$$A = \kappa \cdot e_0 + \xi\,. \tag{7}$$

The tests reported here refer to $S_r = 0.9$ and $I_\sigma = 900\,\text{kPa}$. For this set of values we obtain $\kappa = -0.31$ and $\xi = 0.47$. The influence of S_r on κ and ξ is part of the ongoing investigation. The tests further show that the effect of e_0 on the parameter B is very weak and can be neglected. Here, $B = -0.88$ and $\zeta = 0.12$, that yields from equation (6) a value $m = 0.39$.

Figure 1 shows the quality of the approximation via the constitutive model described above by comparing results from five single tests.

For computing the plastic strain increments $\mathrm{d}\varepsilon_{ij}^P$ we assume an associated flow rule

$$\mathrm{d}\varepsilon_{ij}^P = \lambda\{h\} \tag{8}$$

with λ denoting the unspecified (positive) scalar multiplier, and

$$\{h\} = \left\{\frac{\partial f}{\partial s_{ij}} - \left(\frac{\partial f}{\partial s_{ii}} - D\right)\frac{\delta_{ij}}{3}\right\}, \tag{9}$$

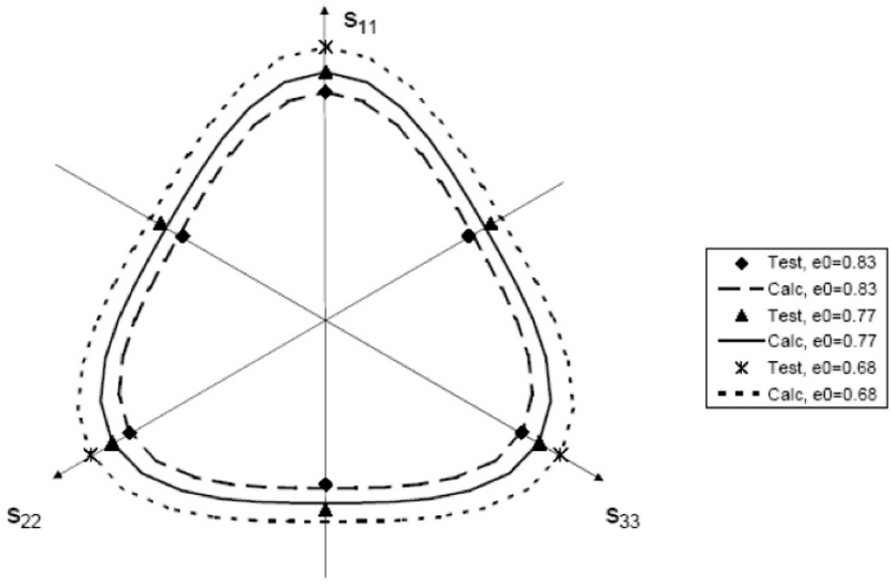

Fig. 1. Test results at failure and prediction by constitutive law in the deviatoric plane for $I_\sigma = 900\,\text{kPa}$, $S_r = 0.9$ at three values of the void ratio e_0

s_{ij}, s_{ii} are the deviatoric stress components and δ_{ij} is Kronecker's Delta.

During hardening λ is assumed to be independent of e_0

$$\lambda = \frac{\left\{\frac{\partial f}{\partial \sigma}\right\}^T [C] \cdot \{\mathrm{d}\varepsilon\}}{\left\{\frac{\partial f}{\partial \sigma}\right\}^T [C]\{h\} - \left\{\frac{\partial f}{\partial e^p}\right\}^T \{h\}} \tag{10}$$

where e^p_{ij} is the plastic deviatoric strain.

The stiffness matrix $[C]$ is defined in terms of the elastic parameters K and G. D is the dilatation parameter defined by

$$D = \frac{\mathrm{d}I_\varepsilon}{\mathrm{d}II^{0.5}_{ep}} \tag{11}$$

with $I_\varepsilon = \varepsilon_{11} + \varepsilon_{22} + \varepsilon_{33}$ and II_{ep} denoting the plastic component of $II_e = e^2_{11} + e^2_{22} + e^2_{33}$ with e_{ii} being the deviatoric strain components.

The test results reported herein show that the dilatation parameter D is almost independent of the degree of saturation and the stress state, as demonstrated in Fig. 2. It can be seen that there is a tendency of increase with increasing void ratio.

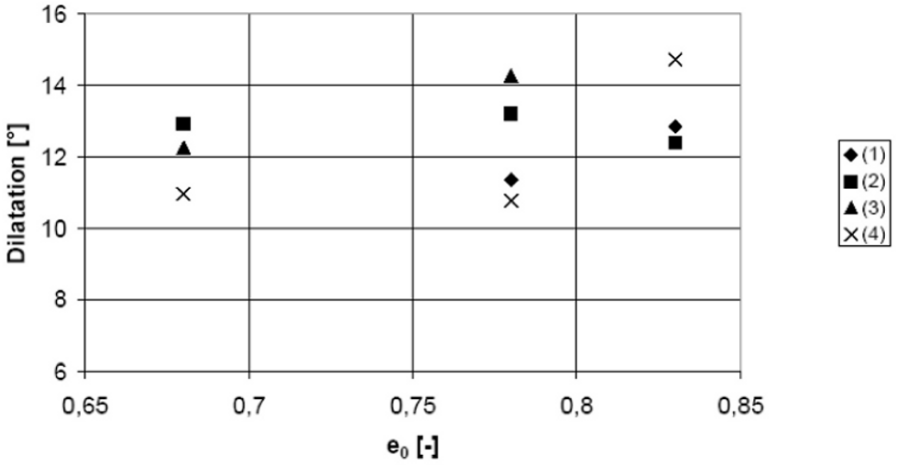

Fig. 2. Variation of the dilatation parameter D with initial void ratio at various combinations of degree of saturation and stress state: (1) $S_r = 0.85$, $I_\sigma = 300\,\text{kPa}$; (2) $S_r = 1$, $I_\sigma = 300\,\text{kPa}$; (3) $S_r = 0.9$, $I_\sigma = 900\,\text{kPa}$; (4) $S_r = 0.85$, $I_\sigma = 900\,\text{kPa}$

4 Conclusions

A constitutive model capable of describing the nonlinear elasto-plastic stress-strain-relationship for partially saturated cohesive soils is presented. Volume change behaviour during deviatoric loading is also included in the present formulation while prediction of collapse is not possible. The effects of initial void ratio and degree of saturation are assessed on the basis of triaxial tests.

Further tests are in progress to investigate the influence of degree of saturation and overconsolidation ratio on the parameters defining the yield surface as well as the dilatation parameter.

Acknowledgment

The presented investigations have been carried out as a part within the research group "Mechanics of partially saturated soils" funded by the German Science Foundation (DFG). This support is greatly appreciated.

References

Alonso EE, Gens A, Josa A (1990) A constitutive model for partially saturated soils, Géotechnique 40(3):405–430

Becker A (2002) Stoffmodell und numerisches Modell für zyklisch beanspruchte, teilgesättigte Sande. Dissertation, FG Bodenmechanik & Grundbau, TU Kaiserslautern

Bishop AW (1959) The principle of effective stress, Tecknish Ukebland 106(39): 859–863

Blatz JA, Graham J (2003) Elastic-plastic modelling of unsaturated soil using results from a new triaxial test with controlled suction, Géotechnique 53(1):113–122

Khalili N, Geiser F, Blight GE (2004) Effective stress in unsaturated soils: Review with new evidence, Int J Geomech, 4(2):115–126

Schwarz V, Becker A, Vrettos C (2006) An initial study on the viscous behaviour of a partially saturated kaolinite clay based on triaxial tests. In: Miller GA, Zapata CE, Houston SL, Fredlund DG (eds) Proc. 4th Int Conf on Unsaturated Soils, Arizona, ASCE, Geotechnical special publication No. 147, pp 1811–1820

Stutz P (1973) Comportement elasto-plastique des milieux granulaires. In: Sawczuk A (ed) Foundations and Plasticity. Noordhoff, Leyden, pp 37–49

Weckbecker W (1993) Beitrag zur Berechnung oberflächennaher Tunnel. Dissertation, Fachgebiet Bodenmechanik & Grundbau, TU Kaiserslautern

Wheeler SJ, Sivakumar V (1995) An elasto-plastic critical state framework for unsaturated soil, Géotechnique 45(1):35–53

Effect of Capillary and Cemented Bonds on the Strength of Unsaturated Sands

Fabien Soulié, Moulay Saïd El Youssoufi, Jean-Yves Delenne, and Christian Saix

Laboratoire de Mécanique et Génie Civil, UMR UMII-CNRS 5508, Université Montpellier II, cc048, place E. Bataillon, 34095 Montpellier cedex 5, France
soulie@lmgc.univ-montp2.fr, elyous@lmgc.univ-montp2.fr, delenne@lmgc.univ-montp2.fr, saix@lmgc.univ-montp2.fr

Summary. The cohesive interactions between grains play a prevailing role in the mechanical behaviour of unsaturated granular materials such as fine sands. These interactions are generally bonds of various natures that evolve according to the surrounding hygrothermic conditions. We study the case where the liquid present in the material is a water solution saturated with sodium chloride. The bonds are then of capillary type and the cohesive interactions are mainly attractive. In this case, the mechanical strength in an unconfined compression test is relatively low. At low relative humidity, the phase change of water involves a crystallization of salt at the contact points between grains generating thus bonds of solid type. The mechanical strength of the material is thus enhanced. An experimental study of the variation of the mechanical strength during the crystallization of salt allowed us to show two distinct cohesive regimes: capillary and cemented. The transition between these two regimes does not seem to be correlated with the mass of the crystallized salt, but rather with the residual degree of saturation. An analysis of these results is proposed by comparison with numerical simulations based on the discrete element approach.

Key words: capillarity, cementation, evaporation, compression test

1 Introduction

In the case of granular soils such as sands, the interstitial liquid can be at the origin of the macroscopic cohesion of material. For low contents of liquid, liquid bridges are formed between grains. The hydrous field corresponding to these contents of liquid is often described as "pendular". The presence of liquid bridges between grains generates attractive capillary forces that appear at the macroscopic scale by a cohesion which is nevertheless relatively weak (Soulié et al. 2006). Under the effects of the surrounding hygrothermic conditions, water can evaporate, thus modifying the concentration in solutes. In cases of extreme concentration, these solutes crystallize, which leads to the

formation of local cemented bonds. This phenomenon creates an improved cohesion at the macroscopic scale, directly related to the cementation degree. The macroscopic mechanical behaviour of granular materials thus results from local phenomena that develop at a local scale. The knowledge of the evolution of the cohesive bonds from a liquid state (liquid bridge) to a solid state (cemented bond) constitutes a major stake for a better understanding of the mechanical behaviour of these materials.

At the local scale, the study of the formation of liquid bridges and capillary forces generated between grains gave rise to an extensive literature and several models of capillary cohesion were proposed (Soulié et al. 2006, Mikami et al. 1998, Willett et al. 2000). The case of cemented bonds was also considered and models of mechanical behaviour of cemented bonds were proposed at the local scale (Delenne et al. 2004).

The objective of this work is to study the mechanical behaviour of a cohesive bond the nature of which evolves according to the environmental conditions. If it is possible to follow, at a local scale, the evolution of a cohesive bond from the liquid state to a solid state during the progressive evaporation of solvent (Farber et al. 2003), it is particularly difficult to study in a same time the evolution of its mechanical behaviour. For this reason, in a first approach, we were interested in the evolution of the macroscopic cohesion of a wet granular material during the evaporation of solvent (water) and thus during the crystallization of the solute (sodium chloride). In this first approach, cohesion will be characterized by the compressive strength of cylindrical granular samples.

2 Experiments: Preparation of the Samples and Protocol of Test

The samples are prepared with Ventoux sand. The sand is first washed and dried, and then filtered to keep only grains the diameters of which are in the range 0.4 mm to 0.8 mm (Fig. 1**a**). This granular material is closely mixed with an aqueous solution including water and a solute that can crystallize during the evaporation of water. The aqueous solution used is saturated with sodium chloride (NaCl) and named in the following saturated brine. This solution contains 35.6 g of NaCl for 100 g of water. The sensitivity of this

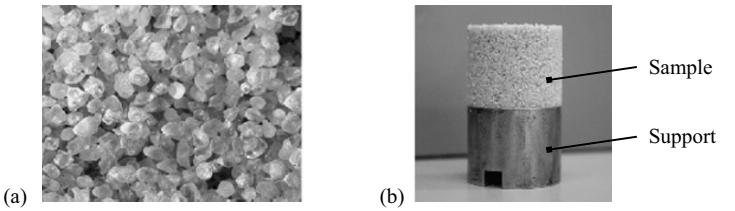

Fig. 1. (**a**) Ventoux sand, (**b**) sample just after preparation

maximum concentration to temperature is low (Kaufmann 1960, Langer and Offermann 1982). The initial gravimetric content of saturated brine of the granular samples is obtained by mixing in a tight box the suitable mass of saturated brine and mass of dry granular material. The samples (diameter 25 mm and height 17 mm, Fig. 1**b**) are prepared in a cylindrical mould.

Hence, each sample is initially a three-phase material including:

- a solid phase (denoted by S) composed of grains (sand),
- a liquid phase (denoted by L) composed of water and dissolved NaCl of mass $m^{\mathrm{L}}_{\mathrm{NaCl}}$.
- a gaseous phase composed of air and water vapor with negligible mass compared to the two other phases.

In this initial state, the samples are particularly delicate to handle since their cohesion and mechanical strength are solely ensured by weak capillary forces between grains. Because of this brittleness, particular experimental precautions were necessary in order to avoid damage to the samples.

According to hygrothermic conditions of the atmosphere, water can evaporate. This leads to a thermodynamic disequilibrium of the solution that results in an excess of NaCl in an already saturated solution. Thermodynamic equilibrium is recovered through the crystallization of NaCl and thus the formation of solid NaCl deposits of a total mass $m^{\mathrm{S}}_{\mathrm{NaCl}}$.

Three series of samples are prepared respectively for three liquid contents of saturated brine: 3%, 5% and 7%. These liquid contents are selected in the hydrous field corresponding to the "pendular state", for which liquid bridges between grains ensure the mechanical integrity of the sample. The samples are weighed just after preparation (the corresponding mass is noted m_i), then put to dry under conditions controlled in temperature $T = 20°\mathrm{C}$ and in relative humidity $\mathrm{RH} = 43\%$.

The samples are taken at various durations varying from 15 minutes to 20 hours, then weighed (mass m_f), before being submitted to an unconfined compression test until rupture. The difference in mass $(m_f - m_i)$ enables us know the mass of evaporated water and thus the mass of crystallized NaCl. The unconfined compression test is carried out using a "low capacity" press allowing to test samples with low dimensions and with forces up to 50 N with an accuracy of 0.01 N.

3 Results and Discussions

The mass of "retained" water in the sample, even after a long time of drying, is proportional to the initial content of saturated brine, and thus to the initial mass of water. For each of the three initial contents of saturated brine, only 93% of the mass of water initially introduced can evaporate. The remainder "is trapped" during the crystallization of NaCl.

The observation of the samples makes it possible to highlight three different localizations of the NaCl deposits:

- a crystallization at the surface of samples, which corresponds to the phenomenon of efflorescence,
- at the surface of the grains, isolated crystals are formed and growth but they do not directly contribute to the creation of cohesive bonds between grains,
- at the contacts between grains, crystals are mobilized in the formation of solid bridges, and then directly contribute to intergranular cohesion.

The tests were carried out on 60 samples. The "low capacity" press allows us to obtain the evolution of the compressive force according to the axial displacement.

Figure 2 presents typical curves of the compressive force versus the axial displacement, for samples with an initial content of saturated brine equals to 5%, for a short time of drying (15 min) and a long time of drying (20 h). The curve obtained for short times of drying shows a continuous evolution of the compressive force with the axial displacement. The deformation of the sample is progressive during the test, the behaviour appears to be of ductile plastic type. The values obtained for the compressive force are relatively low and correspond to a cohesion of capillary type. In the case of a long time of drying, we can observe a peak force with a significant intensity and for a weak axial displacement. The behaviour of this type of samples (cemented ones) is of fragile type: a clear rupture of the sample appears at the same time as the peak force during the compression test. In both cases, the maximum compressive force can be defined without ambiguity. All the samples have the same geometrical configuration, and the maximum compressive force can so be used to characterize the mechanical strength of the granular materials.

Figure 3 presents a synthesis of the 60 tests carried out for the contents of saturated brine 3%, 5%, and 7%. This figure shows the evolution of the maximal force according to the mass of crystallized NaCl. We can note that, whatever the initial content of saturated brine, the obtained results have the

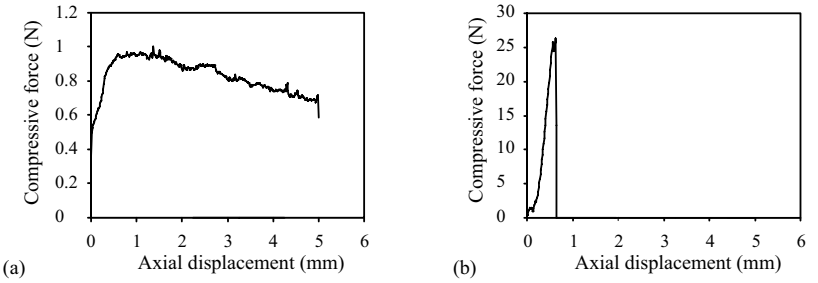

Fig. 2. Compressive force versus axial displacement for samples with an initial content of saturated brine equals to 5%. Duration of drying: (**a**) 15 min, (**b**) 20 h

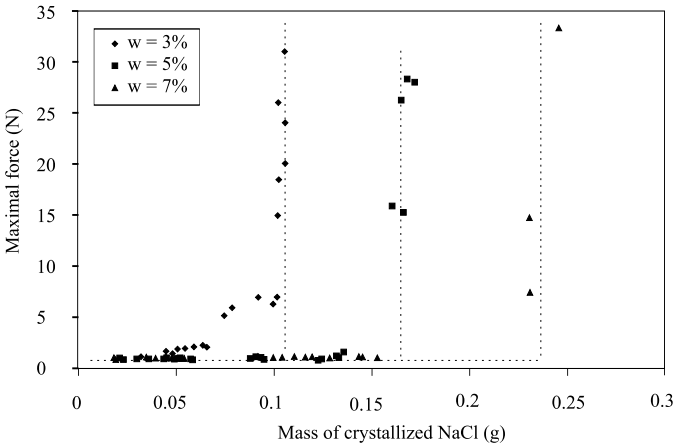

Fig. 3. Maximal compressive forces versus mass of crystallized NaCl for the three initial contents of saturated brine

same feature. At the initial state, the mechanical strength of the granular samples results from the only phenomenon of capillary cohesion, which gets a low cohesion to the material and thus a low rupture strength. Independently of the initial brine content, the rupture strength remains low in spite of the increasing mass of crystallized NaCl. When it reached a critical value, different from the initial brine content, the rupture strength increases considerably reaching values from 30 to 35 times higher than the initial strength.

We can note that the mechanical strength of the granular samples does not depend on the quantity of crystallized NaCl. Indeed, Figure 3 shows, for a same mass of crystallized NaCl, the maximal compressive force is not necessary the same, it also depends on the initial content of saturated brine.

In order to limit the influence of the initial content of saturated brine, we define a crystallization index i_c:

$$i_c = \frac{m^{\mathrm{S}}_{\mathrm{NaCl}}}{m_{\mathrm{NaCl}}} \tag{1}$$

where m_{NaCl} is the NaCl mass present in the sample ($m_{\mathrm{NaCl}} = m^{\mathrm{S}}_{\mathrm{NaCl}} + m^{\mathrm{L}}_{\mathrm{NaCl}}$). This index is equal to 0 if NaCl is completely dissolved and equals to 1 if all the NaCl is crystallized. The variation of the maximal compressive force according to the crystallization index is presented in Fig. 4 for the three initial contents of saturated brine. This figure clearly highlights the existence of two zones:

- the first zone for which the maximal force seems to be constant and thus does not depend on the mass of crystallized NaCl,
- the second zone for which the maximal force sharply increases for $i_c \geq 0.85$.

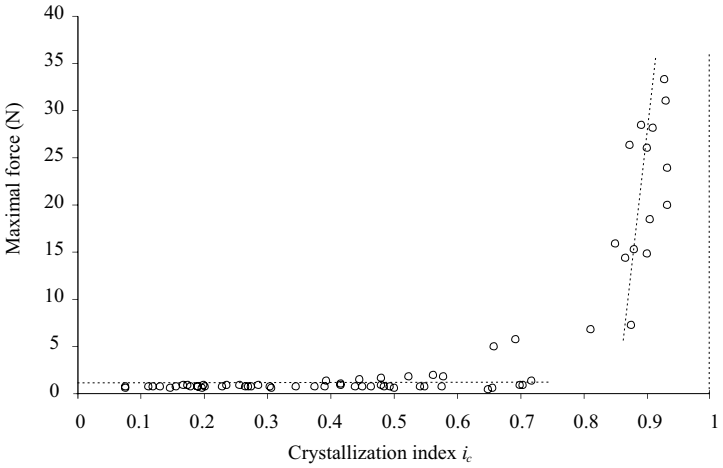

Fig. 4. Maximal compressive force versus crystallization index for the three initial contents of saturated brine ($w = 3\%$, 5% and 7%)

It is remarkable that these zones are well defined whatever the initial content of saturated brine. They correspond to two distinct modes: the capillary mode (first zone) and the cemented mode (second zone). It is also interesting to note that the limit value of the crystallization index (i.e. $i_c = 1$) is never reached. This should be related to the limit value of the mass of water being able to evaporate, which corresponds to 93% of the total mass of water introduced into the sample.

Observations at the local scale of the evolution of bridges showed that a change of nature, from liquid to solid, is a slow complex process. NaCl crystals are initially formed at the liquid-gas interface on grains; these crystals enlarge and support the growth of other crystals and then form a crystalline area which preferentially grows along the liquid-gas interface. This evolution of the cohesive bridges is illustrated in Fig. 5. This type of evolution was also observed for other types of aqueous solutions frequently used by pharmaceutical industry (Farber et al. 2003). Solid cohesion is effective only when the connectivity of the crystallized deposit is established between the two grains, which explains the importance of the capillary zone (first zone in Fig. 4). This importance is also due to the existence of the phenomena of efflorescence and

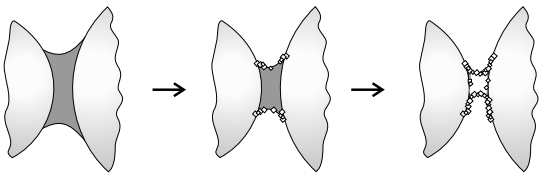

Fig. 5. Schematic representation of the evolution of a bridge of saturated brine

isolated crystallization which form deposits of crystallized NaCl that do not directly contribute to intergranular cohesion.

4 Numerical Approach

A first numerical study is carried out for a better understanding of the behaviour of unsaturated sands during drying. To achieve this, a 2D numerical code, based on the Discrete Element Method initially developed by Cundall and Strack (1979), is used to simulate an unconfined compression test on a 2D polydisperse granular sample the configuration of which is similar to the experimental samples. In addition to the traditional contact and friction interactions between grains, explicit models, formulated at the local scale, allow us to account for the limiting behaviours observed in Sect. 3: respectively, the model of capillary cohesion (Soulié et al. 2006) and of cemented cohesion (Delenne et al. 2004). In the central zone of the samples, the cohesive interactions are of the capillary type, while in the peripheral zone, cohesion is governed by the model of cementation. The thickness of the peripheral zone increases with time, it follows the crystallization front that progresses from the periphery towards the heart of the sample. The rupture thresholds of cemented bonds increases with time, thus representing the hardening of former bonds.

Figure 6 shows the evolution of the normalized maximal force versus the crystallization index both for the experimental case and for the numerical case. The normalized maximal force corresponds to the obtained maximal macroscopic force divided by the maximal macroscopic force at the initial state (just after the preparation of the sample, when the integrity of the sample is only ensured by capillary cohesion). Even if some discrepancies exist, this first

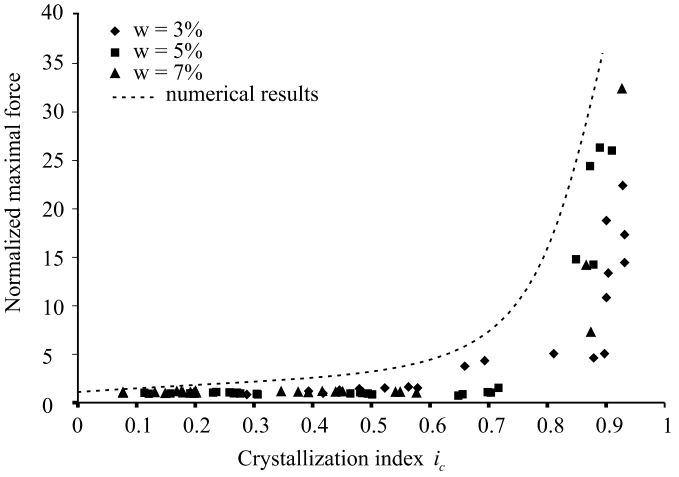

Fig. 6. Numerical results versus experimental results

numerical study in a 2D configuration supplies results in good agreement with experimentally obtained data. Such a kind of approach should be extended to other configurations, especially to 3D situations.

5 Conclusion

An experimental study made it possible to estimate the effect of the crystallization of a solute (NaCl) on the mechanical resistance of an unsaturated sand. The results obtained clearly showed the existence of two markedly distinct modes: a capillary mode and a cemented mode. In order to characterize the dependence between mechanical resistance and crystallization, the importance of the crystallization index i_c in the evolution of the maximal compressive force was highlighted.

The influence of the crystallization index was underlined by the successful comparison of experimental results and numerical results supplied by a series of 2D simulations. A thorough study should allow us to complete this analysis in order to specify laws of macroscopic behaviour including physicochemical parameters. The contribution of the discrete approaches is particularly promising to study the scale-up from the physical phenomena at the microscopic scale to the observable behaviour at the macroscopic scale. The objective is to propose a local law of cohesion in the case of a cohesive bond the nature of which evolves according to the environmental conditions. The central idea is to generalize the methodologies employed in the cases of capillarity (Soulié et al. 2006, Willett et al. 2000) and cementation (Delenne et al. 2004, Jiang et al. 2006) to a unified representation of the cohesive bond interpolating between these two limits with internal variables that evolve according to environmental conditions.

References

Cundall PA, Strack ODL (1979) A discrete numerical model for granular assemblies, Géotechnique 29(1):47–65

Delenne JY, El Youssoufi MS, Cherblanc F, Bénet JC (2004) Mechanical behaviour and failure of cohesive granular materials, Int J Numer Anal Meth Geomech 28:1577–1594

Farber L, Tardos GI, Michaels JN (2003) Evolution and structure of drying material bridges of pharmaceutical excipients: Studies on a microscope slide, Chem Eng Sci 58:4515–4525

Jiang MJ, Yu HS, Harris D (2006) Bond rolling resistance and its effect on yielding of bonded granulates by DEM analyses, Int J Numer Anal Meth Geomech 30:723–761

Kaufmann DW, editor (1960) Sodium chloride, the production and properties of salt and brine. Reinhold Publishing Corporation, New York

Langer H, Offermann H (1982) On the solubility of sodium chloride in water, J Cryst Growth 60:389–392

Mikami T, Kamiya H, Horio M (1998) Numerical simulation of cohesive powder behavior in a fluidized bed, Chem Eng Sci 53(10):1927–1940

Soulié F, Cherblanc F, El Youssoufi MS, Saix C (2006) Influence of liquid bridges on the mechanical behaviour of polydisperse granular materials, Int J Numer Anal Meth Geomech 30:213–228

Willett CD, Adams MJ, Johnson SA, Seville JPK (2000) Capillary bridges between two spherical bodies, Langmuir 16:9396–9405

Determining the Shear Strength of Unsaturated Silt

Shulin Sun[1] and Huifang Xu[2]

[1] Department of Geological and Geotechnical Engineering, College of Civil Engineering, Hohai University, 1 Xikang Road, Nanjing 210098, China
slsun@hhu.edu.cn
[2] Department of Geology and Geophysics, University of Wisconsin-Madison, Madison, WI 53706, USA hfxu@geology.wisc.edu

Summary. In order to determine shear strength of fine-grained unsaturated soils, a new design of a shear box for a modified direct shear device is described where a desired matric suctions is added easily with a hanging column. Simple principles were employed to develop the direct shear testing device so that it would be robust, easy to use, and readily assembled and disassembled for testing and maintenance. Tests were conducted with sandy silts under several net normal stresses ($\sigma_n u_a$) for different desired matric suction ($u_a - u_w$). The results show that unsaturated shear strength and friction angle (ϕ^b) is consistent with results from prediction procedure (Fredlund and Barbour 1996) and estimated friction angle (ϕ^b) based on a soil-water characteristic curve (SWCC) of the sandy silt, respectively.

Key words: unsaturated soil, matric suction, direct shear, shear strength, shear box

Introduction

Shear strength of unsaturated soils can be determined by using both laboratory tests and empirical methods. Some experimental methods were conducted by using both the triaxial equipment modified to allow the control or measurement of pore air pressure (u_a) and pore water pressure (u_w) (Ho and Fredlund 1982, Toll 1990, Rassam and Williams 1999), and the modified direct shear devices with suction controls (Escario and Saez 1986, Gan et al. 1988, Nishimura and Fredlund 2001). The experimental studies were of time consuming and difficult to perform although the experiment results were found to be consistent with the shear strength equation proposed by Fredlund et al. (1978) as follows:

$$\tau_f = c + (\sigma_n - u_a)\tan\phi' + (u_a - u_w)\tan\phi^b \tag{1}$$

where

- τ_f is the shear strength of an unsaturated soil;
- c is the effective cohesion of the soil;
- ϕ' is the effective angle of shearing resistance for a saturated soil;
- ϕ^b is the angle of internal friction with respect to the matric suction;
- σ_n is the total stress;
- u_a is the pore air pressure;
- u_w is the pore water pressure;
- $(u_a - u_w)$ is the matric suction;
- $(\sigma_n - u_a)$ is the net normal stress.

Due to the above reason, several semi-empirical shear strength functions were proposed to predict the shear strength of unsaturated soils (Vanapalli et al. 1996, Fredlund and Barbour 1996, Oberg and Sallfors 1997, Khalili and Khabbaz 1997, Bao et al. 1998). Rohm and Vilar (1995) proposed a hyperbolic relationship to fit matric suction and the experimental strength data. Abramento and Carvalho (1989) used an experimental function as a curve-fitting technique for their experimental data. Fredlund and Barbour (1996) provided a means of estimating the shear strength function from the soil-water characteristic curve by using the saturated shear strength parameters as the starting values. These empirical procedures or/and approaches described in the literatures for predicting the shear strength of unsaturated soils, based on limited number of experimental data, may or may not be suitable for all types of soils. This paper is to describe a simple experimental technique to determine the shear strength of unsaturated, fine-grained soils by using modified direct shear testing device that was conventionally used for measuring the shear strength of saturated soils.

A modified direct shear testing device described in this paper is different from those described in literatures (Escario 1980, Ho and Fredlund 1982, Gan et al. 1988, Escario and Juca 1989, Wheerler and Sivakumar 1992, Vanapalli et al. 1996). Gan et al. (1988) proposed control of matric suction with variation of pore air pressure (u_a) and a pore water pressure (u_w) as zero. During a shear testing with Gan et al. (1988) method, a matric suction ($u_a - u_w$) was positive. Cares must be taken to avoid contamination a high air-entry porous disk with vacuum grease and to ensure there were no air leaks in a ceramic disk (Vanapalli et al. 1996). In this paper, the modified direct shear testing device is easy to measure the shear strength of unsaturated soils with different pore water pressures (u_w). A principle that applies desired matric suction to saturated soil specimen is based on the method in ASTM D 6836–03 (2004) and leak-free pressure plate extractor for measuring the SWCC proposed by Wang and Benson (2004), and the matric suction ($u_a - u_w$) is negative pressure during shear testing.

Modified Direct Shear Testing Device

A modified direct shear testing device for measuring shear strength of unsaturated soils is similar to direct shear testing for measuring shear strength of saturated soils. It consists of shear loading device, normal loading device, shear force measurement device, and horizontal and vertical displacement measurement device (Fig. 1). The shear loading device is applied to the specimen with sufficient capacity and controls to deform the specimen at a uniform rate of displacement with an electric motor. A shear force is determined by a shear force sensor. The normal loading device is capable of maintaining constant force for the entire testing duration, and a normal force is applied by a lever loading yoke which is activated by fixed weights. Horizontal and vertical displacement is determined by using displacement transformers.

Shear box. There is a difference between an unsaturated direct shear testing apparatus and a saturated direct shear testing device. The shear box used in unsaturated direct shear testing is able to maintain desired matric suction in the soil specimen during shear testing. It is made of bronze with an outflow port at the bottom for drainage and control of a matric suction (Fig. 2). The

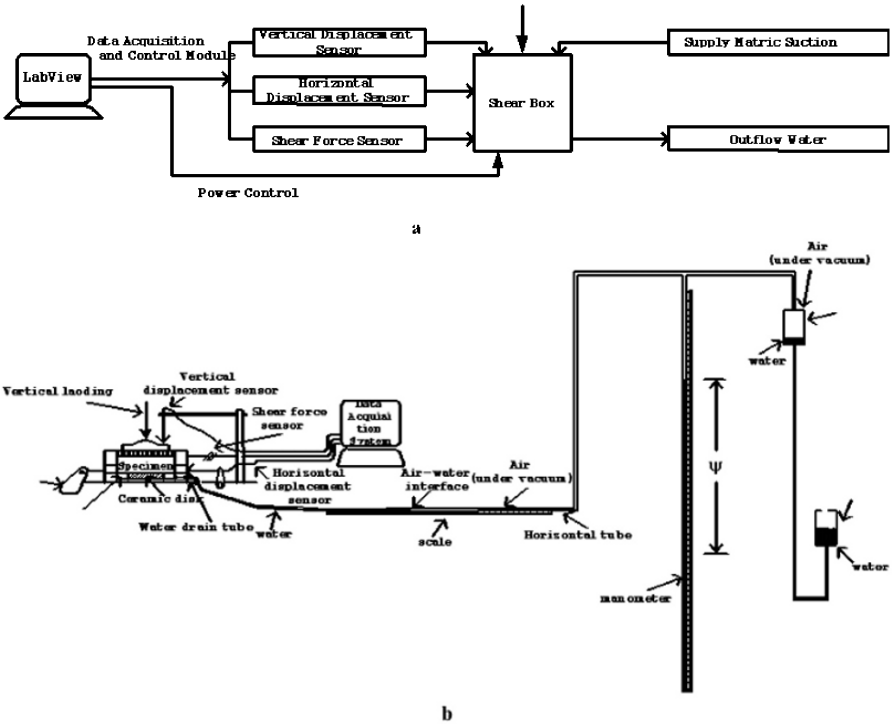

Fig. 1. (a) Flexible boundary direct shear test setup. (b) A negative-pressure unsaturated direct shear testing apparatus

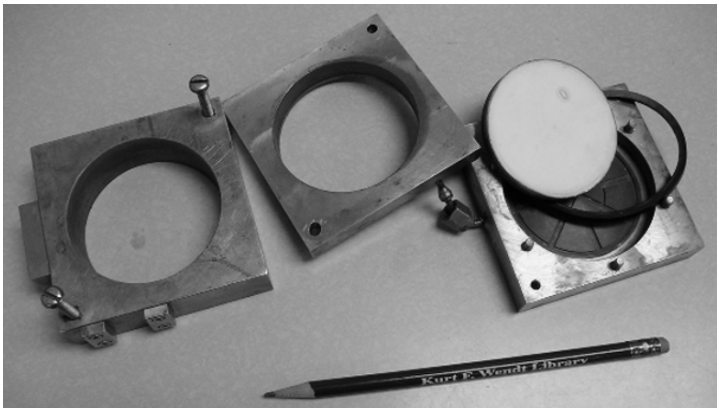

Fig. 2. A Photograph of the unsaturated shear box

shear box is divided vertically by a horizontal plane into two halves of equal thickness which are fitted together with alignment screws. The shear box is also fitted with gap screws, which control the space (gap) between the top and bottom halves of the shear box. The bottom half consists of a Buna-N square O-ring, a ceramic disk, and upper and lower chambers arranged with screws. The Buna-N square O-ring (Wang and Benson 2003), is placed at about the intermediate edge of the ceramic disk between the upper chamber sidewall and the lower chamber base.

Hanging column Adding a matric suction. A saturated specimen adds a suction with hanging column, which is conducted following method A in ASTM D 6836–03 (2004), Standard Test Methods for Determination of the Soil Water Characteristic Curve for Adsorption Using a Hanging Column. The shear box is attached to a small-bore horizontal tube for adding desired matric suction directly by applying a vacuum to the water in the horizontal measurement tube using water reservoirs set at different elevations before shear testing (Fig. 1(**b**)). During the shear testing, the pore air pressure remains at atmospheric pressure and the small-bore horizontal tube measures outflow (Fig. 1(**b**)).

Shear Device, Loading, Shear force measuring, Vertical displacement, and Horizontal displacement as specified in Test Method ASTM D 6836–03 (2004).

Procedures

Before placing the saturated specimen in the shear box, a ceramic disk is saturated by flooding the base of the shear box with some water. The ceramic disk is maintained in water until the removal of air in the ceramic disk, and the water is flushed out through a water drain tube below the ceramic disk. The shear box is dried by using a sponge except the saturated ceramic disk

and the water drain tube. Petrolatum is used at the interface of shear surfaces to ensure that the water did not leak out and friction force at the contacted interface between upper and lower parts of the shear box is set zero.

The saturated soil specimen is placed carefully into the shear box, and then before the desired matric suction applied to the specimen, the horizontal tube is connected with the water drain tube and reading of a air-water interface in the horizontal tube on the scale is recorded after the horizontal tube is poured with small amount of water.

A matric suction ranges provided by the hanging column, is between 0 and 35 kPa. The desired matric suction $(u_a - u_w)$ is added to the specimen by moving a lower reservoir and changing water level showed on a manometer, and the specimen was gradually desaturated with a outflow of water in the specimen through the water drain tube. A reading of the air-water interface is taken when the outflow of water in the specimen ceases. A desired vertical loading does not apply to the specimen until the air-water interface forwarded along the horizontal tube is stable for 1 hr.

When vertical loading is applied to the unsaturated specimen, the water in specimen begins to flow out and the air-water interface moves forward. It may take for about 1 hr that the water stops flowing out, and reading of the interface is taken. After readings from sensors that measure shear force, horizontal and vertical displacement, were checked out, a shear test began with a displacement rate of 0.0096 mm/min. Each unsaturated shear testing takes about $14 \sim 15$ hr with a matric suction and a vertical loading values for each time.

Testing Experiment

Saturated specimen preparation. The 150.6 g dry weight of Boardman soils was taken for the test (Table 1). According to calculation, the water content of a saturated soil specimen is 29.7%, and the weight of water adds to the dry soil specimen for testing is 44.7 g. A saturated soil specimen is made by mixing the dry soil specimen with 44.7 g of water.

Shear box preparation. A ceramic disk at the bottom of a shear box is saturated by filling water into the lower part of the shear box and removing air in the ceramic disk, and a water drain tube connected to the ceramic disk

Table 1. Properties of Boarsman Soil for Tests

Type of a soil	Dry weight Ws (g)	Specific gravity Gs	Dry unit weight γ_d (kN/m^3)	Plasticity ω_P (%)	Water content of saturated soil (%)	Weight of water added (g)
Sandy silt	150.6	2.65	14.52	23	29.7	44.7

is filled with water. An upper part of the shear box is fit to the lower part with screws after petrolatum is used on the contact surface between the upper and the lower. The saturated soil specimen is then put carefully into the shear box.

Adding a desired matric suction. The water drain tube is connected with a horizontal tube filled with water after the shear box is put on a shear machine. Desired matric suction is added to the saturated soil specimen by decreasing a highness of a lower reservoir, and the soil specimen is gradually changed into unsaturated soil specimen with an outflow of water along the water drain tube. The desired matric suction is successfully applied in an hour later after the outflow is ceased. A soil water characteristic curve (SWCC) of the sandy silt was measured and is shown in Fig. 7.

Applied a normal stress. A desired normal stress is applied to the unsaturated soil specimen by using fixed weight while the water was out flowing along the water drain tube. It needs to wait about 1 hr for applying the normal stress.

Shear testing. A shear force sensor, two horizontal and vertical displacement sensors are checked, and screws fitted to the shear box is taken off before shear testing began.

Testing results. The unsaturated direct shear testing is conducted by using four net normal stresses with three matric suctions. The variation of shear strength with net normal stress at different matric suction was displayed in Fig. 3. The x-axis represents the net normal stresses and the y-axis represents the unsaturated shear strength. All the experimental data is shown by using different symbols. Figure 3 shows the straight line with a slope of about 36.9°, which is independent of the matric suction.

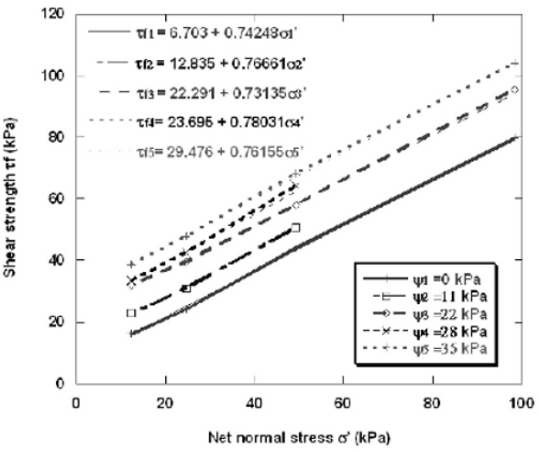

Fig. 3. Shear strength versus net normal stress with different matric suction

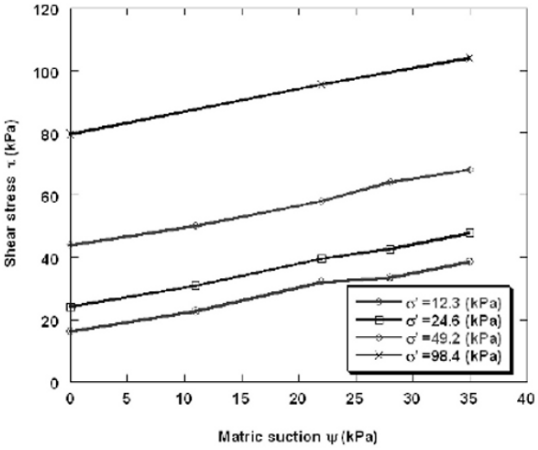

Fig. 4. Shear strength versus matric suction with different net normal stress

Figure 4 presents shear strength in terms of the variation with applied matric suction at different normal stress. The x-axis represents the matric suction, and the y-axis represents the shear strength. The variation in shear strength with respect to matric suction is linear at lower matric suction range, and nonlinear at higher matric suction range. The curves with different normal stress show same trend. The slope of the lines is about 36.6°, and the slope of the nonlinear is less than 36.6°. The shear strength measured is comparable with results from prediction procedure by Fredlund and Barbour (1996). Figure 5 indicates the tendency of measured shear strength basically fits the predicted values.

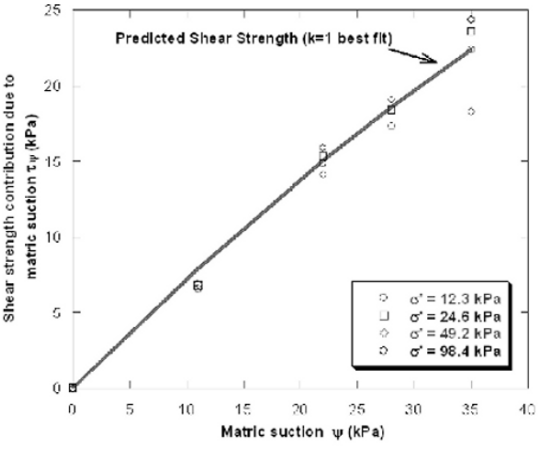

Fig. 5. Comparison between measured and predicted variation of shear strength versus matric suction

Measured frictional angle ϕ^b. According to the results described above (Fig. 3 and Fig. 4), the parameters for the shear strength of unsaturated sandy silt are listed in Table 2 where net normal stress $(\sigma_n - u_a)$ and matric suction $(u_a - u_w)$ are applied to the unsaturated soil specimens, and the shear strength (τ_f) is calculated by using shear force, which is measured with the sensor (Fig. 1) during testing, divided by the shear area. The shear strength (τ_f) equals saturated shear strength (τ_s) when applied desired matric suction is zero. Unsaturated shear strength (τ_ψ) is equal to shear strength (τ_f) minus saturated shear strength (τ_s). The cohesive strength (**c**) taken from Fig. 3 is intercept with the τ_f axis (Fig. 3). The friction angle (ϕ^b) with respect to matric suction is calculated with the equation (2). An average of the effective friction angle (ϕ') for the saturated soil is 36.6°. Figure 6 indicates the variation of ϕ^b with the matric suction. It should be noted that the ϕ^b decreases gradually as the increasing of the desired matric suction, and the ϕ^b is less than the ϕ' of the saturated soil.

$$\phi^b = \arctan\left\{\frac{\tau_f - [c + (\sigma_n - u_a)\tan\phi']}{u_a - u_w}\right\} \tag{2}$$

Table 2. Measured parameter of the shear strength for the unsaturated sandy silts

	Normal stress $(\sigma n - u_a)$ (kPa)	Suction $(u_a - u_w)$ (kPa)	Shear stress τ_f (kPa)	τ_{sat}	τ_ψ	c	$\tan\phi'$	ϕ'	$\tan\phi^b$	ϕ^b
	12.3	0	16.17	16.17	0.00	6.70	0.77	37.59		
	12.3	11	22.76	16.17	6.58	6.70	0.77	37.59	0.60	30.89
Test 1	12.3	22	32.08	16.17	15.90	6.70	0.77	37.59	0.72	35.86
	12.3	28	33.50	16.17	17.33	6.70	0.77	37.59	0.62	31.75
	12.3	35	38.56	16.17	22.38	6.70	0.77	37.59	0.64	32.60
	24.6	0	24.14	24.14	0.00	6.70	0.71	35.33		
	24.6	11	30.95	24.14	6.81	6.70	0.71	35.33	0.62	31.75
Test 2	24.6	22	39.52	24.14	15.38	6.70	0.71	35.33	0.70	34.96
	24.6	28	42.58	24.14	18.44	6.70	0.71	35.33	0.66	33.37
	24.6	35	47.75	24.14	23.60	6.70	0.71	35.33	0.67	34.00
	49.2	0	43.89	43.89	0.00	6.70	0.76	37.09		
	49.2	11	50.80	43.89	6.91	6.70	0.76	37.09	0.63	32.14
Test 3	49.2	22	58.03	43.89	14.14	6.70	0.76	37.09	0.64	32.73
	49.2	28	64.19	43.89	20.30	6.70	0.76	37.09	0.73	35.94
	49.2	35	68.13	43.89	24.24	6.70	0.76	37.09	0.69	34.71
	98.4	0	79.60	79.60	0.00	6.70	0.74	36.53		
Test 4	98.4	22	95.47	79.60	15.87	6.70	0.74	36.53	0.72	35.80
	98.4	35	103.97	79.60	24.37	6.70	0.74	36.53	0.70	34.85

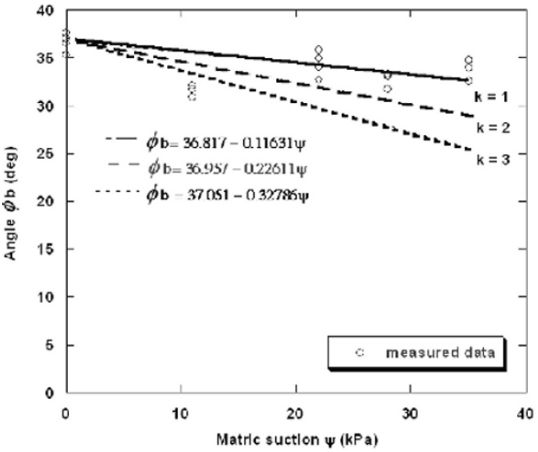

Fig. 6. Measured and estimated friction angles ϕ^b

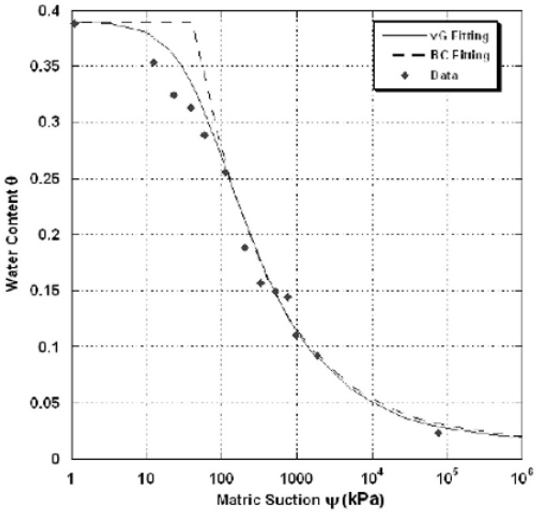

Fig. 7. The SWCC of the sandy silt

Estimated friction angle ϕ^b. The friction angle ϕ^b was estimated from the soil-water characteristic curve (SWCC). According to the estimation the shear strength function provided by Fredlund and Barbour (1996), the estimated formula of ϕ^b is followed:

$$\phi^b = \arctan\left\{\left(\frac{\theta - \theta_r}{\theta_s - \theta_r}\right)^k \tan\phi'\right\}$$

or

$$\phi^b = \arctan\left\{(\Theta)^k \tan\phi'\right\} \tag{3}$$

where ψ = matric suction applied to soil specimens; θ = the volumetric water content at any suction $(u_a - u_w)$; θ_r = the volumetric water content at residual conditions; θ_s = the volumetric water content at saturation, $\Theta = (\theta - \theta_r)/(\theta_s - \theta_r)$, the normalized volumetric water content; $k = 1$, 2, and 3.

The SWCC of the sandy silt was measured with a hanging column apparatus. A saturated specimen was prepared and suction (ψ was applied to remove the water from the soil. The change in the volumetric water content was monitored with increasing suction. Then the suction was slowly decreased and the increase in volumetric water content was recorded. The Brooks-Corey and van Genuchten models were fit to the SWCC data using a least squares optimization scheme with Solver in Excel. The SWCC is shown in Fig. 7, and the results of the friction angle ϕ^b estimated are listed in Table 3 illustrated in Fig. 6. Figure 6 indicates the variation of the friction angle ϕ^b with matric suction at different $k = 1$, 2, 3, which is consistent with the measured ϕ^b, but the estimated friction angle is smaller than the measured angle.

Table 3. Estimated parameter of the shear strength for the unsaturated sandy silts

ψ (kPa)	θ	θ_r	θ_s	Θ	$k = 1$		$k = 2$		$k = 3$	
					$\tan\phi^b$	ϕ^b	$\tan\phi^b$	ϕ^b	$\tan\phi^b$	ϕ^b
0	0.360	0.025	0.36	1	0.74	36.64	0.74	36.64	0.74	36.64
11	0.349	0.025	0.36	0.97	0.72	35.73	0.70	34.83	0.67	33.94
22	0.333	0.025	0.36	0.92	0.68	34.37	0.63	32.16	0.58	30.03
28	0.324	0.025	0.36	0.89	0.66	33.58	0.59	30.65	0.53	27.87
35	0.313	0.025	0.36	0.86	0.64	32.60	0.55	28.80	0.47	25.30

The shear strength contribution due to matric suction (τ_ψ was plotted in Fig. 5, which was equal to $(u_a - u_w)\tan\phi^b$ from experimental results (see Eqn. (1)), or $[(u_a - u_w)\{(\Theta)(\tan\phi')\}]$ from the semi-empirical prediction procedure(see Eqn. (3)).The variation of shear strength with respect to different matric suction is nonlinear for tested suction range.

Summary and Conclusions

This paper describes a new device for determining the shear strength of unsaturated fine-grained soils. Simple principles were employed to develop the direct shear testing device so that it would be robust, and easy to use, and readily assembled and disassembled for testing and maintenance. A testing of a sample was conducted with sandy silts under the net normal stresses $(\sigma_n - u_a)$ of 12.3 kPa, 24.6 kPa, 49.2 kPa, and 98.4 kPa for matric suctions $(u_a - u_w)$ of 0 kPa, 11 kPa, 22 kPa, 28 kPa, and 35 kPa. The measured results show that the unsaturated shear strength and the friction angle (ϕ^b) with

respect to the matric suction are consistent with the results from prediction procedure (Fredlund and Barbour 1996) and estimated friction angle (ϕ^b) based on SWCC of the sandy silt, respectively.

Acknowledgments

The authors thank the support provided by colleague of the Geo-Engineering Program and Geological Engineering Program, Department of Civil & Environmental Engineering, University of Wisconsin-Madison, and for the help of Mr. X. Wang in conducting laboratory testing, and for thoughtful and insightful comments of Professor Craig H. Benson.

References

ASTM D 3080–03 (2003) Standard Test Method for Direct Shear Test of Soils Under Consolidated Drained Conditions, Annual Book of ASTM Standards, ASTM

ASTM D 6836–03 (2004) Standard Test Methods for Determination of the Soil Water Characteristic Curve for Adsorption Using a Hanging Column, Pressure Extractor, Chilled Mirror Hygrometer, and/or Centrifuge, Annual Book of ASTM Standards, ASTM

Abramento M, Carvalho CS (1989) Geotechnical Parameters for the Study of Natural Slopes Instabilization at 'Serra do Mar' Brazil. In: Proc 12th Int Conf Soil Mechanics and Foundations Engineering. Rio de Janeiro 3:1599–1602

Bao CG, Gong B, Zan L (1998) Properties of Unsaturated Soils and Slope Stability of Expansive Soils, Key Note Lecture, UNSAT 98, 2nd Int Conf Unsaturated Soils, Beijing

Escario V (1980) Suction controlled penetration and shear tests. In: Proc 4th Int Conf on Expansive ASCE Publication. Denver 2:781–797

Escario V, Juca JFT (1989) Strength and deformation of partly saturated soils. In: Proc 12th Int Conf on Soil Mechanics and Foundation Engineering. A. A. Balkema, Bookfield, MA 2:43–46

Escario V, Saez J (1986) The shear strength of partly saturated soils, Geotechnique 36(3):453–456

Fredlund DG, Morgenstern NR, Widger RA (1978) The shear strength of unsaturated soils, Can Geotech J 15(3):313–321

Fredlund MD, Barbour SL (1996) The Relationship of the Unsaturated Soil Shear Strength Function to the Soil-Water Characteristic Curve, Can Geotech J 33(3):440–448

Fredlund DG, Morgenstern NR (1977) Stress State Variables for Unsaturated Soils, ASCE J Geotech Eng Div 103(GT5):447–466

Gan JKM, Fredlund DG, Rahardjo H (1988) Determination of the Shear Strength Parameters of an Unsaturated Soil Using the Direct Shear Test, Can Geotech J 25:500–510

Ho DYF, Fredlund DG (1982) Increase in shear strength due to suction for two Hong Kong soils. In: Proc ASCE Geotech Conf, Engineering and Construction on Tropical and residual soils. Honolulu, Hawai, U.S.A., January 11–15 pp 263–295

Khalili N, Khabbaz MH (1997) A unique relationship for χ for the determination of the shear strength of unsaturated soils, Geotechnique 48(5):681–687

Nishimura T, Fredlund DG (2001) Failure envelope of a desiccated unsaturated silty soil. In: Proc 15th Int Conf Soil Mech Geotech Eng. Istanbul 1:615–618

Oberg A-L, Sallfors G. (1997) Determination of shear strength parameters of unsaturated silts and sands based on the water retention curve, Geotech Test J 20:40–48

Rassam DW, Williams DJ (1999) A relationship describing the shear strength of unsaturated soils, Can Geotech J 36:363–368

Rohm SA, Vilar OM (1995) Shear strength of an unsaturated sandy soil. In: Alonso EE, Delage P (eds) Proc 1st Int Conf Unsaturated Soils. Paris 1:189–193

Toll DG (1990) A framework for unsaturated soil behavior, Geotechnique 40(1):31–44

Vanapalli SK, Fredlund DG, Pufahl DE, Clifton AW (1996) Model for the prediction of shear strength with respect to soil suction, Can Geotech J 33(3):379–392

Wang X, Benson CH (2004) Leak-free pressure plate extractor for measuring the soil water characteristic curve, Geotech Testing J 27(2):163–172

Wang X, Benson CH (2003) Pressure Plate Extractor, United States Patent No. 6,718,835

Wheerler SJ, Sivakumar V (1992) Development and application of a critical state model for unsaturated soils, In: Houlsby GT, Schofield AN (eds) Proc Wroth Mem Symp Predictive Soil Mechanics, ASCE, New York. Oxford

Factors Affecting Tensile Strength Measurement and Modified Tensile Strength Measuring Apparatus for Soil

Surendra Bahadur Tamrakar[1], Toshiyuki Mitachi[2], and Yasuo Toyosawa[1]

[1] Japan National Institute of Occupational Safety and Health, Kiyose, Tokyo, Japan tamrakar@s.jniosh.go.jp, toyosawa@s.jniosh.go.jp
[2] Graduate School of Engineering, Hokkaido University, Hokkaido, Japan mitachi@eng.hokudai.ac.jp

Summary. In this paper tensile strength measuring apparatus developed by Tamrakar et al. (2005a,b) was used to measure the tensile strength of one dimensionally consolidated saturated NSF-clay and statically compacted unsaturated mixtures of NSF-clay, CFP-silt and Toyoura-sand. Tensile strength (q_t) obtained from the tensile tests were compared with the unconfined compressive strength (q_u). It was observed that the ratio q_u/q_t lied within the range of 2 to 3 for saturated NSF-clay and 4 to 16 for compacted mixtures. Effect of specimen thickness within the tensile mold, number of compaction layers and tensile pulling rates on the tensile strength were also examined. Comparing the specimen thickness within the tensile mold, it was found that the specimen having 5 cm thickness gave the minimum value. Also, tensile strength increased with the increase in the number of compaction layers. As in other shear strength, increment in the tensile strength was observed beyond tensile pulling rate of 0.34 mm/min. But below this pulling rate also, some increments were observed.

Key words: tensile strength, tensile apparatus, compacted soil, tensile pulling rate

Introduction

Most of the vertical slopes get failed with the development of tensile crack on the top of the slope. Also, many earth dams, embankments, pavements, etc. where soil layers are compacted, are failed due to the development of tensile cracks. Prediction of probable position and depth of tensile crack is necessary to protect the property and loss of lives of workers at the construction site. In order to explain the position and depth of tensile crack, an accurate measurement of tensile strength of soil is necessary. Very few researches (e.g. Suzuki et al. 1998, Yao et al. 2002, Ono et al. 2003) have been made to measure the tensile strength of soils having lower tensile values. Recently, Nahlawi et al. (2004) and Tamrakar et al. (2005a,b) have introduced a new tensile strength

measuring apparatus which measures the tensile strength directly. One developed by Nahlawi et al. (2004) could be mainly used for compacted clayey and stiff soils only whereas the one developed by Tamrakar et al. (2005a,b) seems to be easy to use and simple to handle and could be used for both compacted unsaturated and highly saturated soils.

Tamrakar et al. (2005a,b) measured the maximum tensile strength of Kanto loam around $50 \sim 60\%$ of water content and showed the ratio of unconfined compression strength and tensile strength around 12.5 which varied with the water content. They also showed the effect of amount of finer particles and their size on tensile strength. Possible measurement of tensile strength for saturated NSF clay was also shown.

In this paper, tensile apparatus (type-A tensile mold) developed by Tamrakar et al. (2005a,b) was used to measure the tensile strength of saturated and unsaturated soils. Also, the effect of number of compaction layers, thickness of the specimens and tensile pulling rate on the tensile strength was studied. Unconfined compression tests were also performed to compare their values with tensile strength.

Test Apparatus

Tensile test apparatus shown in Fig. 1 consists of horizontal platform upon which apparatus box having two halves; fixed box and movable box, is placed. Inside this box, two tensile molds are placed. The inner shape of this mold is like "C" structure and it holds the specimen. Two molds are screwed to the apparatus boxes separately. One box of the apparatus is fixed to the horizontal platform while the other box can move freely on the horizontal platform. To

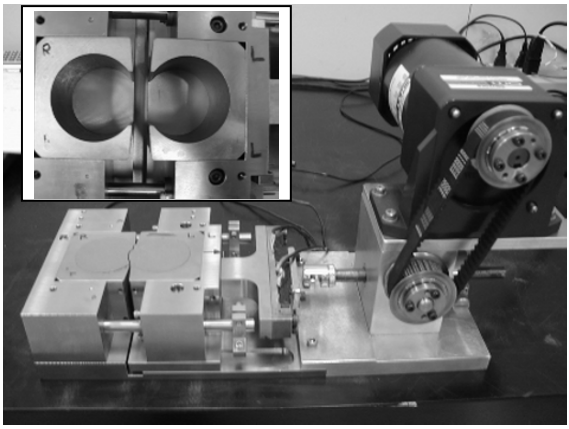

Fig. 1. New tensile strength measuring apparatus (inset : tensile molds) (Tamrakar et al. 2005a,b)

reduce the friction, linear sliding roller is placed between the movable box and platform. Movable box is pulled away in horizontal direction until the soil specimen fails in tension with tensile crack appearing at the middle of the specimen where two halves of the mold is attached. Load cell placed between the movable box and motor axis measures the tensile load. This tensile load divided by the area of the tensile crack perpendicular to horizontal pulling direction, gives the tensile stress. These molds can be easily changed as they are connected to the main apparatus by the screws only. The total surface area of this mold is 38.5 cm^2. The minimum width at the constricted section of this mold is 3 cm and the depth is 5 cm.

The apparatus box along with the mold and platform can be completely separated from the motor for preparing the specimen before the test. Compacted soil specimen is prepared within this mold by direct static compression. Once the specimen is ready within the mold for the test, then it is connected to motor shaft. Between the motor shaft and movable apparatus box, there are some attachments where load cell is kept.

Materials and Specimen Preparation

Kanto loam, NSF-clay and the mixtures of NSF-clay, CFP-silt and Toyoura-sand were taken as test materials. NSF-clay is commercially available clay which consists of Pyrophylite, CFP-silt (100) is crushed form of Silica sand and Toyoura-sand is also commercially available standard Japanese sand. Grain size distribution curves and index properties for these soils are shown in Fig. 2 and Table 1. Now onwards, NSF-clay, CFP-silt and Toyoura-sand are

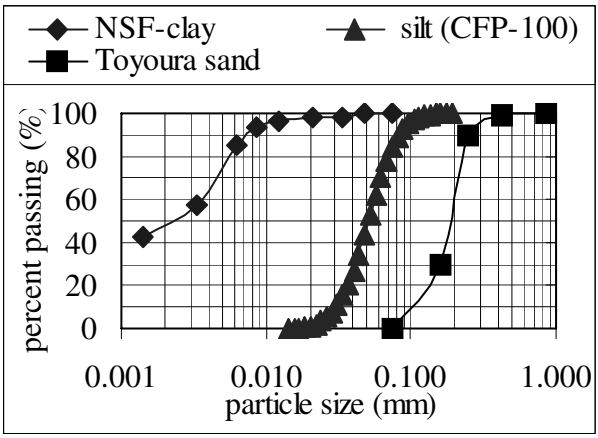

Fig. 2. Grain size distribution curves

Table 1. Properties of test materials

Materials	Density soil solid g/cm^3	Dry density max g/cm^3	Dry density min g/cm^3	w_L (%)	w_P (%)
NSF-clay	2.78			55.1	30.6
Silt (CFP-100)	2.66	1.59	1.17		
Toyoura sand	2.64	1.65	1.34		

represented by clay, silt and sand, respectively. For saturated test specimen, consolidated clay specimens were used where as mixtures of clay, silt and sand in different proportions were used for unsaturated compacted specimens. Tables 2 and 3 show the proportions and test conditions for different mixtures.

Before preparing the specimens, at first, tensile molds were fixed into the apparatus box and screwing was done between the movable box and apparatus horizontal plate so that movable box would be fixed. To reduce the friction between the specimen and the inner wall of the tensile mold, thin film of grease was applied over its inner surfaces. After the insertion of the consolidated specimen in case of saturated specimens or after the completion of compaction in case of compacted specimens into the tensile mold, load cell is set up towards the pulling side of mold box. Finally, the screws which are earlier fixed to prevent the movement of movable box of the apparatus are un-screwed.

Table 2. Test materials for mixtures of clay, silt and sand

Dry density (g/cm^3)	NSF-clay %	CFP-silt %	Toyoura-sand %	q_u (kPa)	q_t (kPa)	q_u/q_t
	25	—	75	21.1	3.2	6.5
	40	—	60	55.9	6.6	8.4
1.50	50	—	50	74.4	7.8	9.5
	60	—	40	79.1	8.6	9.2
	75	—	25	131.3	12.1	10.9
	25	75	—	64.3	6.9	9.3
	40	60	—	100.0	8.4	11.9
1.50	50	50	—	97.8	8.5	11.5
	60	40	—	132.2	10.3	12.9
	75	25	—	182.2	11.7	15.5
	—	25	75	6.6	1.4	4.6
	—	40	60	12.9	2.2	6.0
1.40	—	50	50	16.4	2.7	6.1
	—	60	40	18.7	3.0	6.2
	—	70	30	26.7	3.9	6.9

Table 3. Mixing proportions and testing conditions for clay ∼ sand mixtures

Specimens	Mixing ratio (by wt.)	w (%)	Controlled: dry density (g/cm^3)	Controlled: compaction stress (kPa)	Controlled: dry density (g/cm^3)	Testing Conditions
clay ∼ sand	3:1	10.0	1.50			No. of layers[(1)]
clay ∼ sand	3:1	10.0	1.50			Thickness[(2)]
clay ∼ sand	1:3	10.0		200	1.54	Pulling rate[(a)]
clay ∼ sand	3:1	10.0		200	1.26	
clay ∼ sand	3:1	10.0	1.50			Pulling rate[(b)]
clay ∼ sand	1:3	10.0	1.50			

[(1)] one, two and four layer-compaction, [(2)] 1.25, 2.5, 3.75 and 5 cm
[(a)] 0.01, 0.09 and 0.34 and 0.88 mm/min, [(b)] 0.17, 0.34 and 0.88 mm/min

Saturated specimens were prepared by pre-consolidating the slurry of the clay material in a separate, special consolidation mold. Two-way drainage with one dimensional consolidation was done. Once the consolidation was over, consolidation mold with consolidated specimen was placed over the tensile mold. Centering of molds was done by guiding support screws which were attached to the fixed portion of the apparatus box. By pushing the shaft of the consolidation mold slowly, consolidated specimen was allowed to insert into the tensile mold. Once the full depth (5 cm) insertion was completed, then the specimen was cut and its upper surface was trimmed.

In case of compacted specimens, at first, materials were thoroughly mixed with required distilled water and kept in an air tight plastic bag and sealed so that water was uniformly distributed throughout the materials. Specimens were prepared either under constant stress or under constant dry density conditions. In both the conditions, compacted specimens were prepared by directly and statically compressing the prerequisite amount of soil kept within the tensile mold of the apparatus, using bellophragm cylinder. Collar was generally placed over the tensile mold to prevent falling out of soil from the mold. Specimens were compacted keeping the dry density, water content and thickness of the specimens constant. Thickness, number of compaction layers and tensile pulling rates were varied depending upon the test conditions.

In case of unconfined compression test, saturated specimens were prepared by pre-consolidating the clay specimens in an ordinary consolidometer where as unsaturated compacted specimens were prepared in a normal splitting mold either under constant stress or constant dry density condition. Generally, one layer compaction was done. But to see the effect of numbers of layer of compaction, some specimens were prepared with one, two, three, four, five and ten layers.

Test Conditions

Tests in which specimen thickness was maintained at 5 cm with one-layer compaction and pulled under 0.34 mm/min tensile pulling rate, were considered as reference tests. All the tests of saturated specimens are reference tests. Saturated specimens of clay were prepared under 100, 200 and 300 kPa. Water content, density, degree of saturation, etc. is shown in Table 4.

Table 4. Saturated sol specimens conditions and test results

Specimen type	NSF-clay				
Preconsolidation pressure (kPa)	100	200	200	300	300
Soil unit weight (kN/m^3)	27.23	27.23	27.23	27.23	27.23
Water content w (%)	55.51	45.03	46.65	45.61	42.84
Degree of saturation S_r (%)*	98.40	97.20	96.70	98.75	96.00
q_t (kPa)	13.54	18.34	20.64	25.35	27.04
q_u (kPa)	29.81	52.81	52.81	77.12	77.12
q_u/q_t	2.20	2.88	2.56	3.04	2.85

* for tensile test

In case of unsaturated specimens, test conditions were changed depending upon the type of tests. Mixtures of clay, silt and sand specimens were prepared by mixing them in different proportions as shown in Tables 2 and 3. Specimens were compacted keeping their dry density, water content and specimen thickness constant. In case of tests where the effect of specimen thickness was studied, specimens were prepared by one-layer static compaction and they were pulled with 0.34 mm/min. In this case specimen thickness varied from 1.25 to 5 cm. Similarly, where the effect of number of layers of compaction was studied, specimens were prepared with one-layer, two-layers, three-layers and four-layers of static compactions, keeping the overall specimen thickness to be around 5 cm and pulling them under 0.34 mm/min. In case of the tests where the effect of tensile pulling rate was studied, specimens were prepared by one-layer static compaction with specimen thickness of 5 cm. In this case, tensile pulling rate was varied from 0.09 to 1.75 mm/min.

Unconfined compression test for saturated specimens were prepared by trimming the pre-consolidated specimens whereas unsaturated compacted specimens were prepared using ordinary splitting mold. Other than those for the effect of number of compacted layers, all the compacted specimens were prepared by one-layer static compaction using bellophragm cylinder. Other conditions such as dry density and water content were kept same as those for tensile compacted specimens. Compacted layers were prepared with 1, 2, 3, 4, 5 and 10 layers. Compaction time allowed for each layer was around one minute. The height and depth of specimen for both saturated and unsaturated

cases were 10 cm and 5 cm, respectively. Unconfined compression tests were conducted at constant displacement rate of 0.1 mm/min.

Results and Discussions

Figure 3 shows the photographs before (**a**) and after (**b**) the tensile failure tests for clay ∼ sand (3:1) and clay ∼ sand (1:3), respectively. Clear and straight tensile crack (failure line) could be seen. In Figure 3 (**c**) and (**d**), failure planes (tensile crack plane) after the tests were shown. Clear and smooth failure surfaces could be seen.

Tensile stress ∼ displacement curves obtained for the saturated specimens of clay (pre-consolidated under 100, 200 and 300 kPa) are shown in Fig. 4. As shown, with the increase in consolidation pressure, there is increase in tensile strength. Small variation in the test result might have occurred either during the transferring of the consolidated specimen from the pre-consolidometer to tensile mold or during the trimming of the specimen surface. In addition, variation in the water content (degree of saturation) or the friction between the inner wall of the consolidation mold and slurry material during the pre-consolidation might also have affected small change in their strength. Henceforth, proper attention must be paid during the specimen preparation.

Stress ∼ displacement curves for clay ∼ silt ∼ sand (1:1:1) obtained from tensile test and unconfined compression tests were shown in Figs. 5 (**a**) and (**b**), respectively. Clear peak for tensile stress as well as unconfined compressive stress could be seen. Here, tensile stress measured was shown in negative value. From now onwards, tensile strength values would be shown as positive values.

Table 4 shows the tensile strength and unconfined compression strengths obtained for saturated specimens. Increase in both tensile and unconfined compression strengths with the increase in the consolidation pressure could

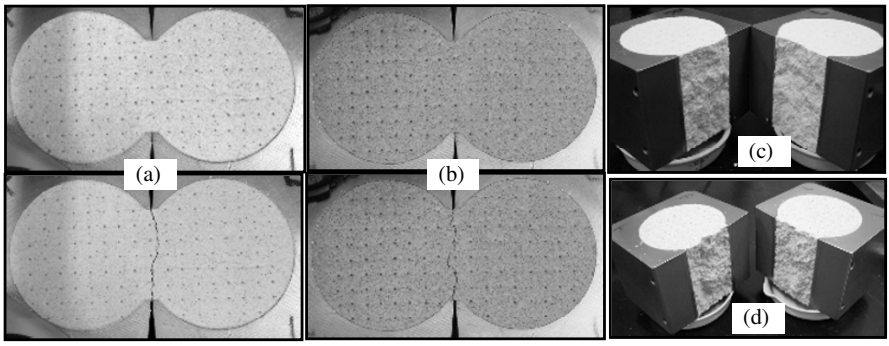

Fig. 3. Photographs before and after the tensile failure. (**a**) and (**c**) clay ∼ sand mixture (3:1) and (**b**) and (**d**) clay ∼ sand mixture (1:3)

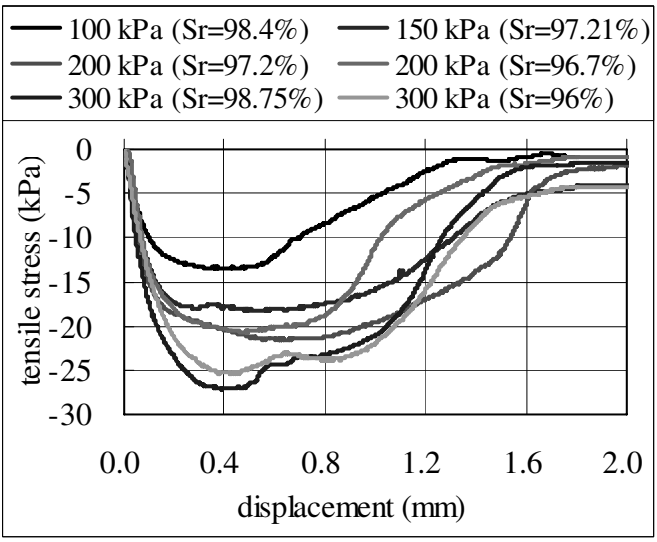

Fig. 4. Tensile stress ∼ displacement curves for consolidated NSF-clay

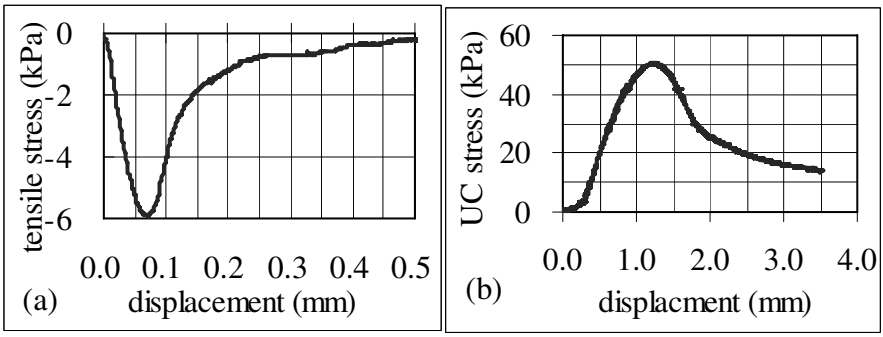

Fig. 5. Stress ∼ displacement curves for clay ∼ silt ∼ sand (1:1:1) mixture (**a**) tensile test and (**b**) unconfined compression test

be seen. It was observed that the ratio of q_u/q_t for saturated clay varied from $2 \sim 3$. Another type of NSF-clay used by Tamrakar et al. (2005a,b) had shown the average ratio as 6. All the test specimens shown in Table 4 have more than 93% of degree of saturation. Degree of saturation (S_r) shown in the Table 4 was calculated by using unit wet of soil solid, total weight of the specimen inside the tensile mold and the water content of the specimen after failure. As it is difficult to measure the area of the specimen directly, the total area of the specimen was considered to be same as that of the tensile mold. Thickness of the specimen was measured once the trimming was done after transferring the consolidated specimen into the tensile mold. It was assumed that the specimen

tightly fits into the mold. Ratio of q_u and q_t for clay $\sim$ silt $\sim$ sand (1:1:1) specimen was found to be 8.6. In Table 2, tensile and unconfined compression strengths measured for different mixtures are shown. It could be seen that the ratio of q_u/q_t for the unsaturated mixtures varied from 4 to 16. Tamrakar et al. (2005a,b) had also measured the similar ratio of q_u/q_t for Kanto loam which varied from 10 to 13 (Tamrakar et al. 2005a,b).

Effects of specimen thickness are shown in Fig. 6. Here, tensile strength values for different specimen thicknesses are shown. Decrease in the tensile strength with the increase in the specimen thickness could be seen. Specimen having 5 cm thickness, i.e., the thickness of tensile mold, showed the minimum tensile strength. Here, specimens were compacted only once for all the thicknesses. Therefore, uniformity in the density is more in case of specimen which had the minimum thickness. Irrespective of specimen thickness, tensile pulling for each test was done from the mid-height of the tensile mold. With the change in the thickness, resultant pulling direction might have changed, hence affecting the strength.

The effect of number of layers of compaction to tensile strength is shown in Fig. 7. During this test, 5 cm thick specimens were prepared by compacting predetermined amount of specimen within the tensile mold in one-layer, two-layer, three-layer and four-layer. Clay-sand mixture (3:1, $w = 10\%$ and rd $= 1.5\,\mathrm{g/cm^3}$) showed the increment in tensile strength with the increase in the number of compaction layers. One-layer compaction gave the minimum value than those obtained for two, three and four-layer compaction. With the increase in number of compaction layers, more uniformity of density through out the specimen takes place and this will increase the strength of the specimen. Similar test result was seen in case of unconfined compression test shown in Fig. 8 where test specimens were prepared by statically compacting the same amount of clay-sand mixture (1:3, $w \sim 10\%$, compaction pressure 50, 100 and 200 kPa) with 1, 2, 3, 4, 5 and 10 layers. As shown in Fig. 8, at the beginning, sudden increase in q_u strength was seen but the rate of increment decreased with the increase in the number of layers. As obvious,

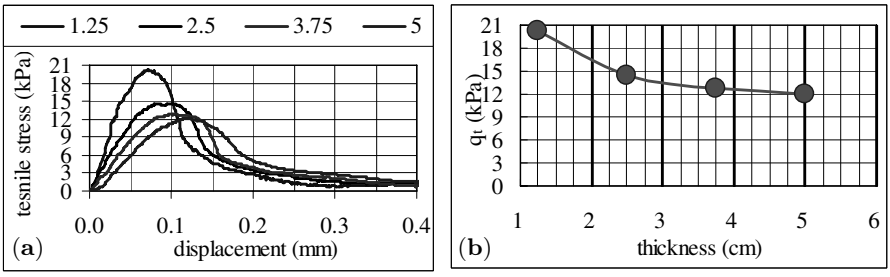

Fig. 6. Effect of thickness on q_t (**a**) stress $\sim$ displacement curves and (**b**) tensile strength

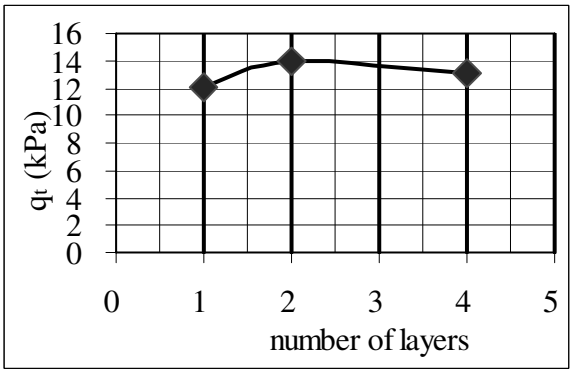

Fig. 7. Effect of number of compaction layers on q_t for clay ∼ sand mixture (3:1)

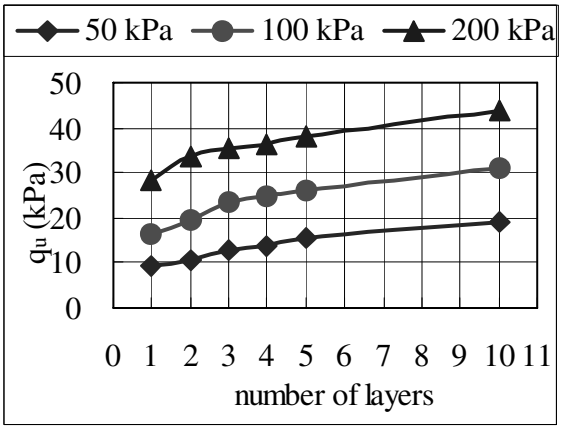

Fig. 8. Unconfined compression test results for clay ∼ sand mixture (3:1)

with the increase in number of layers of compaction, more uniformly dense specimens were obtained which makes the bonding between the soil particles more strong and hence, strength is increased.

Figure 9 shows the tensile strength test results of different soils conducted at different pulling rates which varied from 0.01 to 1.75 mm/min. In Fig. 9(**a**) clay-sand mixtures (1:3 and 3:1) prepared under 200 kPa were shown where as in Fig. 9(**b**) same soil specimens prepared under constant dry unit were shown. Comparing the tensile strength of each specimen with respect to tensile pulling rate, variation in the strength with the change in the pulling rate could be observed for all types of soil specimens. It was observed that the tensile strength measured in the range of 0.1 to 0.34 mm/min pulling rate gave the minimum value. In contrary to this, tensile strength measured at the higher and lower tensile pulling rates than 0.1 mm/min showed larger values.

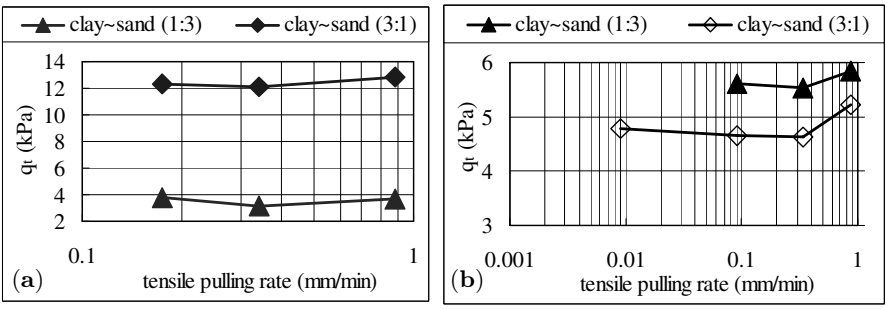

Fig. 9. Effect of tensile pulling rate on tensile strength under controlled: (**a**) pressure; (**b**) dry density

This difference in the tensile strength might have occurred while pulling the specimens where soil particles are attached to each other either by suction or internal bonding or cohesion. Tamrakar et al. (2005a,b) had discussed about the relationship between the tensile strength and suction to some extent. Effect of suction at higher and lower tensile pulling rates are yet to be studied. Increment in the tensile strength at higher tensile pulling rate is obvious as in any other shear strength. One reason for the increment at very low pulling rates might be due the dryness on the surface of the specimen as it takes very long time. Other reasons are yet to study.

Conclusions

From the tests conducted for saturated and statically compacted unsaturated soils, following points could be concluded:

1. Stress-displacement curves obtained for both saturated and compacted unsaturated specimens show the possibility of measuring tensile strength with the apparatus used here.
2. Ratio of unconfined compression strength and tensile strength (q_u/q_t) for NSF-clay was found to be $2 \sim 3$. For unsaturated soils this ratio varied from 4 to 16 depending upon the type and water content of the soil.
3. From the test results of clay-sand mixture (3:1), it was found that 5 cm thick specimen gave the minimum tensile strength in comparison to other specimens having thickness smaller than 5 cm. Therefore, it is recommended to pull the specimen from its mid-height.
4. Effect of number of layers of compaction (one-layer, two-layer and four-layer) on tensile strength was also studied. It was found that with the increase in the number of compaction layers, there was increase in tensile strength. Similar result was obtained in case of unconfined compression

test also. Increment in the strength might have occurred due to increase the uniformity of density distribution throughout the specimen.

5. Effect of tensile pulling rate for variety of unsaturated soil specimens was carried out. It was found that with the increase in the tensile pulling rate beyond 0.34 m/min, tensile strength also increases. But below this pulling rate also, some increments were observed.

Acknowledgements

This research is partially carried out under the Health and Labor Sciences Research Grants of Ministry of Health, Labor and Welfare, Japan.

References

Nahlawi H, Chakrabarti S, Kodikara J (2004) A direct tensile strength testing method for unsaturated geomaterials, Geotech Test J 27(4):356–361

Ono N, Mochizuki A, Kurosaki H, Ueno K (2003) Trial tests with compressive and tensile strength measuring apparatus. In: 58th annual meeting of Japanese Society of Civil Engineers:337–338 (in Japanese)

Suzuki T, Umei T, Sunaga F (1998) A research on the tensile strength of cement treated soils. In: 53rd annual meeting of Japanese Society of Civil Engineers:600–601 (in Japanese)

Tamrakar SB, Toyosawa Y, Mitachi T, Itoh K (2005) Tensile strength of compacted and saturated soils using newly developed tensile strength measuring apparatus, Soils and Foundations 45(6):103–111

Tamrakar SB, Mitachi T, Toyosawa Y, Itoh K (2005) Development of a New Soil Tensile Strength Test Apparatus. In: Geo-Frontiers 2005, Site Characterization and Modeling (GSP 138), ASCE

Yao S, Masui T, Ito A (2002) The relationship between tensile strength and the state of water in Kaolin clay. In: 47th symposium on Geotechnical symposium:127–132 (in Japanese)

The Tensile Strength of Compacted Clays as Affected by Suction and Soil Structure

Rainer M. Zeh[1] and Karl Josef Witt[2]

[1] Geotechnisches Institut AG, Hochstrasse 48, CH-4002 Basel, Switzerland
rainer.zeh@geo-online.com
[2] Bauhaus-University Weimar, Geotechnical Engineering, Department of Civil Engineering, Coudraystr. 11c, D-99423 Weimar, Germany
kj.witt@bauing.uni-weimar.de

Summary. This paper describes the influence of soil structure and soil suction on the tensile strength of a compacted clay. Laboratory tensile strength tests were carried out on a medium plastic clay. The soil samples were prepared by compacting a soil-water mixture of predetermined water content. The soil samples were either wetted or dried to different water contents corresponding to several suction levels. The test results showed an increase in the tensile strength with higher suction values and that samples compacted at different compaction states reach different magnitudes of tensile strength values.

Key words: direct tensile strength tests, different compaction states, SWCC, tensile strength, E-modulus, influence of soil structure and suction

Introduction

The tensile strength of soils is usually not taken into account when solving typical geotechnical problems. It plays an important role in connection with the examination of compacted clay cracking (Morris et al. 1992) in landfill liners or in cores of dam embankments, for example.

The tensile strength has relatively often been analysed in literature (e.g. Tang and Graham 2000, Snyder and Miller 1985, Ajaz and Parry 1975, Satyanarayana and Rao 1972, Farrell et al. 1967), but the initial states, such as density or soil structure, were often unequal. In addition, the testing methods also varied. The tensile strength of soils can be measured by direct or indirect testing devices, such as bending tests, punch tests, centrifuge or triaxial cell tests, etc.

In this paper, a method to measure the direct tensile strength of compacted clays is described. Furthermore, the test results correspond with a number of investigations (e.g. Nagaraj and Miura 2001, Vanapalli et al. 1999) which

have shown that soil-water interaction and soil structure generally have a great influence on soil properties.

Soil Structure

It is known that the engineering properties of fine grained (clayey) soils are closely related to the soil-water interaction (e.g. Nagaraj and Miura 2001, Mitchell 1993). A number of investigations indicated that the water (content) absorbed by the clayey soils (clay aggregates and particles) correlates to other soil properties like shear strength or compressibility.

Figure 1**a** shows a sketch with a typical structure of fine grained soils – sand, silt, clay aggregates (clusters) and pores with different sizes. The clay aggregates (e.g. Fig. 1**b**) consist of clay particles which are formed by face to face (parallel), edge to edge (normal) or mixed orientations – size between 0.01 to 1 µm. The orientation depends on the clay type, water content, soil preparation, etc. Clays compacted wet of Proctor optimum have a dispersed structure (parallel), with small inter-aggregate pores, compacted dry of Proctor

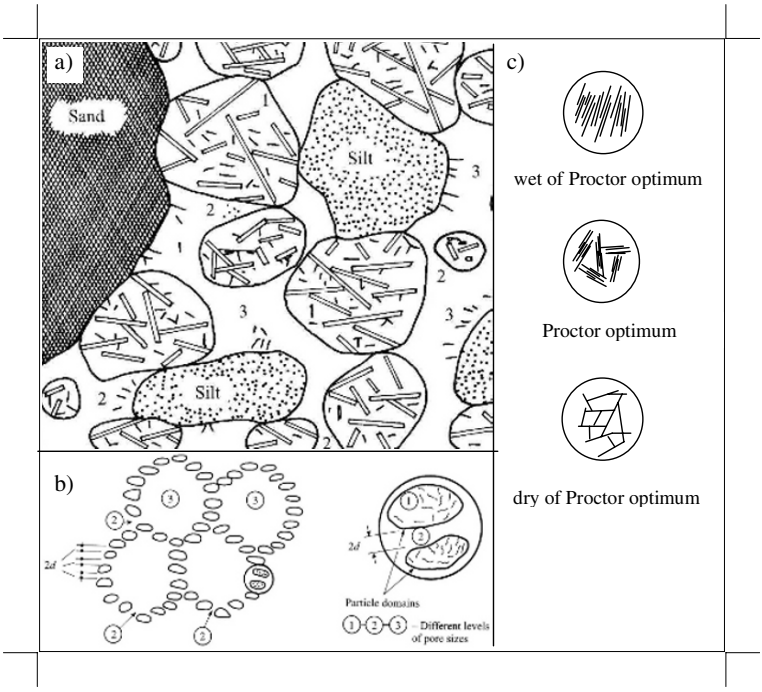

Fig. 1. a) fine grained soil structure – 1: intra-aggregate pores, 2 (3): inter-aggregate (large enclosed) pores, **b**) possible micro fabric of clays (modified from Nagaraj and Miura 2001), **c**) orientation of clay particles

optimum a meta-stable flocculated structure (normal), with larger and more inter-aggregate pores, and compacted at Proctor optimum a mixture of both structures (Fig. 1**c**). Therefore, the number and the size of pores as well as aggregates are strongly influenced by the conditions during compaction.

Depending on the definition of pores (Cuisinier and Laloui 2004, Nagaraj and Miura 2001, Diamond 1971), intra-aggregate pores (1 in Fig. 1**a**) have a maximum diameter of 0.002 to 0.01 µm. The size of the inter-aggregate pores is 0.01 to 0.1 for the small pores, large enclosed pores are up to 10 µm (2 and 3 in Fig. 1**a**).

The water trapped in intra-aggregate pores is mainly influenced by particle surface forces. The inter-aggregate pore water is dominated by capillary forces.

In relation to shear or tensile strength of soils, the number and size of the pores conduct difference magnitudes of strengths. In general, soils with only small pores exhibit higher strengths than soils with large pores or soils with different pores. The particle orientation also governs the obtainable strength. Parallel soil fabrics (dispersed structures), as in the case of clays compacted wet of Proctor optimum, have preponderant small pores and exhibit higher shear or tensile strength values by increasing suction values.

Test Procedure and Soil Characteristics

Tensile Strength Tests

The samples were prepared in a Proctor mould with constant conditions for each series (3 layers, 25 blows, standard hammer, Proctor optimum or 97% wet/dry of Proctor optimum) which created a cylinder of 150×120 mm. Therefore, the initial soil structure per series remained the same. The cylindrical soil samples were cut in 3 slices, which had been individually prepared to hollow cylinders of 90 × 24 mm (inner diameter 8 mm) by carefully trimming the slices and drilling a hole (Fig. 2). The hollow-cylindrical samples were stored for about 48 h to ensure homogeneous conditions. The samples were slowly and regularly air-dried or wetted (spray bottle) – between they were always stored in waterproof bags – until the designated water content value (or corresponding suction) was obtained (about 14 to 21 days). Finally, the samples were weighed and coated in wax to detect the volume by dip-weighing. The centre of the inner hole was later filled with a filter textile and a modified dowel was glued in both sample ends with epoxy resin. Two small hooks drilled in the dowels were used to apply the tensile forces in the sample.

The tensile strength tests were run in a modified triaxial apparatus by measuring the tensile force and the strain. The samples were normally torn apart with $v = 0.001$ mm/s until rupture occurred. Besides, the water content at the rupture zone was measured to determine the suction level by using the SWCC of the soil (Zeh 2006).

Soil Characteristics

In this paper, test results of a medium plasticity clay called Plessa (Pl) are presented. The soil properties are shown in Table 1.

Table 1. Soil properties of clay Plessa (Pl)

Parameters		Values
Clay/silt/sand content		46.4/52.8/0.8%
Liquid/plastic limit w_l/w_p		49.7%/21.3%
Plasticity index I_p		28.4%
Specific gravity ρ_s		2.676
Proctor density/water content	at optimum	$1.696\,\mathrm{g/cm^3}$/17.7%
	at wet (97%) of optimum	$1.645\,\mathrm{g/cm^3}$/21.5%
	at dry (97%) of optimum	$1.645\,\mathrm{g/cm^3}$/14.3%
Shear strength φ'		25.0°
Cohesion c'		$16.8\,\mathrm{kN/m^2}$

To convert the water contents into suction values, shrinkage curves and soil-water characteristic curves (SWCC) were necessary as described before (Zeh and Witt 2005a,b). Figure 3 represents the SWCC of clay Plessa, Proctor compacted (called p18–100o) with a fitting curve by Fredlund and Xing (1994). The curves of samples compacted wet or dry of Proctor optimum (called p21–97f and p14–97tr) also show strong similarities. The SWCCs were determined by the well-known axis-translation technique and chilled-mirror hygrometer measurements (Leong et al. 2003).

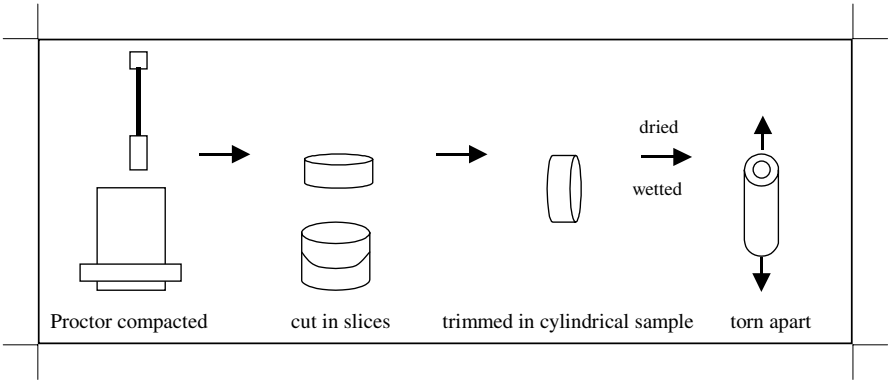

Fig. 2. Schema sample preparation

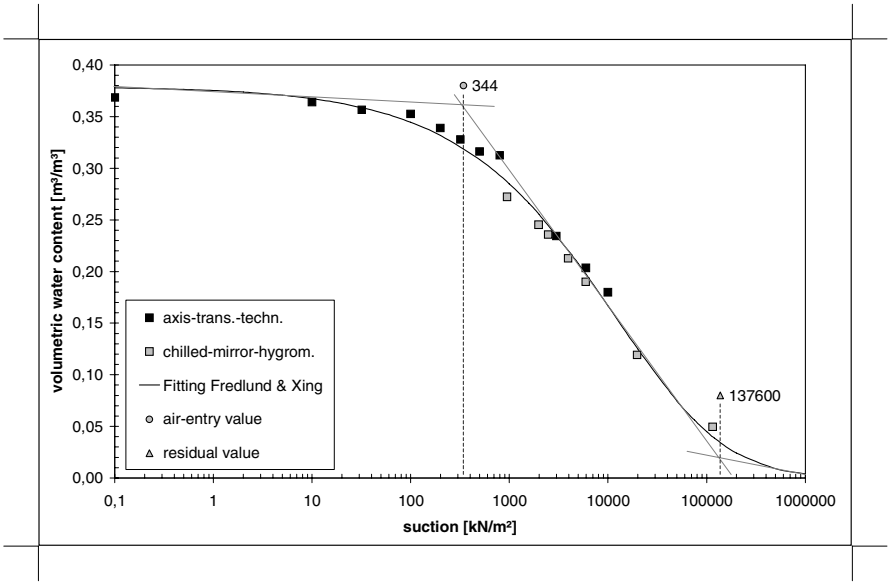

Fig. 3. Soil-water characteristic curve of clay Plessa, compacted at Proctor optimum, fitted with Fredlund and Xing (1994)'s equation

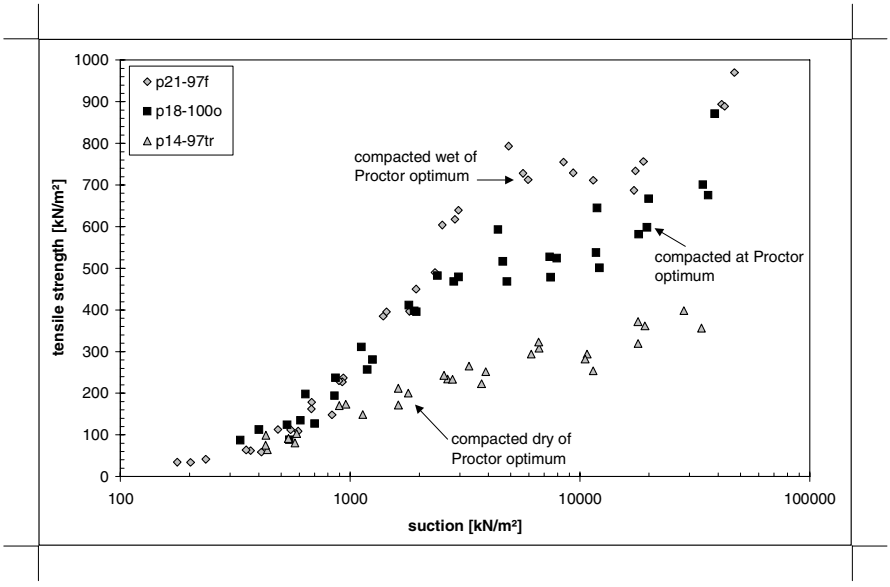

Fig. 4. Tensile strength of clay Plessa in dependence on the soil structure and the suction

Test Results

Figure 4 presents the results of the suction versus tensile strength relationships of all samples tested in the study. As can be seen in Fig. 3 until suction values of about 600 kN/m^2 all samples show a similar development of the tensile strength. Beyond this value, the samples compacted dry of Proctor optimum have a much smaller increase in the tensile strength than the samples compacted wet of optimum or at Proctor optimum. The samples compacted wet of optimum and at Proctor optimum have also a similar tensile strength increase up to a suction of about 1150 kN/m^2; beyond this value, the "wet" samples exhibit higher tensile strength values.

A comparison of the obtained tensile strength at a suction value of about 11,000 kN/m^2, as an example, represents very well their difference as well as the big influence of the soil structure (and pore sizes) as described above. The dry densities (determined by the tensile strength tests) as shown in Fig. 5 verify the smaller difference in tensile strength of the samples compacted wet of optimum or at Proctor optimum and the greater one of the samples compacted dry of Proctor optimum, respectively.

However, the influence of the soil structure is hardly visible in Fig. 6 which represents the E-modulus in dependence on the suction. The values scatter very distinctively. The E-modulus is calculated by strain and stresses during the tensile strength tests – a secant modulus of 80% and 15% stresses or rather strains at failure.

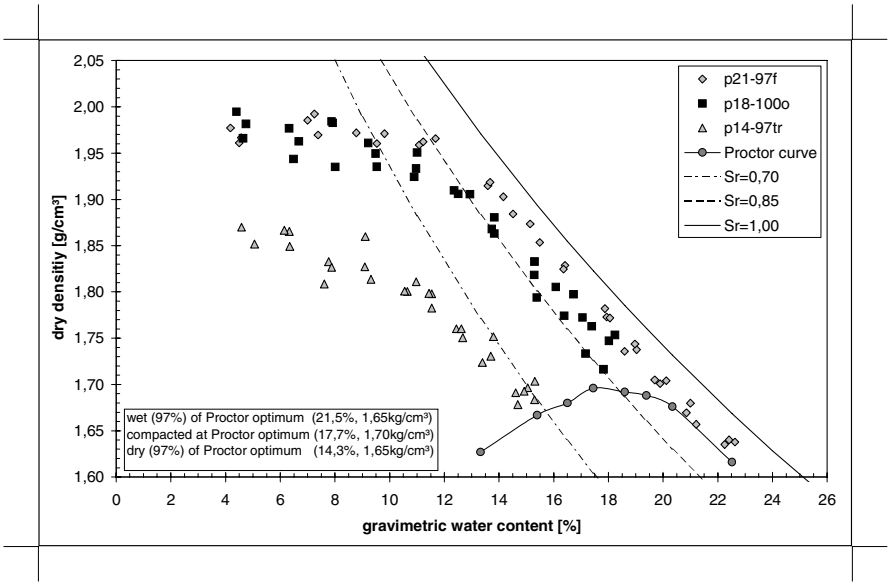

Fig. 5. Dry density (determined by the tensile strength tests) and Proctor curve of clay Plessa

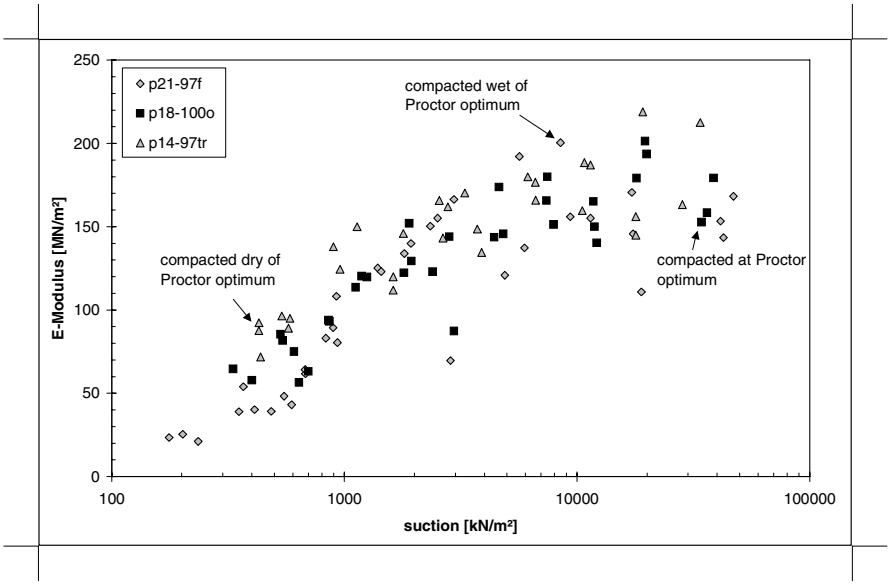

Fig. 6. E-modulus (clay Plessa) in dependence on the soil structure and the suction

Conclusions

The direct tensile testing method presented is very appropriate for examining the tensile strength of compacted clays (or other fine grained soils) exposed to different suctions (water contents). The test procedure is quite simple, whereas the sample preparation needs some practice.

The results of the tensile strength tests clearly showed the effect of soil-water interaction on the tensile strength and the E-modulus. Besides, the soil structure has surprisingly an influence only on the tensile strength. These results and tendencies described have to be verified on further soils and soil structures, respectively.

References

Ajaz A, Parry RHG (1975) Stress-strain behaviour of two compacted clays in tension and compression, Géotechnique 25(3):495–512

Cuisinier O, Laloui L (2004) Fabric Evolution of an Unsaturated Compacted Soil During Hydromechanical Loading. In: Schanz (ed) Unsaturated Soils – Experimental Studies, Vol I. Springer Proceedings in Physics 93, Springer, Berlin:147–158

Diamond S (1971) Microstructure and pore structure of impact compacted clays, Clays and Clay minerals 19:239–249

Farrell DA, Greacen EL, Larson WE (1967) The Effect of Water Content on Axial Strain in a Loam Soil Under Tension and Compression, Soil Sci Soc Amer Proc 31:442–450

Fredlund DG, Xing A (1994) Equations for the soil-water characteristic curve, Can Geotech J 31(3):521–532

Leong EC, Tripathy S, Rahardjo H (2003) Total suction measurement of unsaturated soils with a device using chilled-mirror dew-point technique, Géotechnique 53(2):173–182

Mitchell JK (1993) Fundamental of soil behaviour. John Wiley & Sons, NY

Morris PH, Graham J, Williams DV (1992) Cracking of drying soils, Can Geotech J, 29:263–277

Nagaraj TS, Miura N (2001) Soft clay behaviour – analysis and assessment. Balkema, Rotterdam

Satyanarayana B, Rao KS (1972) Measurement of Tensile Strength of Compacted Soil, Geotech Eng 3:61–66

Snyder VA, Miller RD (1985) A pneumatic fracture method measuring the tensile strength of unsaturated soils, Soil Sci Soc Am J 49:1369–1374

Tang GX, Graham J (2000) A method for testing tensile strength in unsaturated soils, Geotech Testing J 23(3):377–382

Vanapalli SK, Fredlund DG, Pufahl DE (1999) The influence of soil structure and stress history on the soil-water characteristics of a compacted till, Géotechnique 49(2):143–159

Zeh RM, Witt KJ (2005a) A direct testing method for the tensile strength of compacted clays. In: Int Symp Advanced Experimental Unsaturated Soil Mechanics, Trento, Italy, June 2005

Zeh RM, Witt KJ (2005b) Suction-controlled Tensile Strength of Compacted Clays. In: 16th ICSMGE Osaka, Japan, September 2005

Zeh RM (2006) Die Zugfestigkeit bindiger Böden als Kriterium der Rissgefährdung mineralischer Oberflächenabdichtungen. Dissertation (PhD Thesis), Fakultät für Bauingenieurwesen, Bauhaus-Universität Weimar (submitted)

Part IV

Temperature Effects

Modified Isochoric Cell for Temperature Controlled Swelling Pressure Tests

Yulian Firmana Arifin and Tom Schanz

Laboratory of Soil Mechanics, Bauhaus-University Weimar, Germany
yulian-firmana.arifin@uni-weimar.de, tom.schanz@uni-weimar.de

Summary. This paper focuses on the effect of moderately high temperature on the swelling pressure of compacted bentonite and bentonite-sand mixtures which are among the material used as buffer material in high level waste repository. Modified isochoric cell was used to measure the swelling pressure of the material at 80°C. Two different methods were utilized in order to implement two transport mechanisms of water molecules in compacted mixtures. The equipment set-up, verification, and experimental programs adopted in this study are described. The results obtained are presented and discussed.

Key words: swelling pressure, isochoric cell, temperature effects, bentonite–sand mixtures

Introduction

Emplaced high level wastes will emit quite significant amount of heat which is thought to change coupled hydro-mechanical behaviour of the buffer element used in the waste disposal facility. Swelling pressure, which is a representation of both hydraulic and mechanical behaviour of the material and indicates the performance of the sealing material, is one of important behaviour that should be investigated in case when increase in temperature in the waste repository is of concern.

Pusch et al. (1990) stated that the increase in temperature of a bentonite decreased the hydration force due to a reduction in the number of hydrates in the smectite surface within bentonite and increased the osmotic pressure in the molecular system. These led to reduction or increase in the swelling pressure of compacted bentonite depending on the dominant factor happen in the type of bentonite used. On the other hand, the increase in temperature may cause the smectite mineral to become unstable and transform to more stable silicate phases. The transformation processes are known as illitisation, cementation, and chloritisation processes (Wersin et al., in press). These may lead to reduction in swelling pressure of the compacted bentonite.

Earlier investigations show that the increase in temperature induced insignificant increase in the swelling pressure of bentonite (e.g., Pusch et al. 1990 for Na-bentonite, Cho et al. 2000 for Ca-bentonite). On the other hand, the reverse is also true (e.g., Pusch et al. 1990 for Ca-bentonite, Lingnau et al. 1996 for Na-bentonite, and Villar and Lloret 2004 for FEBEX bentonite which is mainly Ca-Mg-bentonite). However, the temperature effects on the swelling pressure of bentonite remain important in the assessment of long-term performance of the whole repository construction. The investigation into the temperature effects on the behaviour of bentonite provides insight into understanding the hydro-mechanical processes taking place in the bentonite in relation to its use as barrier material. The results of such a research will provide fundamental data concerning the parameters to be used in the modelling since the long-term behaviour of the material are to be predicted using available sophisticated numerical tools.

In this study, the effects of moderately high temperature on the swelling pressure of a calcium-type bentonite were investigated. Modified isochoric cell was used to measure swelling pressure of the material by means of constant volume test. The elevated temperature up to 80°C was used in this study since up to now most HLW repository concepts are designed based on a design criterion that a maximum temperature of 90°C is considered for bentonite buffer (SKB 1999). Two types of test; namely, one step swelling pressure test and multi-step swelling pressure test, were performed to study the two mechanisms of water molecules transports (i.e., in fluid phase and in vapour phase). The equipment set-up, verification, and techniques adopted are described. The results obtained as well as the comparison with the swelling pressure measured at room temperature are presented and discussed.

Equipment and Verification

The constant volume test performed in this study was conducted using isochoric cell developed at the Technical University of Barcelona (UPC) Spain. The cell was used to measure swelling pressure of compacted bentonite and bentonite–sand mixture from low to high density at room temperature by Villar et al. (2001) and Agus and Schanz (2005a). The cell was modified by installing a flexible wire heater attached to the outer wall of the cell. The heater was controlled using a proportional integral differential (PID) temperature with programmable ramp and soak temperature features. Two small thermocouples were installed in a hole drilled through the top cap of the cell for measuring the temperature of the specimen during experiment. The swelling pressure was measured using a load cell connected to a handled meter.

Figure 1 shows the schematic diagram of the one-step swelling pressure test. In this test, the cell was connected to a water column filled with distilled water. A flexible wire temperature-controlled heater was also installed in the water column to monitor the temperature of the water used in the permeation.

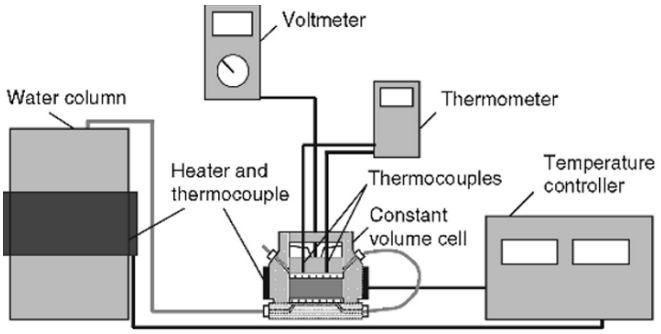

Fig. 1. Schematic drawing of the one-step swelling pressure test

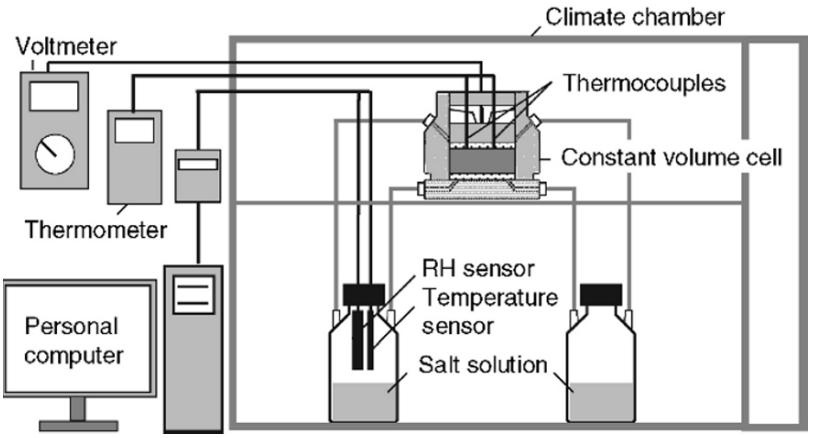

Fig. 2. Schematic drawing of the multi-step swelling pressure test

Figure 2 shows the schematic drawing of the multi-step swelling pressure test. Vapour equilibrium technique (VET) was used in this test whereby the total suction of the specimen was reduced by increasing the relative humidity of the vapour in the specimen's pore space. Similar method was also adopted by Agus (2005) using the same cell in the tests at room temperature.

The multi-step swelling pressure test in this study was performed in a climate chamber that could control temperature to $\pm 0.1^{\circ}$C. The cell was connected to two Erlenmeyer flasks filled with salt solution. A relative humidity and temperature sensor were installed to one of the Erlenmeyer flasks to monitor the relative humidity of the water vapour above the salt solution in the flask that was used to induce relative humidity to the specimen. The sensor (together with a temperature sensor) was connected to a digital data display connectable to a personal computer. The sensor used has an excellent performance not only at room temperature but also at moderately high temperature (Agus and Schanz 2005b, Arifin et al. 2006a).

Prior to use, the deformation of the cell ring and the load cell due to the non-isothermal test conditions were studied and verified so that the effects can be taken into account. Increasing temperature resulted in decreasing zero offset of the load cell calibration curve. However, the intercept of the calibration curves, which was also used for calculating the swelling pressure, does not show significant change. The coefficient of thermal expansion of the cell used in this study was found about $1.58 \times 10^{-5}/°\mathrm{C}$, which is closed to the coefficient of linear thermal expansion of stainless steel (AISI, $\alpha_r = 1.60 \times 10^{-5}/°\mathrm{C}$). Small deviation from the value is expected since the non-steel components of the cell also affect the thermal behaviour of the cell as a whole. The change in void ratio, Δe, due to the change in radial ring deformation can be approximated using the following equation (Romero 1999)

$$\Delta e = (1 + e_0)\left(\frac{(2\alpha_r - \alpha_s)\Delta T}{1 + \alpha_s \Delta T}\right) \tag{1}$$

where e_0 is initial void ratio, α_r is the coefficient of thermal expansion of the ring, α_s is volumetric thermal dilatation of the clay particle ($\alpha_s \approx 2.9 \times 10^{-5}/°\mathrm{C}$, Horseman and McEwen 1996), and ΔT is temperature change (in this study $\Delta T = 60°\mathrm{C}$). By inserting all known parameters, equation (1) can be simplified to be the following equation:

$$\Delta e = 0.0002(1 + e_0)\,. \tag{2}$$

The change in the dry density of the specimen tested due to the change in void ratio can be computed using equation (3), which is derived from substituting equation (2) to the first derivative of the relationship between dry density and void ratio.

$$\Delta \rho_d = -0.0002 \rho_d \tag{3}$$

where $\Delta \rho_d$ is dry density change in $\mathrm{Mg/m^3}$, and ρ_d is initial dry density of specimen. Although the swelling pressure result is an exponential function of dry density of specimen (Villar and Lloret 2004, Agus and Schanz 2005a), it is clear that the swelling pressure change due to thermal deformation of the ring and thermal dilatation of the clay particles is not significant provided that corrections are applied to the specimen's dry density.

Material Used

The materials used in this study were calcium-type bentonite, Calcigel, and mixtures of Calcigel and quartz sand. The bentonite used has specific gravity of 2.8, the liquid limit of 180%, and the plastic limit of 33%. The monmorillonite content of the bentonite used is 50–60% with a specific surface area of $651\,\mathrm{m^2/g}$ (Agus 2005). The quartz sand used has specific gravity of 2.65 with a specific surface area of $0.25\,\mathrm{m^2/g}$. Two types of specimens were prepared

with different bentonite contents (on a dry mass basis); namely, 50B/50S bentonite–sand mixture with a bentonite content of 50% and 100B for pure bentonite. The sand was sieved through 2-mm sieve openings before mixing. The specimen conditions used in this study are summarized in Table 1.

Table 1. Specimen conditions of one step swelling pressure test

Specimen	w (%)	ρ_d (Mg/m^3)	Specimen	w (%)	ρ_d (Mg/m^3)
100B–1	9	1.43	50B/50S–2	17	1.77
100B–2	9	1.26	50B/50S–3	20	1.66
100B–3	9	1.05	50B/50S–4	25	1.49

Heavily compacted 50B/50S prepared by Gesellschaft für Anlagen und Reaktorsicherheit (GRS) were used in the one-step swelling pressure test (i.e., denoted as 50B/50S–1 in the subsequent sections) and multi-step swelling pressure test. The specimens had an average initial dry density of 2.0 Mg/m^3, initial water content of 9%, and initial total suction of 22000 kPa (Agus and Schanz 2006a).

Swelling Pressure Measurement

One-Step Swelling Pressure Test

The test commenced by placing the specimen in the cell. The temperature of specimen was elevated by heating the cell using the temperature-controlled heater. The temperature increment should be slow enough to avoid temperature difference between the cell and the specimen. Rapid temperature increment results in decreasing the relative humidity of the air space which is existed in the cell (e.g. porous disks) due to increase its saturation water vapour (Arifin et al. 2006a, Agus and Schanz 2006b). Some amount of water from the specimen will evaporate to balance this condition. Trial tests had been done to determine the appropriate rate of temperature increase. Figure 3 shows the difference temperature between the cell and the specimen at different rate of temperature increase. For rapid temperature increase (i.e., 20°C/min) as shown in dashed line, the specimen temperature reached 80°C several minutes after the cell temperature had reached 80°C. From the trial tests performed, it is found that the appropriate rate of temperature increase is 0.016°C/min (or 1°C/hour) where the temperature of the cell and the specimen reached 80°C at the same time.

After the temperature of both the cell and the specimen had reached 80°C, warmed distilled-deaired water was circulated through the bottom and the top boundaries of specimen. Warmed water was used in this study with a reason

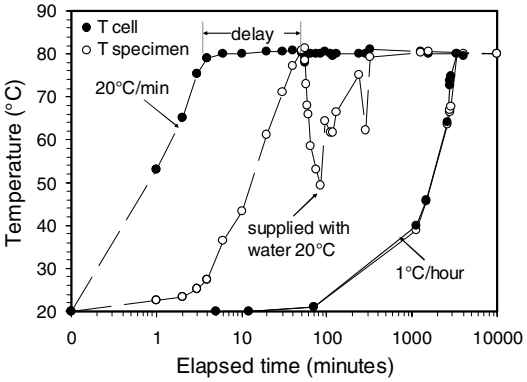

Fig. 3. Investigation of the rate of temperature and supplied water to the specimen temperature

that the use fresh water decreases the temperature of the specimen as also shown in Fig. 3. The decrease in the water temperature due to heat release in the water circulation line was anticipated by increasing the water temperature in the water supply column up to 86°C. During the test, the swelling pressure of the specimen was measured using the handled voltmeter. The equilibrium was reached after the swelling pressure readings stabilised for a significant period of time.

Multi-Step Swelling Pressure Test

The heavily compacted 50B/50S specimens prepared by Gesellschaft für Anlagen und Reaktorsicherheit (GRS) were tested following the multi-step swelling pressure test method. After the arrangement shown in Fig. 2 had been set up, the specimen was placed in the cell and the temperature of the chamber was gradually increased at a rate of 0.01°C/min which was much lower than the rate used in the one-step swelling pressure test for anticipating temperature gradient between the specimen, the cell and the salt solution. The molal and saturated sodium chloride solutions were used to induce relative humidity to the specimen. The use of molal and saturated sodium chloride solutions for controlling suction (or relative humidity) at room temperature and moderately high temperature (i.e., 80°C) was verified by Arifin et al. (2006b). It was found that the technique is applicable provided that the temperature gradient in the system is minimised. The swelling pressure development, specimen temperature, and relative humidity and temperature of salt solution were periodically recorded. The results obtained were compared with those of the earlier investigation performed at room temperature and reported by Agus (2005).

Result and Discussion

Figures 4(**a**) and 4(**b**) show swelling pressure development versus elapsed time plotted in semi-logarithmic scale performed with one-step swelling pressure test for 100B and 50B/50S specimens, respectively. The swelling pressure recorded after distilled water supply show rapid increase rapidly at earlier stage of the test for both specimens. Generally, after the swelling pressure maximum was reached (i.e., after about 100 hours duration), the swelling pressure of the 100B specimen slightly decreased possibly due to meta-stable of structure of the compacted pure bentonite at low water content, whereas the swelling pressure of the 50B/50S specimen remained constant. According to the figures, the swelling pressure development of the specimens tested at 80°C was more rapid than that of the specimens tested at 20°C. Agus and Schanz (2005a) found that the rate of swelling pressure development is a function of the initial total suction of the compacted specimen tested. However, the increase in temperature causes decrease in total suction in compacted bentonite (Villar and Lloret 2004, Romero et al. 2000) and in compacted bentonite–sand mixtures (Arifin et al. 2006a). Therefore, the faster of swelling pressure development rate of specimen tested at 80°C may most probably be due to preconsolidation effects induced by heating.

Figure 4 shows also that the magnitude of swelling pressure of the specimens tested at 80°C was smaller than that of the specimens tested at 20°C. The result agrees well with the results reported by Pusch et al. (1990), Villar and Lloret (2004), Lingnau et al. (1996). According to Pusch et al. (1990), the effects of temperature on the swelling pressure depend on the net of two opposite effects (i.e., the increase in osmotic pressure and the decrease in hydration force). The increase in the osmotic pressure leads to increase in swelling pressure, whereas the decrease in the hydration force causes decrease in swelling pressure. Since the number of flakes of Ca-bentonite is considerably

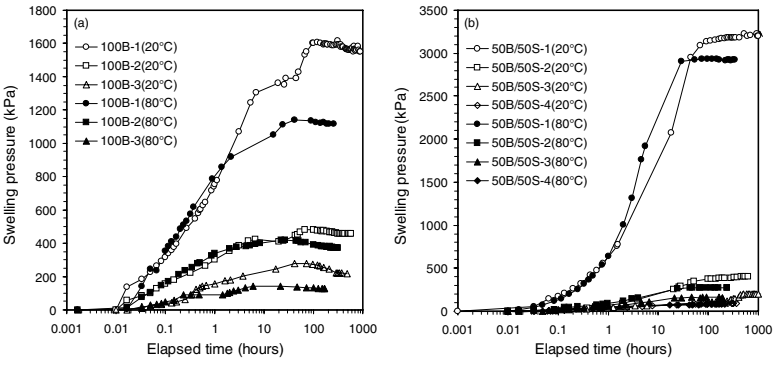

Fig. 4. Development of swelling pressure as a function of time for: (**a**) 100B specimen, and (**b**) 50B/50S specimen (one step tests)

high (higher than that of Na-bentonite), the increase in temperature affects the hydration force more significantly than the osmotic pressure. The effects of the reduction in the hydration force are more pronounced than the increase in the osmotic pressure. Therefore, the increase in temperature results in reducing swelling pressure.

Figure 5 shows the development of swelling pressure at 80°C followed by cooling to the room temperature (i.e., ±20°C) for the test at 80°C. According to the figure, the decrease in swelling pressure due to increase in temperature is reversible. The swelling pressure of the specimen tested increased and reached an equilibrium value which is very close to the swelling pressure performed at 20°C. Therefore, temperature-induced transformation of smectite to non-expandable illite layers is not evident in the range of temperature and time duration considered in this study. However, prolonged heating may induce such transformation which requires further investigation.

Figure 6(**a**) shows the swelling pressure of the 100B and 50B/50S specimens plotted against the mixture dry density. As expected and supported by other's findings such as Komine and Ogata (2003) and Agus and Schanz (2005a), the swelling pressure of the specimens shows exponential function against mixture dry density. As depicted in the figure, the curve of swelling pressures obtained for the specimens tested at 80°C is located below the curve of swelling pressure obtained for the specimens tested at 20°C. The reduction of swelling pressure due to increase in temperature of pure bentonite specimens appears to be higher than that of the 50B/50S specimens. Agus and Schanz (2005a) found that the swelling pressure of compacted bentonite–sand mixtures with different bentonite contents is a function of bentonite dry density. The bentonite dry density ($\rho_d^{\text{bentonite}}$) is computed by assuming that the soil void in the compacted bentonite–sand mixtures only belongs to the bentonite (Komine and Ogata 2003):

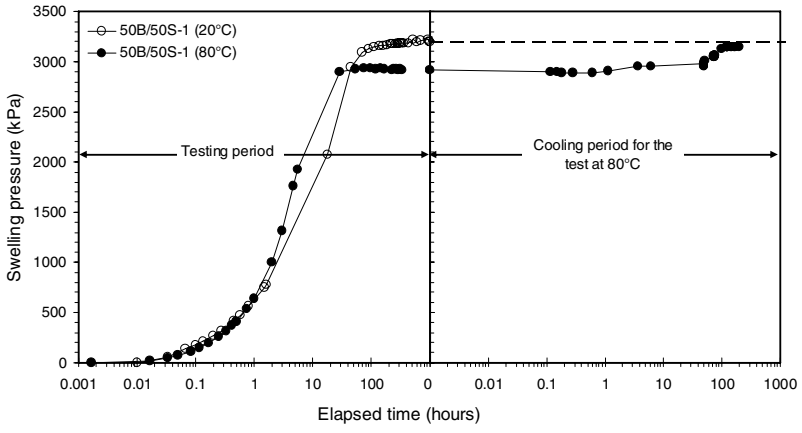

Fig. 5. Development of swelling pressure after tested at 80°C

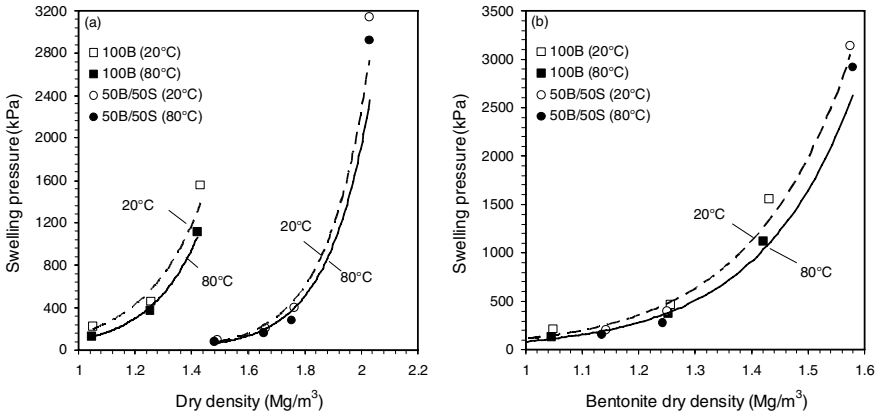

Fig. 6. (**a**) Swelling pressure as a function of dry density, and (**b**) swelling pressure as a function of bentonite dry density

$$\rho_d^{\text{bentonite}} = \frac{r_{bs}\rho_d}{(1 + r_{\text{bs}}) - (\rho_d / G_s^{\text{sand}})} \tag{4}$$

where r_{bs} is the bentonite–sand mass ratio, ρ_d is mixture dry density in Mg/m^3, and G_s^{sand} is the specific gravity of sand.

Figure 6(**b**) shows the relationship between swelling pressure and bentonite dry density for the compacted bentonite and compacted bentonite–sand mixtures. Allowing slight scatters in the data, the curve of swelling pressure for the 50B/50S specimens tested at 80°C coincides with that for the pure bentonite specimens. It indicates that at 80°C the swelling pressure of bentonite–sand mixtures also shows similar trend as the swelling pressure curve obtained at 20°C. The increase in temperature only affects the magnitude of the swelling pressure which represents the effects of temperature on the bentonite mineral in the mixture. Therefore, the presence of sand in the mixture is expected to give benefit in reducing the temperature effects or the reduction in swelling pressure due to elevated temperature.

Figure 7 shows the swelling pressure development of highly compacted bentonite–sand mixture performed using VET at 80°C together with the evolution of the relative humidity of salt solution used as measured using the relative humidity. The good performance of the testing system is indicated by the constant relative humidity throughout the test as shown in the figure.

According to Fig. 7, the swelling pressure tested using VET shows slow development at earlier stage of test. The swelling pressure increased rapidly after 50 hours and reached equilibrium after 200 hours. Ignoring the magnitude of the swelling pressure, the results indicate a delay when compared with the development of swelling pressure when the specimens were tested using water in its liquid phase (i.e., in the one-step swelling pressure test). The delay was probably caused by the retarding transport mechanism of water

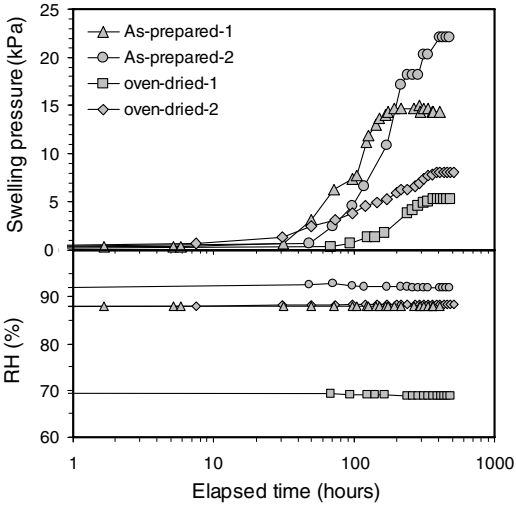

Fig. 7. Swelling pressure development from the multi-step swelling pressure test

molecules in the vapour form which occurs when using VET in the test. The water molecules first migrate into the open voids in the specimen and are subsequently absorbed when in contact with the exposed surfaces of clay clusters (Pusch 2001, Agus 2005). A water potential gradient (suction) that exists between the inter-aggregate and intra-aggregate pore-water and the mixture permeability at micro and macro scales control the mechanism of water movement from the exposed surface of the clay clusters to the intra-cluster pores (Agus and Schanz, in print). These postulations also seem to be true at an elevated temperature of 80°C as indicated by the results presented herein.

Figure 8 shows the development of swelling pressure with decreasing suction for the as-prepared 50B/50S specimens (i.e., those prepared by GRS) and oven dried 50B/50S specimen performed in this study. The oven-dried specimen as referred to herein is basically the GRS-prepared specimen which was oven-dried prior to test. The data of the swelling pressure development obtained for the same material tested at room temperature (i.e., ±20°C) and reported by Agus (2005) using two different methods (i.e., axis translation technique (ATT) and vapour equilibrium technique (VET)) are also plotted for comparison.

According to Fig. 8, the difference between the swelling pressures performed at room temperature and the swelling pressure performed at 80°C appears obscure since the development of swelling pressure is insignificant up to a suction of about 1000 kPa. Agus (2005) states that the insignificant swelling pressure development might be due to a delayed 'true' equilibrium in the specimen by considering the water movement mechanism mentioned above. In addition, the corresponding water content of the specimens at the

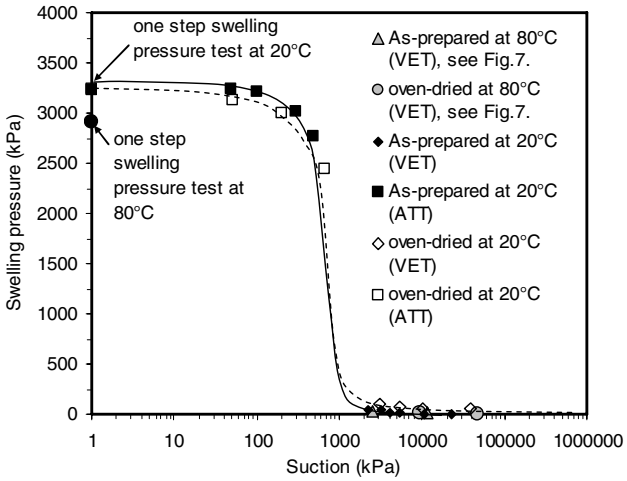

Fig. 8. Swelling pressure versus suction following wetting obtained using the multi-step swelling pressure test

suction range applicable in this method is close to the shrinkage limit of the material reported by Agus and Schanz (2006a) (i.e., 9.8%). The increase in water content with decreasing suction at the range of suction used in VET does not result in significant change in the void ratio of the specimen. As a result the pressure required to keep the void ratio constant (or swelling pressure) when the specimen is wetted is also low.

Conclusion

The swelling pressure test at a moderately high temperature using modified isochoric cell has been presented. The equipment verification and the swelling pressure test procedures (i.e., the one-step swelling pressure test and the multi-step swelling pressure test) performed in this study have been described. The results have been presented and compared to the swelling pressure results obtained at room temperature performed in this study and previous study. The increase in temperature results in reduction in swelling pressure. The reduction of swelling pressure performed in this study is reversible. It seems to be mainly caused by the reduction in the hydration force of the bentonite in the specimens tested. Thus, for the bentonite–sand mixtures, the increase in temperature affects only the bentonite. The presence of sand in the mixture gives benefit as expected to reduce the temperature effects. The transport mechanism of water molecules controlled the development of swelling pressure of the heavily compacted bentonite–sand mixture specimens not only at 20°C but also at 80°C. The increase in swelling pressure of the as-prepared specimen and the oven-dried specimen performed using VET method was insignificant

which is due to the limitation of suction range applicable using the VET. The water content corresponding to the suction values used is close to the shrinkage limit of the specimen. Thus, further investigation using ATT should be performed to investigate the behaviour of the specimen at the lower suction range (i.e., $< 1000\,\mathrm{kPa}$).

Acknowledgment

The research is funded by Bmbf project: Experimentelle und numerische Untersuchungen zum Langzeit-verhalten von Abschlussbauwerken: Thermo-Hydraulisch-Mechanisch-Chemisch gekoppelte Systeme. FKZ: 02C1104.

References

Agus SS (2005) An experimental study on hydro-mechanical characteristics of compacted bentonite–sand mixtures. Ph.D. Thesis, Bauhaus-University Weimar

Agus SS, Schanz T (2005a) Swelling pressure and total suction of compacted bentonite–sand mixtures. In: Proc Int Conf on Problematic Soils, Cyprus, pp 61–70

Agus SS, Schanz T (2005b) Comparison of four methods for measuring total suction. Vadose Zone Journal. Special section: Soil Water Sensing. Soil Science Society of America 4(4):1087–1095

Agus SS, Schanz T (2006a) Drying, wetting, and suction characteristic curves of a bentonite–sand mixture. In: Proc 4th Int Conf on Unsaturated Soils, Arizona, USA, pp 1405–1414

Agus SS, Schanz T (2006b) Discussion of paper "Free energy of water-suction-in filter papers" by R. Bulut and W.K. Wray, Geotechnical Testing Journal, ASTM 29(6)

Agus SS, Schanz T (in print) Discussion of paper "Parameters affecting soil-water characteristic curves of fine-grained soils" by Thakur VKS, Sreedeep S, Singh DN, J Geotech and Geoenvir Engrg ASCE 132(11)

Arifin YF, Agus SS, Schanz T (2006a) Temperature Effects on Suction Characteristic Curve of Bentonite-Sand Mixtures. In: Proc 4th Int Conf on Unsaturated Soils, Arizona, USA, pp 1314–1325

Arifin YF, Agus SS, Schanz T (2006b) Drying-wetting behavior of compacted bentonite–sand mixtures as also affected by temperature. In: Proc Int Conf on Geo-Environmental Engineering 2006, Kyoto, Japan, pp 63–69

Cho WJ, Lee JO, Kang CH (2000) Influence of temperature elevation on the sealing performance of the potential buffer material for a high-level radioactive waste repository, Annals of Nuclear Energy 27:1271–1284

Horseman ST, McEwen TJ (1996) Thermal constraints on disposal of heat-emitting waste in argillaceous rocks, Eng Geol 41:5–16

Komine H, Ogata N (2003) New equations for swelling characteristics of bentonite-based buffer materials, Can Geotl J 40:460–475

Lingnau BE, Graham J, Yarechewski D, Tanaka N, Gray MN (1996) Effects of temperature on strength and compressibility of sand-bentonite buffer, Engineering Geology 41:103–115

Pusch R, Karlnland O, Hokmark H (1990) GMM-a general microstructural model for qualitative and quantitative studies of smectite clays. SKB Technical Report 90–43, Stockholm, Sweden

Pusch R (2001) The microstructure of MX-80 clay with respect to its bulk physical properties under different environmental conditions. SKB Technical Report TR–01–08, Stockholm, Sweden

Romero E (1999) Characterisation and thermo-hydro-mechanical behaviour of unsaturated Boom-clay: an experimental study. Ph.D. Thesis, Universidad Politécnica de Cataluña, Barcelona

Romero E, Gens A, Lloret A (2000) Temperature effects on water retention and water permeability of an unsaturated clay. In: Rahardjo, Toll, Leong (eds) Proc of Unsaturated Soils for Asia. Balkema, Rotterdam

SKB (1999) SR-97: Waste, repository design and site. SKB Technical Report TR–99–08, Stockholm, Sweden

Villar MV, Rivas P, Campos R, Lloret A, Romero E, Mariano A (2001) First report on thermo-hydro-mechanical laboratory tests. Report 70–IMA–L–0–86

Villar MV, Lloret A (2004) Influence of temperature on the hydro-mechanical behaviour of a compacted bentonite, Applied Clay Science 26:337–350

Wersin P, Johnson LH, McKinley IG (in press) Performance of the bentonite barrier at temperatures beyond 100°C: A critical review, Physic and Chemistry of the Earth

Some Aspects of the Effect of the Temperature on the Behaviour of Unsaturated Sandy Clay

Moulay Smaine Ghembaza[1], Said Taïbi[2], and Jean-Marie Fleureau[3]

[1] Laboratory of Soil Mechanics and Structure, University Djillali Liabès, Faculty of the Engineer, BP 89, 22000 Sidi Bel Abbès, Algeria ghembaza_moulay@yahoo.fr
[2] Laboratory of Mechanics, Physics and Geosciences, University of Le Havre, BP 540, 76058 Le Havre Cedex, France Said.Taibi@univ-lehavre.fr
[3] Laboratory MSS-Mat, Ecole Centrale de Paris, 92295 Châtenay-Malabry cedex, France Jean-Marie.Fleureau@ecp.fr

Summary. The paper describes experimental results on triaxial paths at high temperature concerning an unsaturated clay ($w_L = 38\%$, $I_P = 19$ and $C_c = 0.23$). Unsaturated drained triaxial compression tests on normally consolidated samples were carried out at constant temperatures varying from 22 to 80°C. Desaturation of samples were carried out by the imposition of suctions using the osmotic method. This required the development of a new triaxial cell equipped with a collar heating and an osmotic pedestal which allows the circulation of an osmotic solution of Poly Ethylen Glycol (PEG) 6000, in contact with the sample via a dialysis membrane. The principal phenomena simultaneously related on the temperature and saturation were highlighted, in particular the hardening of material on isotropic path, a secant modulus which decreases with temperature and increases with suction, a light reduction in the maximum stress on deviator path at high temperature and the increase in this maximum stress when suction increases.

Key words: unsaturated triaxial path, normally consolidated, temperature, suction, THM behaviour, osmotic method

1 Introduction

The study of the thermo-hydro-mechanical behaviour of saturated and unsaturated soils is a very complex problem, and it is often useful to uncouple the effects of temperature, mechanical loading and negative pore water pressure or suction. This problem was tackled by several authors, either by comparing the soil mechanical behaviour at various temperatures under isothermal conditions, or by varying the temperature under constant stress. The main conclusions of these studies are as follows:

- On normally consolidated path, an increase in temperature results in a densification of the soil. On oedometric and isotropic normally consolidated

paths, the temperature causes a reduction in the void ratio (Fleureau and Kheirbek-Saoud 1992, Rahbaoui 1996) whereas, on an overconsolidated path, the temperature causes a dilation Belanteur et al. (1997), Sultan et al. (2002).

- In the case of overconsolidated soils, one observes that an increase in the temperature erases the overconsolidation of the material (Rahbaoui 1996).
- An increase in temperature reduces the mechanical strength of soils (Sultan et al. 2002, De Bruyn 1999, Belanteur et al. 1997). Other authors show an increase in the mechanical strength with temperature (Tanaka et al. 1997). In this case, a detailed attention must be given to the type of studied material, its initial state and its mode of preparation to clarify these contradictions.
- A few authors show that temperature reduces the value of the slope M in the plan $[p'; q]$ plane (De Bruyn 1999). However, others show little or no influence of the temperature on the value of M, and sometimes a slight increase of this parameter (Tanaka et al. 1997).

Concerning the THM behaviour of the unsaturated soils, very few results exist in the literature. This is due to the complexity of the experiments, their duration and the number of parameters to be controlled (El Youssoufi et al. 2002). Recent works show on the one hand, a reduction in suction when the temperature increases for a given water content (Romero 1999) and, on the other hand, an increase in strength with temperature for a given suction (Jamin 2003).

This paper presents experimental results allowing the study of the effect of the temperature on the behaviour of unsaturated clay on triaxial paths.

2 Materials and Experimental Devices

The material used is a mixture made up of kaolinite (90%), Hostun RF sand (5%) and silica (5%). The percentages were elaborate after several granulometry curves on various proportions. This combination has a continuous granulometry curve. This mixture will be called "sandy clay." The principal characteristics are given in Table 1.

The study of unsaturated triaxial paths according to the temperature required the development of a triaxial cell of 3.5 MPa of confining pressure (Fig. 1). The heating system is composed of a heating insulated collar with an internal diameter of 146 mm and a 230 mm height, developing a power of

Table 1. Description of the material used

Material	w_L (%)	I_P (%)	% $< 80\,\mu$m	% $< 2\,\mu$m	$d_{10}\,\mu$m	d_{60}/d_{10}
Sandy Clay	38	19	95	53	0.2	21

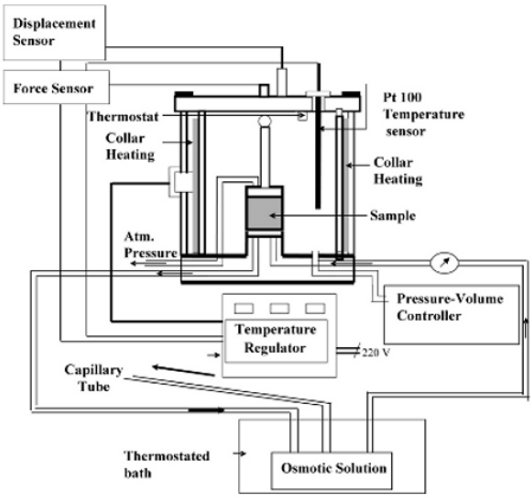

Fig. 1. Unsaturated triaxial cell with controlled temperature and imposed negative pore water pressure by the osmotic technique

1800 W. This collar comes to wrap an aluminum hollow roll. The imposition of a given temperature to the sample is controlled by an electronic regulator of temperature and a Pt100 probe. A thermocouple is used to measure the imposed temperature. Regulation and measuring equipment was developed. Like system of safety, thermostats were fixed in various places of the cell. To impose or control pressures and volumes, three pressure-volume controllers were used. The axial loading is carried out using a 25 kN loading frame. This instrumentation is controlled via a HP station.

In addition, a special pedestal at the bottom of the sample was developed to make it possible to impose negative pore water pressures using the circulation of a PEG solution in contact with the sample via a dialysis membrane. A brass plate, 2.5 mm in thickness and 35 mm in diameter, perforated by holes of 1.5 mm in diameter, comes to cap the cell pedestal. This plate serves as basis for the sample. Between the perforated plate and the sample, a disc of dialysis membrane is placed over the perforated plate. In order to prolong the lifespan of the dialysis membrane and to avoid its degradation by the bacteria naturally present in the soil, a small quantity of benzoic acid, acting like an anti-bacterial, was added to the PEG solution. In addition, the imposition of a negative pore water pressure in the soil sample using the osmotic technique is based on the assumption that the air pressure within the sample is equal to the atmospheric pressure. This condition is ensured by putting the draining circuit at the top of the sample to the atmospheric pressure. To maintain a constant concentration of the osmotic solution in the circuit, a circulation between the chamber of the pedestal and an external tank is carried out by means of a peristaltic pump of low flow.

3 Results and discussion

3.1 Effect of Temperature on Pre-Consolidation Stress in Isotropic Paths

To study the effect of temperature on the preconsolidation pressure, several tests were carried out at four values of temperature (22, 40, 60 and 80°C). Samples were first preconsolidated at isotropic effective stress $p' = 200\,\text{kPa}$, then heated at different temperatures. At equilibrium, isotropic effective stress was increased with a constant temperature. The preconsolidation stress p'_c is evaluated as the stress value at the intersection of the two linear parts of the compression curves (logarithm of mean effective stress versus void ratio). One observes a quasi linear decrease of the preconsolidation pressure when the temperature increases (Fig. 2). This is in agreement with the results from the literature (Sultan et al. 2002, Cekerevac and Laloui 2004). Cekerevac and Laloui (2004) suggested a semi-logarithmic expression to describe this decrease

$$\sigma'_c(T) = \sigma'_c(T_o)\{1 - \gamma \log[T/T_o]\}\,. \tag{1}$$

3.2 Effect of Temperature on Secant Modulus

E_{50} Secant modulus is defined as

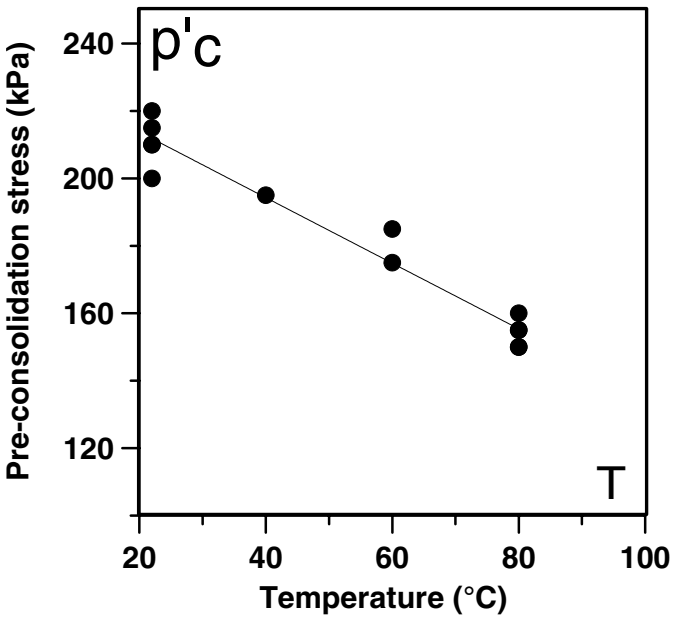

Fig. 2. Influence of temperature on preconsolidation pressure

$$E_{50\%} = \frac{q_{\max}/2}{\varepsilon_{50\%}} \,. \tag{2}$$

where, $q_{\max}$ is the maximum deviatoric strength and $\varepsilon_{50\%}$ is the axial strain corresponding to 50% of maximum deviatoric strength.

Deviatoric loading tests on triaxial paths were carried out at three values of temperatures (22, 60 and 80°C). Figure 3 shows the variation of secant modulus versus effective confining stress. One observes that for a given temperature, the secant modulus increases with effective confining stress. For a given effective confining stress, the secant modulus decreases when the temperature increases. The variation of secant modulus versus confining stress follows Hertz's law $E = \alpha(\sigma'_3)^n$ (Biarez and Taibi 1997), parameterized in temperature. Table 2 summarizes the parameters α and n according to the studied temperatures.

For unsaturated tests, several deviatoric loading tests were carried out on unsaturated samples at both constant suction and temperature. Figure 4 shows the variation of secant modulus versus suction for two values of temperature (22 and 80°C). The total confining stress was maintained equal to 1250 kPa. It is noted that the secant modulus increases with suction following a bi-logarithmic law $E = \beta(u_w)^m$ (Fleureau and Kheirbek-Saoud 1992). In addition, for a given suction, secant moduli at $T = 80$°C are lower than those

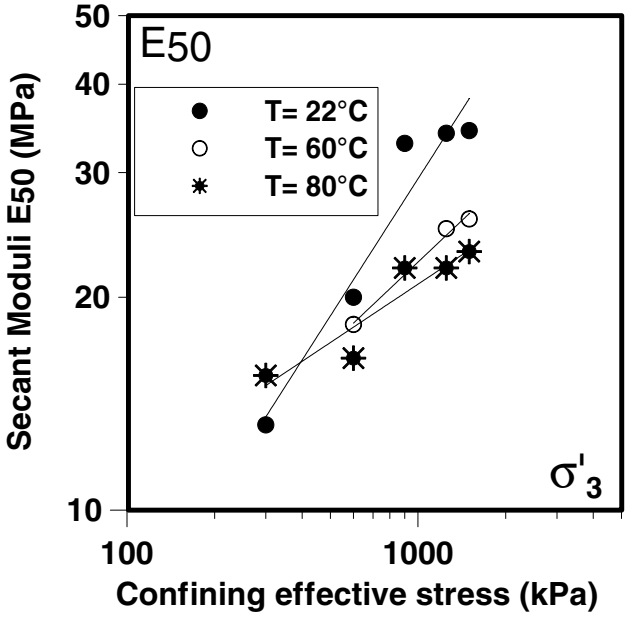

Fig. 3. Variation of secant modulus versus effective confining stress for three temperature

Table 2. Parameters α and n according to the studied temperatures

Temperature (°C)	n	α
22	0.64	0.086
60	0.39	2.63
80	0.27	14

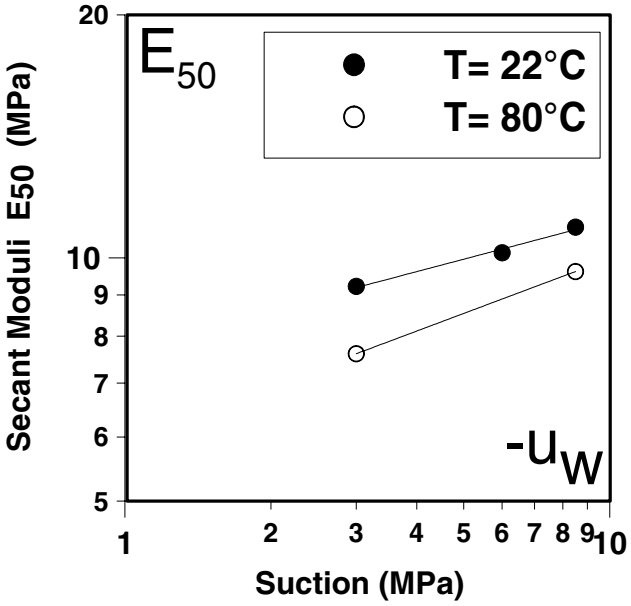

Fig. 4. Variation of secant modulus versus suction for two values of temperature (22 and 80°C)

corresponding to $T = 22°\text{C}$. In all the cases, one notes a loss of rigidity when the temperature increases.

3.3 Effect of Temperature on the Shear Strength

Figure 5 shows an example of results of unsaturated triaxial compression tests on a normally consolidated sandy clay for two imposed suctions $s = -u_w$ (3 and 8.5 MPa) and two temperatures (22 and 80°C) in $[p + s, q]$ plan. It is noticed that the envelope of maximum strengths decreases when the temperature increases and for a given temperature, maximum strength increases with suction (Wiebe et al. 1998, Ghembaza 2004).

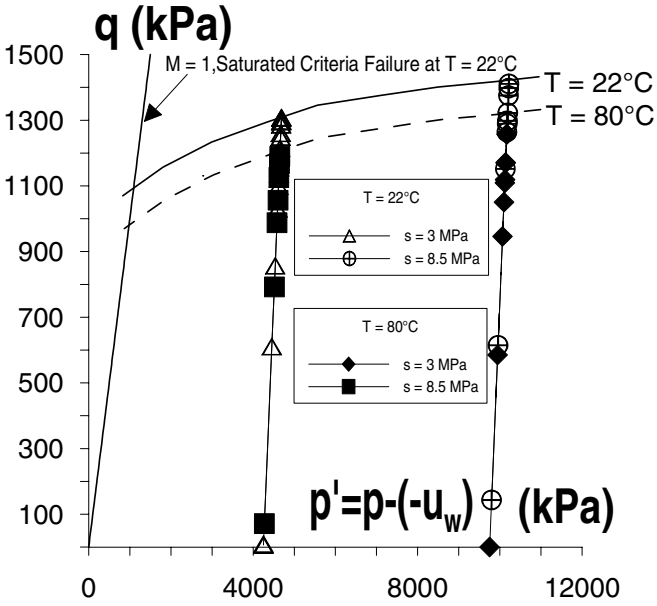

Fig. 5. Unsaturated triaxial compression tests on a normally consolidated sandy clay for two imposed suctions (3 and 8.5 MPa) and two temperatures (22 and 80°C) in $[p + s, q]$ plan

4 Conclusion

The results of laboratory study using a temperature controlled triaxial cell have been presented. Thermal effects on the mechanical behaviour of unsaturated sandy clay were analyzed by comparing tests at various temperatures and suctions. In the case of saturated soils, the preconsolidation pressure decrease when the temperature increases. This observation is in agreement with the results from the literature. It is about a negative hardening. In the case of unsaturated soils, the preconsolidation pressure increases with suction for a given temperature. It is about a hydrous hardening. For a null suction, the secant modulus follow a Hertz law $E = \alpha(\sigma' 3)n$ with n decreasing when the temperature increases. For a non-null suction, the secant modulus increases with suction. For a given suction, this modulus decreases when temperature increases. In the case of unsaturated soils, the maximum strength decreases when the temperature increases, in spite of the hardening produced by the negative pressure. This strength increases with the suction, at a given temperature.

References

Belanteur N, Tachrifet S, Pakzad M (1997) Etude des comportements mécanique, thermo-mécanique et hydromécanique des argiles gonflantes et non gonflantes fortement compactéesm Revue Française de Géotechnique 78:31–51

Biarez J, Taibi S (1997) Les modules en mécanique des sols. Journée du CFMS 'Les essais de laboratoires' 22 Janvier 1997

Cekerevac C, Laloui L (2004) Experimental study of thermal effects on the mechanical behaviour of a clay, Int J Numer Meth Geomech 28:209–228

De Bruyn D (1999) Influence d'une élévation de température sur le comportement physique et mécanique de l'argile de boom dans le cadre de la problématique de galeries d'enfouissement de déchets radioactifs. PhD Thesis, Université Catholique de Louvain

El Youssoufi MS, Jamin F, Saix C (2002) Quelques aspects du comportement hydromécanique lors de la saturation de l'état sec, Bulletin du GFHN Milieux poreux et transferts Hydriques 48:141–146

Fleureau JM, Kheirbek-Saoud S (1992) Strength of compacted soils in relation to the negative pore pressure, Revue Française de Geotechnique 59:57–64

Ghembaza MS (2004) Etude du comportement thermo-hydro-mécanique des sols argileux soumis à une pression interstitielle négative, Thèse de Doctorat, Université du Havre, France

Jamin F (2003) Contribution a l'étude du transport de matière et de la rhéologie dans les sols non saturés a différentes températures. Thèse de Doctorat, Université de Montpellier II, France, 260 p

Rahbaoui A (1996) Modélisation du comportement Thermo-Mécanique des argiles saturées : Application au stockage des dechéts radioactifs. Thèse de doctorat, Université d'Orléans, 293 p

Romero EM (1999) Characterization and thermo-hydro-mechanical behaviour of unsaturated boom clay and experimental study. PhD Thesis, Univ Polytech Catalunya, Barcelona

Sultan N, Delage P, Cui YJ (2002) Temperature effects on the volume change behaviour of Boom clay, Engineering Geology 64:135–145

Tanaka N, Graham J, Crilly T (1997) Stress-strain behaviour of reconstituted illitic clay at different temperatures, Engineering Geology 47:339–350

Wiebe B, Graham J, Tang GXM, Dixon D (1998) Influence of pressure, saturation, and temperature on the behaviour of unsaturated sand-bentonite, Can Geotech J 35:194–205

Influence of Temperature on the Water Retention Curve of Soils. Modelling and Experiments

Simon Salager, Moulay Saïd El Youssoufi, and Christian Saix

LMGC UMR CNRS 5508, Université Montpellier 2, Place Eugène Bataillon
34095 Monpellier Cedex 5, France
salager@lmgc.univ-montp2.fr, elyous@lmgc.univ-montp2.fr,
saix@lmgc.univ-montp2.fr

Summary. We investigate the influence of temperature on the retention curve of soils. This curve represents the constitutive relation between water content w and suction s, for a given temperature T and a given void ratio e. We present a model based on the differential of suction as a function of T, w and e. When adjusted for a retention curve obtained at a given temperature, this model enables to predict this curve for any temperature. In parallel, we carried out experiments on a clayey silty sand by using a pressure cell immersed in a thermostatic bath. The model was validated by several tests on the clayey silty sand at 20 and 60°C. The application of the model to data found in the literature confirms its predictive power for a wide range of porous materials. These results allow us to plot the retention surface, from experimental tests obtained at a given temperature and from modelling. It can be considered as a generalization of the classical retention curve. Finally, we discuss the influence of the void ratio variation during experiments on the curve predicted by the model.

Key words: retention curve, thermo-hydric behaviour, pressure cell, soil, porous media

1 Introduction

Water retention curve is the constitutive relation between suction s and water content w or water volume fraction θ or degree of saturation S_r. This relation is always done for a given temperature T and a given void ratio e. The general shape of this curve depends particularly on the porosity, the pore-geometry characteristics, the grain-size distribution, and the nature (granular or clayey) of the material. Besides its capability to describe the hydraulic behaviour, some authors used it to yield the coefficient of permeability (Fredlund et al. 1994, Van Genuchten 1980) or to analyse shear strength for unsaturated soils (Fredlund et al. 1995). Finally, water retention curve gives a conceptual

framework to understand the hydraulic behaviour of an unsaturated porous media at a given temperature. However, several environmental problems like energy structures (Saix 1987, Laloui et al. 2003), nuclear waste storage in deep clay (Olchitzky 2002), require to take into account the temperature variable in the analysis of hydraulic behaviour. In particular, it is necessary to study the temperature dependence of water retention curve.

This paper presents a contribution to the characterization of the thermo-hydraulic behaviour of unsaturated porous media. From a water retention curve obtained experimentally at a given temperature, a theoretical model allows to predict this curve for other temperatures, reducing then extensively experimental tests to get water retention curve at several temperatures.

The model was validated by the authors on experiments realized on a ceramic and on a clayey silty sand. Its application to other data found in literature confirms its predictive power for a wide range of porous media.

2 Constitutive Thermo-Hydraulic Model

Several mechanisms can be proposed to explain the influence of temperature on the hydraulic behaviour: thermal expansion of the different phases, surface tension of water (liquid phase consists of pure water only), and contact angle variations (Bachmann and Van Der Ploeg 2002). Our model is based on the development of the differential of suction s with respect to the three independent variables: water volume fraction θ (volume of water per unit apparent volume), temperature T and void ratio e. To avoid hysteresis problem, we consider here only the drying path from a saturated state.

We can then express the suction differential by the relation:

$$\mathrm{d}s = \left(\frac{\partial s}{\partial \theta}\right)_{T,e} \mathrm{d}\theta + \left(\frac{\partial s}{\partial T}\right)_{\theta,e} \mathrm{d}T + \left(\frac{\partial s}{\partial e}\right)_{T,\theta} \mathrm{d}e\,. \tag{1}$$

This relation can be explained by expressing the different partial derivative of s from physical relations. The water volume fraction can be written as a function of the specific weight of solid phase ρ_s^*, the specific weight of the liquid phase ρ_e^*, the water content w (mass of water per unit mass of dry soil), and the void ratio:

$$\theta = \frac{\rho_s^* w}{\rho_e^*(1+e)}\,. \tag{2}$$

From relation (2), it is possible to express the differential $\mathrm{d}\theta$, by introducing the volumetric thermal expansion coefficient of water β_e and the volumetric thermal expansion coefficient of the solid phase β_s. That leads to the relation:

$$\mathrm{d}\theta = \frac{\rho_s^*}{\rho_e^*(1+e)}\mathrm{d}w + \frac{\rho_s^* w}{\rho_e^*(1+e)}(\beta_e - \beta_s)\mathrm{d}T - \frac{\rho_s^* w}{\rho_e^*(1+e)^2}\mathrm{d}e\,. \tag{3}$$

Equation (2) also allows us to write:

$$\left(\frac{\partial s}{\partial \theta}\right)_{T,e} = \frac{\rho_e^*(1+e)}{\rho_s^*}\left(\frac{\partial s}{\partial w}\right)_{T,e}. \tag{4}$$

In the context of studies of water retention in porous media, it is common to use Jurin's law which express the suction as a function of the surface tension of water σ_s, the mean pore radius r, and the contact angle ϕ.

$$s = \frac{2\sigma_s \cos\phi}{r}. \tag{5}$$

From equation (5), we can express the derivative of suction with respect to temperature:

$$\left(\frac{\partial s}{\partial T}\right)_{\theta,e} = \frac{s}{\sigma_s}\frac{\mathrm{d}\sigma_s}{\mathrm{d}T} - s\tan\phi\frac{\mathrm{d}\phi}{\mathrm{d}T}. \tag{6}$$

Relation (6) takes into account the fact that the surface tension of water and the contact angle are only dependent on temperature. Introducing relations (3), (4), and (6) in equation (1), we obtain the final form of the differential of suction:

$$\begin{aligned}\mathrm{d}s = F_w\mathrm{d}w + \left(F_w w(\beta_e - \beta_s) + \frac{s}{\sigma_s}\frac{\mathrm{d}\sigma_s}{\mathrm{d}T} - s\tan\phi\frac{\mathrm{d}\phi}{\mathrm{d}T}\right)\mathrm{d}T \\ + \left[\left(\frac{\partial s}{\partial e}\right)_{T,\theta} - \frac{F_w w}{(1+e)}\right]\mathrm{d}e\end{aligned} \tag{7}$$

where F_w is the reciprocal of the slope of the retention curve for a given temperature ($F_w = \left(\frac{\partial s}{\partial w}\right)_{T,e}$). The right-hand side of the relation (7) expresses three terms reflecting the respective contributions of the variations of water content, temperature and void ratio, to the infinitesimal variations of suction. The first and the second terms show strong coupling between suction, water content and temperature. In the case of low deformable materials, the third term become negligible in respect to the others. Its experimental determination during the thermo-hydro-mechanical path is not easy. In addition, the infinitesimal variations of void ratio, are understood here without external mechanical stress, the deformations are thus limited. In a first approach, this term will be neglected. The relevance of this choice will be discussed thereafter. In the same way, the variation of the contact angle versus temperature is very difficult to measure. One can found few results in literature about this subject. Thus, in our experimental validation of the model, this variation will not be taken into account. Futhermore, the volumetric thermal expansion coefficient of the solid phase is assumed to be negligible, compared with volumetric thermal expansion coefficient of water. Under these assumptions, relation (7) can be written in the simplified form (8):

$$\mathrm{d}s = F_w dw + \left(F_w w\beta_e + \frac{s}{\sigma_s}\frac{\mathrm{d}\sigma_s}{\mathrm{d}T}\right)\mathrm{d}T. \tag{8}$$

Finally, from a retention curve obtained at a temperature T_0, the relation (8) allows to predict, for each suction value, the water content variation as a function of the temperature variation. Thus, we obtain the water retention curve for any temperature T.

3 Experimenal Validation

3.1 Experimental Device and Materials

For model validation, several tests were done with an experimental pressure cell, regulated in temperature (Fig. 1). Suction is applied using the air overpressure method (Jamin 2003). The sample is placed in an airtight cell for which the air pressure is regulated by pneumatic system. It is put on a porous ceramic plate with an high air-entry pressure to allow the continuity of the liquid phase between the sample and the hydraulic system. The airtight cell is immersed in a thermostatic bath, where the temperature ranges from 20 to 70°C.

In the experimental part, we used two materials:

- The first is a ceramic, with a specific weight of 2738 kg.m^{-3}, a dry density of 1870 kg.m^{-3} and a void ratio of 0.464. Before each loading, the samples are saturated with chemically pure water. At saturation, water content is 16.9% at 20°C.

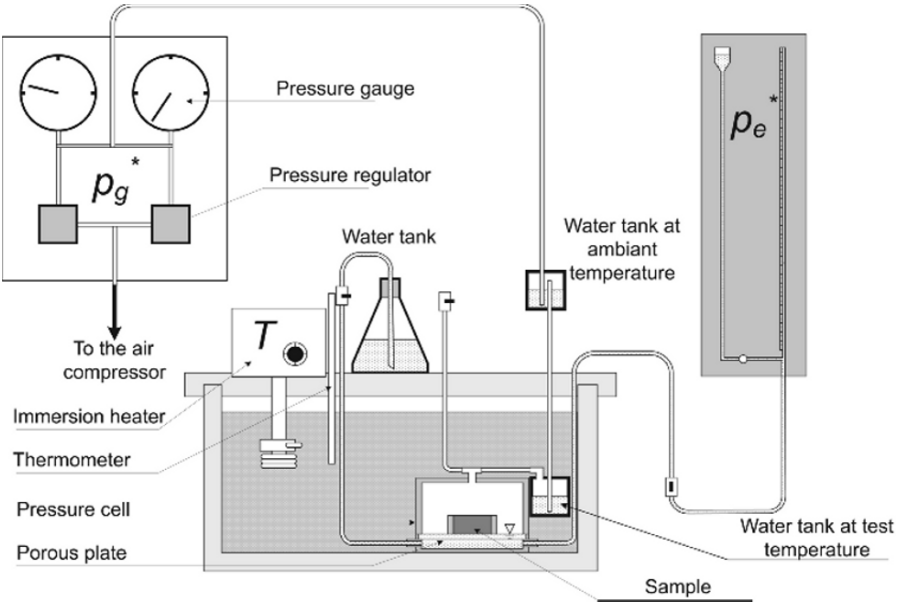

Fig. 1. General scheme of the pressure cell in its environment

- The second is a clayey silty sand with a specific weight of 2650 kg.m^{-3}. The samples are compacted in order to arise a dry density of 1500 kg.m^{-3}. That corresponds to a void ratio of 0.767. The saturated initial state corresponds to a water content of 28.9% at 20°C.

3.2 Results and Discussion

Figure 2 shows the experimental water retention curve of the ceramic obtained at 20 and 60°C. Figure 3 gives the same results for the clayey silty sand. These curves are modelled from experimental data using the fitting function proposed by Fredlund and Xing (1994). Retention curve at 20°C is used as a reference for the modelling described in Sect. 2. For a temperature of 60°C, results of modelling are shown in Fig. 2 for the ceramic and in Fig. 3 for the clayey silty sand. Retention curves, obtained from experiments and modelling, are very similar in both cases. For the clayey silty sand, one can note a divergence after a suction which corresponds to the transition between funicular state and pendular state (Fig. 4). Indeed, the liquid phase is not continuous anymore in the pendular state.

To complete the validation, we applied our model to data found in the literature for two different clays:

- The first is a FoCa compacted clay (Imbert et al. 2005). Its major component is an interstratified clay of 50% calcium beidellite and 50% Kaolinite. It has a liquid limit of 112%, a plastic limit of 50% and a specific weight of 2675 kg.m^{-3}.
- The second is an artificially prepared clay obtained from natural Boom clay (Romero et al. 2001). It is a moderately swelling material (20–30% kaolinite, 20–30% illite and 10–20% smectite) which has a liquid limit of 56%, a plastic limit of 29% and a specific weight of 2700 kg.m^{-3}.

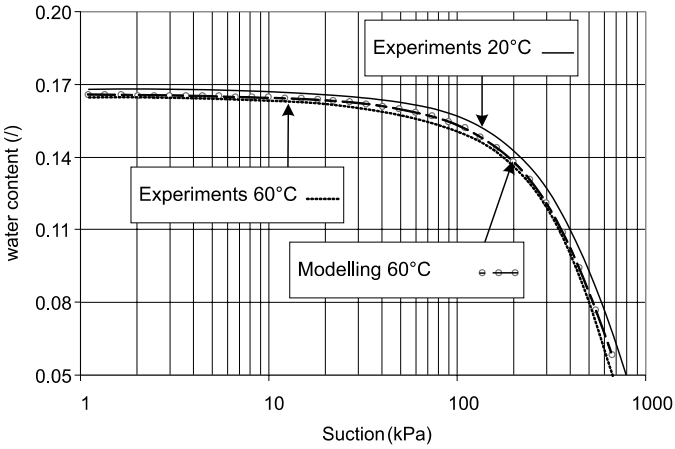

Fig. 2. Water retention curves for the ceramic: experiments and modelling

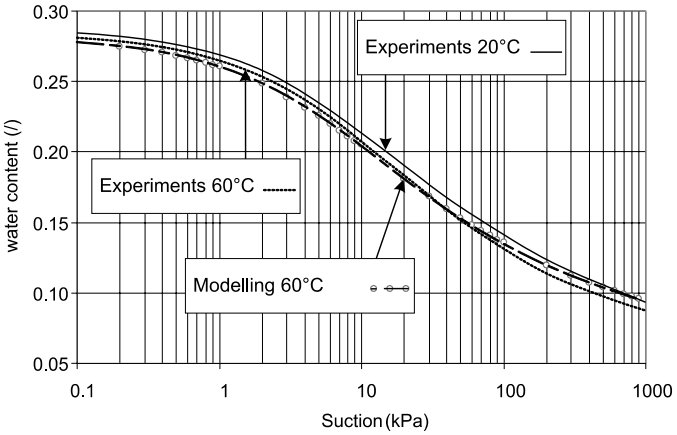

Fig. 3. Water retention curves for the clayey silty sand: experiments and modelling

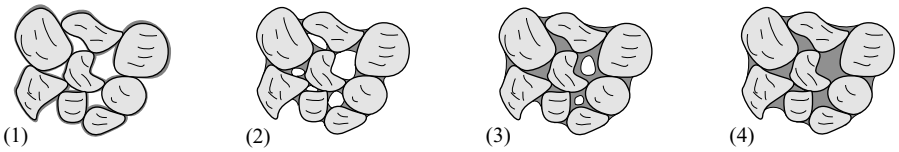

Fig. 4. Different hydraulic states: (1) Hygroscopic state: the gas phase is continuous but not the liquid phase; (2) Pendular state: continuity of each phase is not ensured; (3) Funicular state: the liquid phase is continuous but not the gas phase, (4) Saturated state

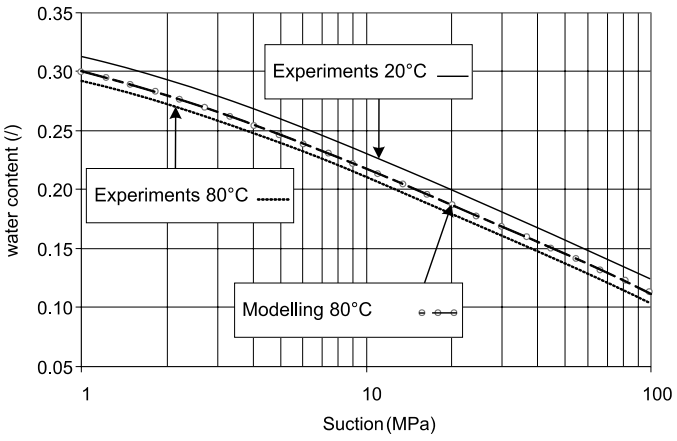

Fig. 5. Water retention curves for the FoCa compacted clay (Imbert et al. 2005): experiments and modelling

Figure 5 shows the results obtained for the FoCa compacted clay; the temperatures of the tests were 20 and 80°C. We can note on this figure that experimental results at 80°C are in good agreement with the modelling results.

Figure 6 gives Romero's results (Romero et al. 2001) on the Boom clay. These tests were made for two different temperatures (22 and 80°C) and for a dry unit weight of $16.7\,\mathrm{kN.m^{-3}}$. In this case, our model is still in good agreement with experimental data. Other results obtained by Romero et al. (2001), in the same conditions but with a dry unit weight of $13.7\,\mathrm{kN.m^{-3}}$, were well predicted by the model. The hypothesis which could result in neglecting the third term of the relation (7) with respect to the others seems acceptable. In fact, although the variation of void ratio can be not negligible on the whole test, it does not seem necessary to take into account explicitly this variation in the calculation. Indeed, the determination of the reciprocal slope of the water retention curve F_w integrates implicitly the contribution of the gradual deformation of the material during the hydraulic path.

Comparison between modelling and experimental results, for four different materials, demonstrates the capability of relation (8) to predict retention curve for any temperature from a retention curve made at a given temperature. Finally, these results allow us to plot a water retention surface $w = w(s, T)$. This surface obtained from experimental tests at a given temperature and from modelling, can provide a conceptual framework to understand thermo-hydraulic behaviour of unsaturated porous media.

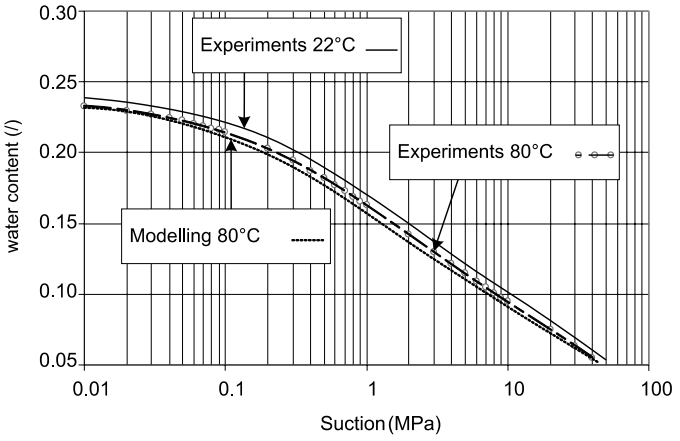

Fig. 6. Water retention curves Boom clay (Romero et al. 2001): experiments and modelling

4 Conclusion

We investigated the influence of temperature on the water retention curve of soils. We presented a model based on the differential of suction as a function of temperature, water content and void ratio. When adjusted for a water retention curve obtained at a given temperature, this model enables to predict this curve for any temperature. In parallel, we carried out experiments on a clayey silty sand and on a ceramic by using a pressure cell immersed in a thermostatic bath. The model was validated by several tests on these two materials at 60°C. The application of the model to data found in the literature confirmed its predictive power for a wide range of porous materials. These results allowed us to plot the water retention surface, from experimental tests obtained at a given temperature and from modelling. It can be considered as a generalization of the classical retention curve.

References

Bachmann J, Van Der Ploeg RR (2002) Soil Sci 165:468–478

Fredlund DG, Xing A (1994) Can Geotech J 31:521–53

Fredlund DG, Xing A, Huang S (1994) Can Geotech J 31:533–545

Fredlund DG, Xing A, Fredlund MD, Barbour SL (1995) Can Geotech J 32:440–448

Imbert C, Olchitzky E, Lassabatère T, Dangla P, Courtois A (2005) Engineering Geology 81:269–283

Jamin F (2003) Contribution à l'étude du transport de matière et de la rhéologie dans les sols non saturés à différentes températures. PhD Thesis , Université Montpellier 2, Montpellier

Laloui L, Moreni M, Vulliet L (2003) Can Geotech J 40:388–402

Olchitzky E (2002) Couplage hydromécanique et perméabilité d'une argile gonflante non saturée sous sollicitations hydriques et thermiques. PhD Thesis, Ecole Nationale des Ponts et Chaussées, Paris

Romero E, Gens A, Lloret A (2001) Geotechnical and Geological Engineering 19:311–332

Saix C (1987) Contribution à l'étude des sols non saturés en température. Application à l'exploitation thermique des sous-sols. PhD Thesis, Université Montpellier 2, Montpellier

Van Genuchten MT (1980) Soil Sci Soc Am J 44:892–898

Thermo-Hydro-Mechanical Behaviour of Compacted Bentonite

Abbass Tavallali[1], Anh-Minh Tang[2], and Yu-Jun Cui[2]

[1] Department of Civil Engineering, Katholieke Universiteit Leuven, Heverlee, Belgium Abbass.Tavallali@bwk.kuleuven.be
[2] Ecole Nationale des Ponts et Chaussées, CERMES, Paris, France tang@cermes.enpc.fr, cui@cermes.enpc.fr

Summary. Like every human activity, the nuclear activities generate waste. Because of the particular characters of the nuclear waste, a special geological formation and also plug material for storage of the high level nuclear waste is necessary.

The plug material plays an important role in confining the radioactive waste. Therefore, one needs a material with the character of very low permeability and a good capacity of holding the radionuclides. The compacted bentonite will thus be employed as such plug material. So it is very important to evaluate the swelling characters of compacted bentonite.

Here, it is presented an experimental study of thermo-hydro-mechanical behaviour of compacted bentonite of MX–80, based on tests carried out in an isotropic high-pressure cell (60 MPa) in the range 20 and 80°C (±0.1°C). The results present the deformation of compacted bentonite as a function of temperature, suction and pressure.

Key words: nuclear waste, temperature effects, compacted bentonite, MX–80, swelling soils, suction, laboratory tests

1 Introduction

Swelling soils such as bentonite have recently attracted increasing attention as back-filling (buffer) materials for high-level nuclear waste (Swedish Nuclear Fuel Supply Co./Division KBS 1983, Yong et al. 1985, Bucher and Mayor 1989).

High-density compacted bentonite (Fig. 1) in the form of blocks has also been proposed as sealing material in high-level radioactive waste repositories, as it provides very low permeability, high exchange capacity, sufficient thermal conductivity, and adequate mechanical resistance (Lloret et al. 2003).

The function of buffer material is to create an impermeable zone around the canister containing the high-level nuclear waste, since nuclear waste must be kept separate from the surrounding environment (Komine and Ogata 1996).

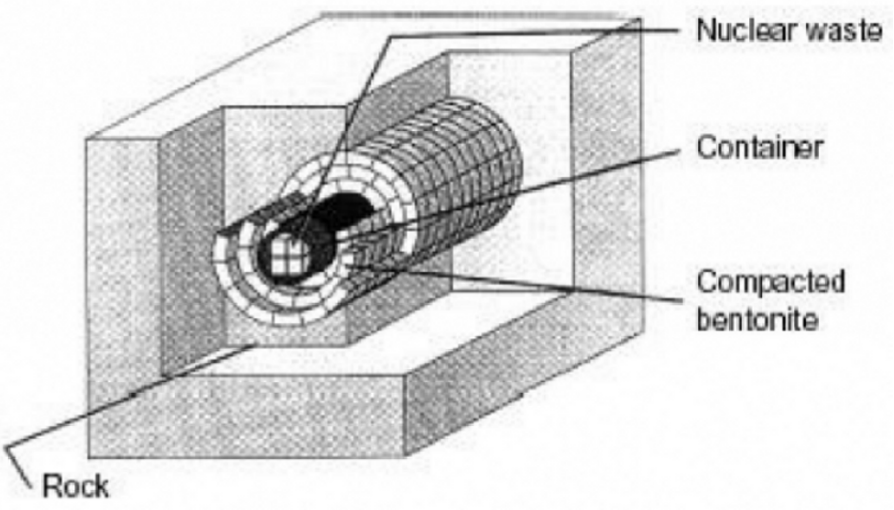

Fig. 1. Proposed engineered barrier made up of compacted bentonite clay for a radioactive waste repository (Lloret et al. 2003)

The buffer materials must have swelling properties because cracks in the surrounding rocks may appear and need to be filled up. Compacted bentonite will therefore be used as buffer material (Komine and Ogata 1996). To develop buffer materials using compacted bentonite, it is important to evaluate the swelling characteristics of compacted bentonite.

2 Materials and Methods

In this study MX–80 is selected to evaluate the thermo-hydro-mechanical behaviour of compacted bentonite. It is focused on thermal volume-change of MX–80 at different states of suction and pressure. The characteristics of MX–80 are presented in Table 1. MX–80 (Pusch 1982) is a Na^{+}–Ca_2^{+} smectite with a clay fraction ($< 2\,\mu m$) of 85% and a montmorillonite fraction of about 80–90% of this fraction. The remaining silt fraction mainly consists of quartz and feldspars, with some micas, sulphides, and oxides (Marcial et al. 2002).

The tests were performed in temperature-controlled high-pressure isotropic cells (temperature and pressure varied between 20 and 80°C ± 0.1°C, and 0–60 MPa, respectively), connected to GDS pressure volume controllers. Volume changes were obtained from the GDS monitoring of the all round water exchanges (Sultan et al. 2000).

Initially MX–80 is in the powder shape. To dry the powder and to stabilize the initial conditions, a desiccator containing saturated salt solutions of K_2CO_3 is used. The suction was controlled by imposing controlled humidity conditions in desiccator containing saturated salt solutions. In the vapour

phase method of controlling suction, saturated salt solutions are used to control the relative humidity of the atmosphere of desiccators in which the sample is placed (Marcial et al. 2002). This powder is dried under the suction of 113 MPa (Table 2). When the mass of the powder does not change during a few days, it can be said that stabilization is finished. With this suction the water content is about 10%.

For this study, disc-shaped samples with a diameter of 80 mm and a height of 12 ± 2 mm were needed. The procedure of the compaction and then machining were used to produce the samples (Tavallali 2005).

In the compaction step, loading up to the 40 MPa is carried out stage by stage (0.1–0.2–0.5–1–2–5–10–20–40 MPa). For each stage it is necessary to wait until the volume of water which left GDS becomes constant. The duration of this step is about six hours. In this part, suction in the sample changes because of changing the volume of void under isotropic compression. Then to reach the initial suction, the sample is placed in the desiccator containing saturated salt solutions of K_2CO_3 (relative humidity of 44% and the suction of 113 MPa). For machining it is necessary to be sure that the mass of compacted sample is stabilized (similar way for powder of MX–80). By a special machine in CERMES, it is possible to have a cylindrical sample with a diameter of 80 mm. Then by sawing manually every 12 mm, a disc of 80 mm in diameter and 12 mm in height is produced. It is important to put the discs immediately in the preceding desiccator to reach the initial suction of 113 MPa.

To evaluate the thermo-hydro-mechanical behaviour of unsaturated compacted bentonite, having the samples with different suctions is necessary. With different salt solutions it is possible to have different suctions. In humidifying

Table 1. Identification parameters of MX–80 (Marcial et al. 2002)

Mineralogy	85% Na–Ca smectite
Liquid limit, w_L (%)	520
Plastic limit, w_P (%)	62
Plasticity index, I_P	458
Unit mass of the solids, ρ_s (Mg/m^3)	2.65

Table 2. Salts used in the vapour phase method of controlling suction (Marcial et al. 2002)

Salt	Suction (MPa)
K_2SO_4	4.2
KNO_3	9
NaCl	38
$NaNO_2$	57
$Mg(NO_3)_2$	82
K_2CO_3	113

Table 3. Test program of thermal isotropic compression

Test	Initial conditions		Loading			
	ρ_d	Suction	1		2	
	(g/cm3)	(MPa)	P (MPa)	T (°C)	P (MPa)	T (°C)
Iso 8*	1.421	39	0.1	25	50	25
Iso 9	1.203	9	0.1	25	0.1	80
Iso 10	1.422	39	0.1	25	5	25
Iso 11	1.205	9	0.1	20	50	20
Iso 12	1.206	9	0.1	25	0.1	80
Iso 13	1.421	39	0.1	25	5	25

*There is a cycle of 25–75–25°C at $P = 5$ MPa

the samples, suction change must be stage by stage. For example to decrease the suction from 113 MPa to 9 MPa it is necessary to use salt solutions of $Mg(NO_3)_2$, $NaNo_2$, NaCl, KNO_3 (82, 57, 38, 9 MPa, respectively) stage by stage. Changing the salt solutions only after mass stabilization of the bentonite is possible.

Table 3 shows the test program carried out in this study. As in this study the vapour phase method of controlling suction is used, when the temperature in a test is 25°C (the temperature of environment), the same salt solution which is already used to humidify the sample is used, even in the fast increase or decrease of temperature (approximately 10 h). It is supposed that in these two cases suction does not change. But when it is plan to increase the temperature and to stabilize it during 1 or 2 months, suction increases and thus it is necessary to use another salt solution (that already has used to humidify the sample). For example when initial suction is 9 MPa (by using salt solution KNO_3) and test must carry out in 80°C, it is necessary to use the salt solution K_2SO_4 with the suction of 4.2 MPa. Because when the temperature increases, suction increases and will be roughly equal to initial suction (9 MPa) and thus the test carry out under constant suction. With this condition one can evaluate the influence of the temperature on the behaviour of compacted bentonite.

3 Test Results

The aim of this study is to evaluate the thermal volume-change behaviour of the bentonite. The volume changes were measured by monitoring the exchanges of the water contained in the cell (Sultan 1997) using a pressure–volume controller (GDS) of high capacity (60 MPa maximum pressure). Figure 2 shows the effect of heating on the thermal volumetric strain of the bentonite. This figure shows the results for the tests Iso 8, Iso 9 and Iso 12.

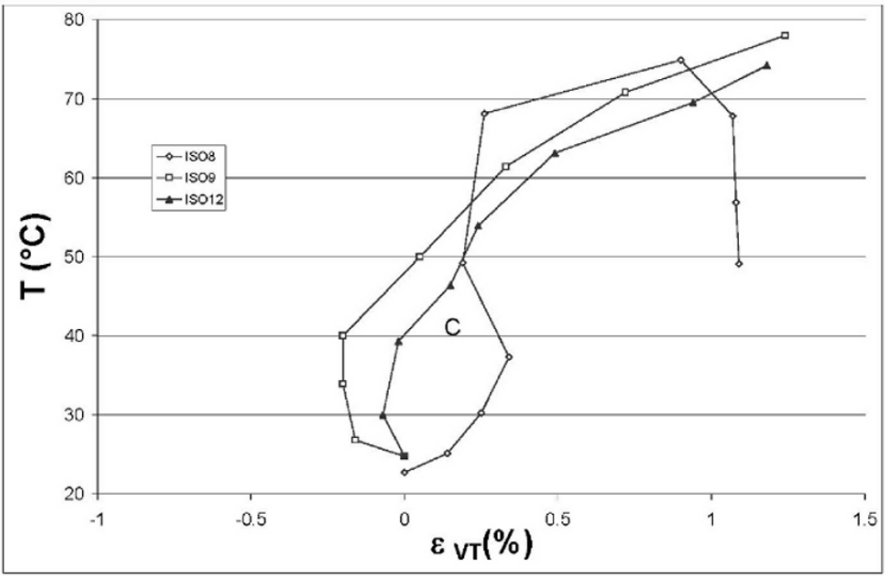

Fig. 2. Temperature effect on the thermal volume-change for the tests Iso 8, Iso 9 and Iso 12

Figure 2 shows that heating the samples Iso 9 and Iso 12 initially produced a small thermal dilation until 40°C. Then when the temperature exceeds 40°C, a thermal contraction can be observed. Also this figure shows that volume strain is very small and therefore temperature change of the environment can easily influence this deformation. This problem exists for the test Iso 8 until 50°C. In spite of that, the thermal volume behaviour of the bentonite in test Iso 8 is similar to the tests Iso 9 and Iso 12. The important point in the test Iso 8 is the irreversible thermal volume strain behaviour of bentonite. In this test when the temperature was decreased a very small thermal contraction was continued.

Figure 3 shows the variation of the void ratio according to pressure. This figure presents the results for the tests Iso 8, Iso 10, Iso 11 and Iso 13. A cycle of heating–cooling on the sample Iso 8 is applied. In spite of that, Figure 3 shows that the variations of void ratio of the samples Iso 8, Iso 10 and Iso 13 under the applied pressures of 0.1 MPa to 5 MPa are roughly identical. Thus it can be concluded that the thermal volume–change is smaller than the volume–change by the pressure. These three samples (Iso 8, Iso 10 and Iso 13) have the same suctions of 39 MPa but the suction of the sample Iso 11 is 9 MPa. By comparing these four samples it can be concluded that the influence of suction on the volume-change is considerable. The results show that the effect of suction on the volume–change is larger than the effect of the temperature.

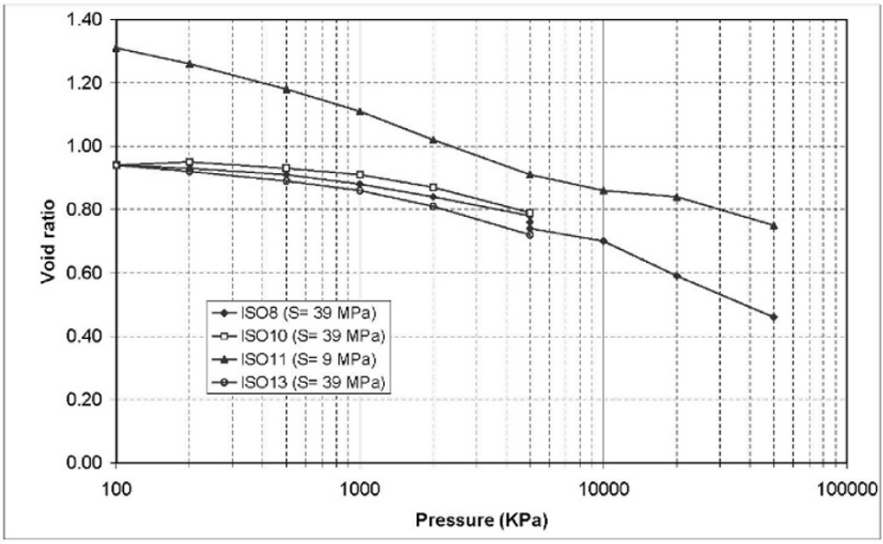

Fig. 3. Variation of void ratio in the function of pressure for the tests Iso 8 (cycle of 25–75–25°C at $P = 5$ MPa), Iso 10, Iso 11 and Iso 13

4 Conclusion

Figures 2 and 3 give some of the thermo-hydro-mechanical behaviour of compacted bentonite. They can be summarized as follows:

1. The samples under the heating have a small dilation until 40°C and then contract and during cooling a small contraction continue, in agreement with Sultan et al. (2000).
2. The cycle of the heating–cooling of the sample is irreversible, in agreement with Sultan et al. (2000).
3. The thermal volume–change of bentonite under the effect of the temperature is very small (approximately 1%).
4. The thermal volume–change in comparison to effects of the pressure is negligible, in agreement with Campanella and Mitchell (1968) and Cui et al. (2000).
5. By comparing the result of this study with the result of saturated clays (Cui et al. 2000) it can be concluded that the thermo-hydro-mechanics behaviour of unsaturated compacted bentonite is similar to the saturated soil.
6. The thermal volumetric deformation in comparison with the effects of suction is negligible.
7. When suction increases the initial void ratio and the slope of the $e - \log p$ diagram decrease, in agreement with Lloret et al. (2003).

References

Bucher F, Mayor PA (1989) Medium-scale experiments on high-compacted bentonite. In: 12th international Conference on Soil Mechanics and Foundation Engineering, Rio de Janeiro 1:583–585

Campanella RG, Mitchell JK (1968) Influence of temperature variations on soil behaviour, J Soil Mech Found Div, ASCE 94:709–734

Cui YJ, Sultan N, Delage P (2000) A thermomechanical model for saturated clays, Can Geotech J 37:607–620

Komine H, Ogata N (1996) Prediction for swelling characteristics of compacted bentonite, Can Geotech J 33(1):11–22

Lloret A, Villar MV, Sànchez M, Gens A, Pintado X, Alonso EE (2003) Mechanical behaviour of heavily compacted bentonite under suction changes, Géotechnique 53(1):27–40

Marcial D, Delage P, Cui YJ (2002) On the high stress compression of bentonites, Can Geotech J 39:812–820

Pusch R (1982) Mineral-water interactions and their influence on the physical behaviour of highly compacted Na bentonite, Can Geotech J 29:1044–1059

Sultan N, Delage P, Cui YJ (2000) Comportement thermomécanique de l'argile de Boom, CR Acad Sci Paris Série II b 328:457–463

Sultan N (1997) Étude du comportement thermo-mécanique de l'argile de Boom: expériences et modélisation. Ph.D. Thesis École nationale des ponts et chaussées

Swedish Nuclear Fuel Supply Co./Division KBS (1983) Final storage of spent nuclear fuel-KBS-3, III barriers. Swedish Nuclear Fuel Supply Co./Division KBS Technical Report pp 9:1–16:12

Tavallali A (2005) Comportement thermo-hydro-mécanique de la bentonite compactée non saturée, Rapport de stage, École nationale des ponts et chaussées

Yong RN, Boonsinsuk P, Yiotis D (1985) Creep behaviour of a buffer material for nuclear fuel waste vault, Can Geotech J 22:541–550

Retention Curves of Two Bentonites at High Temperature

María Victoria Villar and Roberto Gómez-Espina

CIEMAT, Avd. Complutense 22, 28040 Madrid, Spain
mv.villar@ciemat.es, roberto.gomez@ciemat.es

Summary. Two methods were developed to determine the retention curve for a fixed dry density and at high temperature. The materials used are the MX–80 and the FEBEX bentonites. The retention capacity of the FEBEX bentonite is higher than that of MX–80, i.e. for a given suction and dry density, the water content of the FEBEX bentonite is higher. However, the difference between both bentonites becomes smaller towards the lower suctions. In both bentonites the retention capacity has decreased as temperature increased, and the difference in the retention capacity of the two bentonites became less important at high temperature.

Key words: bentonite, temperature, retention capacity, density, water retention curve

1 Introduction

The work presented here has been done in the context of projects related to the study of the bentonite engineered barrier in high-level radioactive waste (HLW) repositories. Most probably the bentonite will be placed in the repository in the form of compacted blocks around the waste containers. Since the barrier will be manufactured with the clay at its hygroscopic water content, the bentonite will initially have degree of saturation lower than 100%. Due to the heat produced by the radioactive decay of the wastes, the barrier will be subjected to temperatures of up to around 100°C, depending on the particular disposal concept.

One of the properties that have to be known to analyse and model the hydration of the bentonite barrier is its water retention capacity. Previous investigations have shown that the retention curve (or water adsorption isotherm), for the same initial conditions of the material, differs significantly depending on the volume restriction imposed to the sample during the determination. Since the state of the bentonite in the barrier will be mostly confined, the methods developed to determine the retention curve must keep the volume of

the material constant (Villar and Lloret 2004). They must also try to reproduce the temperatures expected in the barrier.

The materials tested are two bentonites compacted to high densities: the MX–80 and the FEBEX. Both have been selected by different countries as reference materials for the sealing of HLW repositories.

2 Material

Two bentonites have been used in this investigation: the Spanish FEBEX bentonite and the American MX–80 bentonite.

The FEBEX bentonite comes from the Cortijo de Archidona deposit (Almería, Spain) and its characterisation can be found in ENRESA (1998, 2000), Villar (2002), Fernández (2003). The smectite content of the FEBEX bentonite is higher than 90% ($92 \pm 3\%$) and it contains variable quantities of quartz ($2 \pm 1\%$), plagioclase ($2 \pm 1\%$), K-felspar, calcite and opal-CT. The CEC varies from 96 to 102 meq/100 g, and the major exchangeable cations are Ca (35–42 meq/100 g), Mg (31–32 meq/100 g), Na (24–27 meq/100 g) and K (2–3 meq/100 g). The hygroscopic water content in equilibrium with the laboratory atmosphere is $13.7 \pm 1.3\%$.

The MX–80 bentonite is extracted from Wyoming (USA). It is a worldwide known material supplied in the form of powder homoionised to sodium. The MX–80 bentonite consists mainly of montmorillonite (65–82%). It also contains quartz (4–12%), feldspars (5–8%), and smaller quantities of cristobalite, calcite and pyrite. The CEC is 74 meq/100 g, and the major exchangeable cations are Na (61 meq/100 g), Ca (10 meq/100 g) and Mg (3 meq/100 g). The hygroscopic water content at laboratory conditions is 9%.

3 Methodology

3.1 Cell Method

To determine the water retention curve at constant volume, avoiding the swelling of the clay in wetting paths, special cells were designed (Villar 2002, Villar and Lloret 2004). The cells consist of a stainless steel cylindrical body with two perforated covers joined by bolts. Granulated clay is compacted directly inside the cell ring at room temperature using static uniaxial compaction. The length of the specimen is 1.2 cm and its cross section area is 11.34 cm^2.

The cells are placed in desiccators with a sulphuric acid solution or with a NaCl solution. There are temperature-dependent experimental relations between the concentration of the solution and its water activity (a_w). The calculation of suction on the basis of relative humidity ($RH = a_w/100$) is accomplished through Kelvin's equation. For the cell method the suction is,

therefore, imposed controlling the relative humidity. The cells allow the exchange of water in the vapour phase between the clay and the atmosphere of the desiccators. Once the water content of the clay is stabilized (approximately after 2 to 3 months), the solution in the desiccators is changed in order to apply a different suction. To determine the curve at different temperatures, the desiccators are placed inside ovens.

3.2 Sensor/Cell Method

The drawback of the cell method is the duration of the test, because the time to reach equilibrium at a given suction is very long. To overcome this drawback, another method to determine the retention curve at constant volume and at different temperatures has been developed (Villar et al. 2005, 2006). It consists on mixing the clay with a given quantity of deionised water and compacting this mixture to obtain a bentonite block whose relative humidity is measured by means of a capacitive sensor while the block is kept inside a hermetic cell made out of stainless steel.

The wetted clay is kept for two days in a plastic bag to allow homogenisation of the moisture and afterwards, a block is compacted to the desired density. The dimensions of the block are equal to the internal dimensions of the cell, which are 7 cm diameter and 10 cm height. A hole is drilled in the central, upper part of the block to insert the capacitive sensor and the cell is closed. The external wall of the cell is covered with a silicone-rubber laminated heater that fixes the temperature all over the cell. After measuring the RH of the bentonite corresponding to the laboratory temperature, the temperature of the external heating mat is increased from 40 to 120°C in intervals of 20°C. Afterwards, the temperature is decreased according to the same pattern. Each target temperature is kept for about two days. The accuracy of the humidity sensor is ±1% over the range 0–90% RH and ±2% over the range 90–100% RH.

4 Results

4.1 FEBEX Bentonite

The sensor/cell method has been used to measure the change of suction of the FEBEX bentonite compacted at nominal dry density of 1.60 g/cm^3 during heating/cooling. The average equilibrium values of suction measured for each temperature are plotted in Fig. 1 and they show a decrease of the retention capacity with temperature.

The retention curve at constant volume was determined for the bentonite compacted to nominal dry density of 1.60 g/cm^3 and temperatures of 20 and 80°C using the constant volume cells (Lloret et al. 2004, Villar and Lloret 2004). The initial water content of the samples was the hygroscopic one (about

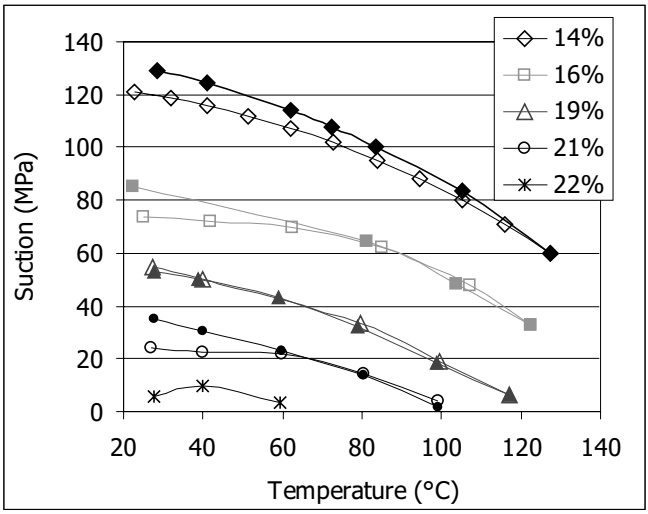

Fig. 1. Equilibrium suction measured during heating/cooling in blocks of FEBEX bentonite compacted at 1.60 g/cm^3 with different water contents (*filled symbols*: cooling)

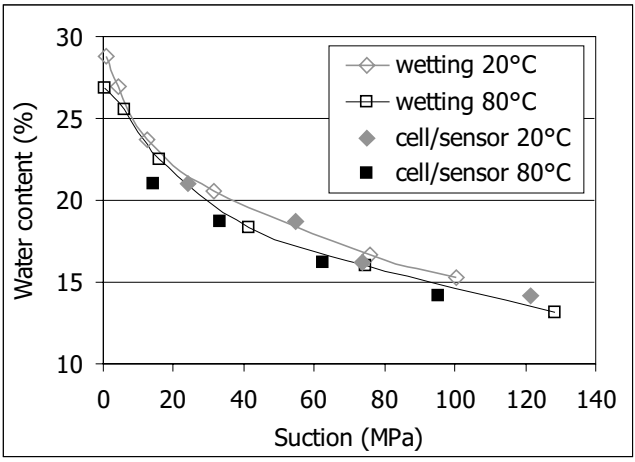

Fig. 2. Retention curves obtained with two methods for the FEBEX bentonite compacted at 1.60 g/cm^3

14%). The results obtained are shown in Fig. 2. A wetting path was followed from the suction corresponding to the hygroscopic water content of the bentonite (100–130 MPa) to 1 MPa. The results shown in Fig. 2 under the label *wetting* are in fact the average of the results obtained in the wetting paths followed in two cells. Figure 2 shows also some of the results obtained with

the cell/sensor method. A good agreement between the results obtained with the two methods is observed, although at 80°C, the suctions measured with the hygrometers for a given water content are higher than expected according to the results obtained in cells.

4.2 MX–80 Bentonite

The sensor/cell method has been used to measure the change of suction of MX–80 bentonite compacted at nominal dry density of 1.60 g/cm^3 during heating/cooling (Villar et al. 2006). The average equilibrium values of suction measured for each temperature are plotted in Fig. 3 and show a decrease of the retention capacity with temperature, as well as hysteresis between heating and cooling.

The retention curves of MX–80 compacted at different densities were also obtained in a previous investigation using the cell method (Villar 2005). Figure 4 shows the results obtained at 60°C with the cell method and with the sensor/cell method for the bentonite compacted at dry density 1.60 g/cm^3.

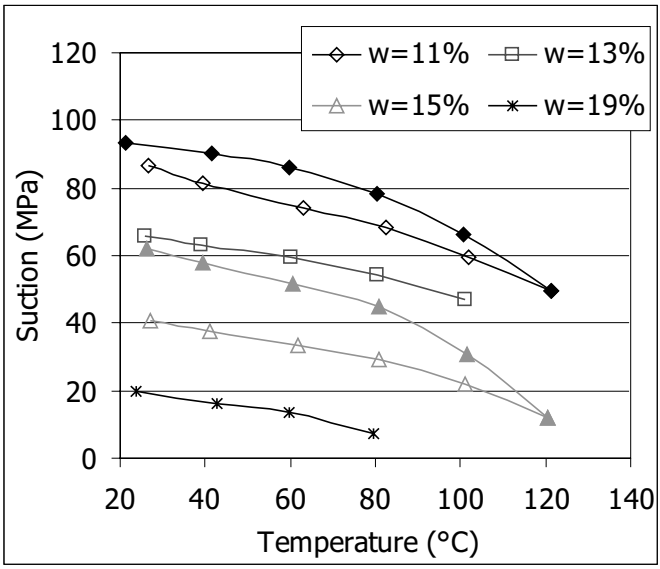

Fig. 3. Equilibrium suction measured during heating/cooling in blocks of MX–80 bentonite compacted at 1.60 g/cm^3 with different water content (*filled symbols*: cooling)

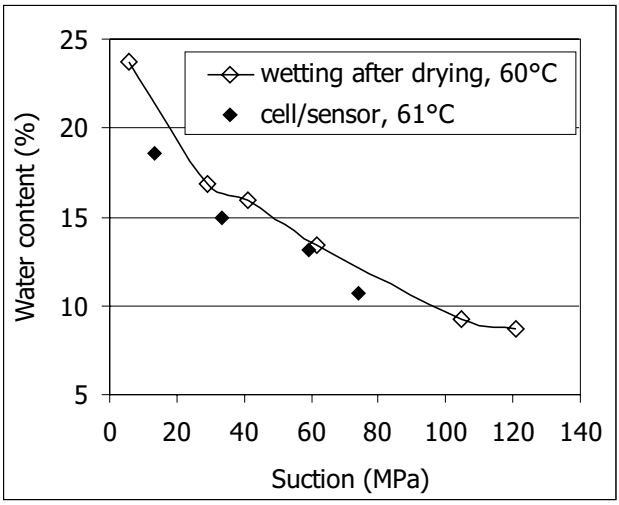

Fig. 4. Retention curves obtained at 60°C with two methods for the MX–80 bentonite compacted at 1.60 g/cm^3

5 Summary

Two methods have been used to determine the retention capacity at high temperature of two bentonites compacted to high density. The results obtained with both methods are coherent, although, for a given suction and temperature, there is a trend to find a lower water content with the "cell/sensor method" than with the cell method.

A decrease of retention capacity with temperature has been observed for the two bentonites. As well, for a given temperature, the suction measured in the sample is higher during cooling than when it was heated. This difference is less important for the FEBEX bentonite.

Some of the results for the two bentonites are plotted together in Fig. 5 in the form of retention curves. Also, the retention capacity of the FEBEX bentonite for a given temperature is higher than that of MX–80, i.e. for a given suction, the water content of the FEBEX bentonite is higher. The difference tends to attenuate for the lower suctions and high temperatures. It must be recalled that FEBEX bentonite has mainly divalent cations in the exchange complex (though the quantity of Na is also important) and MX–80 is predominantly sodic.

The effect of dry density on the water retention capacity has been checked in previous investigations (Villar and Lloret 2004, Villar et al. 2006). For the two bentonites and in terms of water content the effect of dry density is imperceptible for suctions higher than 10 MPa. For lower suctions, i.e. for high RH and when the specimen is approaching saturation, the lower the dry density of the bentonite, the higher the water content for a given suction.

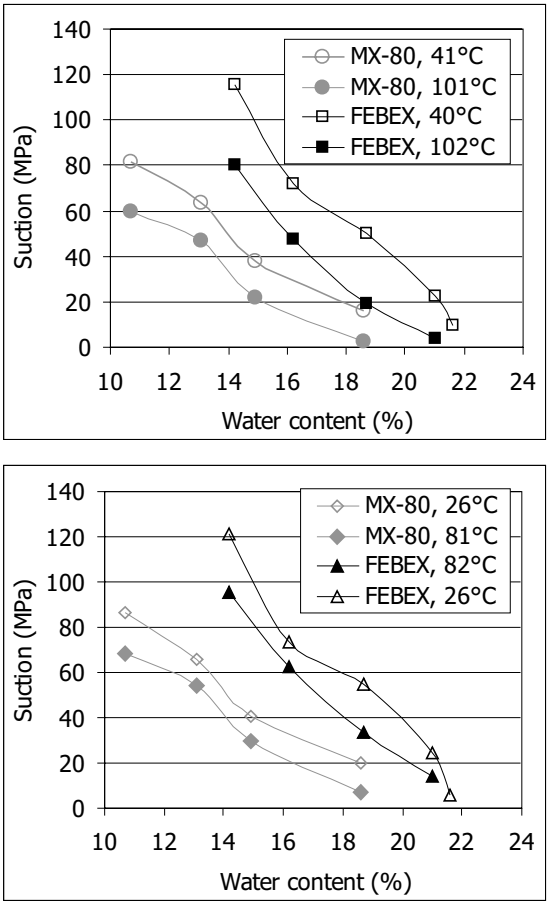

Fig. 5. Retention curves at various temperatures for MX–80 and FEBEX bentonites compacted to nominal dry density 1.60 g/cm^3

Nevertheless, the influence of density seems to be less important for the MX–80 than for the FEBEX bentonite (Villar et al. 2005).

References

ENRESA (1998) FEBEX. Bentonite: origin, properties and fabrication of blocks. Publicación Técnica ENRESA 4/98, Madrid

ENRESA (2000) FEBEX Project. Full-scale engineered barriers experiment for a deep geological repository for high level radioactive waste in crystalline host rock. Final Report. Publicación Técnica ENRESA 1/2000, Madrid

Fernández AM (2003) Caracterización y modelización del agua intersticial en materiales arcillosos: Estudio de la bentonita de Cortijo de Archidona. Ph.D. Thesis, Universidad Autónoma de Madrid, Madrid (In Spanish)

Lloret A, Romero E, Villar MV (2004) FEBEX II Project. Final report on thermo-hydro-mechanical laboratory tests. Publicación Técnica ENRESA 10/04, Madrid

Villar MV (2002) Thermo-hydro-mechanical characterisation of a bentonite from Cabo de Gata. A study applied to the use of bentonite as sealing material in high level radioactive waste repositories. Publicación Técnica ENRESA 01/2002, Madrid

Villar MV (2005) MX–80 bentonite. Thermo-hydro-mechanical characterisation performed at CIEMAT in the context of the Prototype Project. Informes Técnicos CIEMAT 1053, Madrid

Villar MV, Lloret A (2004) Influence of temperature on the hydro-mechanical behaviour of a compacted bentonite, Applied Clay Science 26:337–350

Villar MV, Martín PL, Lloret A (2005) Determination of water retention curves of two bentonites at high temperature. In: Tarantino A, Romero E, Cui YJ (eds) Advanced experimental unsaturated soil mechanics. EXPERUS 2005. A.A. Balkema Publishers, London pp 77–82

Villar MV, Gómez-Espina R, Martín PL (2006) Behaviour of MX–80 bentonite at unsaturated conditions and under thermo-hydraulic gradient. Work performed by CIEMAT in the context of the TBT project. Informes Técnicos CIEMAT 1081, Madrid

Part V

Volumetric Behaviour – Expansive Materials

Experimental Study on Shrinkage Behaviour and Prediction of Shrinkage Magnitudes of Residual Soils

Sarita Dhawan[1], Anil Kumar Mishra[2], and Sudhakar M. Rao[1]

[1] Department of Civil Engineering, Indian Institute of Science, Bangalore 560012, India sarita@civil.iisc.ernet.in, msrao@civil.iisc.ernet.in
[2] Department of Bio-production and Environmental Sciences, Faculty of Agriculture, Kyushu University, Fukuoka 812-8581, Japan anilk.iisc@gmail.com

Summary. The present study examines the shrinkage behaviour of residually derived black cotton (BC) soil and red soil compacted specimens that were subjected to air-drying from the swollen state. The soil specimens were compacted at varying dry density and moisture contents to simulate varied field conditions. The void ratio and moisture content of the swollen specimens were monitored during the drying process and relationship between them is analyzed. Shrinkage is represented as reduction in void ratio with decrease in water content of soil specimens. It is found to occur in three distinct stages. Total shrinkage magnitude depends on the type of clay mineral present. Variation in compaction conditions effect marginally total shrinkage magnitudes of BC soil specimens but have relatively more effect on red soil specimens. A linear relation is obtained between total shrinkage magnitude and volumetric water content of soil specimens in swollen state and can be used to predict the shrinkage magnitude of soils.

Key words: residual soils, clay mineralogy, compaction conditions, shrinkage, prediction, volumetric water content

Introduction

Residually derived clay soils like black cotton (BC) soil and red soil in India cover around 32% of the total landmass. These generally occur in the semi-arid regions and are problematic to engineering structures because of their tendency to heave during wet season and shrink during dry season. The magnitude of these movements being dependent upon several factors still poses a challenge for estimation.

Shrinkage is an important phenomenon in clayey soils. It occurs at lower humidity and higher temperatures prevalent during the dry seasons. Methods

to predict the shrinkage magnitude of soils are useful in anticipating shrinkage settlements of soils. The present study examines the shrinkage behaviour of two residual clay soils namely, BC soil and red soil upon drying of the compacted specimens after swelling. The swollen specimens were allowed to shrink until the mass of the dried specimens became nearly constant. Void ratios and water content of the specimens were monitored during the drying process. Relationships between void ratio and water content are analyzed to evaluate shrinkage behaviour of the soil specimens. Based on the factors influencing the shrinkage, relation is developed to predict shrinkage magnitudes of clay soils from the swollen state.

Materials and Methods

For the present study, BC soil was procured from Davangere district, Karnataka and red soil from the site of Indian Institute of Science, Bangalore. These soils were air-dried and pulverized to pass IS 425 μm sieve prior to use. The BC soil mainly contains montmorillonite clay mineral (Shivananda 2003) while the red soil contains kaolinite mineral (Revanasiddappa 2000). The physical properties of the soils were determined as per IS codes and are listed in Table 1.

Table 1. Physical properties of residual soils

Soil	Liquid limit (%)	Plastic limit (%)	Shrinkage limit (%)	Plasticity Index	Clay (%)	Silt (%)	Sand (%)	USCS symbol
BC	84	23	10	61	55	29	16	CH
Red	39	19	15	20	24	16	60	CL

Compaction curves of the soils were determined by the Standard Proctor method as per IS code. For the present study four compaction conditions were chosen. These are:

1. Maximum Dry Density (MDD) & Optimum MoistureContent (OMC)
2. 95% MDD & OMC
3. MDD & 5% dry of OMC
4. 95% MDD & 5% wet of OMC

These conditions were chosen to bring out the significance of variations in the initial compaction condition on the shrinkage behaviour of the soil specimens and are listed in Table 2.

Determination of Shrinkage of Compacted Soil Specimens

The soils were mixed at the desired water content and were statically compacted in rings of 75 mm diameter to 14 mm height at the desired dry density.

Table 2. Compaction conditions of soil specimens

Compaction condition		BC soil	Red soil
MDD & OMC	Dry density [Mg/m^3]	1.42	1.73
	Water content [%]	28	18
95% MDD & OMC	Dry density [Mg/m^3]	1.35	1.64
	Water content [%]	28	18
MDD & 5% dry of OMC	Dry density [Mg/m^3]	1.42	1.73
	Water content [%]	23	13
95% MDD & 5% dry of OMC	Dry density [Mg/m^3]	1.35	1.64
	Water content [%]	28	23

Details of experimental setup can be found in Sarita (2003). The specimen assembly was placed in a tray, inundated with distilled water and allowed to swell under 6.25 kPa pressure. After two days of inundation, water was removed and the specimens were allowed to air-dry at $32 \pm 3°C$ under the applied pressure. During drying process, the mass, height and diameter of each specimen were measured regularly. The reduction in volume and mass are used to calculate the void ratio and water content of the specimen at any stage of drying from the relations:

$$\Delta e = \frac{\Delta v}{V_0} \times (1 + e_0)\,, \tag{1}$$

$$w = \frac{m_d - m_s}{m_s} \times 100 \tag{2}$$

where V_0 and e_0 are the volume and void ratio of the specimen in the swollen state, m_s is dry mass of soil used for specimens, Δv and Δe are the change in specimen volume and void ratio at any stage of drying, m_d and w are the mass and water content of the specimen at any stage of drying. The drying process was terminated when the mass of the specimens became nearly constant. The time taken for complete air-drying of the specimens was about two months. At each compaction condition of a soil, triplicate specimens were used and their average was taken for calculations.

Results and Discussion

Shrinkage Behaviour of Compacted Specimens

Variation in void ratio with decrease in water content upon drying the swollen BC soil specimens is shown in Fig. 1. The shrinkage of the specimens occur in three stages. In stage one termed as Initial Shrinkage (IS), a small change in void ratio occurs with reduction in water content. The IS region is followed by the Primary Shrinkage (PS) region where the void ratio rapidly decreases

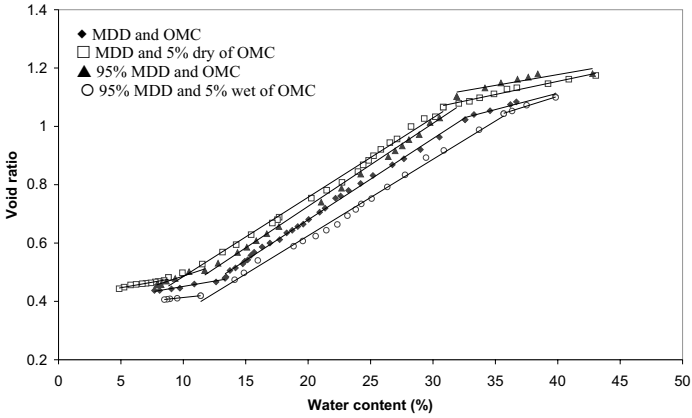

Fig. 1. Void ratio variation with water content during shrinkage of compacted BC soil specimens after swelling

with reduction in water content in a linear manner. Majority of soil shrinkage occurs during PS. After PS, the Residual Shrinkage (RS) sets in with marginal changes in void ratio due to rearrangement of particles on reduction of water content. The degree of saturation reduces in all the three stages of drying implying that total volume decreases at a slower rate than volume of water during the entire drying process.

The magnitude of Initial Shrinkage for the BC soil specimens is calculated as:

$$\text{IS } (\%) = \frac{(e_0 - e_{\text{IS}})}{(1 + e_0)} \times 100 \tag{3}$$

where e_0 and e_{IS} are void ratio of specimen in the swollen state and at end of IS, respectively. The Primary shrinkage is defined as:

$$\text{PS } (\%) = \frac{(e_{\text{IS}} - e_{\text{PS}})}{(1 + e_{\text{IS}})} \times 100 \tag{4}$$

where e_{PS} is void ratio of the specimen at end of PS region.

The Residual shrinkage is defined as:

$$\text{RS } (\%) = \frac{(e_{\text{PS}} - e_{\text{RS}})}{(1 + e_{\text{PS}})} \times 100 \tag{5}$$

where e_{RS} is void ratio at end of RS and simply corresponds to the final void ratio of specimen obtained during drying.

The swell and shrinkage stage parameters of the BC soil specimens are summarized in Table 3. The PS dominates the Total shrinkage (TS) magnitudes. The PS and TS magnitudes of the BC soil specimens vary within

Table 3. Shrinkage magnitudes of BC soil specimens

Compaction condition	w_0 [%]	Sr_0 [%]	e_0	e_{IS}	e_{PS}	e_{RS}	IS [%]	PS [%]	RS [%]	TS [%]
MDD & OMC	39.8	96.6	1.10	1.04	.48	.44	3.0	27.5	2.9	33.4
95% MDD & OMC	42.8	97.1	1.18	1.10	.51	.46	3.6	28.4	3.3	35.3
MDD & 5% dry of OMC	43.0	98.0	1.18	1.07	.47	.44	5.0	29.0	1.6	35.6
95% MDD & 5% wet of OMC	39.8	97.1	1.10	1.04	.42	.41	2.6	30.5	0.9	34.0

Sr_0 Degree of saturation at end of swelling

the narrow limits. Interestingly, the void ratio of swollen specimens varies marginally irrespective of initial compaction conditions.

The changes in void ratio with reduction in water content upon drying the swollen red soil specimens are plotted in Fig. 2. The specimens shrink in three stages same as observed for BC soil.

Same as for BC soil, there was continuous reduction in degree of saturation during entire drying process. The magnitudes of IS, PS, RS were calculated for the red soil specimens from Eqs (3)–(5) and are listed in Table 4 along with swollen state parameters.

Data in Table 4 show that the PS magnitude ranges from 3.8 to 8.2% and TS magnitudes from 6.9 to 11.8%. The trend of variations in PS and TS magnitudes suggests that besides the swollen void ratio, the shrinkage magnitudes of the red soil specimens are influenced by some other soil parameter as well.

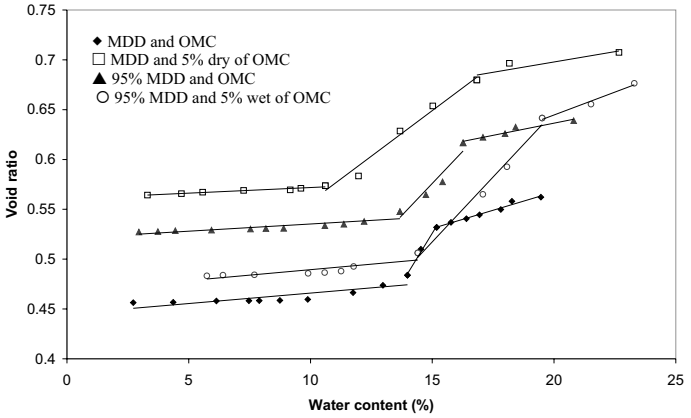

Fig. 2. Void ratio with water content during shrinkage of compacted red soil specimens after swelling

Table 4. Shrinkage magnitudes of red soil specimens

Compaction condition	w_0 [%]	Sr_0 [%]	e_0	e_{IS}	e_{PS}	e_{RS}	IS [%]	PS [%]	RS [%]	TS [%]
MDD & OMC	19.5	92.8	.56	.53	.47	.46	1.9	3.8	1.2	6.9
95% MDD & OMC	20.8	87.3	.64	.62	.55	.53	1.3	4.3.	1.3	6.9
MDD & 5% dry of OMC	22.7	85.9	.71	.68	.57	.56	1.6	6.3	0.6	8.5
95% MDD & 5% wet of OMC	23.3	92.3	.68	.64	.51	.48	2.1	8.2	1.5	11.8

Prediction of Total Shrinkage Magnitudes

Examination of the shrinkage behaviour of various soil specimens had revealed that the void ratio and degree of saturation of swollen specimens play important role in determining TS magnitudes. Soil specimen with larger e_0 and Sr_0 experienced a larger magnitude of TS on drying. Such behaviour may be anticipated as soils with high water content and void ratios experience large magnitudes of shrinkage (Yong and Warkentin 1975, Chen 1988). Also the TS exhibited by the soil specimens have a bearing with their Atterberg limits and hence depend on the clay mineral present in soil. The BC soil specimens with high Atterberg limits (w_L = 84%, I_p = 61%) exhibit high shrinkage magnitudes (33.4 to 35.6%).The red soil specimens with low Atterberg limits (w_L = 39%, I_p = 20%) exhibit shrinkage magnitudes ranging from 6.9 to 11.8%.

Total shrinkage magnitudes are analyzed as function of both swollen porosity and degree of saturation. From volume-mass relations for soils, the product of porosity and degree of saturation represent the volumetric water content (θ) of the soil. Fig. 3 correlates the TS magnitudes with θ after swelling of the soil specimens. A correlation coefficient of 0.997 is exhibited by the plot in Fig. 3. The trend of result in Fig. 3 suggests that the TS magnitude of a specimen from swollen to air-dried state may be predicted by knowing the θ of the specimen after swelling.

The relation between TS and swollen θ of the soil specimens follow the linear relation:

$$\mathrm{TS} = 154.6 \times \theta - 45.6\,. \tag{6}$$

Use of Eq. (6) allows the prediction of total shrinkage of soils from the swollen condition by air-drying. This equation is expected to be valid for soils having liquid limits ranging from 40 to 90% and plasticity index ranging from 20 to 60%. These ranges of Atterberg limits are typical for clayey soils in arid regions that are susceptible to swelling and shrinkage upon moisture content fluctuations.

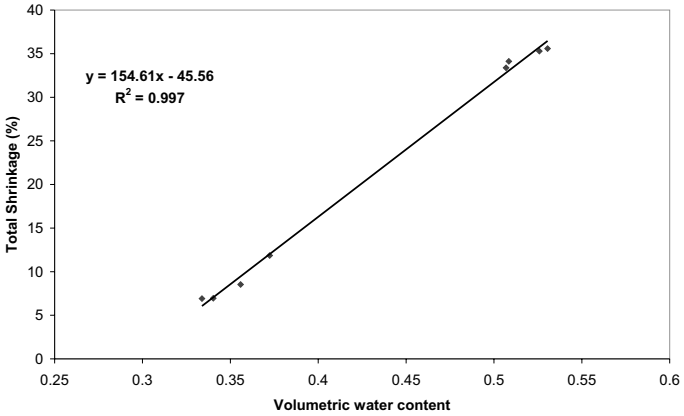

Fig. 3. Relationship between Total shrinkage magnitudes with volumetric water content of swollen specimens

Conclusions

The following major conclusions emerged from the study. Soils shrink in three distinct stages, namely, Initial Shrinkage, Primary Shrinkage and Residual Shrinkage. In the first and third stage, there was little reduction in void ratio with reduction in water content compared to the second stage where the void ratio decreased rapidly. The degree of saturation reduced in all the three stages of drying. The swollen void ratio and degree of saturation of specimens play an important role in controlling the total shrinkage magnitudes. Total shrinkage magnitudes can be predicted using swollen volumetric water contents by equation $\mathrm{TS} = 154.6 \times \theta - 45.6$.

References

Chen FH (1988) Foundation on expansive soils. Elsevier, New York

IS: 2720-Part 4 (1985) Indian standard methods of test for soils: Grain size analysis. BIS, New Delhi

IS: 2720-Part 5 (1985) Indian standard methods of test for soils: Determination of liquid limit and plastic limit. BIS, New Delhi

IS: 2720-Part 6 (1972) Indian standard methods of test for soils: Determination of shrinkage factors. BIS, New Delhi

IS: 2720-Part 7 (1980) Indian standard methods of test for soils: Determination of water content-dry unit weight relation using light compaction. BIS, New Delhi

Revanasiddappa R (2000) Collapse behaviour of red soils of Bangalore district. Ph.D. thesis, Indian Institute of Science

Sarita (2003) An experimental study of shrinkage behaviour and SWCC relations of clays. MSc (Engg) thesis, Indian institute of Science

Shivananda P (2003) Role of lime-soil reactions and environmental factors in the engineering behaviour of lime-amended expansive clays. Ph.D. thesis, Indian Institute of Science

Yong RN, Warkentin BP (1975) Soil properties and behavior. Elsevier, New York

Assessment of Swelling Deformation of Unsaturated Kaolinite Clay

Markus Dobrowolsky and Christos Vrettos

Division of Soil Mechanics and Foundation Engineering,
Technical University of Kaiserslautern, Kaiserslautern, Germany
dobrow@rhrk.uni-kl.de, vrettos@rhrk.uni-kl.de

Summary. The swelling behaviour of kaolinite clay is systematically investigated by means of two types of oedometer devices suitably modified to measure the variation of swelling pressure in dependence of the vertical and volumetric strain. A wide range of values for initial void ratio as well as initial and final degree of saturation has been covered. Based on the experimental results approximate equations for the swelling deformation are derived that are implemented in a FEM-Code. The application to a typical situation in practice is demonstrated by the numerical solution of the respective boundary value problem.

Key words: unsaturated soils, expansive soils, swelling, oedometer tests, numerical modelling

1 Introduction

Swelling of unsaturated cohesive soils may lead to high pressures and deformations of geotechnical structures. So far, publications on swelling of geomaterials refer to rocks (Wittke 2003) or to mudstone (Von Wolffersdorff and Heidkamp 2005, Heidkamp and Katz 2004).

The aim of the investigation presented herein is the measurement of the volume and pressure changes of swelling cohesive soils in dependence of the moisture content and the void ratio. The influence of the constraints on geotechnical structures due to swelling caused by the non-stationary moisture diffusion in the ground is then analysed by the Finite-Element-Method using an appropriate soil model.

In the following, the constitutive relation proposed for modelling the volume change is formulated, the developed oedometer apparatus are described and representative test results are given. Numerical simulations of element tests and of a boundary value problem are also presented.

2 Constitutive Relation for Volume Change

The volume change behaviour due to swelling is described here in terms of the first stress and strain invariants by the following relationship:

$$I_{\varepsilon}^{SW} = I_{\sigma,\max}^{SW}(e_0, S_{r,0}, S_{r,\infty}) \cdot f(I_{\sigma}), \qquad I_{\sigma,0} \leq I_{\sigma} \leq I_{\sigma,\max}^{SW} \tag{1}$$

$$I_{\varepsilon}^{SW} = 0, \qquad I_{\sigma} > I_{\sigma,\max}^{SW} \tag{2}$$

where $I_{\sigma,\max}^{SW}$ is the maximum swelling pressure under constant volume conditions, I_{ε}^{SW} is the swelling strain, I_{σ} is the actual stress, e_0 is the initial void ratio, $S_{r,0}$ is the degree of saturation at the begin of the swelling phase, and $S_{r,\infty}$ the accordingly value at the stress level $I_{\sigma,\max}^{SW}$.

3 Test Material, Equipment, and Procedure

The material chosen for the tests is kaolinite clay of medium to high plasticity and is described in detail by Dobrowolsky and Becker (2002) and Dobrowolsky and Vrettos (2005). The swelling potential of this material is classified as low to medium. The test material has been investigated in the past and allows also the accurate measurement of the soil water suction at relatively low levels using standard techniques.

Two new modified oedometer devices have been developed to determine the parameters in the constitutive equation (1).

With the first oedometer, called oedometer A, it is possible to determine separately the axial and radial pressure. This apparatus as well as test results are described elsewhere (Dobrowolsky and Vrettos 2005).

The second oedometer device, called oedometer B, is designed for 100 mm diameter specimens with a thickness of 50 mm. A rubber membrane is mounted on the inner side of the oedometer allowing the control and the measurement of radial pressure and deformation. The space between membrane and ring is filled with glycerin. The axial pressure is recorded by a load cell. Thus, this apparatus works similar to conventional triaxial equipment.

Results are reported here only for tests carried out in oedometer B. The preparation technique of the soil sample and its optimization is described in detail by Dobrowolsky (2003). Tests have been carried out for selected values of the initial and the final degree of saturation, and of the initial void ratio.

The correlation between I_{ε}^{SW} and I_{σ}^{SW} is investigated. Through watering from $S_{r,0}$ to $S_{r,\infty}$ under constant volume the maximum swell stress $I_{\sigma,\max}^{SW}$ is imposed to the sample. An isotropic deformation I_{ε}^{SW} is then stepwise allowed through control of vertical and radial strain. During this process the actual swelling pressure I_{σ}^{SW} is measured. This leads to swell pressure-strain relationships as exemplarily shown in Figs 1 and 2.

Additional tests have been carried out in different devices to determine the characteristics of the water transport through the soil sample.

The soil–water suction ψ is determined by the pF value, where pF = $\log[\psi/(1\,\text{cm water column})]$. Up to a value of pF = 3 measurement is performed by using a miniature tensiometer placed in the middle of the specimen in the oedometer. The hydraulic relations for values pF > 3 are determined by means of i) the axis – translation method in a pressure plate cell ($3 \leq \text{pF} \leq 4$) and ii) the vacuum desiccator method (pF > 4). In the pressure plate cell tests are performed by dewatering and subsequent watering allowing the identification of hysteretic behaviour in the soil–water–characteristic–curve SWCC. The vacuum desiccator method allows only dewatering and is used here only for the sake of completeness since pF > 4 lies outside the range of the degree of saturation investigated ($S_{r,0} \geq 0.7$). In addition to the SWCC the unsaturated hydraulic conductivity K_u is needed to determine the water transport characteristics of this particular soil type. The variation of K_u with degree of saturation, void ratio, and temperature is taken from Wendling (2004).

4 Test Results

It can be shown that the swell pressure at a constant volume is of isotropic nature, cf. Dobrowolsky and Vrettos (2005). The results presented in that paper lead to the following approximation for $I^{SW}_{\sigma,\max}$:

$$I^{SW}_{\sigma,\max} = 3.29 \cdot p_a \cdot \exp(3.65 \cdot S_{r,\infty} - 4.7 \cdot e_0) \cdot (S_{r,\infty} - S_{r,0})^{(0.95 \cdot S_{r,\infty} - 0.54)} \quad (3)$$

where p_a is the atmospheric pressure. The above equation is valid for $0.68 \leq e_0 \leq 0.88$; $0.6 \leq S_{r,0} \leq 1.0$ and $0.78 \leq S_{r,\infty} \leq 1.0$.

The experimentally determined variation of swelling strain with normalized swelling pressure is approximated by equation (4) that is depicted in Fig. 1 for the range of values investigated:

$$I^{SW}_{\varepsilon} = \frac{a}{\left(\frac{I_\sigma}{I^{SW}_{\sigma,\max}}\right)^b} \log\left(\frac{I_\sigma}{I^{SW}_{\sigma,\max}}\right), \qquad I_{\sigma,0} \leq I_\sigma \leq I^{SW}_{\sigma,\max} \quad (4)$$

whereby a and b are functions of e_0, and of $I^{SW}_{\sigma,\max}$ normalized to the imposed isotropic initial pressure $I_{\sigma,0} = 27\,\text{kPa}$:

$$a = (-0.021 \cdot e_0 + 0.01)\frac{I^{SW}_{\sigma,\max}}{I_{\sigma,0}}\,, \quad (5)$$

$$b = -0.096 + (0.257 \cdot e_0 - 0.131)\frac{I^{SW}_{\sigma,\max}}{I_{\sigma,0}}\,. \quad (6)$$

A significant increase of the swell strain I^{SW}_{ε} occurs with decreasing stress I_σ. It can be seen that the increase of swell strain is stronger for lower values of void ratio. Results from other tests not reported herein show that the swelling potential of the soil sample increases with decreasing initial degree of saturation.

5 Numerical Simulations

General Considerations

We assume that material used in the study is homogeneous and isotropic. A nonlinear elastic – ideal plastic stress–strain–relationship is assumed for the mechanical loading. Swell deformations are superimposed after completion of initial loading. Investigations presented by the authors Dobrowolsky and Vrettos (2005) show that the swell–shrinkage behaviour of the test material at a specific swell pressure level is approximately linear elastic.

In the following, the plastic deformations are left-out for the sake of simplicity. Thus, the total strain is:

$$\mathrm{d}\varepsilon = \mathrm{d}\varepsilon^{el} + \mathrm{d}\varepsilon^{SW} \,. \tag{7}$$

The elastic relationship between the stress increment and the strain increment is given by

$$\mathrm{d}\sigma^{el} = \left[D^{el,m}\right] \cdot \mathrm{d}\varepsilon^{el} + \left[D^{el,SW}\right] \cdot \mathrm{d}\varepsilon^{SW} \tag{8}$$

where $[D^{el,m}]$ is the stiffness matrix for the mechanical elastic behaviour and $[D^{el,SW}]$ is the matrix for the elastic swelling behaviour.

The FEM-code ABAQUS Version 6–4 is used for the analysis. The following general relationship between maximum volumetric swelling strain and degree of saturation is already built in:

$$\Delta\varepsilon^{SW}_{jj,\max} = \frac{1}{3}\left[\varepsilon_v^{SW}(S) - \varepsilon_v^{SW}(S^I)\right], \qquad j = 1,2,3 \tag{9}$$

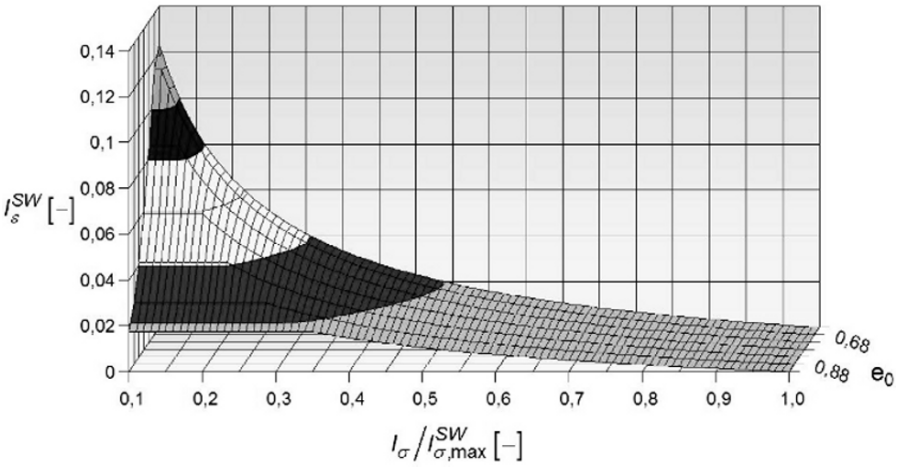

Fig. 1. Swelling strain I_ε^{SW} vs. normalized swelling stress $I_\sigma / I_{\sigma,\max}^{SW}$ for various values of void ratio e_0 and $S_{r,0} = 0.7$, $S_{r,\infty} = 1.0$, $T = 20°\mathrm{C}$

whereby S and S^I are the actual and initial degree of saturation, respectively. The above relation describes unhindered swelling. During our tests the strain is controlled and stress is measured. Thus, by setting $I_\sigma = I_{\sigma,0}$ and for small values of $I_{\sigma,0}$ equations (3)–(4) approximately correspond to the relationship given by equation (9). The value $I_{\sigma,0} = 27\,\text{kPa}$ used in the tests is the lowest practicable stress level.

The stiffness matrix $[D^{el,m}]$ is obtained in terms of the modulus of elasticity E and the Poisson's ratio ν. For the modulus of elasticity we selected a stress dependent relationship derived from the equation for the small strain shear modulus used in dynamic analysis (Hardin 1978):

$$E = C \cdot f(e) \cdot \left[\frac{I_{\sigma'}}{3 \cdot p_a}\right]^{0.5} \cdot p_a \cdot \frac{1}{2 \cdot (1+\nu)}\,. \tag{10}$$

For Poisson's ratio we set $\nu = 0.3$. For small strains the constant $C = 625$. A value $C = 156$ yields a good fitting of the test results and corresponds to a reasonable approximation of the secant modulus at the strain levels under consideration.

The swell-stress dependent swell modulus Q (bulk modulus) to be used in $[D^{el,SW}]$ is obtained from the test results, as exemplarily given in Fig. 1.

Simulation of Laboratory Tests

First, the appropriateness of the relationships given above is checked by simulation of representative laboratory tests carried out in oedometer A and B.

The simulation starts with initial conditions given by $S_{r,0} = 0.7$ and $e_0 = 0.78$. At first, an equilibrium step is computed during which suction as well as self-weight are imposed. In the next step the model is watered from the bottom at constant volume to $S_{r,\infty} = 1.0$. After that, a prescribed deformation is imposed stepwise: axial deformation in odoemeter A and volumetric deformation in oedometer B, respectively. Figure 2 compares the results of the tests and of the numerical simulation. The variation of the swell modulus Q (bulk modulus) yields a good fitting of the curve.

Simulation of a Footing on Expansive Soil

The application to a typical situation in engineering practice is demonstrated by the numerical solution of the boundary value problem of an axisymmetric footing on an expansive soil. The footing with radius of 1.0 m and thickness of 0.4 m is placed on the surface of a homogeneous soil with initial conditions $e_0 = 0.68$ and $S_{r,0} = 0.7$. The size of the model is 5 m in half-width by 4 m in depth. Underneath the base of the model a porous water-bearing layer is assumed. The footing is loaded by force of 200 kPa after the equilibrium step is completed and the self-weight of footing and soil is applied. In the next step the groundwater rises within in the water-bearing stratum up to the

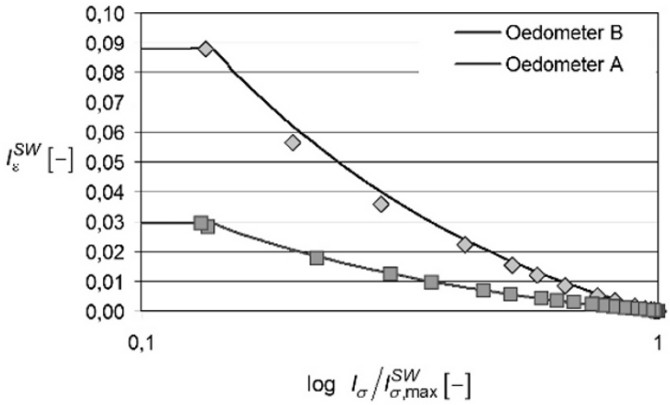

Fig. 2. Volumetric swell strains I_ε^{SW} vs. actual stress I_σ normalized to $I_{\sigma,\max}^{SW}$ for $e_0 = 0.78$, $S_{r,0} = 0.7$, $S_{r,\infty} = 1.0$, $T = 20°\mathrm{C}$. The solid lines describe equation (4), the data points are for the numerical simulation

bottom of the expansive soil. This is simulated by setting suction equal to 0 at the interface between soil and water-bearing stratum. The suction-free front propagates upwards through the soil and leads to its saturation and consequently to swelling. The time the water from the water-bearing stratum is allowed to penetrate the soil is assumed to last 150 days.

Figure 3 displays two snapshots of the vertical heave before and after saturation, respectively. The vertical heave of the foundation amounts to 17 cm while the vertical heave of the ground at the side of the mesh is 30 cm. The differential heave of 13 cm due to swelling is noteworthy.

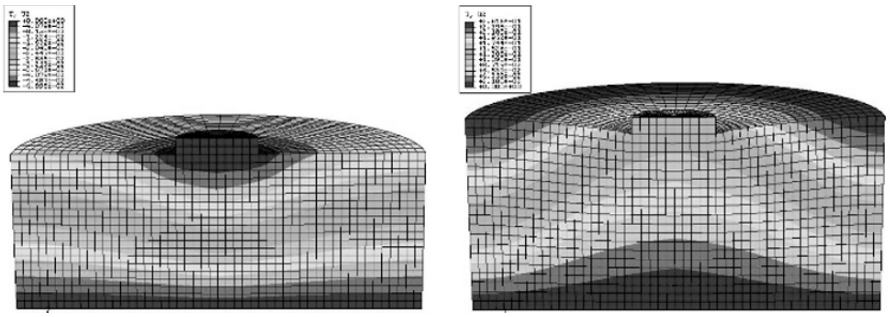

Fig. 3. Vertical heave before and after watering from the bottom

6 Conclusions

A wide range of tests have been performed to determine the water transport characteristics in the soil and the associated swell pressure vs. swell strain relationship of the cohesive material. The numerical simulations show the capability of the proposed analytical expressions to describing the swell behaviour.

Acknowledgements

The investigation presented herein has been carried out within the frame of a project funded by the German Science Foundation dealing with mechanics of unsaturated soils. This support is greatly appreciated.

References

Dobrowolsky M, Becker A (2002) Adsorptions- und Desorptionsverhalten durchströmter bindiger Böden. 4. Workshop Teilgesättigte Böden, Schriftenreihe Geotechnik, Bauhaus-Universität Weimar, Heft 8:71–76

Dobrowolsky M (2003) Volume change behavior of cohesive soils. Proc Int Conf From Experimental Evidence towards Numerical Modeling of Unsaturated Soils, Weimar I:227–239

Dobrowolsky M, Vrettos C (2005) Swell and shrink tests in modified oedometer apparatuses, Advanced Experimental Unsaturated Soil Mechanics, Trento, Italy, pp. 163–168

Von Wolffersdorff P-A, Heidkamp H (2005) Quellverhalten diagenetisch verfestigter Tonsteine in den Einschnitten der Neubaustrecke Nürnberg – Ingolstadt der Deutschen Bahn AG, Universität Kassel, Festschrift zum 60. Geburtstag Prof. Kempfert, Schriftenreihe Geotechnik, Heft 18:35–52

Hardin BO (1978) The nature of stress-strain behavior of soils. Proc ASCE Spec Conf on Earthq Eng Soil Dyn, Pasadena I:3–90

Heidkamp H, Katz C (2004) The swelling phenomenon of soils – Proposal of an efficient continuum modelling approach. Proc ISRM Regional Symposium EUROCK & 53rd Geomechanics Colloquium, Verlag Glückauf, pp. 743–748

Hibbit, Karlson & Sorensen, Inc. (2002) ABAQUS/Standard User's Manual, Version 6–4, Pawtucket, RI, USA

Wittke M (2003) Begrenzung der Quelldrücke durch Selbstabdichtung beim Tunnelbau im anhydritführenden Gebirge, Dissertation, Fakultät für Bauingenieurwesen, TH Aachen

Wendling S (2004) Untersuchungen zur Entstehung von Austrockungsrissen in mineralischen Deponieabdichtungen, Dissertation, Heft 10, Fachgebiet Bodenmechanik und Grundbau, TU Kaiserslautern

Suction and Collapse of Lumpy Spoilheaps in Northwestern Bohemia

Vladislava Herbstová[1], Jan Boháč[1], and Ivo Herle[2]

[1] Department of Engineering Geology, Charles University, Albertov 6, 12843 Prague, Czech Republic herbsto1@natur.cuni.cz, bohac@natur.cuni.cz
[2] Institut for Geotechnik, Technical University Dresden, D-01062 Dresden, Germany ivo.herle@mailbox.tu-dresden.de

Summary. Large spoilheaps of overburden from open-cast coal mining in Northwestern Bohemia offer a space for development. However, they exhibit unfavourable features such as collapse potential caused by the lumpy structure with high overall void ratios. Suction oscillations contribute to the structure degradation by the intervoids closure. The paper presents in-situ suction monitoring and laboratory investigation of the collapse potential of spoilheaps.

Key words: lumpy structure, intervoids closure, suction, collapse potential

1 Introduction

An intensive open-cast coal mining in Northwestern Bohemia produces a large amount of spoil. The brown coal deposit is typically in the depths of 80–200 m. The overburden – mainly clays to stiff fissured claystones – are disintegrated through mining into lumps or blocks ranging in size from centimetres up to tenths of centimetres. The blocks are subsequently end-dumped without any compaction to the bodies of spoilheaps, which reach up to 100 m in height but typically a few tens of metres. The extent of clayfills in Northwestern Bohemia reaches about 100 km^2 (see Fig. 1). The spoilheaps are gradually reclaimed and nowadays when there is a lack of building sites the areas of landfills offer reasonable space for development.

2 Structure of the Spoilheap Soil

The freshly filled spoilheap material has the form of a lumpy soil. The total porosity of such material consists of the primary voids of the clayey lumps sc. intragranular porosity (reaching typically about $n = 40\%$ reported by Feda (1998)) and the voids between the lumps sc. intergranular porosity. The total porosity of such material, which reaches up to 70%, is given by

Fig. 1. Extent of non-engineered spoilheaps within the Czech Republic

$$n_{\text{tot}} = n_i(1 - n_e) + n_e \tag{1}$$

where n_e and n_i are intergranular and intragranular porosities. The state of freshly filled spoilheap is therefore granular (see Fig. 2 left) which is confirmed by its high angle of repose (typically of about 40°). The clayey blocks deposited to the spoilheaps are overconsolidated not only by the current depths but also by the geological history – considerable denudation. Hurník (1978) refers that the thickness of denudated layers in the Miocene could reach 70 to 300 m.

The excavated overburden is filled in a dry way and therefore the intervoids are typically air-dry while the intravoids of lumps exhibit almost full saturation by its natural water content of about $w = 34\%$. Due to the granular nature of freshly filled material there is no suction within the intervoids and some suction within the intravoids in the lumps, where the negative pore water pressures developed first due to water-level sinking and subsequently due to unloading by exploitation. Further suction within the lumps is affected by the weather dependent moisture changes. The intervoids form the preferential paths for surface water. So the freshly filled spoilheaps are highly permeable until the structured soil degrades.

Fig. 2. Spoilheap just after filling (left) and about 10 years after filling (right)

The initially lumpy structure of the soil degrades with the increasing load. The intervoids close up due to plastic straining of relatively weak lumps. In greater depths the interporosity vanishes. In lower depth wetting-drying suction cycles are the main agent, which causes the structure degradation. Through the structure degradation clayfill material changes back into more or less homogeneous soil. The overall hydraulic conductivity decreases with increasing degree of structure degradation. Figure 2 right shows the aged spoilheap material of about 10 years after filling, where some lumps are already degraded into finer mass.

3 Field Suction Measurement

The classic type of jet-fill tensiometers is used for monitoring in-situ suction changes at two spoilheaps near Ústí nad Labem (at the site of a highway construction) and at the site of mine Bílina (see Fig. 1). The lengths of tensiometers used are 0.5–2 metres.

Very low or zero suctions and even positive values of pore water pressure have been measured at the spoilheap near Ústí nad Labem (Fig. 3), which indicates the fully saturated conditions. The zero suctions correspond to practically no collapse potential measured in the laboratory for the particular landfill (see Sect. 4.1).

At the spoilheap of the mine Bílina the tensiometers are installed in a moderate slope. The measured suctions (Fig. 4) reached maximum values of about 90 kPa in late autumn. It is however the limit of negative pore pressures that can be measured by this type of gauges due to cavitation, e.g. Fredlund and Rahardjo (1993). In late winter and spring the suction dropped to the values close to zero even in the deeper gauges. The seasonally dependent cyclic suction changes cause the disintegration of the clay lumps, which leads to the intervoids closure.

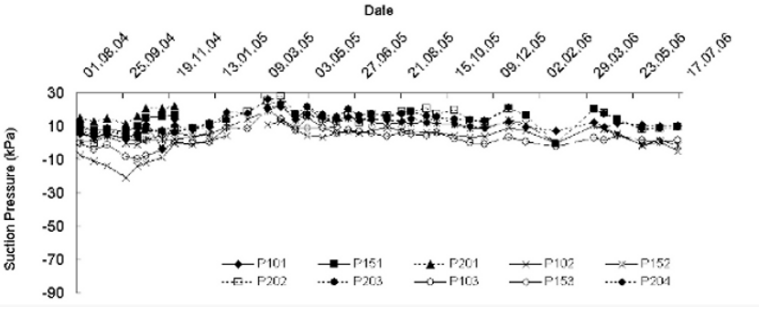

Fig. 3. Suction field measurements at the site near Ústí nad Labem

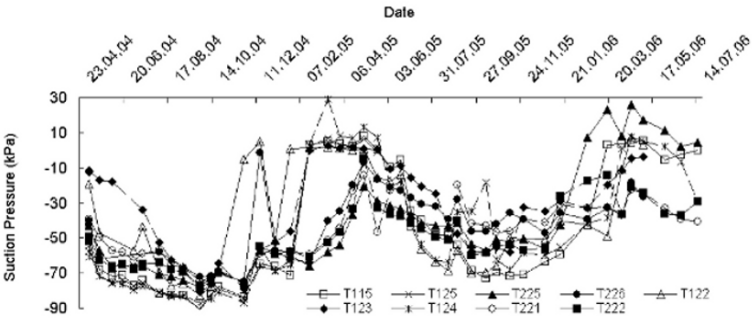

Fig. 4. Suction field measurements at the site of Bílina mine

4 Collapse Potential

The high overall porosity of the freshly filled material causes an open structure which is potentially susceptible to collapse. Charles and Watts (1996) gave three criteria for fills to qualify as particularly vulnerable to collapse compression: the fill

- was not subject to a heavy compaction,
- was placed relatively dry and has never been fully saturated or above a critical degree of saturation,
- is under relatively low stress.

At least in the early stages after landfilling the present clayey spoilheaps fulfill all three criteria. Two sets of tests on undisturbed and lumpy samples have been carried out to investigate the collapse vulnerability of spoilheaps.

4.1 Laboratory Tests on Undisturbed Samples

The collapse potential was investigated at the site of highway construction near the town Ústí nad Labem (see Fig. 1). The highway is crossing the reclaimed spoilheaps in overall length of about 12 km. The particular spoilheap is about 40 years old and in a high degree of homogenization and interporosity decrease but the collapse potential could still be expected. The soils were clays of high plasticity, average $w_L = 59\%$ (from 56 to 62%), $w_P = 28\%$ (27–31%), activity $I_A = 0.9$ (0.77–1.03).

Double oedometer tests were carried out according to Abelev (1959), Cui et al. (1998), Jennings and Knight (1957). Two "identical" specimens are placed into the oedometer and during the test one specimen is maintained at the original water content (referred to as "unsaturated" specimen, marked with unsat in Fig. 5), the second one is inundated at low total vertical pressure ("saturated" specimen, marked with sat in Fig. 5). Some curves needed to be transposed (marked with trans in Fig. 5) to the same initial void ratios as

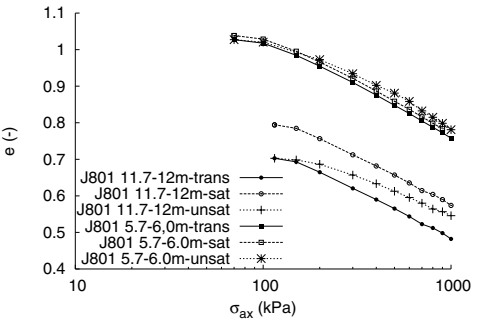

Fig. 5. Double oedometer tests on undisturbed samples

suggested by Jennings and Knight (1957). The divergence of the two stress-void ratio curves indicates the magnitude of collapse due to wetting.

In total 44 pairs of oedometer specimens were evaluated in classic type of oedometer rings (100 mm diameter, 30 mm hight). In total 24 specimens exhibited some collapse, and only two of them were classified as moderately collapsible according to ASTM (2003a). Twenty specimens exhibited a negative value of collapse index which indicated swelling. The standard double oedometer tests did not confirmed any collapse potential.

Matric suction was determined using filter paper method according to ASTM (2003b). Values mainly did not exceed suctions over 100 kPa, and were possibly caused by unloading through sampling. For more detail see Herbstová and Boháč (2005).

There was a scatter in the initial void ratios of undisturbed samples, which could refer to some remaining nonhomogeneity of the aged spoilheap. Therefore, more detailed field testing should be carried out to study collapse vulnerability in an appropriate scale to capture the nonhomogeneity of the clayfill material.

4.2 Laboratory Tests on Lumpy Samples

The second set of tests was carried out on the artificially prepared compacted and loose samples of lumpy clayfill material. The material used for testing was the spoilheap soil from the Bílina mine (see Fig. 1) sampled about 4–5 years after filling. The drying-wetting weathering processes already caused some disintegration of bigger lumps into finer mass. In order to carry out the tests in standard types of oedometer rings (d = 50–100 mm, h = 20–30 mm) the spoilheap material with reduced grain size was used (Fig. 6 left). The soil was sieved through a 5 mm sieve which could cause a difference between the initial overall void ratio of the natural and sieved material but the main feature of the lumpy structure was maintained.

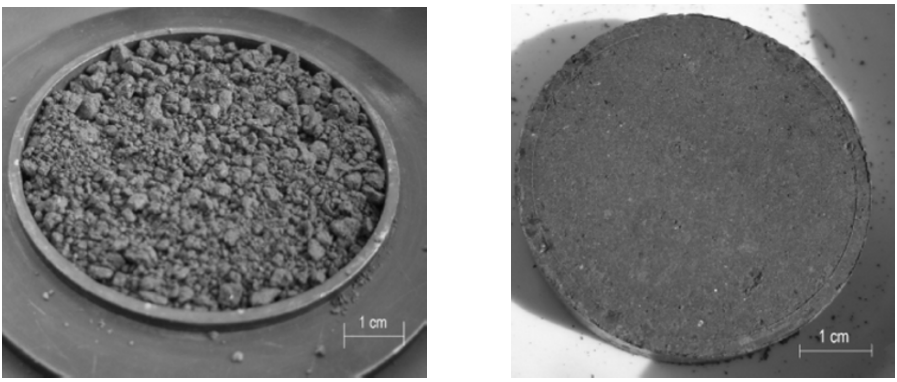

Fig. 6. The lumpy material before the test (left) and after the test (right)

Figure 7 shows the results. The samples inundated at $\sigma_{ax} = 10\,\text{kPa}$ are marked with s. Two sets of the tests with samples of natural water content ($w = 34\%$) were carried out on loose and compacted (marked with c in Fig. 7) soil. The collapsibility index was determined using

$$i = (e_{\text{unsat}} - e_{\text{sat}})/(1 + e_{\text{unsat}}) \tag{2}$$

where e are void ratios natural moisture and inundated samples at each loading step. The collapse potential was estimated with its maximum of $i = 20.2\%$ at $\sigma_{ax} = 100\,\text{kPa}$ for loose samples and $i = 15.9\%$ at $\sigma_{ax} = 200\,\text{kPa}$ for initially compacted samples, which indicates severe degree of collapse potential according to ASTM (2003a).

Collapse potential vanishes at vertical confining pressures of about $\sigma_{ax} = 1000\,\text{kPa}$, where saturated and natural moisture compression lines unite. Above this pressure the slope of NCL of natural moisture samples changes and so the character of the soil. In the region of $\sigma_{ax} \geq 1000\,\text{kPa}$ the interporosity vanishes and the compressibility is controlled just by the intragranular voids.

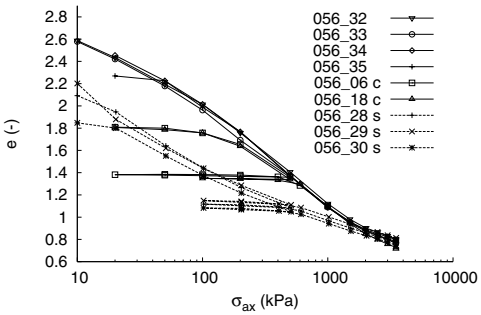

Fig. 7. Double oedometer tests on structured compacted and loose samples

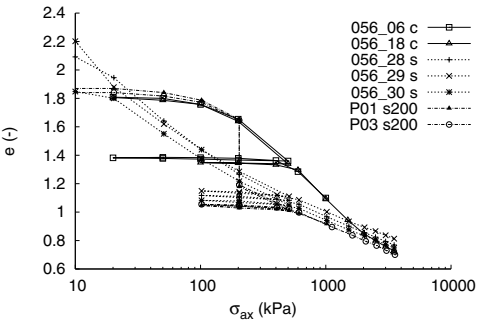

Fig. 8. Double oedometer tests on structured initially compacted samples and collapse under wetting at 200 kPa

After the sample dismantling at the end of test no obvious structure was visible. The material was homogenized in both natural moisture and saturated states (Fig. 6 right).

To confirm the collapse potential indicated by double oedometer tests the standard method for estimating collapse potential according to ASTM (2003a) was used. The samples prepared by compaction with natural water content were inundated at $\sigma_{ax} = 200\,\text{kPa}$ (tests no. P01 and P03 in Fig. 8). The collapse potential estimated through the standard method fits well to the double oedometer curves, which confirms the severe collapse vulnerability of initially lumpy structured samples.

Severe collapse potential was indicated by the tests on model lumpy soil contrary to negligible collapse potential estimated on undisturbed samples. One possible explanation would be that the site, where undisturbed samples were taken, is in a high degree of homogenization so the intervoids are already closed up and the lumpy structure vanished in the whole profile due to suction cycles, overburden and possible collapse under wetting. There was also no suction present (see Sect. 3). On the other hand, the significant scatter in initial void ratios of undisturbed samples indicates some remaining inhomogeneity of the aged material. Field testing should be carried out to fully exclude collapse risk.

5 Conclusions

Spoilheap material is highly collapse susceptible due to its open structure mainly in the early stages after landfilling. There are two main agents causing the degradation of the original open structure: overburden and drop of suction. In greater depths the overburden causes plastic straining and decrease of the total porosity of the material. However even under under low surcharge pressures the lumpy material changes back into more homogeneous soil, and the

suction oscillations due to weather are considered responsible for it. The drop of suction within intravoids causes the decrease of the strength of the lumps. On wetting, the intravoid high suctions vanish, the lumps become softer and the structure collapses.

At the site of Bílina mine the seasonally dependent suction oscillations were recorded through standard type of tensiometers reaching in late autumn its maximum of about 90 kPa. On the other hand at the site of highway construction near Ústí nad Labem there has been no or negligible suction through the whole monitored period. It corresponds well with the fact that there was no collapse potential indicated by laboratory investigation at this site.

Acknowledgements

The first author is grateful for the financial support by the research grants GAUK 6/2006/R and GAUK 331/B-GEO/PřF. A part of the laboratory investigation was carried out at the Technical University, Dresden, during the stay of the first author supported by the grant no. D-CZ 21/05-06 PPP of DAAD-AV ČR.

References

Abelev YM (1959) Collapse of macro-porosity loamy (loess) soil, Research Inst NIIOPS, Moscow, Proc No 37:5–25

ASTM (2003a) Standard Test Method for Measurement of Collapse Potential of Soils. ASTM D5333–03

ASTM (2003b) Standard Test Method for Measurement of Soil Potential (Suction) Using Filter Paper. ASTM D5298–03

Charles JA, Watts KS (1996) The assesment of the collapse potential of fills and its significance for building on fill, Proc Instn Civ Engng Geotech Engng 119:(1)15–28

Cui YJ, Delage P, Alzoghbi P (1998) Microstructure and collapse behaviour of a loess from Northern France. Proc 2nd Int Conf Unsat'98. Internat Acad Publishers, Beijing Vol 1:31–36

Feda J (1998) Fragmentary clay – a difficult waste material, Eng Geol 51:77–88

Fredlund DG, Rahardjo H (1993) Soil Mechanics for Unsaturated Soils. John Wiley and Sons Inc., New York

Herbstová V, Boháč J (2005) Laboratory investigation of the collapsibility of a clayey spoil heap soil. In: Proc GEOPROB 2005, Int Conf on Problematic Soils. Famagusta, Cyprus, Vol 2:715–722

Hurník S (1978) Reconstruction of the Thickness of Overlying Complex in North Bohemian Brown-Coal Basin (Miocene), J Geol Min 23(3):265–276 (in Czech)

Jennings JE, Knight K (1957) The additional settlement of foundations due to a collapse of structure of sandy subsoils on wetting. Proc 4th ICSMFE 316–319

Oedometer Creep Tests of a Partially Saturated Kaolinite Clay

Piotr Kierzkowski

Division of Soil Mechanics and Foundation Engineering, Technical University of Kaiserslautern, Kaiserslautern, Germany pkierz@rhrk.uni-kl.de

Summary. In the following paper an influence of several state parameters on one dimensional time-dependent material behaviour of an unsaturated soil is presented. For identification of parameter values, laboratory experiments were performed. Standard oedometric compression tests were carried out to investigate stress-strain-time relationships. Apart from the degree of saturation the initial void ratio vary as parameters. For measuring the matrix suction a tensiometer is mounted inside the specimen. A detailed description of the equipment used and the test procedures are given in the paper. The tests reported here were carried out with a kaolinite to determine parameter values, depending on different state variables. The characteristic behaviour of unsaturated samples observed during consolidation and creeping is shown in a series of figures. Parameters like C_c, C_s and C_α are used in constitutive model that can simulate both consolidation processes as well as creep phenomenon for partially saturated clay in a single consistent analysis.

Key words: kaolinite, oedometer, creep, partially saturated clay, suction

1 Introduction

Cohesive soils belong to geomaterials with a distinct viscous behaviour. They are often used as mineral seal in landfills. Viscosity is connected with physic-chemical properties of adhesive water and with the contact properties between soil particles. Time-dependent behaviour is plays an important role during creep of slopes or flowing of banks often leading to instabilities. The creep settlement has been a research topic over the last four decades (Bjerrum 1967, Berre and Iversen 1972, Leroueil et al. 1985, Yin 1999, Niemunis and Krieg 1996). In engineering practise, two hypotheses have been adopted for the estimation of the creep settlement. One assumes that secondary consolidation occurs only after the primary consolidation is completed, while another one assumes that creep occurs during the entire consolidation process. In partially saturated soils suction dominates the behaviour and there is lack of experimental evidence for this type of soil. A series of oedometer tests with direct

measurement of suction have been carried out to assess the characteristics of secondary consolidation. The equipment developed for this purpose, the testing procedure and selected results are described next.

2 Test Material

The material used for the tests is a kaolinite clay which is described in detail by Dobrowolsky and Becker (2002).

The clay mineral fractions as well as the relevant soil properties are listed in Table 1. Looking from the mineralogy site view clay minerals belong to the layer silicates. The difference between them and normal silicates is that they have a higher dispersion, sorption- and ion exchangeability. They consist of tetrahedrons and octahedrons that are arranged in layers, corresponding to a so-called sheetstructure.

Table 1. Clay fractions and soils properties

Clay minerals	Kaolinite $> 40\%$ Illite $< 20\%$ Smectite $< 5\%$
Liquid limit	$w_L = 51.3\%$
Plastic limit	$w_P = 22.4\%$

3 Test Equipment and Test Procedure

The creep behaviour of kaolinite was investigated during the secondary compression settlement in an oedometer device, cf. Fig. 1. The cylindrical specimen has a diameter of 100 mm and a height of 19 mm. It is located in 2 mm thick metal ring. The metal ring is brushed in the inner face with silicon fat to reduce friction. Two porous stones are placed on the top and bottom of the specimen.

Variation of suction is measured using UMS-tensiometer type T5-10, cf. Fig. 2. Measurement range is between -85 kPa and 100 kPa. The application of tensiometer measurement technique requires that the values of initial void ratio e_0 and degree of saturation S_r do not yield suction values lower that -85 kPa. A different technique like the axis translation method is here not applicable. To enforce this maximum level of suction the initial degree of saturation was kept higher than 0.90 and the initial void ratio higher than 0.70. The tensiometer is installed through the bottom of the specimen in vertical position, cf. Fig. 4.

Fig. 1. Oedometer

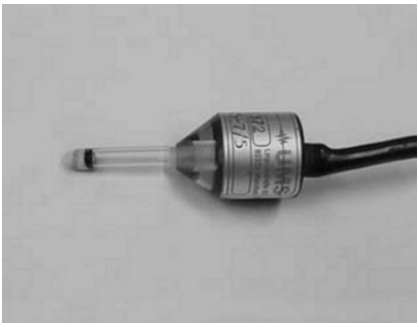

Fig. 2. Tensiometer

Fig. 3. Oedometer with plexiglas cover

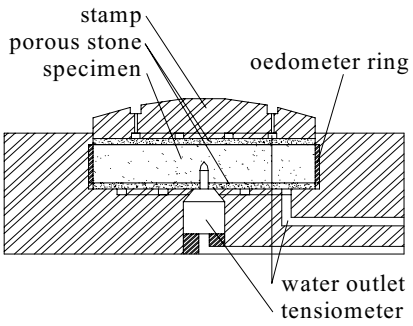

Fig. 4. Oedometer with position of tensiometer

Loading and unloading cycles as in conventional tests have been carried out. Each test consisted of a total of 14 loading/unloading stages with the following sequence: 12 → 25 → 50 → 100 → 200 → 100 → 50 → 100 → 200 → 400 → 200 → 100 → 50 → 25 kPa. The duration of the creep stage depends on the suction development and took in average three to four days. During the test the settlement and suction changing was measured. The axial settlements were recorded using the electronic displacement transducer. Accuracy of measurement is 0.01 mm.

Both temperature and air moisture during the test were kept constant. Both were measured and controlled with temperature- and moisture sensors. To achieve constant air conditions the whole equipment was placed in special plexiglass box, cf. Fig. 3. The air moisture during the test was about 90% in order to prevent drying or swelling of the soil sample that is accompanied by an unintentional suction change. Temperature was kept at 22°C.

4 Test Results

A typical test result in terms of variation of vertical strains with time is shown in Fig. 5.

After completion of primary consolidation, secondary creep settlement is observed at all stress levels. The beginning of creep is defined as the time when the suction reaches a stable value, cf. Fig. 6. The suction responds immediately after loading. It increases fast and then gradually reduces in value. The variation of suction with time for the test is displayed in Fig. 7. It can be seen that after a certain amount of time (approx. 1800 s) it reaches an almost constant value.

In order to define appropriate values for the stress dependent deformation moduli effective stresses σ' are defined following Bishop (1959)

$$\sigma' = \sigma - u_a + \chi(u_a - u_w) \tag{1}$$

where: u_a – pore air pressure
u_w – pore water pressure
χ – coefficient depending on degree of saturation
σ – total stress

The difference between pore air pressure and pore water pressure is defined as suction. The effective stress in ground may thus be higher than the total stress. Soil parameters like E-modulus or consolidation coefficient C_c are evaluated with such defined stress.

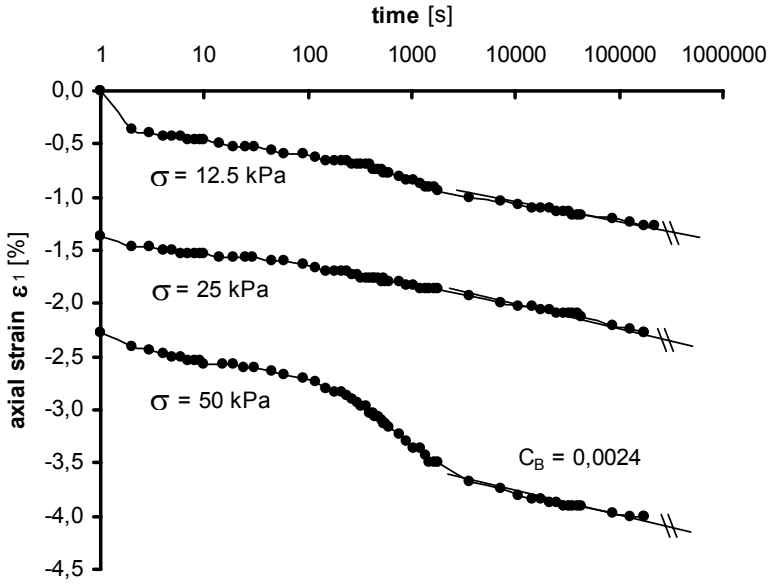

Fig. 5. Variation of strains with time for $e_0 = 0.78$, $S_{r0} = 0.95$, $T = 22°\mathrm{C}$

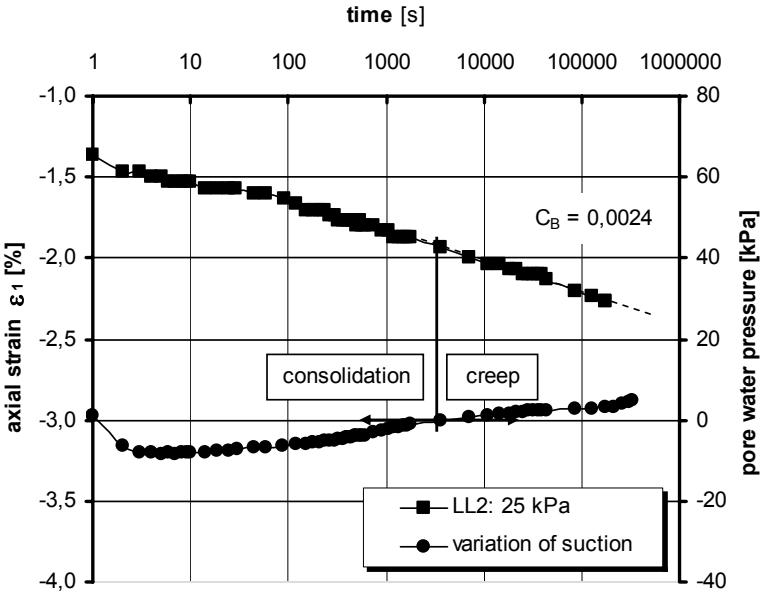

Fig. 6. The beginning of creep

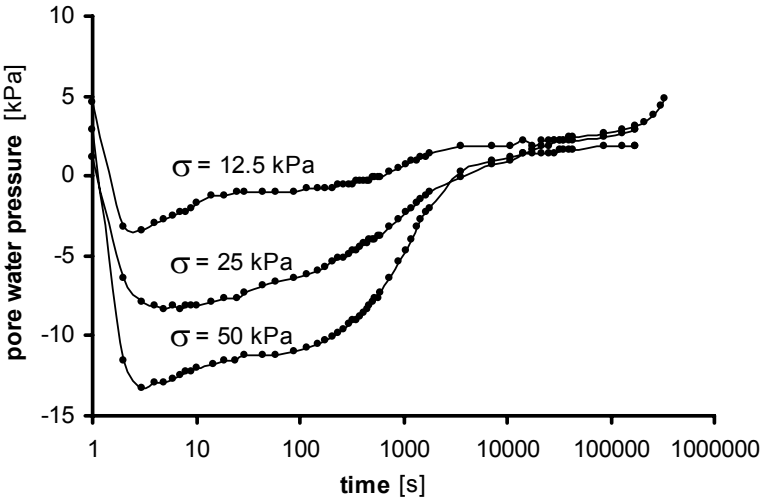

Fig. 7. Variation of suction during creep

When the curve is plotted in the graph: void ratio during the one level against logarithmic time scale, then it passes into the straight line after the consolidation. The slope of this straight line is described with secondary compression index C_α:

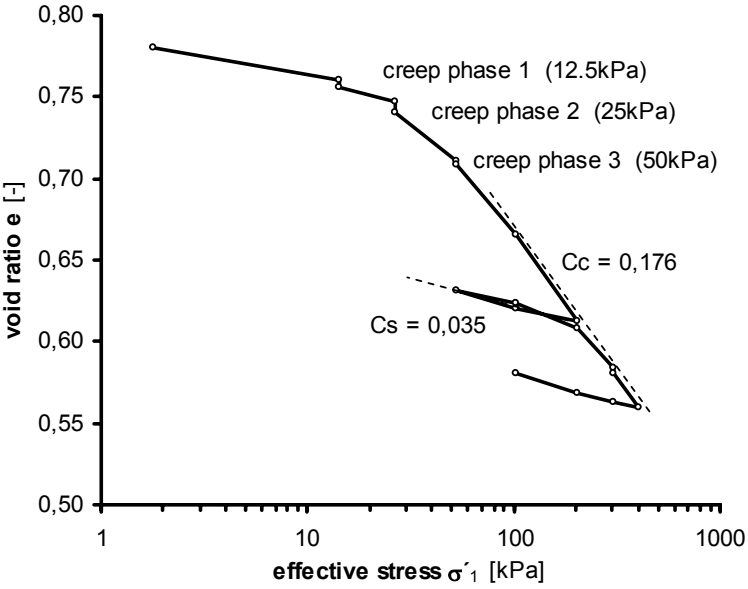

Fig. 8. Loading-unloading paths and creep phases

$$e_1 - e_2 = C_\alpha \log \frac{t_2}{t_1}. \tag{2}$$

This parameter can be replaced by Buisman-factor C_B. There is the following relations between them:

$$C_\alpha = C_B(1 + e_0). \tag{3}$$

5 Conclusions

The results show that stress-strain behaviour in first loading range can be described with a straight line (slope C_c) well accurately. The consolidation coefficient does not depend on stress level also.

Time-strain curves show a typical S-form of consolidations curve only in saturation range. The specimen is partially saturated at the first loading levels and air only is pushed away. Pore water stays inside. Decreasing of void ratio leads to increasing of degree of saturation. Only at higher stress level, the water is pushed away and the consolidations curve takes a classic S-form. The end of consolidation t_p was observed after 30 minutes, respectively.

The creep strain under $\sigma = \text{const}$ in all tests increases linear with logarithm of time. The creep index C_α is constant during the creep phase. Therefore there is sufficient to carry out the creep test so long, till the straight line forms (slope C_α) in time-axial strain graph definitely.

According to the tests, 3–4 days (150 t_p) are enough to determine C_α definitely. Longer tests duration brings no further information about creep behaviour. The creep index has the same value for all loading levels. It does not depend also on the stress.

References

Berre T, Iversen K (1972) Oedometer tests with different specimen heights on a clay exhibiting large secondary compressionn, Geotechnique 22(1):53–70

Bjerrum L (1967) Engineering geology of Norwegian normally consolidated marine clays as related to the settlements of buildings, Geotechnique 17(2):83–118

Buisman K (1936) Results of long-duration settlement tests. In: Proceedings 1st International Conference on Soil Mechanics and Foundation Engineering, Cambridge, Mass. Vol.1, pp. 103-107

Dobrowolsky M, Becker A (2002) Adsorptions- und Desorptionsverhalten durchströmter bindiger Böden. 4. Workshop Teilgesättigte Böden, Schriftenreihe Geotechnik der Bauhaus-Universität Weimar, Heft 8, pp. 71–76

Krieg S (2000) Viskoses Bodenverhalten von Mudden, Seeton und Klei, Heft 150, Veröffentlichung des Institutes für Bodenmechanik und Felsmechanik der Universität Fridericiana in Karlsruhe

Leroueil S, Kabbaj M, Tavenas F, Bouchard R (1985) Stress-strain-strain rate relation fot the compressibility of sensitive natural clays, Geotechnique 35(2):159–180

Niemunis A, Krieg S (1996) Viscous behaviour of soil under oedometric conditions, Can. Geotech. J. 33:159–168

Yin J-H (1999) Non-linear creep of soils in oedometer tests, Geotechnique 49(5):669–707

Analysis of the Expansive Clay Hydration under Low Hydraulic Gradient

Marcelo Sánchez[1], María Victoria Villar[2], Antonio Lloret[3], and Antonio Gens[3]

[1] Department of Civil Engineering, Strathclyde University, U.K.
marcelo.sanchez@strath.ac.uk
[2] CIEMAT, Madrid, Spain mv.villar@ciemat.es
[3] Technical University of Catalonia (UPC), Barcelona, Spain
Antonio.Lloret@upc.edu, antonio.gens@upc.edu

Summary. Engineered barriers made up of compacted expansive clays are a basic component of the systems for the isolation of high-level radioactive waste (HLW). The barrier is initially unsaturated and during hydration the hydraulic gradient varies from high values (i.e. higher than 50000) at the beginning of the wetting to very low values (practically zero when reaching stationary conditions). The values of bentonite permeability are frequently obtained at the laboratory under high hydraulic gradients (i.e. higher than 15000), necessary to induce a measurable flow. A drawback of this practice is that the applied hydraulic gradients are very far from those (expected) in actual conditions. So, the experimental results obtained might not be realistic in many cases, affecting the reliability of the numerical analysis. To advance in the knowledge of expansive clays behaviour this work presents an experimental and numerical study. The hydraulic permeability of FEBEX clay samples has been measured under low injection pressures. This work presents the modelling of infiltration laboratory tests designed to reproduce the thermo-hydro-mechanical conditions of large-scale tests. The evolution of the tests is analysed and discussed in detail using non-standard flow models which consider the presence of a threshold gradient and thermo-osmotic effects.

Key words: expansive clays, thermo-hydraulic cell tests, numerical modelling, non-standard flow models

1 Introduction

The long-term behaviour of low permeability (expansive) clays under low hydraulic gradient is not well-know, especially when the hydration takes place under non-isothermal and confined conditions, which are the expected conditions in high-level radioactive waste repositories (HLW). A trend to a very low rate of hydration, compared to the expected or predicted one, has been

observed in a number of large scale tests designed to study the behaviour of clay barriers intended for the isolation of HLW. A virtually locking of the hydration has been detected in the 'FEBEX mock-up', a large scale heating test that is being carried at CIEMAT laboratories (FEBEX Project 2000). An important part of the clay barrier is still unsaturated after eight years of hydration.

Standard thermo-hydro-mechanical (THM) models under-predict the saturation of the clay barrier (Sánchez and Gens 2005). Similar behaviour has been detected in the ITT test, a large-scale in-situ experiment carried out by AECL (Atomic Energy of Canada Limited). An unexpected very low saturation was achieved at the end of the test. Modelling evidences that a conventional THM formulation cannot match the experimentally measured values (Thomas et al. 2003). The trend to a very low hydration rate observed at advanced stages of these experiments, causes significant differences between models predictions and measurements. This problem affects strongly the reliability of the long-term predictions, especially the one related to the time required to reach the full saturation of the barrier, which is a key variable in the design of engineered barriers.

This work presents an experimental and numerical study oriented towards the identification of THM processes and phenomena that can explain the unexpected clay behaviour introduced above. The behaviour of unsaturated FEBEX bentonite in two infiltration tests, performed under thermal gradient and at isothermal conditions reported in Villar and Gómez-Espina (2006) are analysed herein. In particular, this work focuses on the study of the effect of 'non-Darcian behaviour' and 'thermo-osmotic flow' on the evolution of these tests. In addition, a series of laboratory tests have been carried out to explore the validity of Darcy's law at low hydraulic gradients in samples of FEBREX bentonite. A basic THM formulation (Olivella et al. 1994) has been extended to consider these two non-standard flow models (i.e., no linearity of Darcy's law and thermo-osmotic flows). The infiltration tests are critically analysed by comparing the experimental data and the model results obtained with the extended formulation.

2 Basic THM Formulation

The clay behaviour during the infiltration tests is very complex due to the THM processes and couplings that take place during the simultaneous heating and hydration. A full description of the THM formulation adopted in the analysis is presented in Olivella et al. (1994). The formulation incorporates the main thermal, hydraulic and mechanical phenomena. The problem is approached using a multi-phase, multi-species formulation that expresses mathematically the main THM phenomena in terms of: i) balance equations, ii) constitutive equations and iii) equilibrium restrictions.

The following mass balance equations are considered in the approach: i) water mass balance; ii) air mass balance and iii) solid mass balance. In addition the balance of energy and the balance of momentum have been considered. Two equilibrium restrictions have been considered: the psychometric law, which establishes the concentration of water vapour in the gas phase; and Henry's law, which gives the concentration of air dissolved in the liquid phase. Finally the constitutive models establish the link between the dependent variables and the state variables. Concerning the hydraulic problem, the generalized Darcy's law relates the unsaturated flow with the fluid pressures through the following expression:

$$\mathbf{q}_\alpha = -\mathbf{K}_\alpha \left(\nabla P_\alpha - \rho_\alpha \mathbf{g}\right) \tag{1}$$

where P_l and P_g are liquid (l) and gas (g) phase pressures, respectively, ρ_α is the phase density ($\alpha = l, g$) and $\mathbf{g}$ is the gravity vector. The permeability tensor, $\mathbf{K}_\alpha$ depends on fluid viscosity, degree of saturation (relative permeability law) and pore structure (intrinsic permeability). Figure 1**a** presents the variation of intrinsic permeability with porosity adopted in this work.

The retention curve establishes the link between the degree of saturation and suction. A modified van Genuchten law has been adopted (Fig. 1**b**):

$$S_l^= \left[1 + \left(\frac{s}{P_o}\right)^{\frac{1}{1-\lambda_o}}\right]^{-\lambda_o} \quad f_d : f_d = \left(1 - \frac{s}{P_d}\right)^{\lambda_d} \tag{2}$$

where s is the suction, P_o is the air entry value and λ_o is a model parameter. The function f_d is included to obtain more suitable values at high s.

It has been assumed that the diffusion flows are ruled by Fick's law (i.e. water vapour diffusion in gas phase and air diffusion in water) and that the heat conduction is governed by Fourier's law. To describe the mechanical

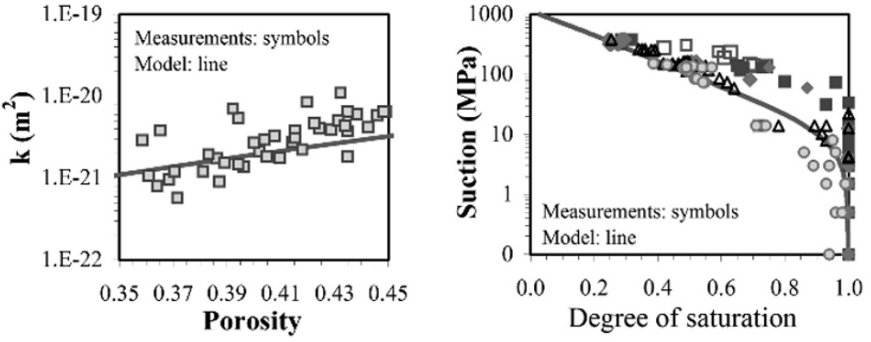

Fig. 1. FEBEX bentonite constitutive laws: **a**) variation of saturated permeability with porosity, **b**) retention curve

behaviour the Barcelona Basic Model (BBM) has been adopted (Alonso et al. 1990). All the laws and parameters used in the analysis are presented in detail in Sánchez and Gens (2005).

The system of equations is solved in a coupled way. One unknown (or state variable) is associated to each balance equation. Then, from the state variables, the dependent variables are calculated using the constitutive equations or the equilibrium restrictions. In this way the finite element program `CODE_BRIGHT` Olivella et al. (1996) has been developed. This code has been used to perform the numerical analysis presented herein.

3 Infiltration Tests

The infiltration tests are being performed by CIEMAT in cylindrical cells, whose internal diameter is 7 cm and inner length 40 cm (Fig. 2). They are made of Teflon to prevent as much as possible lateral heat conduction, and externally covered with steel semi-cylindrical pieces to avoid the deformation of the cell by bentonite swelling. The material tested has been unsaturated FEBEX bentonite, which is the clay used in the FEBEX Project to manufacture the blocks of the FEBEX large scale tests.

The FEBEX clay was compacted with its hygroscopic water content (around 14%) at an initial nominal dry density of 1.65 g/cm^3. Granitic water is injected through the upper lid of the cell at a pressure of 1.2 MPa. In one of the tests (GT40) the clay is being heated through the bottom surface at a temperature of 100°C. The other test (I40) is being carried out at isothermal conditions. The cells are instrumented with sensors of relative humidity and

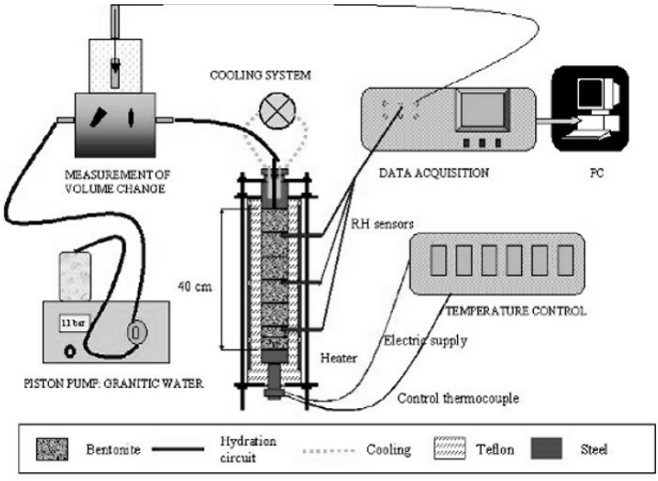

Fig. 2. Experimental setup for the infiltration tests

temperature placed inside the clay at three different levels separated 10 cm. The water intake and the relative humidity and temperature evolution at different levels inside the clay are being measured online.

4 Numerical Modelling

The modelling has been focused on the analysis of the temperature and relative humidity. In relation to the water intake, only one analysis is presented, due to problems occurred in its measurement. The study of these tests has the additional interest to check whether the, already explained, problems in the hydration rate observed in the FEBEX mock-up and ITT tests are also present in these cells. The initial and boundary conditions of the model have been imposed in order to be as close as possible to the experiments. An initial suction of 120 MPa has been adopted, which corresponds approximately to the relative humidity of 42% registered by the sensors inside the bentonite just before hydration. An initially uniform temperature of 23°C has been assumed. Initial hydrostatic stresses of 0.15 MPa have been adopted. Regarding the boundary conditions a temperature of 100°C is imposed in the GT40 cell at the contact between heater and bentonite (the bottom of the cell), while a constant water pressure of 1.2 MPa is imposed at the other end of the cell (upper part). The thermal boundary condition along the sample has been adopted in order to adjust the temperature field, in that sense an external temperature of 23°C has been fixed with a radiation coefficient of 1 (one).

Three main cases have been considered. Firstly, a 'base case' has been adopted using the basic formulation presented in Sect. 2. The constitutive laws adopted in the base case are the same one used in the analysis of the mock-up test (Sánchez and Gens 2005). The second and third cases studied correspond to the application of non-standard flow models developed to explain the slow hydration observed in test GT40.

4.1 Base Case

The results of the isothermal cell (I40) measurements and modelling are shown in Fig. 3. The evolution of relative humidity in different positions and also the water intake is well captured by the model. Figure 4 presents the results of the thermo-hydraulic cell (GT40). The thermal field is quite well reproduced considering that the variations of temperature due to the changes in the laboratory temperature are not taken into account in the simulations. In terms of relative humidity, the model captures qualitatively the main trend of behaviour, that is, an increasing saturation in the zones close to the hydration boundary and, in zones close to the heater, an initial wetting, due to the condensation of the water vapour coming form the bottom, and then a drying. However, the model predicts a quick hydration after the drying, while the experiment shows practically constant values of relative humidity in the three

measured positions. This is a trend similar to the one observed in the mock-up test, with a kind of locking of the hydration of the clay. To explain this unexpected behaviour, two non-standard flow models and the corresponding numerical analyses are introduced in the following sections.

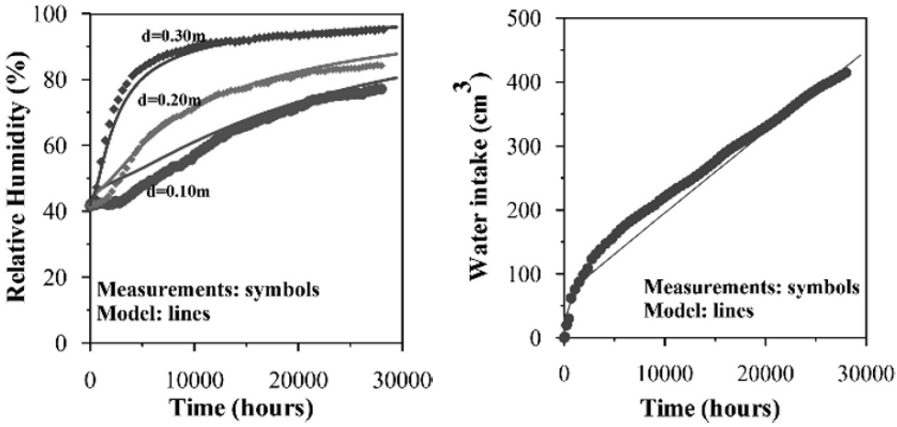

Fig. 3. Isothermal cell (I40): **a**) evolution of the relative humidity, **b**) water intake (d is the distance from the heater)

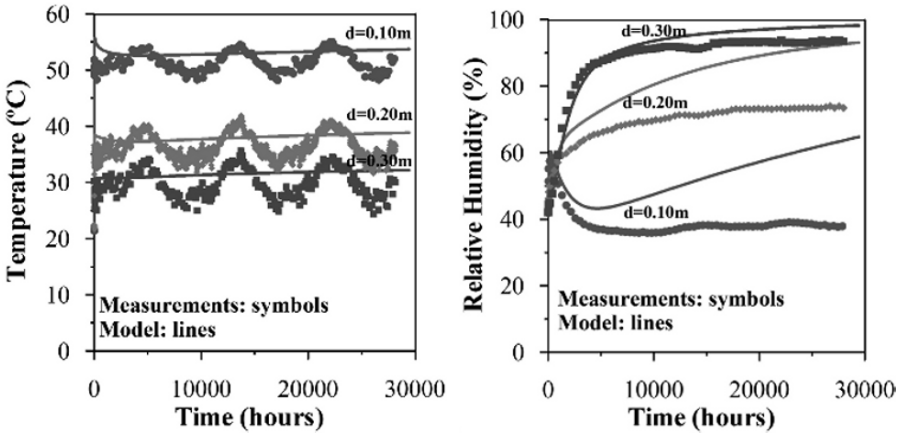

Fig. 4. Thermo-hydraulic cell (GT40): **a**) evolution of temperature, **b**) relative humidity (d is the distance from the heater)

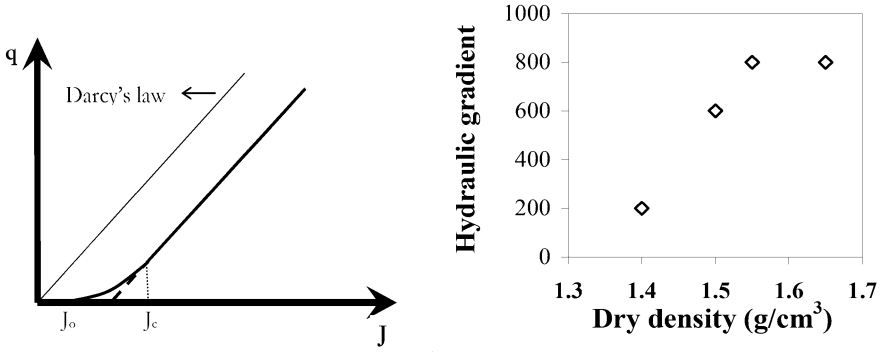

Fig. 5. a) Threshold gradient phenomenon. **b**) Minimum hydraulic needed to get measurable flows as a function of the dry density of the FEBEX bentonite

4.2 Non-Darcian Flow Behaviour

Experimental evidences show that under low hydraulic gradients (J), Darcy's simple relationship does not rule the liquid flow in some soils.

The strong clay-water interactions in clayed soils are suggested to explain this non-Darcian flow behaviour. In this work the law adopted considers two characteristic gradients (Fig. 5**a**): the threshold hydraulic gradient (J_o) and the critical hydraulic gradient (J_c). J_o is the hydraulic gradient below which no flow occurs. J_c is the hydraulic gradient below which flow occurs but it is not Darcian. If the hydraulic gradient is higher than J_c, Darcy's law applies (Dixon et al. 1992). The average hydraulic gradient applied to obtain the permeability of FEBEX bentonite shown in Fig. 1**a** was 15200. To clarify the effect of hydraulic gradient on the value of hydraulic conductivity, the hydraulic conductivity of FEBEX clay samples has been measured under low hydraulic gradients and injection pressures

The hydraulic gradients applied range from 200 to 7200. No measurable outflows have been obtained for certain hydraulic gradients depending on the dry density of the bentonite. These values are shown in Fig. 5**b** and could be regarded as threshold hydraulic gradients, since no flow has been obtained below these gradients. The dispersion found when hydraulic gradients lower than 1000 are applied could indicate that the critical gradient for this bentonite would be around this value (Villar and Gómez-Espina 2006).

Figure 6**a** shows the results obtained using a threshold gradient model. The base case results are also presented in dot lines. The following considerations have been taken into account: i) a threshold gradient equal to 50 (this is a common value found in the literature), ii) a critical gradient close to 1500; and iii) a power law for the range of hydraulic gradient with non-Darcian's flow. This model can reproduce very well the trend to a very low hydration observed in test GT40. On the other hand, the model underestimates the hydration in the isothermal cell.

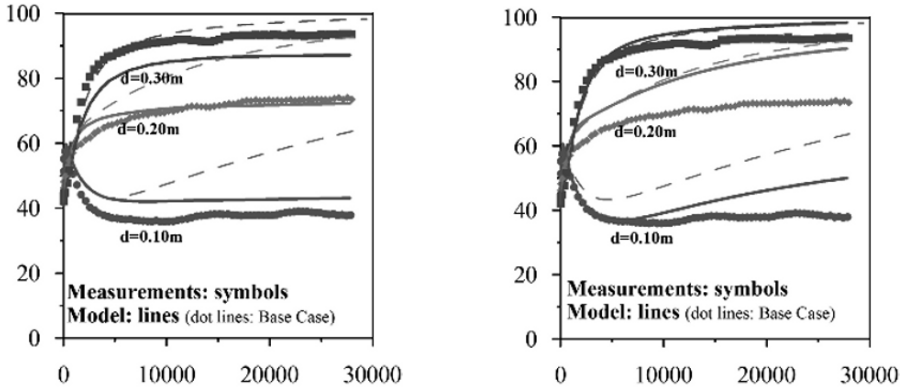

Fig. 6. Evolution of the relative humidity in the thermo-hydraulic cell (GT40): **a**) threshold hydraulic gradient model, **b**) thermo-osmosis flow model (d is the distance from the heater)

Flow	Gradients		
	Hydraulic Head	**Chemical Concentration**	**Temperature**
Fluid	**Darcy's Law** (Hydraulic Conduction)	Chemical Osmosis	**Thermo Osmosis**
Solutes	Ultra Filtration	**Fick's Law** (Diffusion)	Soret Effect (Thermal Diffusion)
Heat	**Thermo Filtration** (Isothermal Heat Transfer)	Dufour Effect	**Fourier's Law** (Thermal Conduction)

Fig. 7. Direct and coupled flow processes

4.3 Thermo-Osmosis Effects

The hydraulic gradient is the main force influencing the movement of water in soils. It is, however, not the only one. Figure 7 presents all the different kinds of flow (except the electrical component) that can occur in a porous media and the corresponding gradient responsible for the movements. Generally, the non-diagonal coefficients are relatively small and negligible compared to the diagonal terms and the coupled processes can be ignored. However there are certain problems in which, due to their particular conditions, the coupled processes may play a more influential role. The thermal conditions imposed on the thermo-hydraulic cell correspond to a practically constant thermal gradient during the test. In contrast, the hydraulic gradient is very high at the beginning of the test, but diminishes with the hydration of the barrier. The liquid flows associated with these two gradients have opposite directions.

Generally, the advective flow (Darcy's law) is the dominant flow. However, at advanced stages of the test (when the hydraulic gradient becomes smaller), it is possible that coupled phenomena (thermo-osmotic flow) could have a noticeable effect on the behaviour of the system, causing a trend to slow down the hydration in the zones close to the heaters. On the other hand, this phenomenon would not influence the isothermal cell.

Fig. 6**b** shows the results of the modelling considering thermo-osmotic flow. The base case results are also presented in dot lines. It is worthy to note the lack of experimental data concerning the phenomenological coefficient associated with thermo-osmotic effects. The thermo-osmotic constant adopted is $5.0 \times 10^{-12}\,\mathrm{m^2/K/s}$ and falls in the range of possible values found in the literature. A good agreement (qualitative) with the observations can be observed in zones close to the heater. Near the hydration front the measured trend is not well captured. The results of the isothermal cell do not change under this hypothesis.

5 Conclusions

The analyses of two infiltration tests have been presented in this work. First the results of a 'base case' using a 'standard THM model' have been presented. The results obtained with this model are not satisfactory, especially when the comparisons with the thermo-hydraulic cell are analysed. Threshold hydraulic gradient and thermo-osmotic effects have been included in the formulation, these being two plausible phenomena that could explain the unexpected trends observed in this kind of experiments. The results obtained are very interesting since a physical interpretation for the unexpected behaviour has been done. Each of these phenomena does not exclude the others and it is possible that an explanation for the whole behaviour of the system would require the combinations of some of them. These analyses show the need of improving the 'classical THM formulation' when complex processes, as those developed in the thermo-hydraulic cells, are studied.

References

Alonso E, Gens A, Josa A (1990) A constitutive model for partially saturated soils, Géotechnique 40:405–430

FEBEX Project (2000) Full-scale engineered barriers experiment for a deep geological repository for high level radioactive waste in crystalline host rock (Final project report EUR 19612 EN EC Brussels)

Dixon D, Gray M, Hnatiw (1992) Critical gradients and pressures in dense swelling clays, Can Geotech J 29:1113–1119

Olivella S, Carrera J, Gens A, Alonso EE (1994) Non-isothermal multiphase flow of brine and gas through saline media, Transp in porous media 15:271–293

Olivella S, Gens A, Carrera J, Alonso EE (1996) Numerical formulation for a simulator (CODE-BRIGHT) for the coupled analysis of saline media, Engineering Computations 13:87–112

Sánchez M, Gens A (2005) Final Report on THM modelling. FEBEX II (UPC-Geomechanical Group, ENRESA Report: 70-UPC-L-5-015)

Thomas H, Cleall P, Chandler N, Dixon D, Mitchell H (2003) Water infiltration into a large-scale in-situ experiment in an underground research laboratory, Géotechnique 53:207–224

Villar MV, Gómez-Espina R (2006) Deliverable 3.2.9: Progress report on laboratory tests performed by CIEMAT (WP3.2 NF-PRO Report). Madrid, 47 pp

Moisture Effects on Argillaceous Rocks

Chun-Liang Zhang and Tilmann Rothfuchs

Gesellschaft für Anlagen- und Reaktorsicherheit (GRS),
Theodor-Heuss-Strasse 4, 38122 Braunschweig, Germany
chun-liang.zhang@grs.de, tilmann.rothfuchs@grs.de

Summary. In view of the disposal of high level radioactive waste in argillaceous rocks various laboratory experiments have been performed at GRS's geotechnical laboratory on samples drilled from the Opalinus clay at the Mont Terri Rock Laboratory in Switzerland and the Callovo-Oxfordian argillite at the Bure site in France. This paper focuses on experimental studies of moisture effects on the clay rocks including the relationship between suction and water content, reaction on de- and re-hydration, and the self-sealing potential of the examined materials. The results indicate that the clay rocks react very sensible to a moisture change. Wetting and drying caused significant swelling and shrinking. After re-saturation, highly damaged samples exhibited a very strong reduction in gas-permeability from 10^{-16}–$10^{-17}\,m^2$ to 10^{-21}–$10^{-22}\,m^2$, indicating a high self-sealing capacity of the studied argillaceous rocks.

Key words: clay rock, moisture, swelling, shrinking, self-sealing

Introduction

Argillaceous formations are being investigated worldwide as host medium for the disposal of high level radioactive waste, because of their favourite properties. Argillaceous rocks are highly consolidated and usually characterized by very low permeabilities. Their high swelling capacity and visco-plasticity provide a high potential for sealing cracks, pre-existing ones as well as new ones created by construction of underground repositories. Additionally, argillaceous rocks also offer a high sorption capacity for most radionuclides. Because of the very low permeability and low hydraulic gradients in argillaceous formations, diffusion dominates the water and radionuclide transport. Consequently these properties lead to a reliable long-term isolation of disposed radioactive waste.

During the construction and operation phase of a repository, the ventilation of the openings by relatively dry air and the subsequent backfilling with unsaturated materials will lead to evaporation of the pore water from the surrounding rock. After closure of the repository, the previously de-hydrated rock

mass will take-up water again from the saturated area. De- and re-hydration may alter the rock properties because of the high sensitivity of the clay minerals in the rocks. This issue has been intensively investigated at GRS's geotechnical laboratory in the frame of several national and international research projects.

Studied Materials

For the laboratory experiments, a number of cores were drilled with compressed air from the Opalinus clay at the Mont Terri Rock Laboratory in Switzerland and from the Callovo-Oxfordian argillite at the Bure Underground Laboratory in France. The sedimentary argillaceous rocks are overconsolidated. The main mineral compositions of the rocks are clay minerals, quartz, and carbonates (Pearson et al. 2003, Lebon and Ghoreychi 2000). The other properties such as grain density, dry density and water content were measured on the samples by drying at 105°C. The basic characters of the clay rocks are summarized in Table 1. Both studied clay rocks have very similar properties.

Table 1. Petrophysical properties of the studied argillaceous rocks

Property	Opalinus clay at Mont Terri	Callovo-Oxfordian argillite at Bure
Clay content (%)	58–76	40–45
Carbonate content (%)	6–24	20–30
Quartz content (%)	5–28	20–30
Water content (%)	6.7	7.7
Grain density (g/cm^3)	2.71	2.70
Dry density (g/m^3)	2.34	2.25
Porosity (%)	15.1	16.5

Water Retention

In highly-consolidated clay rocks, a very significant portion of the water is adsorbed on mineral surfaces. The adsorbed water is so strongly bound that it may not be able to participate in advective transport under normally-encountered pressure gradients. However, the adsorbed water is able to move out thermodynamically from the pores at high external suction. In contrast to that, external water can also be taken-up by unsaturated clays. The process of de- and re-hydration is controlled by the relation between suction and

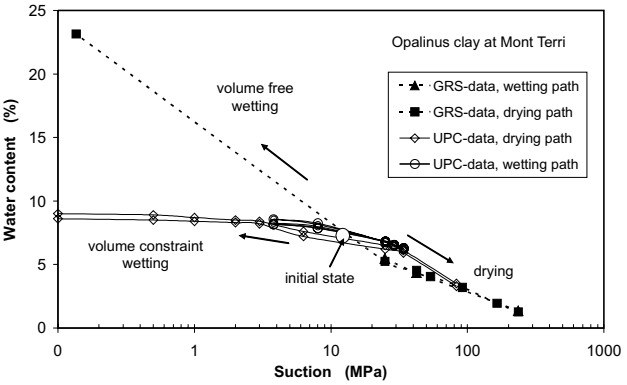

Fig. 1. Water retention curve of the Opalinus clay

water content (water retention curve). For the Opalinus clay, the water retention curve was determined on unconstraint samples placed in desiccators at different values of relative humidity adjusted by means of salt solutions. The result is illustrated in Fig. 1 in comparison with other data on constraint samples (Munoz et al. 2003). It is evident that the water content decreases as the external suction is high and conversely increases at low suctions. It is also obvious that the unconstraint samples took-up a significant amount of water of up to $w = 24\%$ at null suction over 100 days, accompanied by expansion.

Swelling Pressure

As well known, swelling in clays is the physico-chemical process due to interactions between water and particle surface, which cause adsorption of water on the internal and external surfaces of clay minerals, forming electrostatic double-layers. In highly-consolidated natural clay rocks, the double-layers are usually overlapping in the narrow spaces between particles. The interparticle water-films are thus assumed to carry the lithostatic stress (Rodwell et al. 1999). The average disjoining pressure acting in the water-films is equivalent to the swelling pressure, which is usually measured on volume-constraint samples by wetting with liquid water or water vapor. In conventional tests, the swelling pressures obtained on clay rocks are limited to below 2 MPa (Lebon and Ghoreychi 2000, Zhang et al. 2004), much lower than the lithostatic stresses at the sampling depths. GRS (Zhang et al. 2004) has developed a new method for the determination of the swelling pressure of argillaceous rocks. Figure 2 shows schematically the test principle and a test result obtained on a sample of the Callovo-Oxfordian argillite, which was taken at the depth of 455 m below the surface, corresponding to an overburden stress of about 11 MPa.

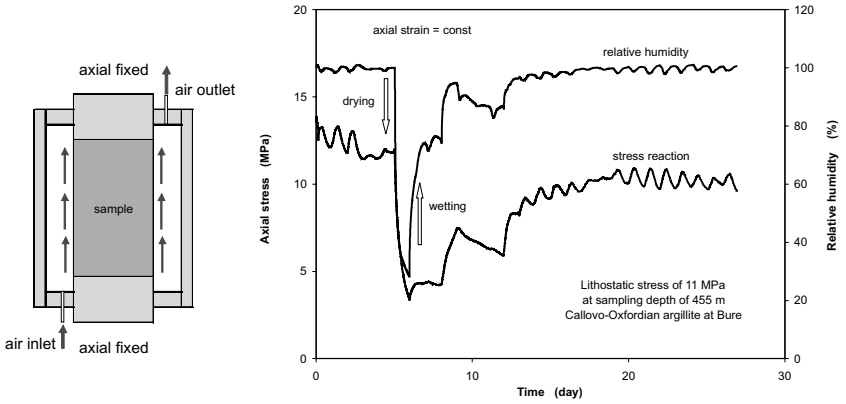

Fig. 2. Swelling pressure of an argillaceous sample under axially-fixed and laterally-unconstraint conditions

The sample was first uniaxially loaded to 13 MPa and then the axial strain was fixed. Under the axially-fixed and laterally-unconstraint conditions, the sample was wetted by pumping water vapor to it for five days, then dried by pumping dry air for one day, and finally wetted again for 20 days. In the first wetting phase at 100% relative humidity, the axial stress was stabilized at about 12 MPa. The subsequent drying however caused a very quick drop of the stress tending to zero. Conversely, the following wetting led the axial stress to rise again. At an elevated humidity of 100%, the axial stress reached about 10 MPa and remained at this level over the long test duration. The periodical variation of the stress is well correlated to the fluctuation of the humidity which was in turn induced by temperature changes. Obviously, the stress reaction or the build-up of swelling pressure is controlled by the amount of the pore water adsorbed on the minerals. When fully re-hydrated, the swelling pressure reaches its maximum, which is almost equal to the lithostatic stress at the sampling depth. Additionally, it is also interesting to point out that the swelling pressure σ_1 was built-up in the fixed axial direction at the laterally-unconstraint condition, $\sigma_2 = \sigma_3 = 0$. This means that this pressure is probably not a scalar quantity and should be represented by a second-rank tensor (Rodwell et al. 1999).

Swelling and Shrinking Strains

In addition to the swelling pressure, swelling and shrinking deformations of the clay rocks have also been examined on samples under different loading conditions. Figure 3 illustrates the measurements of a swelling strain test on an Opalinus clay sample at an axial stress of $\sigma_1 = 1$ MPa and null lateral stress ($\sigma_2 = \sigma_3 = 0$). The sample was dried and wetted by circulating dry air and water vapor at different temperatures between 24 and 58°C over 1 year.

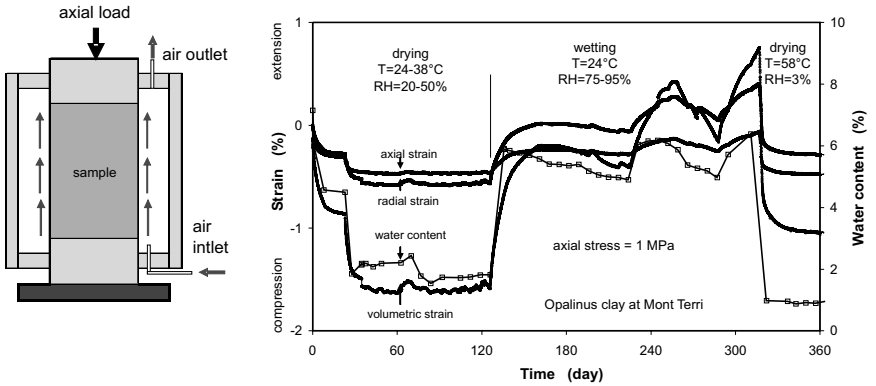

Fig. 3. Swelling/shrinking of an argillaceous sample at low axial load

It can be clearly seen that axial, radial and volumetric strains of the sample varied significantly with the changes in water content which resulted from the changes of the environmental temperature and humidity. The first drying at $T = 24$–$38°$C and RH = 20–50% caused a rapid reduction of the water content from 6.7% to 1.3%. In correlation with the water release, a large shrinkage took place in all directions to a volumetric reduction of 1.6%. When the water content remained constant, the strains were nearly not changed. Elevating the humidity to RH = 75–95% increased the water content to 4.5–5.5%. Correspondingly, the sample expanded so strongly that the pre-shrinkage is almost fully recovered. Drying again at 58°C and the resulting humidity of 3% led to a quick evaporation of the pore water and reduction of the water content to $w = 0.5\%$, resulting in a strong collapse of the pores leading to a volumetric reduction of 1.75%.

Figure 4 presents the measurements of swelling/shrinking deformations of other samples of the Callovo-Oxfordian argillite at a high axial stress of 15 MPa. After a long-term creep over 9 months, the saturated samples were exposed to relatively dry air of RH $= 24 \pm 4\%$. Under the highly-dried condition, the pore water evaporated from the samples, leading to a rapid collapse of the pores equal to a compaction of 0.3%. The slight swelling and shrinking strains observed over the further test duration are well correlated with the fluctuation of the water content.

The above experimental observations suggest that a) the argillaceous rocks have a high swelling capacity; b) the swelling/shrinking deformations in the clay rocks are dependent on two factors, namely the amount of water uptake and release as well as the confining stress; and c) the swelling and shrinking strains are reversible under the tested conditions.

In addition, the mechanical stiffness and strength of the argillaceous rocks are also strongly determined by the water content, as shown in Fig. 5. The air-dried sample exhibited a high compressive strength of ~ 42 MPa and a failure strain of $\sim 2\%$, about two times higher than that strength of 24.5 MPa and

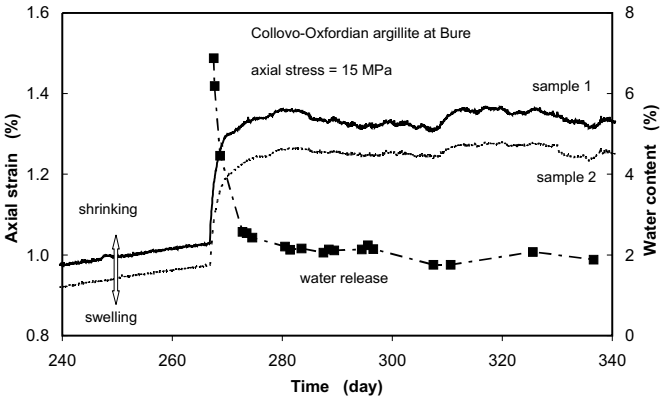

Fig. 4. Swelling/shrinking of an argillaceous sample at a high axial load

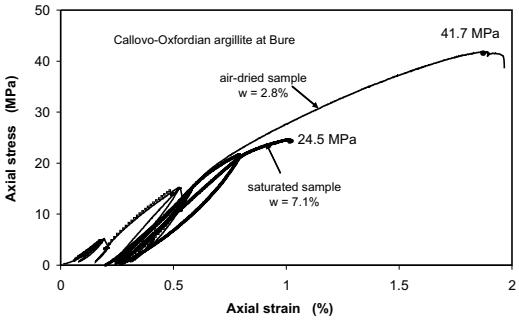

Fig. 5. Stress-strain curves of saturated and air-dried argillaceous samples

of 1.0%, respectively, of the saturated sample. The high strength of the dried clay rocks is probably induced by the increased friction resistances between the grains with very thin or no water-films. However, the large compressive strains of the dried clay rocks are mainly due to the collapse of the de-saturated pores.

It is also to be noted that drying often gives a rise to cracks in the clay rocks, depending on the confining stress. The cracks are usually concentrated along the bedding planes.

Self-Sealing

As an indicator for self-sealing, the gas permeability was measured on a number of samples. Figure 6 compares the gas-permeaiblities obtained on two highly-damaged samples of the Callovo-Oxfordian argillite before and after water injection. The permeabilities measured at a confining stress of 1.5 MPa before the water injection decrease steadily from $4 \cdot 10^{-16}$–$9 \cdot 10^{-17}\,\mathrm{m}^2$ to

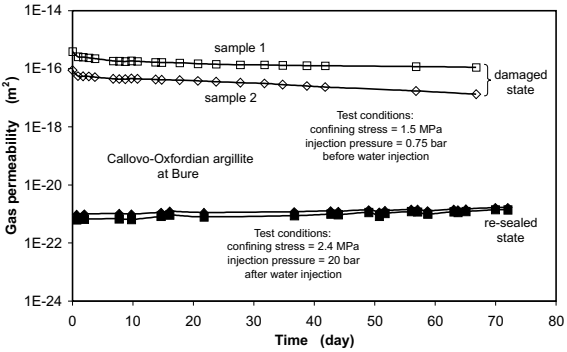

Fig. 6. Gas-permeabilities of highly-damaged argillaceous samples before and after water injection

$1 \cdot 10^{-16}$–$1 \cdot 10^{-17}\,\mathrm{m}^2$ over two months. After that, synthetic pore water was injected to both ends of the samples at 10–15 bars for more than 5 months, but no water outflow was observed. Subsequently, gas was injected again over another two months, during which very low permeabilities were recorded between $5{\cdot}10^{-22}$ and $2{\cdot}10^{-21}\,\mathrm{m}^2$. These values are about five orders of magnitude lower than those before the wetting.

In fact, the water is so strongly bound on the surfaces of the clay particles and so completely occupies the narrow pores that it can not be removed by the gas (or water) injected under the applied pressure gradients. The observation of the permeability reduction due to re-hydration suggests a high self-sealing capacity of the clay rocks.

Conclusions

The experimental findings on the Opalinus clay and the Callovo-Oxfordian argillite suggest that the argillaceous rocks react very sensible to moisture change. In the tests, it was observed that:

- re-hydration produced significant swelling strains even at high confining stresses and large swelling pressures carrying the lithostatic stresses;
- in contrast, de-hydration caused shrinking and stress reduction;
- swelling and shrinking strains are reversible in the tested conditions; and
- re-hydration by liquid water led to a large reduction in gas-permeability of highly-damaged samples from 10^{-16}–$10^{-17}\,\mathrm{m}^2$ to 10^{-21}–$10^{-22}\,\mathrm{m}^2$, indicating a high self-sealing capacity of the studied argillaceous rocks.

Acknowledgements

The authors gratefully acknowledge the funding by the German Federal Ministry of Economics (BMWi) and by the Commission of the European Communities (CEC) under a number of contracts. The support from ANDRA by providing the samples is also gratefully acknowledged.

References

Pearson FJ, Arcos D, Bath A et al. (2003) Mont Terri Project – Geochemistry of Water in the Opalinus Clay Formation at the Mont Terri Rock Laboratory

Lebon P, Ghoreychi M (2000) French Underground Research Laboratory of Meuse/Haute-Marne: THM Aspects of Argillite Formation. In: EUROCK2000, Aachen, 27–31 March 2000

Munoz JJ, Lioret A, Alonso E (2003) Characterization of hydraulic properties under saturated and non saturated conditions, VE-Experiment

Rodwell WR, Harris AW, Horseman ST et al. (1999) Gas Migration and Two-Phase Flow through Engineered and Geological Barriers for a Deep Repository for Radioactive Waste. EC/NEA Status Report, EUR 19122 EN

Zhang CL, Rothfuchs T, Moog H et al. (2004) Thermo-Hydro-Mechanical and Geochemical Behaviour of the Callovo-Oxfordian Argillite and the Opalinus Clay. GRS-202, ISBN 3-931995-69-0

Part VI

Retention Behaviour

Results from Suction Controlled Laboratory Tests on Unsaturated Bentonite – Verification of a Model

Ann Dueck

Clay Technology AB, Ideon, SE-223 70 Lund, Sweden ad@claytech.se

Summary. Highly compacted bentonite has been proposed as buffer material in the Swedish concept for the disposal of nuclear waste. A laboratory program with focus on hydro-mechanical properties of unsaturated highly compacted bentonite has been running and one part included changes in volume. The results could be used to determine different moduli but are presented here as a verification of a model covering the impact of confinement on the retention properties.

The tests were performed with suction control, which was achieved by the vapour equilibrium technique. The applied relative humidity was approximately 85% in the tests presented in this paper. The tests were done both as constant load tests with a change in relative humidity and as tests with constant relative humidity and a change in the applied load. The load was applied axially and the maximum constant load corresponded to an axial stress of 20 MPa. Also the radial stress was measured. All tests started from a compacted condition with a water content of 10% and a void ratio of approximately 0.6.

The investigation showed that the model, which was mainly based on constant volume tests, also seems to be valid after volume change since good agreement was achieved between measured and calculated results in the presented examples.

Key words: model, bentonite, unsaturated, water retention, relative humidity

1 Background

Highly compacted bentonite is proposed as buffer material in the Swedish concept for the disposal of nuclear waste. Although bentonite is expected to become saturated, it is important to understand the saturation process. A laboratory study with mainly constant volume tests was presented by Dueck (2004, 2006b) and new tests involving volume change have now been made.

Test results and interpretations of different moduli (swelling/shrinkage modulus and compression modulus) and different retention curves are presented by Dueck (2006a). However, in this paper examples from the test results have been used to show that a model proposed by Dueck (2004) and

Dueck and Börgesson (2006) is valid also after the volume change exemplified here. The model describes the relationship between swelling pressure, suction, void ratio and degree of saturation and was mainly based on results from constant volume tests.

2 Material and Test Methods

2.1 Material

The material is a commercially available sodium bentonite with a quality symbol MX-80 from American Colloid Co. The bentonite has montmorillonite as the dominating smectite clay mineral.

The particle density $\rho_s = 2.78\,\mathrm{Mg/m^3}$ and water density $\rho_w = 1.0\,\mathrm{Mg/m^3}$ were used for evaluation of void ratio and degree of saturation from measured variables (see e.g. Börgesson et al. 1988, 1995).

2.2 Determination of Retention Curves

The appearance of the retention curve depends to some extent on the initial water content (e.g. Dueck 2004). The retention curve is represented by the relative humidity RH vs. water content w (the mass of water divided by the mass of solids). The retention curve determined under free swelling condition and starting with an initial water content deviating from 0% is called the specific retention curve. Specific retention curves with initial water contents of 10%, 17% and 27% were determined with a method described by Wadsö et al. (2004) using 10 g samples placed in pans hanging from lids in glass jars. The sample weight is monitored by below balance weighing.

Measurements were carried out at seven different RH values (11%, 33%, 59%, 75%, 85%, 93%, 98%). These RH values were achieved using various saturated salt solutions (LiCl, $MgCl_2$, NaBr, NaCl, KCl, K_2SO_4) except in the case of $RH = 93\%$ where an aqueous unsaturated NaCl solution was used. The RH values were taken from Greenspan (1977) and the vapour pressure above the unsaturated 2 molal NaCl solution was taken from Clarke and Glew (1985). The jars were placed in laboratory room climate with a temperature of $20 \pm 0.5°\mathrm{C}$.

2.3 Determination of Volume Change Properties

The volume change properties were investigated in oedometers especially designed for this purpose. With this equipment it is possible to apply constant load and constant suction to a sample. Both the load and suction are measured together with the deformation of the sample. The applied load was in the range 0 to 20 MPa. After the test, the water content and void ratio were measured.

The equipment consists of a steel ring around the sample with filters on both sides. A piston and a force transducer are placed vertically above the sample. A piston and a force transducer are also placed radially through the steel ring. The sample has a diameter of 35 mm and a height of approximately 14 mm.

The constant suction is generated by the vapour equilibrium technique, where saturated salt solutions generate a specified relative humidity. The samples are exposed to the humidified air in a circulation system where air is pumped from the box with the salt solution to the steel ring enclosing each sample. The air passes in grooves above and below the filter stones.

In order to be able to use the relative humidity tabulated for the salt it is necessary to avoid temperature gradients in the equipment including the compartment with the salt solution. To avoid this problem, the relative humidity adjacent to the sample was measured and this value was used for the evaluation. Three saturated salt solutions were used (NaCl, KCl and K_2SO_4) which generate different RH (75%, 85%, 98%) at 20°C. In this paper only the results from tests with $RH = 85\%$ are analysed.

Powder samples with the initial water content 10% were compacted and placed in each oedometer ring. The initial void ratio was approximately 0.6.

Two different test types were performed; test types 1 and 2. In both test types the dependent (observed) variables were volume and water content. In test type 1 the independent (the varied) variable was the applied load and in test type 2 the independent variable was RH.

3 Results

3.1 Retention Curves

The test results from measurements of specific retention curves with free swelling samples are shown in Fig. 1. Results from Dueck (2006a) with the initial water content equal to 10% are presented together with results from Dueck (2004) with initial water contents of 17% and 27%. From the initial water content both drying and wetting takes place.

A continuous formulation of the specific retention curve was necessary for the analysis. A mathematical relation according to Eq. (1) was previously formulated by Kahr et al. (1990). Eq. (1) was used with different constants (a, b) to coincide with the measured values representing the different initial water contents; 10% (6.3, 0.16), 17% (7.25, 0.2) and 27% (7.5, 0.2). The constants are only valid and were only used in ranges shown in Fig. 1.

$$w = (a - \ln[-(10^{-6} \cdot \rho_w \cdot R \cdot T/\omega_w) \cdot \ln(RH/100)])/b \tag{1}$$

In Eq. (1) w is the water content (%), T is the temperature (K), R the universal gas constant (8.31432 J/(mol K)) and ω_v the molecular mass of water

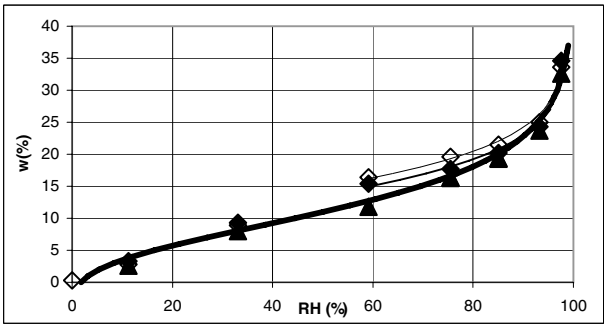

Fig. 1. Retention curves. The points represent laboratory results from Dueck (2006a) and Dueck (2004). Lines are derived from to Eq. (1). The initial water contents are 10% (▲), 17% (♦) and 27% (◇)

vapour (0.018 kg/mol). The relative humidity is defined as $RH = 100 \cdot (p/p_s)$ where p is the partial pressure of pore-water vapour and p_s is the saturation pressure of water vapour over a flat surface of pure water at the temperature T.

3.2 Volume Change Properties

Examples of test results are shown in Fig. 2. The chosen tests were performed at $RH \sim 85\%$. Two tests are shown from each test type and both mean stress (solid lines) and axial stress (broken lines) are plotted vs. void ratio. The mean stress P_{mean} is calculated from axial P_{axial} and radial P_{radial} stresses according to Eq. (2).

$$P_{\text{mean}} = (P_{\text{axial}} + 2 \cdot P_{\text{radial}})/3 \tag{2}$$

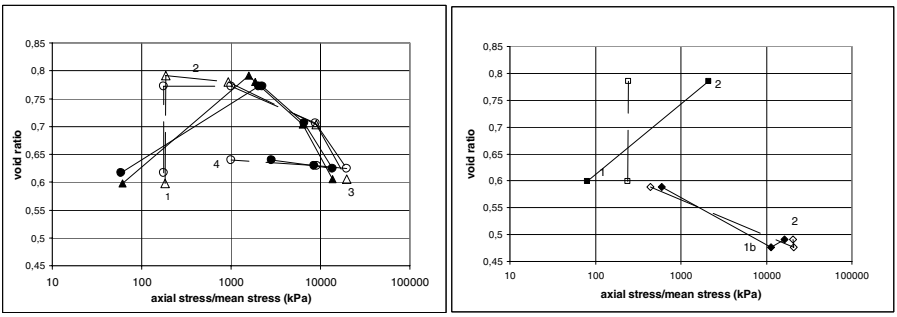

Fig. 2. Axial stress (*broken lines*) and mean stress (*solid lines*) vs. void ratio at $RH = 85\%$ from **a.** two tests from test type 1 (*left figure*) and **b.** two tests from test type 2 (*right figure*). Initial state (1), large load applied (1*b*), swelling (1–2), loading (2–3), unloading (3-4)

In test type 1 a small load (approximately 100 kPa) was initially applied (point 1). The radial stress was initially zero. The air with controlled RH was applied subsequently, which caused an increase in radial stress and a swelling (2). After equilibrium the load was increased in steps (2–3) and the deformation was continuously measured. Finally, one of the samples was unloaded (3-4).

In test type 2 the final load was initially applied (1) (in this case 100 kPa and 20,000 kPa). In the latter case this caused the radial stress to increase and the volume to decrease (1b). The air circulation was applied subsequently and the sample was brought to equilibrium with the deformation measured (2).

4 Analysis

4.1 Model

The model used includes mainly two equations, equations (3) and (4), which relate the variables stress, relative humidity, water content and void ratio. It was proposed by Dueck (2004) and mainly based on tests with constant volume conditions. The included relationships are further described by Dueck and Börgesson (2006).

Equation 3 describes the relation between the mean stress P, the actual relative humidity RH_{act} in the sample and the relative humidity according to the retention curve at actual water content RH_{ret}. The retention curve is derived from Eq. (1) with the constants a and b corresponding to the appropriate water content.

$$P(RH_{\text{act}}, w) = -\frac{R \cdot T \cdot \rho_w}{\omega_v} \cdot \ln \frac{RH_{\text{ret}}(w)}{RH_{\text{act}}} \tag{3}$$

Equation (4) describes the relation between the mean stress and the degree of saturation S_r at a specified void ratio e. The initial degree of saturation of the unloaded sample $S_{r,\text{ini}}$ is included. The swelling pressure at saturation P_{ret} can be calculated from the retention curve (5) which includes the void ratio e and the water content at saturation w_s (6).

$$P(S_r, e) = \frac{S_r - S_{r,\text{ini}}}{1 - S_{r,\text{ini}}} \cdot P_{\text{ret}}(e) \tag{4}$$

$$P_{\text{ret}}(e) = -\frac{R \cdot T \cdot \rho_w}{\omega_v} \cdot \ln \frac{RH_{\text{ret}}(w_s)}{100} \tag{5}$$

$$w_s = 100 \cdot \frac{e \cdot \rho_w}{\rho_s} \tag{6}$$

4.2 Evaluation According to the Model

The evaluation was made in steps. From the measured variables RH and P at a specific time the water content w, void ratio e and degree of saturation

S_r were calculated from Eqs. (3)–(6). Since the equations are not explicitly expressed in the unknown variables, void ratio was assumed and iterations made until agreement was achieved between the calculated and measured stress P.

The calculated and measured results are compared in Fig. 3. The mean stress is plotted vs. measured void ratios (filled symbols) and vs. calculated void ratios (unfilled symbols). Good agreement is shown between the measured and calculated results.

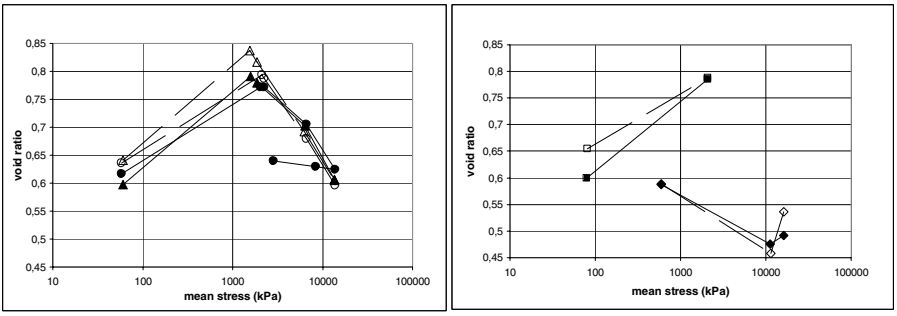

Fig. 3. Mean stress vs. measured void ratio (*filled symbols*) and calculated from the model (*unfilled symbols*). **a**. two tests from test type 1 (*left figure*) and **b**. two tests from test type 2 (*right figure*)

In the calculations only loading was considered, not unloading. At loading the retention curve according to Eq. (1) corresponding to the actual calculated water content at the start of the loading was used. The constants a and b were then interpolated from the values valid for initial water contents 17% and 27%. Only small changes in water content were calculated with the model during loading.

Good agreement was also shown between measured and calculated void ratio from most of the tests performed at $RH = 75\%$ and 98%. Further evaluation will be made.

5 Conclusions

Suction and stress controlled laboratory tests on swelling samples of compacted unsaturated bentonite have been made. The resulting measured volume change was compared to volume change calculated from measured relative humidity and mean stress with a model presented by Dueck and Börgesson (2006). The model was mainly based on results from constant volume tests but the presented results show good agreement between calculated and measured void ratio also after volume change.

Acknowledgement

This paper is a result of work funded by the Swedish Nuclear Fuel and Waste Management Company (SKB).

References

Börgesson L, Hökmark H, Karnland O (1988) Rheological properties of sodium smectite clay, SKB Technical Report TR 88–30

Börgesson L, Johannesson L-E, Sandén T, Hernelind J (1995) Modelling of the physical behaviour of water saturated clay barriers; laboratory tests, Material models and finite element application, SKB Technical Report TR 95–20

Clarke ECW, Glew DN (1985) Evaluation of the Thermodynamic Functions for Aqueous Sodium Chloride from Equilibrium and Calorimetric Measurements below 154°C. J Phys Chem Ref Data 14(2):536–537

Dueck A (2004) Hydro-mechanical properties of a water unsaturated sodium bentonite, laboratory study and theoretical interpretation. PhD Thesis, Lund Institute of Technology, Sweden

Dueck A (2006a) Hydro-mechanical properties of unsaturated MX–80, laboratory study 2005–2006. Report in progress

Dueck A (2006b) Laboratory results from hydro-mechanical tests on a water unsaturated bentonite. Submitted for publication

Dueck A, Börgesson L (2006) Model suggested for an important part of the hydro-mechanical behaviour of a water unsaturated bentonite. Submitted for publication

Greenspan L (1977) Humidity fixed points of binary saturated aqueous solutions, Journal of research of the national Bureau of Standards, A. Physics and Chemistry, 81A(1):89–96

Kahr G, Kraehenbuehl F, Stoeckli HF, Mûller-Vonmoos M (1990) Study of the water-bentonite system by vapour adsorption, immersion calorimetry and X-ray techniques: II. Heats of immersion, swelling pressures and thermodynamic properties, Clay Minerals 25:499–506

Wadsö L, Svennberg K, Dueck A (2004) An experimentally simple method for measuring sorption isotherms, Drying Technology 22(10):2427–2440

Variation of Degree of Saturation in Unsaturated Silty Soil

Ali R. Estabragh[1] and Akbar A. Javadi[2]

[1] Faculty of Soil and Water Engineering, University of Tehran, Karaj 31587-77871, Iran a.estabragh@gmail.com
[2] School of Engineering, Computer Science and Mathematics, University of Exeter, EX4 4QF, UK a.a.javadi@exeter.ac.uk

Summary. This paper presents the results of an experimental study on variation of degree of saturation of a compacted unsaturated silty soil during isotropic loading and unloading. A series of laboratory experiments have been conducted in a double-walled triaxial cell (and a conventional triaxial cell for saturated samples) on samples of a compacted silty soil. In the experiments the soil samples were subjected to isotropic consolidation followed by unloading under constant suction. The results show that during consolidation a significant increase in degree of saturation was observed. In contrast, during subsequent isotropic unloading, where only a very small elastic component of swelling occurred, the changes of degree of saturation were very modest. Comparison has been made between the experimental and theoretical prediction using a relationship proposed in the literature.

Key words: unsaturated soils, suction, degree of saturation, consolidation, unloading

1 Introduction

It is generally understood that unsaturated soils have a high suction by virtue of their partial saturation and the resulting capillary actions, and its magnitude is related to the water content or degree of saturation.

Gallipoli et al. (2003) and Buisson and Wheeler (2000) indicated that the relationship between the degree of saturation, S_r, and suction, s, for a given soil is non-unique because the variation of the void ratio in deformable soils results in changes in the void dimensions and also in changes in the connecting passageway between them. This, in turn, causes corresponding variation in the soil water characteristic curve. As changes in void ratio affect the soil water characteristic curve, irreversible changes of degree of saturation will occur during loading and unloading of mean net stress if there is an irreversible change of void ratio.

Bishop and Blight (1961) used the concept of state surface in order to represent the volume change of unsaturated soils. Matyas and Radhakrishna (1968) found the state surface for a mixture of flint powder and kaolin. Their tests involved either isotropic or anisotropic compression for examining the validity of stress state variables that were suggested by Bishop and Blight (1963). They plotted the results of the both tests series in terms of void ratio, e, and S_r against s and mean net stress, p'. Matyas and Radhakrishna (1968) presented experimental data defining state surfaces which related e and S_r to p' and s.

Fredlund (1979) was the first to suggest the mathematical expression for the state surfaces for void e and water content, w. Lloret and Alonso (1985) also proposed equations for state surfaces for void ratio and degree of saturation and their equation for degree of saturation is as follows:

$$S_r = a - \tanh(bs)(c + dp') \tag{1}$$

where a, b, c and d are soil constants. They reported that the above equation gives better predictions at low stress levels however it does not satisfy saturated condition when suction approaches zero. In this paper, the variation of degree of saturation during loading and unloading is studied and the application of equation (1) in prediction of degree of saturation of unsaturated soils is examined in the light of a comprehensive experimental study.

2 Experimental Study

2.1 Soil Properties

The soil used in the testing programme was a silty soil with low plasticity. The soil comprised 5% sand, 90% silt and 5% clay and had a liquid limit of 29% and plasticity index of 19%. The results of the standard proctor compaction test indicated a maximum dry density of 1.74 $\mathrm{Mg/m^3}$ at an optimum water content of 14.5%.

2.2 Test Procedure and Program

Compacted samples were prepared using a compaction mould designed specifically for static compaction. The compaction was done in nine layers in a compression frame at a fixed displacement rate of 1.5 mm/min to a maximum vertical load of 400 kPa. The samples were 76 mm high and 38 mm in diameter. All samples were compacted in an identical fashion in order to produce the same initial soil fabric in each test. The samples produced by this method were found to be very uniform.

2.3 Experimental Apparatus

A Bishop Wesely triaxial cell was modified to a double walled cell for measuring the volume change of the samples. The pore air pressure was controlled by applying an air pressure through a line from the top of the sample. Pore water pressures were measured through a high air entry disk at the bottom of the sample. The axis translation technique (Hilf 1956) that was adapted for triaxial testing by Bishop and Donald (1961) was used for creating the desired suction in the samples. Four GDS controller units were used to apply the pressures in the apparatus. All the experimental data were recorded continuously by a computer.

2.4 Experimental Procedure

Equalization

The first stage of the tests involves equalization. The purpose of the equalization tests was to create a desired suction in a sample by allowing the pore air pressure and pore water pressure to equalize to the applied air pressure and back pressure respectively. At this stage by applying the required air and water pressures the samples were brought to the desired value of suction (zero, 100, 200 and 300 kPa).

Ramp Consolidation and Unloading

After the sample was equalized at a specified suction (zero, 100, 200 or 300 kPa) and mean net stress, it was loaded isotropically under the constant suction (air back pressure and water back pressure were kept constant) to a pre-selected value of mean net stress. The process of ramped consolidation was used to limit the excess pore water pressure generated at the top face of the sample (Estabragh and Javadi 2004). The sample was then unloaded isotropically in ramp procedure to a predefined lower value of mean net stress.

3 Results and Discussion

A set of experiments were carried out on the samples of unsaturated silty soil. The results of variation of degree of saturation during loading and unloading at constant suctions of 0, 100, 200 and 300 kPa are shown in Fig. 1. During, isotropic loading when large plastic reductions in void ratio occurred, a significant increase in the degree of saturation was observed. In contrast, during subsequent isotropic unloading, when only a very small elastic swelling occurred, the changes of degree of saturation were very small. The results of irreversible changes of degree of saturation presented by Zakaria (1995), Romero (1999) and Gallipoli et al. (2003) strongly support theses findings.

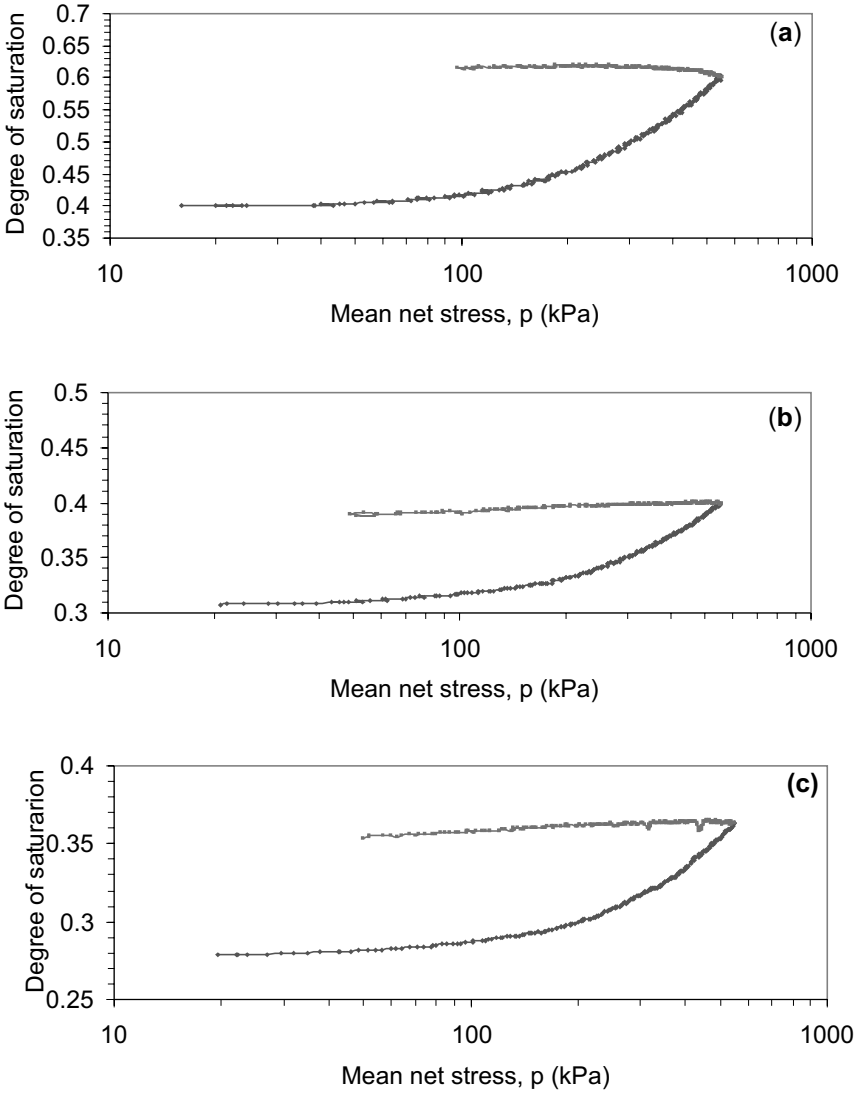

Fig. 1. Isotropic loading-unloading tests at: (**a**) $s = 100\,\text{kPa}$; (**b**) $s = 200\,\text{kPa}$; (**c**) $s = 300\,\text{kPa}$

As the specific volume, v, decreases the dimensions of voids and of connecting passageways between voids tend to decrease, so that a higher value of suction is required to produce a given degree of saturation. Figure 1 shows that the main variation in degree of saturation occurred after the yield point as the great proportion of deformation occurs after yielding. Estabragh and Javadi (2004) performed a comprehensive set of isotropic compression tests on soil

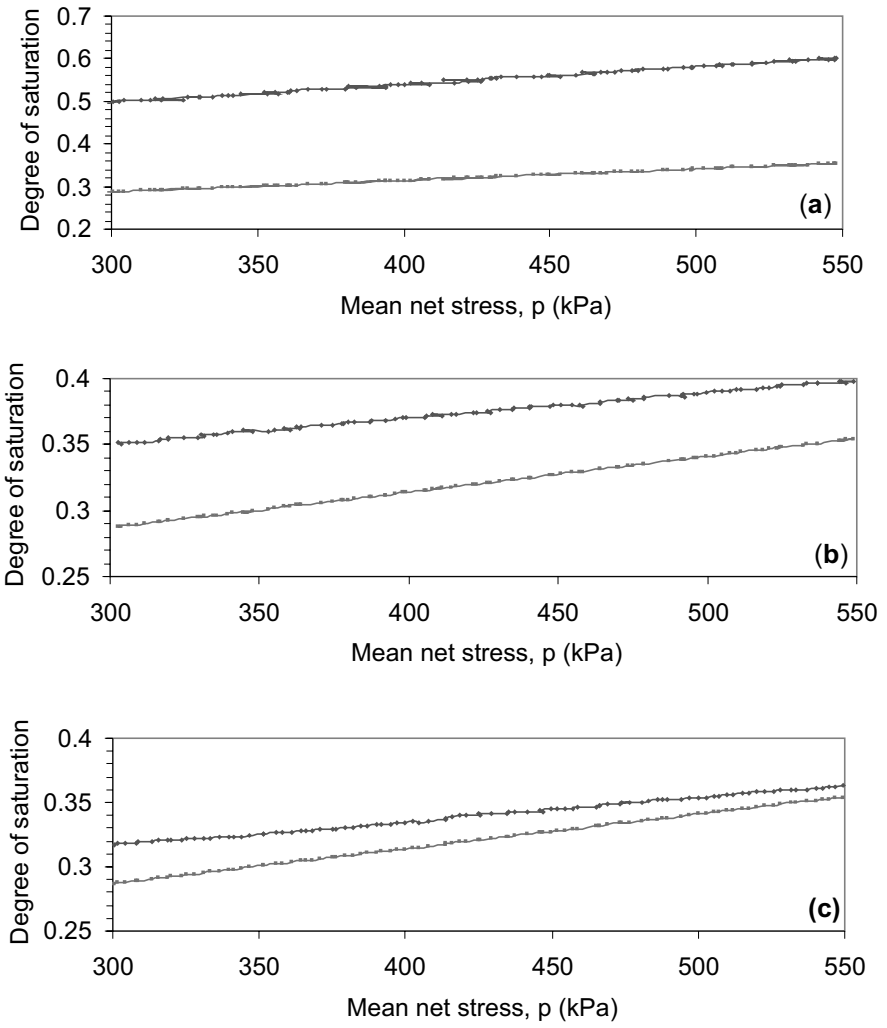

Fig. 2. Experimental and predicted values of S_r on isotropic normal compression lines at: (**a**) $s = 100\,\text{kPa}$; (**b**) $s = 200\,\text{kPa}$; (**c**) $s = 300\,\text{kPa}$

samples at different values of suction (0,100,200 and 300 kPa). The analysis of the experimental results indicated that, for the range of stresses considered, the normal compression lines at constant suction follow a linear relationship in the semi-logarithmic plane of $e - \ln p'$.

It was also shown that the variations of degree of saturation for post yield stresses are on straight line similar to the normal compression lines.

The results were analyzed using the conventional state surface expression for degree of saturation, suggested by Lloret and Alonso (1985) (equation (1)).

A value of 1 was used for the parameter a (in order to predict full saturation at zero suction), and the values of b, c and d were found by fitting the experimental isotropic normal compression lines at constant suctions of 100, 200 and 300 kPa. For each suction the values of S_r were predicted from equation (1). Figure 2 shows the experimental and predicted variations of degree of saturation during post yield sections of isotropic loading at three different values of suction 100, 200 and 300 kPa. It appears that equation (1) provides a reasonable match at $s = 200$ and 300 kPa but the match is not so good at $s = 100$ kPa. This behaviour is similar to that reported by Gallipoli et al. (2003). They developed a simplified version of the equation that was proposed by Van Genuchten (1980) for prediction the variation degree of saturation in unsaturated soils during loading and unloading. They also examined applicability of equation (1) for predicting the variation of degree of saturation and concluded the accuracy of the predictions for some suctions were not reasonable.

4 Conclusion

The results show that significant changes in S_r occurred during isotropic loading, even though the suction was held constant This can be attributed to the influence of volumetric strain as the main changes of S_r coincide with the post yield sections of loading stages when large changes of v were occurring.

Corresponding simulations were also performed with a conventional state surface expression for S_r. The results demonstrate that, where as a state surface expression can match the observed variation of S_r for a particular type of stress path (by selection of suitable parameter values); it is incapable of representing the variation of S_r for the full range of stress paths. This indicates that an alternative explicit form of state surface expression for S_r might provide a better match to the isotropic normal compression behaviour at different values of suction.

References

Bishop AW, Blight GE (1961) Strength and consolidation characteristics of compacted soils. Ph.D Dissertation, University of London

Bishop AW, Blight GE (1963) Some aspects of effective stress in saturated and unsaturated soils, Geotechnique 13(3):177–197

Bishop AW, Donald IB (1961) The experimental study of partly saturated soil in the triaxial apparatus, Proc 5th Int Conf Soil Mech Paris 1:13–22

Buisson MSR, Wheeler SJ (2000) In: Tarantrno A, Mancuso C (eds) Inclusion of hydraulic hysteresis in a new elasto-plastic framework for unsaturated soils. In experimental evidence and theoretical approaches in unsaturated soils 109–119

Estabragh AR, Javadi AA (2004) Effect of compaction pressure on consolidation behaviour of unsaturated soil, Can Geotech Eng J 41:540–550

Fredlund DG (1979) Appropriate concepts and technology for unsaturated soil, Can Geotech Eng J 16:121–139

Gallipoli S, Wheeler SJ, Karstunen M (2003) Variation of degree of saturation in deformable unsaturated soil, Geotechnique 53(1):105–112

Hilf JN (1956) An investigation of pore water pressure in compacted cohesive soils. Technical Memorandum No. 654, Bureau of Reclamation, USDI, Denver, Colorado

Lloret A, Alonso EE (1985) State surface for partially saturated soils. Proc 11th Int Conf Soil Mech Found Engng San Francisco 2:557–562

Matyas EL, Radhakrishna HS (1968) Volume change characteristics of partially saturated soils, Geotechnique 18(4):432–448

Romero E (1999) Characterisation and thermo-hydromechanical behaviour of unsaturated boom clay: an experimental study. PhD Thesis, Universitat politecnical de catalurya, Spain

Van Genuchten MT (1980) A closed-form equation for predicting the hydraulic conductivity of unsaturated soil. Soil Science Soc Am J 44:892–898

Zakaria I (1995) Yielding of unsaturated soil. PhD Thesis, University of Sheffield, UK

Mechanical Behaviour of Compacted Scaly Clay During Cyclic Controlled-Suction Testing

Camillo Airò Farulla[1], Alessio Ferrari[1], and Enrique Romero[2]

[1] Università degli Studi di Palermo, Italy
airo@diseg.unipa.it, ferrari@diseg.unipa.it
[2] Universitat Politècnica de Catalunya, Spain
enrique.romero-morales@upc.edu

Summary. Scaly clays are stiff and highly fissured soils due to their complex geological history. Owing to these characteristics, they may be placed and compacted as excavated, to obtain a material with adequate engineering properties, suitable as core material in earth dams and in waste isolation fills.

With reference to these engineering applications, an exhaustive experimental programme is developed to characterise the hydro-mechanical behaviour of this compacted material under a variety of controlled-suction paths.

This paper presents selected test results, focusing on the interpretation of specific behavioural features of the volume change of this complex material; namely, the strain accumulation and the volumetric irreversible features developed during suction cycling at different stress levels.

Key words: compacted tectonised clay, wetting–drying cycle, controlled suction oedometer, strain accumulation, elastic strain, microstructural elastic compression index

Introduction

Scaly clays are strongly tectonised and are composed of small stiff clayey fragments (scales), almost always angular, whose size ranges from a few millimetres to some centimetres.

Owing to their structural characteristics and natural water content these clays may be placed and compacted as excavated to obtain a material with low permeability and appreciable shear strength and stiffness, suitable as construction material in many Civil Engineering applications. In Sicily these materials were used, successfully, for the core of two dams built in the early sixties and are often used for isolation of industrial and domestic waste banks (Airò Farulla and Valore 1993).

In these cases because of construction management and environmental fluctuations, compacted scaly clay fills may be subjected to cyclic and strong drying and wetting paths during different stages of their design life.

Clayey soils undergo an increase in volume during water uptake, but also experience an important amount of shrinkage on water removal, which give rise to the accumulation of compression or expansion strains during suction cycles.

Several studies and research programmes have been developed on this subject (Dif and Bluemel 1991, Day 1994, Alonso et al. 2005); however, very few experimental studies have been reported in the literature with respect to liquid water transfer in cyclic wetting and drying tests under controlled conditions in the low suction range.

The objective of the research presented in this paper is focused on the investigation of the volume change response of compacted scaly clay samples subjected to several wetting and drying cycles in controlled suction oedometers. Oedometer tests were carried out under different values of constant vertical net stress, and wetting and drying cycles were performed varying applied matric suction between 10 and 800 kPa.

The volume change response of the samples is discussed and interpreted within the context of the elasto-plastic model proposed by Gens and Alonso (1992) and Alonso et al. (1999) (BExM: Barcelona Expansive Model).

Experimental Programme

Tested Material

Tested samples were prepared using a scaly clay outcropping near Palermo. The material is a kaolinitic-illitic clay with liquid limit $w_l = 58\%$ and plasticity index $I_p = 30\%$. The specific gravity is $G_s = 2.78$.

The air-dried clay with a hygroscopic water content $w_h = 0.05$ was disaggregated by a rubber pestle, and the *fraction* passing at n° 4 ASTM sieve was selected. Distilled water was added and carefully mixed. After a curing time of 2 or 3 days, samples were compacted dynamically with a non standard Proctor procedure to a target dry density. Compaction energy was approximately $0.71\,\mathrm{MJ/m^3}$.

Some of the physical characteristics of the tested samples are collected in Table 1.

Controlled-Suction Technique and Experimental Programme

The test programme included five cyclic wetting and drying tests at constant net vertical stress, σ_v, carried out of by means of two controlled-suction oedometers designed at the Geotechnical Laboratory of the UPC (Technical

Table 1. Initial characteristics of the tested samples

Sample	w_0	γ_{d0} [kN/m^3]	e_0	S_0
A1	0.156	17.17	0.59	0.73
A2	0.151	17.68	0.54	0.77
A3	0.151	17.59	0.55	0.76
A4	0.143	18.15	0.50	0.79
B2	0.150	18.25	0.50	0.84

University of Catalonia, Barcelona, Spain). Each oedometer is equipped with a ceramic disk with 1.5 MPa nominal air entry value.

Suction was applied by means of the axis translation technique, keeping a constant air pressure, $u_a = 1000$ kPa, and varying the applied water pressure, u_w, according to the air overpressure technique (Romero 2001).

Due to the high values of the control air pressure and of the degree of saturation of the tested samples, the translation of the air pressure to the reference value was accomplished, under water undrained conditions, with a very careful step by step procedure in order to minimise the volumetric deformation of the soil skeleton and the variation of the initial matric suction of the samples (Airò Farulla 2004, Airò Farulla and Ferrari 2005).

The displacements measured during the axis translation steps were in the order of a few microns and the variations in the degree of saturation were negligible.

After the reference air pressure translation, initial suction was applied ($s = 800$ kPa), and, when samples reached equilibrium, the selected vertical net stresses (100, 200, 300 and 400 kPa), were applied.

The first wetting path started at the end of the stress-induced consolidation process by reducing the applied suction to 10 kPa. Subsequent drying-wetting reversals in the suction interval of 10–800 kPa were then applied. Each equalisation step lasted until the rate of straining had reduced to a limit strain rate equal to or lower than 0.1%/day.

To reduce test duration, suction was changed in a single step in the interval 10–800 kPa. Four to six cycles were applied for each vertical stress.

In order to assess the reliability of the adopted procedure, in test B2 each wetting and drying step was accomplished limiting suction increment to 200 kPa. Because this procedure resulted in a very large test length, only three suction cycles were applied.

Water content and saturation degree variations were determined by measuring water inflow or outflow with a burette with a resolution of 0.02 cm^3. Displacements were measured with a micrometer with a resolution of 1 μm. The tests were performed at a constant temperature of $T = (20 \pm 1)$°C.

Stress-Path Followed

The different stress paths followed in the test programme are indicated in the (σ_v, s) plane (Fig. 1).

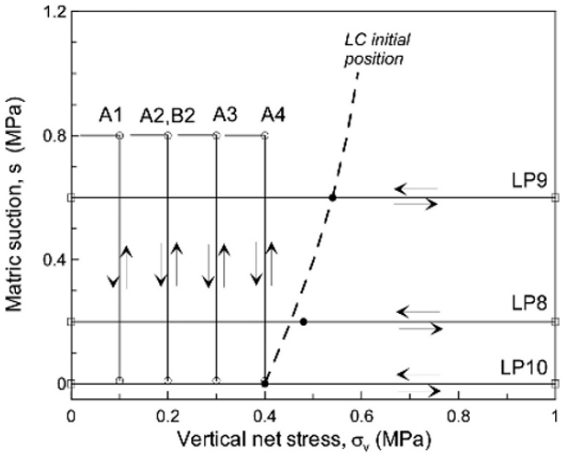

Fig. 1. Stress paths followed and LC yield locus for the as-compacted material

The drying-wetting paths were selected taking into account the position of the yield locus LC related to the as compacted material properties (Alonso et al. 1990). To determine the LC yield curve position in the (σ_v, s) plane, a complementary test programme was developed, including two constant suction loading and unloading oedometer tests ($s = 200$–$600\,\mathrm{kPa}$), and a loading-unloading oedometer test on a compacted sample that was previously saturated under constant volume (isochoric) conditions.

As shown in Fig. 1, applied vertical stress were lower or equal to the yield stress for saturated conditions, in order to investigate the behaviour of the soil in the "swelling region" bounded by the LC curve.

Test Results and Interpretation

Complementary Tests

Parameter values determined in the complementary tests are collected in Table 2, where σ_{v0} is the yield vertical net (or effective for the saturated sample) stress; λ is the slope of the virgin compression line (e–$\ln\sigma_v$ plane) and κ is the elastic (unloading-reloading) compression index (e–$\ln\sigma_v$ plane).

Table 2 reports, also, suction values (s) applied during the loading-unloading cycles, water content (w_0), void ratio (e_0) and dry density (γ_d) of the as-compacted samples.

Table 2. Initial characteristics of the tested sample and parameter values determined in the complementary tests

Sample	w_0	γ_{d0} [kN/m^3]	e_0	s [kPa]	σ_{v0} [kPa]	λ	κ
LP10	0.150	18.33	0.49	0	400	0.083	0.034
LP8	0.155	17.66	0.54	200	480	0.079	0.030
LP9	0.160	17.97	0.52	600	540	0.065	0.020

The best fit of the experimental points on the s–$\lambda(s)$ plane, according to equation:

$$\lambda(s) = \lambda(0)\left[r + (1-r)\mathrm{e}^{-\beta s}\right] \tag{1}$$

allowed determining: $r = 0.74$ and $\beta = 2.07\,\mathrm{MPa}^{-1}$.

The yielding locus, LC, in the (σ_{v0}, s) plane (Fig. 1) was determined by fitting the experimental points according to equation:

$$\frac{\sigma_{v0}}{\sigma_{vc}} = \left(\frac{\sigma^*_{v0}}{\sigma_{vc}}\right)^{\frac{\lambda(0)-\kappa}{\lambda(s)-\kappa}} \tag{2}$$

where σ^*_{v0} is the yield vertical effective stress for the saturated sample and σ_{vc} a reference stress fixed equal to 180 kPa for the best fitting of the experimental points. Even if data collected in Table 2 pointed out dependence with applied suction, κ was supposed a constant parameter equal to 0.030.

Cyclic Wetting-Drying Tests

Wetting and drying volumetric deformations at equilibrium are plotted in Fig. 2 for each applied vertical net stress. Compressive strains are considered positive.

The first wetting path results in sample expansion for $\sigma_v = 100$–$300\,\mathrm{kPa}$, while sample A4 ($\sigma_v = 400\,\mathrm{kPa}$) swells at the beginning of the equalization step and then collapses – an expected behaviour due to the proximity to the LC curve plotted in Fig. 1. Swelling and collapsing strains are quite similar, so that final volumetric strain is almost nil ($\varepsilon_v = 0.02\%$).

Successive suction increase from 10 kPa to 800 kPa induces a significant shrinkage in all samples. Volumetric contraction strains along this path are in the range of 2%, almost independent from applied vertical net stress. As a consequence, in the first suction cycle a quite different material volumetric behaviour in wetting and in drying may be detected for the different stresses applied. However, as the subsequent wetting-drying cycles are applied the differences between two successive wetting-drying volumetric strains become smaller, and the soil tends, clearly, towards a reversible or "elastic" state. This trend is better appreciated in Fig. 3 where the absolute values of the

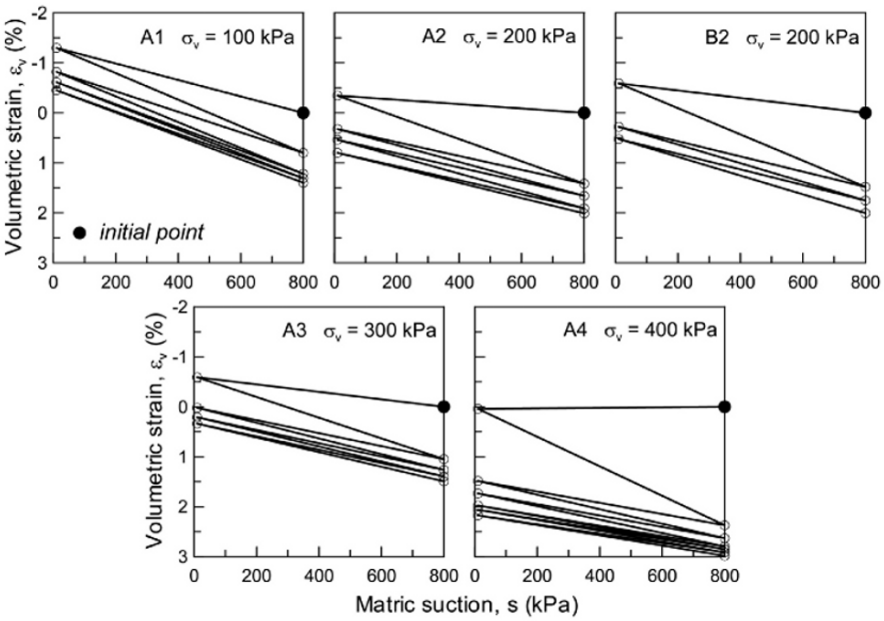

Fig. 2. Volumetric strains in cyclic controlled suction oedometer tests

volumetric strains either in expansion or compression are plotted versus the cycle number.

As the number of cycles increases, shrinkage strain intensity reduces and swelling strain increases, so that their difference tends to zero. However, shrinkage strains are greater than swellings and the material accumulates irreversible compression before the final reversible condition is achieved.

Usually four cycles are sufficient to achieve the final reversible condition (Fig. 3).

These results presented in Figs 2–3 provide data to investigate the ability of the BExM (Gens and Alonso 1992, Alonso et al. 1999) to model soil behaviour against cyclic suction changes. Before this is done, however, some simplifying hypotheses have to be formulated in the double structure approach in order to facilitate parameter determination (Alonso et al. 2005). These are: suction induced elastic deformations are considered only as microstructural deformations, and any suction induced macrostructural elastic deformations are ignored. During the application of drying and wetting cycles the SI (suction increase) and SD (suction decrease) yield surfaces are assumed always activated and macrostructure undergoes only coupled plastic deformations.

According to these hypotheses the total volumetric deformation increment ($\Delta\varepsilon_v$) measured at the end of each wetting or drying step may be considered as the sum of the elastic microstructural deformation increment indicated with superscript m and the coupled plastic strain increment denoted with

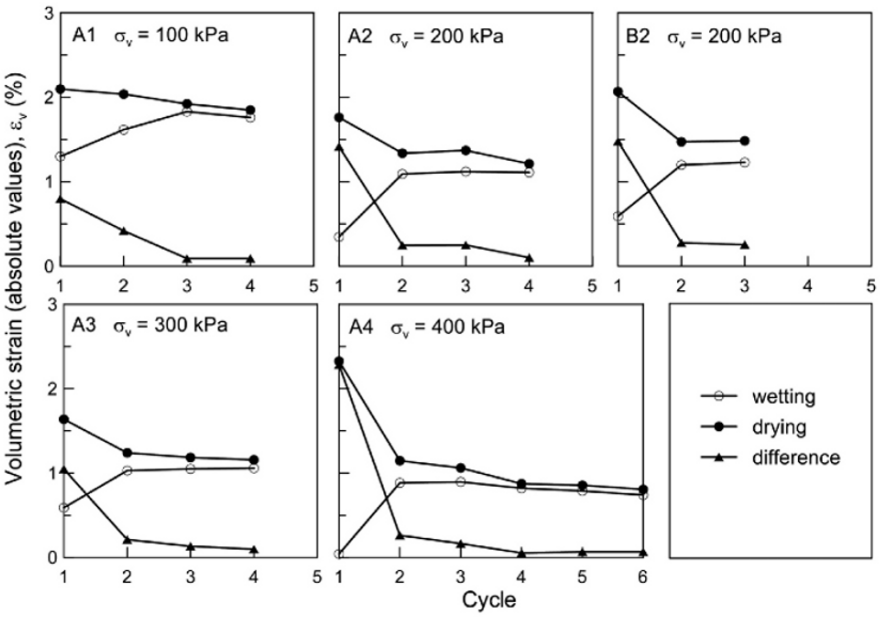

Fig. 3. Evolution of the absolute values of the volumetric strains with the number of controlled suction cycles

superscript c:

$$\Delta\varepsilon_v = (\Delta\varepsilon_v^m)^e + (\Delta\varepsilon_v^c)^p \,. \tag{3}$$

The elastic components, extrapolated from the total volumetric deformations measured in the last applied cycles when irreversible swelling or shrinkage strain increments were negligible, are represented in Fig. 4**a** versus the vertical net stress.

Elastic volumetric strain induced by a change in suction from an initial value s_i to a final value s_f, can be expressed as (Alonso et al. 2005):

$$(\Delta\varepsilon_v^m)^e = \frac{\kappa_m}{1+e_0} \ln\left(\frac{\sigma_v + s_f}{\sigma_v + s_i}\right) \tag{4}$$

where κ_m is the microstructure elastic (unloading-reloading) compression index.

Equation (4) was used to derive the microstructural elastic index, κ_m, for each of the four vertical net stresses applied. The calculated values, represented in Fig. 4**b** versus vertical net stress, belong to a very narrow range (0.011–0.013); the mean value, $\kappa_m = 0.012$, may be assumed as the constant value of the loading-unloading compressibility index of the microstructure.

If the elastic components are subtracted from the total final strain increments given in Fig. 3, coupled plastic volumetric components may be obtained and their evolution with the applied suction cycles could be investigated.

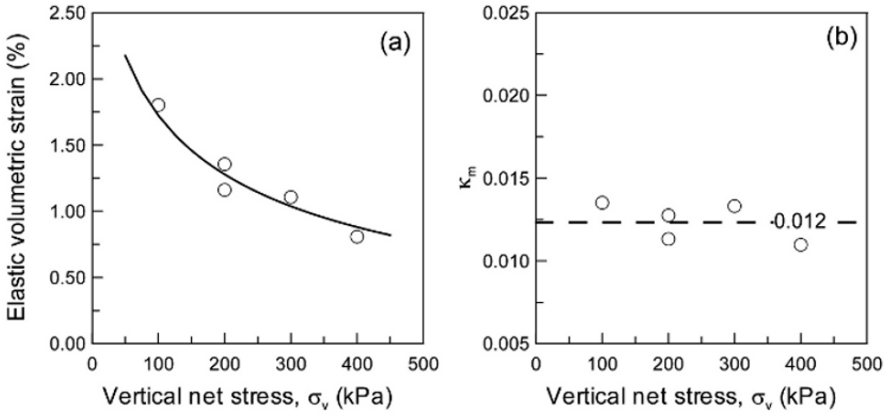

Fig. 4. Elastic volumetric strains (**a**) and microstructural elastic index (**b**) vs vertical net stress

As an example in Fig. 5 plastic volumetric strain increments versus cycle number are plotted for A2 and B2 samples.

Plastic strain increments both in drying and in wetting are positive. It means that during wetting even if measured total volumetric strain increment is negative (swelling), macrostructure experiences a moderate plastic compression. This plastic compression is associated with the invasion of the macrostructure by the active microstructure (Alonso et al. 1999).

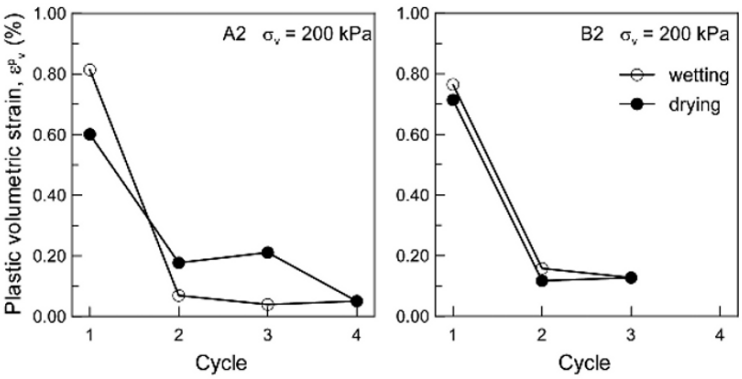

Fig. 5. Evolution of computed plastic volumetric strain increments with the number of cycles

Conclusions

A systematic experimental programme was carried out to study the effect of applying controlled-suction cycles using axis translation technique on compacted scaly clay. Selected test results were presented, which showed strain accumulation and volumetric irreversible features developed during suction cycling at different stress levels.

Test results have been interpreted within the framework of an elastoplastic constitutive model (BExM) described in Alonso et al. (1999), which uses a double structure approach. Collected results enable to calculate the constant loading-unloading compressibility index of the microstructure according to this model.

As previously noted, test B2 was carried out in order to assess the influence of the suction increment intensity on test results. Analysed results show that very little differences may be detected between A2 and B2 test results. From this point of view, cycling suction in a single step results in a reliable procedure in wetting-drying tests, even if this procedure is not lacking in shortcomings when parameter of the model are to be determined.

Owing to cyclic suction variations material accumulates shrinkage for all the intensities of constant net vertical stress applied. However, a few cycles are needed to achieve an "elastic" or reversible condition, in which total volumetric strain increment in wetting and in drying are almost equal. During wetting macrostructure experiences moderate plastic (coupled) compressions, which are associated with the invasion of the macrostructure by the active microstructure. Plastic volumetric strain increments at macroscopic level are slightly masked by the dominant microstructural volumetric strains of the active clay.

References

Airò Farulla C (2004) Comportamento idraulico e meccanico dell'argilla a scaglie compattata del nucleo delle dighe Scanzano e Rossella. In: AGI, XXII Conv Naz di Geotecnica, Palermo, 22–24 September, 445–452

Airò Farulla C, Ferrari A (2005) Controlled suction oedometric tests: analysis of some experimental aspects. In: Tarantino, Romero, Cui (eds) Advanced Experimental Unsaturated Soil Mechanics. Taylor & Francis Group, London, 43–48

Airò Farulla C, Jommi C (2005) Suction controlled wetting-drying cycles on a compacted scaly clay. In: Proc Int Conf on Problematic Soils, 25–27 May, East Medit Univ, Famagusta, N. Cyprus

Airò Farulla C, Valore C (1993) Some aspects of the mechanical behaviour of compacted tectonized clays. In: Anagnastopulos et al. (eds) Geotech Eng Of Hard Soils – Soft Rocks. Balkema, Rotterdam, 335–342

Alonso EE, Gens A, Josa A (1990) A constitutive model for partially saturated soil, Géotechnique 40(3):405–430

Alonso EE, Vaunat J, Gens A (1999) Modelling the mechanical behaviour of expansive clays, Engineering Geology 54:173–183

Alonso EE, Romero E, Hoffmann C, Garcia-Escudero E (2005) Expansive bentonite-sand mixtures in cyclic controlled-suction drying and wetting, Engineering Geology 81:213–236

Day RW (1994) Swell-shrink behaviour of compacted clay, J Geotech Eng 120(3):618–623

Dif AE, Bluemel WF (1991) Expansive soils under cyclic drying and wetting. Technical note, Geotech Testing J 14(1):96–102

Gens A, Alonso EE (1992) A framework for the behaviour of unsaturated expansive clays, Can Geotechnical J 29:1013–1032

Romero E (2001) Controlled-suction technique. In: Gehling WYY, Schnaid F (eds) Proc 4th Symp Brasil Solos Nao Saturados, Porto Algre, Brasil, 535–542

Prediction of Soil–Water Characteristic Curve Based on Soil Index Properties

Navid Ganjian[1], Yadollah Pashang Pisheh[2], and Seyed Majdeddin Mir Mohammad Hosseini[2]

[1] University of Tehran, Iran nganjian@ut.ac.ir
[2] AmirKabir University, Iran ypashangpisheh@aku.ac.ir, smmirhos@aku.ac.ir

Summary. The measurement of soil parameters for the unsaturated soil constitutive models needs extensive laboratory tests. For most practical problems, it has been found that approximate soil properties are adequate for analysis. Thus, empirical procedures to evaluate unsaturated soil parameters would be valuable. The soil–water characteristic curve (SWCC) can be used to estimate various parameters used to describe unsaturated soil behavior. The SWCC is a relationship between soil suction and some measure of the water content. It can be measured or predicted based on soil index properties. Estimation based on index properties is highly desirable due to its simplicity and low cost.

In this paper, a new model for predicting the SWCC based on soil index properties and Van Genuchten equation is presented. The comparisons show that the SWCC predicted by this model is in a good agreement with the experimental results.

Key words: unsaturated soils, soil–water characteristic curve (SWCC), matric suction, water content

1 Introduction

Unsaturated soil mechanics has received wide attention across geotechnical communities because of its practical importance. The investigation of unsaturated soils behavior requires evaluating the particular behavior parameters in these soils. A theoretical basis for unsaturated soil mechanics has been established over the past three decades. The constitutive equations for volume change, shear strength, and flow through unsaturated soil have become generally accepted in geotechnical engineering (Fredlund and Raharjo 1993). The fundamental accepted principal in this theory is that the unsaturated soil behavior could not be described just by making use of one stress state variable; in other words, both the net normal stress, $(\sigma - u_a)$, where σ is the total stress and u_a is the pore-air pressure, and the matric suction, $(u_a - u_w)$, where u_w is the pore-water pressure, are generally required for the constitutive models.

As a result, evaluation of suction is most essential to assess the unsaturated soil behavior.

Suction evaluating in direct measure needs to time consuming and costly laboratory tests, so estimation of suction with indirect methods based on other parameters such as water content would be considered. Consequently, the soil–water characteristic curve (SWCC) that defines degree of saturation corresponding to particular suction in a soil is widely used to estimate unsaturated soil properties. Through the practical applications of the soil–water characteristic curve, prediction of shear strength, water storage, and permeability coefficient may be pointed out. Figure 1 provides a qualitative illustration of the benefits derived from using estimated unsaturated soil property functions (Fredlund 2000). Estimates of the unsaturated soil property function are shown to provide a significant increase in the accuracy of the engineered designs, for a nominal increase at the soil investigation and testing stage. The accuracy of the output from an analysis depends strongly upon the independent variable being computed.

There are different methods to evaluate the soil–water characteristic curve. However, these methods are divided to two general branches: laboratory and estimating methods. The researchers, with taking account of the general form of SWCC, have suggested some equations to approximate these curves. Such equations basically consist of two or three constant evaluated by making use of either suction laboratory results in various water contents or statistical relations based on other soil properties. According to existing difficulties in evaluation of these curves experimentally and noticeable variability, the estimation of such parameters has widely been used by many of researchers.

In current study, an estimating model has been proposed for cohesive soils to evaluate the constant parameters of equation suggested by Van Genuchten (1980) based on soil index parameters. These parameters are, however, the plasticity index, PI, and the percentage passing 200# sieve, W. Using

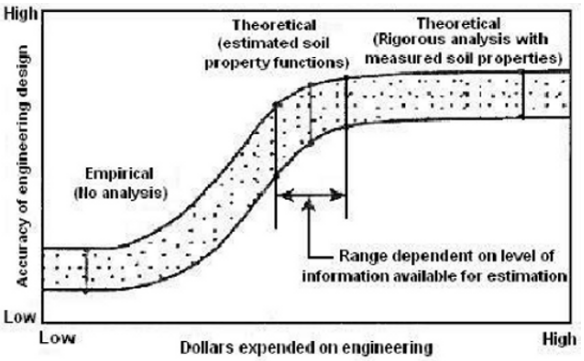

Fig. 1. Qualitative representation of the benefits derived from using estimated unsaturated soil property functions

statistical approach on the collection experimental results, some equations have been proposed for estimation of the mentioned constants parameters and corresponding SWCC.

2 Definitions

The behavior of unsaturated soils is strongly related to the pore size geometry and the pore size distribution. The soil–water characteristic curve is defined as the relationship between water content and suction for the soil (Williams et al. 1983). In soil science, volumetric water content is most commonly used, and in most of researches the soil–water characteristic curve has been suggested as a relationship between volumetric water content and matric suction. The volumetric water content is the ratio of the water volume in the soil to the total volume as below:

$$\theta = \frac{V_w}{V_t} = \frac{V_w}{V_v} \cdot \frac{V_v}{V_t} = S \cdot n = \frac{S \cdot e}{1 + e} \tag{1}$$

where θ = volumetric water content, V_w = water volume within the soil, V_t = total volume of soil, V_v = volume of pores in soil, S = degree of saturation, n = porosity ratio, and e = void ratio.

The suction may be either the matric suction of the soil, $u_a - u_w$, or total suction (i.e., matric plus osmotic suction).

Figure 2 shows a typical plot of a soil–water characteristic curve for a silty soil, along with some of its key characteristics. The air-entry value of the soil is the matric suction where air starts to enter the largest pores in the soil. The residual water content is the water content where a large suction change is required to remove additional water from the soil. The main curve shown in this figure is a desorption curve. The adsorption curve differs from

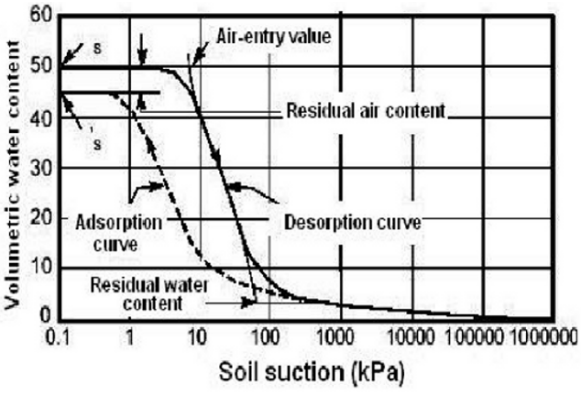

Fig. 2. Typical soil–water characteristic for a silty soil

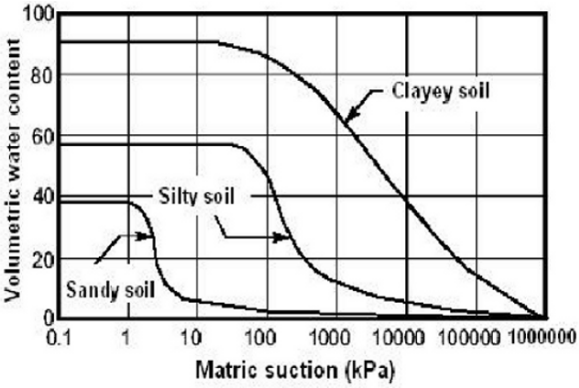

Fig. 3. Soil-water characteristic curves for sandy soil, silty soil, and clayey soil

the desorption curve as a result of hysterics. The end point of the adsorption curve may differ from the starting point of the desorption curve because of air entrapment in the soil. Both curves have a similar form; however, this paper considers the desorption curve.

Typical soil–water characteristic curves for different soils are shown in Fig. 3. The saturated water content, θ_S, and the air-entry value, $(u_a - u_w)_b$, generally increase with the plasticity of the soil. Other factors such as stress history also affect the shape of the soil–water characteristic curves.

3 Methods of Obtaining SWCC

The options for obtaining SWCC can be generally classified as:

a) Experimental methods, based on fitting a curve through a number of points obtained doing direct tests measure the pore water pressure in the soil on the different water content conditions. The development of a SWCC for a particular soil from suction measurements can require several tests and can take some time to obtain all the necessary data. In order to facilitate the efficient determination of the SWCC, several mathematical models have been developed to describe the SWCC for a particular soil from just a few points. On the other hand, many application of the SWCC require that it be differentiated or integrated and be continuous. Some of the fitted functions that have been proposed are summarized in Table 1. Generally, the equations in Table 1 have been validated for certain soils and ranges in suctions. The process of fitting experimental suction data to one of the proposed equations requires a minimum number of experimentally obtained suction measurements, depending upon the number of unknown parameters in the chosen function.

Table 1. Some equations proposed for obtaining Soil–Water Characteristic Curve

Reference	Parameter Description	Equation
Assouline et al. (1998)	ψ: capillary head ψ_L: capillary head corresponds to a very low water content, at which the hydraulic conductivity is negligible θ_L: volumetric water content at capillary head ψ_L ξ, η: fitting parameters	$\theta_w = \theta_L + (\theta_s - \theta_L) \times \left[1 - \exp\left[-\xi\left(\frac{1}{\psi} - \frac{1}{\psi_L}\right)^{\eta}\right]\right]$ (2)
Fredlund and Xing (1994)	θ_w: volumetric water content a: a soil parameter which is a function of the air entry value of the soil in kPa b: a soil parameter which is a function of the rate of water extraction from the soil, once the air entry value has been exceeded c: a soil parameter which is a function of the suction at which residual water content occurs in kPa	$\theta_w = C(\psi)\left[\frac{\theta_S}{\ln^c[e+(\psi/a)^b]}\right]$ (3) $C(\psi) = \left[1 - \frac{\ln(1+\psi/\psi_r)}{\ln(1+10^6/\psi_r)}\right]$ (4)
McKee and Bumb (1987)	θ_r: residual volumetric water content a: curve-fitting parameter b: curve-fitting parameter	$\theta_w = \theta_r + \frac{\theta_S - \theta_r}{1+\exp((\psi-a)/b)}$ (5)
Williams et al. (1983)	A: curve-fitting parameter B: curve-fitting parameter	$\ln \psi = A + B \ln \theta_w$ (6)
Van Genuchten (1980)	θ_r: residual volumetric water content a, b, c: soil parameters, as described for equation 3	$\theta_w = \theta_r + \frac{\theta_S - \theta_r}{[1+(\psi/a)^b]^C}$ (7)
Van Genuchten (1980)	θ_r: residual volumetric water content a: a soil parameter which is a function of the air entry value of the soil in kPa b_m: a soil parameter which controls the slope at the inflection point in the SWCC	$\theta_w = \theta_r + \frac{\theta_S - \theta_r}{[1+(\psi/a)^{b_m}]^{(1-1/b_m)}}$ (8)
Farrel and Larson (1972)	α: empirical constant $(u_a - u_w)_b$: air-entry value	$\psi = a \exp[\alpha(\theta_S - \theta_w)]$ (9)
Brooks and Corey (1964)	θ_r: residual volumetric water content a_b: bubbling pressure in kPa b_b: pore size index	$\theta_w = \theta_r + (\theta_S - \theta_r)(a_b/\psi)^{b_b}$ (10)
Gardner (1958)	θ_r: as above a, b: soil parameters, as described for equation 3	$\theta_w = \theta_r + \frac{\theta_S - \theta_r}{1+(\psi/a)^b}$ (11)

Among these equations, equations proposed by Fredlund and Xing, Eq. (3) and Eq. (4), and Van Genuchten, Eq. (7), seem to be fit and more accurate compared to others. So, they have been studied and compared in this paper.

b) Predictional methods, based on the GSD and other soil properties. These methods can be divided in three main categories:
   - The first of these approaches is based upon statistical estimation of water contents at selected matric suction values. These water contents, at each suction value, are correlated to soil properties. This process requires a regression analysis followed by a curve fitting procedure. This approach has been followed by several researchers including Visser (1969), Gupta and Larson (1979), Reddi and Poduri (1997).
   - The second approach includes those methods that correlate, by regression analysis, soil properties with the fitting parameters of an analytical

equation of SWCC. This statistical approach has been followed by many researchers such as Williams et al. (1983), Tomasella and Hodnett (1998). Zapata (1999) proposed relations to predict the constants of Fredlund and Xing equation based on soil index properties. The proposed option of this paper classified in this category.

- The third approach includes the methods that estimate the SWCC using a physics-based conceptual model. It involve physical models based upon the conversion of the GSD (textural information) into a pore-size distribution, which in turn is related to a distribution of water contents and associated pore pressures. This approach was followed by Arya and Paris (1981), Fredlund et al. (1997).

4 Proposed Model for Predicting the SWCC

The studies done by various investigators show that equations proposed by Fredlund and Xing and Van Genuchten predict the SWCC with more conformity compared to experimental results while they do not contain too constants. Using Fredlund equations, the water content of soil always intends to zero at matric suction equal to 10^6 kPa; which it was not confirmed in all soils and it is dubitable. In contrast, Van Genuchten equation seems to predict the residual water content of soils more accurately. So in current study, Van Genuchten equation was selected as the base and its fitting parameters (a, b, and c) were correlated with index properties of fine soils with plasticity index, PI, greater than zero. Using these relations, one can predict the SWCC without doing expensive and time consuming tests. Neglecting the residual water content at high matric suctions compared with the water content of soil, basic equation proposed by Van Genuchten can be rewritten as:

$$S = \frac{1}{[1 + (\psi/a)^b]^c} \,. \tag{12}$$

To establish the relations, a database characterizing approximately 60 soils with PI greater than 2 was assembled from knowledge-based program developed by Soilvision Systems, Ltd as PhD dissertation of Zapata (1999).

For the fine soils, the product of the percentage passing the 200# sieve, as a decimal, was multiplied by the PI as a percentage, to form the weighted PI, W.PI. This parameter selected as the main index soil property for correlation. The reasoning behind this choice is as follows:

The equilibrium soil suction at a given degree of saturation was expected to be proportional to the specific surface area of the soil. The PI is a fair indicator of surface area and the use of PI alone can be considered. However, a soil with a small percentage of highly active clay would have a high PI but only a moderate specific surface area. Therefore, the weighted PI (W.PI) was considered a better index of soil particle surface area for predicting Soil–Water Characteristic Curve.

Using the described database, and fitting Van Genuchten equation for SWCC to the experimental results for each soil, the parameters a, b, and c, were correlated with the weighted PI as the main index parameter. The relations found are as follows:

$$a = 0.0015(\text{W.PI})^3 + 0.1028(\text{W.PI})^2 + 0.5871(\text{W.PI}) + 11.813 \tag{13}$$

$$b = 0.00011(\text{W.PI})^2 - 0.01358(\text{W.PI}) + 1.76987 \tag{14}$$

$$c = -5 \times 10^{-6}(\text{W.PI})^2 - 0.00014(\text{W.PI}) + 0.14745\,. \tag{15}$$

The W.PI parameter in equations (13)–(15) is defined as:

$$\text{W.PI} = \text{Passing\#200} \times \text{PI} \tag{16}$$

where:
Passing 200# = Material passing the 200# U.S. Standard Sieve expressed as a decimal
PI = Plasticity Index of Soil (%)

The SWCC is obtained using proposed model for various soils with W.PI between 1 and 40 are shown in Fig. 4. As it is expected, increasing W.PI, the air-entry value of suction increased.

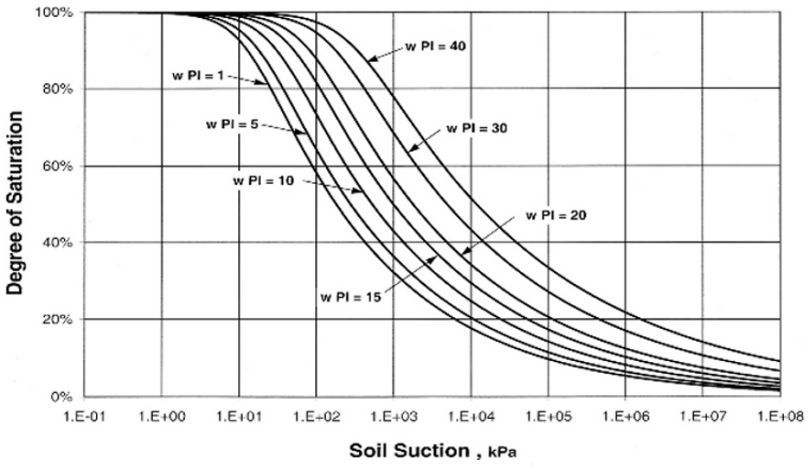

Fig. 4. Predicted SWCC based on W.PI

5 Comparison

To assess the accuracy of proposed model in estimating the soil-water characteristic curve, some comparisons have been made between laboratory suction

tests results with those of mentioned model for various soils. Figs. 5–8 illustrate the results for four different types of soil. The soil characteristics and Van Genuchten equation parameters which have been computed with proposed model equations are shown in Table 2.

Table 2. The soil characteristics and computed parameters

Reference	Constant parameters			Passing 200#	Plasticity index	Dry density	Soil Type
	c	b	a	(W)	(%PI)	(g/cm^3)	
Escario and Juca (1989)	0.129	1.459	167	0.98	31	1.33	Madrid Gray Clay
Escario and Juca (1989)	0.145	1.627	35	0.83	14	1.80	Red Silty Clay
Escario and Juca (1989)	0.147	1.756	12.5	0.13	8	1.91	Madrid Clayey Sand
Zapata (1999)	0.138	1.447	187	0.92	35	1.14	Fountain Hills Clay

As it can be seen in Figs. 5 and 6, the results of proposed model are in a good agreement with those of laboratory tests for clayey soils. The average variance in these samples is about 6%.

For sand sample, Fig. 7, particularly in low suctions, the convergence of results would decrease; however, as it will be discussed later this would be expected respect to the soil type (i.e., very low fine contents and W.PI about 1). Furthermore, comparison between the results of proposed model with those of laboratory tests for Fountain Hills clay, Fig. 8, represents an insignificant convergence in the results; however, this may be explained with respect to the

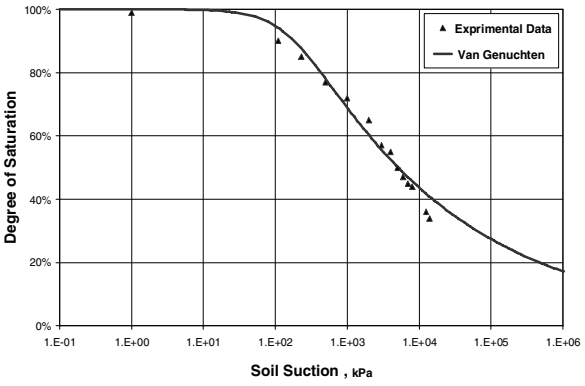

Fig. 5. Comparison between soil-water characteristic curves resulted from proposed model with laboratory results for Madrid Gray clay

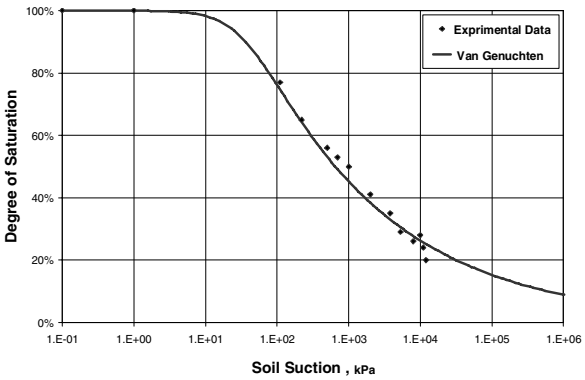

Fig. 6. Comparison between soil-water characteristic curves resulted from proposed model with laboratory results for Red Silty clay

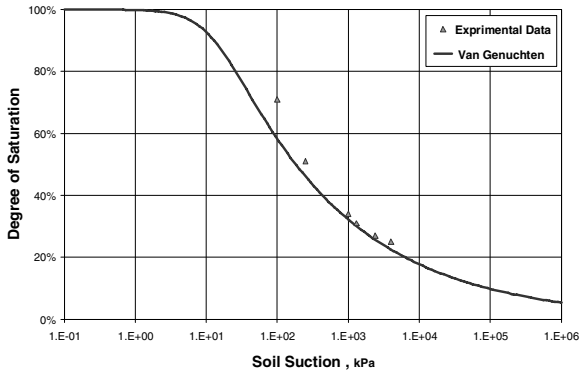

Fig. 7. Comparison between soil-water characteristic curves resulted from proposed model with laboratory results for Madrid Clayey sand

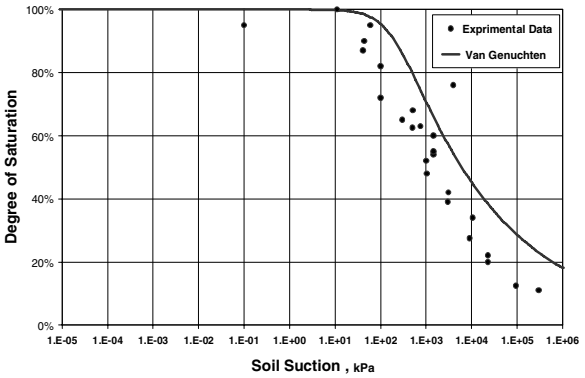

Fig. 8. Comparison between soil-water characteristic curves resulted from proposed model with laboratory results for Fountain Hills clay

very slight dry density about 1.14 g/cm^3 and the high plasticity index in these materials. Also, the distribution of laboratory test results could represent the specific conditions of this soil and furthermore the high probability of errors in the empirical methods. So, current approximating model for clayey soils may not have adequate accuracy for particular soils with special characteristics.

The empirical test results for some of soils that have been assessed in this research and the resulting curves of proposed model are shown in Figs. 9–12. In these figures, the points are representative of tests results and the curves are results of the soil-water characteristic curve for proposed equations in assessed domain. It should be noted that in present study, a database (60 sets of various soil types) have been used; though, according to impossibility and nonnecessity of total data proposal, just 20 selective data from all are shown in mentioned figures. As it can be seen in Fig. 9, for soils with low plasticity index (i.e., silts) and W.PI < 3, the existing variation between the proposed model and the suction tests results are considerable that this may be because of the more effect of aggregate distribution on the soil-water characteristic curve in these materials.

For cohesive soils with $3 <$ W.PI < 30, Figs. 10 and 11, the proposed model predicts the soil-water characteristic curves precisely. Increasing more in W.PI, Fig. 12, the convergence between results decreases in suctions with values greater than 105 kPa. However, this may be the result of existing difficulties in high suction measurements.

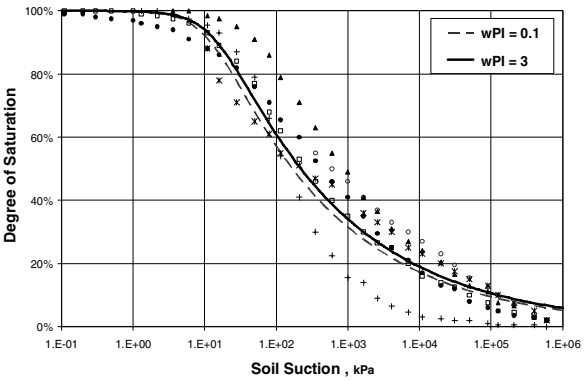

Fig. 9. The empirical and soil-water characteristic curves results for soils with $0.1 <$ W.PI < 3

6 Conclusions

According to extensive practical usage of water retaining curves and existing difficulties in direct evaluation of these curves using laboratory tests, in this

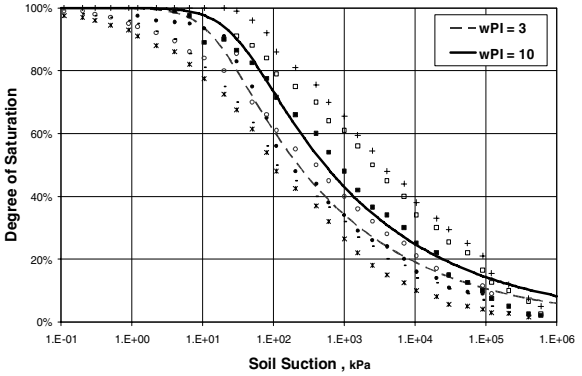

Fig. 10. The empirical and soil-water characteristic curves results for soils with $3 < \text{W.PI} < 10$

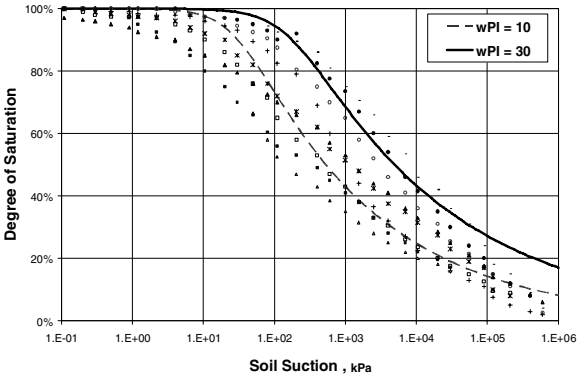

Fig. 11. The empirical and soil-water characteristic curves results for soils with $10 < \text{W.PI} < 30$

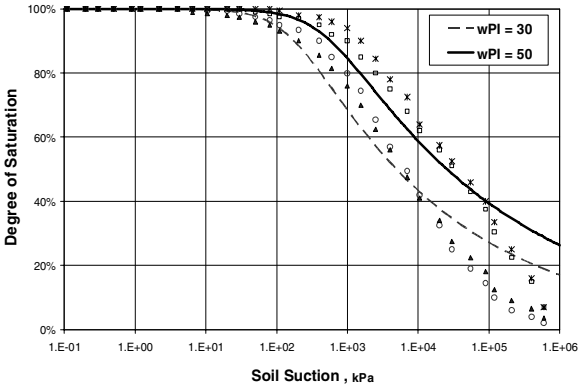

Fig. 12. The empirical and soil-water characteristic curves results for soils with $30 < \text{W.PI} < 50$

paper, based on some index soil parameters, an approximating model for fine soils has been developed. The laboratory tests have been shown that for cohesive soils, product of the plasticity index, PI, in the percentage passing 200# sieve, W, is an appropriate parameter for estimating the soil-water characteristic curves. Therefore, investigating the empirical data of more than 60 various types of soils, some relationships have been developed to approximate the Van Genuchten equation parameters based on W.PI.

The main results concluded from this research are listed below:

- Increasing the parameter of W.PI, the air-entry value will be enhanced, and the soil tendency for water retaining will be increased.
- Respect to existing difficulties in the suction laboratory tests and the variability during tests, the approximating procedures to obtain soil–water characteristic curves by making use of some relations, similar to those represented in this paper, would be proper.
- Comparisons between resulted curves obtained from proposed relations with those of empirical tests represent a good agreement in results; although, this may not exactly be correct for some especial soils (problematic soils).
- For soils with W.PI < 3, the effect of this parameter on soil–water characteristic curves and consequently on the proposed model accuracy is insignificant; thus, other parameters effects such as soil classification would be more considerable.

Acknowledgements

The authors would like to thank Claudia E. Zapata for supplying experimental data and for helpful suggestions.

References

Arya LM, Paris JF (1981) A Physicoempirical Model to Predict the Soil Moisture Characteristic from Particle-Size Distribution and Bulk Density, Soil Sci Soc Am J 45(6):1023-1030

Assouline S, Tessier D, and Bruand A (1998) A Conceptual Model of the Soil Water Retention Curve, Water Resource Research 34(2):223–231

Brooks RH, Corey AT (1964) Hydraulic Properties of Porous Media, Hydrology Papers, 3. Fort Collins, Colorado State University

Escario V, Juca J (1989) Strength and deformation of partly saturated soils. In: Proc 12th Int Conf Soil Mech Found Eng, Rio de Janerio, 3:43–46

Farrell D, Larson W (1972) Modeling the Pore Structure of Porous Media, Water Resource Research 8(3):699–706

Fredlund DG (2000) The implementation of Unsaturated Soil mechanics into geotechnical engineering, Can Geotech J 37:963–986

Fredlund DG, Raharjo H (1993) Soil Mechanics for Unsaturated Soils. Wiley Interscience

Fredlund DG, Xing A (1994) Equations for the Soil–Water Characteristic Curve, Can Geotech J 31(3):521–532

Fredlund M, Fredlund D, Wilson G (1997) Prediction of the Soil–Water Characteristic Curve from Grain–Size Distribution and Volume–Mass Properties. In: Proc 3rd Brazilian Symp on Unsaturated Soils, Rio de Janerio.

Gardner WR (1958) Some Steady State Solutions of the Unsaturated Moisture Flow Equation with Application to Evaporation from a Water-Table, Soil Science 85(4):228–232

Gupta SC, Larson WE (1979) Estimating Soil Water Retention Characteristics from Particle Size Distribution, Organic Matter Percent and Bulk Density, Water Resources Research 15(6):325–339

McKee CR, Bumb AC (1987) Flow-testing coalbed methane production wells in the presence of water and gas. In: SPE Formation Evaluation, December, pp 599–608

Reddi LN, Poduri R (1997) Use of Liquid Limit State to Generalize Water Retention Properties of Fine-Grained Soils, Geotechnique 47(5):1043–1049

Soil Vision User's Guide (Version 1.2) (1997) [Computer Software], Saskatoon, Saskatchewan, Canada, Soil Vision System, Ltd

Tomasella J, Hodnett MG (1998) Estimating Soil Water Retention Characteristics from Limited Data in Brazilian Amazonia, Soil Science, 163(3):190–202

Vanapalli SK, Fredlund DG, Pufahl DE (1996) The Relationship Between the Soil–Water Characteristic Curve and the Unsaturated Shear Strength of a Compacted Glacial Till, Geotechnical Testing J 19(3):259–268

Van Genuchten MT (1980) A Closed-Form Equation for Predicting the Hydraulic Conductivity of Unsaturated Soils, Soil Sci Soc Am J 44:892–898

Visser WC (1969) An Empirical Expression for the Desorption Curve, Water in the Unsaturated Zone:329–335

Williams J et al. (1983) The Influence of Texture, Structure and Clay Mineralogy on the Soil Moisture Characteristic, Australian J Soil Res 21:15–23

Zapata CE (1999) Uncertainty in Soil–Water Characteristic Curve and Impact on Unsaturated Shear Strength Predictions. Ph.D. Thesis, Arizona State University, Tempe, United States

Zapata CE, Houston WM, Houston SL, Walsh KD (2000) Soil-water characteristic curve variability. In: Shackleford CD, Houston SL, Chang N-Y (eds) Advances in Unsaturated Soils, Geotechnical Special Publication No. 99, Reston, ASCE: 84–124

Water Balance and Effectiveness of Mineral Landfill Covers – Results of Large Lysimeter Test-Fields

Wolf Ulrich Henken-Mellies

LGA – Geotechnical Institute, Tillystr. 2, D-90431 Nuremberg, Germany
wolf-ulrich.henken-mellies@lga.de

Summary. Landfills are provided with cover systems in order to separate the waste from the environment and in order to prevent percolation of precipitation and recharge of leachate. The layers of a landfill cover system (restoration profile, drainage layer, compacted clay liner – CCL) have to be specifically designed for long-lasting effectiveness. Special care has to be taken to prevent the CCL from desiccation-cracking due to high matric suction. On a landfill in Northern Bavaria, test fields of some 260 m^2 each were installed with different profiles: The test fields were built according to the recent German landfill ordinance, but with a thicker restoration profile (2.0 m and 1.5 m thick restoration layer, respectively). Water content and matric suction of the soil profiles was measured by FDR-probes and tensiometers. In test field 1 reduction of soil water content during summer was detected down to 1.8 m depth. In test field 2 (1.5 m thick restoration layer) decreasing water content was measured in the CCL, whereas in test field 1 (2.0 m thick restoration layer) the CCL was not affected by loss of water. In conclusion, at the given landfill site only the 2.0 m thick restoration profile is able to effectively shield the CCL from desiccation effects.

Key words: landfill cover, compacted clay liner, lysimeter test field, percolation, matric suction, soil water content

Introduction

Upon completion solid waste landfills are provided with a final cover in order to prevent the migration of contaminants. The cover has to meet two basic requirements: It should be at least as tight as the lining system at the base of the landfill and its ability to minimize percolation should not deteriorate with time.

Landfill covers are exposed to highly variable hydraulic conditions due to seasonally changing weather conditions and influences of vegetation. The upper meters of the pedosphere are dominated by unsaturated conditions. Key element of a landfill cover system is the sealing layer. Most commonly

compacted clay liners are used as sealing layers in Germany, either in combination with a geomembrane or as the only sealing element. Since mineral liners are quite common in landfill cover systems and their proper functioning has to be relied upon for long term use, the problem of preventing desiccation and shrinkage cracks of clayey mineral liners has been paid much attention. The physical phenomena which lead to shrinkage cracks have been studied by laboratory experiments on different soils. Theoretical approaches have been developed, and evidence of desiccation or of the successful prevention of desiccation has been obtained by a number of field trials (Ramke et al. 2002, Witt and Zeh 2004).

This paper presents a field testing program, and intermediate results of ongoing research aimed at a better understanding of the performance of the restoration profile and at specifying its properties required for the prevention of desiccation of the compacted clay liner within the cover system of a sanitary landfill under site specific conditions.

Materials and Methods

Field Site

The field site for this study is situated near the village of Aurach in Northern Bavaria, some 60 km southwest of the city of Nuremberg in a gently hilly region at an elevation of 500 m above sea level. Average annual precipitation at the site is 750 mm, mean annual potential evapotranspiration amounts to 550 mm. Average annual temperature is 9°C. The lysimeter test fields were erected on the slope of a municipal waste landfill, inclined at 14°, exposed towards the south. Vegetation at the site is mainly grass.

Profiles of the Lysimeter Test-Fields

The test fields were placed inside large lysimeters (13×20 m) made of PEHD-geomembranes and drainage composites, allowing collection of surface runoff, lateral drainage and percolation.

The test fields consist of a three-component cover system including a soil cover, a drainage layer and a compacted clay liner. The soil cover consists of locally available sandy loam, but instead of compacting it, care was taken to construct it with little compaction. Thus the soil cover should act as water storage layer. The two profiles of test-field 1 and 2 differ in the thickness of the subsoil layer of the restoration profile, which is 1.8 m in field 1 (thickness of the entire restoration profile of 2.0 m), and 1.3 m in field 2 (thickness of the entire restoration profile of 1.5 m). The drainage layer with a thickness of 0.3 m is made of gravel. The compacted clay liner consists of silt loam (25% clay/50% silt/25% sand; plasticity index 21%). It was constructed in two lifts of 0.25 m each, compacted to $>$ 98% Proctor-density at water content 1–2% below optimum.

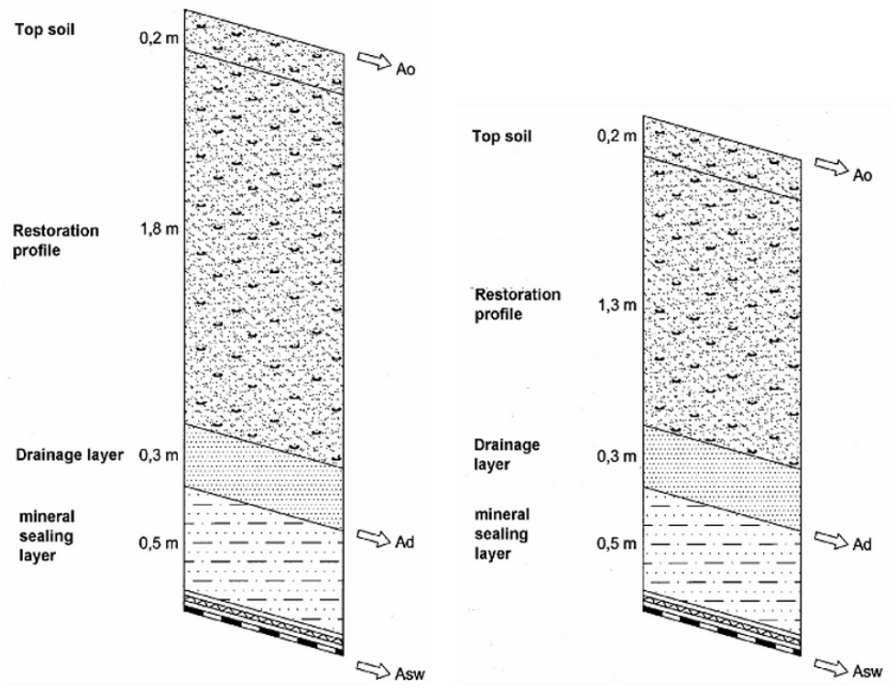

Fig. 1. Profiles of the lysimeter test fields (*left*: field 1; *right*: field 2) at Aurach landfill

Table 1. Properties of soil layers of the test fields

Layer	Thickness	Material	Saturated hydraulic conductivity	Plastic limit; Liquid limit
Top soil and storage layer	2.0 m (#1) 1.5 m (#2)	sandy loam	10^{-6} to 10^{-7} m/s	
Drainage layer	0.3 m	coarse grave	$> 10^{-2}$ m/s	
Compacted clay barrier	0.5 m	silt loam	5×10^{-10} to 2×10^{-9} m/s	20%; 41%

Data Collection

Both lysimeter test fields are equipped with tipping buckets to measure

- Surface Runoff,
- Drainage flow in the drainage layer above the compacted clay liner,
- Percolation through the compacted clay liner.

Matric suction of soil at different depths is measured by tensiometers (pressure transducer tensiometer, type "T 6" by UMS, Munich). Volumetric water

content of soil at different depths is measured by FDR-probes (type "Theta Probe ML2" by Delta-T devices, Cambridge). Temperature of soil at different depths is recorded by thermocoupes. Precipitation and air temperature are recorded at the test field site. Readings of all measuring devices are taken automatically. The data are stored locally on PC and are transferred to the office by GSM.

Results and Discussion

Precipitation and Flow Measurements from Lysimeter

Data from lysimeter 1 for the time period from May 2002 until December 2005 are plotted in Fig. 2. Note that the scale of precipitation on the left side is four times the scale of flows on the right side of the plot. In Central Europe, commonly the precipitation is distributed rather evenly over the year, so the cumulative curve of precipitation (thin black line) shows an almost linear increase.

Surface run-off (dashed line) is generally low. In the long run it plays no important role. Among the measured flows, the discharge from the drainage layer (thick grey curve) has the greatest share. Drainage occurs mainly during winter months from November to April. During summer, the precipitation is

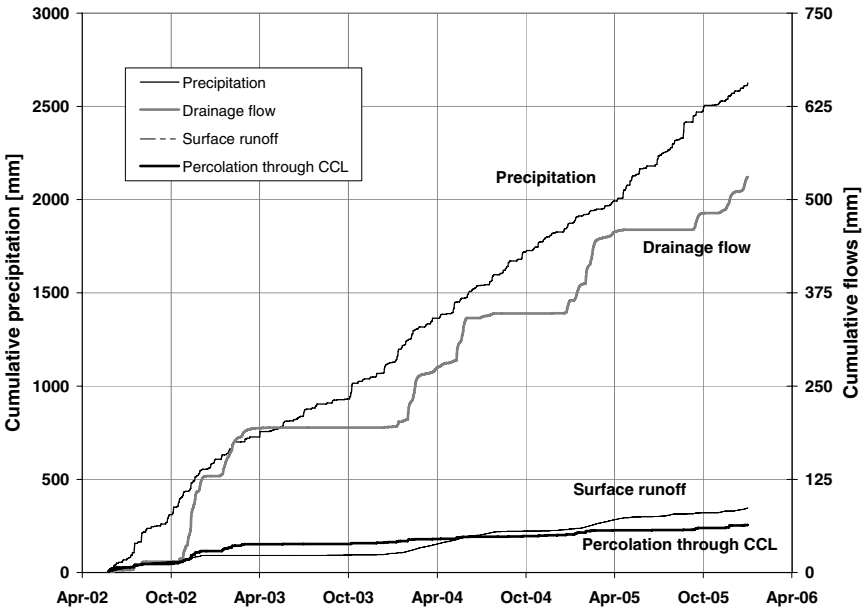

Fig. 2. Precipitation and measured flows at lysimeter test-field 1

partly consumed by evapotranspiration directly and partly stored in the soil layers of the restoration profile for later evapotranspiration, so that there is no drainage flow for a period of several months every year.

Percolation through the compacted clay liner (bold solid curve) occurs simultaneously with lateral drainage. It amounts to about one tenth of the drainage flow. In the water balance of the landfill cover percolation through the CCL amounts to 3% of the total precipitation.

In some other test fields where desiccation of the CCL or GCL took place, the amount of seepage increased and the efficiency of the seals decreased with time (e.g. Melchior 2002). Therefore it is important to take a closer look at the processes which are going on within the layers of unsaturated soil, of which the landfill cover system is composed.

Moisture Content and Matric Suction

Measurements of matric suction (tensiometer measurements) and volumetric moisture content FDR-probe measurements) at different depths within the soil profile are shown in Fig. 3 (for test field 1) and Fig. 4 (for test field 2). The bold lines in both plots represent the probes, which are installed within the CCL (at 2.4 m and 2.6 m in test field 1 and 1.9 m and 2.1 m in test field 2, respectively). The thin lines represent the probes within the storage layer.

During winter season the moisture content of the entire soil profile is generally high ($\theta = 0.35$ to 0.4 in the storage layer and 0.4 to 0.45 in the CCL) and at the same time matric suction is low (generally below 100 hPa). During summer evapotranspiration is usually higher than precipitation and the vegetation extracts water from the soil. The plots show the different response of the soil to the relatively wet summer of 2002 in contrast to the dry summer of 2003:

In 2002 only the tensiometer at 1.0 m depth recorded rapidly increasing matric suction; at greater depths matric suction remained below 100 hPa during summer and fall of 2002. Volumetric moisture content decreased in the upper meter of the soil; below that it almost remained constant. In the dry summer of 2003 the FDR-probes recorded a strong decline in soil water content even at 1.4 and 1.8 m depth. At the same time the tensiometers even at the base of the storage layer recorded an increase of matric suction beyond the measurement range of 700 hPa.

The bold lines represent the measurements within the CCL. In 2002 matric suction and water content showed almost no change at all. During summer of 2003 there was a slight increase in matric suction up to 150–200 hPa and a 1% drop in water content. In comparison with the measurements in the storage layer the diagram shows, that there is an effective hydraulic decoupling between storage layer and CCL.

Figure 4 shows the progress lines of matric suction in the CCL of test field 2 (upper plot) and volumetric water content in the storage layer and in the CCL (lower plot). Again, no critical decrease in water content/increase in

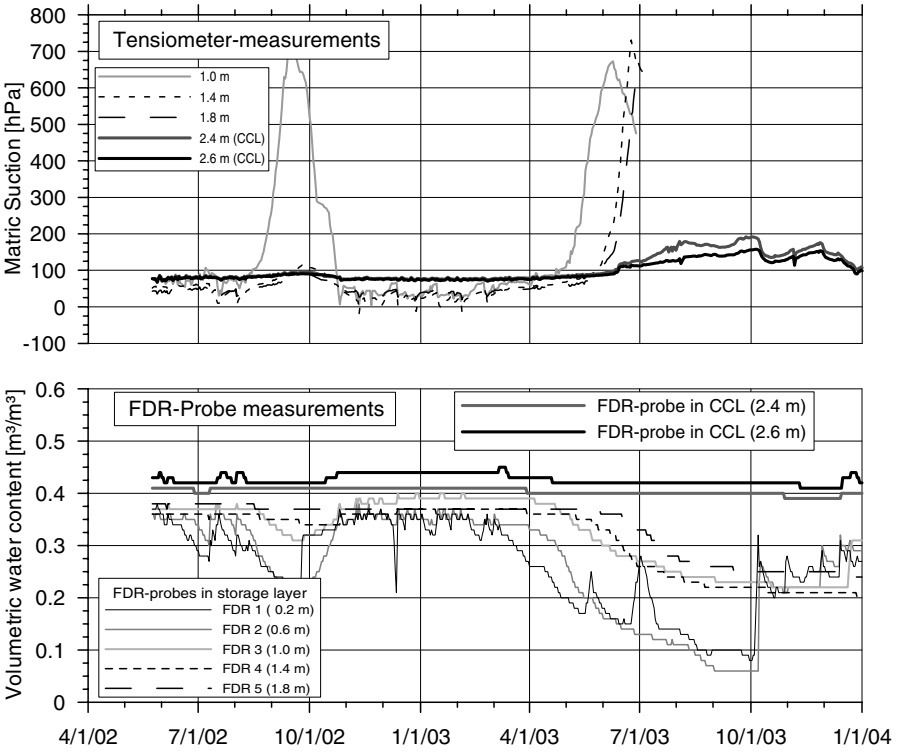

Fig. 3. Results of tensiometer measurements (*upper plot*) and FDR-probe measurements (*lower plot*) at lysimeter test-field 1 for the years 2002 to 2003

matric suction occurred in 2002. But in summer of 2003 water content of the CCL dropped below $0.4\,m^3/m^3$ and at the same time matric suction increased to about 500 hPa.

According to Witt and Zeh (2004) values of matric suction above 250 to 500 hPa are critical with respect to the formation of desiccation cracks in CCLs. The mainly silty material with low to medium plasticity used in this study is less susceptible to cracking than high plasticity clays. The ongoing measurements have not shown any increases of percolation in lysimeter 2 compared to test field 1.

Conclusions

Landfill cover profiles commonly consist of a series of unsaturated soil layers, which are exposed to the dynamics of weather and vegetation. Regulations of EU and Germany recommend a compacted clay layer as sealing component within the design of a landfill cover. In temperate humid climate like in Germany there are periods (generally during winter months) where precipitation

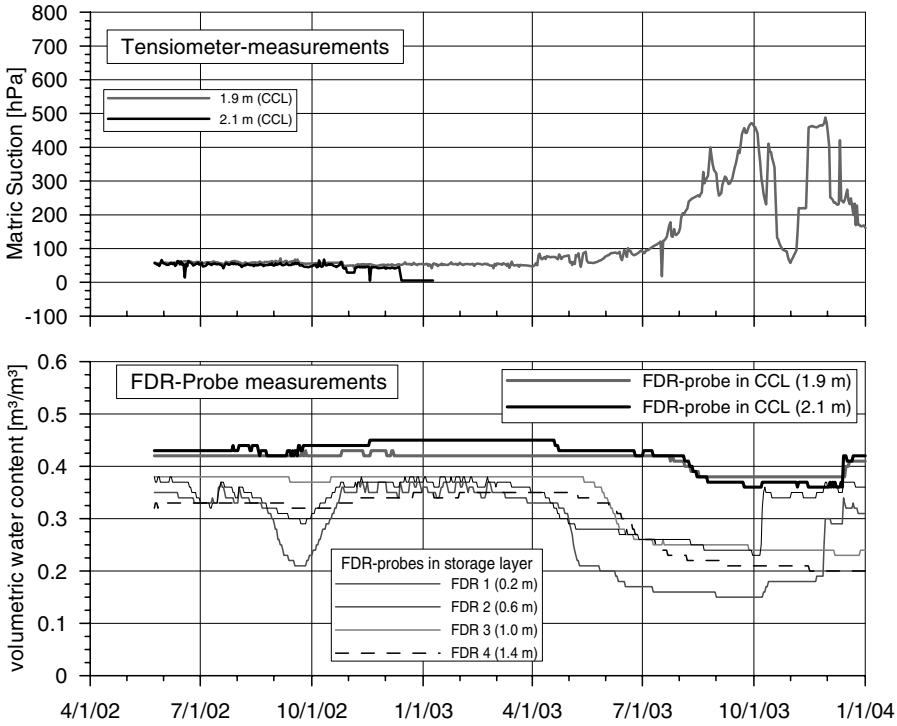

Fig. 4. Results of tensiometer measurements (*upper plot*) and FDR-probe measurements (*lower plot*) at lysimeter test-field 2 for the years 2002 to 2003

exceeds evapotranspiration. In these times low hydraulic conductivity of the CCL is the determining factor for low percolation rates.

In contrast, there are periods during summer and fall, where evapotranspiration exceeds precipitation. The lysimeter measurements show that the periods without drainage flow may last up to nine months. During these periods of time the CCL has to be protected against critical loss of water. This task has to be fulfilled by the top soil or water storage layer. The in-situ-measurements in the soil profiles show an increase in matric suction and at the same time a decrease in water content of the storage layer down to its base at 2.0 m and 1.5 m, respectively. The drainage layer acts as a barrier, which inhibits the capillary rise of water from the CCL to the top soil. In test field 2 with a 1.5 m thick storage layer a reduction of water content of the CCL was detected, which can be attributed to vapour transport through the drainage layer. The temporary reduction of water content did not yet have an adverse effect on the sealing effectiveness of the CCL.

The thickness of the top soil cover should be "> 1 m" according to German and EU regulations. In many cases the actual thickness of the top soil cover is even lower. The results reported here emphasize the importance of a well

designed landfill cover including a thick water storage layer in order to protect the CCL against desiccation.

References

Melchior S (2002) Field studies and excavations of geosynthetic clay barriers in landfill covers. In: Zanzinger et al. (eds) Clay Geosynthetic Barriers. Balkema, Lisse, pp 321–330

Ramke H-G, Gartung E, Heibrock G, Lükewille W, Melchior S, Vielhaber B, Bohne K, Maier-Harth U, Witt K-J (2002) Austrocknungsverhalten mineralischer Abdichtungsschichten in Deponie-Oberflächenabdichtungssystemen. Höxteraner Berichte zu angewandten Umweltwissenschaften, Vol. 03, Höxter

Witt K-J, Zeh R (2004) Maßnahmen gegen Trockenrisse in mineralischen Abdichtungen. In: Kranert (ed) Stuttgarter Berichte zur Abfallwirtschaft 81:83–98

A Retention Curve Prediction for Unsaturated Clay Soils

Mehrez Jamei, H. Guiras, and N. Mokni

Civil Engineering Laboratory, National Engineering School of Tunis (ENIT)
mehrez.jamei@enit.rnu.tn

Summary. In order to obtain the retention curve of unsaturated soil which is defined as the relationship between water content and suction, numerous laboratory tests have been done for many soils with different clay contents. The laboratory tests concern different types of soils; the swelling and not swelling clays (natural clay with high silt content and the bentonite clay). Two complementary experimental ways are conducted. The first which leads to measure suction is based on the filter paper method. The second with the dessicator allows to impose a high suction values.

The paper discusses the theoretical approaches for the grain-size distribution and water retention curve's relation. It discusses also their correlations according to each type of tested soil. The experimental data are used to validate the theoretical model selected in the study. The influence of the different parameters used by the model is also studied.

All the parameters required to run the model can be obtained by performing independent, common laboratory tests and are related to the physical parameters like the initial dry density and the initial void ratio.

After some numerical tests, the direct procedure to obtain the soil-water characteristic curve is improved.

Key words: water retention curve, grain-size distribution, laboratory tests, model, prediction

1 Introduction

The measurement of soil parameters, such us the permeability and shear strength functions, used to describe unsaturated soil behaviour can be expensive, difficult and time consuming. Hence, several models were proposed to predict the hydro-mechanical behaviour of unsaturated soils using soil water characteristic curve (SWCC).

SWCC can be easily estimated using grain size distribution curve. Several methods have previously been proposed for the estimation of the SWCC (Arya and Paris 1981, Haverkamp and Parlange 1986, Fredlund et al. 1997). In the

estimation's methods the effect of swelling was not been addressed. However, swelling compacted clays receive increasing attention as soils which lead to many stability structures problem (shallow foundations, slope stability, etc.). In special applications, some typical clays and bentonite are used as technical buffer materials in geotechnical barriers in order to isolate waste (Börgesson 1985). Therefore, the knowledge of SWCC of swelling soils is of a special interest.

The aim of this paper is to test the Arya and Paris's model for the estimation of the SWCC on swelling soil. The shape of the estimated curve is controlled by the grain size distribution and influenced by the density of the soil. The influence of initial water content, soil structure and stress history, on the SWCC curve was also studied by Vanapalli et al. (1999). It appears that SWCC curve is influenced by initial water content and stress history for the specimens compacted at dry and optimum conditions. However, this influence is not significantly for both high drying conditions (for the high suction ranges) and wet of optimum conditions (for the specimens compacted with wet of optimum conditions).

Unimodal and bimodal models proposed by Fredlund et al. (2000) were used to best fit grain–size distribution data. The fitting method provides a continuous fit of the entire grain size distribution curve including the coarse and fine extremes (Fredlund et al. 2000).

The unimodal form provides methods for accurately representing uniform and well-graded soils.

The equation for the unimodal curve is given as follows:

$$P_p(d) = \frac{1}{\ln\left[\exp(1) + \left(\frac{g_a}{d}\right)^{g_a}\right]^{g_m}} \left[1 - \left[\frac{\ln\left(1 + \frac{d_r}{d}\right)}{\ln\left(1 + \frac{d_r}{d_m}\right)}\right]^7\right] \tag{1}$$

where:

- $P_p(d)$ = percentage by mass, of particles passing a particular size;
- g_a = parameter designating the inflection point on the curve an is related to initial breaking point on the curve;
- g_m = parameter related to the steepest slope on the curve;
- g_n = parameter related to the shape of the curve as it approaches the fines region;
- d_m = diameter of the minimum allowable size particle (mm);
- d_r = parameter related to the amount of fines in a soil;
- d = diameter of any particle size under consideration (mm).

The five parameters in unimodal equation provide a closer fit than previous two-parameter and log-normal equations (Sang II Hwang et al. 2002). It also improves representation of silt and clay soils (Fredlund et al. 2000).

When the soils are gap-grated, it is necessary to consider the use of bimodal equation witch is given as follows:

$$P_p(d) = \left\{ \left[\frac{w}{\left\{ \ln\left[\exp(1) + \left(\frac{a_{\mathrm{bi}}}{d} \right)^{n_{\mathrm{bi}}} \right] \right\}^{m_{\mathrm{bi}}}} \right] + \left[\frac{1-w}{\left\{ \ln\left[\exp(1) + \left(\frac{j_{\mathrm{bi}}}{d} \right)^{k_{\mathrm{bi}}} \right] \right\}^{l_{\mathrm{bi}}}} \right] \right\} \times \left\{ 1 - \left[\frac{\ln\left(1 + \frac{d_{r\mathrm{bi}}}{d}\right)}{\ln\left(1 + \frac{d_{r\mathrm{bi}}}{d_m}\right)} \right]^7 \right\} \quad (2)$$

where:

- a_{bi} = parameter relates to the initial breaking point along the curve;
- n_{bi} = parameter related to the steepest slope along the curve;
- m_{bi} = parameter related to the shape of the curve;
- j_{bi} = parameter related to the second breaking point of the curve;
- k_{bi} = parameter related to the second steep slope along the curve;
- l_{bi} = parameter related to the second shape along the curve;
- $d_{r\mathrm{bi}}$ = parameter related to the amount of fines in a soil.

1.1 Description of the Model

Arya and Paris (1981) presented the first physico-empirical methods to estimate the SWCC. The basic information of the model is the grain size distribution curve. Volumetric water content was calculated basing on an estimation of the pore sizes of the soil. pore radius estimation was based on the assumption of spherical particles and cylindrical pores using the capillary theory. An empirical factor is used to take into account uncertainties in the estimation.

The principle employed to deduce a distribution of pores from a grain size distribution is as follows: the finer particles are the more their stacking spares narrow voids, with each N classes of size of particles (N fractions), a pore is associated (N pores on the whole). The fraction of size R_i is supposed to contain spherical particles. The associated cylindrical pore is supposed to follow the edge of the juxtaposed particles and its length is $l_i = N_i R_i^{\alpha}$ (α is equal to 1 for a rectilinear pore and it is a parameter to be estimated for a natural geometry).

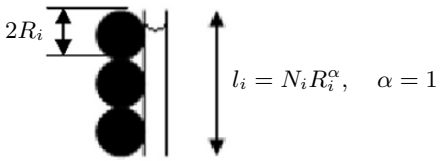

The capillary model used is composed by N independent capillary tubes, from which N couples of values of suction (S), and water content (W) are

calculated. The parameter α is determined by calibration with the experimental data. It may be related to the physical soil parameter like plasticity index (I_p).

1.2 Formulation of the Model

The grain size distribution was divided into N fractions. Individual weight fractions can then be calculated as follows

$$P_i = (g_{i+1} - g_i)\gamma_t \tag{3}$$

where:

- P_i = weight of individual fraction (kg);
- g_i = function representing percent passing versus particle diameter ($i = 1, 2, \ldots, N$);
- N = number of fractions into which grain-size distribution is divided;
- γ_t = total density of the soil sample (kg/m^3).

The calculation of the void ratio is possible once the void ratio is known

$$V_{vi} = \frac{P_i}{G_s \times \gamma_w} \times e \tag{4}$$

where

- e = void ratio;
- ρ_w = density of water;
- G_s = specific gravity of the soil.

The sum of all void ratios can be calculated as follows

$$V_v = \sum_{i=1}^{n} V_{vi}\,. \tag{5}$$

Hence volumetric water content is

$$\theta_{vi} = \frac{\sum_{j=1}^{i} V_{vj}}{V_T}\,. \tag{6}$$

The pore radius is calculated according to the following equation:

$$r_i = R_i \left[\frac{4N_i^{(1-\alpha)}}{6}\right]^{\frac{1}{2}} \tag{7}$$

where:

- r_i = mean pore radius;

- R_i = mean particle radius;
- N_i = the number of spherical particles in the i-th particle-range;
- α = an empirical factor and greater than 1.

Pore radius and soil water pressure:

$$s_i = \frac{2T_S \cos\theta}{\rho_w \times g \times r_i} \tag{8}$$

where:

- s_i = soil water pressure;
- T_s = surface tension of water;
- θ = contact angle;
- ρ_w = density of water;
- g = acceleration due to gravity, and
- r_i = pore radius.

2 Test Program, Results and Analysis

The soils tested are sandy loam, silt loam, and bentonite reconstituted by compaction in the laboratory. The physical and mineralogical properties of tested samples are presented in Table 1.

Table 1. Physical and mineralogical characteristics of soil

Sample designation	Sandy loam	Silty loam	Bentonite
Specific gravity (kN/m^3)	26.8	27.2	27.4
Liquid limit W_l (%)	28.5	51	375
Plasticity index I_p (%)	13.4	26	312
Initial water content W_i (%) (Optimum Condition)	14.5	21	30.2
Dry density γ_d (%) (Optimum Condition)	18	16.4	12.2
Specific surface SST (m^2/g)	—	124	504

2.1 Soil Water Characteristic Curve

Two complementary experimental ways are conducted. The first which leads to measure suction is based on the filter paper method. The second with the dessicator allows to impose a high suction values.

The filter paper method for determining soil water suction consists of placing a small piece of filter paper in direct contact with the soil. Equilibration of moisture is allowed and the filter paper water content, through calibration, is

then related to the soil matric suction. With this method, it is assumed that the salt can move into the filter paper along with the water provided there is adequate moisture and that an osmotic gradient between the buried filter paper and the soil moisture is absent or negligible.

The samples were compacted in a static way under the optimal conditions to have a 30 mm height. We then cut out cubes of 30 mm on sides. The inserted filter papers are initially wet. Once hydrous balance is reached (one month), the samples are weighed, plunged in mercury to determine final volume.

The second method consists in placing small soil cubes of side of 20 mm in a closed enclosure. The relative humidity of the system is imposed by a saline solution. Seven desiccators was prepared, in which was poured one litter of saturated salt solution, and then the samples are placed on the perforated plate. The desiccators are then closed and preserved until hydrous equilibrium is reached. The materials used are compacted in a static way to the Proctor Optimum. Table 2 indicates the salt solution used and corresponding suction.

Table 2. Salt solution

Suction (kPa)	Salt solution
2818	$CuSO_4$,$5H_2O$
7079	KNO_3
12600	$ZnSO_4$,$7H_2O$
22400	KCl
33100	NaCl
56200	$NaNO_2$
158500	$CaCl_2$,$6H_2$

2.2 Free-Swell Odometer System

These tests were carried out according to standard procedure on swelling soil (XP P94–090–1). An odometric cell was used. The sample was initially putted in contact with water. The vertical deformation is measured until stabilization of swelling. The value of the vertical stress necessary to bring back the sample to its initial height (vertical swelling stress) is then measured. The test was performed on a sandy loam for various initial conditions (Fig. 1), and on bentonite under Proctor optimum conditions (Fig. 2). Sandy loam is a non swelling soil.

In the case of bentonite, the stabilization of final swelling is reached after 25 days (Fig. 1). The rate of final swelling exceeds 100%.

For the silt loam compacted under optimal condition, the stabilization of swelling was reached after two days. For low water content the steady state was reached after three days. The rate of final swelling is more important in the case of low initial water content and high dry density. This result was shown by several authors (Guiras 1996).

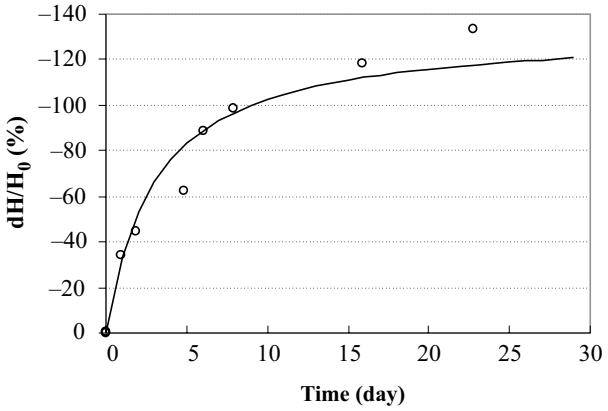

Table of symbols

Symbol	W_i (%) γ_d (kN/m^3)	$\Delta h/h_0$ (%)
—○—	30.2	120
Proctor optimum	12.2	

Fig. 1. Times versus swelling: bentonite

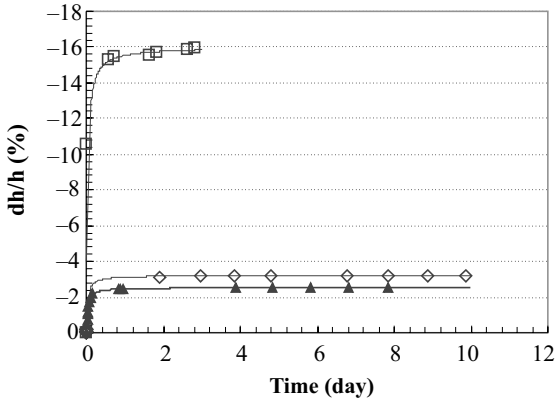

Fig. 2. Times versus swelling: silt loam

3 Prediction of the Experimental Results

The model was tested on the studied soils. The comparisons between the experimental and predicted data are shown in Figs. 3–5. The estimation of a SWCC from grain–size distribution has been attempted for all soil types. The estimated still appear to be quite reasonable in the case of swelling soil (silt

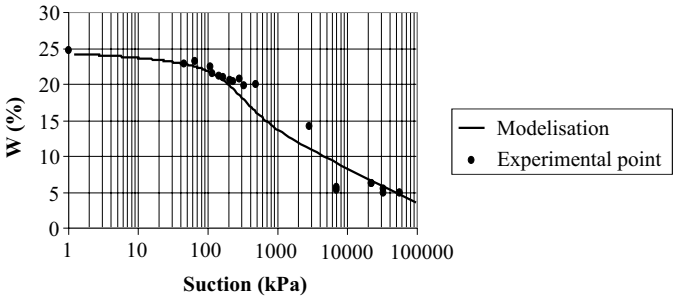

Fig. 3. Comparison of experimental and estimated SWCC for sandy loam

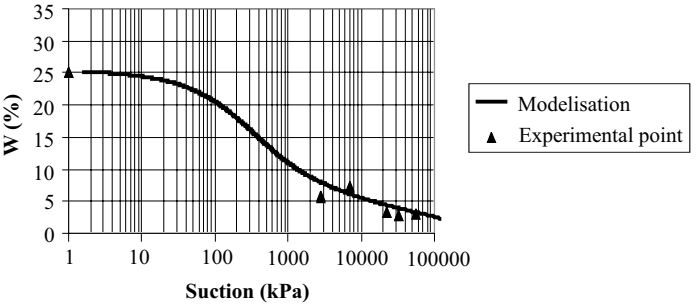

Fig. 4. Comparison of experimental and estimated SWCC for silt loam

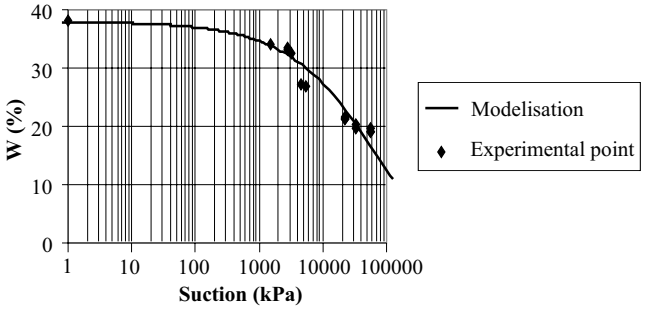

Fig. 5. Comparison of experimental and estimated SWCC for bentonite

Table 3. Estimated α value

Texture	α values
Bentonite (clay)	1.57
Silt loam	1.38
Sandy loam	1.60

Table 4. α values proposed by Arya et al. (1999)

Texture	α values
Clay	1.16
Silt loam	1.15
Sandy loam	1.459

loam and bentonite) and for the non swelling soil like sandy loam. Nevertheless, an estimation of parameter α is necessary to define the natural length of pores. The estimated α value's are shown in Table 3.

The estimated values of α, are different compared to that ones proposed by Arya et al. (1999) for soils with same textural classes (Table 4).

The estimated values performed on swelling soil are higher than the previous values performed on non swelling soil.

The result shows that the Arya and Paris's model provide a good estimation of SWCC of swelling soils if a reasonable estimation of parameter α is made.

4 Conclusion

Estimation of the soil- water characteristic curve from grain size distribution was found to be reasonably reliable for non swelling soil (sand loam) and for swelling soil (silt loam and bentonite). The prediction model of the SWCC curve basing on the grain size distribution curve is well established and it seems that the unimodal equation can be used with success for clay and swelling clay.

The first analytical adjustment is an important step to previous well the SWCC curve.

It seems also, that the Arya and Paris's model predicts well the SWCC curve not only for the sandy and silty soils but also for swelling clays. However, the α parameter must be related to a physical parameter like the plasticity index. Hence, it appears that the lack of complete experimental data to verify the models for the swelling clays remains greatest task at hand.

References

Arya LM, Paris JF (1981) A physicoempirical model to predict soil moisture characteristic from particle-size distribution and bulk density data, Soil Sci Soc Am J 45:1023–1030

Arya LM, Leiji FJ, Van Genuchten MTh, Shouse PJ (1999) Scaling parameter to predict the soil water characteristic from particle size distribution data, Soil Sci Soc Am J 63:510–519

Fredlund MD, Wilson GW, Fredlund DG (1997) Prediction of the soil water characteristic curve from grain-size distribution and volume mass properties. In: 3rd Brazilian symposium on unsaturated soil, Rio de Janeiro, Brazil, April 22–25, 1977

Fredlund MD, Wilson GW, Fredlund DG (2000) An equation to represent grain size distribution, Can Geotech J 37:817–827

Guiras H (1996) Déformabilité des sols argileux non saturés : études expérimentales et application à la modélisation. Thèse de doctorat, Ecole Nationale Supérieure de Géologie de Nancy

Vanapalli SK, Fredlund DG, Pufahl DE (1999) The influence of soil structure and stress history on the soil–water characteristics of a compacted till, Geotechnique 49(2):143–159

Unsaturated-Zone Leaching and Saturated-Zone Mixing Model in Heterogeneous Layers

Samuel S. Lee

D2SI San Francisco Regional Office, Federal Energy Regulatory Commission, San Francisco, CA, USA samuel.lee@ferc.gov

Summary. A screening level model was developed for simulation of pollutant migration through the unsaturated-zone and subsequent mixing within the saturated-zone. This one-dimensional finite difference model simulates the transport processes of liquid-phase advection, liquid- and vapor-phase dispersion, sorption, and decay of the contaminant. The model estimates contaminant concentration in the saturated-zone by using a simple mass balance technique for mixing of the unsaturated-zone leachate with the groundwater. The model can be a useful tool in making preliminary assessments of the potential impacts of contaminants in the subsurface. The model can handle vertical heterogeneity of the soil columns and non-uniform initial contaminant concentration. It was verified by comparing its simulation results to an analytical solution and laboratory soil column experiments. In addition the model was validated against laboratory experiments with three different soil sample sizes of Ottawa quartz sand and 480 ppm saline water as a groundwater contamination source.

Key words: unsaturated-zone, saturated-zone, leaching model, groundwater, modelling, GUI

1 Introduction

Although several computer codes, such as `VLEACH`, `VLEACHSM 2.0`, `EPACML`, etc. can incorporate the heterogeneity of the soil properties often many sites do not have the sufficient degree of details of field-measured data to allow the use of the existing models. Even when there is a site with a reasonable amount of field data, a rigorous parameter estimation and calibration work is often necessary before conducting a comprehensive simulation. This manuscript describes a newly developed model titled Unsaturated-Zone Leaching and Saturated-Zone Mixing Model. The model allows sufficient model simulations and estimation of contaminant concentration with a smaller degree of site sampling, analysis, and parameter estimation than the existing models. It accomplishes it by

employing a one-dimensional (1-D) finite difference scheme for solving the unsaturated-zone transport equation and uses a mass-balanced technique to estimate contaminant concentration in the saturated zone.

Ravi and Johnson (1993) developed a 1-D transport program, titled `VLEACH`, which handles only vertical migration of pollutant in a homogeneous soil column. Later, Lee (1996, 1999a), and Lee and In (2005) developed several versions of `VLEACHSM` by adding the liquid-phase dispersion, decay terms in the unsaturated zone, and the saturation zone mixing into `VLEACH`. This Unsaturated-Zone Leaching and Saturated-Zone Mixing Model is further improved by implementing the heterogeneous soil property and a Graphic User Interface. In addition, the Unsaturated-Zone Leaching and Saturated-Zone Mixing Model allows the specification of two different types (Dirichlet's and Cauchy's) of boundary conditions at the top of the soil column. Using a simple mass-balance technique, the saturated zone module estimates the concentration of contaminants by mixing of leachate from the unsaturated zone with groundwater.

2 Governing Equation and Boundary and Initial Conditions

2.1 Unsaturated Zone Transport

Considering the three equilibrium phases of pollutants in an unsaturated soil column, its 1-D governing transport equation can be expressed as follows:

$$\theta_w \frac{\partial C_w}{\partial t} + \theta_a \frac{\partial C_a}{\partial t} + \rho_b \frac{\partial C_s}{\partial t} = \frac{\partial}{\partial z}\left(\theta_w C_w \frac{\partial C_w}{\partial z}\right) + \frac{\partial}{\partial z}\left(\theta_a C_a \frac{\partial C_a}{\partial z}\right) - \frac{\partial}{\partial z}(q_w C_w) - \mu_w \theta_w C_w - \mu_a \theta_a C_a - \mu_s \rho_b C_s \quad (1)$$

where, C_w denotes the concentration of a contaminant in liquid (water) phase (mg/L), C_a denotes the concentration of a contaminant in vapor (air) phase (mg/L), C_s denotes the concentration of a contaminant in solid phase (mg/kg), θ_a denotes the volumetric water content (volume of water/total volume) (m^3/m^3), θ_a denotes the air-filled porosity (volume of air/total volume) (m^3/m^3), q_w denotes water flow velocity (recharge rate) (m/yr), D_w denotes dispersion coefficient for the liquid phase contaminant in the pore water (m^2/yr). D_a denotes gaseous phase diffusion coefficient in the pore air (m^2/yr), μ_w denotes first order decay rate of a contaminant in water phase (l/yr), μ_a denotes first order decay rate of a contaminant in gaseous phase (l/yr), μ_s denotes first order decay rate of a contaminant in solid phase (l/yr), ρ_b denotes bulk density of the soil (gr/cm^3), z denotes vertical coordinate with positive being downward, and t denotes elapsed time. Several assumptions were considered in the development of (1) as follow: The total porosity

(n) equals the sum of the water filled porosity the air filled porosity. The air flow velocity (q_a) is assumed to be zero. For simplicity, it is also assumed that $\mu_w = \mu_a = \mu_s = \mu$. Instantaneous equilibrium (partitioning) of the contaminant among the phases according to the following linear relationships:

- Liquid-solid phase equilibrium is

$$C_s = K_d C_w \,. \tag{2}$$

- Liquid-gas phase equilibrium is

$$C_a = H C_w \,. \tag{3}$$

In (2) and (3), K_d (ml/g) denotes the distribution coefficient between the solid phase and liquid phase, and H (dimensionless) denotes the partition coefficient between the air phase and water phase. Using the empirical relationship, K_d can be expressed as $K_d = K_{\text{oc}} \cdot f_{\text{oc}}$, where K_{oc} (ml/g) denotes the organic carbon-water partition coefficient and f_{oc} (g/g) denotes the fraction organic carbon of the soil.

The dimensionless form of the Henry's partition coefficient, H, can be determined from the more common form having the units of atmospheres-cubic meters per mole (atm-m^3/mol) using the following equation

$$H = \frac{K_H}{RT} \tag{4}$$

where K_H (atm-m^3/mol) denotes the dimensional form of Henry's Law constant, R denotes the universal gas constant ($R = 8.2 \times 10^{-5}$ atm-m^3/mol K), and T is the absolute temperature in Kelvin (°K = 273.16 + °C).

The dispersion coefficient in the unsaturated zone is regarded as a linear function of the pore water velocity as:

$$D_w = \alpha_L \left(\frac{q_w}{\theta_w} \right) \tag{5}$$

where α_L is the longitudinal dispersivity (feet) of the unsaturated zone.

The gas phase diffusion coefficient (D_a) in the porous medium is calculated by modifying the free air diffusion coefficient using the Millington model (1959):

$$D_a = D_{\text{air}} \frac{(n - \theta_w)^{7/3}}{n^2} \tag{6}$$

where D_{air} denotes the diffusion coefficient of the contaminant in the free air.

By substituting equation (2) and (3) into (1), the governing transport equation can be simplified as:

$$\theta \frac{\partial C_w}{\partial t} = D \frac{\partial^2 C_w}{\partial t^2} + \left(\frac{\partial D}{\partial z} - q_w \right) \frac{\partial C_w}{\partial z} - \left(\frac{\partial q_w}{\partial z} + \mu\theta \right) C_w \tag{7}$$

where $\theta = \theta_w + \theta_a H + \rho_b K_d$ and $D \equiv \theta_w D_w + \theta_a D_a H$.

The initial conditions used in this work to solve equation (7) are given in the following equation

$$C_w(z,t)\big|_{t=0} = \begin{cases} C_s(z,0)/K_d & \text{if } K_d > 0, \\ C_w(z,0) & \text{if } K_d = 0, \end{cases} \tag{8}$$

where $C_s(z,0)$ is the initial solid-phase concentration specified by the user. When the distribution coefficient ($K_d = K_{\text{oc}} \cdot f_{\text{oc}}$) is zero, liquid-phase concentration must be entered as an initial concentration to avoid the program run-time error (division by zero).

The following assumptions are made in the conceptualization of the unsaturated zone:

1. Linear isotherms describe the partitioning of the pollutant among the liquid, vapor, and solid phases with instantaneous equilibrium.
2. Liquid phase dispersion and vapor phase diffusion are combined as one term via the Henry's equilibrium constant.
3. Vapor-phase advection is assumed negligible compared to the infiltrating water velocity and omitted in this screening level model.
4. Contaminant decay is assumed by a first-order process using two constants; one constant for the contaminant decay in the soil, and another constant for the contaminant source reduction.
5. Flow and mixing processes in the capillary fringe is beyond the scope of this work and thus it also assumes that the capillary fringe depth is negligible with respect to the unsaturated column.

The most common types of boundary condition applied at the top of the soil column are either the first type (Dirichlet's) or the third type (Cauchy's). Equation (9) describes these boundary conditions.

$$C_w\big|_{z=0} = \begin{cases} C_0(z=0)\exp(-\gamma t) & \text{if } t \le t_0 \\ 0 & \text{if } t > t_0 \end{cases} \tag{9}$$

or

$$-D\frac{\partial C_w}{\partial z} + q_w C_w\bigg|_{z=0} = \begin{cases} q_w C_0 \exp(-\gamma t) & \text{if } t \le t_0 \\ 0 & \text{it } t > t_0 \end{cases} \tag{10}$$

where C_0 is the liquid phase solute concentration in the infiltration water, γ is the decay rate (1/yr) of the solute source due to either degradation or flushing by the infiltration, and t_0 is the duration of solute release (yr) which can be selected to simulate either "slug" or continuous input.

At the bottom of the soil column, the second type boundary condition (Neuman's) is commonly applied

$$\frac{\partial C_w}{\partial z} = 0 \qquad (z = \infty) \tag{11}$$

In applying this boundary condition, equation (11) is actually implemented at a finite column length (i.e., $z \neq \infty$). To reduce the finite length effect, dummy cells are added at the bottom of the soil column automatically in the numerical calculation in the model. After evaluation of $C_w(z,t)$, the total contaminant mass (M) per unit volume of the soil is calculated as:

$$M(z,t) = M_a + M_w + M_s = [\theta_a H + \theta_w + \rho_b K_d] C_w = \theta C_w \,. \tag{12}$$

2.2 Saturated Zone Mixing

After estimating the liquid phase solute concentration (C_w) at the bottom of the soil column, the mixed concentration in the aquifer can be calculated using a mass-balance technique as below (USEPA 1989, Summers et al. 1980):

$$C_{\text{mix}} = \frac{C_{\text{aq}} q_{\text{aq}} A_{\text{aq}} + C_w q_w A_{\text{soil}}}{q_{\text{aq}} A_{\text{aq}} + q_w A_{\text{soil}}} \tag{13}$$

where C_{aq} is the concentration of horizontal groundwater influx, q_{aq} is the Darcy velocity in the aquifer, A_{aq} is the cross-sectional aquifer area perpendicular to the groundwater flow direction, and A_{soil} is the cross-sectional area perpendicular to the vertical infiltration in the soil column. The aquifer area (A_{aq}) is determined by multiplying the horizontal width of the soil column with the vertical solute penetration depth.

Procedure for the mixing calculation is different depending on the type of soil column arrangement. In the case of the transverse (right angle) arrangement, the mixing calculation is straight forward: simply apply equation (13) at the each mixing element underneath the soil columns. For the parallel arrangement case, however, the mixed concentration at the upgradient cell is considered as an influx concentration to the next cell. The mixing concentration at the next cell is estimated by reapplying the equation (13) using the two inflow concentrations.

The solute penetration depth is the mixing thickness of the contaminant in the aquifer beneath the unsaturated soil column. An estimation of the plume thickness in an aquifer can be made using the relationship below (USEPA 1990):

$$H_d = \sqrt{2\alpha_v L} + B\left[1 - \exp\left(\frac{-L q_w}{q_{\text{aq}} B}\right)\right] \tag{14}$$

where, H_d is the penetration depth (m), α_v is the transverse (vertical) dispersivity (m) of the aquifer, L is the horizontal length dimension of the waste (m), and B is the aquifer thickness (m). In equation (14) the first term represents the thickness of the plume due to vertical dispersion and the second term represents that due to displacement from infiltration water. When implementing this relationship, it is necessary to specify that in the event the computed value of H_d is greater than B, the penetration thickness, H_d is set equal to B.

3 Numerical Implementation

3.1 Unsaturated Zone Leaching

The governing solute transport equation (7) is solved using the finite difference method. Differential equations dealing with liquid contaminant concentration C_w as a function of time and depth are converted into the finite difference equations dealing with the corresponding variable C_i^k centered on time between two time steps:

$$C_w \rightarrow \frac{C_i^{k+1} + C_i^k}{2}, \qquad \frac{\partial C_w}{\partial t} \approx \frac{C_i^{k+1} - C_i^k}{\Delta t} \tag{15}$$

where Δt is the time increment, the subscript i refers to the discretized soil column cell and the superscript k refers to the time level. The subscript w is dropped for simplicity. Converting the other terms into finite difference form, the governing equation can be written as:

$$\begin{aligned}(-M_i + M_i' - N_i)C_{i-1}^{k+1} + (1 + 2M_i + N_i' + L_i)C_i^{k+1} + (-M_i - M_i' + N_i)C_{i+1}^{k+1} \\ = (M_i - M_i' + N_i)C_{i-1}^k + (1 - 2M_i - N_i' - L_i)C_i^k + (M_i + M_i' - N_i)C_{i+1}^k\end{aligned} \tag{16}$$

where the dimensionless constants M_i, M_i', N_i, N_i', and L_i are:

$$\begin{aligned} M_i &\equiv \frac{\Delta t}{2(\Delta z)^2}\frac{1}{\theta_i}D_i\,, & M_i' &\equiv \frac{\Delta t}{2(\Delta z)^2}\frac{1}{\theta_i}\frac{D_{i+1} - D_{i-1}}{4}\,, \\ N_i &\equiv \frac{\Delta t}{4\Delta z}\frac{1}{\theta_i}q_i\,, & N_i' &\equiv \frac{\Delta t}{4\Delta z}\frac{1}{\theta_i}(q_{i+1} - q_{i-1})\,, & L_i &\equiv \frac{\Delta t}{2}\mu\,. \end{aligned} \tag{17}$$

Similarly, the finite difference form of the initial condition for the liquid phase solute concentration is

$$C_i^1 = \begin{cases} (C_s^1)_i/K_d & \text{if } K_d > 0\,, \\ (C_w^1)_i & \text{if } K_d = 0\,, \end{cases} \qquad 2 < i < n-1\,. \tag{18}$$

The finite difference forms of the top boundary conditions for the soil column are:

- First Type Top Boundary Condition

$$\begin{aligned} &C_i^k = \frac{C_s^k(z=0)}{K_d}\exp[-\gamma(k-1)\Delta t]\,, \\ &C_s^k \neq 0 \text{ if } t \leq t_0\,, \\ &C_s^k = 0 \text{ if } t > t_0\,, \end{aligned} \qquad k = 1, 2, \ldots\,. \tag{19}$$

- Third Type Top Boundary Condition

$$C_1^{k+1} - \frac{\Psi'}{\Phi'} C_2^{k+1} = -\frac{\Omega'}{\Phi'} C_2^k + \frac{\Psi'}{\Phi'} C_2^k + \frac{q_w C_0}{\Phi'} \exp(-\gamma t) \tag{20}$$

where

$$\Phi' = \frac{D(2M + L + 1)}{4(\Delta z)(M + N)} + \frac{q_w}{2}\,, \quad \Psi' = \frac{DM}{4(\Delta z)(M + N)}\,,$$
$$\Omega' = \frac{D(2M + L - 1)}{4(\Delta z)(M + N)} + \frac{q_w}{2}\,,$$

and M, N, L were defined in equation (17).

The second type bottom boundary condition is used in this model as follows:

$$\frac{C_n^{k+1} - C_{n-1}^{k+1}}{\Delta z} = 0\,. \tag{21}$$

This work incorporates the development of a `C++` computer code to solve for the values of C_1^{k+1} using the above finite difference form of simultaneous equations by employment of the Thomas algorithm (Press et al. 1992).

3.2 Numerical Stability

Often, the efficiency of a numerical technique is limited due to the instability, oscillation, and mass-balance problems. Several methods have been proposed to determine the stability criteria of finite difference calculation (e.g., Fourier expansion method, matrix method, and other, (Hirsch 1989)). The Fourier expansion method, developed by von Neumann, relies on a Fourier decomposition of the numerical solution in space while neglecting boundary conditions. It provides necessary conditions for stability of constant coefficient problems regardless of the type of boundary condition (Mitchel and Griffiths 1980). The matrix method, however, analyzes the eigenvectors of the space-discretization operator, including the boundary conditions, as a basis for the representation of the spatial behavior of the solution (Hirsch 1989, Ames 1997). Based on the von Neumann method, Crank–Nicolson scheme of finite difference equation can be optimize with:

$$\Delta z < \frac{2D}{q_w}\,, \tag{22}$$

$$\Delta t < \frac{2\theta(\Delta z)^2}{\sqrt{(2D)^2 - (q_w \Delta z)^2}}\,. \tag{23}$$

According to the stability criteria expressed in equations (22) and (23), it is clear that the combined dispersion coefficient (D) must be greater than zero. In natural soil conditions, it is rare to have a value of D as zero or close to zero. Specifically, if there is downward infiltration in the unsaturated zone, hydrodynamic dispersion of contaminant is inevitable. In addition, the air diffusion coefficients of selected organic compounds must also be greater than zero.

3.3 Saturated Zone Mixing

Based on the mass balance principle of equation (13), the mixed solute concentrations are estimated as:

$$C_{mx1} = \frac{q_{w1} L_1 C_{w1} + q_{\mathrm{aq}} \tilde{H}_{d1} C_{\mathrm{aq}}}{q_{mx1} \tilde{H}_{d1}} ,$$
$$C_{mx2} = \frac{q_{w2} L_2 C_{w2} + q_{\mathrm{aq}} \tilde{H}_{d1} C_{\mathrm{aq}} + q_{mx1} \tilde{H}_{d1} C_{mx1}}{q_{mx1} (\tilde{H}_{d1} + \tilde{H}_{d2})} , \tag{24}$$

where $C_{mx(i)}$ is the "Mixed Concentration in Groundwater" and $\tilde{H}$ is the adjusted penetration depth for each column.

4 Program Execution

The hypothetical example with two soil columns of Press et al. (1992) is simulated herein to demonstrate the impact of soil heterogeneity on the spread on the contaminant in the soil.

4.1 Problem Descriptions

The example depicts two soil columns arranged perpendicular to the groundwater flow direction (see Fig. 1). The unsaturated zone soil is divided into four soil layers whose total porosity decreases (from 0.44 to 0.38) and water-filled porosity increases (from 0.26 to 0.32) along with the depth shown in Fig. 1. The bulk density is adjusted according to the total porosity change (contribution from the water content change is disregarded). The soil column 1 has first type top boundary condition. The soil column 2 has third type top boundary condition. This assumed set of parameters are derived based on a filed geologic situation where the total porosity of soil decreases along with the depth due to gravitational pressure while the soil becomes wetter (water-filled porosity increases) along with the depth because water sinks down to the lower layers. Recharge rate q_w is kept constant ($0.3048\,\mathrm{m^3/yr/m^2}$) in order to keep water-filled porosity of each layer constant. Organic content f_{oc} is also kept constant ($0.005\,\mathrm{g/g}$).

4.2 Results

Simulation of a homogeneous soil columns were conducted (Figs. 2 and 3) in order to demonstrate the soil heterogeneity effect on the dispersion of the contaminant. The uniform homogeneous soil properties that were used in the simulations were bulk density of 1.6, total porosity of 0.4, and water filled porosity of 0.3. In both Soil Column 1 and Soil Column 2, the effects of having

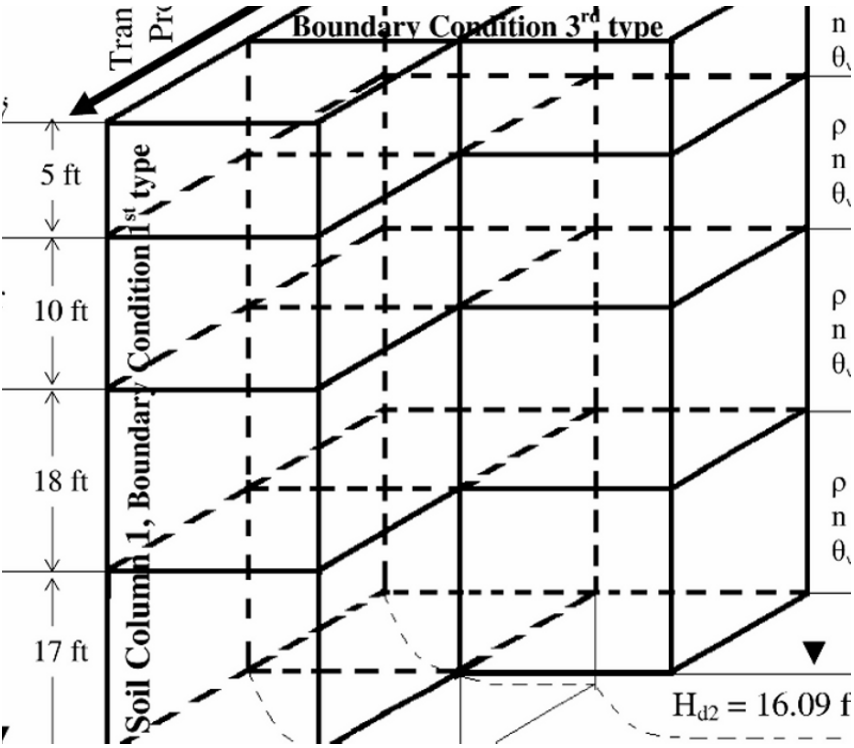

Fig. 1. Profile example problem. Soil column 1 is the first type of boundary condition. Soil column 2 is the third type boundary condition

four different layers instead of one vertically homogenous layer are obvious as shown in Figs. 4 and 5. The liquid-phase contaminant leached deeper in the heterogeneous soil after the same period of time (71 mg/L at −4.572 m in Soil Column 1 at 10 years compared with 28 mg/L for the homogenous case). That is because the total porosity values for the first ($0 \sim -1.524$ m) and second ($-1.524 \sim -4.572$ m) layers are larger than the homogeneous value of 0.4. Also, since the total porosity and water-filled porosity values in the third layer ($-4.572 \sim -10.058$ m) were the same for both the homogenous and the heterogeneous soils, the inclination of the contaminant profile seems to be identical in both case. After 20 years, the contaminant penetrated deeper while keeping a similar profile. After 30 years, the contaminant completely reached the bottom of the unsaturated zone and mixed with the groundwater. Figure 6 depicts the simulation results of mixing the leachate with the ground water.

Figure 7 illustrates a comparison between predicted results of the Unsaturated-zone Leaching and Saturated-zone Mixing Model for simulation of a homogeneous soil column with an analytical transport solution of Cleary and

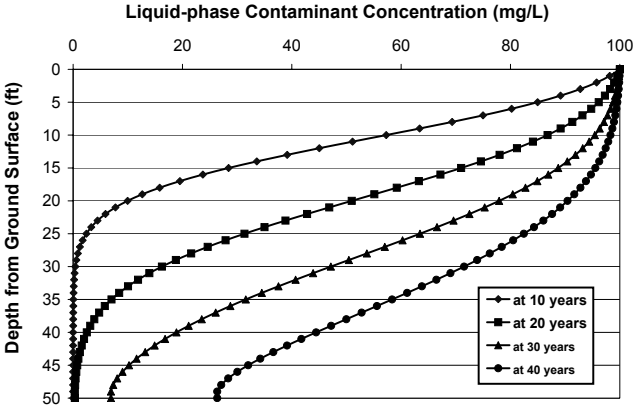

Fig. 2. Simulation results of homogeneous soil column 1, first type of boundary condition at 10, 20, 30, and 40 years of liquid-phase contaminant concentration (mg/L) vs. depth from ground surface (ft)

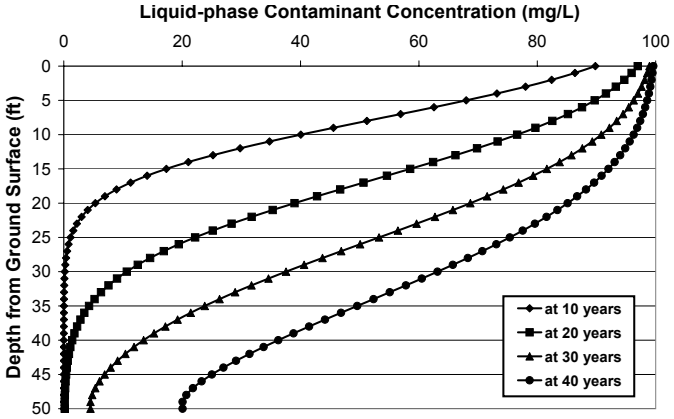

Fig. 3. Simulation results of homogeneous soil column 2, third type of boundary condition at 10, 20, 30, and 40 years of liquid-phase contaminant concentration (mg/L) vs. depth from ground surface (ft)

Ungs (1994). The close matched of the results indicates that the Unsaturated-zone Leaching and Saturated-zone Mixing Model program works correctly in homogeneous case. For the heterogeneous case, Unsaturated-zone Leaching and Saturated-zone Mixing Model results showed reasonable match with column experiment data (Cleary and Ungs 1994), which is available through Internet (`http://www.vadose.net`) (Lee 1999b).

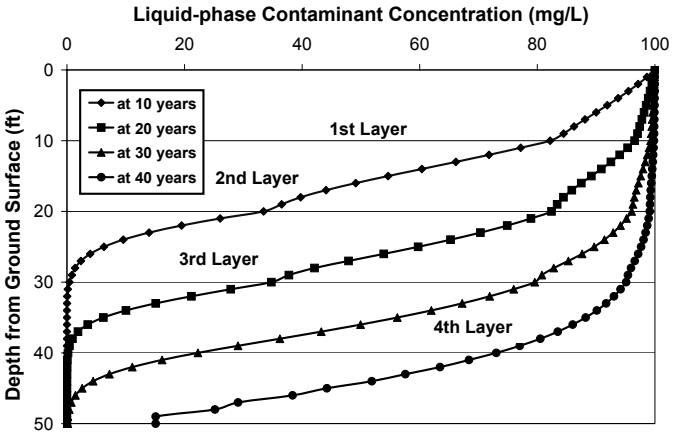

Fig. 4. Simulation results of heterogeneous soil column 1, first type of boundary condition at 10, 20, 30, and 40 years of liquid-phase contaminant concentration (mg/L) vs. depth from ground surface (ft)

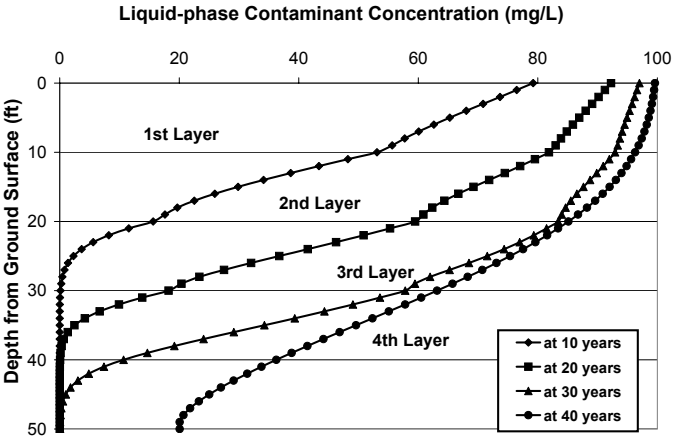

Fig. 5. Simulation results of heterogeneous soil column 2, third type of boundary condition at 10, 20, 30, and 40 years of liquid-phase contaminant concentration (mg/L) vs. depth from ground surface (ft)

5 Summary

Unsaturated-zone Leaching and Saturated-zone Mixing Model was developed. This computer code can handle vertical heterogeneity of soil. The Graphic User Interface used in Unsaturated-zone Leaching and Saturated-zone Mixing Model has made it easy to create the input data file and view the simulation results. Additional benefits stems from the ability to handle the many additional parameters that are needed for vertically heterogeneous soil columns,

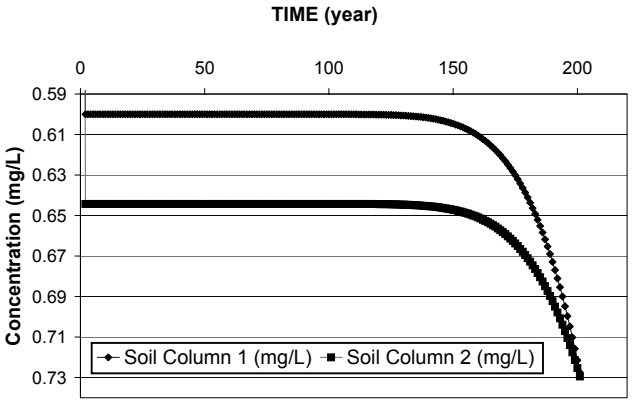

Fig. 6. Simulation results of mixed concentration at the ground water

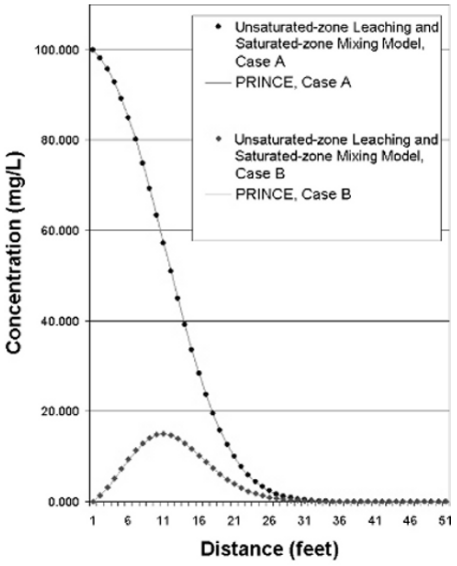

Fig. 7. Verification of Unsaturated-zone Leaching and Saturated-zone Mixing Model with homogeneous soil column by comparing with an analytical solution (PRINCE) modified from Cleary and Ungs (1994). This figure is not referred to in the text!

where a set of parameters is needed to describe the soil properties of each layer.

Verification of the computer code resulted with good match between Unsaturated-zone Leaching and Saturated-zone Mixing Model predictions and an analytical solution (for homogeneous column) and the soil column experiment (for heterogeneous soil). Development of Unsaturated-zone Leaching

and Saturated-zone Mixing Model was funded partially by the United State Environmental Protection Agency.

References

Ames WF (1997) Numerical Methods for Partial Differential Equations, 2nd Ed. Academic Press, New York

Cleary RW, Ungs MJ (1994) PRINCE: Princeton Analytical Models of Flow and Transport, User Guide, Version 3.0, Waterloo Hydrogeologic Software. Waterloo, Ontario, Canada

Hirsch C (1989) Numerical Computation of Internal and External Flows. Vol. 1. Fundamentals of Numerical Discretization. John Wiley & Sons, New York

Lee S (1996) A Screening Level Model for Estimation of Vadose Zone Leaching and Saturated Zone Mixing: VLEACHSM, North American Water and Environment Congress, American Society of Civil Engineers

Lee S (1999a) A Modeling Study on Vadose Zone Leaching, Saturated Zone Mixing, and Groundwater Flow in Heterogeneous Aquifer, Ph.D. Thesis, University of Rhode Island

Lee S (1999b) `http://www.vadose.net`

Lee S, In H (2005) Simulating Groundwater Transport Process Using a Vertical Heterogeneity Model: A Case Study, Lecture Notes in Computer Science 3398:536–544

Millington RJ (1959) Gas Diffusion in Porous Media, Science 130:100–102

Mitchel AR, Griffiths DF (1980) The Finite Difference Method in Partial Differential Equations. John Wiley & Sons, New York

Press WH, Teukolsky SA, Vetterling WT, Flannery BP (1992) Numerical Recipes in FORTRAN, 2nd Ed. Cambridge Univ. Press New York

Ravi V, Johnson JA (1993) VLEACH: An One-Dimensional Finite Difference Vadose Zone Leaching Model, Developed for USEPA, RS Kerr Res Lab, Ada, OK

Summers K, Gherini S, Chen C (1980) Methodology to Evaluate the Potential for Ground Water Contamination for Geothermal Fluid Releases, Prepared by Tetra Tech Inc. for USEPA/IERL, Cincinnati, OH, EPA–600/7–80–117

USEPA (1989) Determining Soil Response Action Levels Based on Potential Contaminant Migration to Ground Water: A Compendium for Examples, Office of Emergency and Remedial Response, Washington D.C., EPA/540/2–89/057

USEPA (1990) Background Document for EPA's Composite Model for Landfills (EPACML), Prepared by Woodward-Clyde Consultants for USEPA, Office of Solid Waste, Washington D.C.

Prediction of SWCC for Coarse Soils Considering Pore Size Changes

Xu Li and Limin Zhang

Department of Civil Engineering, The Hong Kong University of Science and Technology, Clear Water Bay, Hong Kong lixu@ust.hk, cezhangl@ust.hk

Summary. The soil water characteristic curve (SWCC) of a soil is often predicted from the pore size distribution (PSD) of the soil. Experiments show that the PSD may change in the drying or wetting process. It is necessary to consider the pore-size distribution changes in predicting SWCCs.

In this research, different grain-size proportions of completely decomposed granite were separated and then mixed artificially to obtain five soil specimens of different grain-size distributions. These specimens vary from gravel to sand, and silty clay. The SWCCs of these specimens were measured using the axis-translation technique and a Dewpoint psychrometer; and the PSDs of these soil specimens were measured using a mercury intrusion porosimetry (MIP) method. The PSDs obtained from the MIP tests were used to predict the SWCCs, which were compared with the experimental results further.

The PSDs of each soil sample at full saturation and at the end of the SWCC drying test were compared. The PSDs showed a considerable pore-size reduction after soil drying. This phenomenon is referred to as 'pore shrinkage'. A model proposed by Simms and Yanful (2001) was adopted to consider the shrinkage influence in the prediction of the drying SWCC from the PSDs of saturated and dried soil samples. After applying this model, the predicted SWCCs were closer to the experimental SWCCs, especially for fine soils.

For coarse soils, the pore volume with pore diameter larger than a specific value that cannot be measured by MIP tests is large. This volume was estimated and used to correct the predicted SWCC for each coarse soil. With this correction, the predicted SWCCs for coarse soils were also close to the experimental SWCCs.

Key words: SWCC modelling, PSD, pore shrinkage

Introduction

The measurement of soil–water characteristic curve (SWCC) is often time consuming. A traditional method of determining the SWCC using a pressure plate is limited in a narrow suction range. A viable method is to predict SWCC from the pore-size distribution (PSD) of soil.

The nitrogen adsorption and the mercury intrusion porosimetry (MIP) can give PSD curve quantitatively. However, the MIP method has been widely used as a reliable method to measure PSDs of a wide variety of porous solids (Aung et al. 2001). The PSD as measured by MIP has often been advanced as a parameter to help interpret geotechnical behaviors. It has been correlated with saturated hydraulic conductivity (Lapierre et al. 1990), frost heave (Reed et al. 1979), macroscopic volume change (Al-Mukhtar et al. 1996) and SWCC (Prapaharan et al. 1985, Romero et al. 1998).

Based on the PSD from MIP tests, a SWCC can be estimated rapidly in a much wider suction range comparing with the traditional method of determining the SWCC using a pressure plate. But the methodology is still not mature and satisfactory (Simms and Yanful 2004). For example, the PSD changes with soil water content even for a same soil sample. Also, the SWCC prediction method based on the PSD from MIP tests are seldom applied to coarse soils.

Four coarse soils and one fine soil were used in this paper. To investigate the changes in PSD during the soil drying process, a series of MIP tests had been conducted. Also scanning electron microscopy (SEM) tests were used to study the pore geometry of soils qualitatively. Based on the PSDs from the MIP tests, the SWCCs for five soils were predicted with the consideration of the changes of PSD during soil drying and the pore volumes with pore diameters larger than a specific value, which could not be measured in the MIP tests. The predicted SWCCs were further compared with the SWCCs from laboratory tests, which were measured by a pressure plate and a Dewpoint psychrometer.

Materials

Two unimodal soils, one fine soil with an average particle diameter d_{50} of 0.0185 mm and one coarse soil with d_{50} of 6 mm, were 'brewed' from a natural completely decomposed granite (CDG), which was taken from a construction site located at Beacon Hill, Hong Kong. The grain-size distribution (GSD) curves and the grain density function curves are shown in Fig. 1. Firstly, the natural soil was sieved into ten portions according to particle diameter, namely $<$ 0.063 mm, 0.063–0.125 mm, 0.125–0.185 mm, 0.185–0.6 mm, 0.6–2 mm, 2–4.25 mm, 4.25–6 mm, 6–10 mm, 10–14 mm and 14–20 mm. The grain-size distribution of the finest soil–particle portion, which had a maximum soil–particle diameter of 0.063 mm, was measured by the hydrometer tests (BS 1377, part 2. 1990). Secondly, a fine soil was mixed from the finest particle portion with particle diameters smaller than 0.063 mm and the particle portion with particle diameters in range of 0.063–0.125 mm by weight proportions of 0.72 and 0.28. Thirdly, a coarse soil was mixed from all the particle portions following the design GSD (refer to Fig. 1).

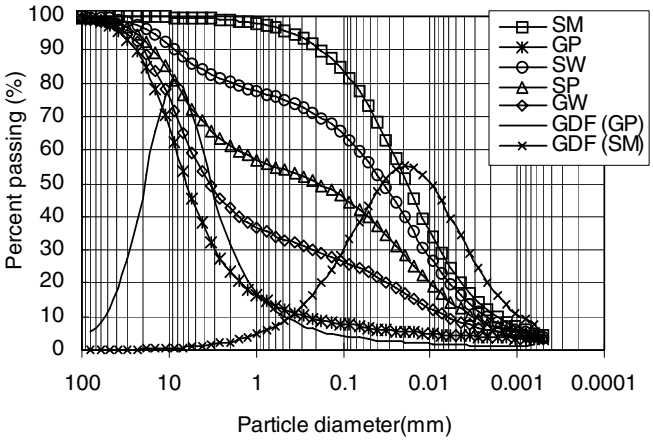

Fig. 1. Grain size distributions of design soils

Further, the fine soil and the coarse soil were mixed into three new soils according to three weight proportions, namely 75% coarse soil mixed with 25% fine soil, 50% coarse soil mixed with 50% fine soil and 25% coarse soil mixed with 75% fine soil.

Basic parameters of these soils were measured and are shown in Table 1. Four types of soil samples were used in the experiments: compacted soil sample (CS), first compacted and then saturated soil sample (SS), oven-dried soil sample (OS) and powder sample (PS). The relative compaction (RC) value, which is defined as the ratio of the dry density to the maximum dry density, was chosen to indicate the soil compaction state.

Table 1. Detailed parameters of five design soils

Soil type	Maximum dry density (g/cm^3)	Optimum water content (%)	Grain size distribution Clay (%)	Silt (%)	Sand (%)	Gravel (%)	Group symbols (ASTM D2487)
1	1.97	9	3.9	3.1	16.7	76.3	GP
2	1.96	11	5.9	18.7	17.9	57.5	GW
3	1.90	13	7.9	34.3	19.1	38.7	SP
4	1.71	18	9.9	49.9	20.3	19.9	SW
5	1.55	21	11.9	65.5	21.5	1.1	SM

Experimental Methods

Scanning Electron Microscopy Tests

SEM was used to study the soil fabric for SM qualitatively. Based on the photographs from the backscattered electron scanning images, the macro-micro fabric at the soil surface could be recognized.

Mercury Intrusion Porosimetry Tests

MIP is routinely and effectively used to evaluate the PSDs of powder and bulk materials with open and interconnected pore structures. Compacted and saturated soil samples (SS) and the oven-dried samples (OS) of five soils (SM, SW, SP, GW and GP) were used to study the changes in PSDs before and after soil drying.

During a MIP test, a dehydrated sample was initially surrounded with mercury at a specific low pressure. Then the surrounded mercury pressure was increased in steps until it reached the system maximum capacity and the intruded volumes of mercury were measured for each pressure increment.

The largest soil sample was limited to 15 cm^3 in the MIP tests. To maintain the homogeneity of soil samples, soil particles with diameters above 10 mm were taken out from the soil when preparing the soil samples for the MIP tests. With the assumption that the remaining part retained the void ratio and PSD of the soil, the density of the soil sample used in the MIP tests was corrected as,

$$\rho_c = \frac{(1-p)\rho}{1-\frac{p\rho}{G_s}} \tag{1}$$

where

ρ = initial soil density;

ρ_c = corrected soil density;

p = weight proportion of the soil particles with diameters larger than 10 mm;

G_s = gravimetric density of the soil solid.

Soil Water Characteristic Curve Tests

The SWCCs of five soils (SM, SW, SP, GW and GP) were measured in the laboratory.

Three devices, a Fredlund SWCC device, a 5-Bar pressure plate extractor and a Dewpoint psychrometer were used to measure the SWCCs. The Fredlund SWCC device was used to measure the wetting and drying SWCC in the suction range of 0–500 kPa. It is similar to traditional one-dimensional pressure plate extractors. The 5-Bar pressure plate extractor was used to measure the drying SWCC in the suction range of 0–500 kPa. With a large sample

container, 300 mm in diameter and 150 mm in height, it is able to measure the SWCCs of large size soil samples and is suitable for coarse soils. The Dewpoint psychrometer was only suitable for measuring the SWCCs of small soil samples or powder soil samples, because of the small sample container, 20 mm in diameter and 12 mm in height. The suction range of the Dewpoint psychrometer was above 500 kPa with an accuracy of ±100 kPa.

Prediction of SWCC Based on the PSD Obtained from MIP Tests

The measured PSD from the MIP tests was used to predict the SWCC. Assuming the pore geometry can be modeled as a bundle of cylindrical tubes, the pore radius r can be calculated by using Jurin's equation (Hillel 1980)

$$r = \frac{2T_{s,\text{water}} \cos \alpha_{\text{water}}}{\psi} = \frac{2T_{s,\text{mercury}} \cos \alpha_{\text{mercury}}}{P} \tag{2}$$

where

ψ = matric suction;
P = mercury injected pressure;
r = entrance pore radius;
$T_{s,\text{water}}$ = surface tension at the water–air interface;
$T_{s,\text{mercury}}$ = surface tension at the mercury–air interface;
α_{water} = contact angle of water–air interface to solid;
α_{mercury} = contact angle of mercury–air interface to solid.

In equation (2), the constants, air/water surface tension $T_{s,\text{water}}$ and mercury/air surface tension $T_{s,\text{mercury}}$ decreased with temperature. For water in contact with air, $T_{s,\text{water}} = 74.2\,\text{mN/m}^2$ at 10°C, $72.0\,\text{mN/m}^2$ at 25°C, and $62.6\,\text{mN/m}^2$ at 80°C. The surface tension of mercury $T_{s,\text{mercury}}$, $472\,\text{mN/m}^2$ at 20°C, is much higher.

Using the symbols used by Simms and Yanful (2002), we define

$$\frac{\partial w(\psi)}{\partial \psi} = vf(\psi) \tag{3}$$

where

$w(\psi)$ = total water content of the soil sample with a suction of ψ;
$vf(\psi)$ = volume fraction of water corresponding to a suction range of $\mathrm{d}\psi$.

Transforming soil suction ψ and mercury intrusion pressure P to pore radius r according to equation (2), one obtains

$$vf(\psi) = vf(r) = vf(P)\,. \tag{4}$$

That is to say, the volume fraction $vf(\psi)$ by drainage of water when the suction increases from ψ to $\psi + \mathrm{d}\psi$ is equal to the volume fraction $vf(P)$ by mercury injection when the mercury intrusion pressure increases from P to $P + \mathrm{d}P$. Also the soil drying process corresponds to a mercury intrusion process.

In the MIP test, the start mercury intrusion pressure P_0 is non-zero. The total water content in a soil sample at suction ψ can be written as

$$w(\psi) = w(0) - \int_0^{\psi} vf(\psi) = w_s - \int_0^{P_0} vf(P) - \int_{P_0}^{P} vf(P) \tag{5}$$

where

w_s = saturated water content of a soil sample;

P_0 = started mercury intrusion pressure;

$vf(P)$ = volume fraction of injected mercury at the mercury intrusion pressure of P.

Limited by the mercury injection pressure ranging from 9.3 kPa to 212 MPa, only pores which have entrance diameters ranging from 0.006 μm to 142 μm can be measured in the MIP tests. There may be a considerable volume of pores with pore entrance diameters larger than 142 μm. For a coarse soil, this volume may be large. This volume is also indicated by the water retention capacity in a suction range of 0 to 2 kPa in the SWCC. If the air entry value (AEV) is larger than 2 kPa, the volume will be 0 and can be ignored. This volume can be estimated by the experimental data and used to correct the predicted SWCC. This correction is referred to as 'P_0 correction.'

In the drying SWCC test, water is gradually removed from soil pores by drainage of the liquid phase, accompanied by pore shrinkage. Earlier research shows that soil shrinkage will change the PSD of the soil sample considerably (Simms and Yanful 2001, 2002). Simms and Yanful (2001) offered a method to model the PSD changes during the SWCC tests based on the assumption that the pores shrunk elastically as water drained from the soil. In this paper, this correction to SWCC prediction was exercised referred to as 'shrinkage correction.'

Results and Discussions

Influence of Water Content on the PSD

SEM photos of an SM SS (RC = 0.85) and an SM OS (RC = 0.85), which was first saturated before it is oven-dried, are shown in Fig. 2. There are much fewer macro pores in the OS. This indicates that most of the macro pores disappear in the process of soil drying.

Under the same soil dry density, the saturated soil sample (freezing dehydration method) and the oven dried soil sample were analyzed by MIP. The PSD curves of the SM SS and the SM OS are shown in Fig. 3. The vertical axis of the figure is the volume frequency, which is defined as the partial derivative of the cumulative injected mercury volume with respect to $\log r$. There were much fewer macro pores (larger than 2 μm) in the SM OS than in the SM SS, which is consistent with the SEM photos shown in Fig. 2. This indicates that

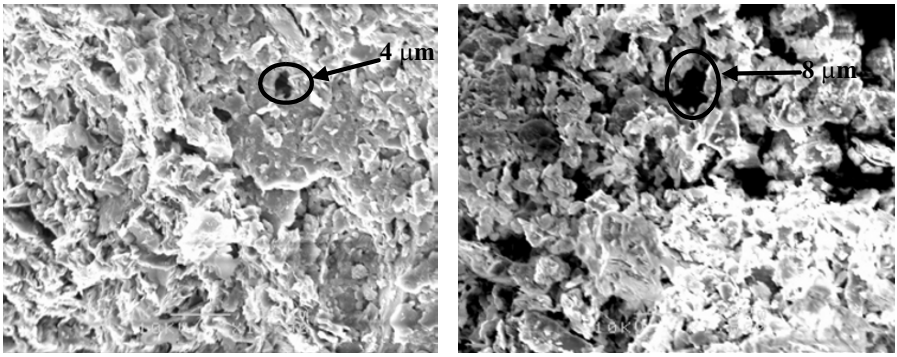

a. Pore geometry of SM OS (RC = 0.85). Scale: 800:1

b. Pore geometry of SM SS (RC = 0.85). Scale: 700:1

Fig. 2. Pore geometry of SM at different water contents

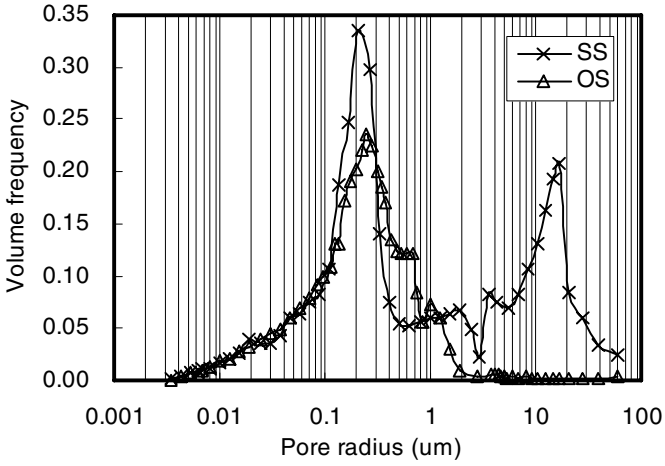

Fig. 3. Pore size distribution curves of SM SS and SM OS (RC = 0.85)

most macro pores with diameter larger than 2 μm disappeared in the drying process of the SM soil sample. A possible reason for this is pore shrinkage. The macro pores may shrink into smaller ones due to the drainage of water in the drying process. At last, only few macro pores are left in the oven-dried SM soil sample. Most of them are surrounded by the smaller pores and cannot be displaced by mercury at low mercury intrusion pressures.

Similar phenomena are found in the comparison of the PSDs of the OS and SS for GP, GW, SP and SW (refer to Fig. 4). General features between the PSD of the SS and the PSD of the OS for a sandy soil or a gravel soil can be summarized as follows:

(1) The PSDs of the SS and the OS are considerably different.

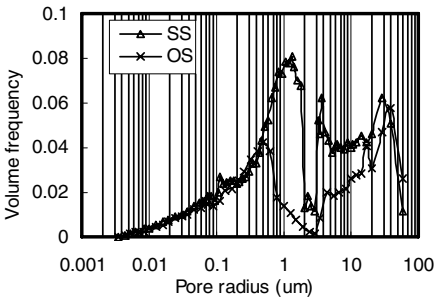

a. Pore size distribution curves for GP

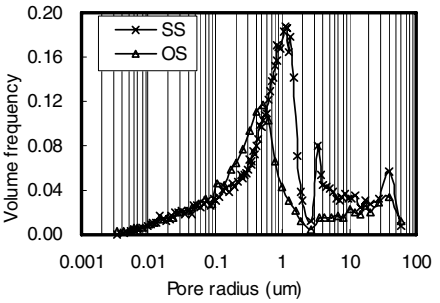

b. Pore size distribution curves for GW

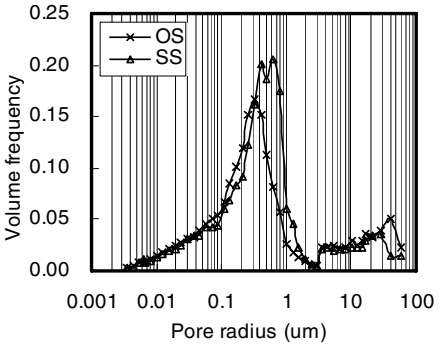

c. Pore size distribution curves for SP

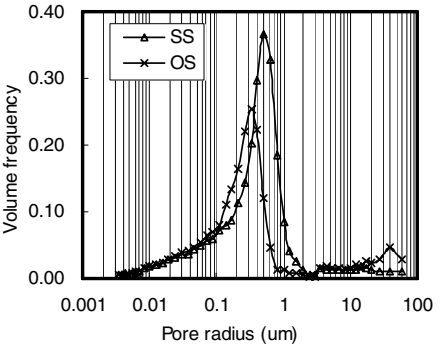

d. Pore size distribution curves for SW

Fig. 4. PSDs of saturated samples and oven-dried samples (RC = 0.85)

(2) Both the PSD of the SS and the OS can be divided into a macro part and a micro part, which has a boundary pore radius of approximately 2 μm. The volume frequencies in the micro part show an obvious peak. The volume frequencies in the macro part are flat without obvious peak.
(3) In the micro part, the peak volume frequency, f_{peak}, and the pore radius at peak volume frequency, r_p, for the SS are larger than those for the OS.
(4) In the micro part, the pores can be divided into three portions by two boundary pore radii r_l and r_u. In the small pore-radius portion, in which the pore radius is smaller than r_l, the volume frequencies of the SS and the OS are same. In the intermediate pore-radius portion, in which the pore radius is larger than r_l but smaller than r_u, the volume frequencies of the SS are smaller than these of the OS. In the large pore-radius portion, in which the pore radius is larger than r_u, the volume frequencies of SS are larger than these of OS.

Features (3) and (4) may be partially induced by shrinkage. If large pores shrunk during the soil drying process, the peak volume frequency and the pore radius at peak volume frequency would decrease. The pore with pore radius

smaller than r_l will not shrink into a smaller one. The upper boundary pore diameter r_u is an apparent radius. The volume of pores with diameter r_u that shrunk from larger pores is equal to the volume of pores with diameter r_u that will shrink into smaller ones. Values of the parameters, f_{peak}, r_p, r_u and r_l were listed in Table 2.

Table 2. Characteristic parameters of PSD for GP, GW, SP and SW

Type of soil sample		r_p (μm)	f_{peak}	r_l (μm)	r_u (μm)
GP, RC = 0.85	SS	1.3	0.080	0.05	0.5
	OS	0.5	0.042		
GW, RC = 0.85	SS	1.1	0.19	0.09	0.7
	OS	0.6	0.12		
SP, RC = 0.85	SS	0.5	0.22	0.04	0.32
	OS	0.23	0.17		
SW, RC = 0.85	SS	0.5	0.37	0.04	0.35
	OS	0.32	0.26		

Notes:
f_{peak} = peak volume frequency in the micro part;
r_p = pore radius at peak volume frequency in the micro part;
r_u = boundary pore radius, above which the volume frequencies of SS were larger than these of OS;
r_l = minimum pore radius of pore shrinkage during soil drainage.

SWCC Prediction Based on the PSD Obtained from MIP Tests

The drying SWCCs of the five soils under the same RC value are put together in Fig. 5. The water retention ability of the five soils increases with the fraction of fine contents in soil.

When the soil suction decreases to 5 kPa, the degrees of saturation of gravel soils, GP and GW, are 0.73 and 0.4. Also the degree of saturation for SW is 0.88 at suction of 5 kPa. That indicates that there are abundant pores with the pore entrance diameter larger than 56 μm (refer to equation (2)). That is to say the pore volume with pore entrance diameter larger than 142 μm for GP, GW and SW, which cannot be measured in MIP tests, should be corrected in the SWCC prediction process. In contrary, the degree of saturation for SM and SP is about 0.99 when the soil suction decreases to 5 kPa. The pore volume with pore entrance diameter larger than 142 μm for SM and SP can be ignored in the SWCC prediction.

The predicted SWCCs of SM are shown in Fig. 6. After the consideration of shrinkage influence (Simms and Yanful 2001), the predicted SWCC is

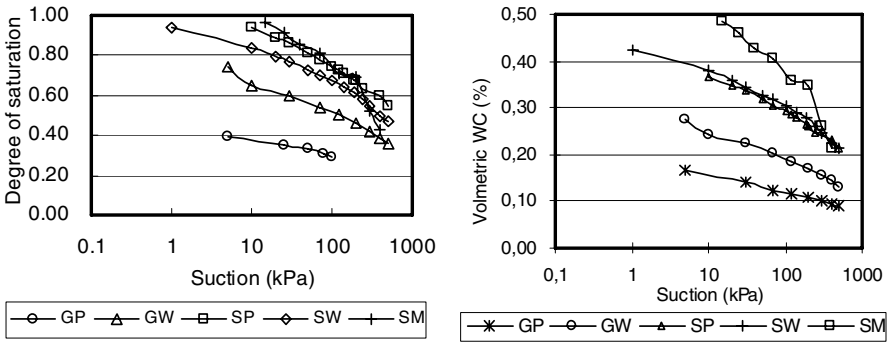

a. Degree of saturation vs. suction

b. Volumetric water content vs. suction

Fig. 5. SWCCs of five soils measured by the soil sample (RC = 0.85)

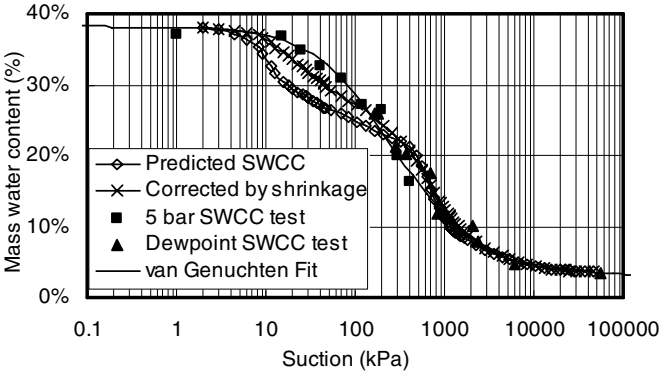

Fig. 6. Predicted SWCCs from PSD for SM (RC = 0.85)

closer to the experiment SWCC. But the predicted AEV, 8 kPa, is less than the AEV from the experiments, 15 kPa. This phenomenon is consistent with Prapaharan et al. (1985) and Simms and Yanful (2001). Prapaharan et al. (1985) gave a possible reason that the clay mineralogy adsorbed to the soil surface and induced a smaller pore diameter at the soil surface in the SWCC tests compared to that in MIP tests. This phenomenon may also be due to the disturbance of the macro pore structures during sample preparation for the MIP tests or due to the inaccuracy of the mercury-air contact angle at the soil surface used in the calculation.

The predicted SWCC for SP is close to that from the experiment (refer to Fig. 7(**a**)). But its shape does not fit the experimental data very well. Also the similarity between the predicted SWCC and the SWCC obtained in the experiment is improved by the shrinkage correction. The P_0 correction is not needed for SP, which is consistent with the experimental SWCCs (refer to Fig. 5(**b**)).

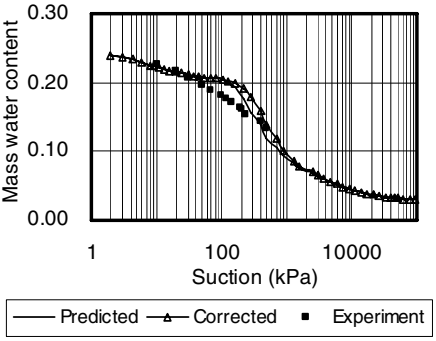

a. Predicted SWCCs from PSD for SP

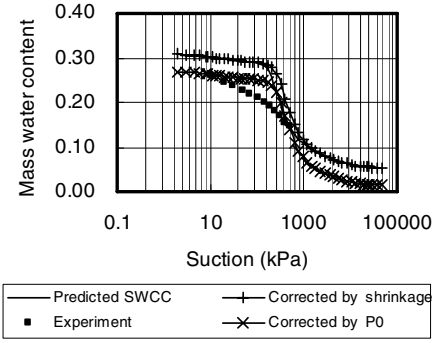

b. Predicted SWCCs from PSD for SW

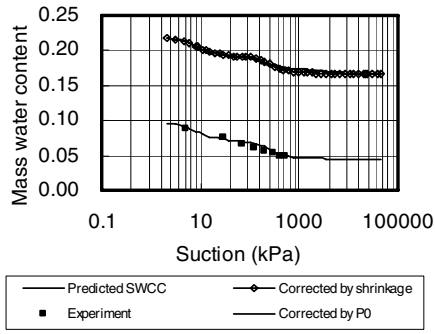

c. Predicted SWCCs from PSD for GP

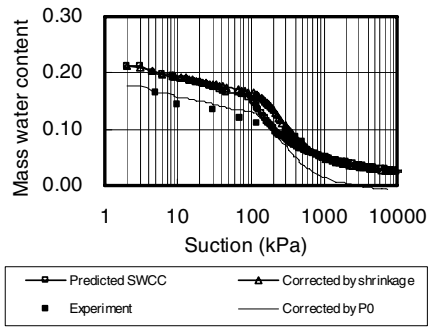

d. Predicted SWCCs from PSD for GW

Fig. 7. Predicted SWCCs from PSDs for GP, GW, SP and SW (RC = 0.85)

The predicted SWCCs from the PSDs of SW, GP and GW are shown in Figs. 7(**b**)–(**d**). Without the P_0 correction, the predicted SWCCs are far away from the experimental SWCCs. With the correction of the pore volume with pore entrance diameters larger than 142 μm, the predicted SWCCs of SW, GP and GW are close to the experimental data. The predicted SWCC of GP is satisfactory. But the shape of the predicted SWCCs of SW and GW are different from that obtained in the SWCC experiments. The influence of shrinkage correction is rather limited for SW, GP and GW.

Summary and Conclusions

A series of MIP tests and SEM tests were conducted in this paper to investigate the changes of PSD during soil drying. Shrinkage phenomena occurred during the drying process for all five CDG soils.

The PSDs obtained from the MIP tests were used to predict the SWCCs of the five soils. The results demonstrated that this method was effective and

could give a drying SWCC rapidly in a much wide suction range. With the P_0 correction, the predicted SWCCs for the coarse soils were close to the experimental SWCCs. With the shrinkage correction, the predicted SWCC for SM fitted the experimental SWCC quite well.

Acknowledgements

This research was substantially supported by a grant from the NSFC/RGC Joint Research Scheme between the National Natural Science Foundation of China and the Research Grants Council of the Hong Kong SAR (Project No. N-HKUST611/03). The authors are grateful to Prof. D. G. Fredlund for constructive discussions during the course of the study.

References

Al-Mukhtar M, Belanteur N, Tessier D, Vanapalli SK (1996) The fabric of clay soil under controlled mechanical and hydraulic stresses, Appl Clay Sci 11:185–197

Aung KK, Rahardjo H, Leong EC, Toll DG (2001) Relationship between porosimetry measurement and Soil water characteristic curve for an unsaturated residual soil, Geotech Geol Eng 19:401–416

Hillel D (1980) Fundamentals of soil physics. Academic Press Inc., London

Lapierre C, Leroueil S, Locat J (1990) Mercury intrusion and permeability of Louisville clay, Can Geotech J 27:761–773

Prapaharan S, Altschaeffl AG, Dempsey BJ (1985) Moisture curve of compacted clay: mercury intrusion method, J Geotech Geoenv Eng 111(9):1139–1143

Reed MA, Lovell CW, Altschaeffl AG, Wood LE (1979) Frost-heaving rate predicted from pore-size distribution, Can Geotech J 16:463–472

Romero E, Gens A, Lloret A (1998) Water permeability, water retention and microstructure of unsaturated Boom clay, Eng Geol 54:117–127

Simms H, Yanful EK (2001) Measurement and estimation of pore shrinkage and pore distribution in a clayey till during soil–water characteristic curve tests, Can Geotech J 38(4):741–754

Simms H, Yanful EK (2002) Predicting soil–water characteristic curves of compacted plastic soils from measured pore-size distributions, Geotechnique 52(4):269–278

Simms H, Yanful EK (2004) Discussion of the application of mercury intrusion porosimetry for the investigation of soils, including an evaluation of its use to estimate volume change in compacted clayey soils, Geotechnique 54(6):421–426

The Influence of the Pore Fluid on Desiccation of a Deformable Porous Material

Hervé Péron[1], Liangbo Hu[2], Tomasz Hueckel[2], and Lyesse Laloui[1]

[1] Soil Mechanics Laboratory, Ecole Polytechnique Fédérale de Lausanne – EPFL, Station 18, CH-1015 Lausanne, Switzerland
herve.peron@epfl.ch, lyesse.laloui@epfl.ch

[2] Department of Civil and Environmental Engineering, Duke University, Durham, N.C. 27706, U.S.A. lh19@duke.edu, Hueckel@duke.edu

Summary. This paper aims at elucidating the influence of pore fluid properties on the shrinkage strains of deformable materials subjected to drying. Results of isothermal drying tests of two kinds of silts saturated with three different pore fluids are presented. Results show different strain amounts during drying and the final void ratios, depending on pore fluid. The rates of drying are consistent with saturated vapor pressures, while their amount with the surface tension. The shrinkage limit appears also to be controlled by a limitation in skeleton compressibility.

Key words: desiccation, shrinkage, pore fluid properties, unsaturated soil, cracks

Introduction

The study of deformation due to drying is fundamental in the understanding of the patterns of stress generated by the constrained shrinkage and cracking in soils. When drying shrinkage is constrained, reaction forces arising located at the constraints generate stresses, which depend on the amount of shrinkage. Our previous papers (Péron et al. 2006, Hu et al. 2006) revealed how the development of such stress in the elastic domain leads to soil cracking.

Notably, several previous studies established that most of the desiccation shrinkage develops when soil is saturated (Croney and Coleman 1954, Fleureau et al. 1993). The state of full saturation when cracking initiates was hypothesized by several authors (Konrad and Ayad 1997, Abu-Hejleh and Znidarcic 1995, Lloret et al. 1998). Recently, Péron et al. (2006) showed that cracks occur at the end of saturation range or at the early stage of desaturation.

The goal in this work is to investigate a possible relationship between the total amount of shrinkage, its rate and the mechanisms of liquid removal and deformation. In particular, the role of the evaporation flux versus surface tension, in addition to soil compressibility and transport properties are of interest. Slow, constant humidity environment, (isothermal) air-drying of thin

and long rectangular soil slabs was carried out. Two different soil types were used: clayey silt, and a powder of rock. The soils were wetted with three different pore fluids, characterized by distinctly different surface tension, latent heat, saturation vapor pressure and viscosity.

Desiccation Tests

Desiccation Tests Procedure

The silts employed were: a clayey silt (referred to as silt A), and a powder of granite (silt B). They were saturated with three fluids: tap water, and two alcohols: ethanol/water mixture (with a volume ratio of 50%/50%), and ethylene-glycol/water mixture (65%/35%) with the properties shown in Table 1. The two alcohols were used in mixtures with water to avoid flocculation, which is especially acute in pure ethanol. Saturation vapor pressure and latent heat were calculated as for pure mixtures.

Table 1. Properties of fluids used for material preparation

	Pure water	Ethylene-glycol solution	Ethanol solution
Specific Latent Heat [MJ/m^3]	2448	1479	1591
Saturation Vapor Pressure [Pa]	2337	1639	3253
Surface Tension [mN/m]	72.6	56.4[a]	30[a]
Viscosity [cm^2/s]	0.01	0.0423[b]	0.029[b]
Density [g/cm^3]	1	1.071	0.92

[a] Vasquez et al. (1995) J Chem Eng Data 40; Won et al. (1981) J Chem Eng Data 26

[b] Fernandez & Quigley (1988) Can Geotech J 25; Hayduk & Malik (1971) J Chem Eng Data 16(2)

Two silts were used: a clayey silt (referred as silt A) and granite powder (silt B). Particles greater than 90 µm (sandy fraction) have been removed. In silt A, the clay fraction is 25%; clay minerals are illite (10% of the total amount of mineral species), smectite (10%) and chlorite (5%). The liquid limit is $w_L = 31.8\%$, plastic limit $w_P = 16.9\%$, and the unit weight of solid particles is $\gamma_s = 27.1\,\mathrm{kN/m^3}$. Silt B has low clay content (less than 7%, mainly illite and chlorite). The liquid limit is $w_L = 29.5\%$, the plastic limit $w_P = 20.1\%$, and the unit weight of solid particles is $\gamma_s = 27.7\,\mathrm{kN/m^3}$.

The tests were performed in a climate chamber with a controlled relative air humidity and temperature, of 40% and 18°C, respectively. Strains in three

directions were measured with calipers, which were fixed on the support. Average fluid content of the whole cake was recorded versus time by continually weighing an identical cake, dried in the same time in identical conditions as the one used for strain measurement. Details of the tests are reported elsewhere (Péron et al. 2006, Hu et al. 2007).

Density changes (due to the fact that the more volatile fluid of the mixture evaporates faster) were tested for the calculation of void ratio evolution during drying, as well as for the fluid properties determination.

Desiccation Test Results

The main result is the relationship between the void ratio evolution and the volumetric fluid content for both materials plotted in Fig. 1**A** and **B**. In these graphs the thin dotted line denotes the theoretical void ratio evolution under the assumption that the material remains water saturated at constant volume of solids. It is noted that at the beginning of drying, all the curves do not much deviate from this line. However, well before all fluid is evaporated, the shrinkage stopped. The volumetric water content value at that point identified as the shrinkage limit tends to depend on the pore fluid. Void ratio stabilizes finally, reaching a "limiting void ratio." The curves obtained could be conceptualized as piecewise bilinear, with the first part merging with the saturation line, and a second part with void ratio equal to a constant "limiting void ratio."

For either silt, water involves the highest amount shrinkage and ethanol the lowest. Ethylene-glycol induces intermediate values, closer to water in the case of silt B, and closer to ethanol in the case of silt A. Shrinkage in the case of silt A was much more significant for all three liquids, than in the case of silt B. The values of the limiting void ratios exhibit also an apparently wide scatter. In Figure 2 the volume loss of fluids for silt A and B has been plotted versus time. The drying of silt with glycol is significantly slower. The drying

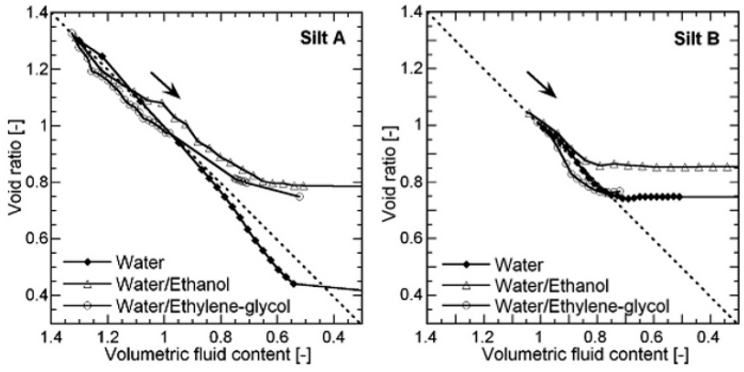

Fig. 1. Void ratio evolution with respect to volumetric fluid content

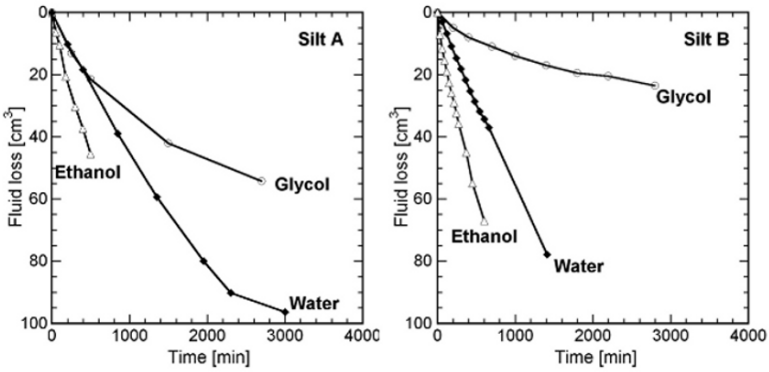

Fig. 2. Fluid loss with respect to time

rates are well correlated with vapor pressure of the permeating liquid: the higher vapor pressure, the higher drying rate.

Discussion

First, it has to be outlined that the rates of fluid removal and void ratio change (Fig. 1 and Fig. 2) follow the order of saturated vapour pressure of the fluids, that is glycol – water – ethanol.

A hypothesis of air-water interface (or contractile skin) is described in Fredlund and Rahardjo (1993). The surface tension associated with the contractile skin results in a reaction force, which is likely to produce compression of the soil structure. For the saturated range, Hu et al. (2007) showed that evaporation at the *external* solid-fluid-air interface is the only driving force of shrinkage. Capillary force exists only at this boundary, as there is no air within the body of the sample. During drying the removal of the pore fluid at the boundary generates an outward transport of fluid, and a consequent fluid content decrease within the medium. That induces a negative pore pressure gradient across the body. That also produces strain and the proportional stress field that is equilibrated at the boundary by capillary forces. Hu et al. (2007) performed a simple numerical simulation of the process in 1D using Biot theory that captures the salient points of the process.

The limiting value of the void ratio change and the total strain variation over the course of drying are left outside of the above model. Shrinkage of unconstrained specimens ceases at a relatively well-defined configuration. The mechanism of this cessation remains an open question. At least for the silt A when wetted with water, the air entry value obtained from an independent evaluation via the water retention curve coincides with the shrinkage limit (see Péron et al. 2006). Nevertheless, in some cases, shrinkage limit may significantly differ from the air entry value; see experimental results of Taibi (1992)

for remolded silt. Fleureau et al. (1993) hypothesise that for low saturation state, the capillary forces between the particles are normal to a plane tangent to the particle at the contact point and thus cannot result in a rearrangement of the soil structure. Other hypotheses on the shrinkage limit, include a locking value of compressive strain, air phase spreading due to either bulk pore water (internal) cavitation or an external air/fluid interface instability followed by fingering. In general, such hypotheses may be linked to the properties of the solid skeleton and of the fluid. In what follows we explore some numerical correlations between the limiting void ratio and void ratio variation during drying and basic fluid properties (surface tension, vapor pressure, latent heat, viscosity). Figures 3–6 present such correlations. The limiting void ratios and void ratio variation values are clearly different for the two materials. They also depend on the permeating fluid. Interestingly, the numerical values of the characteristics of interest for the fluid employed do not follow the same sequence.

For both soils, the value of limiting void ratio, as well as void ratio evolution exhibit similar trends with respect to viscosity, surface tension, saturation vapor pressure and latent heat. However, silt A is clearly more sensitive to pore liquid than silt B. Indeed, the differences in the values of limiting void

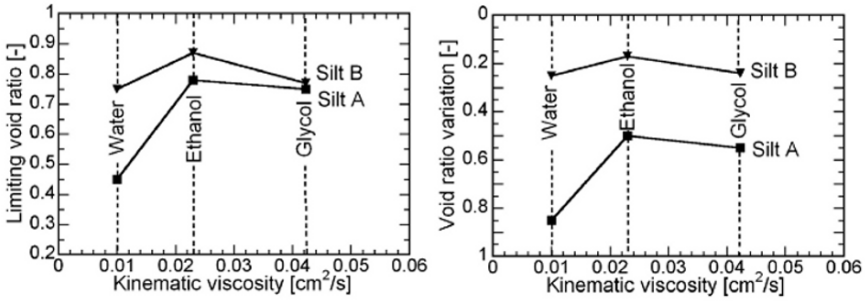

Fig. 3. Limiting void ratio and void ratio variation with respect to viscosity

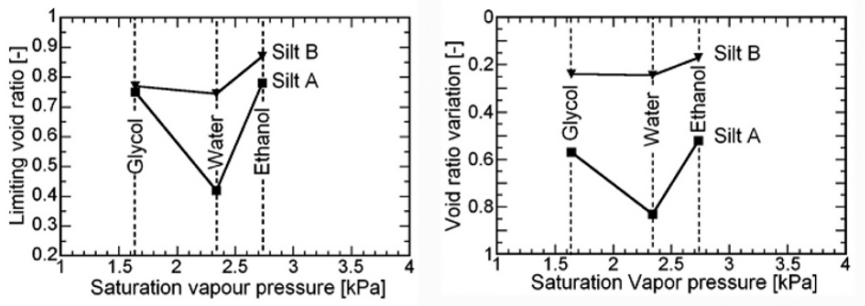

Fig. 4. Limiting void ratio and void ratio variation with respect to vapor pressure

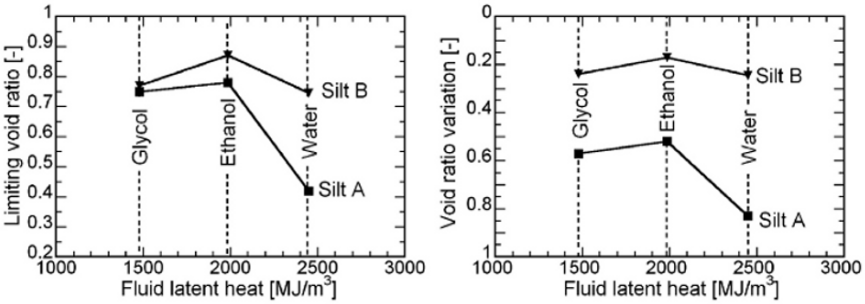

Fig. 5. Limiting void ratio and void ratio variation with respect to latent heat

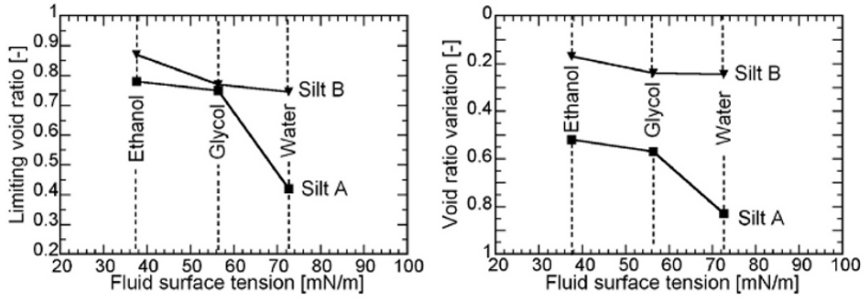

Fig. 6. Limiting void ratio and void ratio variation with respect to surface tension

ratio, as well as void ratio variation in silt B are not substantial. Visibly, the most clear monotonic trend of the void ratio variables is seen for surface tension (Fig. 6). The higher the surface tension the higher the total variation of void ratio and hence the volumetric strain during drying and the lower the limiting void ratio. Early research (Kingery and Francl 1954) assessed a similar trend and showed the final shrinkage of kaolinite clay during drying was a linear function of the surface tension of the pore fluid.

This observation supports the assumption that the shrinkage deformation is controlled by external boundary menisci, which act as a stretched membrane. It must be recognized however, that the capillary forces depend also on the contact angle, which however, is not known at the grain scale.

Viscosity, and hence permeability show much less influence except for a clear difference between the two alcohols and water in silt A (Fig. 3). As these two variables control the fluid flux to the external surface they may have a greater impact on the rate than the total or limiting strain.

Finally, it seems that the clayey character of silt A makes it much more shrinking with water than it is with alcohol as the pore fluid. Earlier tests of Sridharan and Venkatappa Rao (1973) indicate a dramatically lower compressibility of clayey soils permeated with alcohols than with water. This is attributed to the existence of highly deformable electric diffuse double layer

coatings around clay particles in water. Hence, it appears that difference in response of soils to drying in terms of the total shrinkage and limiting void ratio point also to their difference in generating the adsorbed water.

Conclusions and Open Issues

Drying of unconstrained slabs of silts has been tested experimentally. Most of the shrinkage strain occurs in the saturated phase of drying with an evaporative flux at the surface and a perimeter capillary force. Limiting void ratio and void ratio variation correlate well with surface tension confirming a role of surface capillary forces in the process. Clayey silt is more sensitive to pore fluid properties than granite powder. Hence, clay water evaporation mechanism is of particular interest for further investigation. The shrinkage limit appears also to be controlled by a limitation in skeleton compressibility.

Acknowledgment

This work is funded by a cooperation of the US NSF (grant # 0324543) and Swiss NSF (grant 200021–101917).

References

Abu-Hejleh AN, Znidarcic D (1995) Desiccation theory for soft cohesive soils, J Geotech Eng 121(6):492–502

Croney D, Coleman JD (1954) Soil structure in relation to soil suction (pF), J Soil Sci 5:75–84

Fleureau JM, Kheirbek-Saoud S, Soemitro R, Taibi S (1993) Behavior of clayey soils on drying-wetting paths, Can Geotech J 30(2):287–296

Fredlund DG, Rahardjo H (1993) Soil mechanics for unsaturated soils. Wiley-Interscience Publication, John Wiley and Sons, Inc.

Hu L, Péron H, Hueckel T, Laloui L (2006) Numerical and phenomenological study of desiccation of soil. In: Lu N, Hoyos LR, Reddi L (eds) Advances in Unsaturated Soil, Seepage, and Environmental Geotechnics, GSP 148 ASCE:166–173

Hu L, Péron H, Hueckel T, Laloui L (2007) Drying shrinkage of deformable porous media: mechanisms induced by the fluid removal. GeoDenver 2007, GSP ASCE (to appear)

Kingery WD, Francl J (1954) Fundamental Study of Clay: XIII, Drying Behavior and Plastic Properties, J Am Ceram Soc 37(12):596–602

Konrad JM, Ayad R (1997) An idealized framework for the analysis of cohesive soils undergoing deesiccation, Can Geotech J 34:477–488

Lloret A, Ledesma A, Rodriguez R, Sanchez MJ, Olivella S, Suriol J (1998) Crack initiation in drying soils. Unsaturated Soils, Pékin, International Academic Publishers, pp 497–502

Péron H, Laloui L, Hueckel T, Hu L (2006) Experimental study of desiccation of soil, In: Proceedings of the Fourth International Conference on Unsaturated Soils, UNSAT 2006: pp 1073–1084

Sridharan A, Venkatappa Rao G (1973) Mechanisms controlling compressibility of clays and the role of the effective stress concept, Géotechnique, 23(3):359–382

Taibi S (1992) Comportement mécanique et hydraulique des sols partiellement saturés. PhD. Thesis, Ecole Centrale de Paris

Determination of the Soil Water Retention Curve and the Unsaturated Hydraulic Conductivity from the Particle Size Distribution

Alexander Scheuermann and Andreas Bieberstein

Institute of Soil Mechanics and Rock Mechanics, Division of Embankment Dams and Landfill Technology, University of Karlsruhe (TU)
alexander.scheuermann@ibf.uka.de,
andreas.bieberstein@ibf.uni-karlsruhe.de

Summary. Because of the complexity of the metrological determination of the soil water retention curve (SWRC), so-called pedotransfer functions (PTF) have been developed for several years. Mostly these PTF are based on a more or less simple regression analysis using a limited set of data. In such methods the SWRC is predicted with data on the amount of soil components sometimes supplemented by values regarding the density or the amount of organic materials. Only few PTF deal directly with the particle size distribution. In many cases empirical factors are necessary to obtain a prediction for the water retention curve. A new method for determining the soil-hydraulic properties using the pore constriction distribution of a soil has been developed, whereby the pore constriction distribution is derived from the particle size distribution depending on the density of the soil. The contribution will present the new pedotransfer method and shows results in comparison to experimental investigations.

Key words: pedotransfer method, soil water retention curve, hydraulic conductivity, pore model

1 Introduction

Different methods have been developed to estimate the SWRC from the particle size distribution. For this purpose different approaches were used. By making estimations using a simple model for the pore structure, the particle size distribution can be separated into fractions of different sizes. Using this information it is possible to incrementally estimate the SWRC for a predefined bedding of particles within a specific size range (Arya and Paris 1981, Fredlund et al. 2002). The analogy between the progression of the particle size distribution and SWRC makes it possible to reach a direct solution using a functional relationship between both curves (Haverkamp and Parlange 1986). Based on the particle size distribution, newly developed methods calculate the

capillary and adsorptive bound water separately, which are then summarised in order to receive the SWRC (Schick 2002, Aubertin et al. 2003). However, as a rule, these kinds of solutions require additional empirical information which naturally contains uncertainties. A numerical solution for the calculation of the SWRC and the unsaturated hydraulic conductivity has been given by Kitamura et al. (1998). For the calculation they use a statistical distribution for the pore diameter and the pore inclination, which are both derived from the particle size distribution (cf. Kitamura et al. 2000). On the basis of the consideration of sphere packings Zou (2003, 2004) has developed an elegant solution for the estimation of the SWRC because it is purely analytical. However, for this reason this method can only be used at best for uniform soils.

In the following, a method will be briefly introduced, which uses the pore constriction distribution for the calculation of the SWRC for the case of drainage as well as the relationship for the unsaturated hydraulic conductivity. In this connection, the pore constriction distribution will be calculated from the particle size distribution under consideration of the relative density of the soil.

2 Calculation of the Pore Constriction Distribution

The structure of a pore system depending on the density is the most important factor influencing the soil hydraulic parameters. Another relevant geotechnical question regarding pore structures is the ability of materials to pass through pores in a soil. In this connection the suitability of a soil for grouting purposes (Schulze 1992) or questions concerning geotechnical filters (Wittmann 1980, Witt 1986, Schuler 1997) should be mentioned. However, the direct measurement of the pore size distribution is a challenging undertaking. For this reason very early first approaches have been developed in order to estimate pore size distributions from more easily measurable parameters like the particle size distribution.

A procedure of this kind has been developed by Silveira (1965). It considers a particle group consisting of three touching spherical grains. With this consideration he assumes from the beginning the densest condition of a soil (hexagonal packing). In the space between the grains a spherical pore can be subscribed which touches every three grains representing the pore constriction of this group. As a basis for the selection of the grain sizes Silveira uses the particle size distribution finer by weight, which has been criticised by Ziems (1969) since the introduction of the procedure, because of the underestimation of the finer part of the soil. For a similar procedure Ziems used the particle size distribution finer by amount (quantity distribution).

Schuler (1997) has finally developed the procedure, which is the basis for the calculation of the pore constriction distribution. As a basis for the selection of grains, he uses the particle size distribution finer by surface (surface distribution). Additional modifications carried out by Schuler are as follows:

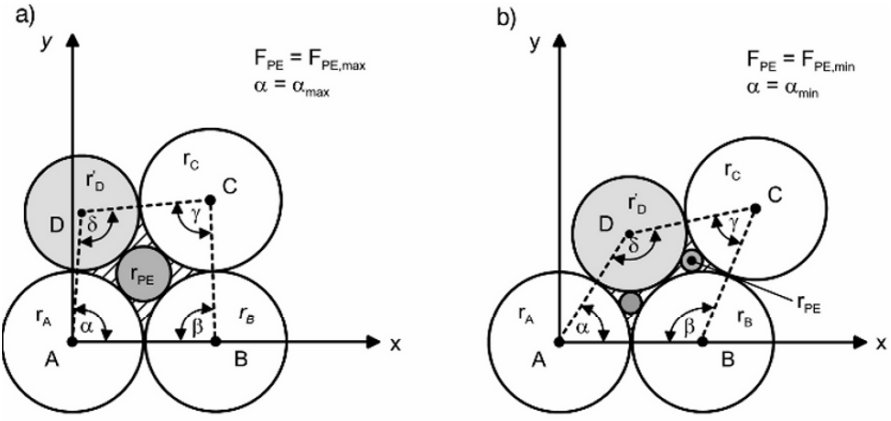

Fig. 1. Calculation of pore constrictions within a pore space consisting of four particles **a**) for the lowest relative density $D = 0$ and b) for the highest relative density $D = 1$

- Experimental investigations have shown that most of the pores are formed by four particles (Witt 1986 (pore imprints) and Glantz 1997 (magnetic resonance imaging)). Due to this observation instead of three particles Schuler considers a group of four particles as shown in Fig. 1.
- When a pore constriction is formed by four particles, the probability that the centre of each spherical grain is located in one intersection is very low, which is verified by observations according to Witt. Due to these observations it is assumed that one particle is shifted in the third dimension, while the radius of this particle is decreased in the two dimensional consideration of Fig. 1 to $r'_D = r_D \cdot (2/3)^{0.5}$ (cf. grey particles (D) in Fig. 1). In Figure 1 it is assumed that all particles have the same radius ($r_A = r_B = r_C = r_D$).
- For a pore constellation (group of particles with specific positions) as shown in Fig. 1 spaces with different sized areas are possible. If particles A and B touch each other, the densest packing of the four particles will be obtained and the angle α as well as the area F_{PE} of the space between the particles then have their lowest values (cf. Fig. 1**b**)). As the values for α increase also the area F_{PE} of the space between the particles grows until F_{PE} reaches a maximum (cf. Fig. 1**a**)). Under this condition the constellation reaches its loosest density. Consequently the constellation of particles takes on different densities according to the area of the space between the particles, which can be assigned to the loosest and densest bedding of the particles. In order to take into account the bedding of the soil for the calculation of the pore constrictions, an analogy is introduced between the area F_{PE} of the space between the particles and the porosity n of the soil as shown in equation (1)

$$D = \frac{n_{\max} - n}{n_{\max} - n_{\min}} = \frac{F_{PE,\max} - F_{PE}}{F_{PE,\max} - F_{PE,\min}} \,. \tag{1}$$

As mentioned before, the selection of the grains takes place using the surface distribution. For this purpose, the particle size distribution is divided into sections of equal percentage and for every section a mean diameter of the particle is calculated. As a result every particle diameter has the same probability of occurrence. Because of the consideration of four particles and depending on the amount of sections k chosen for the calculation, a total amount of $Z_k = k^4$ constellations has to be considered. Finally, for each pore constellation two pore constriction radii are subscribed and a mean value characterising the pore is calculated.

The subscription of pores into the space between the particles is a purely geometric problem. In order to improve the efficiency of the calculations, an analytical method is used and integrated into a programme. Calculations with $k = 15$ pore sections are possible, which is very important for the consideration of well graded soils.

Figure 2 shows the result of a calculation of a pore constriction distribution with a relative density of $D = 0.8$ in comparison to experimental results from Witt (1986). The solid line on the right shows the particle size distribution, the long dashed line shows the quantity distribution and the line with dashes

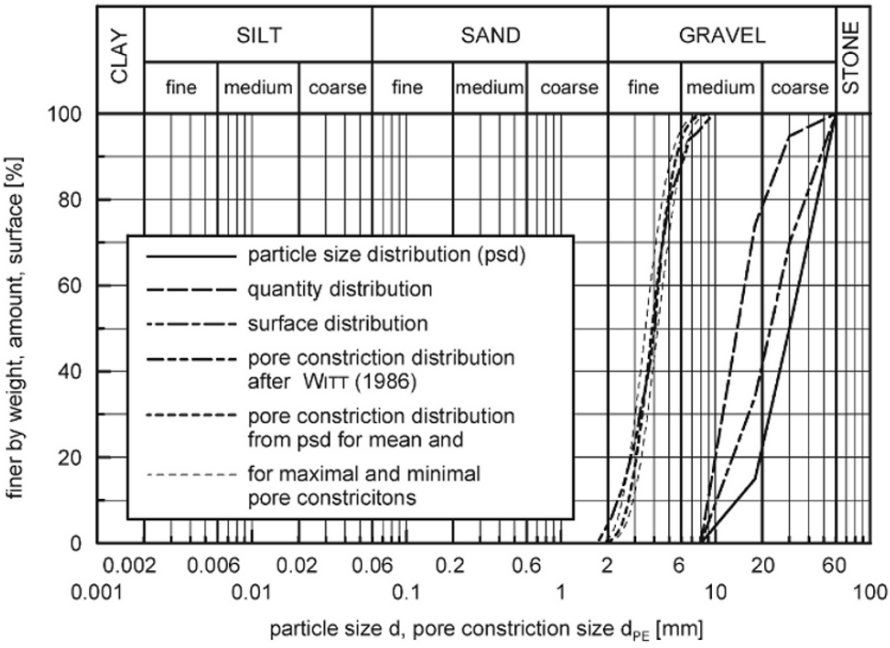

Fig. 2. Comparison between calculated pore constriction distribution and a measured distribution based on silicon pore imprints (according to Witt 1986)

and dots shows the surface distribution. It can be seen from the propagation of the curves that by using the surface distribution the probability of occurrence of finer particles is higher than by using the particle size distribution finer by weight and lower by using the quantity distribution.

The bundle of lines on the left shows the pore constriction distributions finer by amount. The dotted lines represent the results of the calculation. The thick line represents the mean value of the pore constriction and both fine lines represent the limits for maximum or minimum pore constrictions. The experimental result according to Witt is shown by a dashed line with two dots. Witt determined his distribution using silicon imprints of the pores. On the one hand, it is a challenging procedure to assess pore size distributions, but, on the other hand, it is a quite exact one. It can be very clearly recognised that the experimental result is reproduced very well with the calculation, which has already been verified by Schuler (1997). This comparison illustrates the applicability of the introduced procedure for the calculation of the pore constriction distribution depending on the bedding, at least for granular soils.

3 Derivation of Soil Hydraulic Parameters

In the following the required steps for the calculation of the soil hydraulic parameters are presented. The pore constriction distribution constitutes the necessary input data for this calculation, which must be carried out separately. The following calculation examples are presented for a weak gravelly sand, of which the particle size distributions, quantity distribution and surface distribution as well as the calculated distributions for the pore constriction are shown in Fig. 3.

3.1 Soil Water retention Curve (SWRC)

As already mentioned, the SWRC of a soil for the drainage condition is mainly influenced geometrically by the pore constrictions of a soil. The retentive force acting against the drainage of water out of the soil is the capillary force which is activated by the greatest pore with a connection to the free air phase.

Consequently, with the information of the pore constriction distribution, it is possible to determine the capillary forces as isotropic forces acting in a soil. For this purpose the well known equation (2) for the description of the rise of water in a capillary tube is used. In this connection, the so-called capillary rise of water is inversely proportional to the radius of the pore constriction r_{PE}. For the case of drainage (completely wetted surface) it is feasible to assume a value of $\delta = 0°$ for the contact angle (cf. Schubert 1982, Fredlund and Rahardjo 1993). The surface tension σ_{wa} of water to the air phase is a temperature-dependent property, which can be inferred from Table 1. Finally, with the specific weight of water γ_w it is possible to calculate two values for every pore constellation for the capillary rise of water (according to the

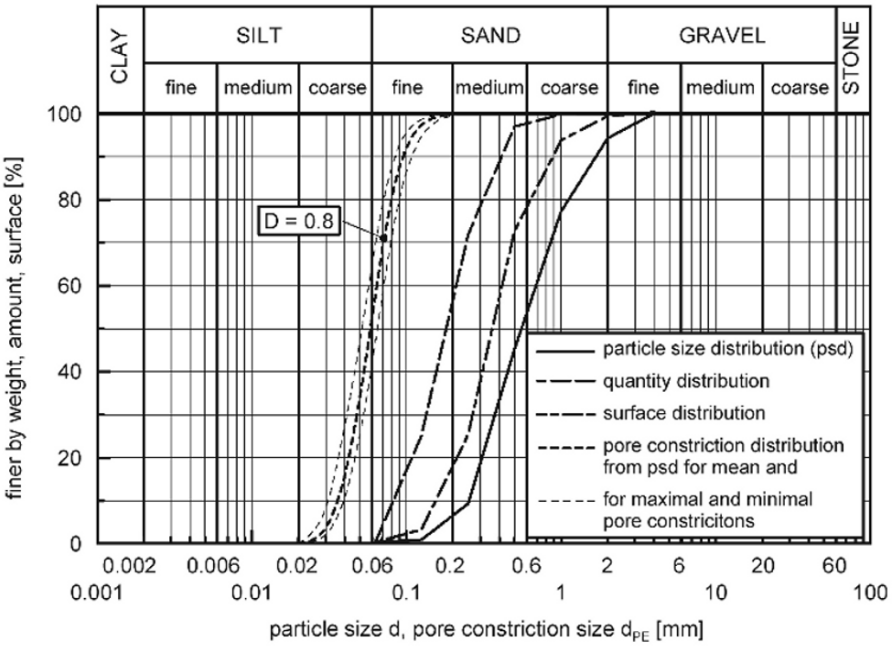

Fig. 3. Particle size distribution, quantity distribution and surface distribution for a weak gravelly sand as well as pore constriction distributions for mean pore constrictions for a relative density of $D = 0.8$ (with variation due to maximal and minimal pore constrictions)

Table 1. Surface tension σ_{wa} of water to air depending on the temperature

Temperature (°C)	10	15	20	30
Surface tension σ_{wa} (N/m)	0.0724	0.0735	0.07275	0.0712

minimum and maximum pore constrictions) as well as a mean value, which is set equal to prevailing capillary forces $|\psi_{PE}|$ due to the a pore constriction:

$$|\psi_{PE}| = \frac{2\sigma_{\mathrm{wa}} \cos \delta}{\gamma_w r_{PE}} \tag{2}$$

The decrease in the water content during drainage is calculated from the loss of water volume, which is set equal to the area loss of the drained pore space for each pore constellation. The sum of the area of all pore spaces equates to $S = 100\%$ saturation. Finally, by presetting the porosity n according to the porosity used for the calculation of the pore constriction distribution (cf. equation (1)), the analogy to the saturated volumetric water content is established.

Without considering water-retention in the pore space, the soil would be completely drained in the calculation. In fact, some water is stored in the contact points or gussets of the particles, which leads to residual water in every pore constellation. However, the water in the gussets of the particles forms a corpus, which is approximated in the 2D-consideration. Furthermore, it is unknown with which radius water is stored in the gussets. Due to these uncertainties, the residual water is considered to be a variable. As an empirical value it is feasible to predefine the residual water content as the sum of all water stored in the gussets of the particles. Another possibility for a predefinition of the water content is the use of a matric suction at which the residual water content will be set (similar to the definition of the field capacity between 60 and 310 hPa). Finally it is also possible to automatically calculate the residual water content using the pore radii of the constrictions of each pore constellation. If the smaller pore constriction of each pore constellation is used for the calculation, an upper limit for the residual water content is obtained and with the use of the smallest pore constriction of all pore constellations, a lower limit is determined. So far adsorptive bound water has been neglected in the calculation.

For a direct estimation of the residual water content or the water content at saturation, data from literature can also be used (e.g. relative values for the water contents by Luckner et al. 1989).

With the procedure presented discrete points of the SWRC are calculated, which can be parameterised using appropriate models like Brooks and Corey (1964) or van Genuchten (1980). Figure 4 shows the result of a calculation (white squares) in comparison to a statically measured SWRC (grey circles) for the weak gravelly sand presented in Fig. 3. Here the saturated water content θ_S was given by the assumed porosity, and the residual water content θ_r was automatically calculated using the smallest pore constriction radius for all pore constellations. Whereas the saturated water content is more or less a given parameter, the residual water content represents a value which can be estimated taking values from experience.

As can be seen in Fig. 4, there is a satisfactorily good match between the measured and the calculated SWRC. In this connection, the calculation of the SWRC was carried out as a prediction for a given porosity n with a resulting relative density D (under consideration of $n_{\max}$ and $n_{\min}$, cf. equation (1)). It can be assumed that the accordance of both curves could be much better with an adapted value for D.

3.2 Unsaturated Hydraulic Conductivity

There are different microscopic approaches for the determination of the unsaturated hydraulic conductivity. Microscopic approaches are based on a pore model and the hydraulic conductivity is calculated by summation of the conductivities of individual capillaries. The most well known model based on a microscopic approach is the model of Mualem (1976) which is the most

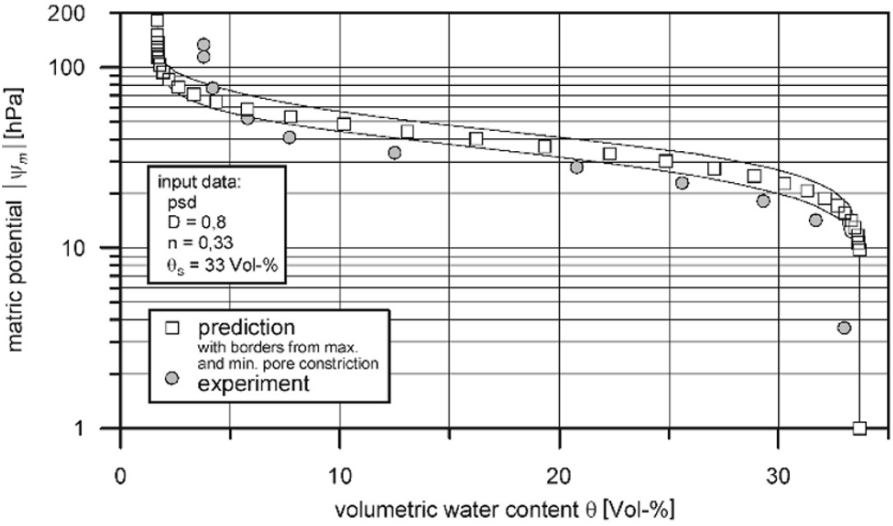

Fig. 4. Comparison between measured and calculated soil water retention curve using the pore constriction distribution for the weak gravelly sand (cf. Fig. 3)

widespread model in combination with the parameterisation of van Genuchten (1980).

For all microscopic approaches specific conditions are assumed which were defined for the first time by Childs and Collis-George (1950):

- The pore size distribution of a soil can be derived from the soil water retention curve.
- For individual pore fragments, the flow model of Hagen-Poiseuille for laminar flow in channel-like capillaries applies (cf. equation (3)).
- Since in the equation of Hagen-Poiseuille the radius of the capillary is used to the power of four, the effective flow resistance in a sequence of pores in series is significantly influenced by the pore with the smallest diameter.
- The total conductivity of a porous media is determined only by sequences of pores in series. Hence a lateral connectivity of pore sequences is neglected.

In this connection, the negative effects of the last two assumptions should counterbalance each other. All microscopic approaches use pore sequences which are combined in a specific way. By the summation of water-bearing pore sequences up to a defined water content or matric suction, it is possible to calculate the unsaturated hydraulic conductivity.

From a statistical point of view, the pore constriction distribution is a representative solution of an arbitrary cut through a soil and, since the pore constriction distribution shows per definition a priori hydraulically active pore openings, it is not necessary to combine them in the sense mentioned above.

This means that for the calculation of the hydraulic conductivity it is feasible to use the equation directly according to Hagen–Poiseuille, as shown in equation (3).

Equation (3) can easily be transformed into a form for the definition of the hydraulic conductivity according to Darcy. Since the term $(\Delta p/l)$ corresponds to the hydraulic gradient i, the flow through a capillary is defined only by the form factor f_{HP} and the dynamic viscosity η. By equitation of equation (3) with the well-known Darcy equation $Q = k_f iA$ equation (4) is obtained, which describes the saturated hydraulic conductivity for all capillaries of number m considered as a bundle representative of a soil with a total surface area of A_B in a representative soil cut.

$$Q = \frac{\Delta V}{\Delta t} = f_{HP} \frac{\Delta p}{l} \frac{1}{\eta} \tag{3}$$

Q	discharge (m^3/s)	l	length of the capillary (m)
ΔV	flow volume (m^3)	η	dynamic viscosity (10^{-6} kNs/m^2) (cf. Table 2)
Δt	time interval (s)		
Δp	pressure difference at the end of the capillary (kN/m^2)	f_{HP}	form factor (m^4), which is $(r_{PE}^4 \pi)/8$ for circular cross section

Table 2. Dynamic viscosity of water depending on the temperature

Temperature (°C)	10	15	20	30
Dynamic viscosity η (10^{-6} kNs/m^2)	1.306	1.138	1.002	0.798

$$k_f = \sum f_{HP,m} \frac{1}{\eta} \frac{1}{A_B} \tag{4}$$

With equation (4) the saturated hydraulic conductivity of a soil considered as a bundle of capillaries is well defined. However, two very important properties of a porous media have been neglected so far, namely the tortuosity of the pore channels and the connectivity among them. In the well known equation according to Mualem, both soil properties are combined in one parameter, for which Mualem originally proposed the constant value 0.5 based on experiments. However, more and more frequently this parameter is being used as a fitting parameter, as a result of which the original physical meaning has been lost. Nevertheless, both the tortuosity and the connectivity are dependent on the water content, which has to be considered in the calculation.

The tortuosity T_0 describes the relationship between the distance of two points L_P and the actual length of the pore channel L_{Pe} between these two

points. Most frequently the tortuosity is defined as shown in equation (5) decreasing the saturated hydraulic conductivity (cf. Bear 1972). For a saturated condition it is feasible to use $T_0 = 2/3$ as a constant value for the tortuosity.

$$T_0 = \left(\frac{L_P}{L_{Pe}}\right)^2 \leq 1 \tag{5}$$

When considering the connectivity it is more difficult, because as a topologic property of a porous medium it must be determined based on microstructural investigations or by using the Euler–Poincaré characterisation (cf. Vogel and Roth 1998). However the connectivity K can be considered in context with the relationship between the specific surface of a porous medium and its pore volume (Vasconcelos 1998). Based on this approach, it is possible to assess a constant value for K assuming constant conditions regarding the pore volume. For this a cubic arrangement of same sized particles with the radius r_P resulting in a maximum pore surface is considered. For such a packing of particles the pore constriction between the particles has a radius of $r_{PE} = 0.4142 r_P$. Finally the connectivity results from the relationship between the inner surface of the pore and the pore length, and a value for the connectivity of about $K = 2.6$ is determined.

The tortuosity decreases the hydraulic conductivity, whereas the connectivity has an increasing influence. However, as mentioned before, both are dependent on the water content or the saturation of the soil, whereby the influence of the saturation prevails over the progression of the unsaturated hydraulic conductivity. As a result of this consideration, the factor f_{TK}, as shown in equation (6), takes into account the influence of tortuosity T_0 and connectivity K as the multiplicand for equation (4). A comparison between the calculated curve and a curve determined using the model according to Mualem/van Genuchten based on experimental data is given in Fig. 5.

$$f_{TK} = T_0 K S^2 = 1.73 S^2 \quad \text{with} \quad S = \frac{\theta}{\theta_S} \tag{6}$$

As can be seen from Fig. 5, there is a satisfactorily good match between the progression of the unsaturated hydraulic conductivity determined with the model of Mualem/van Genuchten and the calculated curve based on the pore constriction distribution. But even more astonishing is the direct match of the saturated hydraulic conductivity calculated with the presented procedure. Naturally the hydraulic conductivity depends on the density of the soil. Concerning this additional factor, for the saturated hydraulic conductivity a variance of $10^{-4} \leq k_f \leq 8 \times 10^{-4}$ m/s is obtained, which is a good estimation of this soil property.

4 Summary and Conclusion

A new procedure for the determination of the soil hydraulic properties based on the particle size distribution has been presented. It uses the pore constric-

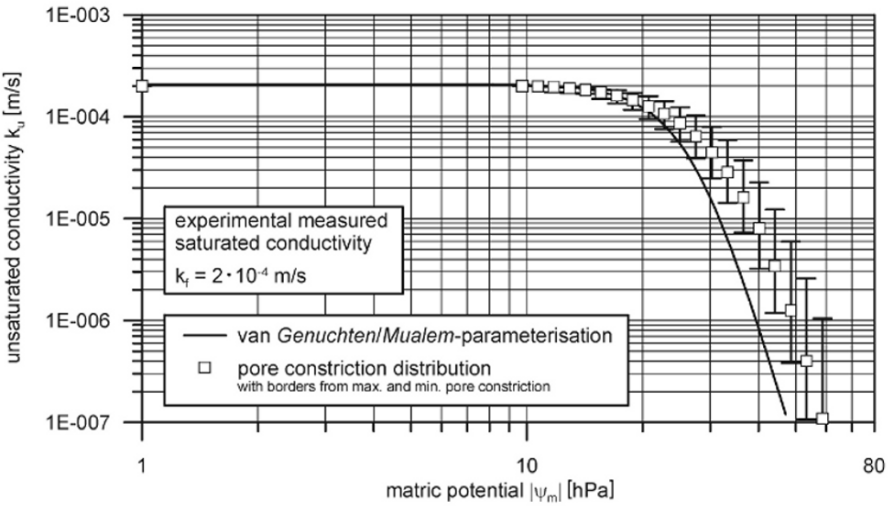

Fig. 5. Progression of the calculated unsaturated hydraulic conductivity from the pore constriction distribution in comparison to the curve determined with the parameterisation according to Mualem/van Genuchten under consideration of the measured saturated hydraulic conductivity of the weak gravelly sand

tion distribution, which has to be calculated separately taking the density of the soil into consideration. Using the equation for the capillary rise of water, the SWRC can be calculated very easily from the pore constriction distribution. The calculation of the unsaturated hydraulic conductivity is based on a consideration of the soil as a bundle of capillaries. In this way it is possible to use the equation according to Hagen-Poiseuille for the flow in capillary tubes, in order to determine the hydraulic conductivity of the soil. However, for this purpose the influence of tortuosity and connectivity must be taken into account.

The comparisons between calculated and measured curves matched satisfactorily well. The introduced procedure was also tested with other granular materials up to silty materials and it was also compared with other pedotransfer functions based on the particle size distribution (cf. Scheuermann 2005). Thus this procedure has proved to be in constant accordance over the range of tested materials.

One great advantage of the procedure presented is its independence from empirical parameters. The shape of both curves of the soil hydraulic properties is the result of the pore constriction distribution, which is directly influenced by the assumed density of the soil. The saturated water content of the SWRC is given by the porosity of the soil, and the residual water content can be automatically calculated or predefined using a measured residual water content or an estimated matric suction.

Furthermore, this procedure also provides a possibility to determine the imbibition SWRC. A concluding step in this connection could be the investigation of the hysteresis of the soil hydraulic parameters.

References

Arya LM, Paris JF (1981) A physicoempirical model to predict the soil moisture characteristic from particle-size distribution and bulk density data, Soil Sci Soc Am J 45:1023–1030

Aubertin M, Mbonimpa M, Bussière, Chapui RP (2003) A model to predict the water retention curve from basic geotechnical properties, Can Geotech J 40: 1104–1122

Bear J (1972) Dynamics of fluids in porous media, Dover Publications, Inc., New York

Brooks RH, Corey AT (1964) Hydraulic properties of porous media, Hydrology Papers, Colorado State University, Fort Collins, Colorado

Childs EC, Collis-George N (1950) The permeability of porous materials, Proc Roy Soc A 201:392–405

Fredlund DG, Rahardjo H (1993) Soil mechanics for unsaturated soils, John Wiley & Son, Inc

Fredlund MD, Wilson GW, Fredlund DG (2002) Use of the grain-size distribution for estimation of the soil-water characteristic curve, Can Geotech J 39:1103–1117

Glantz R (1997) Porennetzwerke von Erdstoff-Filtern – Mathematisch-Morphologische Beschreibung kernspintomographischer Aufnahmen. Ph.D Thesis, Mitteilungen der Abteilung Erddammbau und Deponiebau am Institut für Bodenmechanik und Felsmechanik der Universität Karlsruhe, Heft 9

Haverkamp R, Parlange J-Y (1986) Predicting the water retention curve from particle-size distribution: 1. Sandy soils without organic matter, Soil Science 142(6):325–339

Kitamura R, Fukuhara S, Uemura K, Kisanuki G, Seyama M (1998) A numerical model for seepage through unsaturated soil, Soils and Foundation 38(4):261–265

Kitamura R, Seyama M, Abe H (2000) Investigation of seepage behaviour through unsaturated soil, Unsaturated Soils for Asia. Balkema, Rotterdam, pp 405–408

Luckner L, van Genuchten MTh, Nielsen DR (1989) A consistent set of parametric models for the two-phase flow of immiscible fluids in the subsurface, Water Resour Res 25(10):2187–2193

Mualem Y (1976) Hysteretical models for prediction of the hydraulic conductivity of unsaturated porous media, Water Resour Res 12(6):1248–1254

Scheuermann A (2005) Instationäre Durchfeuchtung quasi-homogener Deiche, Mitteilungen des Institutes für Bodenmechanik und Felsmechanik der Universität Karlsruhe, Heft 164

Schick P (2002) Die pF-Kurve bindiger Böden bei grossen Wasserspannungen, Bautechnik 79(12):842–849

Schubert H (1982) Kapillarität in porösen Feststoffsystemen. Springer-Verlag, Berlin, Heidelberg, New York

Schuler U (1997) Bemessung von Erdstoff-Filtern unter besonderer Berücksichtigung der Parameterstreuung, Mitteilungen des Institutes für Bodenmechanik und Felsmechanik der Universität Karlsruhe, Heft 143

Schulze B (1992) Injektionssohlen – Theoretische und experimentelle Untersuchungen zur Erhöhung der Zuverlässigkeit, Mitteilungen des Institutes für Bodenmechanik und Felsmechanik der Universität Karlsruhe, Heft 126

Silveira A (1965) An analysis of the problem of washing through in protective filters. In: Proc 6th Int Conf on SMFE, Montreal

van Genuchten (1980) A closed-form equation for predicting the hydraulic conductivity of unsaturated soils, Soil Sci Soc Am J 44:892–898

Vasconcelos WL (1998) Connectivity in sol-gel silica glasses, Quimica Nova 21(4):514–516

Vogel HJ, Roth K (1998) A new approach for determining effective soil hydraulic functions, Eur J Soil Sci 49:547–556

Witt KJ (1986) Filtrationsverhalten und Bemessung von Erdstoff-Filtern, Mitteilungen des Institutes für Bodenmechanik und Felsmechanik der Universität Karlsruhe, Heft 104

Wittmann L (1980) Filtrations- und Transportphänomene in porösen Medien, Mitteilungen des Institutes für Bodenmechanik und Felsmechanik der Universität Karlsruhe, Heft 86

Ziems J (1969) Beitrag zur Kontakterosion nichtbindiger Erdstoffe, Dissertation an der Technischen Universität Dresden

Zou Y (2003) Ein physikalisches Modell der pF-Kurve für teilgesaittigte grobkörnige Böden, Bautechnik 80(12):913–921

Zou Y (2004) Ein erweitertes physikalisches Modell der pF-Kurve für teilgesättigte grobkörnige Böden auf primäre Entwässerung und skundäre Be- und Entwässerung, Bautechnik 81(5):371–378

Part VII

Field Applications

Earthquake-Induced Mudflow Mechanism from a Viewpoint of Unsaturated Soil Dynamics

Motoki Kazama and Toshiyasu Unno

Tohoku University, Graduate School of Engineering, 6-6-06, Aoba, Aramaki, Aoba-ku, Sendai, Japan 980-8579
m-kazama@civil.tohoku.ac.jp, unno@soil1.civil.tohoku.ac.jp

Summary. This paper discusses the general liquefaction state of unsaturated soil related to the mudflow type slope failures observed during earthquakes in areas covered with volcanic ash sand deposits. It is found that the volume compressibility of soil structure, the degree of saturation and the confining pressure are key factors governing the liquefaction of unsaturated soils.

Key words: cyclic shear, suction change, air volume change, liquefaction, mudflow

1 Introduction

Japan has had many experiences of mudflow type slope failures involving volcanic sandy soil during the several earthquakes. It has been suspected that most of the soil of the failed slopes was under unsaturated condition. So far, the unsaturated condition has been assumed tacitly safer against cyclic shear because of the high compressibility of the pore air. Therefore, little attentions has been paid to the shear strength reduction of unsaturated soils subjected to cyclic shear in practical engineering. In facts, it is known that when the degree of saturation decreases to 90%, the cyclic shear strength is double that of fully saturated soil under ordinary testing conditions in the case of fine clean sand Yoshimi et al. (1989). In this paper, firstly the necessity of the research on unsaturated soil dynamics is explained. Secondary, the liquefaction state of unsaturated soils as a three phase material is discussed based on the results of cyclic triaxial test for fine clean sand, with pore air and water responses taken into consideration.

1.1 Mudflow Type Slope Failure During Earthquakes

Mudflow type failures of artificial fill and natural slope have occurred during several earthquakes around the world. Such failures occur especially in regions covered with the volcanic ash sandy soil. Las Colinas landslide, which

Fig. 1. Mudflow type slope failure during the 2003 earthquake in Japan

occurred in El Salvador in 2001 earthquake and resulted in the deaths of over 500 people, is a typical example Konagai et al. (2002). Figure 1 shows an example in Japan which occurred during a 2003 earthquake Uzuoka et al. (2004). The collapsed portion was about 40 m wide and 80 m long, with a depth of about 5 m and an averaged original slope angle of about 7 degrees. It is estimated that the volume of the collapsed soil was about 8,100 m^3. The mudflow destroyed some houses in its path, but fortunately, there was no loss of life.

According to the investigation report, the flowed fill material was a pyroclastic sediment that was classified as a volcanic sandy soil with pumice, and it was unsaturated. Therefore, in the first stage of the research, the authors conducted laboratory shaking table tests to examine the change of the water retention nature of this volcanic sand under an unsaturated condition Unno et al. (2006). It was found that the apparent volumetric water content increased by shaking when the water content was at a certain level. The level of water content corresponded to an in-situ one. This observed behaviour is thought to be attributable to the peculiarity of volcanic sandy soil with pumice, and may be related to mudflow-type slope failure.

1.2 Why Is Unsaturated Soil Dynamics Important?

Past experiences implied that the water retention nature of volcanic sandy soil plays an important role in mudflow type slope failures during earthquakes. This can be explained by soil water characteristic curves. Figure 2 shows the comparison of physical properties between an ordinary fine clean sand and volcanic sandy soil. These two soils are actual soils we have used in experiments.

As shown in the figure, because volcanic sand particles have many micro cavities, its capacity to retain water is much larger than fine clean sand. It

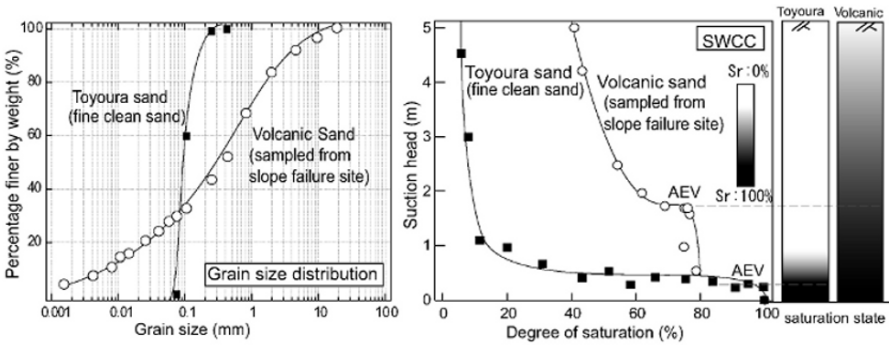

Fig. 2. Comparison of properties between fine clean sand and volcanic sand

results in a high degree of saturation several meters from the free water table. This is a clear indication of the need to study dynamics of unsaturated soils. In the second stage of the research, using the volcanic sandy soil samples from slope failure site, the authors performed cyclic triaxial tests under the unsaturated condition Kazama et al. (2006). In this paper, the general liquefaction state of unsaturated sandy soil is discussed, using a fine clean sand as a representative sand.

2 Cyclic Triaxial Test for Unsaturated Sandy Soils

2.1 Physical Properties of Soils used in the study

As was mentioned in a previous section, for the under unsaturated condition, the cyclic behavior of soils with a high water retention capacity is much more important than that of clean sand from a practical engineering viewpoint. However, the test results of fine clean sand are presented in this section to explain the general liquefaction state for unsaturated soils. Figure 2 shows the grain size distribution of the fine clean sand used in this study. The sand, called Toyoura sand, is representative of fine clean sand in Japan. It has no fine content, and density of soil particle is $2.643\,\mathrm{g/cm^3}$. Its maximum and minimum void ratios are 0.967 and 0.956, respectively. From Figure 2, air entry value can be seen to be 4 to 5 kPa.

2.2 Testing Method

We have conducted cyclic triaxial test for unsaturated soils under the undrained condition and measured the pore air and water pressure responses. The initial soil conditions before cyclic shear loading, such as dry density ($\mathrm{Dr}_0 =$ 60% and 26%), the degree of saturation (0–100%), the confining pressure ($\sigma_{\mathrm{net0}} = 20\,\mathrm{kPa}$ and 60 kPa in target value) and initial suction (0–11 kPa), were the testing parameters.

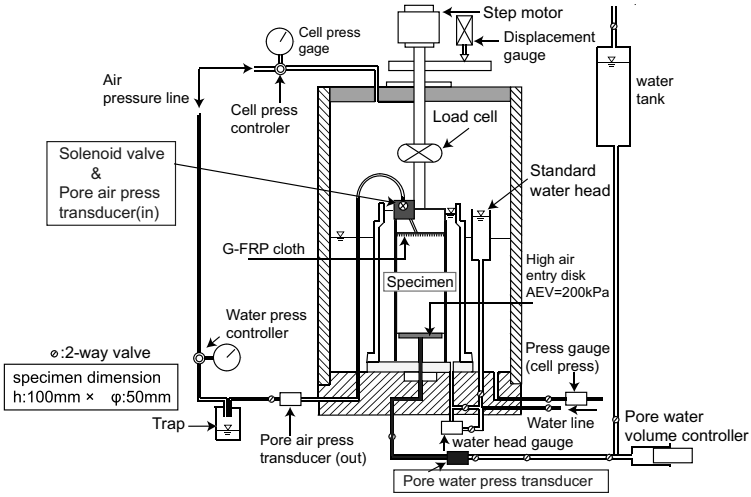

Fig. 3. Cyclic triaxial test apparatus for unsaturated soils

Testing Apparatus

Figure 3 shows a testing apparatus used in this study. The specimens were $d = 50\,\text{mm}$ in diameter and $h = 100\,\text{mm}$ in height. A grass fiber filter and a ceramic disk with an AEV of 200 kPa were installed at the top and bottom of specimen, respectively. The pore air pressure during cyclic shear was measured by the air pressure transducer attached directly above the specimen. A solenoid valve is attached at the right after in order to avoid the effect of the aerial compressibility in the pipe line. The volume of the inner pipe from top of the specimen to the solenoid valve is $0.18\,\text{cm}^3$, which is small enough for accuracy.

Specimen Preparation Method

The method for making the initial condition was as follows. To begin with, 75 cc of water was put into the mold. This corresponds to 95% saturation, or a water content of about 25%. Next, dried sand was dropped through air into the mold. In this condition, the sand absorbs the water, and the specimen becomes a uniform moisture state. In the consolidation process, confining pressure is applied step by step, as shown in Fig. 4. Because of the difficulty controlling the air pressure to achieve the prescribed initial suction state, we controlled the drained water volume. That is, when the target degree of saturation was achieved during a consolidation step, the route of the pore water was closed. After that, the air pressure was controlled to achieve a pore water pressure of 98 kPa (= atmospheric pressure), as shown in Fig. 4.

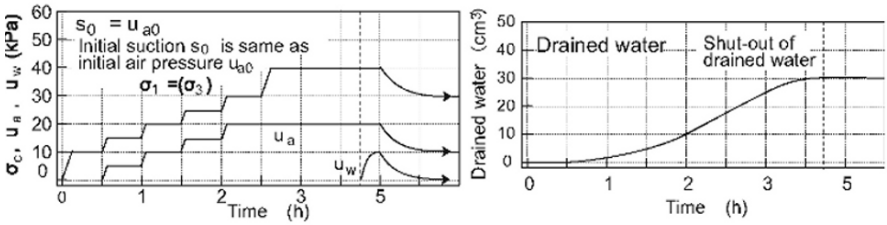

Fig. 4. Specimen consolidation process for achieving initial suction state

Loading Condition

After making the initial isotropical stress state as described, cyclic axial strain was applied under the undrained condition. The axial strain single amplitude of the sinusoidal wave was 0.2, 0.4, 0.8, 1.2, 1.6, 2.0% with every ten cycles. The concept of a strain controlled cyclic shear test is shown in the literature by the first author Kazama et al. (2000). The loading frequency was 0.005 Hz, which was slow enough allow the pore air and pore water response for clean sand to be followed. This point was confirmed in a preliminary test.

Definition of Stress State Variables

It is well known that there are many definitions of effective stress for unsaturated soils. For simplicity, in this study, Bishop's proposed equation was used to evaluate the effective stress Bishop et al. (1960). In the equation, the degree of saturation at initial state was adopted as a suction parameter. Therefore,

$$\sigma'_m = (\sigma_c - u_a) + \frac{S_{r0}}{100}(u_a - u_w) \tag{1}$$

By using the definition above, the effective stress reduction ratio during the cyclic shear can be determined as $1 - (\sigma'_m/\sigma'_{m0})$, where σ'_{m0} is the initial mean effective stress before cyclic shear. This index indicates the degree of effective stress loss ranging from zero to unity, which corresponds that of the initial state to a zero effective stress state due to cyclic shear.

3 Test Results and Discussion

3.1 Representative Test Results

Figure 5 shows an example of a stress strain relationship and an effective stress path for unsaturated soil with a relatively low degree of saturation. It is noteworthy that, even in the case where the degree of saturation is considered relatively small, the soil particle skeleton is degraded by the cyclic shear

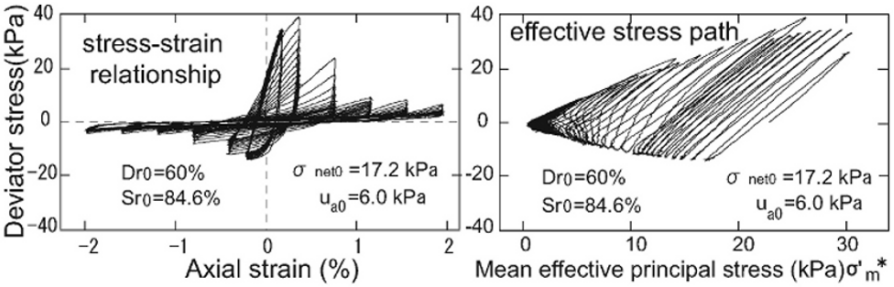

Fig. 5. Test results ($\mathrm{Dr}_0 = 60\%$, $\mathrm{Sr}_0 = 85\%$, $\mathrm{u_{a0}} = 6.0\,\mathrm{kPa}$, $\sigma_{\mathrm{net0}} = 17.2\,\mathrm{kPa}$)

and reaches to the zero effective stress state, thereby causing a failure of the microstructure and engendering the reduction of the soil shear strength.

Figure 6 shows the pore air and water pressure response during the cyclic shear. In the figure, the difference between u_a and u_w, which is indicated by shading in the figure, represents the suction. It is found that pore air pressure gradually increased and reached to the initial mean confining stress at around 3000 seconds. At this point, the net stress reaches zero. The pore water pressure also gradually increased but with relatively large fluctuation and reached the initial mean confining stress at around 7000 seconds. At this point, it can be regarded that netstress and suction contribution to effective stress were completely diminished.

Figure 7 shows the time histories of effective stress reduction ratio for several specimens. As shown in the figure, when the same axial strain history is applied, it is more difficult to reach the effective stress reduction ratio to unity, when the degree of saturation is lower, and the initial confining stress and relative density are higher. Consequently, the final effective stress after cyclic shear of all cases can be written as a function of the initial degree of saturation, as shown in Fig. 8. The liquefaction of unsaturated soils is affected

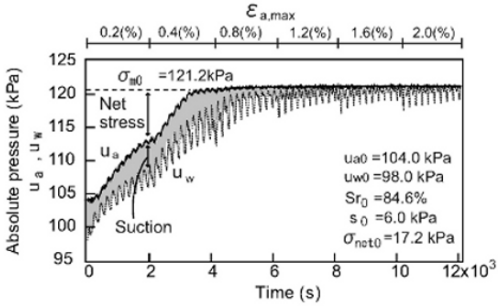

Fig. 6. Time histories of pore air pressure and pore water pressure during the cyclic shear ($\mathrm{Dr}_0 = 60\%$, $\mathrm{Sr}_0 = 85\%$, $u_{a0} = 6.0\,\mathrm{kPa}$, $\sigma_{\mathrm{net0}} = 17.2\,\mathrm{kPa}$)

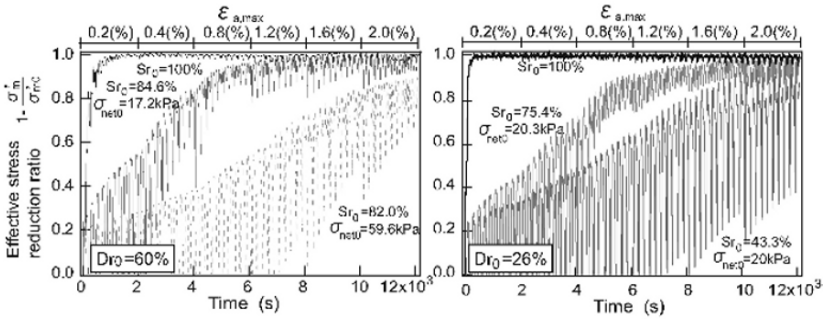

Fig. 7. Time histories of effective stress reduction ratio ($Dr_0 = 60\%$ and 26%)

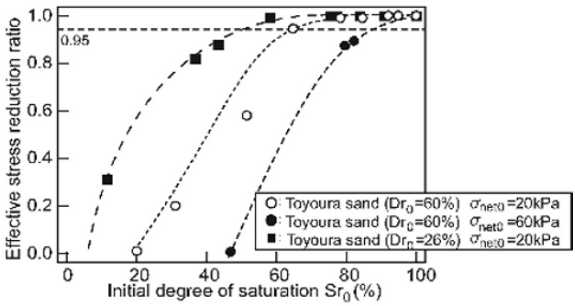

Fig. 8. Effective stress reduction ratio versus the initial degree of saturation

not only by the volume compressibility of the soil structure, which is reflected by dry density, but also by the degree of saturation and the initial confining pressure.

3.2 Discussion on the Liquefaction State for Unsaturated Soils

Based on the test results and equation (1), it can be understood that a complete liquefaction state for unsaturated soils is the condition in which both pore air and water pressure are at the same pressure as the initial mean total confining pressure. If we consider the volume change of pore air ΔV_a between the initial and final full liquefaction states, and if the pore air is assumed to be an ideal gas, the following equation can be obtained.

$$u_{a0} V_{a0} = \sigma'_{m0}(V_{a0} - \Delta V_a) \tag{2}$$

where V_{a0} is the initial volume of pore air. The volume change of pore air ΔV_a represents the volume change of the soil particle structure required to cause complete liquefaction. The relationship expressed in equation (2) can be rewritten by the change of void ratio as follows:

$$e_0 - e_{u_a = \sigma'_{m0}} = \left(1 - \frac{u_{a0}}{\sigma'_{m0}}\right)(1 - S_{r0}/100)e_0. \tag{3}$$

It can be understood that void ratio change required to cause liquefaction is a function of the initial degree of saturation and confining stress.

4 Conclusions

1) Generally speaking, because volcanic sand has a higher water retention capacity than ordinary fine clean sand, the unsaturated zone with a high degree of saturation is thicker. This points to the necessity of further investigations into unsaturated soil dynamics in order to develop an understanding of the mechanism of the mudflow type slope failure.
2) The liquefaction state for unsaturated soil can be defined by the same concept of effective stress used in saturated soil. That is, the liquefaction state is the zero effective stress state.
3) For unsaturated soils subjected to cyclic shear under the undrained condition, both pore air and pore water pressure can reach the initial confining stress, when the volume compressibility of the soil particle structure is high enough.
4) The liquefaction of unsaturated soils is affected not only by the volume compressibility of the soil structure but also by the degree of saturation and initial confining pressure.

References

Bishop AW, Alpan I, Blight GE, Donald IB (1960) Factors controlling the strength of partly saturated cohesive soils, Proc Colorad Conference 503–532

Kazama M, Takamura H, Unno T, Sento N, Uzuoka R (2006) Liquefaction mechanism of unsaturated volcanic sandy soils, J of Geotechnical Engineering, JSCE 62(2):546–561 (in Japanese)

Kazama M, Yanagisawa E, Yamaguchi A (2000) Liquefaction resistance from a ductility viewpoint, Soils and Foundations 40(6):47–60

Konagai K et al. (2002) Las Colinas Landslide Caused by the January 12, 2001 off the Coast of El Salvador Earthquake, J of JAEE 2(1):1–12

Unno T, Kazama M, Uzuoka R, Sento N (2006) Change of moisture and suction properties of volcanic sand induced by shaking disturbance, Soils and Foundations 46(4):519–528

Uzuoka R, Sento N, Kazama M, Unno T (2004) Landslides during the earthquakes on May 26 and July 26, 2003 in Miyagi, Japan, Soil and Foundations 45(4):149–163

Yoshimi Y, Tanaka K and Tokimatsu K (1989) Liquefection resistence of a partially saturated sand, Soils and Foundations, 29(3):157–162

Plate-Load Tests on an Unsaturated Lean Clay

Juan Carlos Rojas[1], Luis Mauricio Salinas[2], and Claudia Sejas[2]

[1] Department of Geotechnical Engineering, University of Naples Federico II, Naples, Italy rojasvidovic@unina.it
[2] Laboratorio de Geotecnia, Universidad Mayor de San Simón, Cochabamba, Bolivia msalinas@fcyt.umss.edu.bo, gtumss@fcyt.umss.edu.bo

Summary. Plate-load tests are a common field method to estimate soil bearing pressure. Classic-result-test interpretations do not consider the matric suction effect. This paper analyzes the matric suction effect in bearing pressure from plate-load tests conducted in a lean clay soil. Seven plate-load tests were carried on in an unsaturated lean clay deposit; two of them were performed in saturated condition to verify the site homogeneity and test repeatability, five of them took into account different matric-suction values. Matric suction along the plate influence zone was monitored with four Jet Fill tensiometers, inserted at 0.1, 0.3, 0.6 and 0.9 m around every test pit. The results show bearing pressure values are highly influenced by matric suction changes.

Key words: plate-load test, bearing pressure, unsaturated soils, field tests

Introduction

The most reliable method to obtain the ultimate bearing capacity at a uniform site is a load test. These kinds of tests are often used to predict the response of buildings foundations and road pavements. If a footing is placed in the capillary zone, the soil below is not fully saturated and a negative pore-water pressure, u_w, is present. However, in the design practice, the bearing capacity of the soil is underestimated because of the actual higher level of stress is not taken into consideration.

The aim of the research was to quantify the effect of matric suction on the in-situ-bearing capacity obtained by means of a plate-load test. A comprehensive experimental testing program was carried out in a field site at Cochabamba, Bolivia on lean clay (CL). Seven tests were conducted under different matric suction values. Matric suction was measured using tensiometers installed at different depths covering the zone of load influence.

Previous Studies

Previous studies considering plate-load tests on unsaturated soils have been published; Table 1 shows a summary of the highlights of these projects. The literature related with deals mainly with four variables: plate size, soil stiffness variation, loading rate and ultimate load definition.

Table 1. Details of plate-load tests performed on unsaturated soils

Author	Soil type	Suction evaluation	Plate base [m]
Steensen-Bach et al. (1987)	sand	tensiometers	$0.1^{\dagger}$, $0.2^{\dagger}$
Larson (1997)	silt	w correlation	0.5^{*}, 1^{*}, 2^{*}
Conciani et al. (1998)	collapsible clay	tensiometers	$0.8^{\dagger}$
Rojas and Salinas (2002)	lean clay	w correlation	$0.8^{\dagger}$
Costa et al. (2003)	clayey sand	tensiometers	$0.8^{\dagger}$
Xu (2004)	expansive clay	w correlation	0.3^{*}
Mohamed and Vanapalli (2006)	sand	tensiometers	0.1^{*}, 0.15^{*}

* square plates; † circular plates

Site Characterization

The test site is located in the city of Cochabamba, Bolivia. Figures 1**a** and 1**b** show the results of cone penetration tests, CPT. The soil profile is presented in Fig. 1**c** to a depth of 3 m. The ground water table was at a depth of about 2.6 m during the cone penetration tests. Fig. 1**c** presents the average results of characterization tests executed in samples gathered from 8 spread points, at profundities of 1.5 m and 2 m.

Figure 2 shows the pressure-plate test data measured by Pardo and Salinas (2006) and the drying branch of the soil-water retention curves, SWRC, obtained following two methods: Fredlund et al. (1997) physico-empirical estimation and Zapata et al. (2000) correlation.

Field Experimental Program

The program was designed with the objective of determining the ultimate bearing capacity of a clayey soil in saturated and unsaturated conditions.

Seven pits, $1.2 \times 3.0\,\mathrm{m}^2$, were excavated up to 1.4 m of depth in order to assure a homogeneous clayey soil profile under the plate and to fulfil ASTM criteria of free space next to the plate (i.e. 4 times the diameter of the plate). Four tensiometers were installed in each pit at depths of 0.1, 0.3, 0.6 and 0.9 m below the base of the pit.

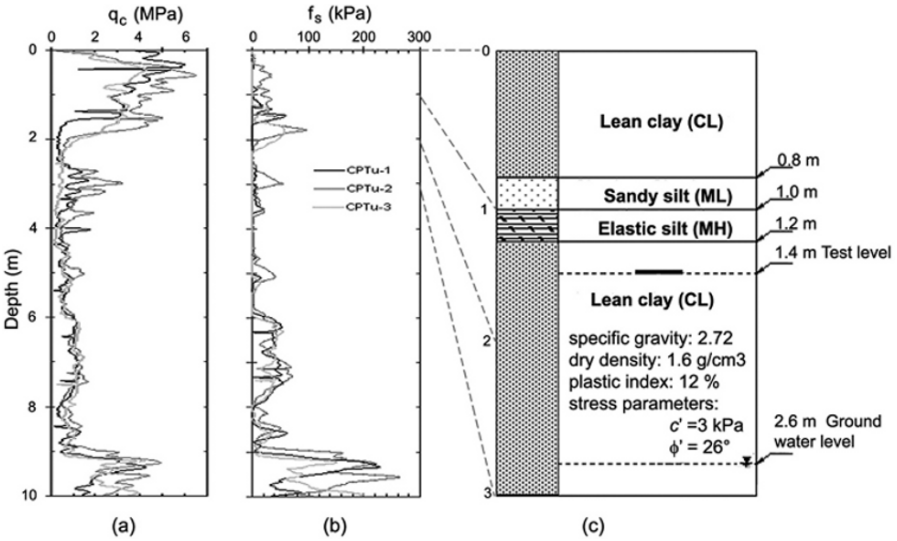

Fig. 1. CPT test results and the first 3 m of soil profile

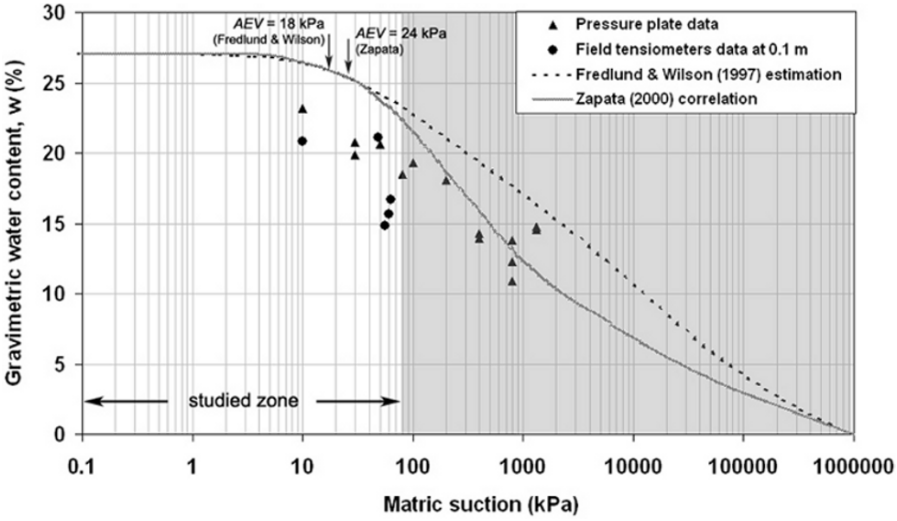

Fig. 2. Estimated soil-water retention curves and matric suctions measurements

Two out of seven excavations (i.e. pits S1 and S2) were filled with water at a constant level and suction was measured; in such a manner the repeatability and deviations of the soil conditions and properties in saturated conditions were verified. It was considered saturation in the soil profile was reached when the suction in the four tensiometers reached the zero value. The rest of the excavations (i.e. pits U1 to U5) were also filled with a constant level of water;

nevertheless, it was taken away before a zero value was observed. This procedure ended up with different suction values in the rest of the five pits.

Seven plate load tests were carried out using a 0.31-m-rigid-circular-steel plate, following ASTM D 1194 standard, a world-wide-accepted procedure. The counter load, 200 kN, was given by a Mercedes Benz truck, prepared by Ap Van Den Berg for this kind of tests. During the execution of each test, measurements of vertical strain were taken until a maximum deformation of 0.03 mm/min for 3 consecutives measurement was read. The number of load increments that was set for the tests was taken with the principle that each increment of load should not be greater than 10% the maximum load to be reached (i.e. 650 kPa due to manometer capacity of the hydraulic jack). In addition, the tests were stopped when the maximum expected pressure was reached or a deformation of 31 mm was observed (i.e. 10% of the plate diameter).

Results and Discussion

The results obtained from CPT tests (Fig. 1) and plate-load tests S1 and S2 (Fig. 3), verified a reasonably repeatability of test results and a low variability of the soil deposit in the selected site.

Figure 3 shows the results of the 7 plate-load tests. As it is expected in this type of soils, none of them show a peak load, therefore, the peak load

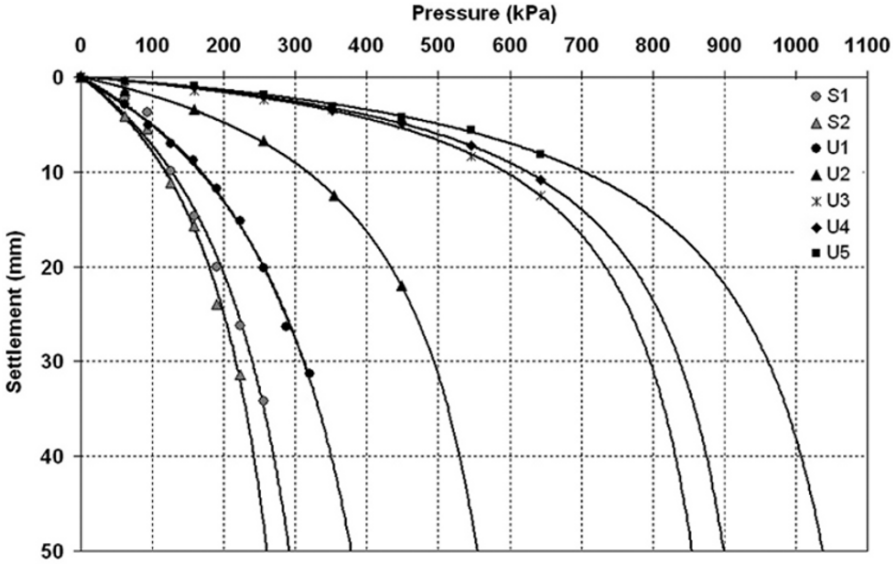

Fig. 3. Pressure-settlement curves

has been estimated by extrapolation of the load-settlement curves using the hyperbolic equation proposed by Kondner (1970).

For homogeneous saturated clay the bearing capacity is considered independent of the foundation breadth. Consoli et al. (1998) determined the effect of footing size on bearing capacity of unsaturated low plasticity clay (CL), and concluded that the effect of the size of the load area in the measured settlement and bearing capacity was shown to be negligible. Thus, the stress-strain characteristics obtained by means bearing capacity do not need corrections. However, the saturated approach assumes constant shear-strain modulus, E, but his variability increases under unsaturated conditions, due to matric suction variations with depth.

The ultimate bearing capacity, q_{PL}, is also defined as the pressure level that corresponds at predefined settlement or to the onset of permanent soil deformation. The standard method ASTM D1194 consider as q_{PL} value the pressure corresponding to a settlement equal to 10% of plate diameter, d. Another criterion is to estimate the q_{PL} value as the stress defined by the intersection of the tangents of the initial and final portions of the pressure-settlement curve, named yield stress criteria (Steensen-Bach et al. 1987, Larson 1997, Consoli et al. 1998, Costa et al. 2003, Xu 2004). Tests S1, S2 and U1, which have the smallest values of suction, present a yield load, the other tests were stopped before the yield load was reached. Table 2 summarizes the bearing capacity values calculated following these criteria.

Additionally, for saturated conditions the theoretical ultimate bearing capacity, q_u, of 115 kPa was calculated using Meyerhof's method. The ratio between the experimental ultimate bearing capacity considering failure criteria, $q_{PL\text{failure}}$, and q_u (Table 2), shows that, for saturated conditions, Meyerhof's

Table 2. Bearing capacity values determined using different criteria

Test	Suction	Bearing capacity [kPa]			$q_{PL\text{unsat}}/q_{PL\text{sat}}$			$q_{PL\text{failure}}/q_u$
	[kPa]	Yield*	ASTM†	Failure	Yield*	ASTM†	Failure	
S1	0	122	244	450	1	1	1	3.9
S2	0	124	220	376	1	1	1	3.3
U1	10	197	316	552	1.6	1.4	1.5	4.8
U2	48	375	499	671	3.0	2.2	1.8	5.8
U3	56	670	802	961	5.4	3.5	2.5	8.3
U4	60	715	844	980	5.8	3.6	2.6	8.5
U5	63	800	968	1112	6.5	4.2	3.0	9.7

* yield stress criteria

† pressure corresponding to 31 mm settlement

$q_{PL\text{unsat}}/q_{PL\text{sat}}$ = ultimate unsaturated − saturated bearing capacity ratio

$q_{PL\text{failure}}/q_u$ = field failure criteria and Meyerhof's method ratio

method greatly under predicts the ultimate bearing capacity, similar results were reported by Larson (1997).

Matric suction values measured before the tests started are summarized in Table 3, together with the water content values measured on samples gathered from similar depths. The matric suction variation during plate loading was not registered, and is not considered in the analysis.

The field values of matric suction-water content, measured at 0.1 m depth, follow approximately the pressure-plate data trend (Fig. 2). This fact is due to the hysteresis of the SWRC. Fredlund et al. (1997) and Zapata et al. (2000) methods provide a main drying curve. By the other hand, the procedure followed by Pardo and Salinas (2006) to condition the undisturbed soil samples before the test (i.e. addition of water on samples surface without reaching the completely saturation) generated a drying scanning curve; then, this SWRC reflects properly the stress history, age, and water changes of the sample. Thus, in the cases were the water content is measured in the field to obtain the matric suction by means of the main drying SWRC, the bearing capacity can be overestimated compared to when the matric suction is determined by measurements in situ.

A representative matric suction value must be defined. In previous works where the matric suction profile was obtained, this value was establish as an average matric suction corresponding to values registered in the stress bulb zone, a depth beneath the plate assumed as $1 \times d$ in Costa et al. (2003) and $1.5 \times B$ in Mohamed and Vanapalli (2006). In this study, the matric suction value registered at 0.1 m depth has been considered as representative of the soil profile, considering the average value does not correspond to experimental evidence and more studies have to be carried on. However, for this case, the average in the stress bulb zone (i.e. $1 \times d$) is almost the same.

The increase of ultimate bearing capacity with matric suction is illustrated in Fig. 4. Due to the scattered points, it is not possible to recognize a clear trend. Mohamed and Vanapalli (2006) and Costa et al. (2003) established that

Table 3. Matric suction and water content values

Test	Matric suction [kPa] at depth [m]				Gravimetric water content [%] at depth [m]		
	0.1	0.3	0.6	0.9	0.1	0.3	0.6
S1	0	0	0	0	27.4	24.5	23.2
S2	0	3	0	0	22.4	23.5	25.8
U1	10	4	13	0	22.8	21.0	22.6
U2	48	38	15	0	21.1	–	–
U3	56	46	4	0	14.8	20.8	22.7
U4	60	53	6	4	15.6	12.1	20.9
U5	63	57	11	0	16.7	9.8	15.2

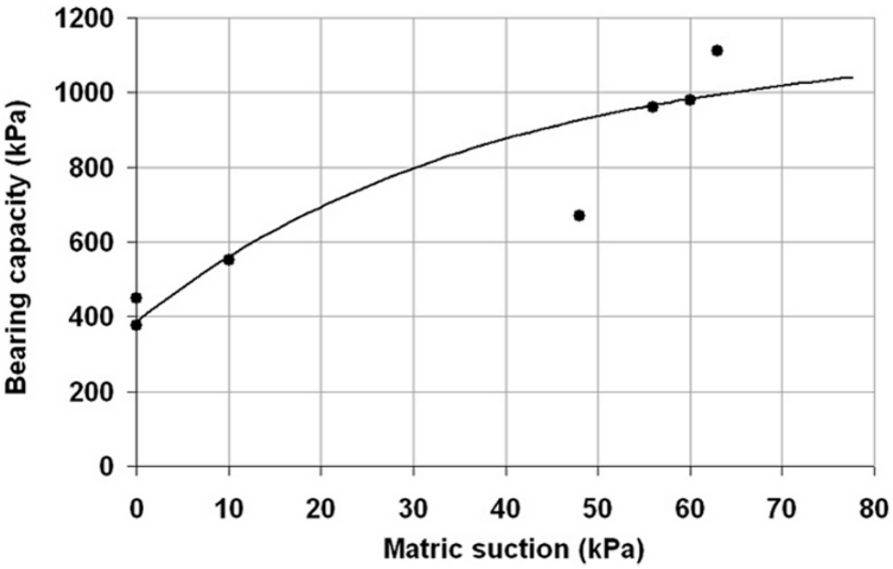

Fig. 4. Variation of bearing capacity at failure with respect to matric suction

the bearing capacity versus matric suction relationship is similar to the shear strength behaviour of unsaturated soils (i.e. a linear increase up to the air entry value and a nonlinear increase beyond the air entry value). Following this criterion, a trend curve has been plotted (Fig. 4).

For the suction range covered in this work (i.e. 0 to 63 kPa), the different criteria to define the ultimate bearing capacity, q_{LP}, does not reflect in the same proportion the matric suction effect (Table 2). For instance, the bearing capacity of U4 test using yield stress criterion is six times higher than the saturated conditions, four considering ASTM norm and three if failure condition is assumed.

Conclusions

The following conclusions are applicable to the results of this experimental program on a lean clay soil.

In order to know the magnitude of suction during a plate load test, it has to be measured in the field. The estimation of the suction by means of the water content of the field might increase its actual value.

For saturated conditions, the ultimate bearing capacity estimated by Meyerhof's theoretical method provided lower values than the ones calculated with the plate load tests.

The different criteria to define the ultimate bearing capacity, q_{LP}, do not reflect the matric suction effect in the same proportion. In the analyzed suction

range, the matric suction effect increase the maximum bearing capacity, from plate-load test, in three to six times, depending on the criteria selected to define the q_{LP}.

The results suggest a considerable contribution of the matric suction to the bearing capacity of the soil.

References

ASTM 1194-94 Standard test method for bearing capacity of soil for static load and spread footings. 2003 Annual book of ASTM Standards 04.08.

Conciani W, Soares MM, Naime JM, Crestana S (1998) Plate load test with CT. In: 2nd International conference on unsaturated soils, Beijing: 333–337

Consoli NC, Schnaid F, and Milititsky J (1998) Interpretation of plate load tests on residual soil site, J Geotechnical and geoenvironmental engineering 124(9): 857–867

Costa YD, Cintra JC, Zornberg JC (2003) Influence of matric suction on the results of plate load tests performed on a lateritic soil deposit, J Geotechnical Testing 26:219–227

Fredlund MD, Fredlund DG, Wilson GW (1997) Prediction of the soil-water characteristic curve from grain-size distribution and volume-mass properties. 3rd Brazilian symposium on unsaturated soils, Rio de Janeiro, Brazil

Kondner RL (1970) Hyperbolic stress-strain response: cohesive soils, J Soil Mechanics and Foundations Division 93:283–310

Larson L (1997) Investigations and load tests in silty soils. Swedish Geotechnical Institute, Report No. 54

Larson L (2001) Investigations and load tests in clay till. Swedish Geotechnical Institute, Report No. 59

Mohamed FMO, Vanapalli SK (2006) Laboratory investigations for the measurements of the bearing capacity of an unsaturated coarse-grained soil. Canadian geotechnical conference, Vancouver 2006 (in print)

Pardo JM, Salinas LM (2006) Curva de retención de agua del suelo (SWRC): Análisis de estimaciones y ajustes. IV Congreso de Ciencia del Suelo, Bolivia

Rojas JC, Salinas LM (2002) Bearing pressure and settlement for a lean clay in saturated and unsaturated conditions. In: Proceedings of 3rd Unsaturated Soils Conference, Recife, Vol. 2:703–708

Steensen-Bach JO, Foged N, Steenfelt JS (1987) Capillary induced stresses – fact or fiction? In: Proceedings 9th European conference on soil mechanics and foundation engineering: 83-89

Xu Y (2004) Bearing capacity of unsaturated expansive soils, J Geotechnical and Geological Engineering 22:611–625

Zapata CE, Houston WN, Houston SL, Walsh KD (2000) Soil-water characteristic curve variability. Advances in unsaturated geotechnical special publication, No. 99

Selfsealing Barriers of Clay/Mineral Mixtures. The SB Project at the Mont Terri Rock Laboratory

Tilmann Rothfuchs, Rüdiger Miehe, Norbert Jockwer, and Chun-Liang Zhang

GRS-Final Repository Research Division, Theodor-Heuss-Strasse 4, D38122 Braunschweig, Germany
Tilmann.Rothfuchs@grs.de, Ruediger.Miehe@grs.de, Norbert.Jockwer@grs.de, Chun-Liang.Zhang@grs.de

Summary. Clay/sand mixtures are currently being investigated at GRS's geotechnical laboratory on their suitability for sealing disposal rooms containing gas generating radioactive waste. It has been found that moderately compacted mixtures may represent a reasonable alternative to highly compacted bentonite envisaged as buffer in various multi-barrier repository concepts. In contrast to highly compacted buffers moderately compacted clay/sand mixtures exhibit a comparably low gas entry/break through pressure in the saturated state while providing an adequate sealing potential due to swelling of the clay minerals in consequence of water uptake from the host rock. The evolution of high gas pressure in the repository near-field due to corrosion of the waste containers will thus be avoided while possible migration of radionuclides from the waste matrix through the buffer will be diffusion controlled. Besides laboratory investigations and mockup testing, full-scale experiments are being conducted at the Mont Terri Underground Rock Laboratory to test and demonstrate the advantageous sealing properties of moderately compacted clay/sand-mixtures under representative in-situ conditions.

Key words: radioactive waste repository, barrier, clay/sand-mixture, swelling pressure, permeability, gas entry pressure

1 Introduction

To completely seal radioactive waste from the biosphere various repository concepts rely on a multiple engineered barrier system (EBS). Some of these concepts involve highly compacted bentonite buffers between the waste containers and the host rock.

Considering these concepts in more detail, there is a concern about gas pressure built-up in the near-field once formation water re-saturates the buffer and leads to start-up of hydrogen gas generation by corrosion of the canisters.

According to Rübel et al. (2003), clay formations like the Opalinus clay provide enough water to completely corrode metallic high-level waste canisters. Up to 481 m^3 of hydrogen gas would be produced per canister by its complete corrosion. Because of the very low permeability of the bentonite buffer after re-saturation, gas migration is hindered and a higher gas pressure may evolve in the repository near field. In case the least principal stress and the tensile strength are exceeded, fracturing and disintegration of the buffer and/or the host rock may take place.

Moderately compacted clay/sand mixtures have been found to represent a suitable alternative to highly compacted bentonite buffer (Jockwer et al. 2000, Miehe et al. 2003). After re-saturation, such mixtures exhibit a comparably low gas entry/break through pressure while providing an adequate sealing potential against intruding water due to swelling of the clay minerals after water uptake from the host rock. By using optimized material mixtures, the parameters of primary interest, such as permeability to gas and water, gas entry pressure in the saturated state, and two phase-flow parameters can be adjusted to the prevailing local conditions of the host rock in a way that the buffer material acts as a gas vent thereby avoiding the generation of higher gas pressure in the repository near field.

The most important properties the material mixtures must fulfil in comparison to those of the host rock are:

- Low permeability to water in the saturated state between 10^{-17} to 10^{-18} m^2 in analogy to the permeability of the excavation disturbed zone (EDZ) in the host rock.
- Gas entry pressure or break-through pressure lower than that of the host rock.
- Higher permeability to gas than that of the host rock after break-through.
- Swelling pressure lower than the least principal stress in the host rock in order not to disturb the integrity of the host rock.

The SB (**S**elf-sealing Clay/Sand-**B**arriers) project started in summer 2003 comprises material characterization in the laboratory as well as the conduction of confirmative mockup test in the laboratory and in-situ experiments at the Mont Terri Rock Laboratory (MTRL) in Switzerland.

2 Laboratory Characterization of Moderately Compacted Clay/Sand-Mixtures

On basis of the experiences gained in the preceding projects the laboratory investigations within the SB-project were focused on samples with clay/sand mixing ratios of 35/65, 50/50, and 70/30. The bentonite used is a commercially available calcium-type, named Calcigel, produced from the company Süd-Chemie AG in Germany. The sand is a quartz sand with grains less than 2 mm. The bentonite has a grain density of 2.7 g/cm^3 and an initial water

content of 8%, while the sand has a grain density of $2.67\,g/cm^3$ and a water content of 1%. Water content was determined by drying the materials in an oven according to DIN 18121–1. The density of the mixtures achieved by mixing bentonite and sand together in an electric mixer ranges from 1.40 to $1.88\,g/cm^3$.

The most interesting parameters such as permeability to gas and water, swelling pressure, gas breakthrough pressure were measured in specially developed oedometer cells of 50 mm diameter and 50 mm.

The gas permeability in the initial dry state was determined by injecting nitrogen gas. The determined data range between $1.23 \times 10^{-13}\,m^2$ (35/65 clay/sand mixture) and $1.16 \times 10^{-15}\,m^2$ (70/30 clay/sand mixture). The water permeability was determined by injecting synthetic clay formation water as well as fresh water and salt brines. The results for the different liquids are compared in Fig. 1. It can be seen that the permeability to water of the mixtures decreases with the clay content and with increasing density. The mixtures with clay/sand ratios of 35/65 and 50/50 exhibit very low permeability to clay water of less than $10^{-17}\,m^2$, and thus meet the above mentioned requirement of 10^{-17}–$10^{-18}\,m^2$ for the seals. It is also interesting to see that the permeability to fresh water is about one order of magnitude lower than that to salt brine and clay water.

The gas break-through pressure of the investigated mixtures ranges between 0.2 and 2.8 MPa and increases clearly with the clay content. Figure 2 depicts as an example a measurement on a moderately compacted 50/50 clay/sand sample. The determined average gas permeability after gas break-through amounts to about $10^{-17}\,m^2$ for 35clay/65sand samples and to about $5 \times 10^{-18}\,m^2$ for 50clay/50sand samples (see Table 1) and is considered sufficiently high in comparison to the permeability of the intact Opalinus clay which is in the order of 10^{-20} to $10^{-22}\,m^2$.

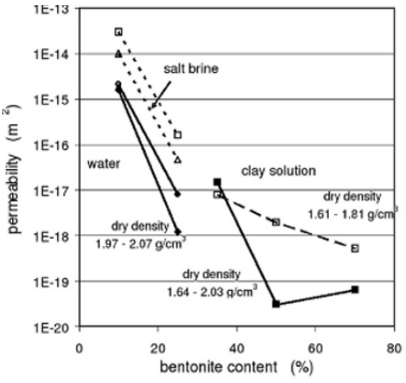

Fig. 1. Permeability of clay/sand mixtures to different fluids as a function of clay content

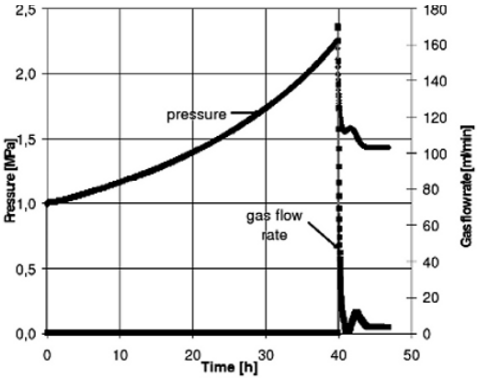

Fig. 2. Gas pressure and flow rate evolution during a gas break-through test of a moderately compacted 50clay/50sand sample

The swelling pressures were measured after full re-saturation with synthetic clay water. The average values of 0.2 to 0.4 MPa are significantly below the upper limit of 2 MPa which represents the least principle stress at MTRL. Average data measured on the moderately compacted clay/sand mixtures are summarized in Table 1.

Table 1. Hydraulic data determined on moderately compacted clay/sand mixtures in comparison to required material properties

Clay/ sand ratio	Dry density (g/cm^3)	Porosity (%)	Gas permeability at dry conditions (m^2)	Water permeability at full saturation (m^2)	Gas breakthrough pressure (MPa)	Gas permeability after gas breakthrough (m^2)	Swelling pressure (MPa)
35/65	1.88	29.8	$1 \cdot 10^{-13}$	$3 \cdot 10^{-17}$ $\sim 9 \cdot 10^{-18}$	0.4 ~ 1.1	$1 \cdot 10^{-17}$	0.2
50/50	1.67	37.7	$5 \cdot 10^{-14}$	$1 \cdot 10^{-18}$ $\sim 4 \cdot 10^{-18}$	0.4 ~ 2.8	$5 \cdot 10^{-18}$	0.3
70/30	1.40	48.0	$1 \cdot 10^{-15}$	$5 \cdot 10^{-19}$	1		0.4
Requirements							
			high	$1 \cdot 10^{-17}$ $\sim 1 \cdot 10^{-18}$	< 2	high	< 2

In general, the investigated mixtures with bentonite contents higher than 30% and with installation densities around 1.9 g/cm^3 meet the requirements that are to be considered in the specific case of the MTRL.

3 In-Situ and Full-Scale Mockup Experiments

The SB in-situ experiments are specially designed to enable the investigation of the sealing properties of moderately compacted clay/sand mixtures which are most important with regard to the long-term evolution of the repository. Four individual experiments will be conducted in boreholes of 0.31 m diameter and 3 m depth drilled from the floor of a test niche of 5 m width, 4 m height and 8 m length (Fig. 3). The lower part of the boreholes, the injection volume, is filled with a porous material (e.g. sand). Above the injection volume a filter frit is placed for ensuring a homogeneous distribution of the injected water over the entire borehole cross section. The clay/sand-seal is installed in several layers to a height of 1 m above the frit. At the top of the seal, a further filter frit is installed for water and gas collection. The whole borehole will be sealed against the ambient atmosphere by a gastight packer. The most upper part of the test borehole is grouted for keeping the packer in place. No instruments

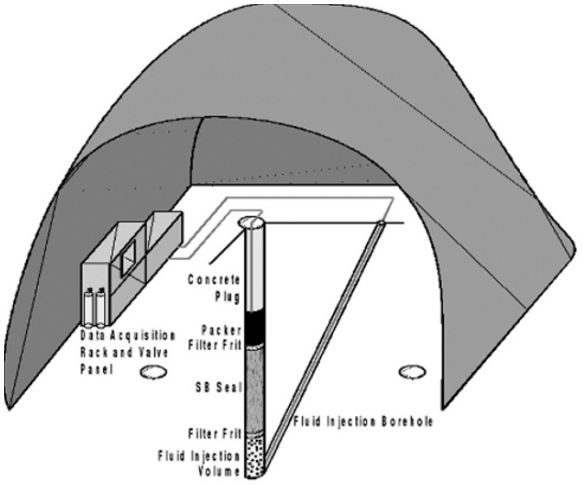

Fig. 3. Principle design of a SB-borehole sealing test

are installed in the SB seal itself to avoid any negative impact on the sealing properties.

For re-saturation of the seal, synthetic clay formation water is injected into the lower injection volume. The water flow through the seal is collected in the upper frit by a further tube running back to the control valve panel where water flow rate and pressure are controlled and measured.

For the design of the in-situ tests, scoping calculations were performed using the FE code CODE-BRIGHT (UPC 2002) developed by the Technical University of Catalonia in Barcelona. In the modelling, gas and water flow are modelled according to Darcy's law, the molecular diffusion of water vapour is governed by Fick's law, the solubility of air in water is controlled by Henry's law, and an elasto-plastic model (BBM) which is able to represent swelling and shrinking features of unsaturated soils is applied for the description of the mechanical behaviour of the mixtures. The parameters were established on basis of preliminary laboratory tests described in (Rothfuchs et al. 2005). Figure 4 illustrates the predicted evolution of water re-saturation of a 1 m long moderately compacted seal of 35% clay and 65% sand in a test borehole. According to the calculation full saturation may be reached at an injection pressure of 1 MPa after about 170 days.

Before going in situ, full-scale mockup tests have been started in March 2005 at the GRS geotechnical laboratory, in order to test proper installation methods for achieving the pre-determined installation density, to determine the time needed to reach full saturation and to determine the permeability to gas and water as well as swelling pressure, gas breakthrough pressure and permeability after re-saturation under ideal laboratory conditions. The first experiment under representative in-situ conditions was started at Mt. Terri in October 2005.

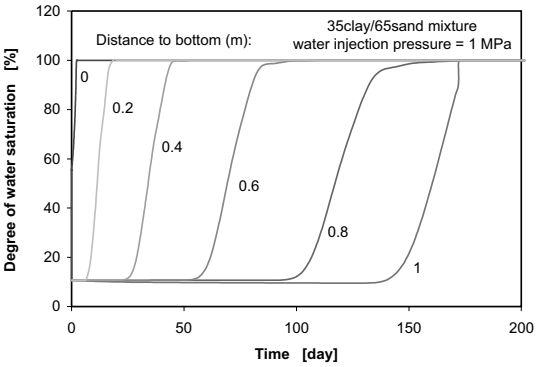

Fig. 4. Predicted evolution of water saturation in a moderately compacted 35clay/65sand seal of 1 m length

In both cases the most promising 35/65 clay/sand mixture has been installed. The installation densities achieved amount to 1.94 g/cm^3 in the mockup and 1.91 g/cm^3 in the in-situ experiment. These values are quite similar to those of the moderately compacted laboratory samples (compare Table 1). At the beginning of both experiments the permeability to gas of the dry material was measured first. The determined values amount to 6.2×10^{-14} m^2 for the mockup and to 3.71×10^{-14} m^2 for the in situ experiment. These values agree very well with the data determined at the small samples in the laboratory (see Table 1).

By June 2006 about 23 litres of water have been injected in the mockup at an injection pressure of 1.1 MPa while an amount of 22 litres has been injected at an injection pressure of 0.4 MPa in the in-situ experiment. While the total pressure evolution is measured at three different levels along the tube wall and at top of the seal in the mockup it is measured in situ only at top of the seal.

While the water pressure sensors mounted along the tube wall in the mockup allow an assessment of the evolution of the seal saturation in the mockup this is not possible in situ since no instruments are allowed in the seal to avoid any bypassing of water along instrument cables. The swelling pressure of the clay/sand mixture, however, which is a useful indicator of the sealing properties, can be assessed in both experiments by observation of the total pressure at the two pressure sensors mounted in both set ups at top of the seal.

Figure 5 shows the pressure evolution in the mockup measured along the tube wall. At the lower level, 14 cm into the seal, the pressure reached rather quickly the level of the injection pressure of about 1.1 MPa. At the middle level the actual value ranges around 1.05 MPa. No pressure increase can be observed so far at the upper level at 86 cm in the seal. One of the sensors at the seal top, however, shows a pressure increase of about 0.04 MPa (Fig. 6)

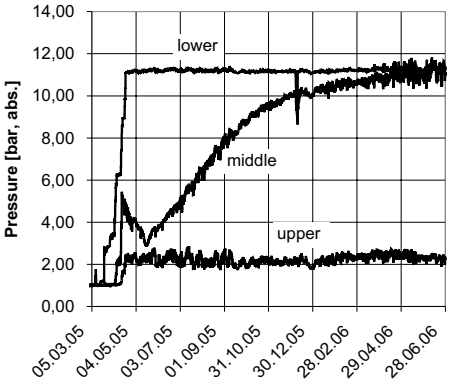

Fig. 5. Evolution of total pressure along the mockup tube wall

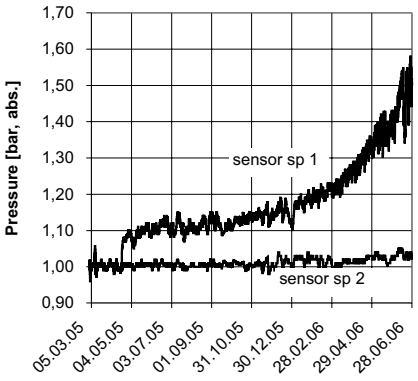

Fig. 6. Evolution of total pressure at top of the mockup-seal

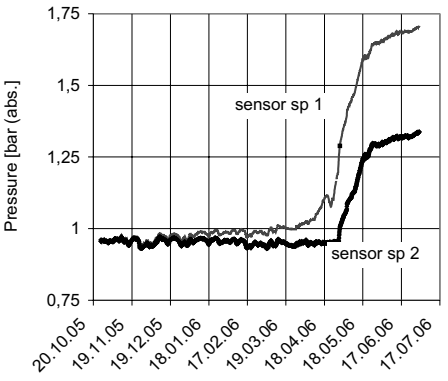

Fig. 7. Evolution of total pressure at top of the in-situ seal

which is quite comparable to a similar pressure increase of about 0.05 MPa observed in situ (Fig. 7).

Figures 6 and 7 indicate that the swelling pressures which will be reached in the mockup and the first in-situ experiment will be in the same order of magnitude as that determined on the laboratory test samples (compare the value of 0.2 MPa Table 1). Thus, similar sealing properties as observed on small samples in the laboratory can be expected in the in-situ experiment.

4 Conclusions

The preliminary results of the running SB mockup and in-situ experiment at the MTRL indicate confirmation of the advantageous sealing properties of moderately compacted clay/sand mixtures preliminarily determined on small samples under ideal conditions in the laboratory. The time needed to reach

full saturation of the test seals in both the mockup and the in-situ experiment, however, seems to exceed the predicted ones significantly. Further efforts will be needed to clarify the observed discrepancies and to achieve appropriate process understandding and model improvements.

Acknowledgements

The authors gratefully acknowledge the funding of the SB-project by the German Federal Ministry of Economics and Technology (BMWi) under contract No. 02E9894 and by the Commission of the European Communities (CEC) under contract No. FI6W-CT-2003-508851.

References

Jockwer N, Miehe R, Müller-Lyda I (2000) Unter-suchungen zum diffusiven Transport in Tonbarrieren und Tongesteinen. Gesellschaft für Anlagen- und Reaktorsicherheit (GRS) mbH, Köln, GRS-167

Miehe R, Kröhn P, Moog H (2003) Hydraulische Kennwerte tonhaltiger Mineralgemische zum Verschluss von Untertagedeponien (KENTON), Gesellschaft für Anlagen- und Reaktorsicherheit (GRS) mbH, Köln, GRS-193

Rothfuchs T, Miehe R, Jockwer N, Zhang C-L (2005) Self-Sealing Barriers of Clay/Mineral Mixtures in a Clay Repository – SB Experiment in the Mt. Terri Rock Laboratory, Gesellschaft für Anlagen- und Reaktorsicherheit (GRS) mbH, GRS-212

Rübel A, Nosek U, Müller-Lyda I, Kröhn P, Storck R (2003) Konzeptioneller Umgang mit Gasen im Endlager, Gesellschaft für Anlagen- und Reaktorsicherheit (GRS) mbH, GRS-205

UPC (2002) CODE-B l media, USER'S GUIDE

Preferential Water Movement in Homogeneous Soils

Alexander Scheuermann and Andreas Bieberstein

Institute of Soil Mechanics and Rock Mechanics, Division of Embankment Dams and Landfill Technology, University of Karlsruhe (TU)
alexander.scheuermann@ibf.uka.de,
andreas.bieberstein@ibf.uni-karlsruhe.de

Summary. Preferential water movement is a frequently observed phenomenon in soil science. Especially on natural slopes hydraulic behaviour can sometimes be observed which arises from preferential water flow. If the soil consists of a more or less homogeneous material, the preferential water movement can be caused only by heterogeneously distributed water. A sprinkler irrigation test on a large scale homogeneous dyke model and corresponding measurement results using different techniques have shown on the one hand, that preferential water flow in the form of fingering possibly occurred during the experiment. On the other hand, lateral water movement due to heterogeneously distributed water content inside the dyke body could be observed. Both phenomena were also investigated in simple laboratory experiments. The contribution presents results from the above mentioned experiment which are analysed and discussed.

Key words: preferential flow, fingering, capillary barrier effect, experimental investigation

1 Introduction

Preferential water flow is mainly seen to arise due to structural heterogeneities of the soil. The random stratification – especially in granular soils – can cause capillary barrier effects governed by the unsaturated hydraulic properties of the underlying coarser soil (Stormont and Clifford 1999). Water movement across the interface occurs in this connection when the matric suction at the interface reaches the so-called breakthrough head of the underlying coarser soil layer, defined as the matric suction when the coarser layer becomes conductive. The matric suction corresponds in this case approximately to the water entry value ψ_{WEV} which can be estimated from the appropriate soil water imbibition curve (Baker and Hillel 1990). In this sense the breakthrough of water only depends on the soil hydraulic properties of the coarser material and

is independent of the properties of the overlying finer soil and the hydraulic boundary conditions.

In a similar manner, preferential water flow in the form of fingering can occur in stratified soils. The development of fingers at the interface of two adjacent layers or at the transition from wet to underlying dry conditions can also be considered as a kind of breakthrough. Fingering is well known as the result of an unstable wetting front (Hill and Parlange 1972) caused by unfavourable conditions above or below the wetting front (e.g. water infiltration during overpressure in the air phase). According to Hillel and Baker (1988), a concentrated water flow in the form of fingering can occur, if the unsaturated hydraulic conductivity at the water entry value $k_u(\psi_{\mathrm{WEV}})$ of the underlying layer or area is higher than the prevailing infiltration rate from above. As is generally known, water infiltrates into a soil much more easily if the soil is in an initially wet condition. Thus in this case the development of fingers depends on the soil hydraulic properties of the underlying layer and the initial moisture condition as well as on the hydraulic boundary conditions.

Consequently both effects are based on the same physical property, namely on the water entry value of the underlying soil. Hence it is not surprising that both phenomena can occur similarly where there are stratified soil conditions (Walter et al. 2000). Differences in the water content distribution can intensify such hydraulic behaviour of soils (Stephens and Heermann 1988). But also in homogeneous soils, preferential flow in the form of lateral water movement can occur due to anisotropic water content distribution (McCord et al. 1991). The triggering factor in this connection is the sudden change of the matric suction at the water front.

2 Observations on the Full-Scale Dyke Model

Measurement results during a sprinkler irrigation test on a full-scale dyke model have indicated that both phenomena possibly occurred simultaneously during the experiment. In this connection, a newly developed moisture measurement technique based on Time Domain Reflectometry (TDR) was applied for the first time on such a scale in order to observe the spatially distributed soil moisture content (Spatial-TDR). Additional laboratory experiments were carried out in order to verify the observations on the dyke model. In the following the dyke model as well as the measuring technique Spatial-TDR will be described. Later on the results from the experiment on the full-scale dyke model will be presented and discussed in comparison to the results of the laboratory experiments.

2.1 Design and Instrumentation of the Model

In order to investigate transient seepage through dykes, the full-scale dyke model in Fig. 1 at the Federal Waterways and Research Institute in Karlsruhe

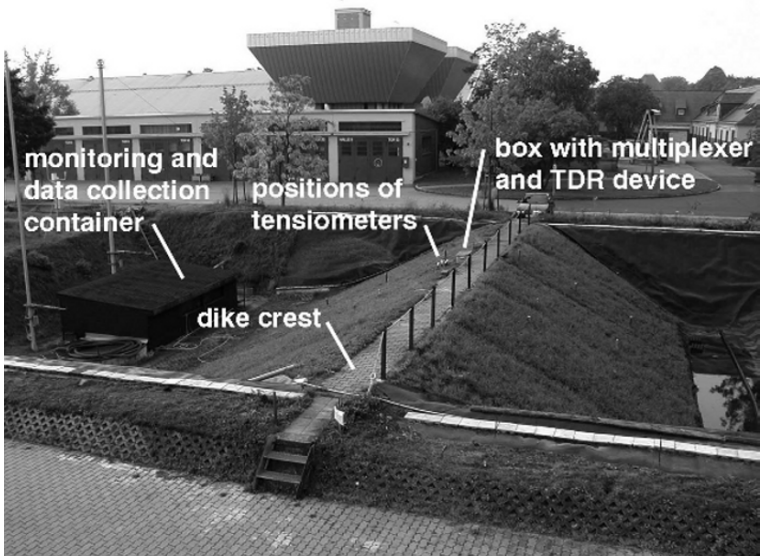

Fig. 1. Full-scale dyke model at the Federal Waterways and Research Institute in Karlsruhe (upstream side on the right)

was made available for the experiment. The dyke is constructed homogeneously with uniform sand (grain size 0.2–2 mm) and is situated on a base consisting of waterproof plastic sheets, so that water infiltrating into the dyke body will flow to a drain at the toe of the downstream slope. The slope inclinations are 1:2.0 on the upstream side and 1:2.25 on the downstream side. Both slopes of the dyke are covered with an approximately 20 cm thick topsoil layer. The discharge of the water collected in the drain is recorded in the monitoring and data collection container.

In order to assess the pore water pressures within the dyke body, the model is equipped with piezometer gauges which are also distributed along the base of the dyke. Furthermore, the condition of the capillary forces can be observed using tensiometers vertically installed in one profile (cf. Fig. 2).

With the aim of observing water content changes within the dyke body, a new monitoring system based on Time Domain Reflectometry (TDR) was installed in the model. The advantage of this system is its high resolution both in space and time which is required for monitoring transient water content changes. The system consists of 12 flat ribbon cables from 1 to 3 m in length which are installed vertically inside the dyke (cf. Fig. 3). They are connected on both sides with coaxial cables to a multiplexer and a TDR-device in a box on the crest of the dyke. Using adapted programmes a conventional PC, located in the container at the toe of the downstream slope, takes over data collection and controlling of the measuring equipment (multiplexer and TDR-device). With this system the data acquisition time for the whole cross

section is only 5 minutes. The changes in water content are determined with a spatial accuracy of about 3 cm and an accuracy of ±2 Vol-% (volumetric water content) compared to independent water content measurements. Below, the TDR measuring method and the modifications for the spatial assessment of the water content along the extended sensors will be described.

2.2 Spatial Time Domain Reflectometry (Spatial-TDR)

Time Domain Reflectometry (TDR) is a widely used method for the determination of the water content in soils. With the conventional method, a fast rise voltage step is launched from a TDR-device into a sensor consisting of two or three wires of non-insulated metallic rods buried into the soil (cf. Fig. 4 on the left). At the transition between coaxial cable and sensor a portion of the signal is reflected. The remaining signal travels along the sensor until it is completely reflected at the open end. An oscilloscope within the TDR-device records the sum of the incident signal and the reflected signal, also called the TDR trace, from which the travel time and the mean wave velocity in the sensor can be determined.

The permittivity of the surrounding soil can be calculated from the wave velocity. The permittivity of the soil is dependent on the dielectric properties of the soil constituents: air (1), grain (3–8) and water (80). Therefore, it is possible to determine the volumetric water content using appropriate calibration functions (e.g. Topp et al. 1980). As the use of non-insulated metallic rods as sensors for TDR measurements in soils is limited to about 1 m, a flat ribbon cable has been developed which can be used in soils over several meters (see Fig. 4 on the right, cf. Hübner et al. (2005)).

The TDR trace contains far more information than the travel time of the reflected signal, since the signal responds also to changes in the water content along the sensor. In order to use this additional information, a three step algorithm has been developed to reconstruct the soil moisture profile from the signal response along the sensor (Schlaeger 2005). This new TDR measurement system consisting of a recorded TDR trace with spatial analysis

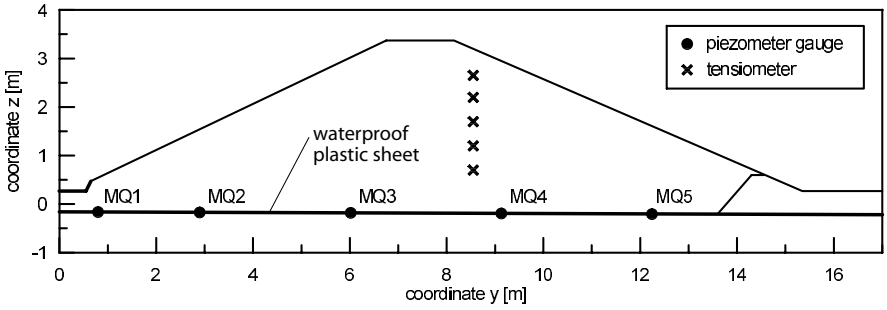

Fig. 2. Positions of piezometer gauges and tensiometers within the dyke body

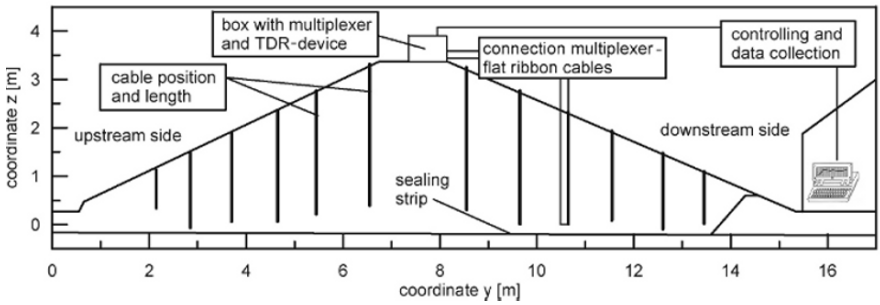

Fig. 3. Positions and lengths of the flat ribbon cables in the cross section of the dyke and schematic description of the measuring system

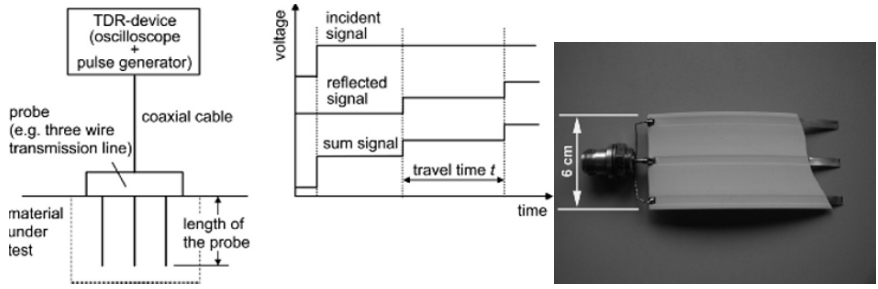

Fig. 4. Left: Basic TDR setup and typical TDR trace (schematic), right: Flat ribbon cable

has already proven its effectiveness in various applications (Hübner et al. 2005, Scheuermann and Bieberstein 2006) and is called as Spatial-TDR.

2.3 Experimental Investigations

The aims of the investigations on the full-scale dyke model were to observe water balance processes and to quantify the influence of the initial water content distribution inside the dyke on the transient seepage in the case of a flood event (cf. Scheuermann and Bieberstein 2005). For this purpose, an extreme precipitation event for Karlsruhe expected to occur once in every 100 years (148 mm in three phases over 72 h) was simulated using sprinkler irrigation equipment. Figure 5 shows the resulting hydrographs of the parameters measured. The grey columns in the graph at the top represent the amount of water irrigated during the experiment and the line in the same graph shows the discharge from the drain measured in the data collection container. The mean saturation is given in the graph below. The small black dots are measured with the Spatial-TDR measuring system and the grey rhombuses are determined manually using a tube probe (IMKO), which is also based on TDR. The next five graphs show the measurement of the matric potential at the tensiometers

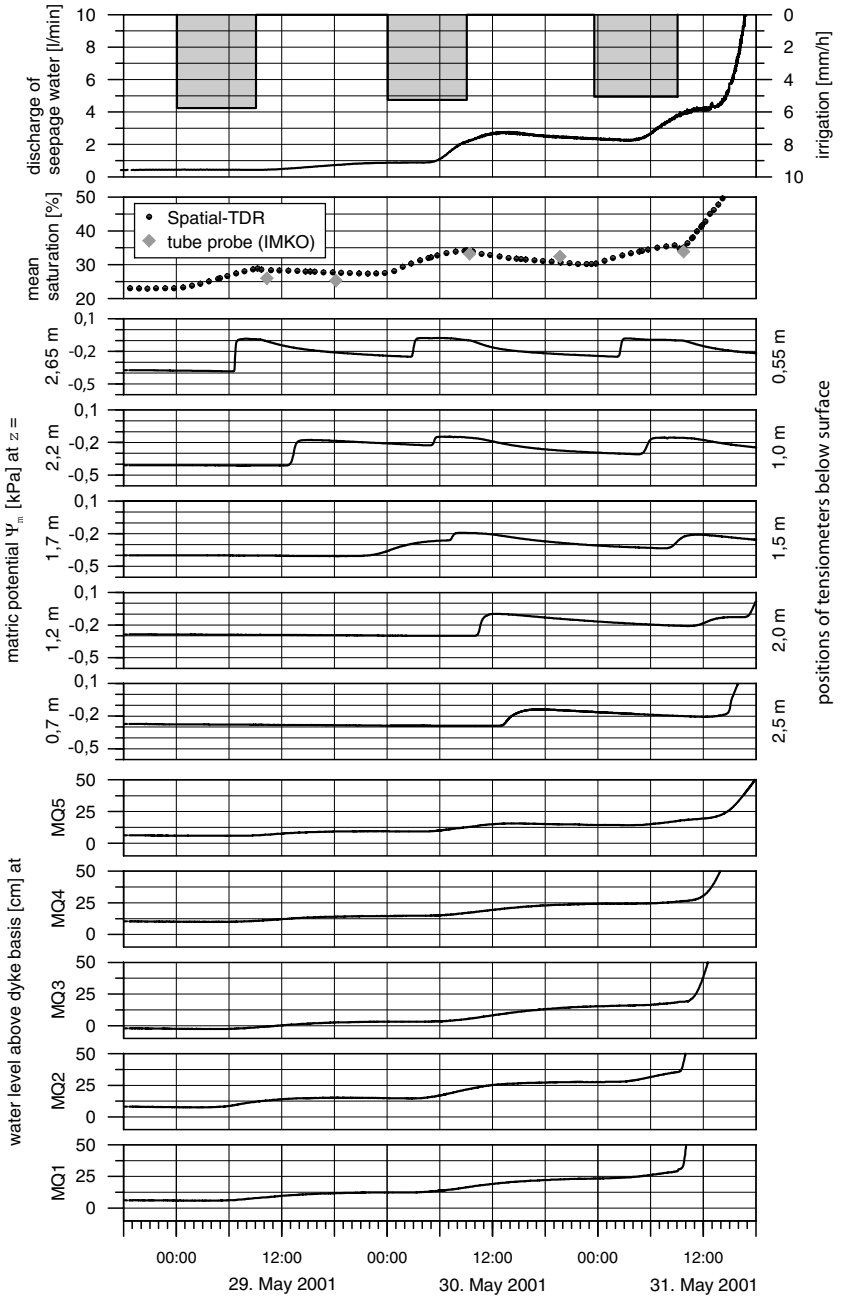

Fig. 5. Temporal evolution of irrigation, discharge, mean saturation, matric potential and water level above dyke base during the irrigation experiment (cf. Fig. 2)

(cf. Fig. 2). The graphs of the tensiometer measurements are arranged starting with the flattest tensiometer at the top and finishing with the one installed in the deepest position. The last five graphs give the measurements of the water level above the dyke base with piezometer gauges. Here the graphs are arranged starting with the piezometer near the drain at the top and finishing with the piezometer on the upstream side (cf. Fig. 2). From the graphs of Fig. 5 the temporal changes of the state variables within the dyke body can be recognised very easily. The first phase of irrigation started at midnight on May 29th. The corresponding saturation distribution is given in Fig. 6**a**). The dotted lines represent the positions of the individual flat ribbon cables together with the measured saturations at these locations (cf. colour bar in Fig. 6). For a better visualisation, the single measurements were interpolated over the observed area in the cross section. The dark colours show the wet zones, whereas the light grey colours represent the more dry zones.

As expected, the mean saturation measured with Spatial-TDR shows the first changes only a few hours after the beginning of the first irrigation phase (cf. Fig. 5). The top tensiometer at a depth of 0.55 m registered the first increase in the matric suction indicating the arrival of the water front approximately 7 h after the start of the experiment. The closed water front, which moves downwards, can be observed very well from the temporal evolution of the matric potential measurements. However the first increase in the water level above the dyke base can be recognised at almost every piezometer gauge after approximately 9 h (see graphs for MQ1 to MQ5 in Fig. 5). At this point in time the water content above the dyke base in the middle of the cross section shows almost no change (cf. Fig. 6**b**)).

One possible explanation for the observation of a rise in the water table near the dyke base without any obvious water content changes directly above the base is preferential water flow in the form of fingering. This phenomenon occurs for example when the moving wetting front reaches an unstable condition, which means that the water front begins to develop concentrated flow paths, the so-called fingers.

After the last irrigation phase (9:00 on May 31st) the saturation distribution of Fig. 6**c**) was measured. It can be seen that despite the high quantity of irrigated water, no homogeneously distributed saturation was reached. In fact the larger part of the water was stored near the surface in the slopes of the dyke (cf. Fig. 6**a**) and **c**)). In these more saturated areas the sand has a higher hydraulic conductivity, so that water can flow laterally to the waterproof sealing at the base of the dyke due to capillary barrier effects. As a consequence, an area in the middle of the cross section remained nearly unchanged (cf. Fig. 6**d**)).

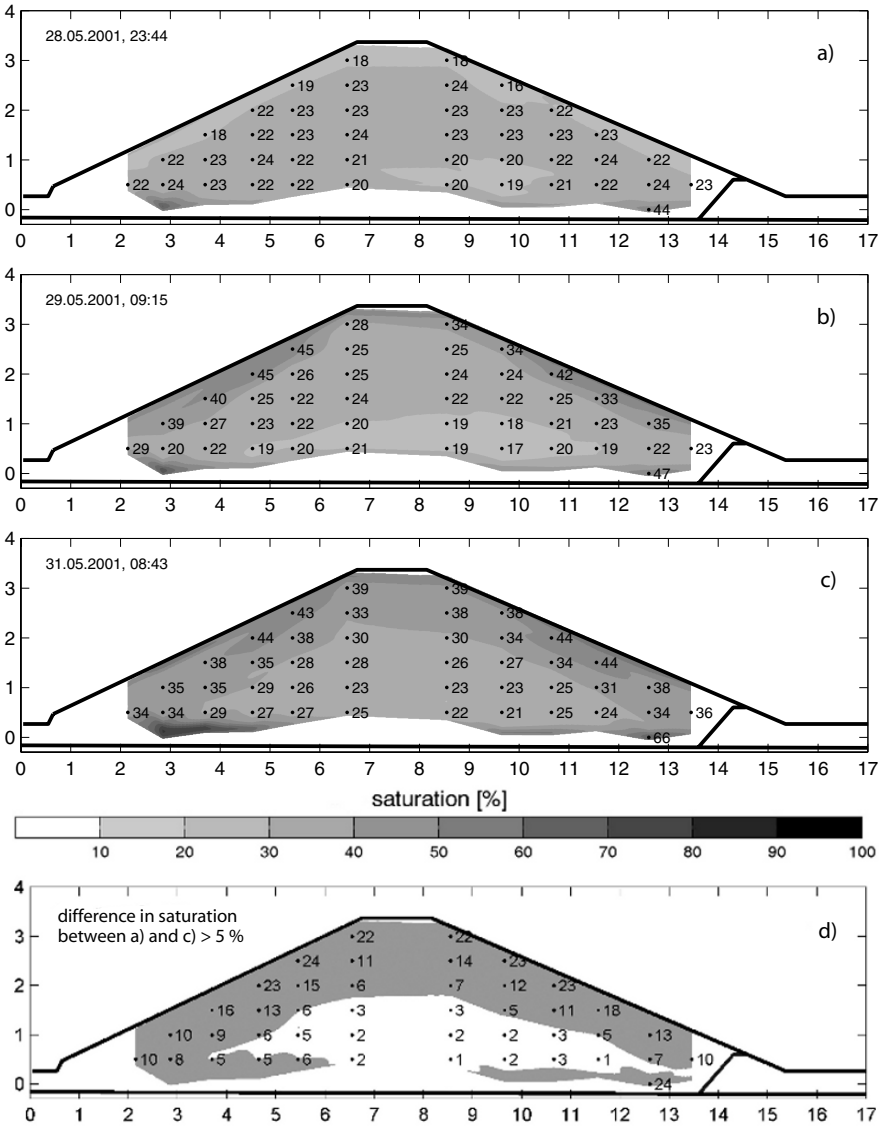

Fig. 6. Distribution of saturation during an irrigation test (148 mm in 72 h) on the full-scale dyke model: **a**) at the beginning of the irrigation test, **b**) after the first irrigation phase 9 h after beginning of the experiment, **c**) at the end of the experiment and **d**) shows the difference in the saturation between **a**) and **c**) during the test (area with changes $> 5\%$ highlighted in colour)

3 Laboratory Investigations

In order to verify the observations on the dyke model, additional laboratory experiments were carried out. The infiltration chamber used is 105 cm in length, 62.5 cm in height and 3 cm in depth. At the base of the chamber, water outlets are located in order to drain water out of the chamber. For the experiments, soil formations of the same material as in the dyke model were placed in the infiltration chamber. The initial condition of the soil within the chamber was always totally dry. At the top of the soil formation, an infiltration system was set up to use drop irrigation of a rate much smaller than the saturated hydraulic conductivity of the material. The infiltration process was recorded with a digital camera. In the following two sections, experiments concerning the phenomena observed are presented.

3.1 Fingering Experiment

For the fingering experiment, a soil formation was constructed in a chamber with a thin horizontal top soil layer. At 11 mm/h the mean infiltration rate during the experiment was approximately 65 times lower than the saturated hydraulic conductivity. Figure 7 shows infiltration fronts at specific

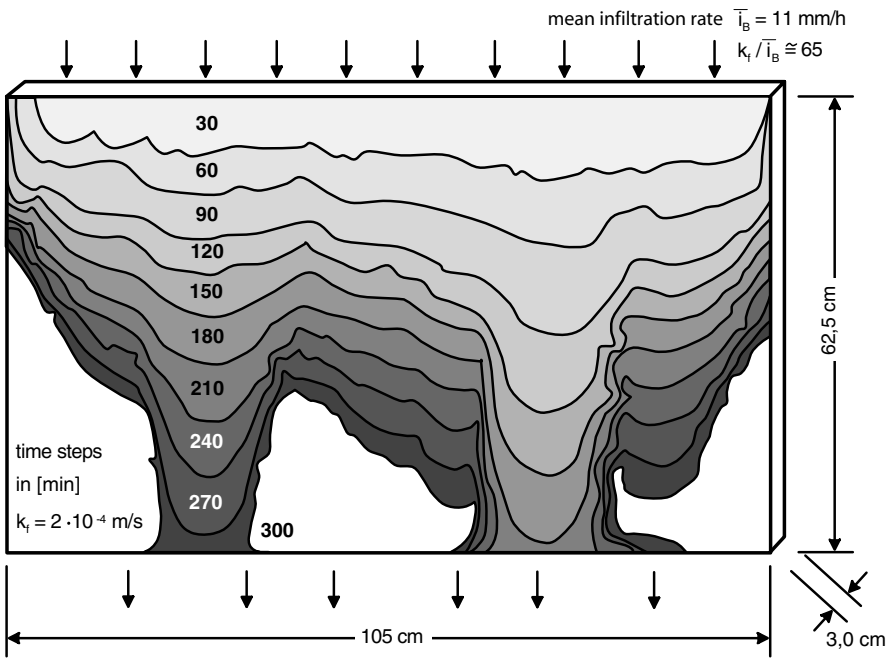

Fig. 7. Experiment on an infiltration chamber in order to investigate the fingering effect: Water fronts at different time intervals

time intervals. The grey scale colouring shows the temporal evolution of the infiltration. From the infiltration fronts, it can be seen very clearly that already after 60 minutes the first finger began to develop on the right side of the chamber. Sixty minutes later the second finger grew out of the infiltration front on the left side. As soon as a finger inclines to develop the water front around the finger starts to decelerate. Similar experiments have shown that almost saturated conditions prevail at the finger tip, whereas at the tail of the finger saturation decreases. As soon as the velocity of the water in the finger decreases, the water content increases and a growth of the finger as well as an accelerated movement of the water front starts in the surrounding material (Kawamoto and Miyazaki 1999). Both could also be observed in the laboratory experiment presented here.

3.2 Experiment on Lateral Water Movement

The soil formation for the investigation on the phenomenon of lateral water movements in inclined slopes was built with a similar slope inclination as the slopes of the full-scale dyke model. As in the experiment described above, the irrigation was set at 6.8 mm/h much lower than the saturated hydraulic conductivity (approx. 100 times). From the temporal evolution of the infiltration fronts, it can be seen very clearly that during the course of infiltration, the water movement was relocated more and more towards the slope, where the water flowed laterally in the direction of the drain. After approximately 200 minutes, water started to flow primarily from the slope to the base. Furthermore, a finger developed underneath the horizontal part of the soil formation on the right side of the infiltration chamber. The disturbed water fronts developed due to small heterogeneities which result from the way the soil formation was constructed.

4 Analysis of Experimental Investigations

As already pointed out in the introduction, both the development of fingering as well as the lateral movement of water due to the capillary barrier effect are based on the same soil hydraulic property, namely the breakthrough head which roughly corresponds to water entry value ψ_{WEV} of the soil. In this connection, the water entry value is equal to the matric potential when the soil becomes wet for the first time. However, physical investigations have proven that in reality the water entry value depends also on the initial condition of the soil (Wang et al. 2000). Also the daily observations have shown that soil becomes wetted much more easily, if it has already been wetted with water.

A method, which uses the inflection point of the imbibition soil water retention curve to determine an effective value for the water entry value, has been given by Baker and Hillel (1990), cf. Fig. 9. With the corresponding unsaturated hydraulic conductivity $k_u(\psi_{\mathrm{WEV}}) = 2.8 \cdot 10^{-5}\,\mathrm{m/s} \approx 100\,\mathrm{mm/h}$

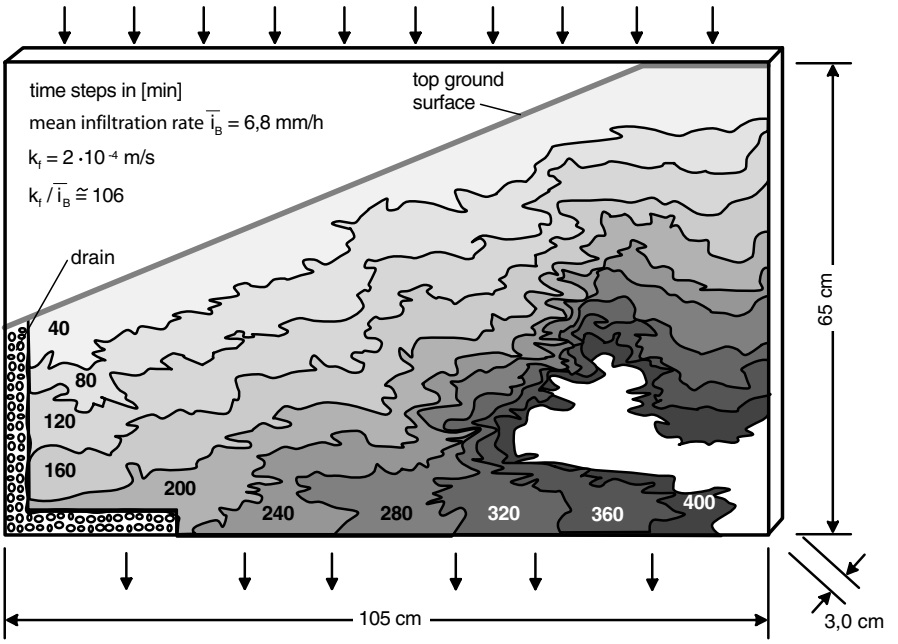

Fig. 8. Experiment on an infiltration chamber in order to investigate lateral water movements due to a capillary barrier effect: Water fronts at different time intervals

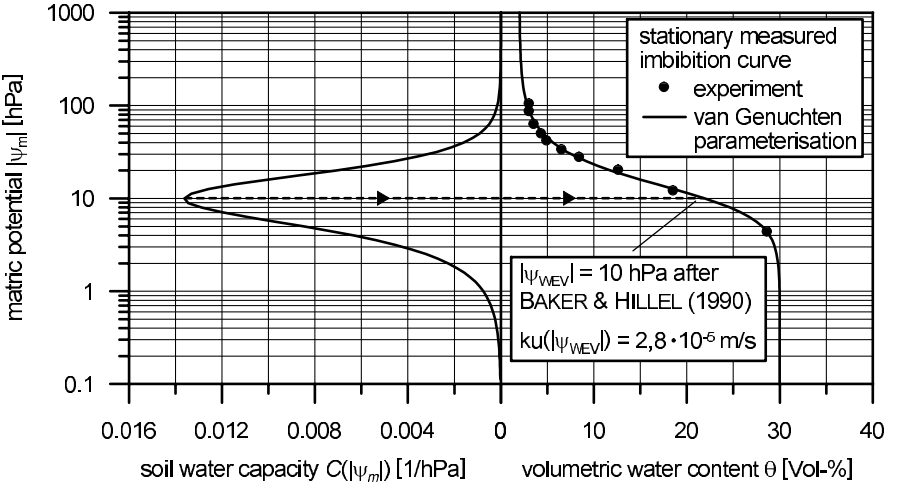

Fig. 9. Estimation of the effective water entry value ψ_{WEV} according to Baker and Hillel (1990) from the imbibition soil water retention curve of the construction material of the full-scale dyke model with experimental results and a van Genuchten parameterisation

(estimated from the soil water retention curve given in Fig. 9 and the saturated hydraulic conductivity $k_f = 2 \cdot 10^{-4}$ m/s with the model by Mualem (1976)) it is possible to estimate the possibility of the occurrence of preferential flow. Using the criterion according to Hillel and Baker (1988), as already mentioned in the introduction, and comparing $k_u(\psi_{\mathrm{WEV}})$ with the infiltration rates of the experiments (5–6 mm/h on the full-scale dyke model, 11 mm/h for the fingering experiment and 6.8 mm/h for the experiment on lateral water movement) it is completely possible that both phenomena could occur during the precipitation experiment on the full-scale dyke model.

5 Summary and Conclusion

A precipitation experiment on a homogeneously built full-scale dyke model at the Federal Waterways and Research Institute in Karlsruhe has shown anomalies, which indicate that preferential water movements in the form of fingering and lateral water movement have possibly occurred. In this connection, a new measuring system for the observation of spatially distributed water contents has provided important information on the hydraulic situation within the dyke body.

In order to verify the observations on the dyke model and to prove the hypothesis of preferential flow, additional laboratory investigations were conducted on an infiltration chamber. Both experiments showed clearly that unsaturated infiltration processes in inclinational soil formations can lead to preferential water movements in the form of fingering and lateral water movement. The appearance of these kinds of preferential flow can be expected, especially if the infiltration rate is lower than the unsaturated hydraulic conductivity at the water entry value.

Whereas the occurrence of lateral water movement could be proven by the moisture measurements using Spatial-TDR, some questions still remains regarding preferential flow due to fingering. The observations of the water level above the dyke base during the experiment indicate the occurrence of fingering. However, the investigations presented could not provide an undisputable proof of fingering.

Against the background of slope failures induced by heavy or extreme precipitation events, the questions concerning water infiltration and water movement processes in natural (hill) or artificial (deposit) slopes play a significant role.

References

Baker RS, Hillel D (1990) Laboratory tests of a theory of fingering during infiltration into layered soils, Soil Sci Soc Am J 54:20–30

Hill DE, Parlange J-Y (1972) Wetting front instability in layered soils, Soil Sci Soc Am Proc, 36(5):697–702

Hillel D, Baker RS (1988) A descriptive theory of fingering during infiltration into layered soils, Soil Science 146(1):51–56

Hübner C, Schlaeger S, Becker R, Scheuermann A, Brandelik A, Schaedel W, Schuhmann R (2005) Advanced measurement methods in Time Domain Reflectometry for soil moisture determination. In: Kupfer K (ed) Electromagnetic Aquametry, Springer, pp 317–347

Kawamoto K, Miyazaki T (1999) Fingering flow in homogeneous sandy soils under continuous rainfall infiltration, Soils and Foundation 39(4):79–91

McCord JT, Stephens DB, Wilson JL (1991) Hysteresis and state-dependent anisotropy in modelling unsaturated hillslope hydrologic processes, Water Resour Res 27(7):1501–1518

Mualem Y (1976) Hysteretical models for prediction of the hydraulic conductivity of unsaturated porous media, Water Resour Res 12(6):1248–1254

Scheuermann A, Bieberstein A (2005) Influence of the initial water content on the transient seepage through dikes. In: International Symposium in Dam Safety and Detection of Hidden Troubles of Dams and Dikes, Xi'an, China, November 1–3

Scheuermann A, Bieberstein A (2006) Monitoring of dams and dikes – water content determination using Time Domain Reflectometry (TDR). In: 13th Danube-European Conference on Geotechnical Engineering, Ljubljana, Slovenia, May 29–31, ISBN 961.90043–8–8, pp 493–498

Schlaeger S (2005) A fast TDR-inversion technique for the reconstruction of spatial soil moisture content, Hydrol Earth Sys Sci 2:971–1009

Stephens DB, Heermann S (1988) Dependence of anisotropy of saturation in a stratified sand, Water Resour Res 24(5):770–778

Stormont JC, Clifford EA (1999) Capillary barrier effect of underlying coarser soil layer, J Geotechnical and Geoenvironmental Engineering 125(8):641–648

Topp GC, Davis JL, Annan AP (1980) Electromagnetic determination of soil water content: Measurements in coaxial transmission lines, Water Resour Res 16(3):574–582

Walter MT, Kim J-S, Steenhuis TS, Parlange J-Y, Heilig A, Braddock RD, Selker JS, Boll J (2000) Funneled flow mechanisms in a sloping layered soil: Laboratory investigation, Water Resour Res 36(4):841–849

Wang Z, Wu L, Wu QJ (2000) Water-entry value as an alternative indicator of soil water-repellency and wettability, J Hydrology 231–232:76–83

Compaction Properties of Agricultural Soils

Anh-Minh Tang[1], Yu-Jun Cui[1], Javad Eslami[1], and Pauline Défossez-Berthoud[2]

[1] ENPC, 6–8 av. Blaise Pascal, F–77455 Marne–la–Vallée Cedex 2, France
tang@cermes.enpc.fr, cui@cermes.enpc.fr, eslami_javad@yahoo.com
[2] INRA, rue Fernand Christ, F–02007 Laon cedex, France defossez@laon.inra.fr

Summary. The compaction of field soils due to repeated rolling of agricultural vehicles is one of the main reasons for the agricultural soil degradation. A good understanding of the compaction properties of these soils is essential for an optimum organisation of agricultural activities, and therefore for environmental protection in terms of nitrate migrations. In the present work, the compaction properties of agricultural soils from four sites in France are studied after experimental data from oedometer tests. In the oedometer tests, a quick loading procedure was applied to simulate the loading of tire rolling. The soils that were initially in unsaturated state were loaded under constant water content condition. The compaction properties of these soils (i.e. the precompression vertical stress, compression index and swelling index) were then determined. The effect of initial dry density and initial water content on these properties is discussed. A possible effect of loading velocity on the apparent compressibility was observed. The results are finally discussed in the context of unsaturated soil mechanics.

Key words: compaction, agricultural soil, oedometer, quick loading, compressibility, dry density, water content

Introduction

Soil compaction induced by vehicle traffic is one of the major problems in modern agriculture. It is well-known that soil compaction increases soil strength and decreases soil hydraulic conductivity, as a result, root penetration is reduced; water extraction becomes more difficult; plants growth is therefore affected. From an economical point of view, this would result in the increase of production cost (Hamza and Anderson 2005, Raper 2005, Chan et al. 2006). Oedometer test is usually used to study the compaction properties of arable soils (Arvidsson and Keller 2004). The main parameters determined from this test are: (i) precompression stress, σ_p; (ii) the slope of the normal consolidation curve, λ; (iii) the slope of the unloading curve, κ. These parameters are useful in the modelling of agricultural soils compaction induced by vehicle

traffic (Berli et al. 2003). As the conventional oedometer test is time consuming, it is common practice to use pedotransfer functions (Imhoff et al. 2004) to estimate the soil mechanical properties. Horn et al. (2005) used this method to predict the mechanical strength of arable soils in Eastern and Western Europe countries at various scales.

In the present work, oedometer tests are performed to study the compaction properties of four soils from France. The effects of dry density and water content on the compressibility of soil are discussed.

Materials and Methods

Soil samples were taken from four sites in France: (1) Mons, La Somme; (2) Epernay, Marne; (3) le Breuil, Nièvre; (4) Avignon, Vaucluse. The soils samples were taken from two different horizons: from the cultured horizon at 0–30 cm and the undisturbed horizon at 30–60 cm depth. The physical properties determined according to the French Standards (AFNOR) are presented in Table 1. The specific gravity was determined using water pycnometer on soil sieved at 2 mm; Atterberg limits were determined with soil sieved at 0.4 mm; and the methylene blue absorption was measured with soil sieved at 0.5 mm. The classification is based on the Atterberg limits.

Prior to oedometer test, the bloc of undisturbed soil from 30–60 cm depth was wetted (by spraying) or dried (in air) to have the desired water content. When the target water content value was reached, the soil bloc was put in a hermetic box during 24 h for homogenisation of water distribution. Finally, the soil sample (70 mm in diameter, 20 mm in height) was trimmed directly from the soil bloc and inserted in the oedometer cell. The soils from 0–30 cm depth were air dried and sieved at 2 mm. Prior to oedometer test, the soils were wetted (by spraying) until the desired water content was reached. They were

Table 1. Physical properties of soils studied

Soil	Mons	Breuil	Epernay	Avignon
Specific gravity, G	2.62	2.56	2.68	2.71
Liquid limit, w_L (%)	32	58	49	31
Plastic limit, w_P (%)	22	51	29	20
Plasticity index, I_P (%)	10	7	20	11
Methylene blue absorption (g/100 g)	1.4	0.4	7.4	2.3
Grain size distribution (%):				
– Clay ($< 2\,\mu$m)	19	19	47	34
– Silt (2–50 µm)	75	23	33	51
– Sand ($> 50\,\mu$m)	6	58	20	16
Classification	Low plasticity clay	High plasticity silt	Low plasticity silt	Low plasticity clay

then stocked in a hermetic box during 24 h for obtaining homogeneous water distribution. Afterwards, the soils was compacted directly in the oedometer cell to the desired dry density.

Vertical normal stresses of 15, 30, 50, 100, 200, 300, 600, and 800 kPa were applied sequentially during loading stage. During unloading stage, the vertical normal stress was decreased from 800 kPa to 600, 300, 200, 100, 50, 30, 15 kPa. Each stress was applied for 5 min and the displacement (accuracy ± 0.001 mm) was read at the end of each step. At the end of test, the soil sample was taken out of the oedometer cell and its dimensions were measured using a calliper (accuracy $\pm$ 0.001 mm). Finally, its water content was determined by oven-drying at 105°C during 24 h. These measurements allowed determining the final void ratio and the degree of saturation. The initial void ratio is calculated by back analysis using final void ratio and total displacement measured.

Experimental Results

The test program and the main results are presented in Table 2. In Figure 1, the results of some test (void ratio and degree of saturation as a function of vertical stress) are shown. It can be observed that the relationship $e - \log \sigma_v$ in the unloading path is linear for all the tests. The swelling index is then calculated from the unloading path as follows: $\kappa = \Delta e / \Delta \ln \sigma_v$ (slopes in Fig. 1 divided by $\ln 10 = 2.3$). In the tests where a clear elasto-plastic behaviour is observed as test 12 (Fig. 1**a**) and test 39 (Fig. 1**d**), the compression index, $\lambda = \Delta e / \Delta \ln \sigma_v$, is calculated from the three last points in the compression curve. In test 16 (Fig. 1**b**) and test 31 (Fig. 1**c**) where a change of the slope can be observed during the compression curve, the maximum value of the slope is taken to calculate the compression index. The precompression stress (σ_p) is calculated as the interception of the compression line and the line that across the initial point and that is parallel to the unloading line. All the parameters obtained (σ_p, λ and κ) are shown in Table 2 with the void ratio (initial, e_i, and final, e_f), the water content (initial, w_i, and final, w_f) and the initial dry density (ρ_i).

In Figure 2, the precompression stress (σ_p), the compression index (λ) and the swelling index (κ) of all soils are drawn as functions of initial water content (w_i) and mean initial dry density (ρ_i). For all tests, a decrease of the precompression stress can be observed when the initial water content increases or when the initial dry density decreases. In addition, the swelling index (κ) seems to be insensible to the initial dry density and the swelling index. In the case of soils from Breuil (Fig. 2**a**) and Mons (Fig. 2**d**), it is observed that at the same water content, looser soil samples (lower dry density) have higher compression index, and that at the same dry density the compression index increases with the water content increase. For the soil from Epernay, Fig. 2**b**, the increase of water content reduces the compression index. In the case of soil from Avignon (Fig. 2**c**), wetting induced an increase following by a decrease

Table 2. Test program and results (Br.: Breuil; Ep.: Epernay; Av.: Avignon; Mo: Mons)

No	Soil	Depth (cm)	e_i	e_f	w_i (%)	w_f (%)	ρ_i (Mg/m^3)	σ_p (kPa)	λ	κ
1	Br.	0–30	1.49	0.85	24.7	24.7	1.03	34	0.225	0.012
2	Br.	0–30	1.43	0.81	18.9	18.2	1.05	45	0.235	0.010
3	Br.	0–30	1.49	0.81	25.3	22.7	1.03	24	0.224	0.012
4	Br.	0–30	1.08	0.73	23.3	22.5	1.23	65	0.153	0.009
5	Br.	0–30	1.16	0.79	24.7	24.7	1.19	67	0.163	0.012
6	Br.	0–30	1.09	0.80	17.9	18.8	1.22	106	0.133	0.009
7	Br.	0–30	0.93	0.76	20.2	19.1	1.33	165	0.111	0.008
8	Br.	0–30	0.99	0.77	24.2	24.2	1.29	129	0.135	0.011
9	Br.	0–30	1.01	0.74	25.8	25.2	1.27	114	0.148	0.010
10	Br.	30–60	1.41	0.83	18.1	17.4	1.06	50	0.259	0.007
11	Br.	30–60	1.24	0.72	24.7	23.8	1.14	35	0.181	0.010
12	Br.	30–60	1.30	0.84	16.3	13.5	1.11	95	0.222	0.006
13	Ep.	0–30	1.44	0.87	37.8	30.4	1.10	26	0.230	0.009
14	Ep.	0–30	1.64	0.84	32.5	28.6	1.02	26	0.358	0.016
15	Ep.	0–30	1.74	0.82	25.6	25.2	0.98	39	0.377	0.014
16	Ep.	0–30	1.27	0.88	37.1	29.7	1.18	29	0.146	0.015
17	Ep.	0–30	1.36	0.86	31.3	28.7	1.14	42	0.241	0.014
18	Ep.	0–30	1.41	0.78	25.6	25.0	1.11	73	0.304	0.010
19	Ep.	0–30	1.17	0.90	37.9	31.5	1.24	32	0.083	0.011
20	Ep.	0–30	1.10	0.82	30.4	28.4	1.28	56	0.133	0.012
21	Ep.	0–30	1.11	0.79	25.1	24.2	1.27	76	0.183	0.012
22	Ep.	30–60	1.16	0.90	32.5	30.6	1.24	60	0.108	0.016
23	Ep.	30–60	1.49	1.15	41.4	39.6	1.08	50	0.151	0.014
24	Ep.	30–60	1.08	0.90	30.2	29.6	1.29	83	0.093	0.013
25	Av.	0–30	1.36	0.66	16.8	16.4	1.15	37	0.247	0.011
26	Av.	0–30	1.24	0.59	22.4	19.5	1.21	19	0.258	0.014
27	Av.	0–30	1.04	0.64	28.7	20.4	1.33	15	0.103	0.015
28	Av.	0–30	1.13	0.63	16.5	16.2	1.27	77	0.228	0.010
29	Av.	0–30	1.10	0.58	22.1	19.5	1.29	26	0.229	0.014
30	Av.	0–30	0.91	0.60	28.5	20.2	1.42	20	0.096	0.014
31	Av.	0–30	1.06	0.64	16.8	16.4	1.32	98	0.212	0.009
32	Av.	0–30	0.98	0.59	21.9	19.6	1.37	28	0.154	0.013
33	Av.	0–30	0.88	0.63	28.2	19.6	1.44	23	0.068	0.013
34	Av.	30–60	0.76	0.60	19.2	18.4	1.54	99	0.089	0.012
35	Av.	30–60	0.80	0.60	23.0	19.2	1.51	77	0.086	0.012
36	Av.	30–60	0.79	0.61	21.0	19.8	1.51	45	0.083	0.014
37	Mo.	30–60	0.59	0.51	12.4	12.4	1.65	106	0.073	0.009
38	Mo.	30–60	0.79	0.63	19.5	19.5	1.46	112	0.109	0.008
39	Mo.	30–60	0.75	0.62	18.2	18.2	1.50	137	0.111	0.008
40	Mo.	30–60	0.78	0.60	29.7	20.5	1.47	68	0.105	0.012
41	Mo.	30–60	0.75	0.57	27.1	19.9	1.50	83	0.106	0.012

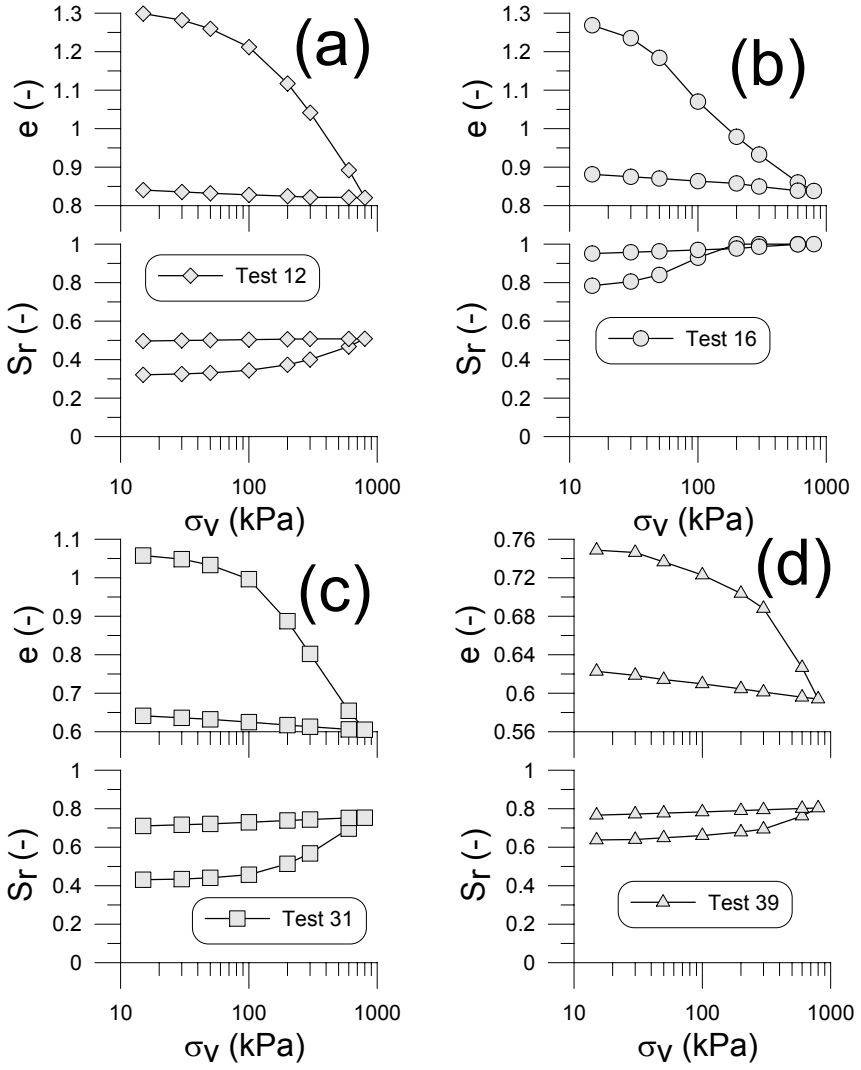

Fig. 1. Void ratio (e) and degree of saturation (S_r) as a function of vertical stress (σ_p): (a) Breuil; (b) Epernay; (c) Avignon; (d) Mons

of compression index in case of loose soils ($\rho_i = 1.25 - 1.35\,\mathrm{Mg/m^3}$). On the contrary, wetting induced only a decrease of compression index in the case of dense soils ($\rho_i = 1.40\,\mathrm{Mg/m^3}$).

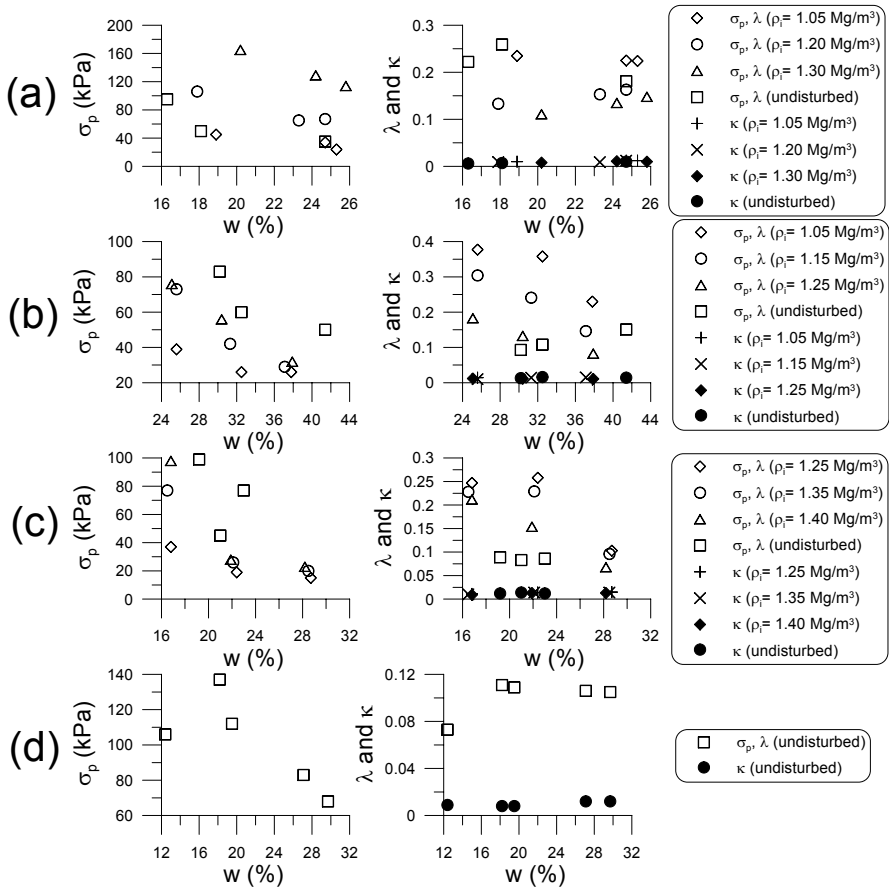

Fig. 2. Precompression stress (σ_p), compression index (λ) and swelling index (κ) as a function of mean initial water content (w_i) and initial dry density (ρ_i): (a) Breuil; (b) Epernay; (c) Avignon; (d) Mons

Discussions

In the domain of unsaturated soil mechanics, it is well-known that the precompression stress of looser soil is lower that that of denser soil. In addition, an increase of water content (that corresponds to a decrease of suction) reduces the soil strength or precompression stress (Alonso et al. 1990).

On the other hand, as the swelling index of soil depends on the stiffness of soil grains, it is independent on the soil density and on the water content in case of low plasticity soils. All these phenomena have been observed on the agricultural soils.

On the contrary, the effect of water content on the compression index observed in the present work is different from that found in the literature. After

Alonso et al. (1990), wetting softens the soil and increases then the compression index. Cui and Delage (1996) observed the same phenomenon on the compacted Jossigny silt. Nevertheless, this phenomenon can be observed only on the soils from Breuil and Mons. This contradiction can be explained by the consolidation mechanism in these tests. Indeed, in geotechnical engineering, a loading duration longer than 24 h is applied to simulate the stress generated by buildings construction. But in the present work, 5 min was applied for each loading stage in order to simulate the stress generated by rolling of agricultural vehicles. In case of plastic soils, as its permeability is low, this duration of 5 min may be not sufficient for water movement within the soil at high saturation degree. In Figure 1**b**, for example, loading increased the degree of saturation and the soil reached saturation state under 200 kPa vertical stress. The change of the compression curve slope observed in this test can be then explained by a partial consolidation of the soil.

In conclusion, wetting softens the soil and increases then the compression index. But this compression index can be reduced also by wetting due to the partial consolidation during short loading duration. This phenomenon depends on the permeability (that is influenced by soil dry density and soil plasticity) and the degree of saturation. The combination of these two trends governs the effect of water content on the compression index.

Conclusions

Oedometer tests were performed on agricultural soils taken from four sites in France. Rapid loading stage (5 min for each stage) was applied to study the soil compaction due to agricultural vehicles traffic. The effect of dry density and water content on the compaction properties of soils was observed. Generally, the soil is more compressible at lower dry density or higher water content. Nevertheless, in case of plastic soils or dense soils, wetting reduces the compression index. The consolidation mechanism was discussed to reveal the effect of loading duration on the compression index.

Acknowledgements

The authors are grateful for the technical assistance of D. Boitez and F. Bornet. This work is part of the French National Projects ANR–ADD and Gessol2. The financial support from the two projects is gratefully acknowledged.

References

Alonso EE, Gens A, Josa AA (1990) A constitutive model for partially saturated soil, Géotechnique 40(3):405–430

Arvidsson J, Keller T (2004) Soil precompression stress. I. A survey of Swedish arable soils, Soil & Tillage Research 77:85–95

Berli M, Kirby JM, Springman SM, Schulin R (2003) Modelling compaction of agricultural subsoils by tracked heavy construction machinery under various moisture conditions in Switzerland, Soil & Tillage Research 73:57–66

Chan KY, Oates A, Swan AD, Hayes RC, Dear BS, Peoples MB (2006) Agronomic consequences of tractor wheel compaction on a clay soil, Soil & Tillage Research 89:13–21

Cui YJ, Delage P (1996) Yielding and plastic behaviour of an unsaturated compacted silt, Géotechnique 46(2):291–311

Hamza MA, Anderson WK (2005) Soil compaction in cropping systems. A review of the nature, causes and possible solutions, Soil & Tillage Research, 82:121–145

Horn R, Fleige H, Richter FH, Czyz EA, Dexter A, Diaz-Pereira E, Dumitru E, Enarche R, Mayol F, Rajkai K, de la Rosa D, Simota C (2005) SIDASS project. Part 5: Prediction of mechanical strength of arable soils and its effects on physical properties at various map scales, Soil & Tillage Research 82:47–56

Imhoff S, Da Silva AP, Fallow D (2004) Susceptibility to compaction, load support capacity, and soil compressibility of Hapludox. Soil Sci Soc Am J 68:17–24

Raper RL (2005) Agricultural traffic impacts on soil, J Terramechanics 42:259–280

Bearing Capacity of Model Footings in Unsaturated Soils

Sai K. Vanapalli and Fathi M.O. Mohamed

Department of Civil Engineering, 161 Louis Pasteur Str., University of Ottawa, Ottawa, K1N 6N5 Ontario, Canada
vanapall@eng.uottawa.ca, fmoha035@uottawa.ca

Summary. A simple technique is proposed to predict the variation of the bearing capacity of an unsaturated soil with respect to matric suction. This technique is based on extending conventional bearing capacity theory proposed by Terzaghi. The proposed equation in this paper is presented as a functional relationship such that the variation of the bearing capacity of an unsaturated soil with respect to matric suction can be predicted. This technique is developed extending the concepts for predicting the shear strength of unsaturated soils proposed by Vanapalli et al. (1996). Using the approach presented in this paper, the bearing capacity of an unsaturated soil can be predicted using the saturated shear strength parameters, c' and ϕ' and the soil-water retention curve (SWRC).

Key words: bearing capacity, unsaturated soils, shear strength, matric suction, soil–water retention curve, model footings

Introduction

The bearing capacity is one of the key parameters required in the design of shallow foundations. Several approaches are available in the literature for determination of the bearing capacity of soils based on the saturated shear strength parameters (Terzaghi 1943, Meyerhof 1951). However, in several situations, shallow foundations are located above the ground water table where the soil is typically in a state of unsaturated condition. Nevertheless, the bearing capacity of soils is commonly determined assuming fully saturated conditions ignoring the influence of capillary stresses or the matric suction. Due to this reason, estimation of the bearing capacity of shallow foundations using the conventional approaches may not be reliable leading to uneconomical designs.

Foundation designs for unsaturated soils are complex and require not only the soil–structure interaction but also a fundamental understanding of soil behaviour that comprises the combined role of suction and cementation (Schnaid et al. 1995). Several researchers carried out investigations on the bearing capacity of unsaturated soils (Broms 1963, Steensen-Bach et al. 1987, Oloo 1994,

Miller and Muraleetharan 1998, Costa et al. 2003, Mohamed and Vanapalli 2006). All these studies have shown significant contribution of matric suction to the bearing capacity of unsaturated soils. However, limited theoretical research work is reported in the literature with respect to the interpretation of the bearing capacity of unsaturated soils (Fredlund and Rahardjo 1993, Oloo et al. 1997).

Based on the results presented in this study, a semi-empirical equation is proposed to predict the variation of the bearing capacity of unsaturated soils using the saturated shear strength parameters, c' and ϕ' and the SWRC. The equation presented in this paper is developed extending the concepts for predicting the shear strength of unsaturated soils proposed by Vanapalli et al. (1996). The proposed equation is also extended for other model footings studies reported in the literature that includes both coarse-grained and fine-grained soils. The studies presented in this paper show that there is a good comparison between the measured and predicted bearing capacity of model footings.

Test Equipment

Figure 1 shows the details of equipment specially designed at the University of Ottawa for determining the bearing capacity of coarse-grained soils using model footings. All the key features of this equipment are summarized in Mohamed and Vanapalli (2006). This equipment has special provisions to achieve fully saturated and unsaturated conditions of the compacted sand in the test tank. While the water table level in the test tank can be adjusted to the desired level using drainage valves, the capillary tension (i.e., matric suction) variation with respect to depth in the unsaturated soil zone below the model footing can be measured using commercial Tensiometers.

Properties of the Tested Soil

The properties of the soil used in this study were determined in the geotechnical laboratory of the University of Ottawa. The soil was classified using *USCS* as poorly graded sand (SP). The average void ratio after compaction was 0.63 and the dry unit weight was 16.02 kN/m^3. The internal friction angle was 35.3° from direct shear tests. Bolton (1986) studies on sands show that the effective stress and soil density affect the rate of dilatancy of soils and thereby influence the internal friction angle, ϕ'. As the dilatancy of sands has a significant effect on the ϕ' value, it was suggested that the measured ϕ' values can be modified as $\phi' = (\phi' + 0.8$ of dilatancy angle). Some investigators have found that better comparisons can be provided between the measured and computed bearing capacity values by using ϕ' values about 10 to 15% higher than the measured values (Steensen-Bach et al. 1987). Therefore, ϕ'

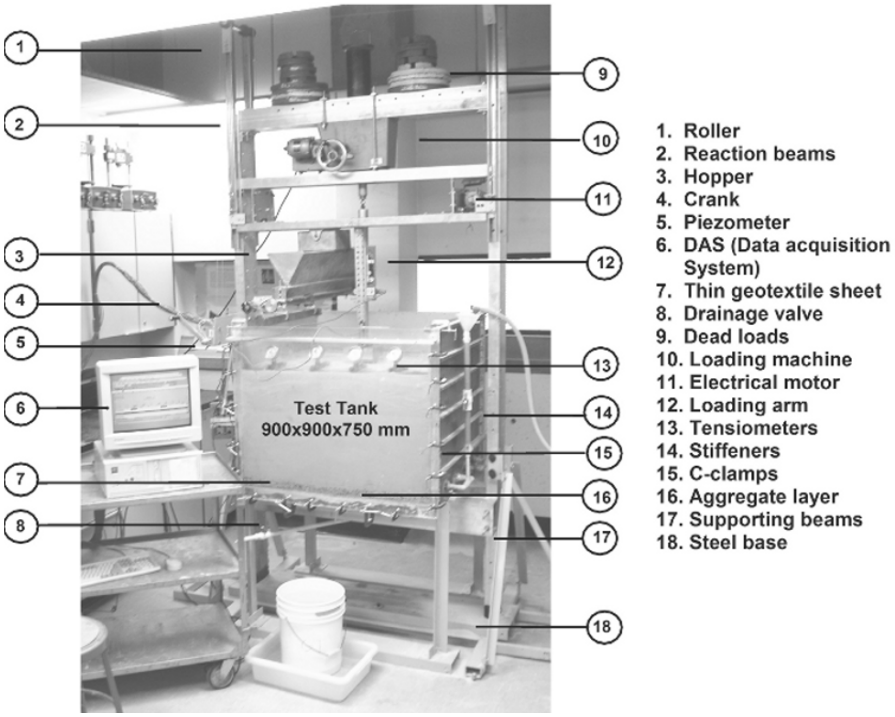

Fig. 1. University of Ottawa Bearing Capacity Equipment (UOBCE)

value which is 10% higher than the measured value (i.e., 39°) was used in this study.

Typical Experimental Results

The relationship between the applied stress and settlement of typical experimental results on a 100 mm × 100 mm square model footing is shown in Fig. 2. This relationship demonstrates that there is a significant increase in the bearing capacity of the model footing due to the contribution of matric suction in the range 0 to 6 kPa for the tested compacted, coarse-grained soil. The analysis presented in this paper is based on the average matric suction value in the proximity of the stress bulb. The procedure used for the determination of the average suction value is detailed using Fig. 3.

The variation of the matric suction with respect to depth underneath the model footing is non-linear as shown in Fig. 3 (left hand side). The variation of matric suction in the capillary zone above the ground water table (GWT) is typically hydrostatic (see right hand side of Fig. 3) for coarse-grained soils. The experimental results supported this generally observed behavior and indirectly

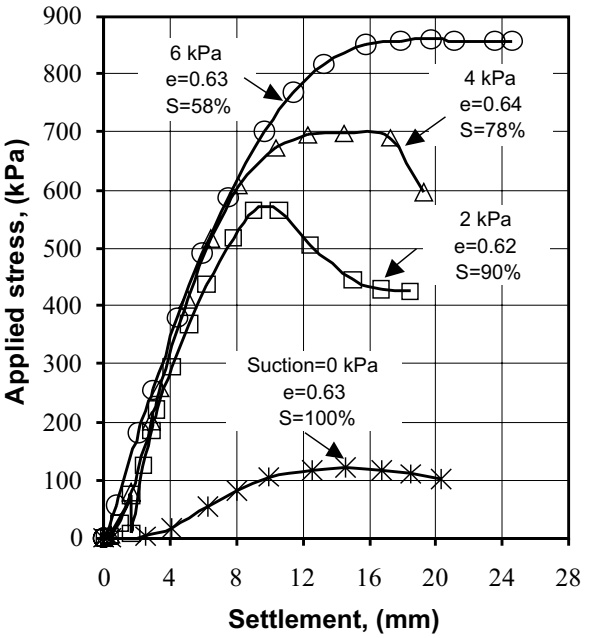

Fig. 2. The relationship between the applied stress versus settlement for 100 mm × 100 mm square model footing

demonstrated that the Tensiometers performed well. As the significant soil stresses are typically distributed over a depth of $1.5B$ (Poulos and Davis 1974 and Chen 1999) the matric suction value is considered as the average value of $(u_a - u_w)_1$ (matric suction close to the surface of the footing) and $(u_a - u_w)_2$ (matric suction value at the bottom of the stress bulb) as shown in Fig. 3.

The Measured and the Predicted SWRC

Figure 4 shows the soil–water retention curve (drying curve) plotted as a relationship between the degree of saturation, S and the matric suction, $(u_a - u_w)$ using three different methods. Two direct methods were used for measuring the SWRC's. The first method constituted the measurement of the SWRC directly from the test tank. The SWRC was also measured using the Tempe cell in the laboratory, which formed the second method. More details of the procedures used in the determination the SWRC are available in Mohamed and Vanapalli (2006). The third method for estimation of the SWRC was based on the procedure summarized in Vanapalli and Catana (2005). This procedure uses one measured point (i.e., water content and matric suction) along with data obtained from the grain size distribution curve. Figure 4 shows that

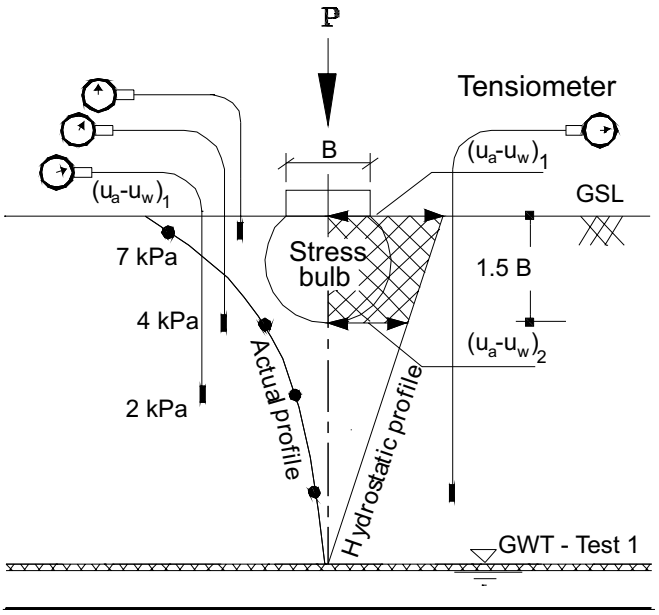

Fig. 3. Schematic to demonstrate the procedure used for determining the average matric suction below the footing

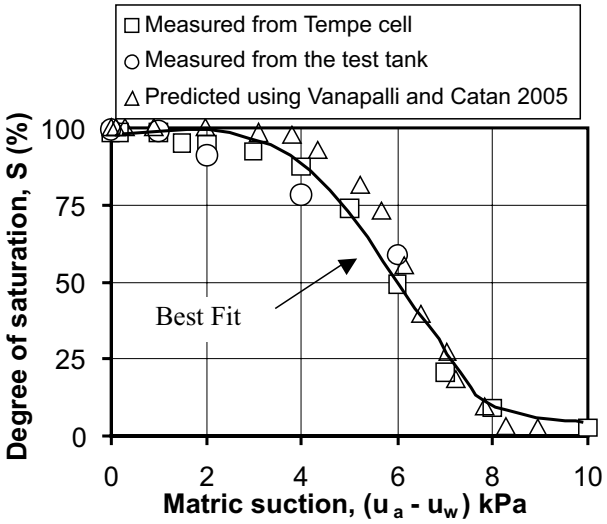

Fig. 4. Measured SWRC from the Tempe cell and test tank along with the estimated SWRC

there is a good agreement between the SWRC's using all the three methods. The objective of the determination of the SWRC was to understand its relationship with the bearing capacity of unsaturated soils similar to the shear strength of unsaturated soils.

Bearing Capacity of Unsaturated Soils

Terzaghi (1943) proposed an equation for computing the bearing capacity of shallow strip footings extending Prandtl (1921) assumptions for the soil failure mechanism. This equation is valid for strip footings resting in a homogenous soil and subjected to vertical loading.

$$q_u = c' N_c + q N_q + 0.5 B \gamma N_\gamma \tag{1}$$

where:
q_u = ultimate bearing capacity, kPa
q = overburden pressure, kPa
c' = effective cohesion, kPa
N_c, N_q, N_γ = bearing capacity factors due to cohesion, surcharge and unit weight, respectively
γ = soil unit weight, kN/m^3
B = footing width, m

Equation (1) can be written as given below for interpreting the bearing capacity of surface footings taking account of the influence of the shear strength contribution due to matric suction for unsaturated soils:

$$q_u = [c' + (u_a - u_w) \tan \phi^b] N_c + 0.5 B \gamma N_\gamma. \tag{2}$$

Vanapalli et al. (1996) proposed a relationship for estimating the shear strength contribution with respect to matric suction, $\tan \phi^b$ using the SWRC and the saturated shear strength parameters as $\tan \phi^b = S^\kappa \tan \phi'$, where S is the degree of saturation. This term, $S^\kappa \tan \phi'$, takes account of the non-linear variation of the shear strength of unsaturated soils using a fitting parameter, κ. Extending the concepts of shear strength of unsaturated soils proposed by Vanapalli et al. (1996), equation (2) can be used to predict the bearing capacity of unsaturated soils which desaturate on application of matric suction

$$q_u = [c' + (u_a - u_w) S^\psi \tan \phi'] N_c \xi_c + 0.5 \gamma B N_\gamma \xi_\gamma \tag{3}$$

where:
ψ = bearing capacity fitting parameter
ξ_c, ξ_γ = shape factors due to cohesion and unit weight (from Vesić 1973)

The fitting parameter, ψ used in equation (3) is referred as a bearing capacity fitting parameter in the remainder of the paper. The bearing capacity contribution due to matric suction can be obtained from a part of

equation (3), which is equal to $(u_a - u_w)S^{\psi} \tan \phi'$. This is similar to predicting the shear strength contribution due to matric suction using the expression $[(u_a - u_w)S^{\kappa} \tan \phi']$ from Vanapalli et al. (1996). Similar to prediction of the shear strength of unsaturated soils, the contribution of matric suction to the bearing capacity can be determined using the SWRC.

The philosophy of using the fitting parameter, ψ in the bearing capacity of unsaturated soils is similar to using the fitting parameter, κ for predicting the shear strength of unsaturated soils. Due to this reason, the limitation of using equation (3) in the prediction of the bearing capacity of unsaturated soils is similar to using the equation proposed by Vanapalli et al. (1996) for the prediction of the shear strength of unsaturated soils. In other words, equation (3) can only be used for predicting the bearing capacity when the experimental results are available. To alleviate such a limitation for the shear strength of unsaturated soils, Vanapalli and Fredlund (2000) and Garven and Vanapalli (2006) provided a relationship between κ versus plasticity index, I_P for predicting the shear strength of unsaturated soils. Such a relationship will be useful to obtain fitting parameter value from the plasticity index, I_P of the soil.

In the present study, the same philosophy has been extended to propose a relationship between the bearing capacity fitting parameter, ψ and plasticity index, I_P such that the bearing capacity of unsaturated soils can be predicted without the experimental results.

Equation 3 will take the form as equation 4 for interpreting the experimental results of the square model footing by including Vesić (1973) shape factors. Close observation of this equation shows that the equation has been modified to take account of the air-entry value, $(u_a - u_w)_b$. Up to the air-entry value, the contribution of matric suction to the bearing capacity is equal to $(u_a - u_w)_b(\tan \phi' - S^{\psi} \tan \phi')$. The form of this term is similar to $(u_a - u_w)_b(\tan \phi' - \tan \phi^b)$, which was derived by Oloo (1994). The bearing capacity contribution due to matric suction $\tan \phi^b$ in this term has been replaced with the term $S^{\psi} \tan \phi'$ (see equation 4):

$$q_u = [c' + (u_a - u_w)_b(1 - S^{\psi}) \tan \phi' + (u_a - u_w)_{\mathrm{AVR}} S^{\psi} \tan \phi'] \times N_c \left[1.0 + \left(\frac{N_q}{N_c}\right)\left(\frac{B}{L}\right)\right] + 0.5B\gamma N_{\gamma} \left[1.0 - 0.4\left(\frac{B}{L}\right)\right] \quad (4)$$

where
$(u_a - u_w)_{\mathrm{AVR}} = \frac{1}{2}[(u_a - u_w)_1 + (u_a - u_w)_2]$ as defined in Fig. 3,
$(u_a - u_w)_b$ = air entry value, kPa.

The bearing capacity factors due to cohesion, N_c, surcharge, N_q and unit weight, N_{γ} were developed by several researchers (Terzaghi 1943, Meyerhof 1951, Vesić 1973, Kumbhokjar 1993). The bearing capacity factors of N_c and N_q proposed by most of the investigators are approximately the same. For this reason, the bearing capacity factors, N_c and N_q originally proposed by Terzaghi (1943) using the limit equilibrium method were used in the analysis. There is no general consensus with respect to the bearing capacity factor

due to unit weight, N_γ. The N_γ values proposed by various investigators are significantly different (Terzaghi 1943, Meyerhof 1951, Vesić 1973). Kumbhokjar (1993) has undertaken an extensive study and proposed N_γ values based on numerical analysis which are relatively higher in comparison to other N_γ values reported in the earlier literature. This study also shows that bearing capacity computations provide better comparisons with the measured bearing capacity values using the proposed N_γ values. For this reason, the bearing capacity factor, N_γ values proposed by Kumbhokjar (1993) are used in this study.

Comparison between the Measured and Predicted Bearing Capacity of Unsaturated Soils

Equation (4) is used in the prediction procedure to provide comparisons with the measured values of bearing capacity for typical model square footings. The model footings were subjected to static vertical loads in the UOBCE both under saturated and unsaturated conditions. Different values of capillary suction (i.e., matric suction) were achieved by varying the water table level in the test tank (Fig. 1).

Figure 5 shows comparisons between the measured and predicted values of the variation of bearing capacity with respect to matric suction for the compacted coarse-grained sand studied. There is a reasonably good comparison between the measured and predicted bearing capacity values. However, the predicted values are slightly lower than the measured bearing capacity values. These differences may be attributed to the assumption used in the procedure

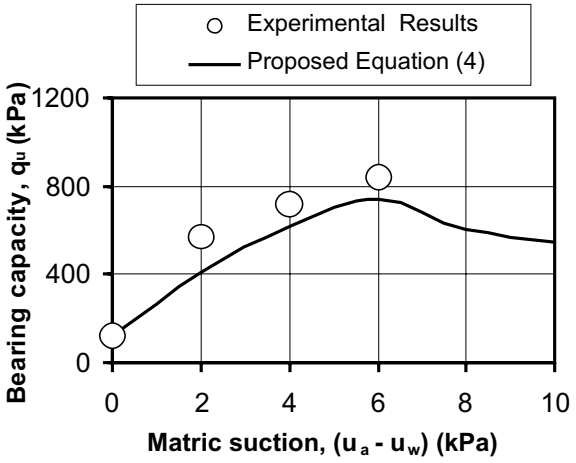

Fig. 5. Comparison between the measured and predicted bearing capacity versus matric suction for 100 mm × 100 mm footing

for the estimation of the average matric suction values below the footing, which typically results in the lower contribution of matric suction compared to the actual value. Similar trends were observed for the measured and predicted values of bearing capacity for four other soils data from the literature. For this reason, the proposed prediction procedure may be summarized to be conservative as the measured bearing capacity is slightly higher than the predicted bearing capacity.

All the above observations are derived from the results of model footings tested in a laboratory environment. More details of the analysis and comparisons between the measured and predicted bearing capacity of the other four soils could not be provided in this paper due to space limitations.

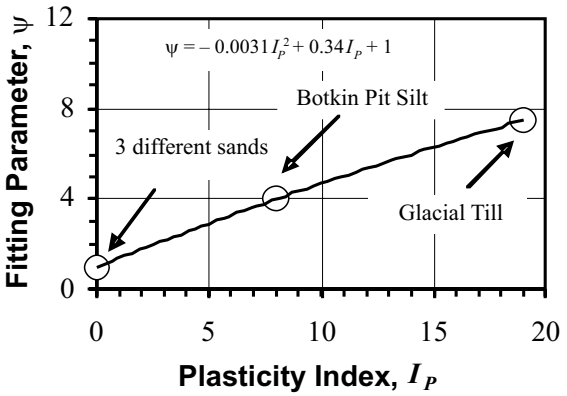

Fig. 6. Relationship between the bearing capacity fitting parameter, ψ and plasticity index, I_p

The bearing capacity fitting parameter, ψ value was equal to 1 for all the three sandy soils studied and higher values were required for the other fine-grained soils. Based on results of the study undertaken through this research program on five soils, a relationship was developed between the bearing capacity fitting parameter, ψ and the plasticity index, I_P (Fig. 6 and equation (5))

$$\psi = 1.0 + 0.34I_P - 0.0031I_P^2. \tag{5}$$

Conclusions

In this paper, a simple technique is proposed for predicting the bearing capacity of unsaturated soils using the saturated shear strength parameters, c' and ϕ' and the SWRC. The results of the study suggest that there is a good comparison between the measured and predicted bearing capacity values. The framework is based on studies undertaken on model footings and shows considerable promise for extending it to field studies.

Acknowledgements

The authors thank the General Public Committee of Higher Education in Libya (G.P.C.H.E) for providing the financial support to F.M.O. Mohamed during this research program. The authors would like to acknowledge the funding received from National Sciences and Engineering Research of Canada (NSERC) for this project. Thanks also go to C. Catana, graduate student from the Department of Civil Engineering, University of Ottawa for his assistance.

References

Bolton MD (1986) The Strength and Dilatancy of Sands, Geotechnique 36(1):65–78

Broms BB (1963) The Effect of Degree of Saturation on the Bearing Capacity of Flexible Pavements, Highway Research Record 71:1–14

Chen FH (1999) Soil Engineering, Testing, Design and Remediation. CRC Press LLC, N.W., Boca Raton, Florida, USA

Costa YD, Cintra JC, Zornberg JG (2003) Influence of Matric Suction on the Results of Plate Load Tests Performed on a Lateritic Soil Deposit. Geotechnical Testing Journal, 26(2):219–226

Fredlund DG, Rahardjo H (1993) Soil Mechanics for Unsaturated Soils, 1st Ed. Wiley, New York

Garven E, Vanapalli SK (2006) Evaluation of Empirical Procedures for Predicting the Shear Strength of Unsaturated Soils. Proceedings of the Fourth International Conference on Unsaturated Soils, Carefree, Arizona, American Society of Civil Engineers Geotechnical Special Publication 147(2):2570–2581

Kumbhokjar AS (1993) Numerical Evaluation of Terzaghi's N_γ. Journal of Geotechnical Engineering, American Society of Civil Engineers 1999(3):598–607

Meyerhof GG (1951) The Ultimate Bearing Capacity of Foundations, Geotechnique 2:301–332

Miller GA, Muraleetharan KK (1998) In Situ Testing in Unsaturated Soil. Proceedings of the Second International Conference on Unsaturated Soils, Beijing, China, Vol. 1:416–421

Mohamed FMO, Vanapalli SK (2006) Laboratory Investigations for the Measurement of the Bearing Capacity of an Unsaturated Coarse-Grained Soil. 59th Canadian Geotechnical Conference, BC, Vancouver (in print)

Oloo SY (1994) A Bearing Capacity Approach to the Design of Low Volume Traffic Roads. Ph.D. Thesis, University of Saskatchewan, Canada

Oloo SY, Fredlund DG, Gan JK-M (1997) Bearing Capacity of Unpaved Roads. Canadian Geotechnical Journal 34:398–407

Poulos HD, Davis EH (1974) Elastic Solutions for Soil and Rock Mechanics, John Wiley and Sons, New York

Prandtl L (1921) Eindringunsfestigkeit und Festigkeit von Schneiden. Z. Angew. Math. Mech. 1(4):15–20

Schnaid F, Consoli NC, Cudmani RO, Militistsky J (1995) Load-settlement response of shallow foundations in structured unsaturated soils. Proceedings of the First International Conference of Unsaturated Soils, Paris, France 999–1004

Steensen-Bach JO, Foged N, Steenfelt JS (1987) Capillary Induced Stresses – Fact or Fiction? Nineth ECSMFE, Groundwater Effects in Geotechnical Engineering, Dublin 83–89

Terzaghi K (1943) Theoretical Soil Mechanics. John Wiley and Sons, New York

Vanapalli SK, Fredlund DG, Pufahal DE, Clifton AW (1996) Model for the Prediction of Shear Strength with respect to Soil Suction. Canadian Geotechnical Journal 33:379–392

Vanapalli SK, Fredlund DG (2000) Comparison of Empirical Procedures to Predict the Shear Strength of Unsaturated Soils Using the Soil-Water Characteristic Curve, Geo-Denver 2000. American Society of Civil Engineers, Geotechnical Special Publication 99:195–209

Vanapalli SK, Catana MC (2005) Estimation of the Soil–Water Characteristic Curve of Coarse-Grained Soils Using One Point Measurement and Simple Properties. Proceedings of an International Symposium on Advanced Experimental Unsaturated Soil Mechanics 401–410

Vesić AS (1973) Analysis of Ultimate Loads of Shallow Foundations. Journal of the Soil Mechanics and Foundation Division, ASCE 99(SM1):45–73

Influence of Soil Suction on Trench Stability

Valerie Whenham[1], Monika De Vos[1], Christian Legrand[1], Robert Charlier[2], Jan Maertens[3], and Jean-Claude Verbrugge[4]

[1] Geotechnical Division, Belgian Building Research Institute (BBRI), Brussels, Belgium valerie.whenham@bbri.be, monika.de.vos@bbri.be, Christian.legrand@bbri.be
[2] GeomaC Department University of Liège (ULg), Liège, Belgium Robert.Charlier@ulg.ac.be
[3] Department of Civil Engineering, Catholic University of Leuven (KUL), Leuven, Belgium jan.maertens.bvba@skynet.be
[4] Laboratoire Jacques Verdeyen Université Libre de Bruxelles (ULB), Brussels, Belgium jverbrug@ulb.ac.be

Summary. A research project on the stability of temporary trenches in unsaturated soil is carried out in Belgium. The main objective of the project is to evaluate the seasonal variations of suction in the soil and to quantify the consequences of these suction variations on trench stability. Within the framework of the research, a full scale instrumented test trench with vertical sides has been excavated in June 2004 at the site of BBRI, characterized by quaternary loam (Limelette, Belgium), to compare calculations with full-scale observations. As expected first failures occurred during the winter, when suction in the soil was minimal. This paper presents the details of this experiment.

Key words: temporary, trench, slope stability, suction, full-scale experiment

1 Introduction

Common methods applied in Belgium for designing trenches and evaluating slope stability do not take into account the effects of suction when present in silty and sandy unsaturated soils. The suction is one of the reasons that steeply inclined slopes remain stable, while this stability can not be proven by common design rules. Because of the large occurrence of unsaturated loam and sand soils (possibly after water lowering) during excavations, a research project on the stability of temporary trenches in unsaturated soil is carried out in Belgium, with the financial support of the federal ministry of Economical Affairs. The main objective of the project is to assess the influence of precipitations on trench stability. In a first approach, it is assumed that the influence of precipitations on slope stability can be related to the variations of the suction in the soil. In order to evaluate this approach, theoretical predictions – based

on "easily applicable" measurement systems, soil characterization procedures and calculation methods that can be promoted in the practice – were compared with full-scale observations obtained from the trench test experiments that are presented in this paper.

2 Geotechnical Context

2.1 Selection of a Site

Because of the large occurrence of unsaturated loam in Belgium, the site of BBRI at Limelette where the subsoil exists out of overlying quaternary loam ($I_p = 10\%$) was selected to carry out the test trench experiments. An extensive geotechnical investigation of the test site is described in Van Alboom and Whenham (2003).

2.2 Preliminary Investigation

In order to evaluate the soil layering in the test area, eight Electrical Cone Penetration Tests (CPT-E) were performed on the selected site. Further a boring with undisturbed sampling was executed to define through laboratory tests the physical and mechanical properties of the soil (Figs 1 and 2).

Gravimetric soil water content profiles were determined in order to characterise the soil layering in terms of water content susceptibility, and a first series of suction measuring devices were placed with the aim to assess the range of suctions developed at different depths as well as the evolution of this suction with the seasons (Fig. 3).

2.3 Additional Soil Characterization Tests

Additional laboratory tests were performed on undisturbed samples in order to allow further interpretation of the experiment. Besides, unsaturated

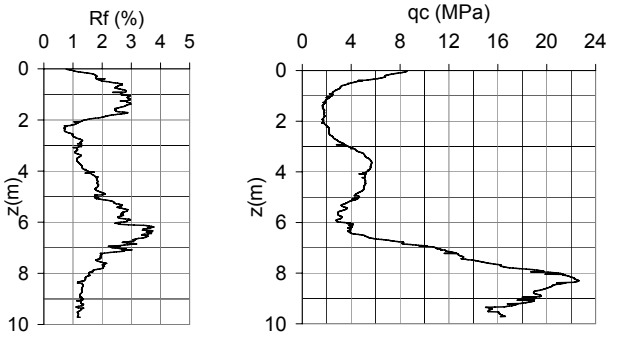

Fig. 1. Average values of the CPT-E results for the test site at Limelette

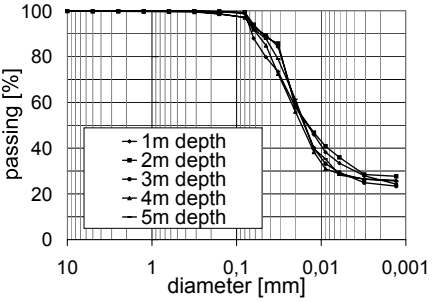

Fig. 2. Grain size distribution curve

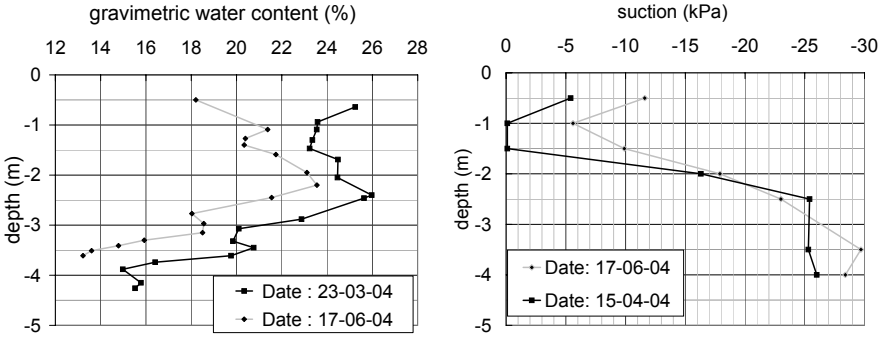

Fig. 3. Gravimetric water content and suction profiles at Limelette (preliminary investigation results)

specimens were tested using a modified triaxial apparatus. Tests were carried out under constant water (CW) conditions, where the specimen was drained with respect to the pore air pressure and undrained with respect to the pore water pressure during shear. Typical derived values of friction angle and cohesion from CU- and CW-triaxial tests are given in Table 1. Soil water retention curves were determined in the laboratory on undisturbed soil samples using the axis translation technique. Results are shown in Fig. 4.

Table 1. Typical results of CU and CW triaxial tests (sampling depth = 1.5 m)

Type of triaxial test	Applied suction s [kPa]	Effective cohesion c' [kPa]	Effective friction angle φ' [°]
CU-test	0	0	32.2
CW-test	20	19.2	35.7
CW-test	50	18.1	35.8

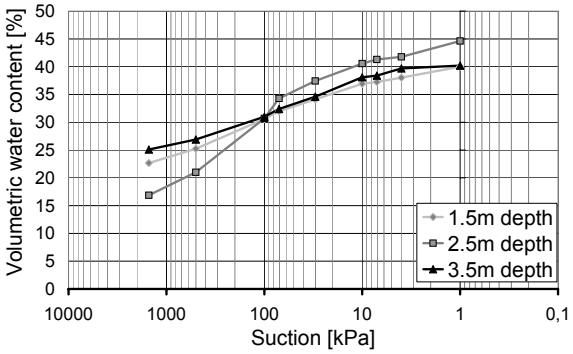

Fig. 4. Soil water retention curves determined on undisturbed soil samples – axis translation technique

3 Test Trench Experiment

3.1 Objective of the Experiment

The objective of the experiment was to observe the influence of the seasonal variations of suction in the soil on the stability of a full scale instrumented trench, and to compare this influence in terms of soil movements and failures with very simple calculation methods proposed in the literature (Fredlund and Rahardjo 1993, Vanapalli and Fredlund 2000). This experiment took place between June 2003 and June 2004.

3.2 Definition of the Geometry of the Test Trench

The geometry of the test trench was established based on the preliminary soil investigation data, taking into account the goal that was to observe the influence of suction degradation on slope stability. A length of 20 m was found to be sufficient in order to avoid 3D effects. Besides, it was calculated that a vertical 3 meters depth trench side would only be stable taking into account the cohesion increase attributable to the suction levels measured in the summer, while suction levels measured in the winter would not be sufficient. It was therefore decided to excavate a test-trench of 20 m length, with vertical 3 m depths sides.

3.3 Instrumentation

Based on the test-trench layout and in order to follow the suction and degree of saturation in the soil, an extensive instrumentation was specified (Fig. 5). Before the excavation was executed, reference tensiometers were placed all around the excavation area, at depths varying from 0.5 m to 3.5 m. Further

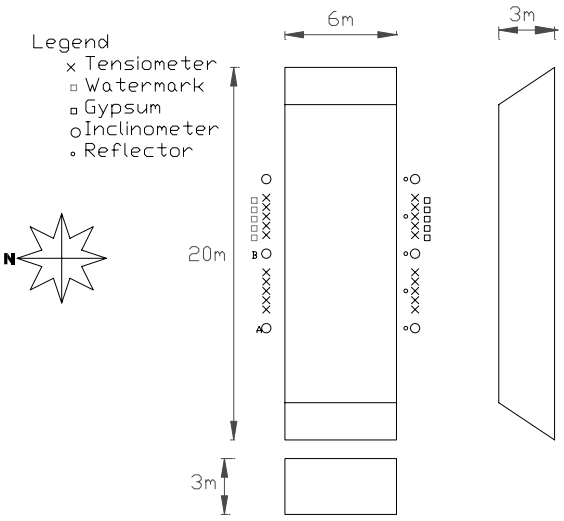

Fig. 5. Test-Trench layout and instrumentation

instrumentation consisted in watermark sensors for suction measurements and gypsum blocs for soil water content evaluation. Besides inclinometer casings and reflectors were installed in order to monitor soil movements.

3.4 Observations

The test trench was excavated in June 2004. Weekly averaged rain measurements obtained for the site as well as averaged suction results are presented in Fig. 6. For shallow measurements, the influence of precipitations on the suction results can clearly be observed. However, below 1.5 m depth, the response to rains in terms of suction variations is significantly "smoothed". From Figure 6, it can also be observed that while it rained much more in the summer, and in particular during the months of July and August, suctions were still measured even in the upper layers due to the evaporation being much more important than in the winter (from December to March).

Settlement and horizontal movements of the trench sides were monitored from June 2004 (before excavation of the test trench) using reflectors and inclinometers. Results of these measurements are shown in Fig. 7. Few displacements were measured, and the degradation of the trench side was observed to be limited to very superficial erosion until first failures occurred.

First failures of the test-trench occurred in January 2005 after heavy rains. These first failures – registered by webcams focussed on the trench sides – were shown to be localized and to occur very suddenly. Further failures occurred during the following days. This first experiment also illustrated the effects of erosion on the inclined sides (see Fig. 8).

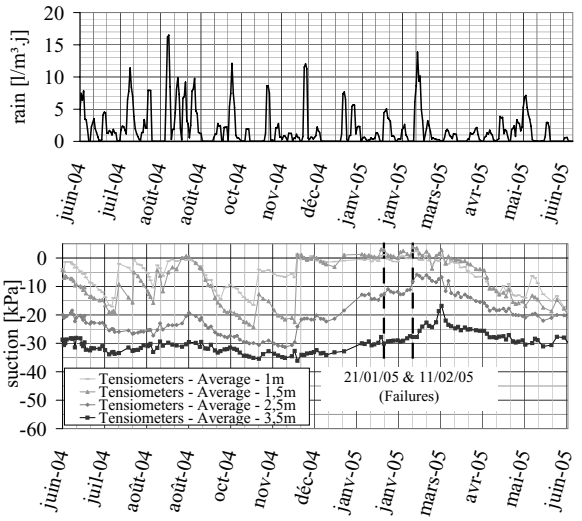

Fig. 6. Rain measurements and Averaged suction measurements

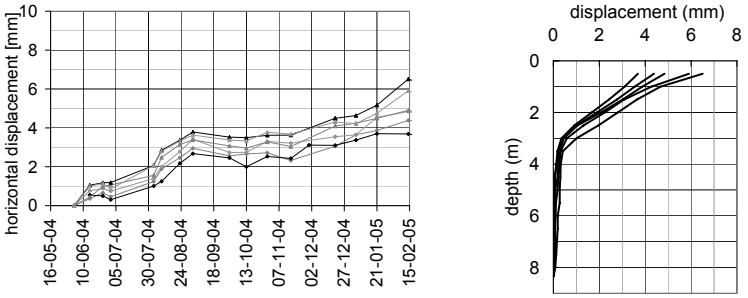

Fig. 7. Inclinometer results (horizontal movements measured at a distance of 1 m from the vertical trench sides): (**a**) movements measured at 0.5 m depth, (**b**) displacement profiles measured after the first trench failures

4 Conclusions

This contribution has given a general overview of an experiment carried out at the site of BBRI, within the framework of a national research project on the influence of precipitations on trench stability. This experiment involved the excavation and monitoring of a full scale instrumented test-trench. As expected, it was observed that the test trench remained stable during the first seven months, while first failures occurred in the winter when suction measurements were minimal.

Fig. 8. Upper left: June 2004 – after excavation of the test trench; Upper right: first localised failures (January 2005); Lower left: eroded inclined sides; Lower right: generalized failures (February 2005)

References

BBRI – Research report (2005) Stabilité des talus: Méthodes de calcul avec prise en compte du degré de saturation du sol, et déduction de règles pratiques pour l'exécution des tranchées et fouilles temporaires, biennale 2003–2005

Fredlund, Rahardjo (1993) Soil mechanics for unsaturated soils, John Wiley & Sons, USA 517 pp

Vanapalli, Fredlund (2000) Comparison of different procedures to predict unsaturated soil shear strength. In: Shackleford C, Houston SL, Chang N-Y (eds) Advances in Unsaturated Soils, Geotechnical Special Publication No. 99. Reston, American Society of Civil Engineers:195–209

Van Alboom, Whenham (2003) Soil investigation campaign at Limelette (Belgium): Results. In: Proc Symp on screw piles in sand – design & recent developments, May 7th 2003, Brussels

Index

SPRINGER PROCEEDINGS IN PHYSICS

66 **The Structure and Conformation of Amphiphilic Membranes**
Editors: R. Lipowsky, D. Richter, and K. Kremer

67 **Nonlinearity with Disorder**
Editors: F. Abdullaev, A.R. Bishop, and S. Pnevmatikos

68 **Time-Resolved Vibrational Spectroscopy V**
Editor: H. Takahashi

69 **Evolution of Dynamical Structures in Complex Systems**
Editors: R. Friedrich and A. Wunderlin

70 **Computational Approaches in Condensed-Matter Physics**
Editors: S. Miyashita, M. Imada, and H. Takayama

71 **Amorphous and Crystalline Silicon Carbide IV**
Editors: C.Y. Yang, M.M. Rahman, and G.L. Harris

72 **Computer Simulation Studies in Condensed-Matter Physics IV**
Editors: D.P. Landau, K.K. Mon, and H.-B. Schüttler

73 **Surface Science**
Principles and Applications
Editors: R.F. Howe, R.N: Lamb, and K. Wandelt

74 **Time-Resolved Vibrational Spectroscopy VI**
Editors: A. Lau, F. Siebert, and W. Werncke

75 **Computer Simulation Studies in Condensed-Matter Physics V**
Editors: D.P. Landau, K.K. Mon, and H.-B. Schüttler

76 **Computer Simulation Studies in Condensed-Matter Physics VI**
Editors: D.P. Landau, K.K. Mon, and H.-B. Schüttler

77 **Quantum Optics VI**
Editors: D.F. Walls and J.D. Harvey

78 **Computer Simulation Studies in Condensed-Matter Physics VII**
Editors: D.P. Landau, K.K. Mon, and H.-B. Schüttler

79 **Nonlinear Dynamics and Pattern Formation in Semiconductors and Devices**
Editor: F.-J. Niedernostheide

80 **Computer Simulation Studies in Condensed-Matter Physics VIII**
Editors: D.P. Landau, K.K. Mon, and H.-B. Schüttler

81 **Materials and Measurements in Molecular Electronics**
Editors: K. Kajimura and S. Kuroda

82 **Computer Simulation Studies in Condensed-Matter Physics IX**
Editors: D.P. Landau, K.K. Mon, and H.-B. Schüttler

83 **Computer Simulation Studies in Condensed-Matter Physics X**
Editors: D.P. Landau, K.K. Mon, and H.-B. Schüttler

84 **Computer Simulation Studies in Condensed-Matter Physics XI**
Editors: D.P. Landau and H.-B. Schüttler

85 **Computer Simulation Studies in Condensed-Matter Physics XII**
Editors: D.P. Landau, S.P. Lewis, and H.-B. Schüttler

86 **Computer Simulation Studies in Condensed-Matter Physics XIII**
Editors: D.P. Landau, S.P. Lewis, and H.-B. Schüttler

87 **Proceedings of the 25th International Conference on the Physics of Semiconductors**
Editors: N. Miura and T. Ando

88 **Starburst Galaxies**
Near and Far
Editors: L. Tacconi and D. Lutz

89 **Computer Simulation Studies in Condensed-Matter Physics XIV**
Editors: D.P. Landau, S.P. Lewis, and H.-B. Schüttler

90 **Computer Simulation Studies in Condensed-Matter Physics XV**
Editors: D.P. Landau, S.P. Lewis, and H.-B. Schüttler